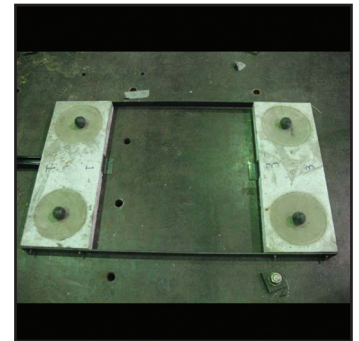
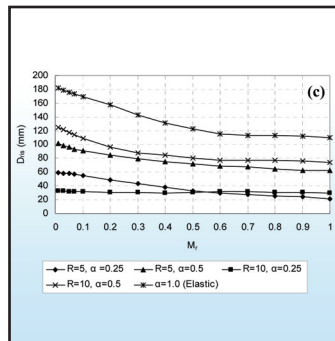


Integrated Design Methodology for Isolated Floor Systems in Single-Degree-of-Freedom Structural Fuse Systems

by

Shenlei Cui, Michel Bruneau and Michael C. Constantinou



Technical Report MCEER-12-0004

June 13, 2012

NOTICE

This report was prepared by the University at Buffalo, State University of New York as a result of research sponsored by MCEER through a grant from the Earthquake Engineering Research Centers Program of the National Science Foundation under NSF award number EEC-9701471 and other sponsors. Neither MCEER, associates of MCEER, its sponsors, the University at Buffalo, State University of New York, nor any person acting on their behalf:

- a. makes any warranty, express or implied, with respect to the use of any information, apparatus, method, or process disclosed in this report or that such use may not infringe upon privately owned rights; or
- b. assumes any liabilities of whatsoever kind with respect to the use of, or the damage resulting from the use of, any information, apparatus, method, or process disclosed in this report.

Any opinions, findings, and conclusions or recommendations expressed in this publication are those of the author(s) and do not necessarily reflect the views of MCEER, the National Science Foundation, or other sponsors.

Integrated Design Methodology for Isolated Floor Systems in Single-Degree-of-Freedom Structural Fuse Systems

by

Shenlei Cui,¹ Michel Bruneau² and Michael C. Constantinou²

Publication Date: June 13, 2012

Submittal Date: April 13, 2012

Technical Report MCEER-12-0004

NSF Master Contract Number EEC 9701471

- 1 Ph.D. Candidate, Department of Civil, Structural and Environmental Engineering, University at Buffalo, State University of New York
- 2 Professor, Department of Civil, Structural and Environmental Engineering, University at Buffalo, State University of New York

MCEER

University at Buffalo, State University of New York

133A Ketter Hall, Buffalo, NY 14260

Phone: (716) 645-3391; Fax (716) 645-3399

E-mail: mceer@buffalo.edu; WWW Site: <http://mceer.buffalo.edu>

Preface

MCEER is a national center of excellence dedicated to the discovery and development of new knowledge, tools and technologies that equip communities to become more disaster resilient in the face of earthquakes and other extreme events. MCEER accomplishes this through a system of multidisciplinary, multi-hazard research, in tandem with complimentary education and outreach initiatives.

Headquartered at the University at Buffalo, The State University of New York, MCEER was originally established by the National Science Foundation in 1986, as the first National Center for Earthquake Engineering Research (NCEER). In 1998, it became known as the Multidisciplinary Center for Earthquake Engineering Research (MCEER), from which the current name, MCEER, evolved.

Comprising a consortium of researchers and industry partners from numerous disciplines and institutions throughout the United States, MCEER's mission has expanded from its original focus on earthquake engineering to one which addresses the technical and socio-economic impacts of a variety of hazards, both natural and man-made, on critical infrastructure, facilities, and society.

The Center derives support from several Federal agencies, including the National Science Foundation, Federal Highway Administration, National Institute of Standards and Technology, Department of Homeland Security / Federal Emergency Management Agency, and the State of New York, other state governments, academic institutions, foreign governments and private industry.

This study investigates methods to reduce floor acceleration demands in buildings with structural fuses. A strategy is proposed that combines passive hysteretic energy dissipation devices (PED) with isolated floors in rooms where acceleration-sensitive equipment is located. Two kinds of isolated floor systems were studied. The first isolated floor system used concrete ball-in-cone (BNC) isolators with rubber and polyurethane spherical solid balls, instead of steel balls, as the rolling balls between the top and bottom concrete bearing plates. A multi-directional spring unit was used as the isolator in second isolated floor system. Characterization tests were conducted on these two isolated floor systems, from single isolator to complete system; and models of single-degree-of-freedom (SDOF) structural fuse frames with these two isolated floor systems were developed. Studies were then conducted to determine the preferred parameter values to be used in design, and to establish how the combined systems behave under different mass ratios of the isolated floor system to the base SDOF structural fuse structure. Finally, combined design concepts considering both the design of the base SDOF structural fuse structure and the design of the isolated floor system on top were developed for each kind of isolated floor system.

ABSTRACT

Various researchers developed general design procedures for the design of structures with structural fuses (i.e., defined as metallic passive hysteretic energy dissipation (PED) devices which are disposable or can be easily replaced after a seismic event). The structural fuse concept, as implemented in these design procedures, requires to concentrate all the seismic damage in the structural fuses, while the bare frame hosting these devices behaves elastically during a seismic event. Past research showed that structures are stiffened when using PED devices as structural fuses, which correspondingly reduces the displacement demands on these structures. Therefore, one benefit of using structural fuses is that displacement sensitive nonstructural components in such buildings can be better protected during seismic events. However, this past research also showed that this may also correspond to an increase in floor acceleration demands. To protect the acceleration sensitive equipments on the floors of such buildings, a possible solution may be to combine the stiffening of structures using PED devices with a strategy of introducing isolated floors in the rooms where such acceleration-sensitive equipment is located. This is the strategy investigated in this report.

Two kinds of isolated floor systems were studied in this research. Characterization tests were first conducted on two kinds of isolated floor systems to define their mechanical behavior properties, from single isolators to complete systems. The experimentally obtained mechanical behavior was then simulated in computer programs. Models of single-degree-of-freedom (SDOF) structural fuse frames with implementation of these two isolated floor systems were developed. A number of parametric studies were then conducted on these combined systems to determine the preferred design parameter values to be used in the design of such structural fuse frames coupled with isolated floors, and to establish how the combined systems behave under different mass ratios of the isolated floor system to the base SDOF structural fuse structure. Finally, combined design concepts considering both the design of the base SDOF structural fuse structure and the design of the isolated floor system on top were developed for each kind of isolated floor system.

ACKNOWLEDGMENTS

This work was supported by the Earthquake Engineering Research Centers Program of the National Science Foundation under Award No. ECC-9701471 to the Multidisciplinary Center for Earthquake Engineering Research (MCEER). The multi-directional spring unit is a proprietary device patented by Dynamic Isolation Systems, Inc. (DIS). The floor isolation system and the springs were provided by DIS for this study. This support is greatly appreciated. Any opinions, findings, conclusions, and recommendations presented in this report are those of the authors and do not necessarily reflect the views of the sponsors.

A new element was developed by Dr. Andrei M. Reinhorn and Dr. Hwa-Sung Roh in IDARC2D, which was used to simulate the unique behavior of the multi-directional spring units. This assistance is gratefully acknowledged.

The experimental part of this research could not have been accomplished without the valuable collaboration of the staff of the Structural Engineering and Earthquake Simulation Laboratory (SEESL) at the University at Buffalo. Sincere thanks to Mark Pitman, Duane Kozlowski, Robert Staniszewski, Christopher Budden, Lou Moretta, Scot Weinreber, Goran Josipovic and Chris Zwierlein for sharing their collective expertise.

TABLE OF CONTENTS

SECTION	TITLE	PAGE
1	INTRODUCTION	1
2	LITERATURE REVIEW	5
2.1	Introduction	5
2.2	Structural Fuse Concept	5
2.3	Base Isolation Bearings.....	9
2.4	Response and Design of Nonstructural Components	13
3	CONCRETE BNC ISOLATOR CHARACTERIZATION TEST	17
3.1	Introduction	17
3.2	Empirical Model for Concrete BNC Isolator	19
3.3	Concrete BNC Isolator Design and Cast	26
3.4	Test Setup	29
3.4.1	Specimen assembly and setup	29
3.4.2	Load program	32
3.4.3	Input program	33
3.4.4	Instrumentation	36
3.4.5	Test protocol	38
3.5	Test Results	43
3.5.1	Results of free-vibration tests	43
3.5.2	Results of force-displacement tests	47
3.5.3	Results of sweep frequency tests	56
3.5.4	Results of dynamic tests using earthquake inputs	63
3.6	Observations	73
4	MULTI-DIRECTIONAL SPRING UNIT CHARACTERIZATION TEST AND PHYSICAL MODEL	75
4.1	Introduction	75
4.2	Multi-directional Spring Unit Description	76
4.3	Test Setup	77
4.3.1	Specimen setup and instrumentation	77
4.3.2	Input program	83
4.3.3	Test protocol	88
4.4	Test Results	89
4.4.1	Results of Test Series 1 and 2	89
4.4.2	Results of Test Series 3	94
4.5	Physical Model of Multi-directional Spring Units	102
4.5.1	General system geometry.....	102
4.5.2	Hysteretic behavior model for pre-tensioned multi-directional spring units	105
4.5.3	Hysteretic behavior model for non-pre-tensioned multi-directional spring units	111
4.6	Sensitivity Study	115
4.7	Observations	121

TABLE OF CONTENTS (CONT'D)

SECTION	TITLE	PAGE
5	ISOLATED FLOOR SYSTEM II CHARACTERIZATION TEST	123
5.1	Introduction	123
5.2	Isolated Floor System II Description	125
5.3	Test Setup	126
5.3.1	Specimen assembly and setup	126
5.3.2	Load program	130
5.3.3	Input program	146
5.3.4	Instrumentation	151
5.3.5	Test protocol	154
5.4	Test Results	157
5.4.1	General	157
5.4.2	Typical results	158
5.4.3	Comparisons	161
5.5	Additional Tests	185
5.6	Further Investigation of Rotation Effect	191
5.7	Importance of Quality Control	195
5.8	Observations	198
6	ISOLATED FLOOR SYSTEM I CHARACTERIZATION TEST	199
6.1	Introduction	199
6.2	Isolated Floor System I Description	200
6.3	Test Setup	206
6.3.1	Specimen assembly and setup	206
6.3.2	Load program	209
6.3.3	Input program	212
6.3.4	Instrumentation	213
6.3.5	Test protocol	217
6.4	Test Results	222
6.4.1	General	222
6.4.2	Typical results	223
6.4.3	Comparisons	226
6.5	Response when Hitting the Wall	268
6.6	Further Investigation of Rotation Effect	269
6.7	Observations	274
7	ANALYTICAL MODELS OF BEHAVIOR OF ISOLATED FLOOR SYSTEMS.....	275
7.1	Introduction	275
7.2	Analytical Model of Isolated Floor System I Behavior	276
7.2.1	Equivalent friction coefficient	276
7.2.2	Analytical model	284
7.2.3	Comparison between results from analytical model and tests	285

TABLE OF CONTENTS (CONT'D)

SECTION	TITLE	PAGE
7.2.4	Sensitivity study	306
7.3	Analytical Model of Isolated Raised Floor System II Behavior	309
7.3.1	Analytical model	309
7.3.2	Comparison between results from analytical model and tests	313
7.3.3	Sensitivity study	323
7.4	Observations	325
8	PARAMETRIC STUDY OF SYSTEMS CONSISTING OF SINGLE-DEGREE-OF-FREEDOM STRUCTURAL FUSE FRAMES AND ISOLATED FLOOR SYSTEMS	327
8.1	Introduction	327
8.2	Development of New Spectra Compatible Acceleration Time Histories	328
8.3	Model Setup and Selection of Parameters	330
8.4	Initial Parametric Study on Coupled Models	335
8.4.1	Isolated Floor System I	335
8.4.2	Isolated Floor System II under lower bound load	339
8.4.3	Isolated Floor System II under upper bound load	345
8.5	Selected Targeted Parametric Studies	350
8.5.1	Parametric study using uncoupled model	350
8.5.2	Parametric study on mass ratio	352
8.5.2.1	Isolated Floor System I	353
8.5.2.2	Isolated Floor System II	361
8.5.3	Explanation of the observed trends	367
8.6	Observations	374
9	DESIGN METHODOLOGY FOR SYSTEMS CONSISTING OF SINGLE-DEGREE- OF-FREEDOM STRUCTURAL FUSE FRAMES AND SOLATED FLOOR SYSTEMS	379
9.1	Introduction	379
9.2	Design Methodology For Systems Consisting of SDOF Structural Fuse Frames and Isolated Floor System I	380
9.2.1	Linear static method	380
9.2.2	Nonlinear response history method	390
9.2.3	Comparison of designs	392
9.3	Design Methodology For Systems Consisting of SDOF Structural Fuse Frames and Isolated Floor System II	392
9.3.1	Linear static method	392
9.3.2	Nonlinear response history method	395
9.3.3	Comparison of designs	396
9.4	Observations	397
10	CONCLUSIONS AND FUTURE RESEARCH	407

TABLE OF CONTENTS (CONT'D)

SECTION	TITLE	PAGE
11	REFERENCES.....	411
APPENDICES (Provided on attached CD)		
A	DESIGN OF ISOLATED FLOOR SYSTEM I	449
B	DESIGN OF CONCRETE BALL-IN-CONE (BNC) ISOLATOR	467
C	ADDITIONAL TEST RESULTS OF ISOLATED FLOOR SYSTEM II	479
D	ADDITIONAL TEST RESULTS OF ISOLATED FLOOR SYSTEM I	519
E	DESIGN OF COMBINED SYSTEMS USING ISOLATED FLOOR SYSTEM I _LINEAR STATIC METHOD	611
F	DESIGN OF COMBINED SYSTEMS USING ISOLATED FLOOR SYSTEM I _NONLINEAR RESPONSE HISTORY METHOD	623
G	DESIGN OF COMBINED SYSTEMS USING ISOLATED FLOOR SYSTEM II _LINEAR STATIC METHOD	635
H	DESIGN OF COMBINED SYSTEMS USING ISOLATED FLOOR SYSTEM II _NONLINEAR RESPONSE HISTORY METHOD	647
I	COMMENTS ON ISOLATED FLOOR DISPLACEMENT DEMANDS	657

LIST OF FIGURES

FIGURE	TITLE	PAGE
2.1	Frame with Nippon Steel BRBs (from Vargas and Bruneau (2006b))	7
2.2	Frame with Star Seismic BRBs (from Vargas and Bruneau (2006b))	8
2.3	BNC Isolator on Top of Third Floor (from Vargas and Bruneau (2006b))	9
2.4	Lead-Rubber Isolator (from Naeim and Kelly 1999)	10
2.5	Double FP Bearing (from Fenz and Constantinou 2008)	10
2.6	BNC Geometries and Corresponding Restoring Laws (from Kemeny and Szidarovszky 1995)	11
2.7	Seismic Isolated Platform with Patented Ball-B-Cone TM Isolators (from Amik et al. 1998)	13
3.1	BNC Bearing: (a) Working Surface; (b) Free Body Diagram of Isolated Weight	20
3.2	Behavior of BNC Bearing with Friction	23
3.3	Behavior of BNC Bearing without Friction	25
3.4	Bearing Plate of Concrete BNC Isolator: (a) Plan and Cross Section Views; (b) Bearing Plates at Maximum Displacement	27
3.5	Bearing Plate Cast: (a) Foam Mold; (b) Foam Mold with Reinforcement; (c) Concrete Pouring	28
3.6	Concrete BNC Isolator Specimen: (a) Bottom Bearing Plates with Balls; (b) Specimen	30
3.7	Specimen Setup_1	31
3.8	Specimen Setup_2	31
3.9	Average Elastic Response Spectrum of Realization VS Target Response Spectrum ($\zeta=5\%$)	34
3.10	Lateral Force-Displacement Relationship of Structural Fuse Frame	35
3.11	Layout of Instrumentation	36
3.12	Results of Free Vibration Tests under Load Case 1: (a) Rubber Balls; (b) Polyurethane Balls	44
3.13	Results of Free Vibration Tests under Load Case 2: (a) Rubber Balls; (b) Polyurethane Balls	45
3.14	Results of Free Vibration Tests under Load Case 3: (a) Rubber Balls; (b) Polyurethane Balls	46
3.15	Results of Free Vibration Tests under Load Case 4: (a) Rubber Balls; (b) Polyurethane Balls	47
3.16	Acceleration-displacement Relationship under Load Case 1_Rubber Balls: (a) 0.05 Hz; (b) 0.2 Hz; (c) 0.8 Hz	49
3.17	Acceleration-displacement Relationship under Load Case 2_Rubber Balls: 0.2 Hz	50
3.18	Acceleration-displacement Relationship under Load Case 3_Rubber Balls: (a) 0.05 Hz; (b) 0.2 Hz; (c) 0.8 Hz	51
3.19	Acceleration-displacement Relationship under Load Case 4_Rubber Balls: 0.2 Hz	52

LIST OF FIGURES (CONT'D)

FIGURE	TITLE	PAGE
3.20	Acceleration-displacement Relationship under Load Case 1_Polyurethane Balls: (a) 0.05 Hz; (b) 0.2 Hz; (c) 0.8 Hz	53
3.21	Acceleration-displacement Relationship under Load Case 2_Polyurethane Balls: 0.2 Hz	54
3.22	Acceleration-displacement Relationship under Load Case 3_Polyurethane Balls: (a) 0.05 Hz; (b) 0.2 Hz; (c) 0.8 Hz	55
3.23	Acceleration-displacement Relationship under Load Case 4_Polyurethane Balls: 0.2 Hz	56
3.24	Acceleration-displacement Relationship under Load Case 1_Sweep Frequency	58
3.25	Acceleration-displacement Relationship under Load Case 2_Sweep Frequency	59
3.26	Acceleration-displacement Relationship under Load Case 3_Sweep Frequency	60
3.27	Acceleration-displacement Relationship under Load Case 4_Sweep Frequency	61
3.28	Torsion Effect of Concrete Isolator under Load Case 2: (a) Rubber Ball; (b) Polyurethane Ball	63
3.29	Acceleration-Displacement Relationship of Concrete Isolator (Rubber Balls, Load Case 1): (a) Subject to Acc1; (b) Subject to Acc2; (c) Subject to Acc3	65
3.30	Acceleration-Displacement Relationship of Concrete Isolator (Rubber Balls, Load Case 3): (a) Subject to Acc1; (b) Subject to Acc2; (c) Subject to Acc3	66
3.31	Acceleration-displacement Relationship of Concrete Isolator (Rubber Balls, Load Case 4): (a) Subject to Acc1; (b) Subject to Acc2; (c) Subject to Acc3	67
3.32	Acceleration-Displacement Relationship of Concrete Isolator (Polyurethane Balls, Load Case 1): (a) Subject to Acc1; (b) Subject to Acc2; (c) Subject to Acc3	68
3.33	Acceleration-Displacement Relationship of Concrete Isolator (Polyurethane Balls, Load Case 3): (a) Subject to Acc1; (b) Subject to Acc2; (c) Subject to Acc3	69
3.34	Acceleration-Displacement Relationship of Concrete Isolator (Polyurethane Balls, Load Case 4): (a) Subject to Acc1; (b) Subject to Acc2; (c) Subject to Acc3	70
3.35	Torsion Effect of Concrete Isolator (Rubber Balls, Acc2): (a) Load Case 1; (b) Load Case 3; (c) Load Case	71
3.36	Torsion Effect of Concrete Isolator (Polyurethane Balls, Acc2): (a) Load Case 1; (b) Load Case 3; (c) Load Case 4	72
4.1	Multi-directional Spring Unit	77
4.2	Multi-directional Spring Unit in Isolated Floor System	77
4.3	Specimen Configuration of Test Series 1: (a) 3-D View and; (b) Side View of the Specimen Setup	80
4.4	Specimen Configuration of Test Series 2: (a) 3-D View and; (b) Side View of the Specimen Assembly and Setup	81
4.5	Specimen Configuration of Test Series 3: (a) 3-D View and; (b) Side View of the Specimen Assembly and Setup	82
4.6	Anchor End Used in Test Series 3	83
4.7	Half Sinusoidal Signal with Frequency of 0.05 Hz	84

LIST OF FIGURES (CONT'D)

FIGURE	TITLE	PAGE
4.8	Half Sinusoidal Signal with Frequency of 0.2 Hz	85
4.9	Complete Sinusoidal Signal with Frequency of 0.05 Hz	85
4.10	Complete Sinusoidal Signal with Frequency of 0.2 Hz	86
4.11	Seismic Floor Displacement Record of 2Acc31wo	86
4.12	Seismic Floor Displacement Record of 3Acc31wo	87
4.13	Seismic Displacement Record of B107050	87
4.14	Seismic Floor Displacement Record of B207050	88
4.15	Test Results of 2627 N/m (15 lb/in) Spring without Pretension	91
4.16	Test Results of 1313 N/m (7.5 lb/in) Spring without Pretension	92
4.17	Test Results of 2627 N/m (15 lb/in) Spring with 51 mm (2 in) Pretension	92
4.18	Test Results of 1313 N/m (7.5 lb/in) Spring with 51mm (2 in) Pretension	93
4.19	Comparison of Realization and Target of Seismic Displacement Record 2Acc31wo (from Test of 2Acc31wo152ww)	95
4.20	Comparison of Realization and Target of Seismic Displacement Record 3Acc31wo (from Test of 3Acc31wo152ww)	96
4.21	Comparison of Realization and Target of Seismic Displacement Record B107050 (from Test of B107050072ww)	96
4.22	Comparison of Realization and Target of Seismic Displacement Record B207050 (from Test of B207050072ww)	97
4.23	Test Results of 2627 N/m (15 lb/in) Spring Units without Pretension	98
4.24	Test Results of 1313 N/m (7.5 lb/in) Spring Units without Pretension	99
4.25	Test Results of 2627 N/m (15 lb/in) Spring Units with 51mm (2 in) Pretension	99
4.26	Test Results of 1313 N/m (7.5 lb/in) Spring Units with 51 mm (2 in) Pretension	100
4.27	Comparison of Original and Modified Results of Test 05152ww	102
4.28	Geometry of Bushing and Cable System under Isolated Floor Displacement: (a) Floor Motion towards the Spring Unit, and; (b) Floor Motion away from the Spring Unit	103
4.29	Comparison of Model Straight Line for 2627 N/m (15 lb/in) Spring and Test Results of 05152wowo	107
4.30	Comparison of Model Straight Lines for 1313 N/m (7.5 lb/in) Spring and Test Results of 05072wowo	107
4.31	Comparison of Model Prediction for 2627 N/m (15 lb/in) Spring Unit and 05152ww Test Results	110
4.32	Comparison of Model Prediction for 1313 N/m (7.5 lb/in) Spring Unit and 05072ww Test Results	110
4.33	Comparison of Model Straight Lines for 2627 N/m (15 lb/in) Spring and Test Results of 05150wowo	112
4.34	Comparison of Model Straight Lines for 1313 N/m (7.5 lb/in) Spring and Test Results of 05070wowo	113
4.35	Comparison of Model Prediction for 2627 N/m (15 lb/in) Spring Unit and 05150ww Test Results	114

LIST OF FIGURES (CONT'D)

FIGURE	TITLE	PAGE
4.36	Comparison of Model Prediction for 1313 N/m (7.5 lb/in) Spring Unit and 05070ww Test Results	114
4.37	Comparison of Behaviors of 2627 N/m Spring Unit under Different r Values ($a = 20$ mm, $f = 18$ N, $\mu_k = 0.171$)	117
4.38	Comparison of Behaviors of 2627 N/m Spring Unit under Different a Values ($r = 31$ mm, $f = 18$ N, $\mu_k = 0.171$)	117
4.39	Comparison of Behaviors of 2627 N/m Spring Unit under Different f Values ($r = 31$ mm, $a = 20$ mm, $\mu_k = 0.171$)	118
4.40	Comparison of Behaviors of 2627 N/m Spring Unit under Different μ_k Values ($r = 31$ mm, $a = 20$ mm, $f = 18$ N)	118
4.41	Comparison of Behaviors of 1313 N/m Spring Unit under Different r Values ($a = 20$ mm, $f = 18$ N, $\mu_k = 0.190$)	119
4.42	Comparison of Behaviors of 1313 N/m Spring Unit under Different a Values ($r = 31$ mm, $\mu_k = 0.190$, $f = 18$ N)	119
4.43	Comparison of Behaviors of 1313 N/m Spring Unit under Different f Values ($r = 31$ mm, $a = 20$ mm, $\mu_k = 0.171$)	120
4.44	Comparison of Behaviors of 1313 N/m Spring Unit under Different μ_k Values ($r = 31$ mm, $a = 20$ mm, $f = 18$ N)	120
5.1	Overview of Isolated Floor System II (without Wall and Steel Edge Plates)	125
5.2	Cable Fixture of the Spring Units	126
5.3	Concrete Footing Slab with Masonry Wall	128
5.4	Fixture of Spring Units	128
5.5	Assembly of Two Modules of the Isolated Floor System	129
5.6	Corner Configuration of Edge Plates in Isolated Floor System II	129
5.7	Overview of Isolated Floor System II Specimen	130
5.8	Top View of Load Case 1	137
5.9	Top View of Load Case 2	138
5.10	Top View of Load Case 3	139
5.11	Top View of Load Case 4	140
5.12	Top View of Load Case 5	141
5.13	Top View of Load Case 6	142
5.14	Top View of Load Case 7	143
5.15	Top View of Load Case 8	144
5.16	Top View of Load Case 9	145
5.17	Top View of Load Case 10	146
5.18	Input of Acc01	148
5.19	Input of Acc02	148
5.20	Input of Acc11	149
5.21	Input of Acc31	149
5.22	Input of Acc002	150
5.23	Top View of Instrumentation Positions	152

LIST OF FIGURES (CONT'D)

FIGURE	TITLE	PAGE
5.24	Rising Bars Fixed on Walking Surface	154
5.25	Results of Test 2Acc11: (a) and (b) Displacement and Acceleration of Shake Table and Isolated Floor, Respectively; (c) Rotation; (d) Acceleration-Displacement Relationship of Isolated Floor System II	166
5.26	Results of Test 2C2 in E-W Direction: (a) and (b) Displacement and Acceleration of Shake Table and Isolated Floor, Respectively; (c) Rotation; (d) Acceleration-Displacement Relationship of Isolated Floor System II	167
5.27	Results of Test 2C2 in N-S Direction: (a) and (b) Displacement and Acceleration of Shake Table and Isolated Floor, Respectively; (c) Rotation; (d) Acceleration-Displacement Relationship of Isolated Floor System II	168
5.28	Results of Test 9C2 in E-W Direction: (a) and (b) Displacement and Acceleration of Shake Table and Isolated Floor, Respectively; (c) Rotation; (d) Acceleration-Displacement Relationship of Isolated Floor System II	169
5.29	Results of Test 9C2 in N-S Direction: (a) and (b) Displacement and Acceleration of Shake Table and Isolated Floor, Respectively; (c) Rotation; (d) Acceleration-Displacement Relationship of Isolated Floor System II	170
5.30	Results of Test 10C2 in E-W Direction: (a) and (b) Displacement and Acceleration of Shake Table and Isolated Floor, Respectively; (c) Rotation; (d) Acceleration-Displacement Relationship of Isolated Floor System II	171
5.31	Results of Test 10C2 in N-S Direction: (a) and (b) Displacement and Acceleration of Shake Table and Isolated Floor, Respectively; (c) Rotation; (d) Acceleration-Displacement Relationship of Isolated Floor System II	172
5.32	Results of Test 2Acc31wo: (a) and (b) Displacement and Acceleration of Shake Table and Isolated Floor, Respectively; (c) Rotation; (d) Acceleration-Displacement Relationship of Isolated Floor System II	173
5.33	Results of Test 2C2wo in E-W Direction: (a) and (b) Displacement and Acceleration of Shake Table and Isolated Floor, Respectively; (c) Rotation; (d) Acceleration-Displacement Relationship of Isolated Floor System II	174
5.34	Results of Test 2C2wo in N-S Direction: (a) and (b) Displacement and Acceleration of Shake Table and Isolated Floor, Respectively; (c) Rotation; (d) Acceleration-Displacement Relationship of Isolated Floor System II	175
5.35	Comparison of Acceleration-Displacement Relationships under Different Inputs and Load Case 1	176
5.36	Comparison of Acceleration-Displacement Relationships under Different Inputs and Load Case 2	176
5.37	Comparison of Acceleration-Displacement Relationships under Different Inputs and Load Case 3	177
5.38	Comparison of Acceleration-Displacement Relationships under Different Symmetric Load Cases and Same Input of Acc11 (with edge plates)	177
5.39	Comparison of Acceleration-Displacement Relationships under Different Symmetric Load Cases and Same Input of Acc31 (with edge plates)	178

LIST OF FIGURES (CONT'D)

FIGURE	TITLE	PAGE
5.40	Comparison of Acceleration-Displacement Relationships under Different Symmetric Load Cases and Same Input of Acc31 (without edge plates)	178
5.41	Comparison of Acceleration-Displacement Relationships Between Symmetric and Eccentric Load Cases under Input of Acc31	179
5.42	Comparison of Acceleration-Displacement Relationships Between With and Without Cover Plates under Load Case 2 When Subjected to Acc31	179
5.43	Comparison of Acceleration-Displacement Relationships in E-W Direction Between With and Without Cover Plates under Load Case 2 When Subjected to C2	180
5.44	Comparison of Acceleration-Displacement Relationships in N-S Direction Between With and Without Cover Plates under Load Case 2 When Subjected to C2	180
5.45	Comparison of Acceleration-Displacement Relationships Between With and Without Cover Plates under Load Case 3 When Subjected to Acc31	181
5.46	Comparison of Acceleration-Displacement Relationships in E-W Direction Between With and Without Cover Plates under Load Case 3 When Subjected to C2	181
5.47	Comparison of Acceleration-Displacement Relationships in N-S Direction Between With and Without Cover Plates under Load Case 3 When Subjected to C2	182
5.48	Comparison of Acceleration-Displacement Relationships Between Spring Units and Whole System under Load Case 2	182
5.49	Comparison of Acceleration-Displacement Relationships Between Spring Units and Whole System under Load Case 3	183
5.50	Results of Test 1Acc31: (a) and (b) Displacement and Acceleration of Shake Table and Isolated Floor, Respectively; (c) Rotation; (d) Acceleration-Displacement Relationship of Isolated Floor System II	184
5.51	Input of B1	186
5.52	Input of B2	187
5.53	Results of Test B107050wo: (a) and (b) are Displacement and Acceleration of Shake Table and Isolated Floor, Respectively; (c) Rotation; (d) Acceleration - Displacement Relationship of Isolated Floor System II	188
5.54	Results of Test B207050wo: (a) and (b) Displacement and Acceleration of Shake Table and Isolated Floor, Respectively; (c) Rotation; (d) Acceleration-Displacement Relationship of Isolated Floor System II	189
5.55	Comparison of Acceleration-Displacement Relationships under Different Inputs (1313 N/m Spring Units)	190
5.56	Comparison of Acceleration-Displacement Relationships Between Spring Units and Entire System under Input of B1	190
5.57	Comparison of Acceleration-Displacement Relationships Between Spring Units and Entire System under Input of B2	191

LIST OF FIGURES (CONT'D)

FIGURE	TITLE	PAGE
5.58	Impact between the Edges of the Edge Plate and the Tile: (a) Edge of the Edge Plate after Impact, and; (b) Edge of the Tile after Impact	196
5.59	Results of Test 2Acc111: (a) Acceleration of Shake Table and Isolated Floor, and; (b) Acceleration-Displacement Relationship of Isolated Floor System II	197
5.60	Removal of Edge Plates	197
6.1	Isolated Floor System I: (a) Plan and Cross Section Views of Isolated Floor System I, and; (b) and (c) Details 1 and 2 indicated in (a)	203
6.2	Configuration of Edge Plate in Isolated Floor System I	204
6.3	Corner Configuration of Edge plates in Isolated Floor System I	205
6.4	Corner Configuration of Edge Plates in Isolated Floor System II	205
6.5	Grid of Steel Angles on Top of Isolators	207
6.6	Inserting of FRP Decking Pieces	208
6.7	Insert Hold Down System (Strongwell, 2003)	208
6.8	Overview of Isolated Floor System I Specimen	209
6.9	Top View of Load 1	211
6.10	Top View of Load Case 10	212
6.11	Top View of Instrumentation positions	215
6.12	Rising Bars Fixed on Walking Surface	217
6.13	Lifting and Fixing of Edge Plates	222
6.14	Results of Test 12ss: (a) and (b) Displacement and Acceleration of Shake Table and Isolated Floor, Respectively; (c) Rotation; (d) Acceleration-Displacement Relationship of Isolated Floor System I	233
6.15	Results of Test 12B1: (a) and (b) Displacement and Acceleration of Shake Table and Isolated Floor, Respectively; (c) Rotation; (d) Acceleration-Displacement Relationship of Isolated Floor System I	234
6.16	Results of Test 12C2 in E-W Direction: (a) and (b) Displacement and Acceleration of Shake Table and Isolated Floor, Respectively; (c) Rotation; (d) Acceleration-Displacement Relationship of Isolated Floor System I	235
6.17	Results of Test 12C2 in N-S Direction: (a) and (b) Displacement and Acceleration of Shake Table and Isolated Floor, Respectively; (c) Rotation; (d) Acceleration-Displacement Relationship of Isolated Floor System I	236
6.18	Results of Test 12B1wo: (a) and (b) Displacement and Acceleration of Shake Table and Isolated Floor, Respectively; (c) Rotation; (d) Acceleration-Displacement Relationship of Isolated Floor System I	237
6.19	Results of Test 12C2wo in E-W Direction: (a) and (b) Displacement and Acceleration of Shake Table and Isolated Floor, Respectively; (c) Rotation; (d) Acceleration-Displacement Relationship of Isolated Floor System I	238
6.20	Results of Test 12C2wo in N-S Direction: (a) and (b) Displacement and Acceleration of Shake Table and Isolated Floor, Respectively; (c) Rotation; (d) Acceleration-Displacement Relationship of Isolated Floor System I	239

LIST OF FIGURES (CONT'D)

FIGURE	TITLE	PAGE
6.21	Results of Test 19C1 in E-W Direction: (a) and (b) Displacement and Acceleration of Shake Table and Isolated Floor, Respectively; (c) Rotation; (d) Acceleration-Displacement Relationship of Isolated Floor System I	240
6.22	Results of Test 19C1 in N-S Direction: (a) and (b) Displacement and Acceleration of Shake Table and Isolated Floor, Respectively; (c) Rotation; (d) Acceleration-Displacement Relationship of Isolated Floor System I	241
6.23	Results of Test 110C1 in E-W Direction: (a) and (b) Displacement and Acceleration of Shake Table and Isolated Floor, Respectively; (c) Rotation; (d) Acceleration-Displacement Relationship of Isolated Floor System I	242
6.24	Results of Test 110C1 in N-S Direction: (a) and (b) Displacement and Acceleration of Shake Table and Isolated Floor, Respectively; (c) Rotation; (d) Acceleration-Displacement Relationship of Isolated Floor System I	243
6.25	Results of Test 22ss: (a) and (b) Displacement and Acceleration of Shake Table and Isolated Floor, Respectively; (c) Rotation; (d) Acceleration-Displacement Relationship of Isolated Floor System I	244
6.26	Results of Test 22B1: (a) and (b) Displacement and Acceleration of Shake Table and Isolated Floor, Respectively; (c) Rotation; (d) Acceleration-Displacement Relationship of Isolated Floor System I	245
6.27	Results of Test 22C2 in E-W Direction: (a) and (b) Displacement and Acceleration of Shake Table and Isolated Floor, Respectively; (c) Rotation; (d) Acceleration-Displacement Relationship of Isolated Floor System I	246
6.28	Results of Test 22C2 in N-S Direction: (a) and (b) Displacement and Acceleration of Shake Table and Isolated Floor, Respectively; (c) Rotation; (d) Acceleration-Displacement Relationship of Isolated Floor System I	247
6.29	Results of Test 22B1wo: (a) and (b) Displacement and Acceleration of Shake Table and Isolated Floor, Respectively; (c) Rotation; (d) Acceleration-Displacement Relationship of Isolated Floor System I	248
6.30	Results of Test 22C2wo in E-W Direction: (a) and (b) Displacement and Acceleration of Shake Table and Isolated Floor, Respectively; (c) Rotation; (d) Acceleration-Displacement Relationship of Isolated Floor System I	249
6.31	Results of Test 22C2wo in N-S Direction: (a) and (b) Displacement and Acceleration of Shake Table and Isolated Floor, Respectively; (c) Rotation; (d) Acceleration-Displacement Relationship of Isolated Floor System I	250
6.32	Results of Test 29C1 in E-W Direction: (a) and (b) Displacement and Acceleration of Shake Table and Isolated Floor, Respectively; (c) Rotation; (d) Acceleration-Displacement Relationship of Isolated Floor System I	251
6.33	Results of Test 29C1 in N-S Direction: (a) and (b) Displacement and Acceleration of Shake Table and Isolated Floor, Respectively; (c) Rotation; (d) Acceleration-Displacement Relationship of Isolated Floor System I	252
6.34	Results of Test 210C1 in E-W Direction: (a) and (b) Displacement and Acceleration of Shake Table and Isolated Floor, Respectively; (c) Rotation; (d) Acceleration-Displacement Relationship of Isolated Floor System I	253

LIST OF FIGURES (CONT'D)

FIGURE	TITLE	PAGE
6.35	Results of Test 210C1 in N-S Direction: (a) and (b) Displacement and Acceleration of Shake Table and Isolated Floor, Respectively; (c) Rotation; (d) Acceleration-Displacement Relationship of Isolated Floor System I	254
6.36	Comparison of Acceleration-Displacement Relationships under Different Inputs and Load Case 1 (Polyurethane Balls)	255
6.37	Comparison of Acceleration-Displacement Relationships under Different Inputs and Load Case 2 (Polyurethane Balls)	255
6.38	Comparison of Acceleration-Displacement Relationships under Different Inputs and Load Case 3 (Polyurethane Balls)	256
6.39	Comparison of Acceleration-Displacement Relationships under Different Inputs and Load Case 2 (Rubber Balls)	256
6.40	Comparison of Acceleration-Displacement Relationships under Different Inputs and Load Case 3 (Rubber Balls)	257
6.41	Comparison of Acceleration-Displacement Relationships under Different Symmetric Load Cases and Input of B1 (with Edge Plates, Polyurethane Balls)	257
6.42	Comparison of Acceleration-Displacement Relationships under Different Symmetric Load Cases and Input of Acc11 (with Edge Plates, Polyurethane Balls)	258
6.43	Comparison of Acceleration-Displacement Relationships under Different Symmetric Load Cases and Input of B1 (with Edge Plates, Rubber Balls)	258
6.44	Comparison of Acceleration-Displacement Relationships under Different Symmetric Load Cases and Input of Acc11 (with Edge Plates, Rubber Balls)	259
6.45	Comparison of Acceleration-Displacement Relationships under Different Symmetric Load Cases and Input of Acc11 (without Edge Plates, Polyurethane Balls)	259
6.46	Comparison of Acceleration-Displacement Relationships under Different Symmetric Load Cases and Input of Acc11 (without Edge Plates, Rubber Balls) ...	260
6.47	Comparison of Acceleration-Displacement Relationships Between Symmetric and Eccentric Load Cases under Input of Acc11 (Polyurethane Balls)	260
6.48	Comparison of Acceleration-Displacement Relationships Between Symmetric and Eccentric Load Cases under Input of Acc11 (Rubber Balls)	261
6.49	Comparison of Acceleration-Displacement Relationships Between With and Without Cover Plates under Load Case 1 When Subjected to B1 (Polyurethane Balls)	261
6.50	Comparison of Acceleration-Displacement Relationships Between With and Without Cover Plates under Load Case 1 When Subjected to Acc11 (Polyurethane Balls)	262
6.51	Comparison of Acceleration-Displacement Relationships Between With and Without Cover Plates under Load Case 2 When Subjected to B1 (Polyurethane Balls)	262

LIST OF FIGURES (CONT'D)

FIGURE	TITLE	PAGE
6.52	Comparison of Acceleration-Displacement Relationships Between With and Without Cover Plates under Load Case 2 When Subjected to Acc11 (Polyurethane Balls)	263
6.53	Comparison of Acceleration-Displacement Relationships Between With and Without Cover Plates under Load Case 3 When Subjected to B1 (Polyurethane Balls).....	263
6.54	Comparison of Acceleration-Displacement Relationships Between With and Without Cover Plates under Load Case 3 When Subjected to Acc11 (Polyurethane Balls)	264
6.55	Comparison of Acceleration-Displacement Relationships Between With and Without Cover Plates under Load Case 1 When Subjected to Acc11 (Rubber Balls)	264
6.56	Comparison of Acceleration-Displacement Relationships Between With and Without Cover Plates under Load Case 2 When Subjected to B1 (Rubber Balls)	265
6.57	Comparison of Acceleration-Displacement Relationships Between With and Without Cover Plates under Load Case 2 When Subjected to Acc11 (Rubber Balls)	265
6.58	Comparison of Acceleration-Displacement Relationships Between With and Without Cover Plates under Load Case 3 When Subjected to B1 (Rubber Balls)	266
6.59	Comparison of Acceleration-Displacement Relationships Between With and Without Cover Plates under Load Case 3 When Subjected to Acc11 (Rubber Balls)	266
6.60	Comparison of Acceleration-Displacement Relationships between BNC Isolator Component and Whole System under Load Case 3 and Input of Acc11 (Polyurethane Balls)	267
6.61	Comparison of Acceleration-Displacement Relationships Between BNC Isolator Component and Whole System under Load Case 1 and Input of Acc11 (Rubber Balls)	267
6.62	Results of Extra Test 13ss in N-S Direction: (a) and (b) Displacement and Acceleration of Shake Table and Isolated Floor, Respectively; (c) Acceleration-Displacement Relationship of Isolated Floor System I	269
7.1	Relationship between Equivalent Friction Coefficient and Average Ball Load on Polyurethane Ball	277
7.2	Relationship between Equivalent Friction Coefficient and Average Ball Load on Rubber Ball	278
7.3	Linear Approximate Relationship between Equivalent Friction Coefficient and Average Ball Load on Polyurethane Ball	281
7.4	Polynomial Approximate Relationship between Equivalent Friction Coefficient and Average Ball Load on Polyurethane Ball	282

LIST OF FIGURES (CONT'D)

FIGURE	TITLE	PAGE
7.5	Power Approximate Relationship between Equivalent Friction Coefficient and Average Ball Load on Polyurethane Ball	282
7.6	Linear Approximate Relationship between Equivalent Friction Coefficient and Average Ball Load on Rubber Ball	283
7.7	Polynomial Approximate Relationship between Equivalent Friction Coefficient and Average Ball Load on Rubber Ball	283
7.8	Power Approximate Relationship between Equivalent Friction Coefficient and Average Ball Load on Rubber Ball	284
7.9	Principle for Concrete BNC Isolators Modeling	285
7.10	Comparison between Results from Analytical Model and Test for Concrete BNC Isolator Using Polyurethane Balls under Load Case 1: (a) Displacement; (b) Acceleration, and; (c) Acceleration-Displacement Relationship	288
7.11	Comparison between Results from Analytical Model and Test for Concrete BNC Isolator Using Polyurethane Balls under Load Case 3: (a) Displacement; (b) Acceleration, and; (c) Acceleration-Displacement Relationship	289
7.12	Comparison between Results from Analytical Model and Test for Concrete BNC Isolator Using Polyurethane Balls under Load Case 4: (a) Displacement; (b) Acceleration, and; (c) Acceleration-Displacement Relationship	290
7.13	Comparison between Results from Analytical Model and Test for Concrete BNC Isolator Using Rubber Balls under Load Case 1: (a) Displacement; (b) Acceleration, and; (c) Acceleration-Displacement Relationship	291
7.14	Comparison between Results from Analytical Model and Test for Concrete BNC Isolator Using Rubber Balls under Load Case 3: (a) Displacement; (b) Acceleration, and; (c) Acceleration-Displacement Relationship	292
7.15	Comparison between Results from Analytical Model and Test for Concrete BNC Isolator Using Rubber Balls under Load Case 4: (a) Displacement; (b) Acceleration, and; (c) Acceleration-Displacement Relationship	293
7.16	Comparison between Results from Analytical Model and Test for Isolated Floor System I without Edge Plates, Using Polyurethane Balls, under Load Case 1 and Input B1: (a) Displacement; (b) Acceleration, and; (c) Acceleration-Displacement Relationship	294
7.17	Comparison between Results from Analytical Model and Test for Isolated Floor System I without Edge Plates, Using Polyurethane Balls, under Load Case 2 and Input Acc11: (a) Displacement; (b) Acceleration, and; (c) Acceleration-Displacement Relationship	295
7.18	Comparison between Results from Analytical Model and Test for Isolated Floor System I without Edge Plates, Using Polyurethane Balls, under Load Case 3 and Input Acc11: (a) Displacement; (b) Acceleration, and; (c) Acceleration-Displacement Relationship	296

LIST OF FIGURES (CONT'D)

FIGURE	TITLE	PAGE
7.19	Comparison between Results from Analytical Model and Test for Isolated Floor System I without Edge Plates, Using Rubber Balls, under Load Case 1 and Input Acc11: (a) Displacement; (b) Acceleration, and; (c) Acceleration-Displacement Relationship	297
7.20	Comparison between Results from Analytical Model and Test for Isolated Floor System I without Edge Plates, Using Rubber Balls, under Load Case 2 and Input B1: (a) Displacement; (b) Acceleration, and; (c) Acceleration-Displacement Relationship	298
7.21	Comparison between Results from Analytical Model and Test for Isolated Floor System I without Edge Plates, Using Rubber Balls, under Load Case 3 and Input B1: (a) Displacement; (b) Acceleration, and; (c) Acceleration-Displacement Relationship	299
7.22	Comparison between Results from Analytical Model and Test for Isolated Floor System I with Edge Plates, Using Polyurethane Balls, under Load Case 1 and Input B1: (a) Displacement; (b) Acceleration, and; (c) Acceleration-Displacement Relationship	300
7.23	Comparison between Results from Analytical Model and Test for Isolated Floor System I with Edge Plates, Using Polyurethane Balls, under Load Case 2 and Input Acc11: (a) Displacement; (b) Acceleration, and; (c) Acceleration-Displacement Relationship	301
7.24	Comparison between Results from Analytical Model and Test for Isolated Floor System I with Edge Plates, Using Polyurethane Balls, under Load Case 3 and Input Acc11: (a) Displacement; (b) Acceleration, and; (c) Acceleration-Displacement Relationship	302
7.25	Comparison between Results from Analytical Model and Test for Isolated Floor System I with Edge Plates, Using Rubber Balls, under Load Case 1 and Input Acc11: (a) Displacement; (b) Acceleration, and; (c) Acceleration-Displacement Relationship	303
7.26	Comparison between Results from Analytical Model and Test for Isolated Floor System I with Edge Plates, Using Rubber Balls, under Load Case 2 and Input B1: (a) Displacement; (b) Acceleration, and; (c) Acceleration-Displacement Relationship	304
7.27	Comparison between Results from Analytical Model and Test for Isolated Floor System I with Edge Plates, Using Rubber Balls, under Load Case 3 and Input B1: (a) Displacement; (b) Acceleration, and; (c) Acceleration-Displacement Relationship	305
7.28	Results of Sensitivity Study for Isolated Floor System I without Edge Plates, Using Polyurethane Balls, under Load Case 2 and Input Acc11: (a) Displacement; (b) Acceleration, and; (c) Acceleration-Displacement Relationship	307
7.29	Results of Sensitivity Study for Isolated Floor System I without Edge Plates, Using Rubber Balls, under Load Case 2 and Input B1: (a) Displacement; (b) Acceleration, and; (c) Acceleration-Displacement Relationship	308

LIST OF FIGURES (CONT'D)

FIGURE	TITLE	PAGE
7.30	Sketch of Modified Hysteretic Damper Brace Element Model	310
7.31	Straight Lines Used to Simulate Physical Model for 2627 N/m Multi-directional Spring Units	312
7.32	Straight Lines Used to Simulate Physical Model for 1313 N/m Multi-directional Spring Units	313
7.33	Values of Force Dropping Factor $-\langle\eta\rangle$ from Physical Model	313
7.34	Comparison of Results between Quasi-static Analysis of Analytical Model and Physical Model for 2627 N/m Spring Unit	315
7.35	Comparison of Results between Quasi-static Analysis of Analytical Model and Physical Model for 1313 N/m Spring Unit	316
7.36	Comparison between Results from Analytical Model and Test for Isolated Floor System II Using 2627 N/m Spring Units, without Edge Plates, and under Load Case 2: (a) Displacement; (b) Acceleration, and; (c) Acceleration-Displacement Relationship	317
7.37	Comparison between Results from Analytical Model and Test for Isolated Floor System II Using 2627 N/m Spring Units, without Edge Plates, and under Load Case 3: (a) Displacement; (b) Acceleration, and; (c) Acceleration-Displacement Relationship	318
7.38	Comparison between Results from Analytical Model and Test for Isolated Floor System II Using 1313 N/m Spring Units, without Edge Plates, and under 50 psf Load: (a) Displacement; (b) Acceleration, and; (c) Acceleration-Displacement Relationship	319
7.39	Comparison between Results from Analytical Model and Test for Isolated Floor System II Using 2627N/m Spring Units, with Edge Plates, and under Load Case 1: (a) Displacement; (b) Acceleration, and; (c) Acceleration-Displacement Relationship	320
7.40	Comparison between Results from Analytical Model and Test for Isolated Floor System II Using 2627N/m Spring Units, with Edge Plates, and under Load Case 2: (a) Displacement; (b) Acceleration, and; (c) Acceleration-Displacement Relationship	321
7.41	Comparison between Results from Analytical Model and Test for Isolated Floor System II Using 2627N/m Spring Units, with Edge Plates, and under Load Case 3: (a) Displacement; (b) Acceleration, and; (c) Acceleration-Displacement Relationship	322
7.42	Results of Sensitivity Study for Isolated Floor System II without Edge Plates, Using 2627N/m Spring Units, under Load Case 2 and Input Acc31: (a) Displacement; (b) Acceleration, and; (c) Acceleration-Displacement Relationship	324
8.1	Comparison between the Average of Elastic Response Spectra from Synthetic Acceleration Time Histories and the Target NEHRP Spectrum (5% of Critical Damping)	330
8.2	Coupled Model	332

LIST OF FIGURES (CONT'D)

FIGURE	TITLE	PAGE
8.3	Uncoupled model: (a) Base SDOF Frame, and; (b) Isolated raised floor	332
8.4	Pushover Curve of Structural Fuse Frame	332
8.5	Average Peak Response of the SDOF Frame from Limited Parametric Study of Combined Systems Using Isolated Floor System I (Polyurethane Balls): (a) to (d) respectively correspond to a values of 0, 0.25, 0.5, and 1.0	338
8.6	Average Peak Response of the SDOF Frame from Preliminary Parametric Study of Combined Systems Using Isolated Floor System II (0 psf Load Case): (a) to (d) respectively correspond to a value of 0, 0.25, 0.5, and 1.0	344
8.7	Average Peak Response of the SDOF Frame from Preliminary Parametric Study of Combined Systems Using Isolated Floor System II (25 psf Load Case): (a) to (d) respectively correspond to a value of 0, 0.25, 0.5, and 1.0	345
8.8	Average Peak Relative Displacement Response of Isolated Floor System I to Structural Fuse Frame (D_{ris}): (a) to (c) Respectively Correspond to Cases with $T=0.25s$, 0.5 s, and 1.0 s	356
8.9	Average Peak Relative Displacement Response of Structural Fuse Frame in Systems Using Isolated Floor System I (D_{rs}): (a) to (c) Respectively Correspond to Cases with $T=0.25s$, 0.5 s, and 1.0 s	357
8.10	Average Peak Absolute Acceleration Response of Isolated Floor System I (A_{absi}): (a) to (c) Respectively Correspond to Cases with $T=0.25s$, 0.5 s, and 1.0 s	358
8.11	Average Peak Absolute Acceleration Response of Structural Fuse Frame in Systems Using Isolated Floor System I (A_{abss}): (a) to (c) Respectively Correspond to Cases with $T=0.25s$, 0.5 s, and 1.0 s	359
8.12	Average Peak Responses of Combined System Using Isolated Floor System I with Rubber Balls ($T=0.5$ s, $R=5$, and $a=0.5$): (a) to (d) Respectively Correspond to Results of D_{ris} , D_{rs} , A_{absi} , and A_{abss}	360
8.13	Average Peak Relative Displacement Response of Isolated Floor System II to Structural Fuse Frame (D_{ris}): (a) to (c) Respectively Correspond to Cases with $T=0.25s$, 0.5 s, and 1.0 s	363
8.14	Average Peak Relative Displacement Response of Structural Fuse Frame in Systems Using Isolated Floor System II (D_{rs}): (a) to (c) Respectively Correspond to Cases with $T=0.25s$, 0.5 s, and 1.0 s	364
8.15	Average Peak Absolute Acceleration Response of Isolated Floor System II (A_{absi}): (a) to (c) Respectively Correspond to Cases with $T=0.25s$, 0.5 s, and 1.0 s	365
8.16	Average Peak Absolute Acceleration Response of Structural Fuse Frame in Systems Using Isolated Floor System II (A_{abss}): (a) to (c) Respectively Correspond to Cases with $T=0.25s$, 0.5 s, and 1.0 s	366
8.17	Analysis Results of Systems Using Isolated Floor System I: D_{ris}	368
8.18	Analysis Results of Systems Using Isolated Floor System I: D_{rs}	368
8.19	Analysis Results of Systems Using Isolated Floor System I: A_{absi}	368
8.20	Analysis Results of Systems Using Isolated Floor System I: A_{abss}	368

LIST OF FIGURES (CONT'D)

FIGURE	TITLE	PAGE
8.21	Displacement Responses of System Using Isolated Floor System I: $M_r = 0.01$	371
8.22	Displacement Responses of System Using Isolated Floor System I: $M_r = 1.0$	371
8.23	Comparison of Displacement Responses of Structural Fuse Frame	372
8.24	Energy Flow Time Histories: (a) and (b) Respectively Correspond to the Histories of Hysteretic Energy of the Isolated Floor System and Hysteretic Energy of the Structural Fuse Frame	374
9.1	Procedure of Linear Static Design Method: Isolated Floor System I	399
9.2	Frame and BRB Properties (from Vargas and Bruneau (2006a))	384
9.3	Behavior of Isolated Floor System I	388
9.4	Procedure of Nonlinear Response History Design Method: Isolated Floor System I	401
9.5	Procedure of Linear Static Design Method: Isolated Floor System II	403
9.6	Behavior of Isolated Floor System II	394
9.7	Procedure of Nonlinear Response History Design Method: Isolated Floor System II	405

LIST OF TABLES

TABLE	TITLE	PAGE
3.1	List of Instrumentation	37
3.2	Free Vibration Test Sequence	39
3.3	Force-Displacement Test Sequence	40
3.4	Sweep Frequency Test Sequence	41
3.5	Sequence of Dynamic Tests Using Earthquake Inputs	42
3.6	Equivalent Friction Coefficient	62
4.1	Test Sequence	90
5.1	Summary of Steel Plates	132
5.2	Summary of Load Cases	133
5.3	Summary of Dimensions and Elements of Structural Fuse Frame (4-Story 3-Bay) ..	150
5.4	Summary of Dimensions and Elements of Structural Fuse Frame Specimen (3-Story 1-Bay)	151
5.5	Summary of Instrumentation Channels	153
5.6	Test Sequences of Isolated Floor System II	156
5.7	Summary of Peak Values of Response Quantities for Isolated Floor System II Having 2627 N/m Multi-directional Spring Units	165
5.8	Rotation Effects_2627 N/m Spring Units	193
6.1	Summary of Instrumentation Channels	216
6.2	Test Sequences of Isolated Floor System I with Polyurethane Balls	219
6.3	Test Sequences of Isolated Floor System I with Rubber Balls	221
6.4	Summary of Peak Values of Response Quantities (Polyurethane Balls)	230
6.5	Summary of Peak Values of Response Quantities (Rubber Balls)	232
6.6	Rotation Effects_Polyurethane Balls	271
6.7	Rotation Effects_Rubber Balls	273
7.1	Squashing Ball Test Results	279
7.2	Experimentally Obtained Values of Equivalent Friction Coefficients	281
8.1	Results from Parametric Studies Using Lower and Upper Bound Isolated Load Values (0 psf to 50 psf)	348
8.2	Results from Parametric Studies Using Lower and Upper Bound Isolated Load Values (25 psf to 50 psf)	349
8.3	Difference of the Results between Uncoupled and Coupled Models for Systems Using Isolated Floor System I (Polyurethane Balls)	351
8.4	Difference of the Results between Uncoupled and Coupled Models for Systems Using Isolated Floor System II (Load Case of 0 psf)	352
9.1	Comparison of Designs_Combined Systems Using Isolated Floor System I	392
9.2	Comparison of Designs_Combined Systems Using Isolated Floor System II	397

CHAPTER 1

INTRODUCTION

Various researchers developed general design procedures for the design of structures with structural fuses (i.e., defined as metallic passive hysteretic energy dissipation (PED) devices which are disposable or can be easily replaced after a seismic event). The structural fuse concept, as implemented in these design procedures, requires to concentrate all the seismic damage in the structural fuses, while the bare frame hosting these devices behaves elastically during a seismic event. This research showed that structures are stiffened when using PED devices as structural fuses, which correspondingly reduces the displacement demands on these structures. Therefore, one benefit of using structural fuses is that displacement sensitive nonstructural components in such buildings can be better protected during seismic events. However, this research also showed that in most cases, this can also correspond to an increase in floor acceleration demands. To protect the acceleration sensitive equipments on the floors of such buildings, a possible solution may be to combine the stiffening of structures using PED devices with a strategy of introducing isolated floors in the rooms where such acceleration-sensitive equipment is located. This is the strategy investigated here.

Two kinds of isolated floor systems (labeled type I and II here) are studied here. When this research started, a number of manufacturers were developing their own isolated floor system and were not in a position to release details on their systems until their patents were issued. For this reason, a special kind of concrete ball-in-cone (BNC) isolators and a corresponding isolated floor system using this kind of concrete isolators were designed and build, which was named Isolated Floor System I, were designed. This special kind of concrete BNC isolator used rubber or polyurethane rolling balls, instead of steel rolling balls, between the top and bottom bearing plates. These balls (rubber or polyurethane) can deform under gravity loads and provide a greater contacting area on the working surface. This is advantageous to avoid damaging the concrete

working surface of the bearing plate and avoid forming grooves on the concrete working surface during motions (as was observed for steel balls rolling on steel surfaces, as described in a later section). These rubber or polyurethane balls, instead of steel rolling balls, can also introduce more damping to this isolation system. Furthermore, from a commercial point of view, the construction of this kind of concrete BNC isolator is relatively inexpensive compared to the steel BNC isolators, and they can be built by any contractor (although the exact cost benefit of these advantages have not been quantified here). Because the mechanical behavior of both the single concrete BNC isolator and the corresponding Isolated Floor System I was unknown, characterization tests were designed and conducted.

After the characterization tests on the single concrete BNC isolator were completed, and just before the characterization tests of Isolated Floor System I started, an isolated floor system by Dynamic Isolation Systems (DIS) became available, which was named Isolated Floor System II as it was obtained after Isolated Floor System I was designed. Proprietary multi-directional spring units provided by DIS were used as isolators in this system. This research project was therefore expanded to include this recently developed system. Considering the sudden immediate availability of Isolated Floor System II, it was first tested from single isolators to complete systems using the shake table facilities in the Structural Engineering and Earthquake Simulation Laboratory (SEESL) at the University at Buffalo. After the tests on the Isolated Floor System II, characterization tests were conducted on the originally developed isolated floor system-Isolated Floor System I.

A great amount of characterization tests were conducted on these two kinds of isolated floor systems to define their mechanical behavior properties (i.e., force-displacement relationships), from single isolators to complete systems. As an added benefit of the systems considered in this study compared to other available systems, note that both isolated floor systems work well under service loads, as they can prevent displacements of the isolated floors under small horizontal loads (e.g., due to normal walking on the floor or even some abrupt movements by users) due to the friction effects present in these systems (from the rolling balls and edge plates in Isolated Floor System I and from the casters and the edge plates in Isolated Floor System II). The experimentally obtained mechanical behavior and properties were then simulated in computer

programs (i.e., SAP2000 for Isolated Floor System I and IDARC 2D for Isolated Floor System II). Models of single-degree-of-freedom (SDOF) structural fuse frames with implementation of these two isolated floor systems were developed. Both coupled and uncoupled models are considered. A number of parametric studies were then conducted on these combined systems to determine the preferred design parameter values to be used in the design of such structural fuse frames coupled with isolated floors, and to establish how the combined systems behave under different mass ratios of the isolated floor system to the base SDOF structural fuse structure. Finally, the design procedures for structural fuse frames developed by Vargas and Bruneau (2006a) were extended to become an integrated design methodology for each kind of isolated floor system, which includes both the design of the base SDOF structural fuse structure and the design of the isolated floor system on top. As an important addition to the previous methodology, if the design of the isolated floor system is not satisfactory, the proposed methodology makes it possible to modify either the design of the SDOF structural fuse frame and/or the design of the isolated floor system to make the integrated systems meet their performance objectives.

In this report, Chapter 2 provides a brief literature review on structural fuse concept, isolation bearings, and response and design of nonstructural components. The characterization tests conducted on single isolators, i.e., the special kind of concrete BNC isolator and the multi-directional spring units, are presented in Chapters 3 and 4, respectively. In Chapter 3, polyurethane and rubber balls were separately used as rolling balls between the top and bottom concrete bearing plates. An empirical model was also developed for the concrete BNC isolator where the rolling friction between the ball and the concrete working surface is significant. In Chapter 4, two sets of multi-directional spring units with different nominal stiffnesses were respectively tested under both sinusoidal and seismic inputs. A new physical model was also developed for this kind of multi-directional spring unit (in collaboration with Dynamic Isolation Systems, Inc.) in this chapter. Chapter 5 shows the details of the tests on Isolated Floor System II which were conducted earlier than those on Isolated Floor System I. The two sets of multi-directional spring units with different nominal stiffnesses presented in Chapter 4 were separately used as isolators in this system. The results from the complete isolated floor system were also compared with the corresponding ones from the single isolator tests. The characterization tests on Isolated Floor System I are presented in Chapter 6. Again the results are compared between

the complete isolated floor tests and the corresponding single concrete BNC isolator tests. Chapter 7 provides the modeling details for both isolated floor systems in computing programs. Chapter 8 presents the results of parametric studies in terms of both the primary design parameters for the base SDOF structural fuse structures and the mass ratio of the isolated floor system to the SDOF structural frame. Some trends in the behavior of the combined systems consisting of the base SDOF structural fuse structure and the isolated floor systems were observed and different methods were used to explain some of these trends. Combined design methodology considering the integrated designs of both the base SDOF structural fuse structure and isolated floor systems were developed to provide guidance for the design of these isolated floor systems for SDOF structural fuse structures. Both linear static and non-linear response history design methods were considered, and results are presented in Chapter 9. Chapter 10 summarizes conclusions from this study.

CHAPTER 2

LITERATURE REVIEW

2.1 Introduction

As mentioned in Chapter 1, the objective of this research is to propose an integrated design procedure to consider both the design of the main structure with structural fuses and the design of the isolated floor system in an integrated manner. Consequently, this chapter provides a brief review of past related research and findings on the structural fuse concept, isolation bearing, and response and design of nonstructural components, presented in Sections 2.2 to 2.4, respectively.

2.2 Structural Fuse Concept

Vargas and Bruneau (2006a) provided a review on the development history of the structural fuse concept. They observed that the structural fuse concept was not consistently defined in the literature. In some of the past research (Roeder and Popov 1977, Fintel and Ghosh 1981, Aristizabal-Ochoa 1986, Basha and Geol 1996, Carter and Iwankiw 1998, Sugiyama 1998, and Rezai et al. 2000, to name a few), the term “structural fuse” was used to define structural elements in which seismic damage concentrated. However, these fuse elements were not typically not disposable or not easy to be replaced after seismic events. In other research, “structural fuses” were elements either used to reduce the nonlinear response of the main structure (Sugiyama 1998) or to keep the main structure (tall buildings in those studies) elastic during earthquakes (Wada et al. 1992, Wada and Huang 1995, and Shimizu et al. 1998).

Vargas and Bruneau (2006a) focused on easily replaceable hysteretic fuses in the perspective of keeping the rest of the structure elastic. In that perspective, they proposed a general design procedures for the design of single-degree-of-freedom (SDOF) structures and multi-degree-of-

freedom (MDOF) structures having structural fuses that consist of metallic passive energy dissipation (PED) devices (such as, buckling-restrained braces, triangular added damping and stiffness device, and shear panel) implemented as disposable (and easy to replace) structural fuses. A set of key parameters (namely, the stiffness post-yielding ratio α , the maximum displacement ductility μ_{\max} , the strength ratio η , and the natural period of the structure T), defined the behavior of the structures with structural fuses. The proposed design procedure was based on this set of key parameters. Through parametric studies and design examples, it was observed that structural fuses are easier to implement when $0.25 \leq \alpha \leq 0.5$ and $\mu_{\max} \geq 5$. Vargas and Bruneau (2006a) also compared the floor acceleration response from structures with structural fuses with those from the corresponding bare frames, and reported that, in most cases, floor acceleration increased when metallic fuses were introduced to the structure – which was somewhat expected.

Experimental validation of the proposed structural fuse design procedure in Vargas and Bruneau (2006a) is presented in Vargas and Bruneau (2006b) using a scaled structure designed in accordance with the design procedures in Vargas and Bruneau (2006a). Figs. 2.1 and 2.2 show the geometry of the specimen used in the experiment, correspondingly tested with Nippon Steel BRBs and Star Seismic BRBs, respectively. Note that a ball-in-cone (BNC) isolator (i.e., ISO-Base™ from WorkSafe Technologies) was also installed on the top of the structure to assess its effectiveness in the protection of nonstructural components, as shown in Fig. 2.3. The test results showed that the seismically induced damage was successfully concentrated on BRBs (i.e., structural fuses) while the beams and columns behaved elastically. It was also found that the BNC isolator was effective to control the acceleration transmitted to nonstructural components.

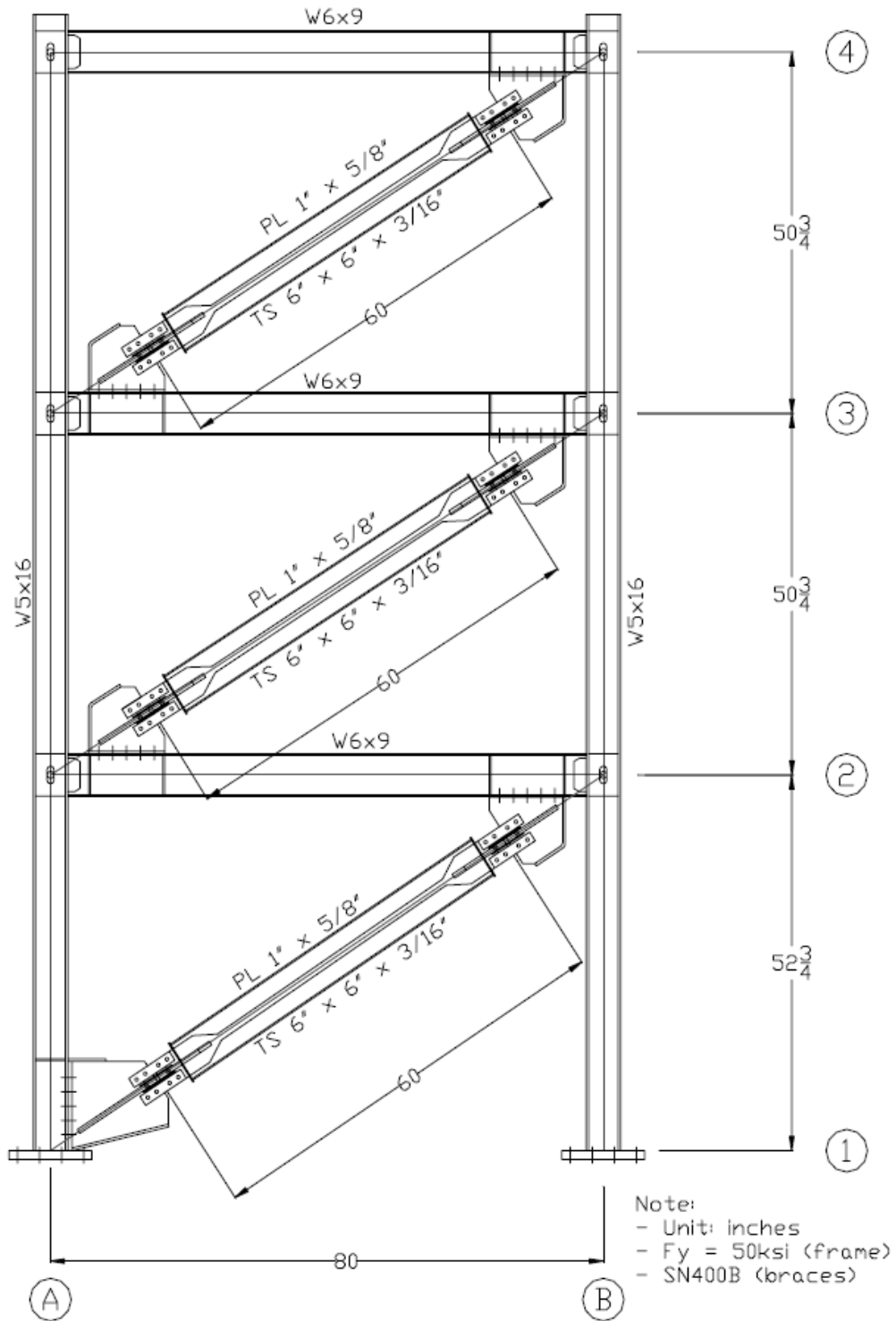


Figure 2.1 Frame with Nippon Steel BRBs (from Vargas and Bruneau (2006b))

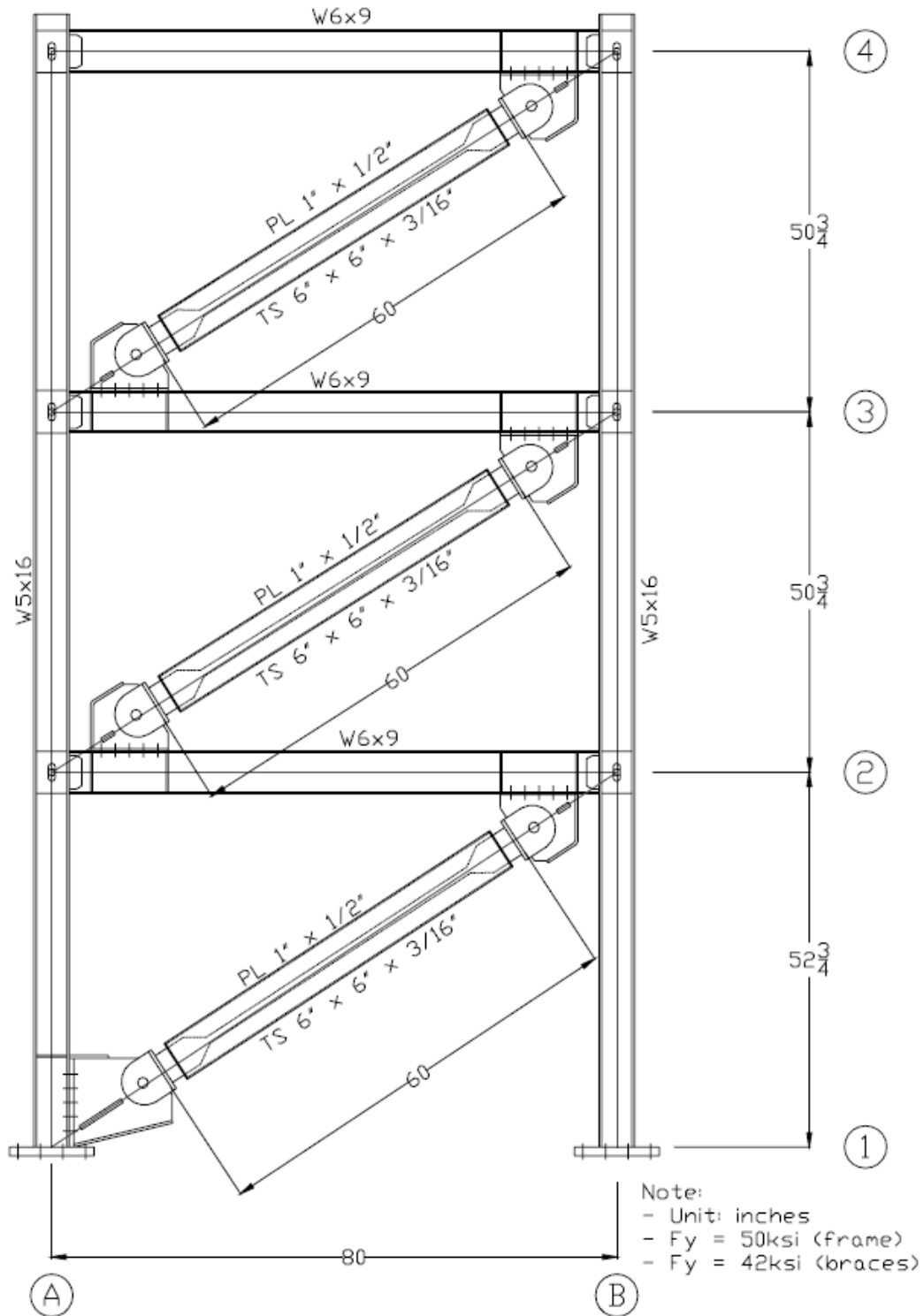


Figure 2.2 Frame with Star Seismic BRBs (from Vargas and Bruneau (2006b))



Figure 2.3 BNC Isolator on Top of Third Floor (from Vargas and Bruneau (2006b))

2.3 Base Isolation Bearings

Extensive research has been conducted in past decades to develop and implement technologies (such as lead-rubber bearings and friction pendulum bearings) for the seismic base isolation of structures (e.g., Kartoum 1987, Koh and Kelly 1987, Kelly 1991 and 2003, Constantinou 1992, Constantinou et al. 1993, Constantinou et al. 1998, Constantinou et al. 1999, Kasalanati and Constantinou 1999, Naeim and Kelly 1999, and Fenz and Constantinou 2006 and 2008, to name a few). The two most common types of seismic isolation bearings used in seismic isolation are elastomeric bearings and friction pendulum (FP) bearings. The elastomeric bearings can be subdivided into three types: low damping rubber bearings, high damping rubber bearings, and lead-rubber bearings (as shown in Fig. 2.4 from Naeim and Kelly 1999). The friction pendulum bearing can be further divided into different kinds of bearings based on the number of sliding surfaces from which the friction comes, such as single FP bearings with one sliding surface and double FP bearings with two sliding surfaces (as shown in Fig. 2.5 from Fenz and Constantinou 2008). Furthermore, a multi-spherical sliding bearing was developed by Fenz and Constantinou

(2008), which is based on the physical principle of FP bearings. In addition, a roller bearing was also developed by Lee et al. (2007) and used in seismic isolation of highway bridges. All these bearings mentioned above are heavy duty bearings and suitable for the seismic isolation of buildings and bridges.

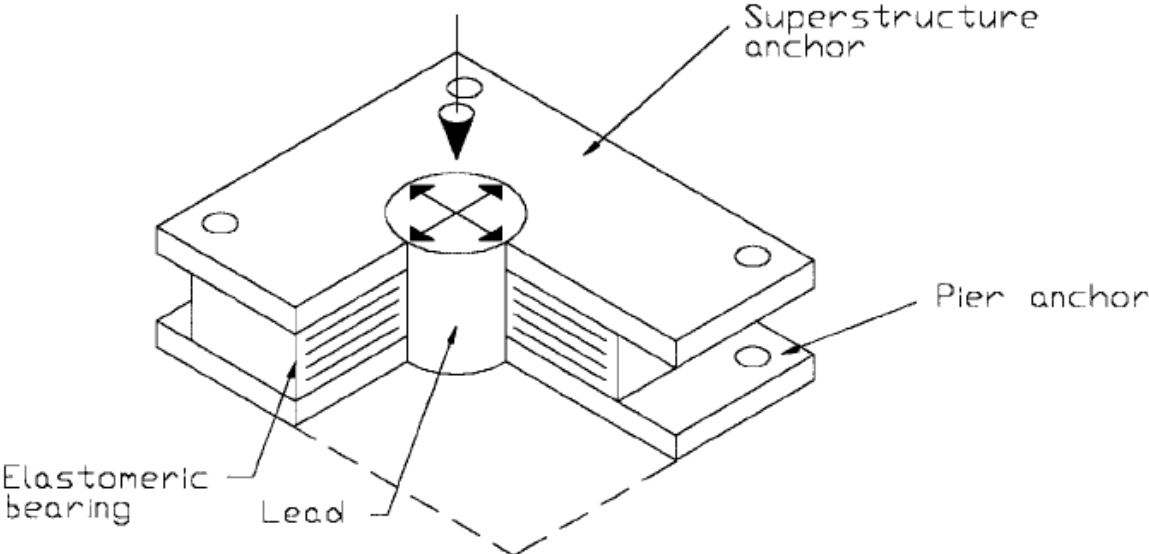


Figure 2.4 Lead-Rubber Isolator (from Naeim and Kelly 1999)

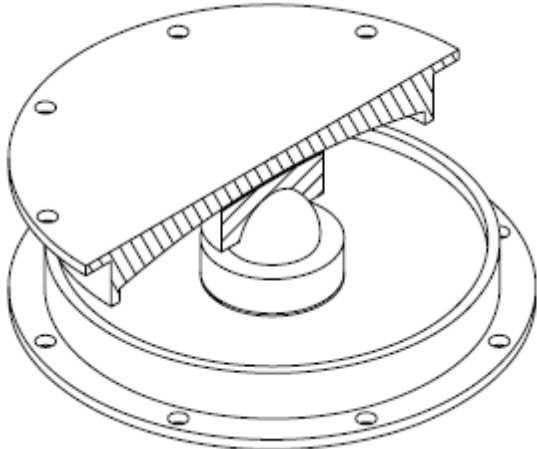


Figure 2.5 Double FP Bearing (from Fenz and Constantinou 2008)

In recent years, there has been a growing interest in isolating only specific equipments or specific rooms on the floors of buildings. Isolating equipment rather than entire buildings can be challenging to the isolation devices described above due to the relatively low mass supported by the isolators. Various systems have been developed to isolate equipments, such as the wire rope systems developed by Demetriades et al. (1992 and 1993) and the systems by Kosar et al. (1993). Another example of the equipment isolation bearings is the ball-in-cone (BNC) isolator (Kemeny and Szidarovszky 1995, Kasalanati et al. 1997, Amick et al. 1998, to name a few). The BNC bearing consists of top and bottom bearing plates together with a spherical ball rolling between the concave working surfaces of these two bearing plates. Both the bearing plates and rolling ball are made of the steel material. The behavior of the BNC isolator is a function of the geometric properties of its working surface. Fig. 2.6 shows three configurations of the working surface, together with the corresponding restoring laws, where, φ is the slope of the conical surface, ε is a factor less than one, x is the displacement of the top bearing plate with respect to the bottom bearing plate, d is the displacement capacity of the BNC isolator, and $\frac{\varepsilon d}{2\varphi}$ is the radius of the spherical part.

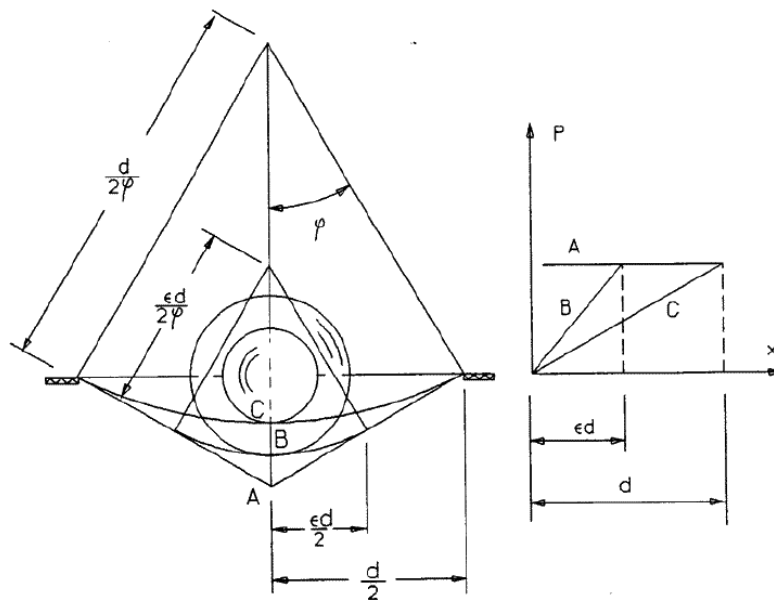


Figure 2.6 BNC Geometries and Corresponding Restoring Laws (from Kemeny and Szidarovszky 1995)

Normally the working surface configuration B in Fig. 2.6 is adopted for a typical BNC isolator where the working surface consists of two parts: a spherical central part and an outside conical surface. Given that the rolling friction (i.e., damping) between the rolling ball and the working surface is negligible, the restoring law is bilinear and elastic as shown in Fig. 2.6. The restoring law of path B shown in that figure can be expressed by the following equations (Kemeny and Szidarovszky 1995),

$$P = \begin{cases} \frac{Wx}{\varepsilon d} \\ \varphi \end{cases} \quad (\text{when } x < \varepsilon d, \text{ i.e., the rolling ball within the spherical central part}) \quad (2.1)$$

$$P = \varphi W \quad (\text{when } x \geq \varepsilon d, \text{ i.e., the rolling ball within the conical surface}) \quad (2.2)$$

Note from Eq. 2.2 that the output seismic force is a constant value and independent of the lateral displacement. Kemeny and Szidarovszky (1995) also claimed the following advantages of the BNC isolators through comparing with rubber bearings: the BNC isolator volume and cost were said to be less than that of the rubber bearings and the BNC isolator was stated to not be affected by aging issues. They also pointed out that the BNC isolator can be coupled with viscous or friction dampers to reduce its seismic displacement.

Kasalanati et al. (1997) experimentally studied the application of BNC isolators in the seismic isolation of a bridge model. Supplemental friction dampers, together with the BNC isolation system, were used in their tests. Two hardness configurations of the BNC bearing plates were studied, respectively. The test results showed that this system could reduce superstructure accelerations and substructure forces and that the hardness of the conical bearing plates had a direct effect on the performance of the isolation system (e.g., the hard steel ball was observed to cause grooves on the surfaces of the low-hardness conical bearing plates due to high stress concentration at the contacting point between these two). A transverse movement of the bearings was also observed to develop even though the input motion was only in the longitudinal direction.

The marketed ISO-Base™ shown in Fig. 2.7 (U.S. Patent No. 5,599,106), which was used in the experiment by Vargas and Bruneau (2006b), is one kind of BNC isolators. The slope of their working surface is typically 0.1. As mentioned in Section 2.2, tests showed that the BNC isolator can be effective to control the acceleration transmitted to nonstructural components.



Figure 2.7 Seismic Isolated Platform with Patented Ball-B-Cone™ Isolators (from Amik et al. 1998)

Lambrou and Constantinou (1994) showed that the seismic isolation of a single equipment can be challenging for traditional isolation bearings (such as elastomeric or sliding bearings) because it is difficult to achieve the desired long period (due to the low weight of the equipment) without introducing special configurations that can be expensive to implement. However, they demonstrated that such isolators could be used if implemented to isolate an entire computer floor system, considered FP bearings with and without adding fluid viscous dampers. Substantial reductions in the response of a generic computer cabinet on the top of the isolated computer floor were observed from their experimental and analytical results (Lambrou and Constantinou 1994).

2.4 Response and Design of Nonstructural Components

A large amount of research has been done in past decades on the seismic response and design of nonstructural components. Several state of the art reviews exist, such as those by Chen and Soong (1988), Soong (1994), Villaverde (1997), and Retamales (2008). Note that nonstructural components are often alternatively called “nonstructural elements”, “secondary structures”, “building attachments”, “secondary systems,” in various references.

The design of nonstructural components has already been addressed by many building codes through specific design forces (e.g., NEHRP 2003, NEHRP 2000, UBC 1997, ASCE7-98, and ASCE7-10, to name a few). However, the deficiencies in these building codes have been recognized by the research community; in particular, they often neglect the interaction between the nonstructural components and the main structure, as shown in FEMA 357, and the nonlinearity of the main structure is typically not considered in building codes (Soong et al. 1993).

Beyond building code issues, extensive research has been conducted in past decades on the response and design of such nonstructural components. A number of methods have been proposed. One is the use of floor response spectrum. In this method, a floor response spectrum is first generated and then is used for the design of the nonstructural components. Extensive research has been conducted to develop simple methods from which floor response spectra can be directly generated, particularly some decades ago when response history analysis of the combined systems was difficult (e.g., Biggs and Roesset 1970, KapurKa and Shao 1973, Peters et al. 1977, Singh 1980, to name a few). However, the floor response spectra method does not consider the interaction between the nonstructural components and the main structure and cannot be rationally applied for the analysis of a secondary structure with multiple points of attachments (Wang et al. 1983). The interaction between the nonstructural component and the primary structure may be negligible when the mass ratio of the nonstructural component to the primary structure is small, but this is not always the case.

Researchers subsequently generated several alternative methods that not only take the interaction into account, but also overcome the practicality problems associated with the response history analysis of the combined systems (e.g., Lee and Penzien 1983, Igusa and Der Kiureghian 1985a and 1985b, Singh and Sharma 1985, Suarez and Singh 1987a and 1987b, Villaverde 1986 and 1991, to name a few). However, all those studies considered linear secondary systems mounted on linear primary systems.

Some research used linear multi-degree-of-freedom (MDOF) secondary systems mounted on an elasto-plastic MDOF primary structure (Villaverde 1987), or studied a combined two-degree-

freedom-system by introducing small nonlinearity into this combined system (Igusa 1990).

It nonetheless remains that further research is needed to develop a simple method (or methods) from which the floor response spectrum can be directly generated in an accurate manner for combined systems with significant nonlinearity (i.e., not only limited nonlinearity) and which also takes into account the interaction between the nonstructural component and the primary structure.

Another method for the design of nonstructural components is the response history method. Although this method is quite straightforward, it was challenging or even impractical several decades ago due to limitations in computational power (Soong 1994, Villaverde 1997), given the facts that: 1) an extensive number of degrees of freedom are included in a combined primary-secondary system; 2) the structural parameters (i.e., mass, stiffness, and damping) of the primary system are quite different from those of the secondary system; and 3) the primary structure is normally designed prior to the secondary system and would have to be reanalyzed every time a change is made in the secondary system. However, response history approach is nowadays possible (and much easier) given that nonlinear response history analysis is available in a number of commercial structural analysis programs.

CHAPTER 3

CONCRETE BNC ISOLATOR CHARACTERIZATION TEST

3.1 Introduction

To protect some of the seismic sensitive nonstructural components typically sitting on the floors of rooms in critical buildings (such as hospitals), a specially designed isolated floor concept is proposed to reduce the acceleration demands on acceleration sensitive components. This concept is to be used as part of a combined solution together with stiffening the structure. In this combined solution, the stiffened structure significantly reduces the drift demands on the displacement sensitive components, and the floor is supported by base isolators to reduce the acceleration demands on the floor during earthquake response. This chapter focuses on defining the isolator properties for the first of two base-isolated floors concepts considered for this purpose. Using these properties, a complete isolated floor system was designed and tested as described in a subsequent chapter.

Here, a special kind of concrete ball-in-cone (BNC) isolator was developed to decrease the acceleration response of the room floor. The design of this concrete BNC isolator was inspired in part by a commercial product marketed by ISO-BaseTM, and described in Vargas and Bruneau (2006b), with two substantial differences as: (i) solid rubber and polyurethane balls were used instead of steel balls rolling between two sets of bearing plates and, (ii) the rolling surfaces were made of concrete. As a result, the properties and findings presented in this report can not (and should not) be inferred to be representative of the performance expected from the ISO-BaseTM

system in similar situations. Recall, as indicated earlier (Chapter 1), that this concept was developed out of necessity in the early phase of this project as manufactures of base isolation devices were working in parallel on developing isolated floor concepts and unwilling to share details of their product until patents were filed. As a result, it is important to recognize that the purpose of the concrete BNC concept is not to develop an alternative competing product, but rather to develop a system for academic purposes for which thorough credible mechanical properties can be obtained and used for the global objectives described earlier without delays.

As such, because this isolator is new in a few different ways, the mechanical properties (such as horizontal acceleration-displacement relationship) of this kind of concrete BNC isolator are unknown and characterization tests are necessary before the whole isolated floor system can be designed and tested.

This chapter presents the details about the test setup and experimental results for these characterization tests. For each kind of balls, four series of test were conducted on individual isolators under different magnitudes of gravity loads, namely free vibration tests, force-displacement tests, sweep frequency tests, and dynamic tests using earthquake inputs. Note that for the dynamic tests using earthquake inputs, both synthetic response spectra compatible acceleration time histories and floor responses of buildings having structural fuse frames of the type described in Vargas and Bruneau (2006a) were adopted as seismic inputs.

An empirical model is developed in Section 3.2 for this special kind of concrete BNC isolator. The description of the concrete BNC isolator is presented in Section 3.3, followed by details on the test setup in Section 3.4. The test results are presented in Section 3.5. The detailed description of the design and test of the complete isolated floor system using this kind of concrete BNC isolators will be presented in subsequent chapters.

3.2 Empirical Model for Concrete BNC Isolator

As described in Chapter 2, BNC isolators have been studied as early as in 1995 by Kemeny and Szidarovszky. All consist of parallel rolling surfaces that translate upon rotation of the ball. The working surfaces are concave, providing self-centering capabilities. Here, building from the experiment by Vargas and Bruneau (2006b) which included an ISO-BaseTM device by WorkSafe Technologies on top of a 3-story structural fuse frame specimen to successfully reduce the acceleration response of nonstructural components, a special kind of concrete BNC isolator is developed. The bearing plates of the concrete BNC isolator are made of concrete material and chosen to be concave, similar to the dimensions of ISO-BaseTM platforms (e.g., the slope of the conical part of the working surface is 1:10). However, the concrete BNC isolator used here adopted 51 mm (2 in) diameter rubber and polyurethane balls (instead of the 38 mm (1.5 in) diameter steel balls used in ISO-BaseTM isolators). The hardness of the rubber balls and polyurethane balls are 70A and 95A, respectively. The advantages gained by using these balls include adding damping to the BNC isolator and avoiding the problem of causing grooves on the working surface of the bearing plates under relatively high isolated loads.

The rolling friction between the ball and the concrete working surface is significant. Therefore, the physical model by Kemeny and Szidarovszky (1995) as described in Section 2.3 for the BNC isolator made of steel material (where the rolling friction is negligible) is not directly useable for the concrete isolator and that a new model is required for this special kind of concrete BNC isolator. The development of an empirical model is shown below.

Fig. 3.1(a) illustrates the geometry of the concrete working surface, which consists of two parts: a spherical central part and an outside conical surface. When the ball rolls within the spherical central part of the working surface, the concrete BNC isolator is equivalent to a double friction pendulum (FP) bearing (Fenz and Constantinou 2006 and 2008) with equal friction coefficient

and equal effective radius of curvature for both spherical surfaces. The only difference between these two lies in the friction type: rolling friction in the concrete BNC isolator and sliding friction in the double FP bearing. So, the empirical model of the concrete BNC isolator under this movement case is similarly derived as following.

The free body diagram of the isolated weight is shown in Fig. 3.1(b), where the rolling ball is within the spherical central area and ascending the concrete working surface. The equilibrium equations in the horizontal and vertical directions can respectively be written as:

$$F - N \sin \gamma_x - N \mu_1 \cos \gamma_x = 0 \quad (3.1a)$$

$$W - N \cos \gamma_x + N \mu_1 \sin \gamma_x = 0 \quad (3.1b)$$

where F is the lateral restoring force; W is the isolated weight; N is the reaction force from the working surface; μ_1 is the rolling friction coefficient between the rolling ball and the concrete working surface; γ_x is the rotation angle corresponding to the ball lateral displacement, x . In addition, M_r in Fig. 3.1(b) is the rolling friction moment.

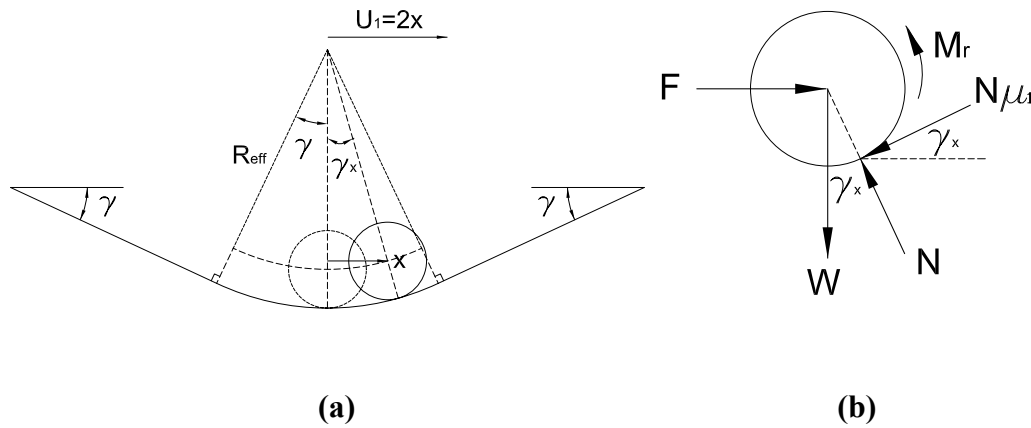


Figure 3.1 BNC Bearing: (a) Working Surface; (b) Free Body Diagram of Isolated Weight

Solving Eq. 3.1b gives,

$$N = \frac{W}{\cos \gamma_x - \mu_1 \sin \gamma_x} \quad (3.2)$$

Substituting Eq. 3.2 into Eq. 3.1a, one obtains,

$$F = \frac{W \sin \gamma_x}{\cos \gamma_x - \mu_1 \sin \gamma_x} + \frac{W \mu_1 \cos \gamma_x}{\cos \gamma_x - \mu_1 \sin \gamma_x} \quad (3.3)$$

Since the rotation angle γ_x is very small (i.e., $\cos \gamma_x \approx 1$ and $\sin \gamma_x = \frac{x}{R_{eff}} \approx \gamma_x$, where R_{eff} is the effective radius of curvature equal to the radius of the spherical central part minus the radius of the rolling ball) when $x < R_{eff} \sin \gamma$ (where γ is the slope of the outside conical surface), and since both μ_1 and γ_x are small values (i.e., $\mu_1 \sin \gamma_x \approx 0$), Eq. 3.3 can be simplified as,

$$F = \frac{Wx}{R_{eff}} + W\mu_1 \quad (3.4)$$

Note that the error induced by the simplifications of $\cos \gamma_x \approx 1$ and $\mu_1 \sin \gamma_x \approx 0$ in Eq. 3.4 is less than 3% even when μ_1 takes an extreme value of 0.2 and γ_x takes its maximum value of 0.1 (i.e., the slope of the outside conical surface).

Since the lateral displacement of the top bearing plate with respect to the bottom bearing plate, U_1 , is twice the lateral displacement of the rolling ball, x , Eq. 3.4 can be expressed as,

$$F = \frac{WU_1}{2R_{eff}} + W\mu_1 \quad (3.5)$$

Note that Eq. 3.5 is valid only when $x < R_{eff} \sin \gamma$ and the rolling ball is ascending the working surface. When the rolling ball is descending along the working surface and $x < R_{eff} \sin \gamma$, the

equation of motion can be obtained as,

$$F = \frac{WU_1}{2R_{eff}} - W\mu_1 \quad (3.6)$$

The acceleration of the isolated components corresponding to the Eqs. 3.5 and 3.6, a_1 , can be obtained by dividing Eqs. 3.5 and 3.6 by the isolated mass,

$$a_1 = \frac{gU_1}{2R_{eff}} + g\mu_1 \quad (\text{when the ball is ascending the working surface}) \quad (3.7)$$

$$a_1 = \frac{gU_1}{2R_{eff}} - g\mu_1 \quad (\text{when the ball is descending the working surface}) \quad (3.8)$$

where, g is the acceleration of gravity.

When the rolling ball reaches the conical part of the working surface (i.e., $x \geq R_{eff} \sin \gamma$), the lateral force, F , becomes a constant value,

$$F = W \sin \gamma + W\mu_1 \quad (\text{when the ball is ascending the working surface}) \quad (3.9)$$

$$F = W \sin \gamma - W\mu_1 \quad (\text{when the ball is descending the working surface}) \quad (3.10)$$

The acceleration of the isolated components corresponding to the Eqs. 3.9 and 3.10 is respectively a constant value as:

$$a_1 = g \sin \gamma + g\mu_1 \quad (\text{when the ball is ascending the working surface}) \quad (3.11)$$

$$a_1 = g \sin \gamma - g\mu_1 \quad (\text{when the ball is descending the working surface}) \quad (3.12)$$

Since the slope of the outside conical surface γ is small (i.e., $\sin \gamma \approx \gamma$ (in rad)), Eqs. 3.11 and 3.12 can be simplified as,

$$a_1 = g\gamma + g\mu_1 \quad (\text{when the ball is ascending the working surface}) \quad (3.13)$$

$$a_1 = g\gamma - g\mu_1 \quad (\text{when the ball is descending the working surface}) \quad (3.14)$$

Based on Eqs. 3.5 and 3.6 and Eqs. 3.9 and 3.10, the force-displacement relationship of the special kind of concrete BNC isolator, where the rolling friction between the rolling ball and the working surface is significant, is shown in Fig. 3.2.

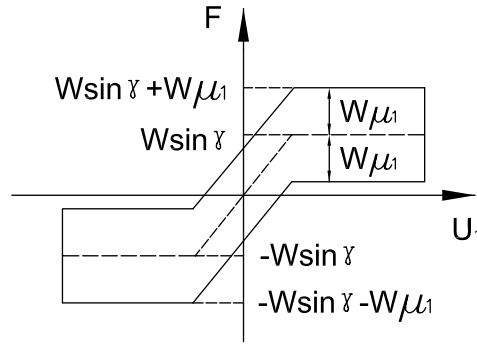


Figure 3.2 Behavior of BNC Bearing with Friction

Note here that the empirical model developed for this special kind of BNC isolator does not physically model the fact that the actual ball is deformed under pressure (i.e., the gravity load on top). However, it is accounted for by this empirical model (even though the ball is shown as idealized round in Fig. 3.1) by calibration of the friction effect between the rolling ball and the concrete working surface, as shown later in this chapter.

Based on the empirical model developed above for the concrete BNC isolator with significant rolling friction between the ball and the concrete working surface, the force-displacement

relationships for the case where the rolling friction is negligible (i.e., $\mu_1 \approx 0$) is also derived here. When $\mu_1 \approx 0$, the friction effect in Eqs. 3.5 and 3.6 for the case when $x < R_{eff} \sin \gamma$ and Eqs. 3.9 and 3.10 for the case when $x \geq R_{eff} \sin \gamma$ can be neglected accordingly and these equations can be simplified and combined as,

$$F = \frac{WU_1}{2R_{eff}} \quad (\text{when } x < R_{eff} \sin \gamma) \quad (3.15)$$

$$F = W \sin \gamma \quad (\text{when } x \geq R_{eff} \sin \gamma) \quad (3.16)$$

Note from Eq. 3.16 that the lateral restoring force is a constant value and independent of the lateral displacement of the BNC isolator.

The acceleration response in Eqs. 3.7 and 3.8 and Eqs. 3.13 and 3.14 can respectively be simplified and combined as:

$$F = \frac{gU_1}{2R_{eff}} \quad (\text{when } x < R_{eff} \sin \gamma) \quad (3.17)$$

$$F = g\gamma \quad (\text{when } x \geq R_{eff} \sin \gamma) \quad (3.18)$$

The force-displacement relationship, based on Eq. 3.15 and 3.16, is shown in Fig. 3.3. It can be noted that it is a bilinear elastic relationship, which corresponds to the central line of the curve shown in Fig. 3.2 (i.e., the friction effect is subtracted from the curve in Fig. 3.2).

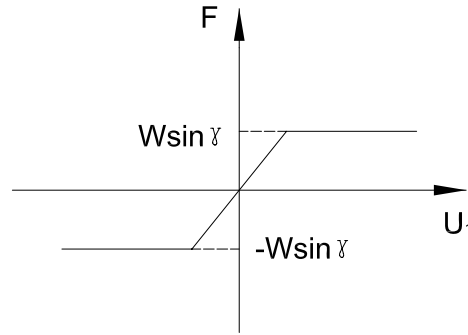


Figure 3.3 Behavior of BNC Bearing_without Friction

A comparison between Eqs. 3.15 and 3.16 (i.e., the empirical model developed here for the case where the rolling friction is negligible) and Eqs. 2.1 and 2.2 (i.e., the physical model by Kemeny and Szidarovszky (1995) for the steel BNC isolator where the rolling friction is negligible) is conducted here and shows that: 1) the lateral displacement of the top bearing plate with respect to the bottom bearing plate (i.e., the displacement of the BNC isolator) is defined as double of the lateral displacement of the center of the rolling ball in the empirical model here and it is taken as double of the lateral distance between the apex of the bearing plate and the contacting point between the rolling ball and the working surface in the physical model by Kemeny and Szidarovszky (1995); 2) Together with the above definitions of BNC isolator displacement in different models, when the ball rolls within the spherical central area, the effective radius of curvature is used in the equations of the empirical model developed here and the radius of the spherical area is used instead in the physical model by Kemeny and Szidarovszky (1995). However, when the radius of the spherical part is large compared to the radius of the rolling ball, these two models are consistent, and; 3) when the ball rolls within the outside conical surface, these two models are same.

3.3 Concrete BNC Isolator Design and Cast

The detailed design calculations for the concrete bearing plates are presented in Appendix B. The dimensions of the designed bearing plates of the concrete BNC isolators are shown in Fig. 3.1. Each plate is 273 mm (10.75 in) wide and 301 mm (28 in) long. The working surface consists of a central spherical surface with radius of 152 mm (6 in) and an outside conic surface with a slope of 1:10 (5.7°). The diameter of the concave surface is 213 mm (8.375 in). The horizontal diameter of the central spherical area is 30 mm (1.2 in). The distance between the centers of the two concave surfaces on each bearing plate is 438 mm (17.25 in). Thickness of the concrete bearing plate is 51 mm (2 in), i.e. still thin enough to be attractive for isolated floor system use. The displacement capacity of the concrete isolators is set to be 178 mm (7 in). To avoid brittle failure of the concrete bearing plates, deformed wires were deployed as reinforcement. The inside reinforcement for all bearing plates consisted of deformed wire (D2.0), with a cross sectional area of 13 mm^2 (0.02 in^2), tied together to form a 51 mm (2 in) square grid cage.

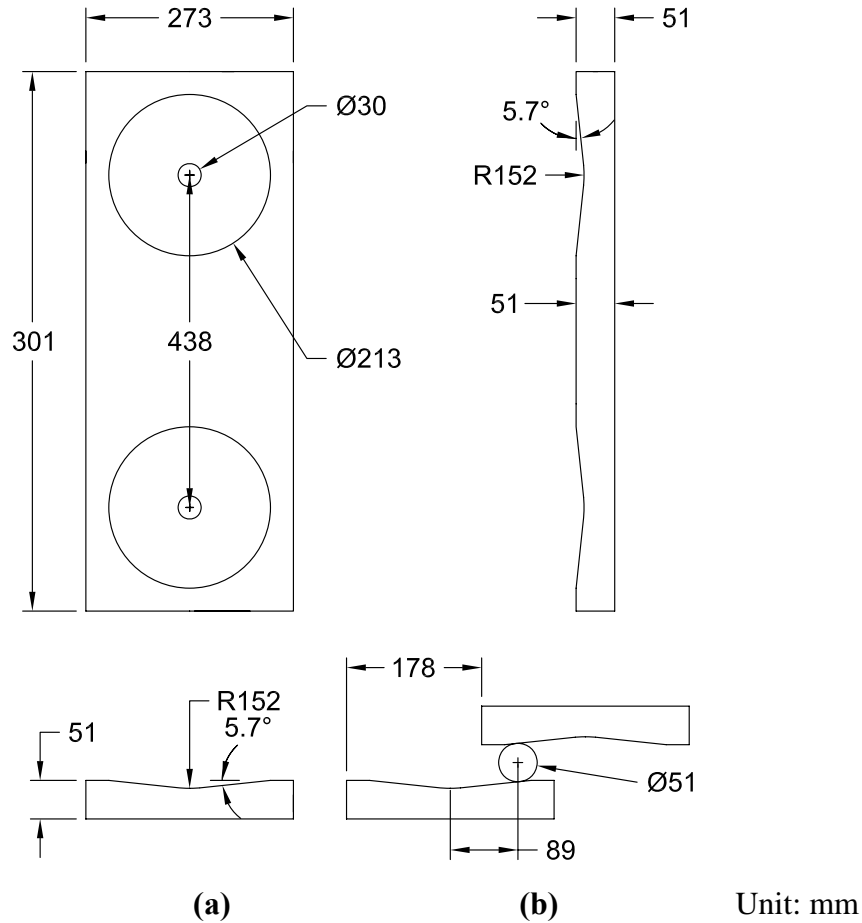


Figure 3.4 Bearing Plate of Concrete BNC Isolator: (a) Plan and Cross Section Views; (b) Bearing Plates at Maximum Displacement

To cast the thin bearing plates with common commercial concrete of 27.58 MPa (4 ksi) compression strength, and to ensure smooth concave surfaces, a ADVA 170 superplasticizer was added to make the concrete mix more flowable and workable. It was added in a ratio of about 35 ml per 72.58 Kg of concrete mix, which is equivalent to 35 ml for two bags (80 lb/bag) of concrete mix. Foam molds donated by Thermal Foams, Inc, as shown in Fig. 3.5, were used instead of traditional wood forms to make the pours easier and faster. The foam material used in these molds is 76 mm (3 in) thick, which is strong and stiff enough to hold the concrete mix inside. The manufacturer's expected tolerance is 3.2 mm (1/8 in) for dimensions and 2 degrees for angles. Measuring the concrete bearing plates after their curing, it was found that the actual

slope of the conic part of the working surface was about 1 degree bigger than the target, which was within the expected tolerance. However, the difference between the actual horizontal diameter of the central spherical area and the target was about 25 mm (1 in), which was bigger than the expected tolerance – this happened because the shape of the central tip part of the bearing plates on the foam molds was hard to make using machine tools. Based on those observations, for possible future applications, the manufacturer recommended to use a more precise manufacturing process, such as a laser mold machine, if more accurate results are desired for both the central part and the outside conical surface of the mold. However, this option was too expensive for the available project budget, and new molds were not made.

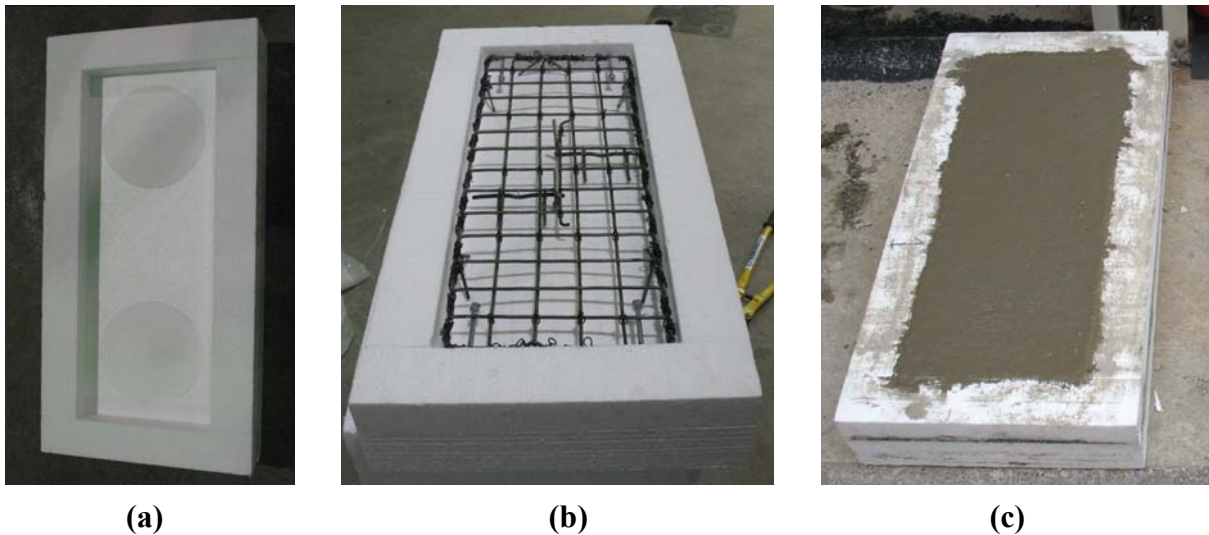


Figure 3.5 Bearing Plate Cast: (a) Foam Mold; (b) Foam Mold with Reinforcement; (c) Concrete Pouring

3.4 Test Setup

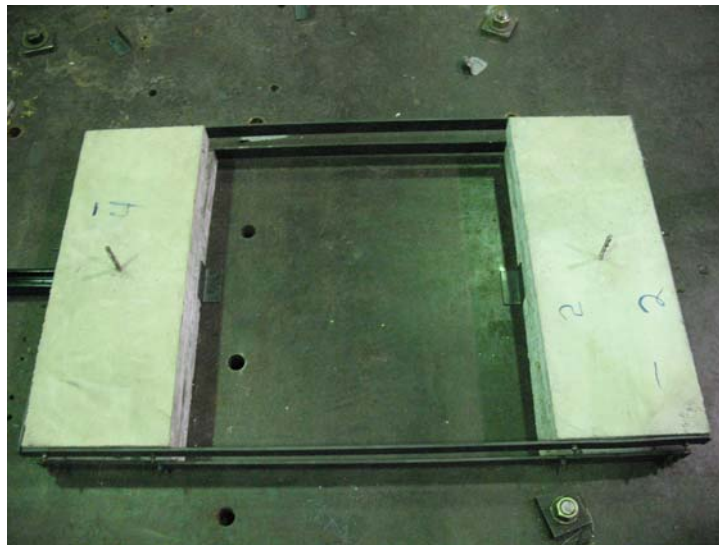
3.4.1 Specimen Assembly and Setup

Eight pieces of concrete bearing plates in total, four top bearing plates and four bottom ones, were cast for this phase of experiment. Four of them with better working surfaces were selected to assemble the concrete BNC isolator specimen as illustrated in Fig. 3.6. The assembly was achieved using steel flat bars, 38 mm (1.5 in) deep and 6 mm (1/4 in) thick. These steel flat bars were bolted onto threaded anchors pre-cast into the concrete bearing plates.

Four series of tests were conducted on this isolator specimen, namely free vibration tests, force-displacement tests, sweep frequency tests, and dynamic tests using earthquake inputs. In all these tests, the bottom bearing plates of the specimen were fixed to the shake table (“Shake Table O” located in the older part of the SEESL laboratory at the State University of New York at Buffalo, http://nees.buffalo.edu/Facilities/Major_Equipment/shaketables.asp) by tack welding some steel angles against the edges of the bottom concrete bearing plates as shown in Fig. 3.7. Note that in the force-displacement tests, a bracket bar (3277 mm long) connected the top bearing plates to the load cell fixed on a stiff column beside the shake table, as shown in Figure 3.8.



(a)



(b)

**Figure 3.6 Concrete BNC Isolator Specimen: (a) Bottom Bearing Plates with Balls;
(b) Specimen**

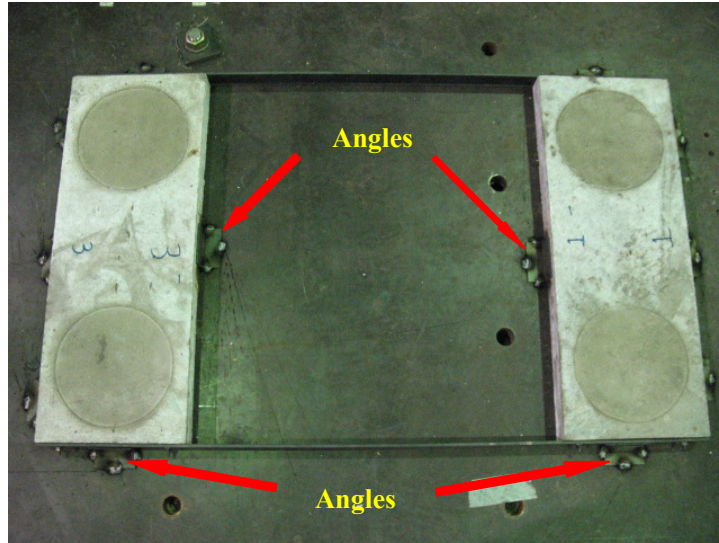


Figure 3.7 Specimen Setup_1

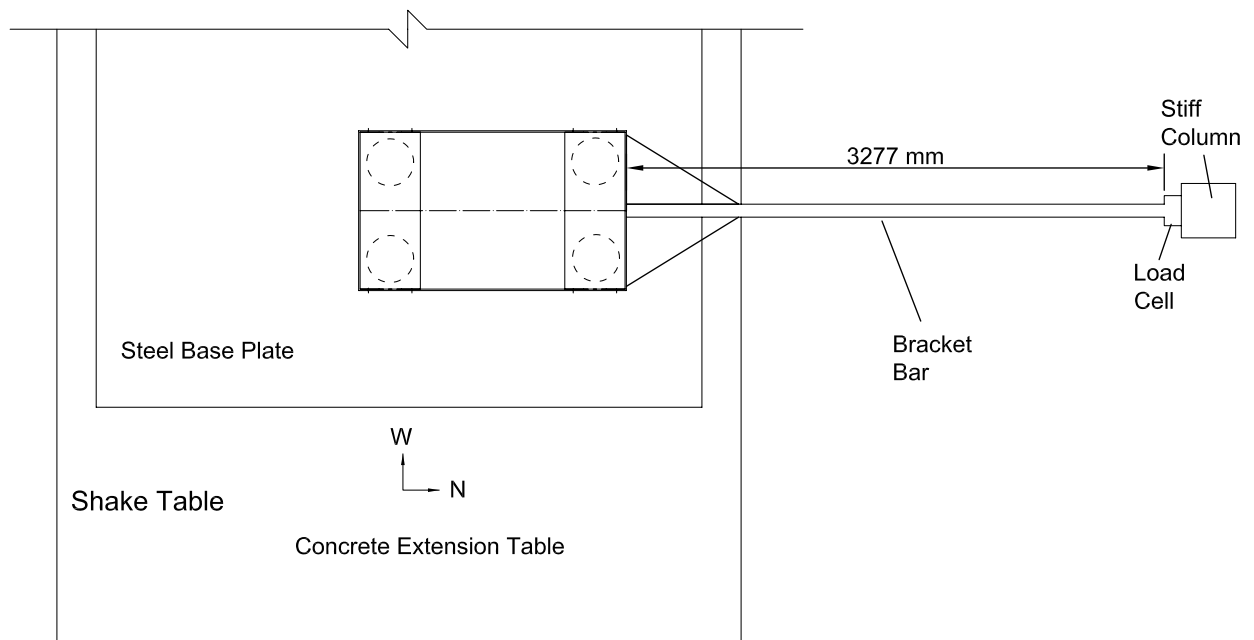


Figure 3.8 Specimen Setup_2

3.4.2 Load Program

The objective of this phase of tests was to characterize the properties of this special kind of BNC isolators, more specifically the horizontal acceleration-displacement relationship under different gravity loads and dynamic regimes. Note that for isolator tests here, “displacement” means the relative displacement of the top bearing plates with respect to the bottom ones, and “acceleration” means the absolute acceleration response of the top bearing plates.

Given the load combinations specified by the “ASCE-7 Minimum Design Loads for Buildings and Other Structures” (ASCE 2005), gravity loads were applied to the isolators to simulate two extreme load cases, namely, $1.2D + L + 1.0E$ and $0.9D + 1.0E$. The specimen selected for the single isolator tests correspond to the middle set of the outside row of the BNC isolators used in the complete isolated floor system described in Appendix A, which carries the maximum load calculated per its tributary area. The target gravity load on the selected set of isolator, corresponding to these two load combinations, were respectively about 6072 N (1365 lb) and 543 N (122 lb), which was applied to the entire isolator, and thus transmitted through 4 balls. Some steel plates were stacked on top of the isolator to achieve these load values. The actual achieved load values were 6512 N (1464 lb) and 689 N (155 lb), respectively, i.e. the difference between the realization and target is within 27% of the target values. To get more information on performance of the isolators under various conditions, two other gravity of 4875 N (1096 lb) and 2393 N (538 lb) achieved by different combinations of these steel plates were also considered, as interpolated values of the previous two extreme load cases. These load cases were denoted as Load Case 1 to Load Case 4, from the smallest to the largest magnitude of the four load values considered.

3.4.3 Input Program

As mentioned before, four series of tests were run on the concrete isolator specimen, namely free vibration tests, force-displacement tests, sweep frequency tests, and dynamic tests using earthquake inputs. The free vibration tests were conducted by manually moving the top bearing plate to its nominal horizontal displacement capacity (i.e., 7 in) and then releasing to let the top bearing plate vibrate freely. In force-displacement tests, the displacement was controlled by the shake table and load cells were used to measure the force transmitted by the bracket. Sweep frequency tests were also conducted using the shake table in displacement control mode. Sine waves were applied with amplitude of either 25 mm, 38mm, or 51 mm (1 in, 1.5 in, or 2 in) progressively sweeping over a frequency range of 7 Hz to 0.4 Hz. For the last set of tests, both earthquake-like synthetic acceleration time histories and structural floor absolute acceleration responses were used as inputs. The following shows the generation of such inputs.

Following the same synthetic acceleration time history generation procedure used by Vargas and Bruneau (2006a), an elastic response spectrum was first defined in accordance with the NEHRP Recommended Provisions for Seismic Regulations for New Buildings and other Structures (NEHRP 2003) for Sherman Oaks, California, and site soil-type class B, which correspond to the site of the Multidisciplinary Center for Earthquake Engineering Research (MCEER) Demonstration Hospital (Yang and Whittaker 2002) chosen for this project. The design spectral accelerations for this site are $S_{DS}=1.3g$, and $S_{D1}=0.58g$ for 2% probability of exceedance in 50 years. For this spectrum, T_s is 0.45 s, and T_0 is 0.09 s. A response spectra compatible acceleration time history was then generated by using the Target Acceleration Response Spectra Compatible Time Histories (TARSCTHS) Code (Papageorgiou et al. 1999) and was used as one of the seismic inputs for dynamic tests of the isolators. This earthquake input is denoted as “Acc1”. This synthetic strong motion record was 15 s in duration. The comparison between the elastic response spectrum for 5% of critical damping corresponding to the response spectra compatible

acceleration time histories and the target NEHRP 2003 elastic response spectrum is shown in Fig. 3.9. Good agreement can be found from this figure.

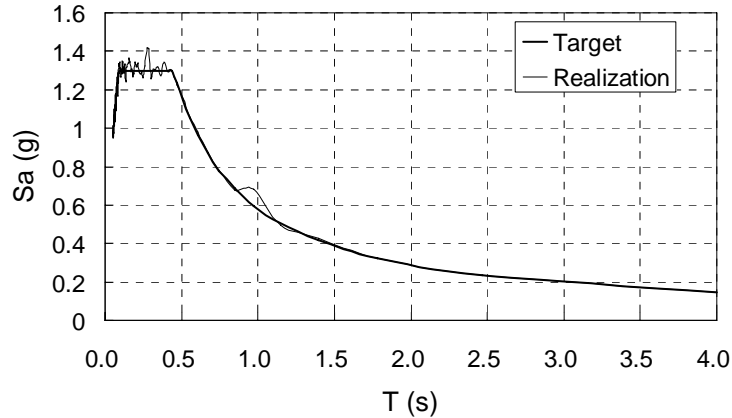


Figure 3.9 Average Elastic Response Spectrum of Realization VS Target Response Spectrum ($\zeta=5\%$)

In the dynamic tests using earthquake inputs, the floor absolute acceleration responses recorded from response history analysis of structural fuse frames were also selected as seismic inputs. One of the structural fuse frames considered here was a one-story one-bay structural fuse frame, which was a design example in Vargas and Bruneau (2006a). The schematic lateral force-displacement relationship for this structural fuse frame is shown in Fig. 3.10. The mass of this frame is $0.35 \text{ kN}\cdot\text{s}^2/\text{mm}$ ($2 \text{ kip}\cdot\text{s}^2/\text{in}$). The initial lateral stiffness of the frame, K_{isf} , is 49.43 kN/mm (282.26 kip/in), and the yield strength, V_{ysf} , is 714.39 kN (160.61 kip). The natural vibration period of this single-degree-of-freedom (SDOF) frame is 0.53 s . The post yielding stiffness ratio is $K_{psf}/K_{isf}=0.25$, where K_{psf} is the frame lateral stiffness after yielding of the metallic energy dissipating element. The equivalent linear viscous damping ratio of the frame is 5% .

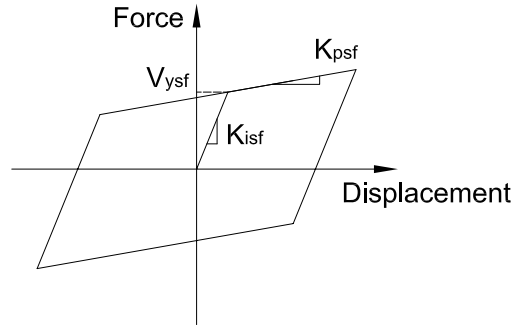


Figure 3.10 Lateral Force-Displacement Relationship of Structural Fuse Frame

This structural fuse frame was modeled in SAP2000 (CSI 2004) with a Wen-plastic link element and a damper link element. It was then subjected to nonlinear response history analysis by using the above response spectra compatible time histories Acc1 as the ground motions. The absolute acceleration response of the floor was recorded and adopted here as one of the seismic inputs to test the concrete isolator in the test series of dynamic tests using earthquake inputs, which is denoted as “Acc2”.

Another structural fuse frame considered was also a one-story one-bay structural fuse frame with a mass of $0.35 \text{ kN}\cdot\text{s}^2/\text{mm}$ ($2 \text{ kip}\cdot\text{s}^2/\text{in}$). The initial lateral stiffness of this frame, K_{ist} , is $2822 \text{ kN}/\text{mm}$ ($16114 \text{ kip}/\text{in}$), and the yield strength, V_{ysf} , is 1290 kN (290 kip). The natural vibration period of this SDOF frame is 0.07 s . The post yielding stiffness ratio is $K_{psf}/K_{ist}=0.25$. The equivalent linear viscous damping ratio of the frame is 5% . This frame was also analyzed in SAP2000, and the absolute acceleration response of the frame floor was recorded and adopted as another floor response seismic input for dynamic tests using earthquake inputs, denoted as “Acc3”. Note that the natural periods of these two structural fuse frames considered here are 0.53 s and 0.07 s , which lie in the ascending range and descending range of the target elastic response spectra (as shown in Fig. 3.9), respectively. This indicates that the frequency contents of these two floor response seismic inputs are different.

3.4.4 Instrumentation

String pots and accelerometers were used to measure the displacement and acceleration responses at different points of the specimen. The instrumentation layout is schematically shown in Fig. 3.11. A total of eighteen channels of data were recorded, among which nine were string pots, and nine were accelerometers. The function of each one is shown in Table 3.1. Note that in the force-displacement tests, an additional data channel was included for the load cell to record the force transmitted by the bracket mentioned in Section 3.4.1. Also note that in the force-displacement tests, three load cells, with calibration scales ranging from low to high, were correspondingly used in the test cases with gravity loads from low to high.

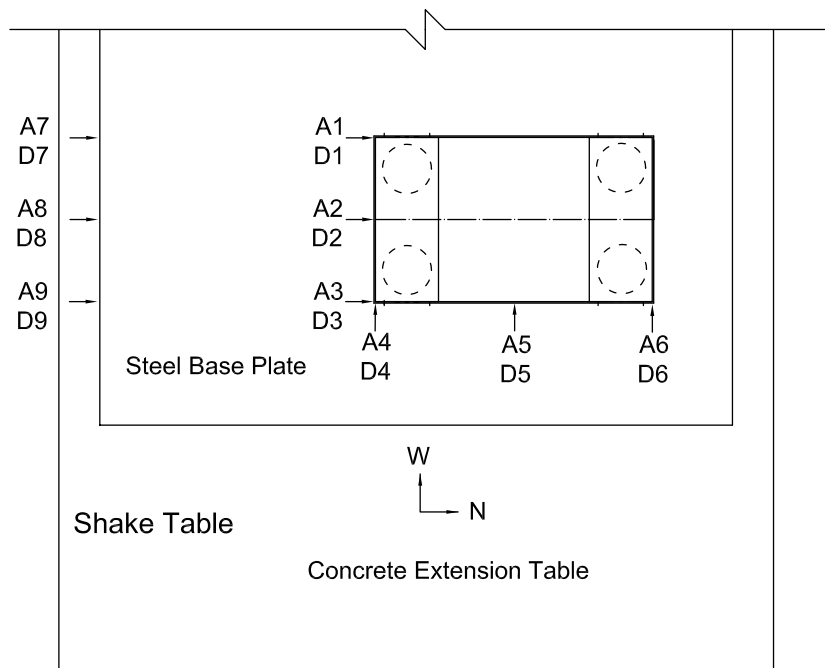


Figure 3.11 Layout of Instrumentation

Table 3.1 List of Instrumentation

#	Name	Type of Sensor	Measure Direction	Note
(1)	(2)	(3)	(4)	(5)
1	A1	Accelerometer	N-S	Top bearing plate, west, south
2	A2	Accelerometer	N-S	Top bearing plate, middle, south
3	A3	Accelerometer	N-S	Top bearing plate, middle, south
4	A4	Accelerometer	E-W	Top bearing plate, East, south
5	A5	Accelerometer	E-W	Top bearing plate, East, middle
6	A6	Accelerometer	E-W	Top bearing plate, East, north
7	A7	Accelerometer	N-S	Shake table, west, south
8	A8	Accelerometer	N-S	Shake table, west, middle
9	A9	Accelerometer	N-S	Shake table, west, north
10	D1	String Pot	N-S	Top bearing plate, west, south
11	D2	String Pot	N-S	Top bearing plate, middle, south
12	D3	String Pot	N-S	Top bearing plate, middle, south
13	D4	String Pot	E-W	Top bearing plate, East, south
14	D5	String Pot	E-W	Top bearing plate, East, middle
15	D6	String Pot	E-W	Top bearing plate, East, north
16	D7	String Pot	N-S	Shake table, west, south
17	D8	String Pot	N-S	Shake table, west, middle
18	D9	String Pot	N-S	Shake table, west, north

3.4.5 Test Protocol

Tables 3.2 to 3.5 show the test sequences for the four series tests: free vibration tests, force-displacement tests, sweep frequency tests, and dynamic tests using earthquake inputs, respectively. Note that the two kinds of balls rolling between the top and bottom concrete bearing plates were separately tested in all the four test series.

Note that because these tests were conducted to generate knowledge on the acceleration-displacement relationship of the isolator, lack of this knowledge made prediction of response during the dynamics tests under earthquake inputs (using simplistic models) unreliable. For safety purposes, the amplitude of the shake table was operated for low amplitude of the dynamic excitations, and the same test was repeated with signals were scaled up gradually until the relative displacement of the top bearing plates with respect to the bottom ones (in at least one test for dynamic tests under earthquake inputs) reached around 127 mm (5 in), or until the input amplitude reached the shake table capacity (whichever came first). Therefore, a total of 112 tests were conducted, but only the results for the last in each series for a given combination of gravity load, isolator type, and ground acceleration corresponding to the cases listed in Tables 3.3 to 3.5 are reported in the rest of this chapter. It is also for this reason that different shake table signal amplitudes were used for cases with rubber balls and cases with polyurethane balls in the sweep frequency test series as shown in Table 3.4.

Table 3.2 Free Vibration Test Sequence

Test # (1)	Ball Type (2)	Load (N) (3)
1	Rubber	689
2	Rubber	2393
3	Rubber	4875
4	Rubber	6512
5	Polyurethane	689
6	Polyurethane	2393
7	Polyurethane	4875
8	Polyurethane	6512

Table 3.3 Force-Displacement Test Sequence

Test # (1)	Ball Type (2)	Weight (N) (3)	Signal Frequency (Hz) (4)	No. of Cycles (5)
1	Rubber	689	0.05	10
2	Rubber	689	0.2	10
3	Rubber	689	0.8	10
4	Rubber	2393	0.2	10
5	Rubber	4875	0.05	10
6	Rubber	4875	0.2	10
7	Rubber	4875	0.8	10
8	Rubber	6512	0.2	10
9	Polyurethane	689	0.05	10
10	Polyurethane	689	0.2	10
11	Polyurethane	689	0.8	10
12	Polyurethane	2393	0.2	10
13	Polyurethane	4875	0.05	10
14	Polyurethane	4875	0.2	10
15	Polyurethane	4875	0.8	10
16	Polyurethane	6512	0.2	10

Table 3.4 Sweep Frequency Test Sequence

Test # (1)	Ball Type (2)	Load (N) (3)	Signal Amplitude (mm) (4)	Frequency Range (Hz) (5)
1	Rubber	689	51	7-0.4
2	Rubber	2393	51	7-0.4
3	Rubber	4875	51	7-0.4
4	Rubber	6512	51	7-0.4
5	Polyurethane	689	25	7-0.4
6	Polyurethane	2393	25	7-0.4
7	Polyurethane	4875	25	7-0.4
8	Polyurethane	6512	38	7-0.4

Table 3.5 Sequence of Dynamic Tests Using Earthquake Inputs

Test # (1)	Ball Type (2)	Load (N) (3)	Seismic Input* (4)
1	Rubber	689	Acc1
2	Rubber	689	Acc2
3	Rubber	689	Acc3
4	Rubber	4875	Acc1
5	Rubber	4875	Acc2
6	Rubber	4875	Acc3
7	Rubber	6512	Acc1
8	Rubber	6512	Acc2
9	Rubber	6512	Acc3
10	Polyurethane	689	Acc1
11	Polyurethane	689	Acc2
12	Polyurethane	689	Acc3
13	Polyurethane	4875	Acc1
14	Polyurethane	4875	Acc2
15	Polyurethane	4875	Acc3
16	Polyurethane	6512	Acc1
17	Polyurethane	6512	Acc2
18	Polyurethane	6512	Acc3

Note* :

Acc1, Spectra compatible ground acceleration;

Acc2, floor acceleration of frame with period of 0.53s;

Acc3, floor acceleration of frame with period of 0.07s.

3.5 Test Results

3.5.1 Results of Free Vibration Tests

As in Vargas and Bruneau (2006b), some free vibration tests were conducted with the expectation that it would allow to quantify the free vibration period and the equivalent viscous damping ratio of the concrete BNC isolator. The displacement history of such free vibration tests are shown in Figs. 3.12 to 3.15. Note that there are two parts in each figure, which correspond to the cases using rubber and polyurethane balls, respectively.

It can first be found from these figures that when the initial displacement (just before releasing the top bearing plate for free vibration) is almost same, there are more motion cycles in the cases using polyurethane balls than the corresponding ones with rubber balls. This indicates that the damping in the cases with rubber balls is bigger than that in the corresponding one using polyurethane balls. It is also observed that, with increases in the magnitude of the gravity load, less motion cycles are found. It indicates that damping increases along with the increases in the gravity load magnitude.

A closer review of these figures reveals that the concrete BNC isolator does not have a constant vibration period. For example, Fig. 3.12 illustrates this phenomenon. In this figure, calculating the period between various points at various amplitudes of vibration, two vibration periods are shown for the case with rubber balls (Fig. 3.12a), and four vibration periods are shown for the case using polyurethane balls (Fig. 3.12b). Consequently, the viscous damping ratio cannot be directly obtained using the classical relationship between the damping ratio and the decay in the free vibration amplitudes proposed for damped structures in dynamic analysis (Chopra 2001). It was also observed that the time needed for the balls to roll from the apex of the spherical part to the point of maximum displacement on the conical part of the working surface is shorter than

that the time taken by the balls to roll back from that peak displacement back to the apex of the spherical part of the working surface. One example is shown in Fig. 3.15. However, this is reasonable and explained by the fact that the acceleration is bigger when the ball ascends the working surface than that when it descends the working surface, as shown by the equations (in Section 3.2) derived from the behavior of this type of isolator.

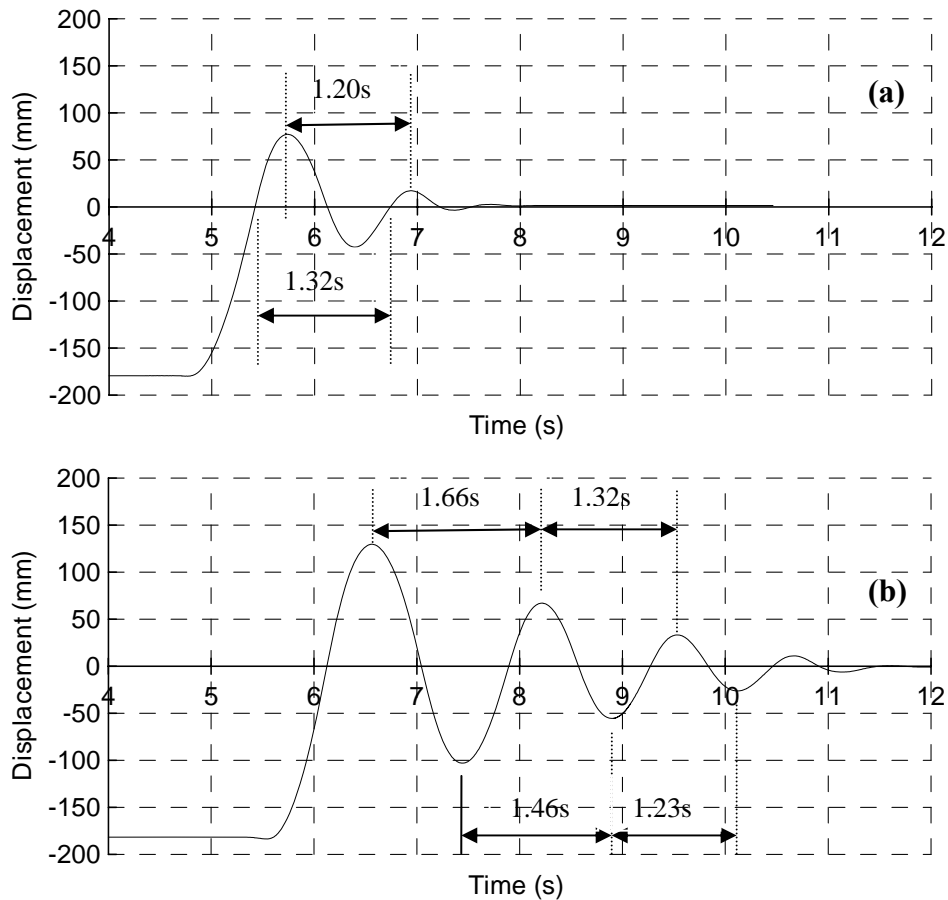


**Figure 3.12 Results of Free Vibration Tests under Load Case 1: (a) Rubber Balls;
(b) Polyurethane Balls**

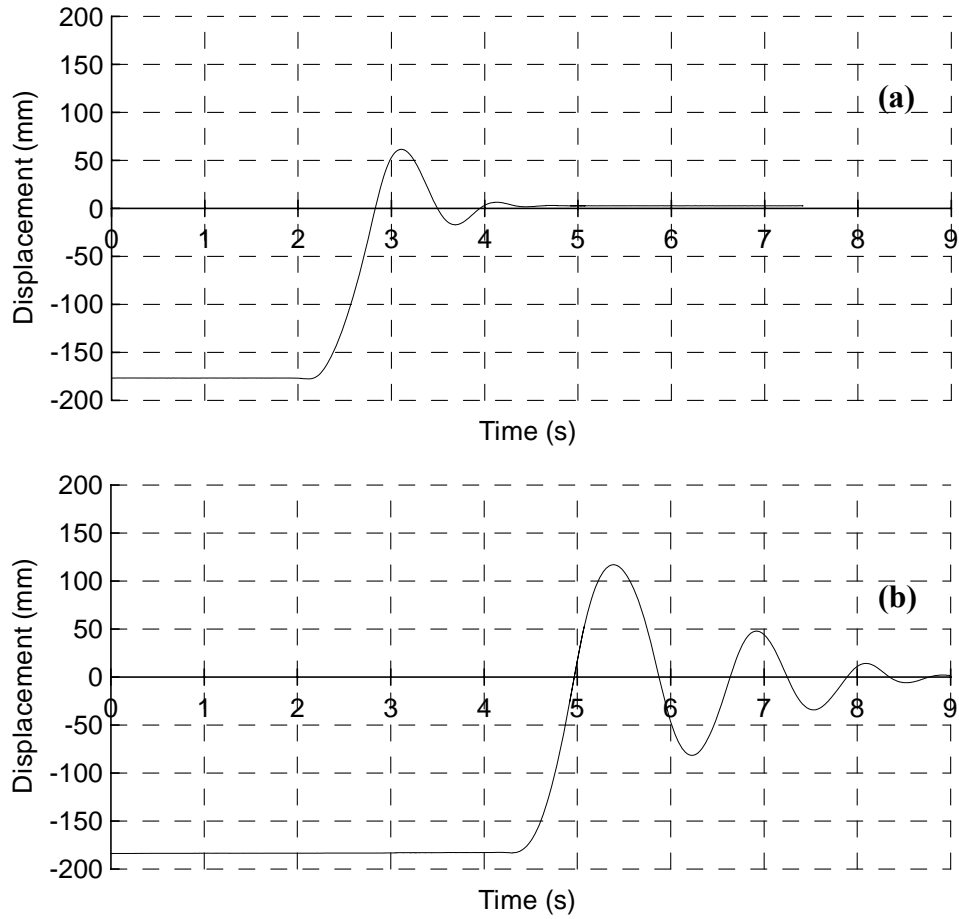


**Figure 3.13 Results of Free Vibration Tests under Load Case 2: (a) Rubber Balls;
(b) Polyurethane Balls**

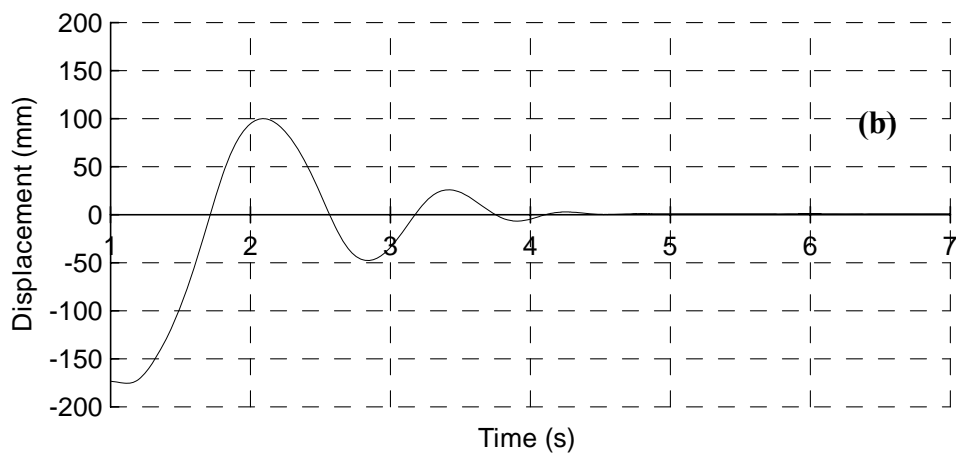
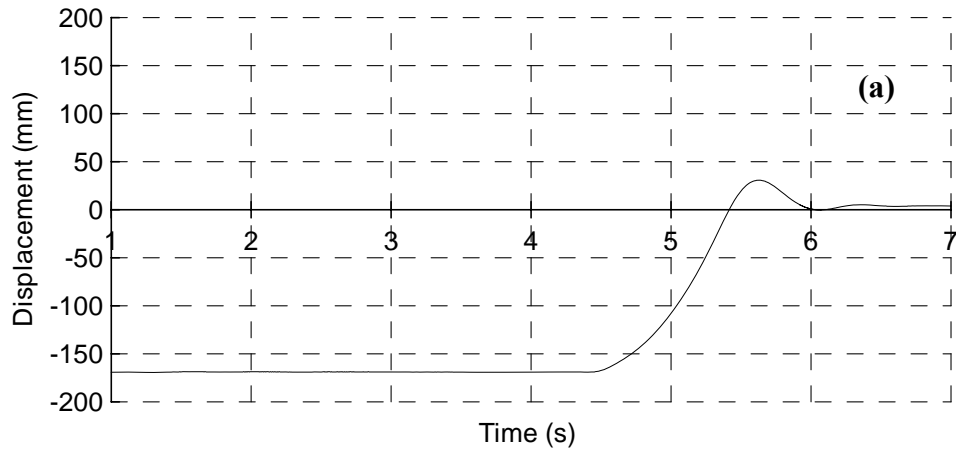


Figure 3.14 Results of Free Vibration Tests under Load Case 3: (a) Rubber Balls; (b) Polyurethane Balls

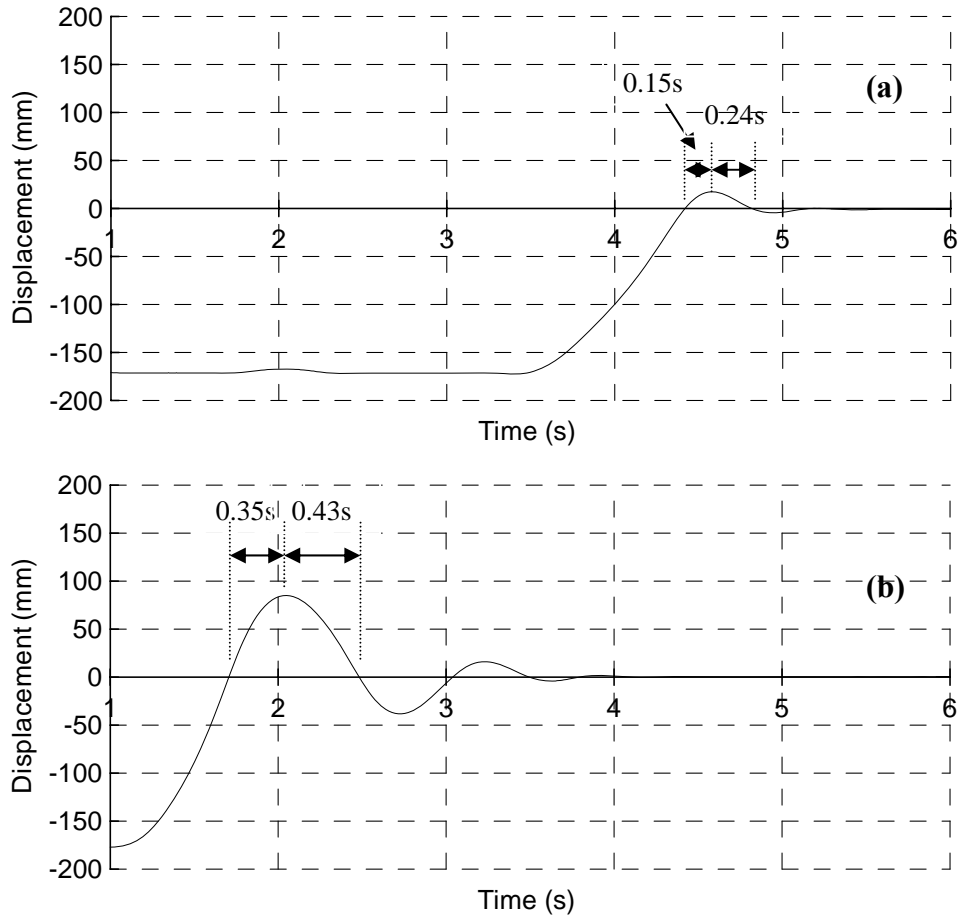


Figure 3.15 Results of Free Vibration Tests under Load Case 4: (a) Rubber Balls; (b) Polyurethane Balls

3.5.2 Results of Force-Displacement Tests

Because the objective of this phase of experiment is to determine the horizontal behavior properties of the concrete isolator, results are presented in terms of acceleration-displacement relationships here. The “acceleration” of isolator here means the horizontal force measured from the load cell divided by the isolated mass including both the self-mass of the top bearing plates and the mass of the steel plates on top. The results of the force-displacement tests are shown in Figs. 3.16 to 3.23. Among these figures, Figs. 3.16 to 3.19 are for cases using rubber balls, and Figs. 3.20 to 3.23 are for cases using polyurethane balls.

From these figures, it is observed that the acceleration-displacement relationship for this kind of isolator forms loops. This indicates that the friction between the rolling ball and the concrete working surface is significant. It is noteworthy that the acceleration-displacement loops for 10 cycles of motions are all stable. Comparison of the isolator behavior under different motions reveals that, for a given gravity load, the loops from sinusoidal motions with different frequencies are almost same, indicating that the behavior of the isolator remains stable under different frequencies of motions, except for some fluctuations in the acceleration-displacement loops observed from the cases where 0.8 Hz motions were applied. These fluctuations may be attributed to the specimen setup. As mentioned in Section 3.4.1, a long bracket bar was used to connect the top bearing plates to the load cell. There is no other constraint to limit the top bearing plates in the transverse direction. The top bearing plates swayed a little bit and the bracket bar vibrated freely during the tests. This may explain the observed fluctuations. In addition, it can be noted as shown in Fig. 3.23, that the center line of the loops is significantly off the one in the other cases using polyurethane balls. Based on the empirical model shown in Section 3.2, the center line of the loops corresponds to the elastic bilinear motion of the BNC isolator, which is defined by the geometry of the working surface. Therefore, the unusual observation in this figure was most probably because a miscalibrated load cell was used in that test case. Unfortunately, it was too late to correct this problem when it was found. Also note that, during the tests, the top bearing plates rose by an amount equal to the lateral displacement times the slope of the working surface. This uplift therefore occurred at the end of the bracket bar connecting the actuator to the specimen, which may also have affected the data read from the load cell. Considering all these issues, the results from this series of force-controlled tests may not be totally exact in terms of numerical values, but the above qualitative observations from these test results remain nonetheless valid.

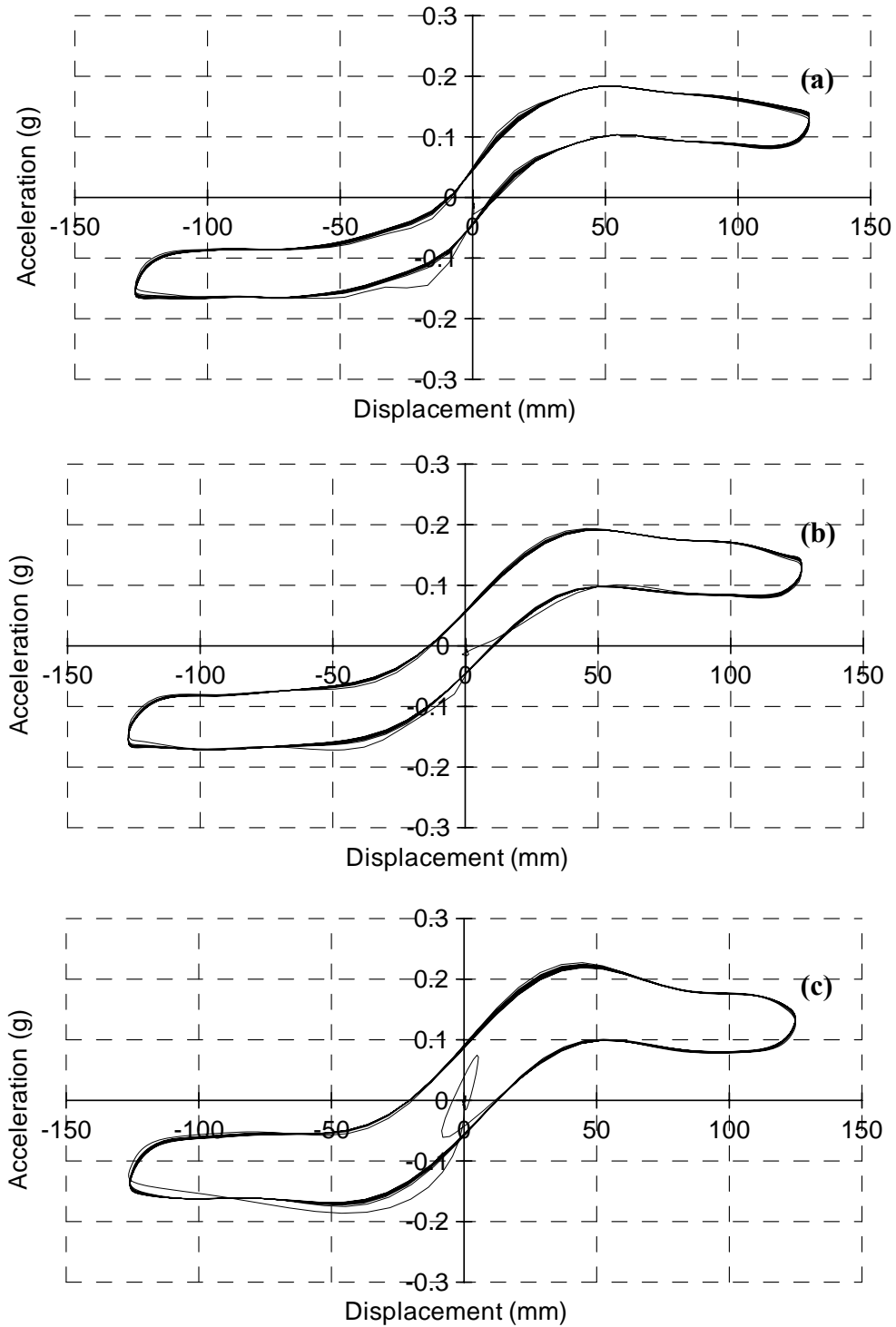
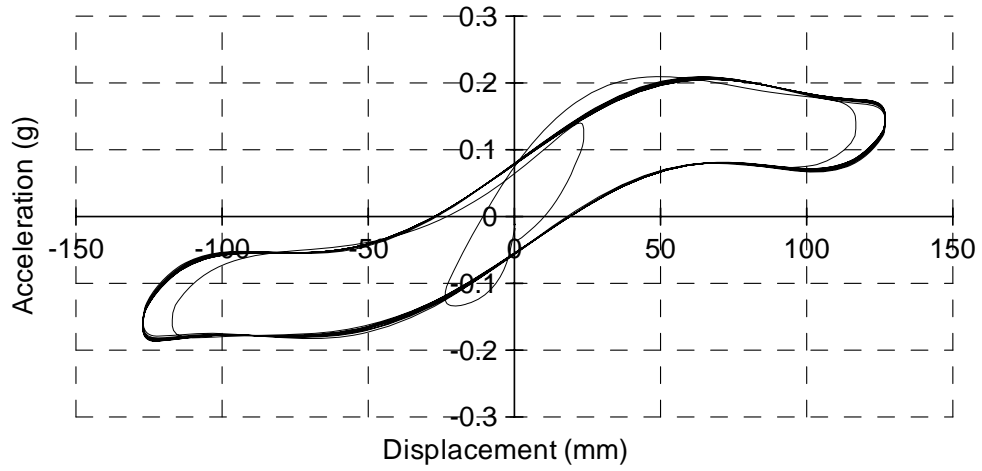


Figure 3.16 Acceleration-displacement Relationship under Load Case 1_Rubber Balls:

(a) 0.05 Hz; (b) 0.2 Hz; (c) 0.8 Hz



**Figure 3.17 Acceleration-displacement Relationship under Load Case 2_Rubber Balls:
0.2 Hz**

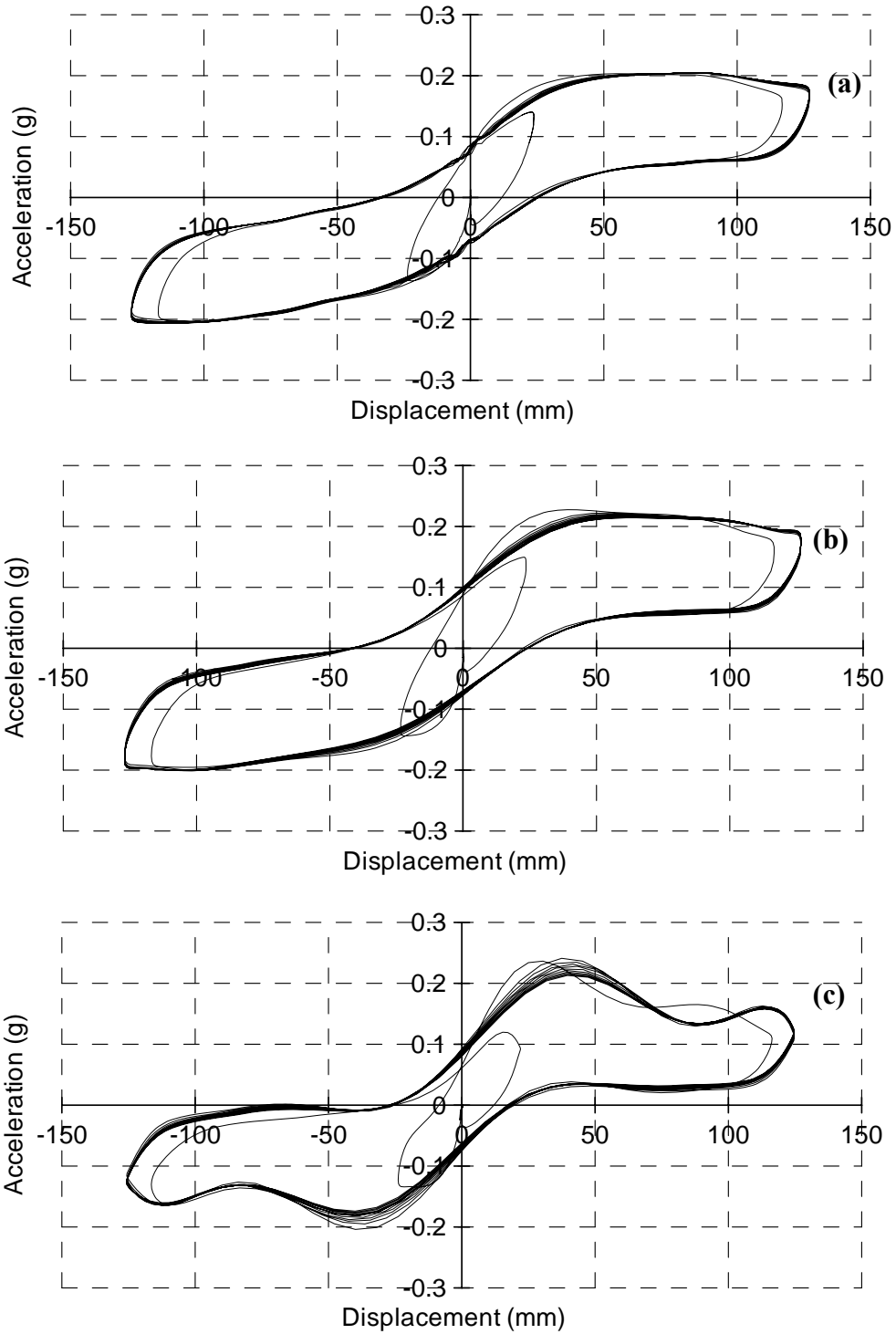
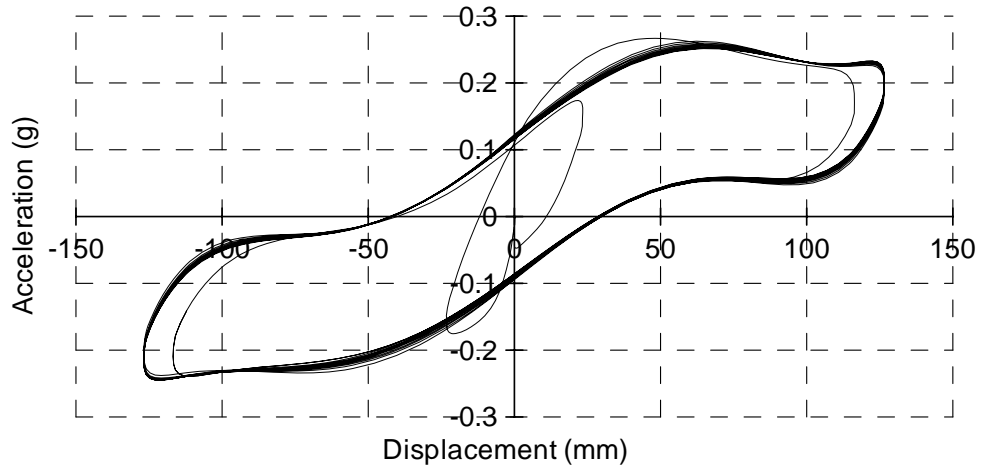


Figure 3.18 Acceleration-displacement Relationship under Load Case 3_Rubber Balls:

(a) 0.05 Hz; (b) 0.2 Hz; (c) 0.8 Hz



**Figure 3.19 Acceleration-displacement Relationship under Load Case 4_Rubber Balls:
0.2 Hz**

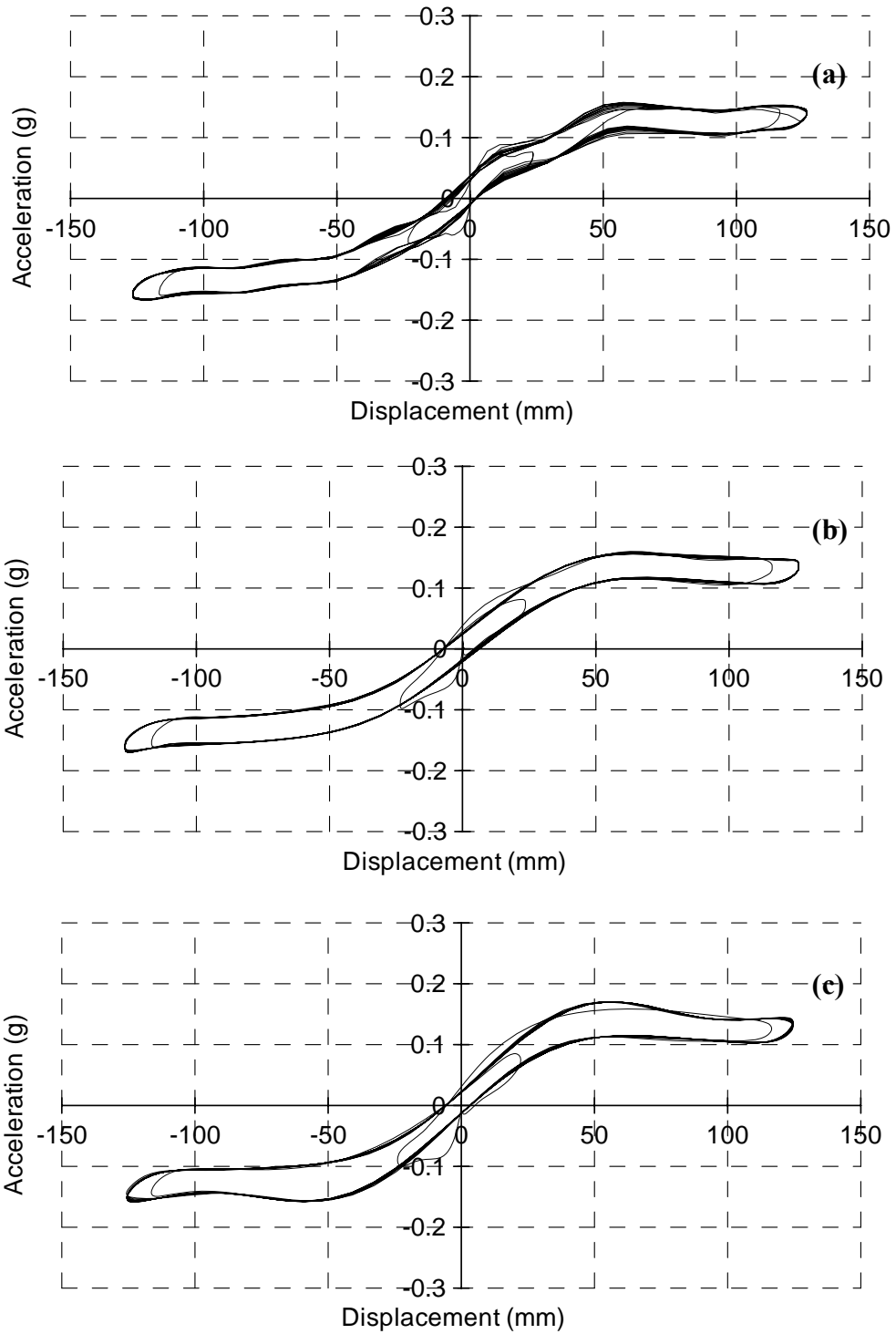
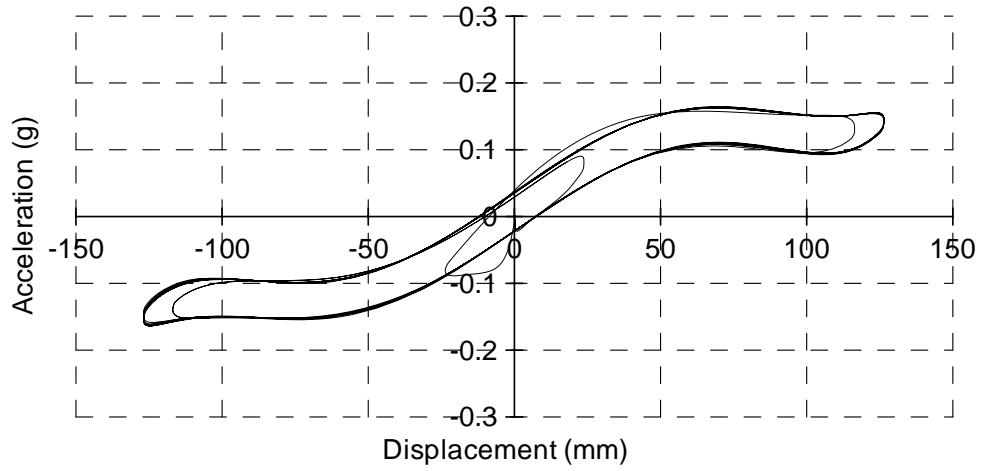


Figure 3.20 Acceleration-displacement Relationship under Load Case 1_Polyurethane Balls:

(a) 0.05 Hz; (b) 0.2 Hz; (c) 0.8 Hz



**Figure 3.21 Acceleration-displacement Relationship under Load Case 2_Polyurethane Balls:
0.2 Hz**

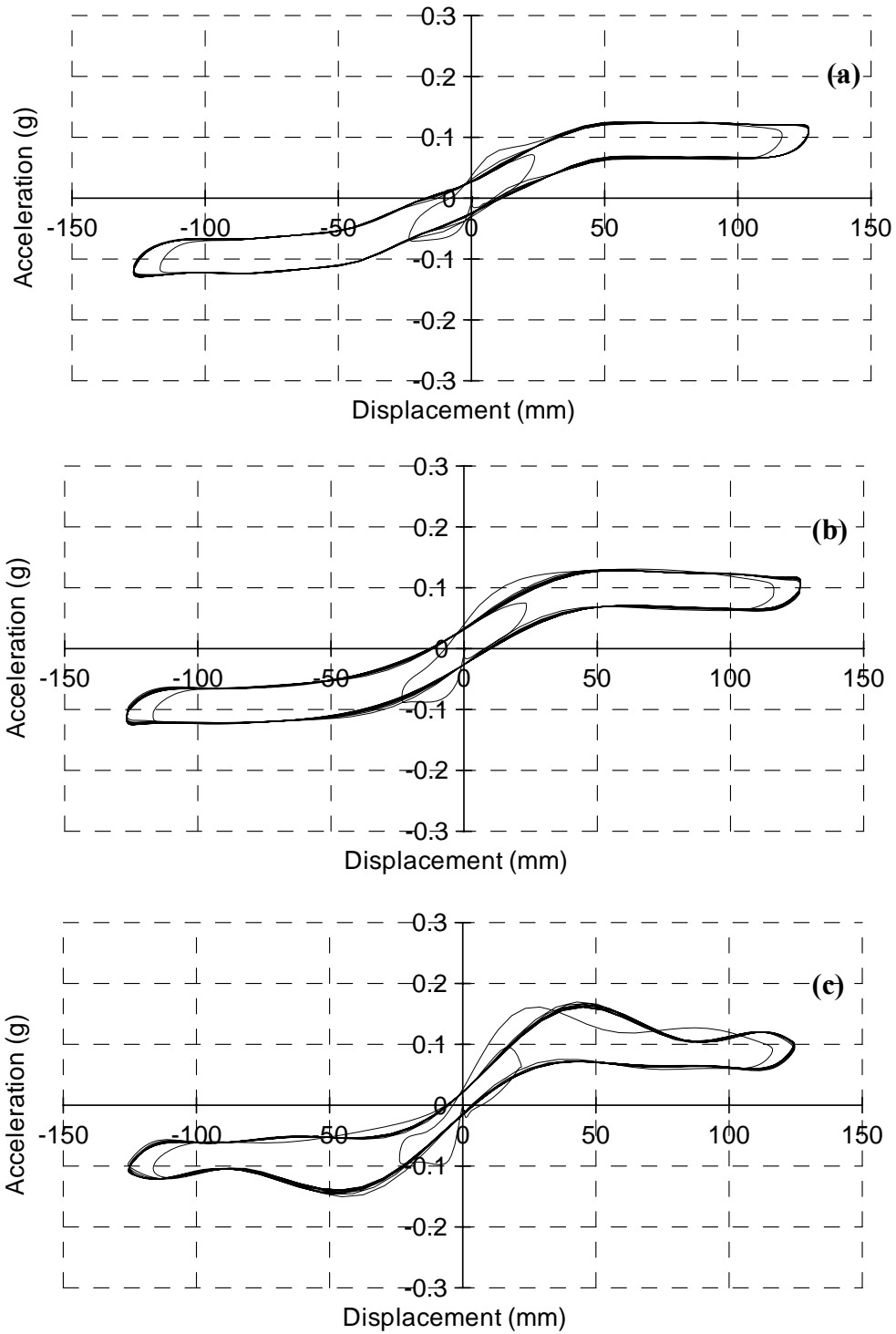
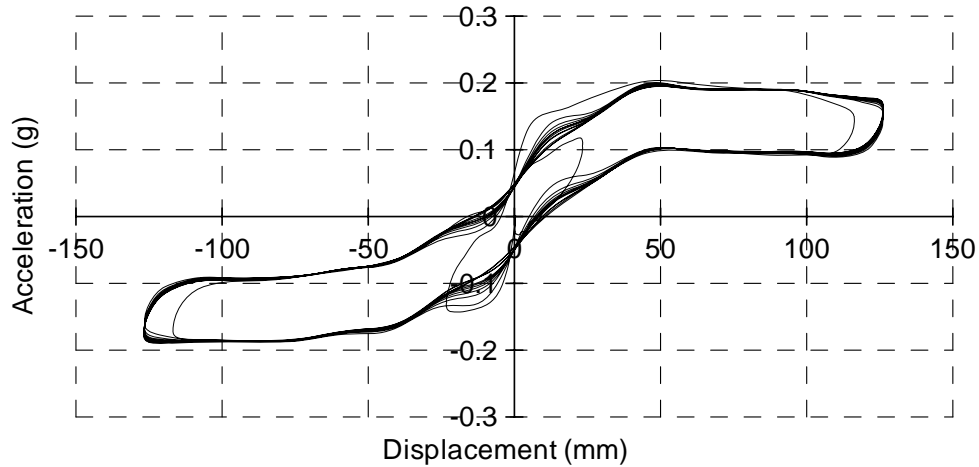


Figure 3.22 Acceleration-displacement Relationship under Load Case 3_Polyurethane Balls:

(a) 0.05 Hz; (b) 0.2 Hz; (c) 0.8 Hz



**Figure 3.23 Acceleration-displacement Relationship under Load Case 4_Polyurethane Balls:
0.2 Hz**

3.5.3 Results of Sweep Frequency Tests

The objective of the sweep frequency tests is to find out the natural vibration period of this special kind of concrete BNC isolator. However, it has been observed in Section 3.5.1 that there is no constant vibration period for this kind of isolator. Although the original purpose of the sweep frequency tests cannot be achieved, these tests can be used to further investigate the behavior of this kind of isolator because the displacement of the isolator in these test are relatively large. The test results are shown in Figs. 3.24 to 3.27. Note that there are two parts in each of these figures, corresponding to the cases using rubber and polyurethane balls, respectively.

Consistent with observations in Section 3.5.2, the effect of friction is also seen in the acceleration-displacement loops here, as shown in Figs. 3.24 to 3.27. Also, the fact that the loops obtained from tests using rubber balls are more voluminous than those corresponding to the tests using polyurethane balls indicates that the friction provided by the rubber balls is greater than that from the polyurethane balls. Here, an equivalent coefficient of friction, μ_e , is defined as the

ratio of half of the ordinate difference at a given displacement on the acceleration-displacement loop to the acceleration of gravity, g . From Figs. 3.24 to 3.27, the equivalent coefficients of friction are estimated and listed in Table 3.6. This friction effect will be further studied in subsequent chapters for the complete isolated floor tests.

Note that the horizontal force-displacement of this isolator may be obtained by multiplying the ordinates of the acceleration-displacement loop by the total isolated mass. Therefore, hysteretic loops are proportional to the acceleration-displacement curves, which means that more energy is dissipated by the rubber balls compared to the polyurethane balls. In addition, it can be found that the peak acceleration response is almost a constant value, as expected by the empirical model in Section 3.2. Finally, the center line of the plateau part of these loops, which is defined by the slope of the conical part of the isolator, is slightly higher than the target $0.1g$. It is about $0.12g$. This is because the slope of the actual working surface is about 1 degree higher than the target as mentioned in Section 3.3.

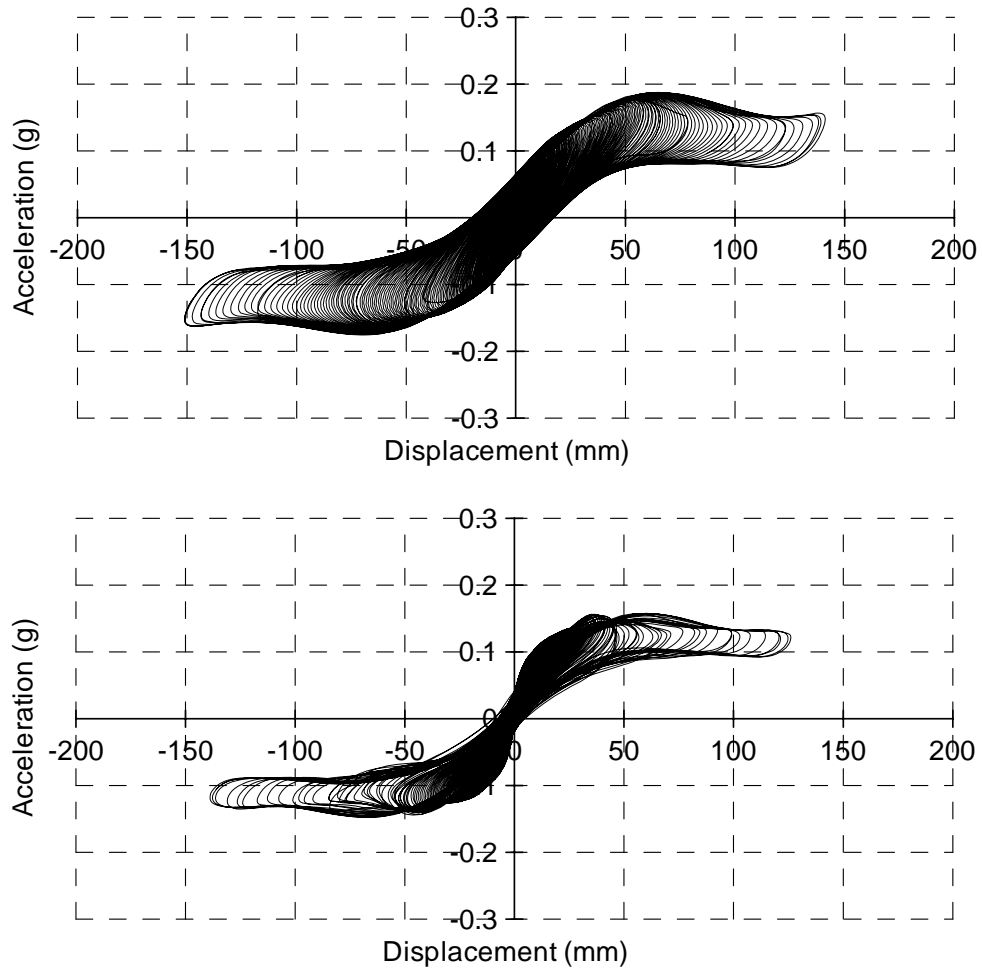


Figure 3.24 Acceleration-displacement Relationship under Load Case 1_Sweep Frequency

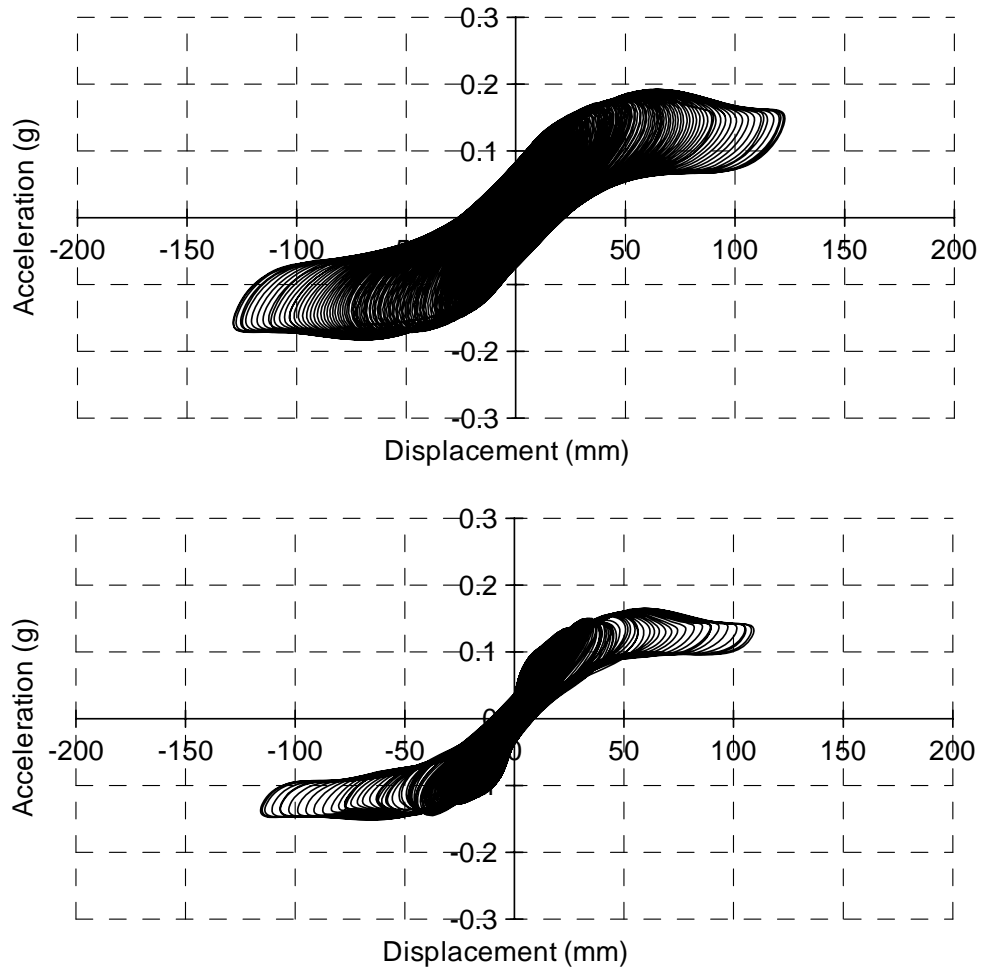


Figure 3.25 Acceleration-displacement Relationship under Load Case 2_Sweep Frequency

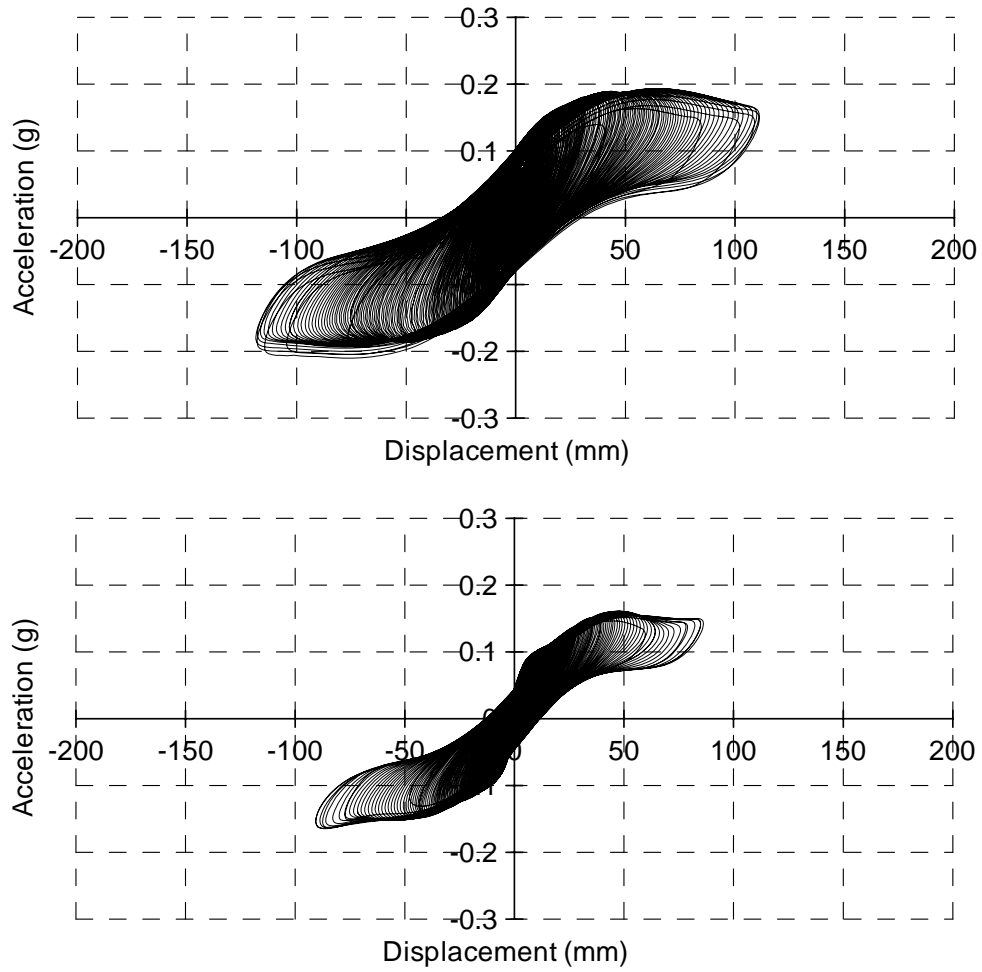


Figure 3.26 Acceleration-displacement Relationship under Load Case 3_Sweep Frequency

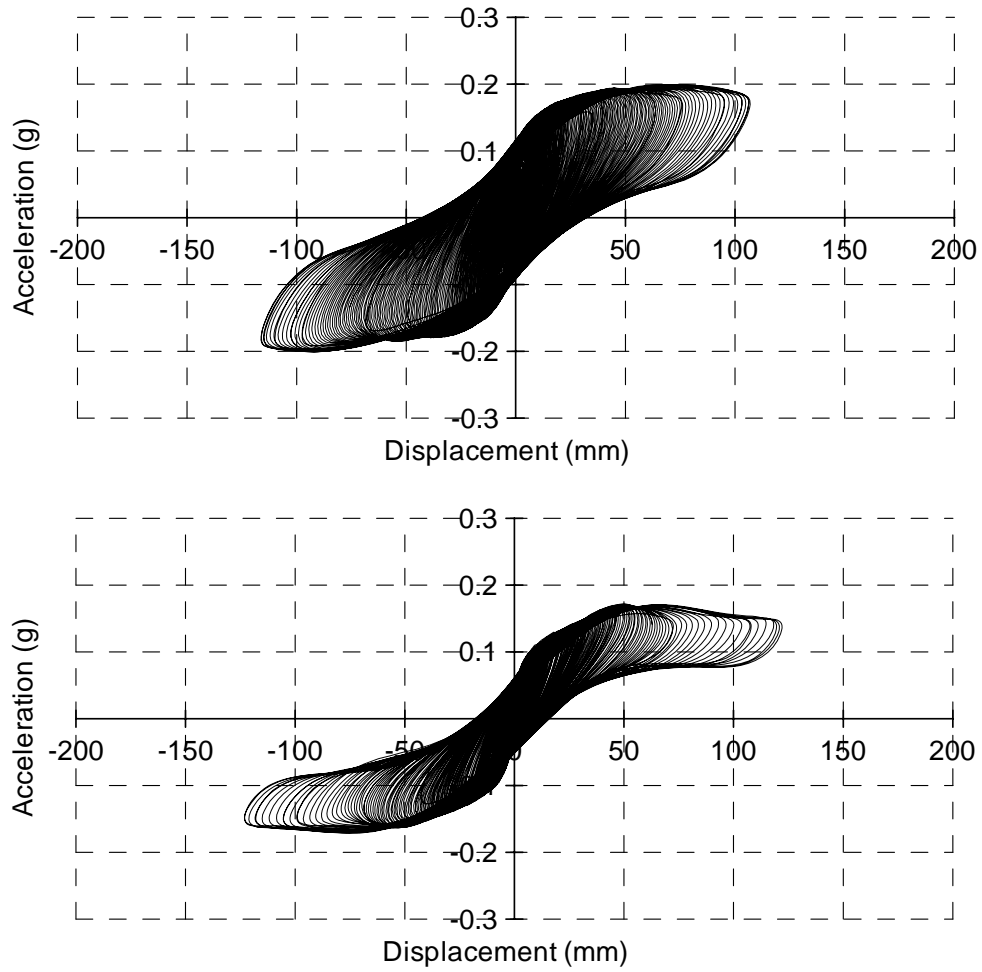


Figure 3.27 Acceleration-displacement Relationship under Load Case 4_Sweep Frequency

Table 3.6 Equivalent Friction Coefficient

Ball Type (1)	Load (N) (2)	μ_e (3)
Rubber	689	0.06
Rubber	2393	0.08
Rubber	4875	0.1
Rubber	6512	0.112
Polyurethane	689	0.022
Polyurethane	2393	0.032
Polyurethane	4875	0.044
Polyurethane	6512	0.05

During the tests, the two top bearing plates exhibited some torsional response. To study this effect, the sweep frequency tests under Load Case 2 are selected as examples here. The displacement difference of the two side corners with string pots D4 and D6 with respect to time are shown in Fig. 3.28. It can be noted that the maximum value of the displacement difference of the two extreme side corners is about 13 mm (0.5 in) for the rubber ball case, and 38 mm (1.5 in) for the polyurethane ball case. The torsion angle is the ratio of the maximum value of the displacement difference between D4 and D6, 38 mm, to the distance of the two string pots, 1168 mm (46 in), which is about 2 degrees. This slight amount of torsion was therefore deemed to be insignificant here. Torsional response will be further studied when considering complete isolated floor system tests as shown in subsequent chapters.

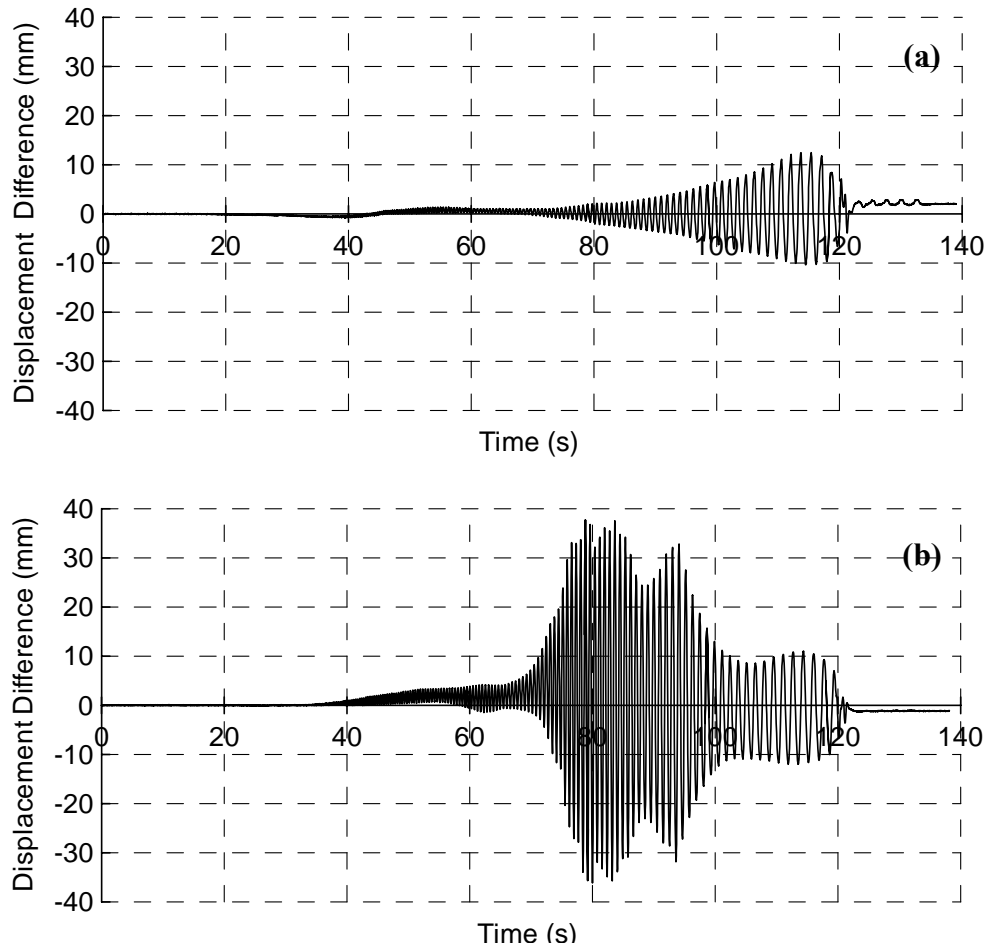


Figure 3.28 Torsion Effect of Concrete Isolator under Load Case 2: (a) Rubber Ball; (b) Polyurethane Ball

3.5.4 Results of Dynamic Tests Using Earthquake Inputs

As in Sections 3.5.2 and 3.5.3, the results of the dynamic tests using earthquake inputs are also shown in terms of acceleration-displacement loops. These are presented in Figs. 3.29 to 3.34. From these figures, the observations from the test results made in Sections 3.5.2 and 3.5.3 are also found here. Furthermore, the values of the equivalent coefficient of friction estimated from these tests are almost same with the corresponding ones found in Section 3.5.3. In addition, as expected, a plateau of peak acceleration response is also observed for each test case here.

As in Section 3.5.3, torsional response was also investigated here. As an example, the displacement difference between D4 and D6 in the cases subjected to Acc2 is shown in Figs. 3.35 and 3.36. It can be noted that the maximum value is about 15 mm (0.6 in), which corresponds to a torsional angle of about 1 degree. Again, it is not significant.

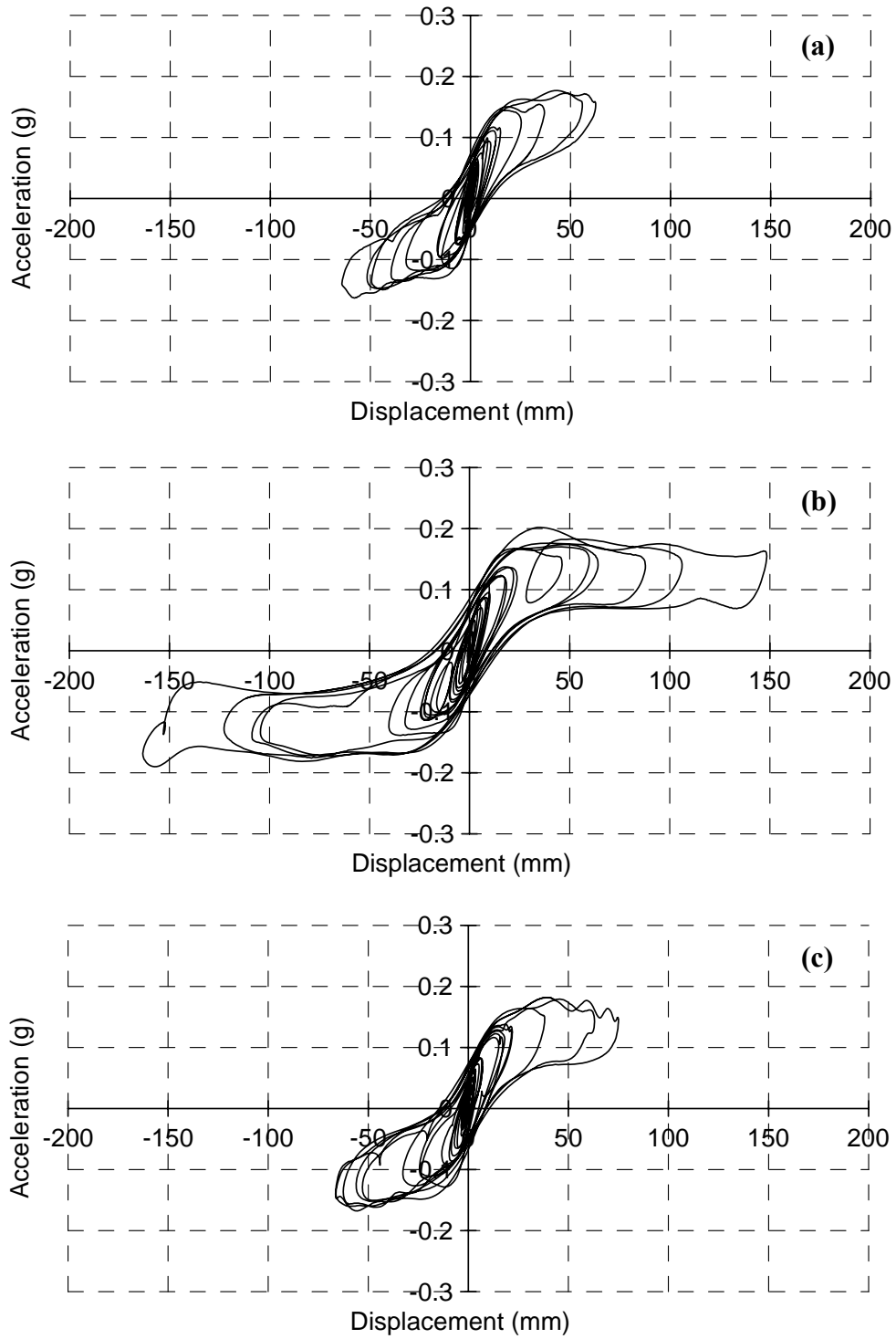


Figure 3.29 Acceleration-Displacement Relationship of Concrete Isolator (Rubber Balls, Load Case 1): (a) Subject to Acc1; (b) Subject to Acc2; (c) Subject to Acc3

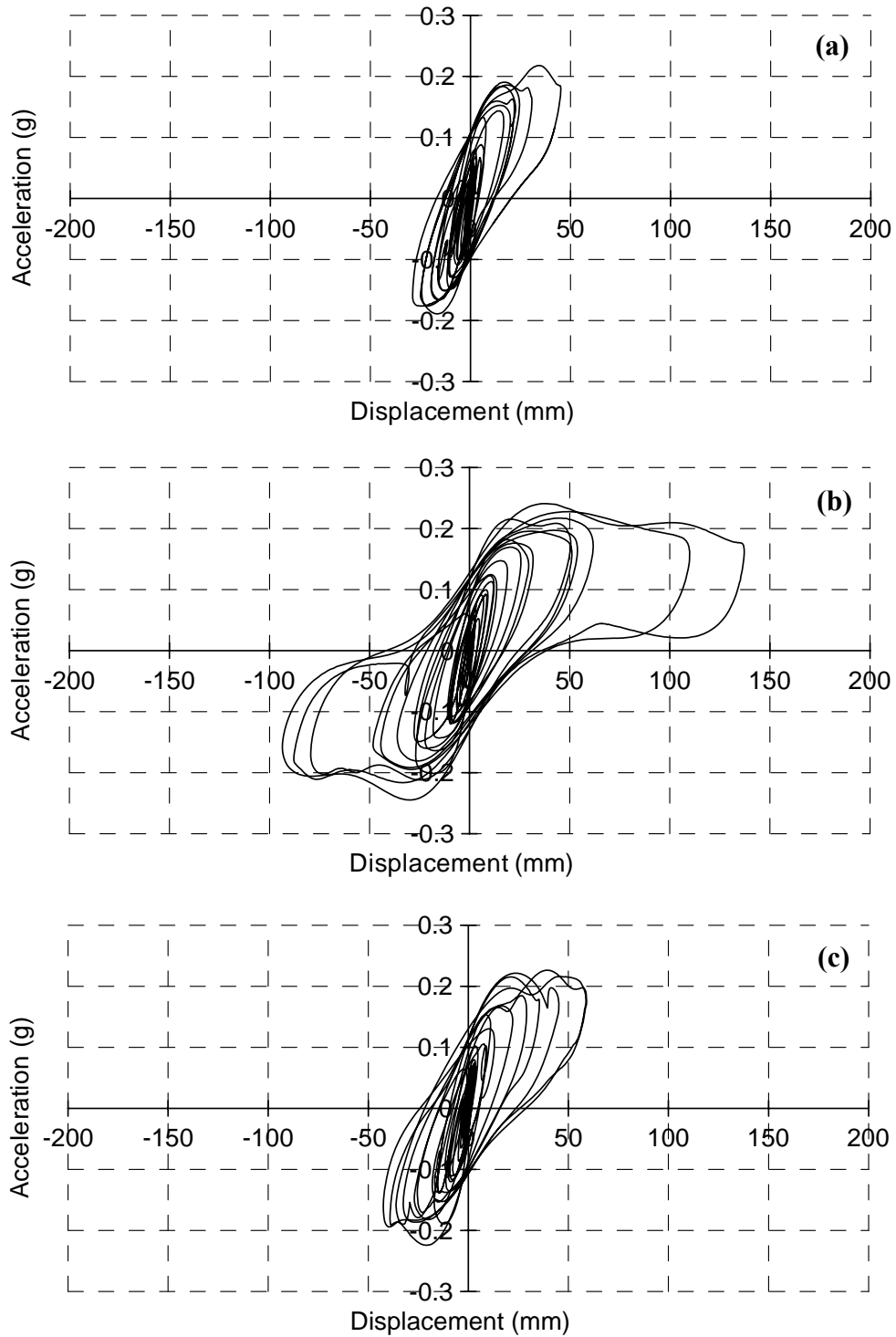


Figure 3.30 Acceleration-Displacement Relationship of Concrete Isolator (Rubber Balls, Load Case 3): (a) Subject to Acc1; (b) Subject to Acc2; (c) Subject to Acc3

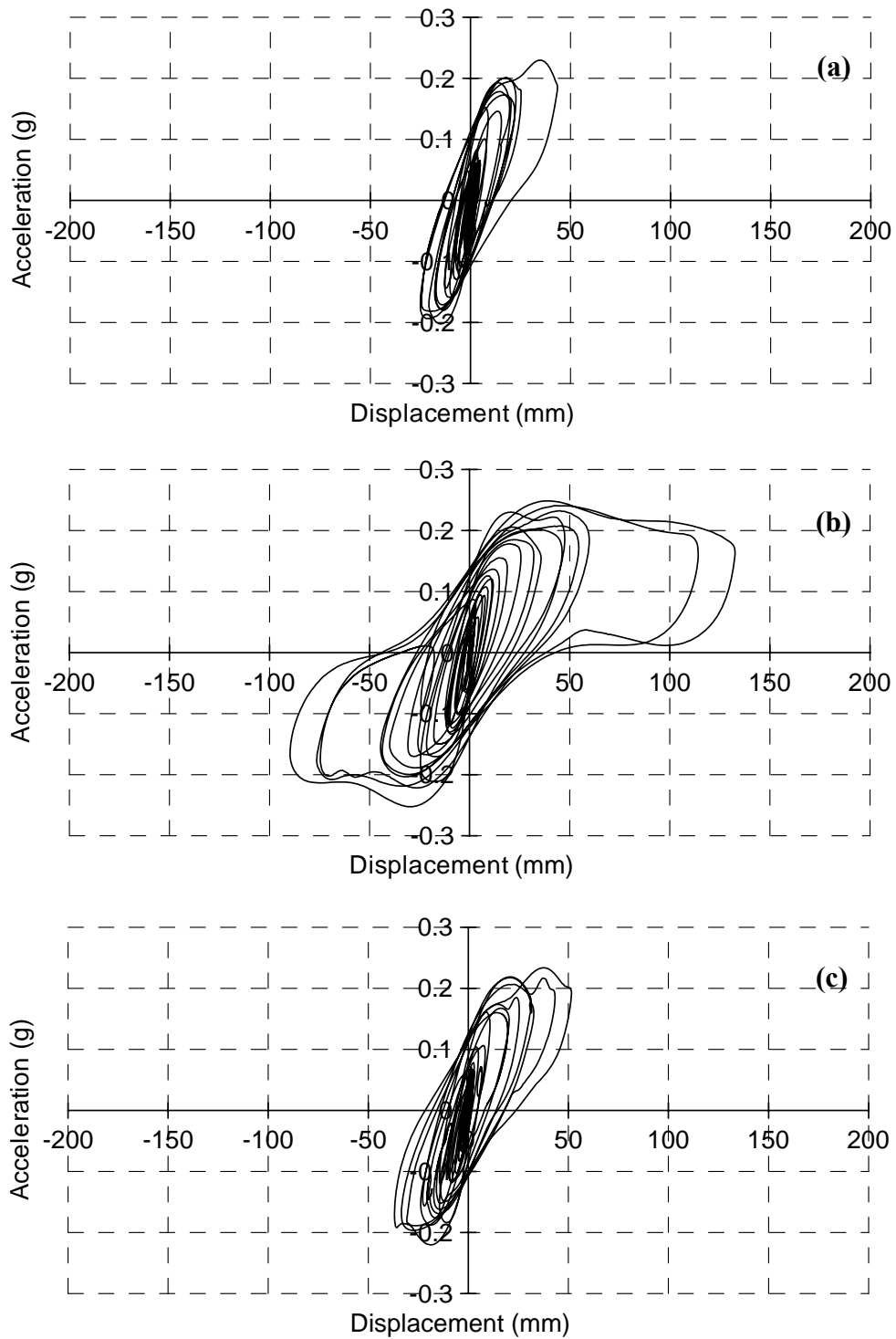


Figure 3.31 Acceleration-displacement Relationship of Concrete Isolator (Rubber Balls, Load Case 4): (a) Subject to Acc1; (b) Subject to Acc2; (c) Subject to Acc3

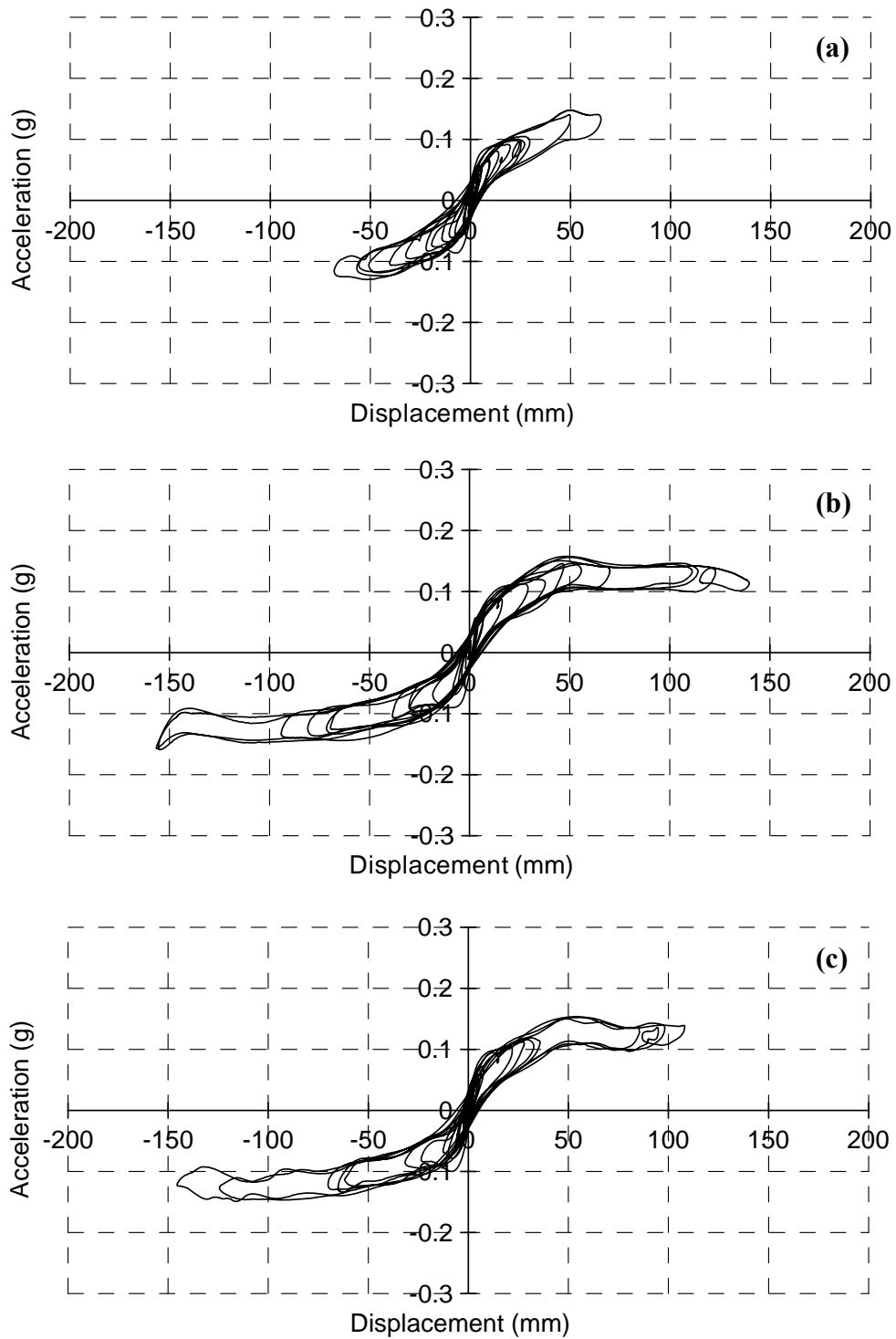


Figure 3.32 Acceleration-Displacement Relationship of Concrete Isolator (Polyurethane Balls, Load Case 1): (a) Subject to Acc1; (b) Subject to Acc2; (c) Subject to Acc3

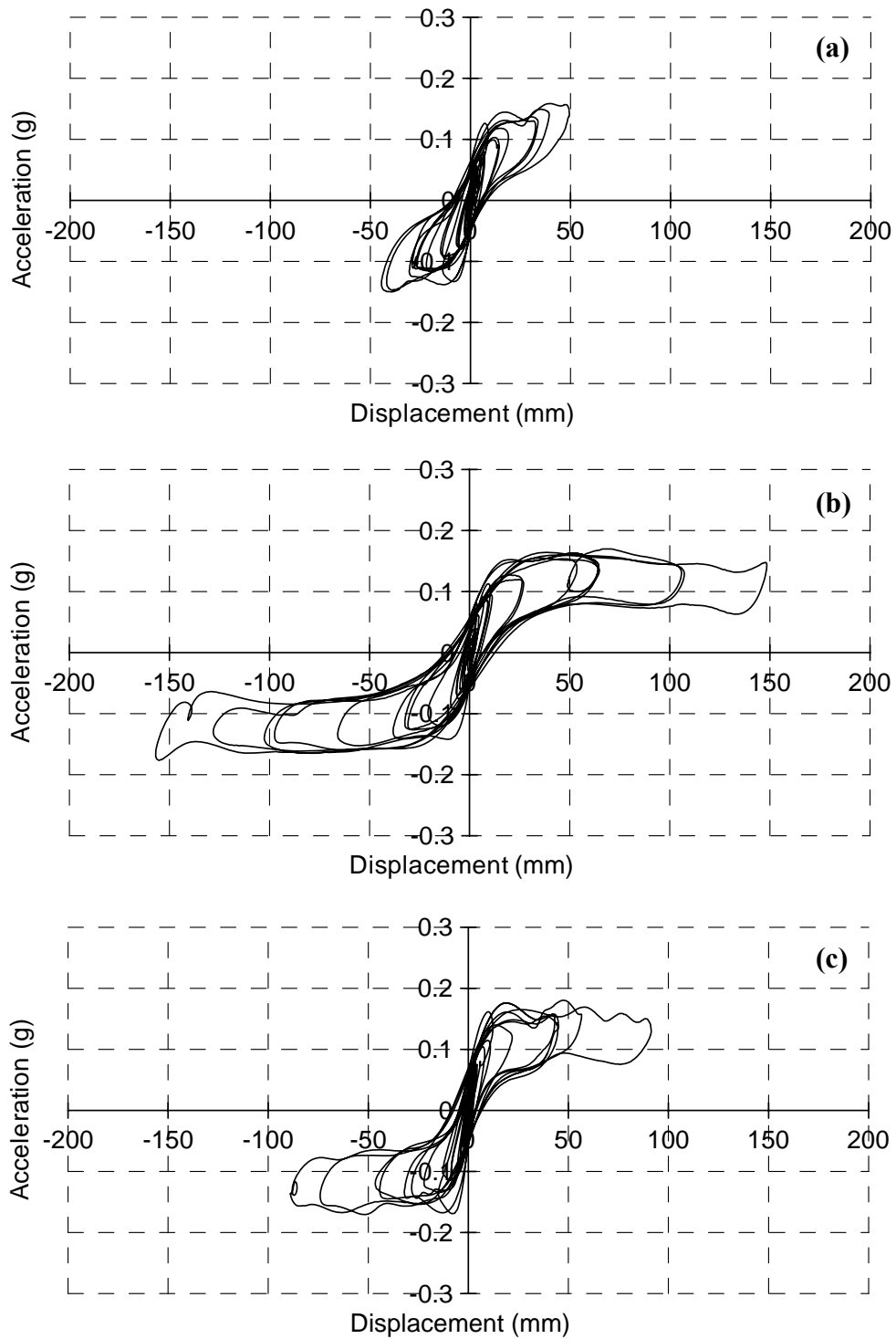


Figure 3.33 Acceleration-Displacement Relationship of Concrete Isolator (Polyurethane Balls, Load Case 3): (a) Subject to Acc1; (b) Subject to Acc2; (c) Subject to Acc3

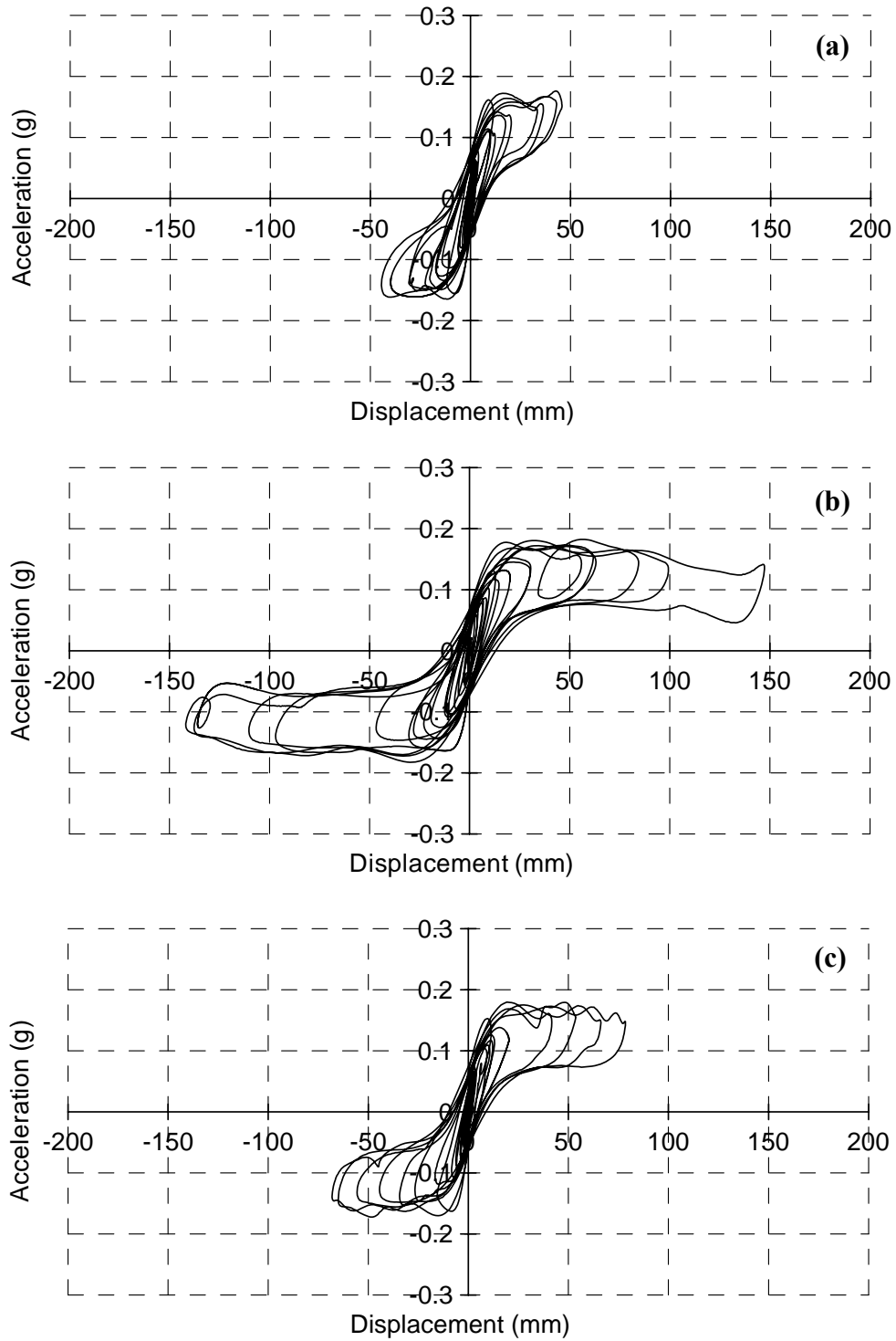


Figure 3.34 Acceleration-Displacement Relationship of Concrete Isolator (Polyurethane Balls, Load Case 4): (a) Subject to Acc1; (b) Subject to Acc2; (c) Subject to Acc3

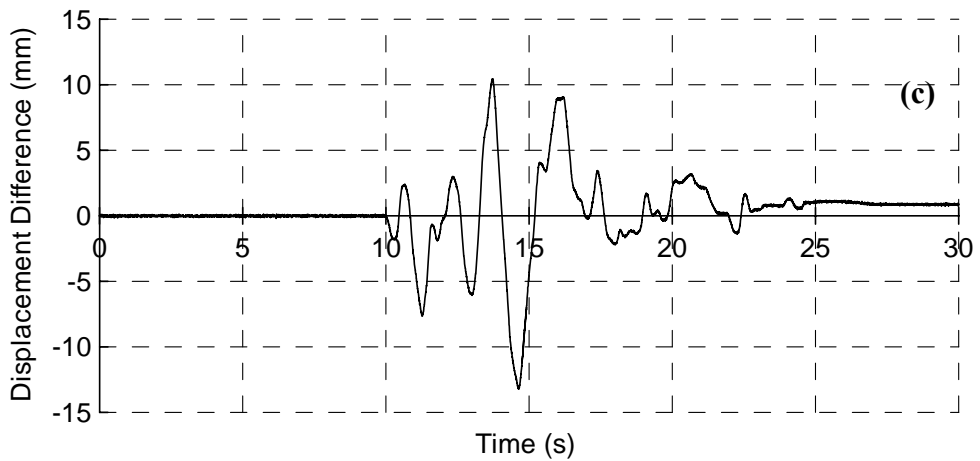
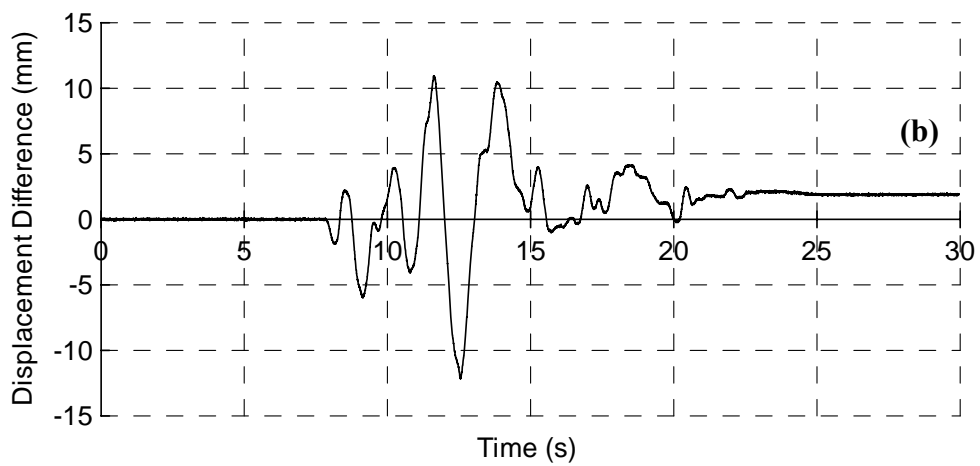
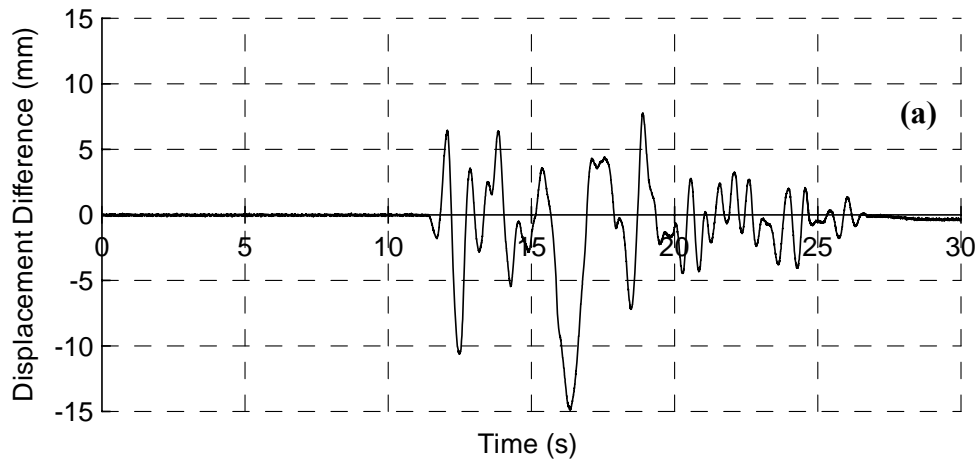
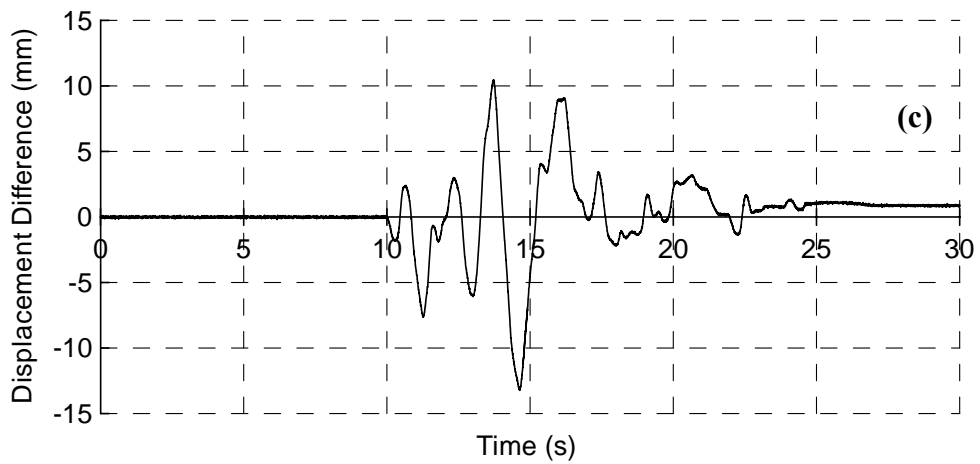
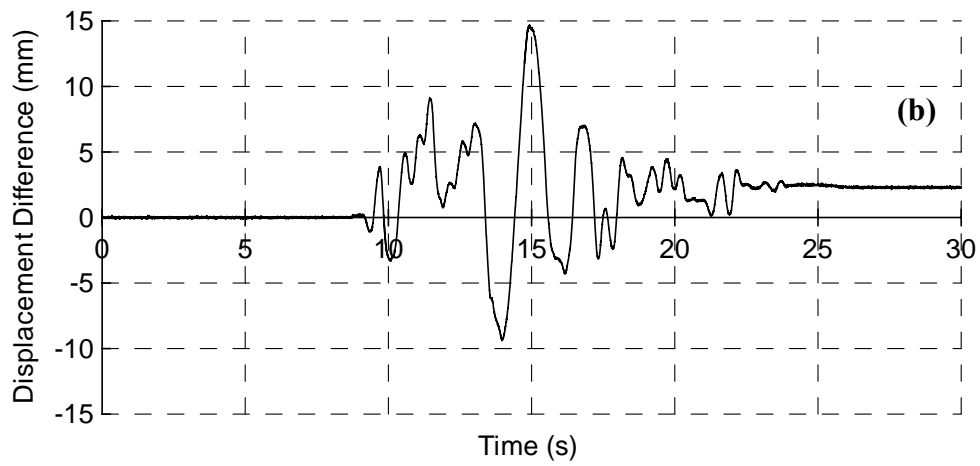
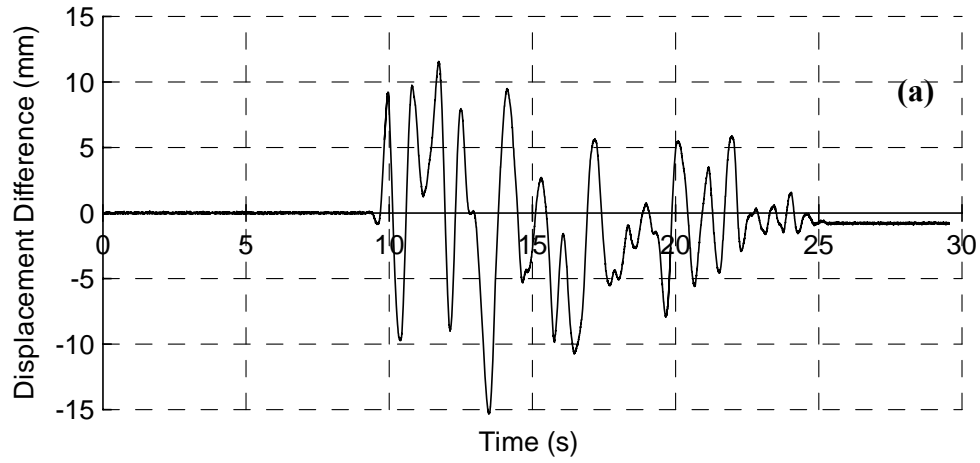


Figure 3.35 Torsion Effect of Concrete Isolator (Rubber Balls, Acc2): (a) Load Case 1; (b) Load Case 3; (c) Load Case 4



**Figure 3.36 Torsion Effect of Concrete Isolator (Polyurethane Balls, Acc2): (a) Load Case 1;
(b) Load Case 3; (c) Load Case 4**

3.6 Observations

In this chapter, an empirical model was first developed for a special kind of BNC Isolator where the rolling friction between the rolling ball and the concrete working surface is significant. Characterization tests conducted to determine the mechanical properties of this special kind of concrete ball-in-cone (BNC) isolator were then presented. The concrete isolator used rubber balls and polyurethane balls between two concrete bearing plates with concave rolling surfaces. For each kind of ball, four series of tests were conducted under different gravity loads: free vibration tests, force-displacement tests, sweep frequency tests, and dynamic tests using earthquake inputs. Note that both response spectra compatible acceleration time histories and floor acceleration responses recorded from the nonlinear response history analysis of typical structural fuse frames were used as seismic inputs for the dynamic tests using earthquake inputs.

The test results show that this special kind of concrete BNC isolator does not have a constant vibration period. So the viscous damping cannot be directly obtained based on the relationship between the viscous damping and the decay in the free vibration amplitude. The test results also show that the behavior of this special kind of concrete BNC isolator is stable under different motions. The friction between the balls and the concrete working surface is found to be significant from the acceleration-displacement loops. Friction is found to be greater in the case using rubber balls than that in the corresponding case using polyurethane balls. It is also found that this friction will be larger with increases in the supported isolated loads. In addition, based on the equations that capture the behavior of this kind of isolator shown at the beginning of this chapter, a plateau of peak acceleration response was observed in the test results.

An equivalent coefficient of friction, μ_e , was also defined in this chapter to catch the friction effect between the rolling ball and the concrete working surface. This factor also provides a basis for building the model of such isolators in computer programs, which is the topic of a subsequent

chapter. The values of μ_e were estimated based on the experimentally obtained acceleration-displacement relationships for all the gravity load cases considered in this chapter.

The friction effect between the rolling balls and the concrete working surface will be discussed more extensively when presenting the test results for the complete isolated floor system, which is the topic of subsequent chapters.

CHAPTER 4

MULTI-DIRECTIONAL SPRING UNIT CHARACTERIZATION TEST AND PHYSICAL MODEL

4.1 Introduction

Chapter 3 described the characterization tests and phenomenological model of a special kind of concrete ball-in-cone (BNC) isolator. This chapter will present the details of the characterization tests and physical model of a special kind of spring unit used to control the response of an isolated floor system manufactured by Dynamic Isolation Systems (DIS), which is referred here as multi-directional spring unit.

To investigate the force-displacement behavior of the multi-directional spring units and to better understand the mechanical properties that define how these spring units work, three series of tests were conducted, from spring components alone to the complete spring unit in its implemented configuration. Two spring units were tested to investigate the repeatability of results. In addition, because the spring units can be built with internal springs with different nominal stiffnesses, tests were conducted sequentially with springs with two different nominal stiffnesses. Both sinusoidal signals (with different amplitudes and frequencies) and seismic floor displacement records (obtained from the tests of isolated floor system presented in Chapter 5) were adopted as inputs to conduct these characterization tests. Furthermore, both without and with pretension initial cases are considered. This chapter presents all the details of these tests, including specimen setup, instrumentation, input program, test protocol, and the test results. The

results from tests subjected to different inputs are also compared to observe whether the behavior of the spring units is stable. Finally, a physical model for this kind of multi-directional spring units is developed. The results obtained from this model are compared with those from the characterization tests. A study is also conducted to investigate the sensitivity of its four primary parameters of the model in capturing the behavior of the spring unit.

4.2 Multi-directional Spring Unit Description

The multi-directional spring units were adopted as isolators to work in an isolated floor system manufactured by DIS, which was tested in the Structural Engineering and Earthquake Simulation Laboratory (SEESL) of University at Buffalo. The complete details of this isolated floor system will be presented in Chapter 5. For the time being, an overview of the multi-directional spring unit and a conceptual sketch of its application in isolated floor system are shown in Figs. 4.1 and 4.2, respectively. From these figures, note that a steel cable connecting the internal spring comes out of the spring unit tube through a bushing. Then, the cable is fixed onto the above isolated floor through another similar bushing welded to the underside of the isolated floor. The steel cable will slide along the bushing in the spring unit during motion of the isolated floor and control the response of the top isolated platform. The surfaces of the two bushings mentioned above are of same shape. It is a revolution surface similar to a “hyperboloid of one sheet” with an exception that it is a half circle that is revolved around a central axis. By analogy, looking at it from above, the shape of the bushing surface looks like the inside surface of the flare of a “trumpet”. In addition, the bushing in the spring unit is made of brass, and the one on the isolated floor is in steel.



Figure 4.1 Multi-directional Spring Unit

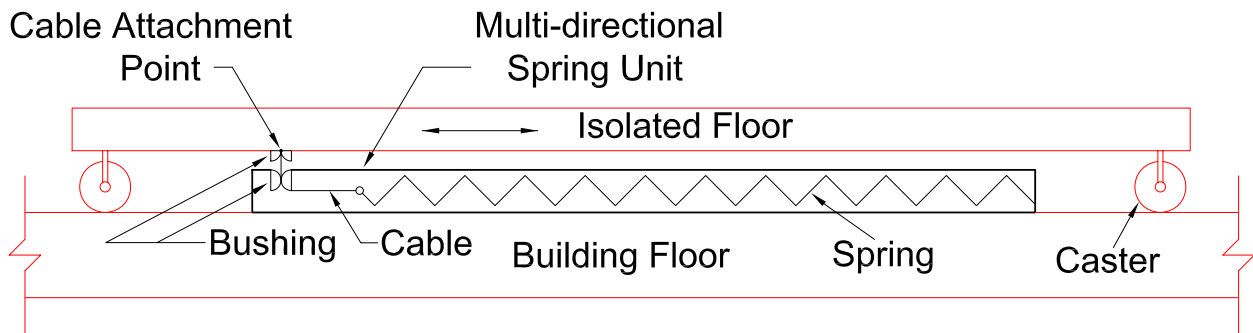


Figure 4.2 Multi-directional Spring Unit in Isolated Floor System

4.3 Test Setup

4.3.1 Specimen Setup and Instrumentation

Hysteretic force-displacement behavior of the spring units is needed to simulate the seismic behavior of these units in computer program. However, to be able to construct this behavior using physical models, the force-displacement relationship of the spring unit as a complete component, as well as that of its individual spring, is required. Therefore, three test series were originally scheduled to accomplish this purpose:

- In Test Series 1, axial tests of individual springs left within the tube, without threading the cable through the bushing of the spring unit, to investigate the behavior of the spring alone;
- In Test Series 2, axial tests of individual springs taken out of the tube to capture the behavior of the spring alone and compare results with those from Test Series 1, in an

attempt to quantify friction between the spring and the tube;

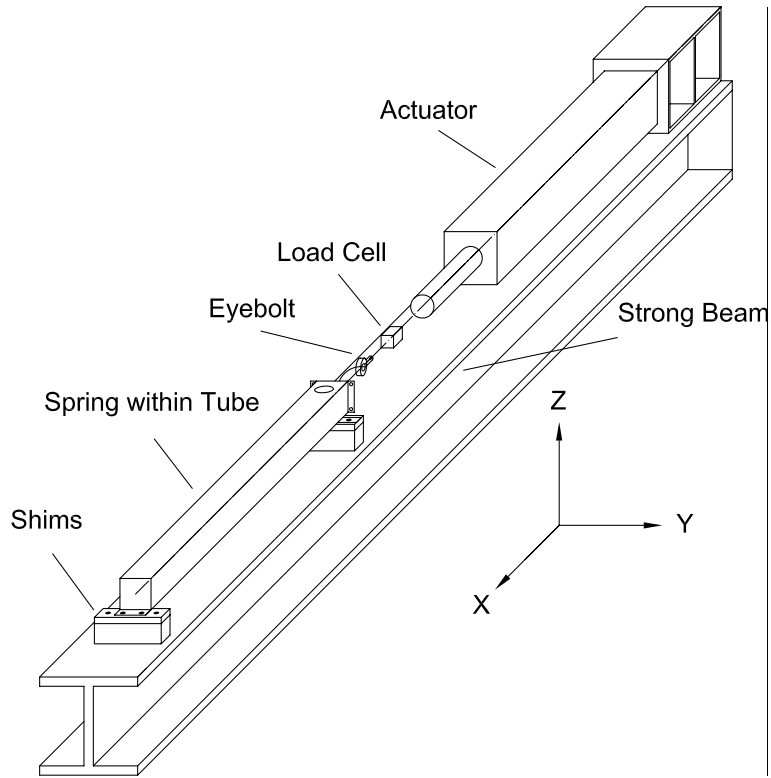
- In Test Series 3, tests of complete spring unit with tube and bushings on. The configuration of the spring unit in these tests was same as the working conditions of the spring units in the tests of the isolated floor introduced in Chapter 5.

During Test Series 1, note that a low rumbling sound, attributed to the friction between the spring and the tube, could always be heard. Furthermore, during the first tests of Test Series 2, it was observed that the spring was sagging downward due to its self-weight, which indicated that the spring was likely always in contact with the tube during its motion when working within its tube. Thus, to better observe the behavior of the internal spring, the setup for Test Series 2 was modified by introducing a steel channel at the same height level corresponding to the bottom surface of the tube in Test Series 1. Under this new setup, the spring could be openly seen, unlike the Test Series 1 tests where the spring was hidden by the tube.

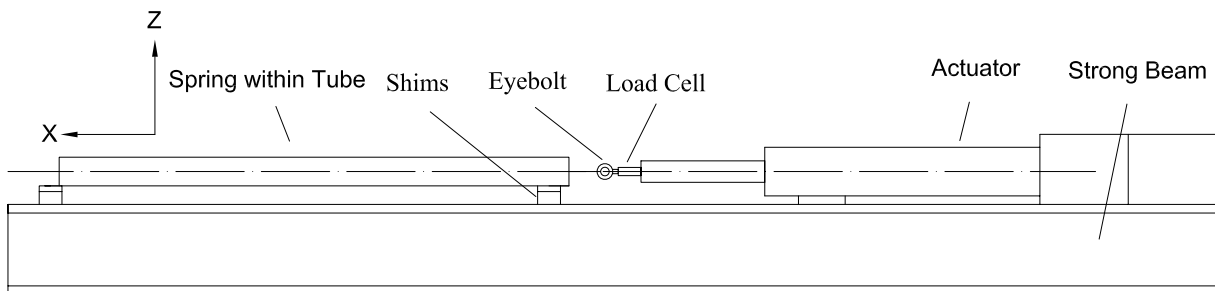
The specimen assembly and setup for each test series (after the modification of Test Series 2) are shown in Figs. 4.3 to 4.5, respectively. As mentioned before, Test Series 1 and 2 were intended to investigate the force-displacement behavior of the spring alone. Hence, the layout of the specimen in these two test series was that the spring, the load cell which was connected to the shaft of the actuator and used to record axial load of the spring, and the shaft of the actuator were aligned on the same axis, as shown in Figs. 4.3 and 4.4. Also, note that the load cell was connected to the specimen cable using an eyebolt, the central line of which also agreed with the common central line of the other parts of the specimen. For Test Series 3, to simulate the working conditions of the spring units as they are installed in the complete isolated floor system (that is itself tested in Chapter 5), an anchor end was manufactured to hold the spring cable in a way that would replicate the conditions of the floor underside attachment point. A photo of the anchor end used in Test Series 3 is shown in Fig. 4.6. A bushing was welded to the bottom plate of the anchor to duplicate the bushing on the isolated floor shown in Fig. 4.2. In the specimen

assembly and setup for this series of tests, the spring unit, the anchor, the load cell used to measure the horizontal load of the spring unit, and the shaft of the actuator were connected in series together. However, the central lines of the load cell and the actuator shaft were different from that of the spring unit which was at a lower level to simulate the working condition of the spring unit in isolated floor system, as shown in Fig. 4.5. Also note, from Fig. 4.5, that the load cell inserted between the actuator and the anchor end manufactured to hold the spring cable, was connected using threaded rods. The spring cable passed through the hole of the bushing of the anchor end and was fixed with small clamps above, as shown in Fig. 4.6. The setup of this series of tests was designed to leave a clear gap of about 20 mm (0.783 in) between the anchor end bushing bottom surface and the top surface of the multi-directional spring unit, to replicate the actual conditions of the spring units in the tested isolated floor system (described in Chapter 5).

As mentioned above, a load cell was used to record the load (i.e. axial load of spring in Test Series 1 and 2 and horizontal load of the complete spring unit in Test Series 3) at the actuator end closest to the cable attachment point. The displacement of the actuator shaft was directly obtained from the recorded actuator motion. Therefore, only two instrumentation channels in total were used for these characterization tests: one for the load cell to measure force, and the other for the actuator to measure the horizontal displacement.

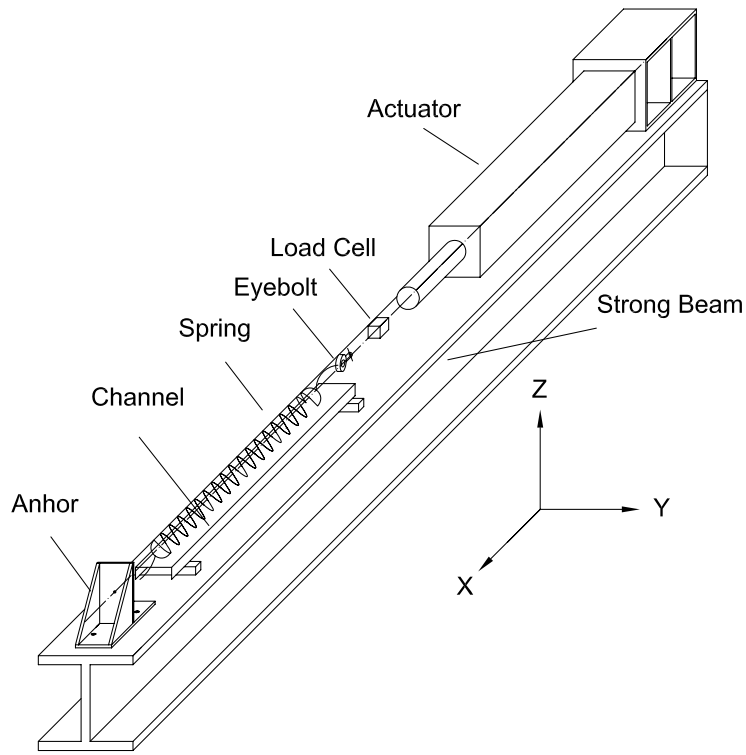


(a)

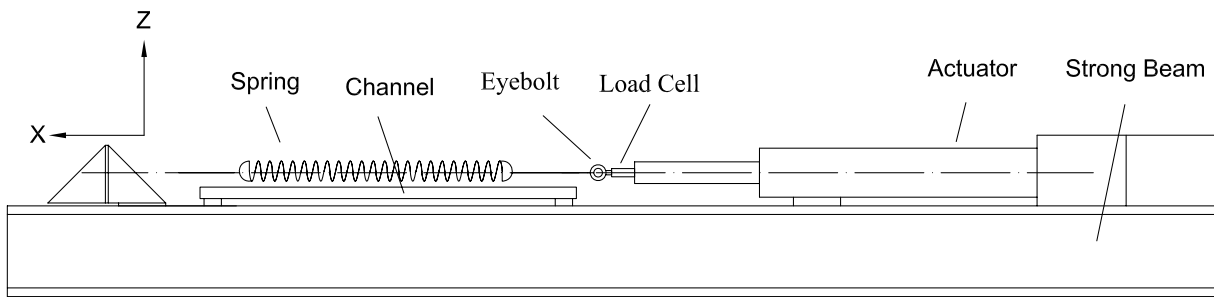


(b)

Figure 4.3 Specimen Configuration of Test Series 1: (a) 3-D View and; (b) Side View of the Specimen Setup



(a)



(b)

Figure 4.4 Specimen Configuration of Test Series 2: (a) 3-D View and; (b) Side View of the Specimen Assembly and Setup

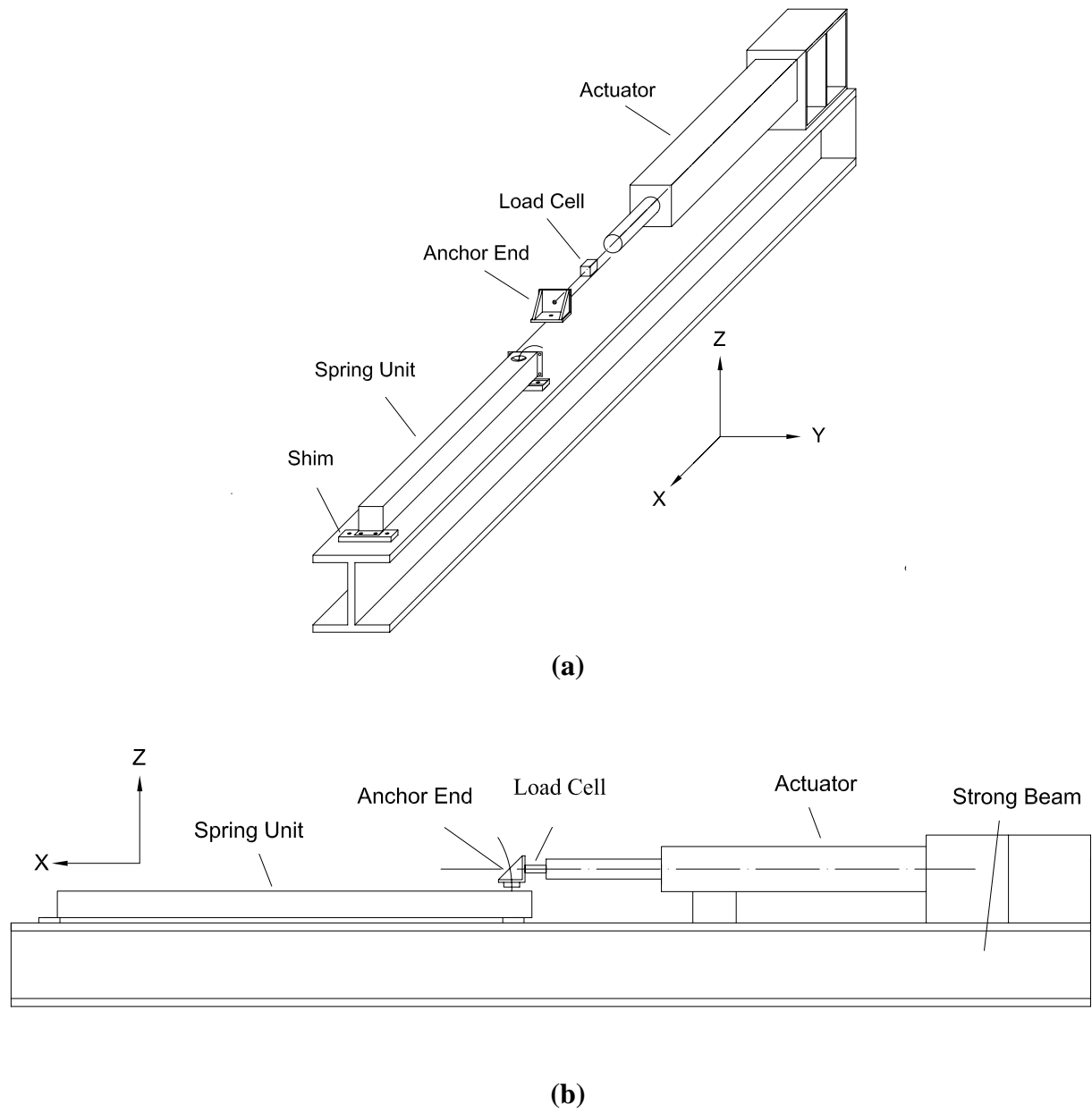


Figure 4.5 Specimen Configuration of Test Series 3: (a) 3-D View and; (b) Side View of the Specimen Assembly and Setup

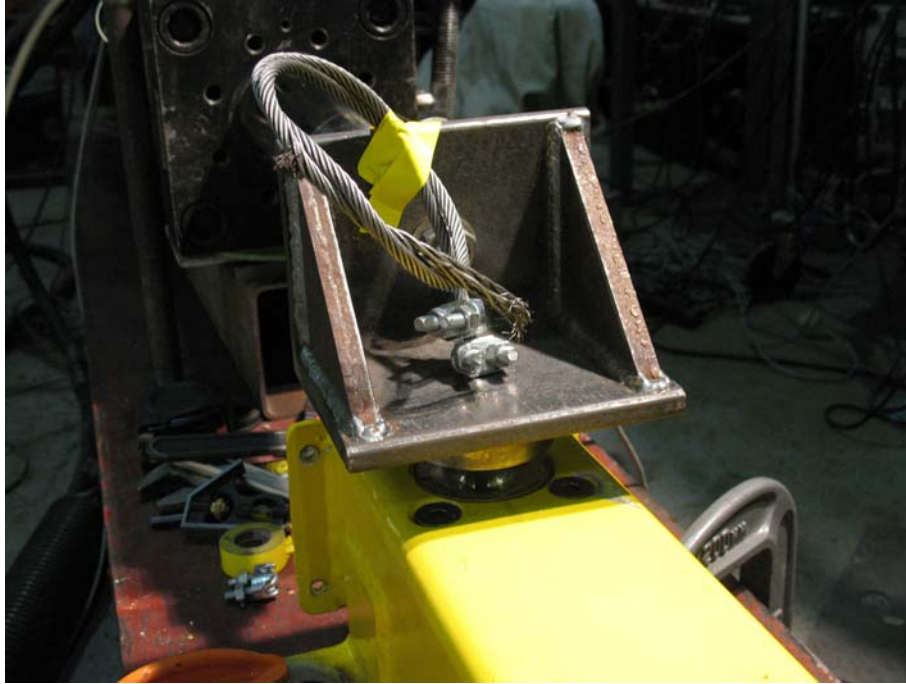


Figure 4.6 Anchor End Used in Test Series 3

4.3.2 Input Program

For the characterization tests of the multi-directional spring unit, two different types of displacement histories were adopted as input signals for the actuator. First, to check whether the behavior of the springs and spring units was stable under cyclic repeated motions, sinusoidal input signals ten cycles long were used. To check whether the behavior of the springs and spring units was sensitive to motion velocity, both 0.05 Hz and 0.2 Hz sinusoidal signals were adopted. Amplitude of displacement was 254 mm (10 in) and 203 mm (8 in) for 0.05 Hz frequency and 0.2 Hz frequency sinusoidal signals, respectively. The difference in maximum stroke reached at different frequencies is a function of maximum velocity that can be applied by the actuator. For those amplitudes of the sinusoidal signals, the velocity at each point of the 0.2 Hz sine wave was 3.2 times that of the corresponding 0.05 Hz wave. Some seismic floor displacement inputs were also adopted as inputs to test the multi-directional spring units. These are relative displacement

histories between the isolated floor and the base floor recorded during the tests of the isolated floor system reported in Chapter 5. These seismic displacement histories are called 2Acc31wo, 3Acc31wo, B107050, and B207050 for reasons that will be described in Chapter 5, and are considered to reflect a representative range of floor response histories.

Note that since Test Series 1 and 2 test the spring alone, which can only be subjected to tension when in the full spring assembly for any direction of isolated floor displacement, only the “pull” half of these sinusoidal signals were adopted for these two series of tests, denoted as half sinusoidal signals as illustrated in Figs. 4.7 and 4.8. For these test series, for the same reasons, the seismic floor displacement histories were not used. For Test Series 3, the complete “pull” and “push” parts of the sinusoidal signals and the seismic displacement records were used. The target inputs adopted in Tests Series 3 are illustrated in Figs. 4.9 through 4.14, respectively.

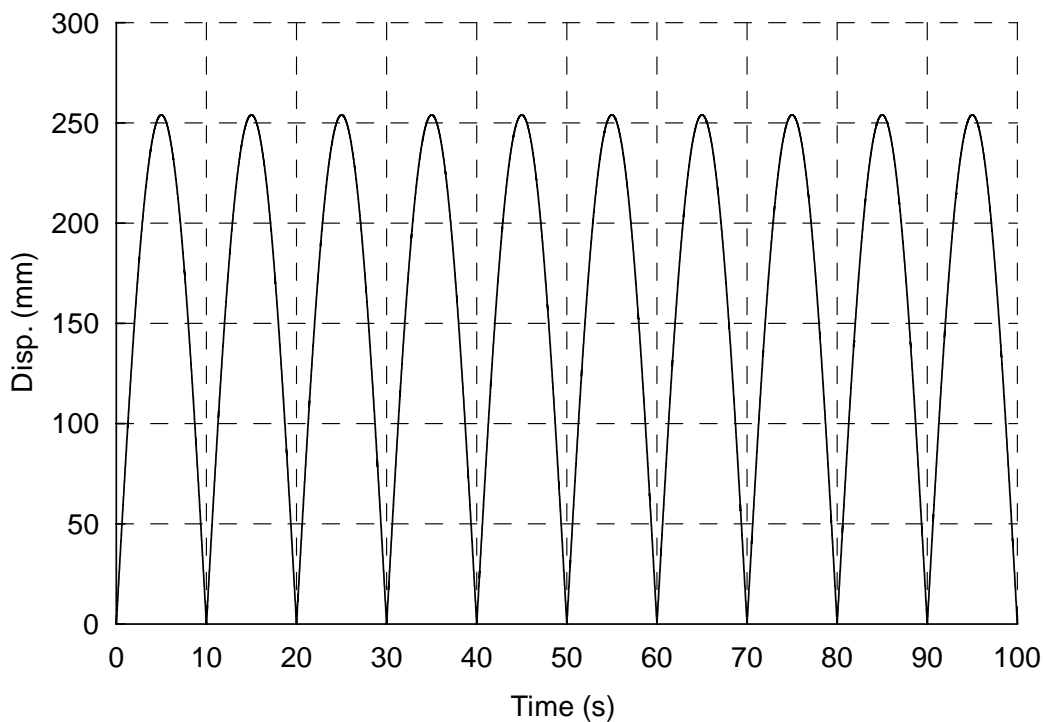


Figure 4.7 Half Sinusoidal Signal with Frequency of 0.05 Hz

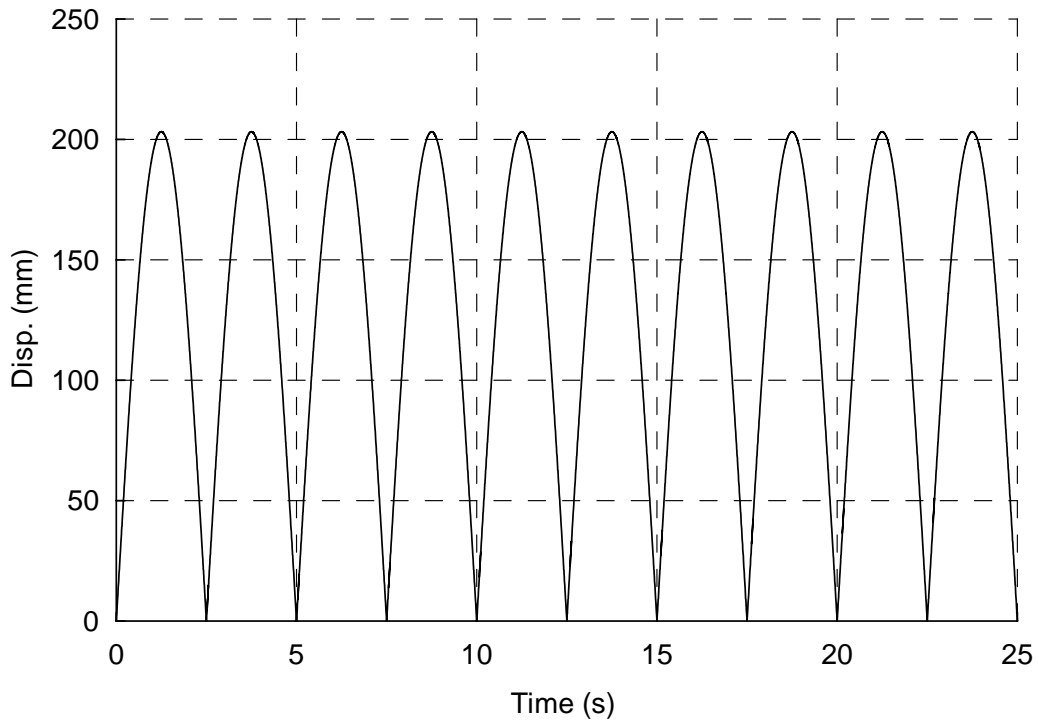


Figure 4.8 Half Sinusoidal Signal with Frequency of 0.2 Hz

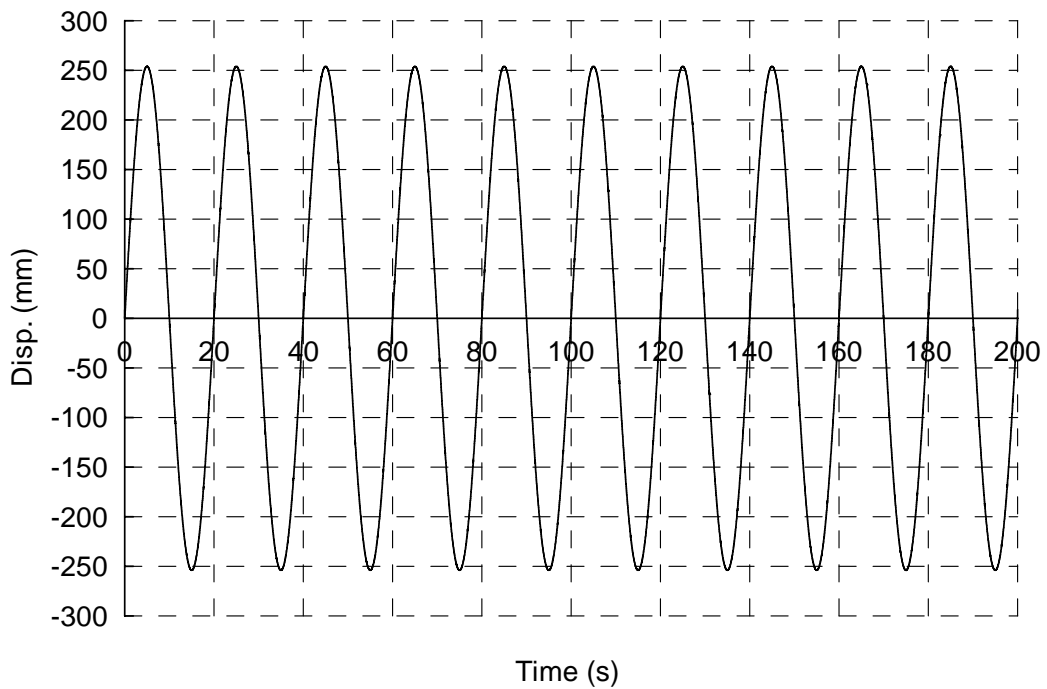


Figure 4.9 Complete Sinusoidal Signal with Frequency of 0.05 Hz

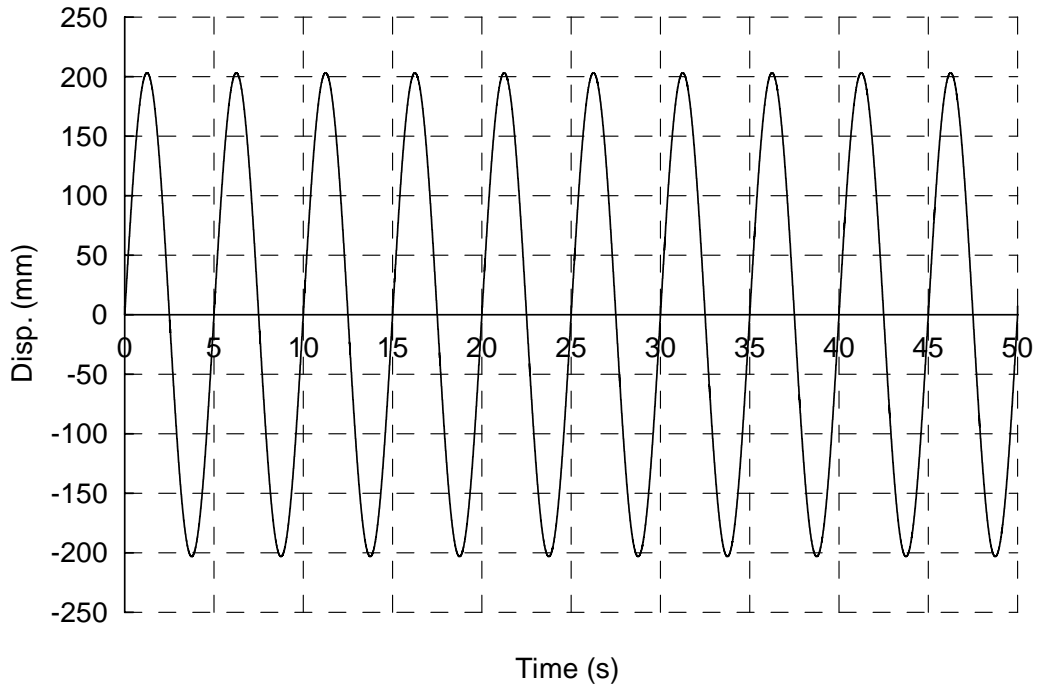


Figure 4.10 Complete Sinusoidal Signal with Frequency of 0.2 Hz

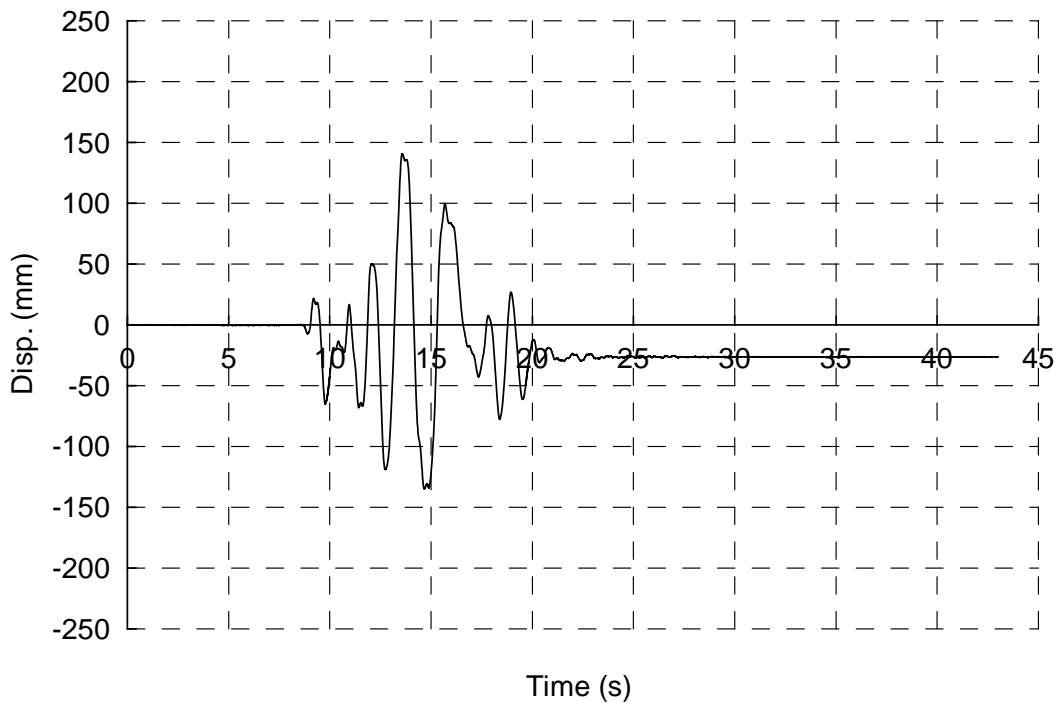


Figure 4.11 Seismic Floor Displacement Record of 2Acc31wo

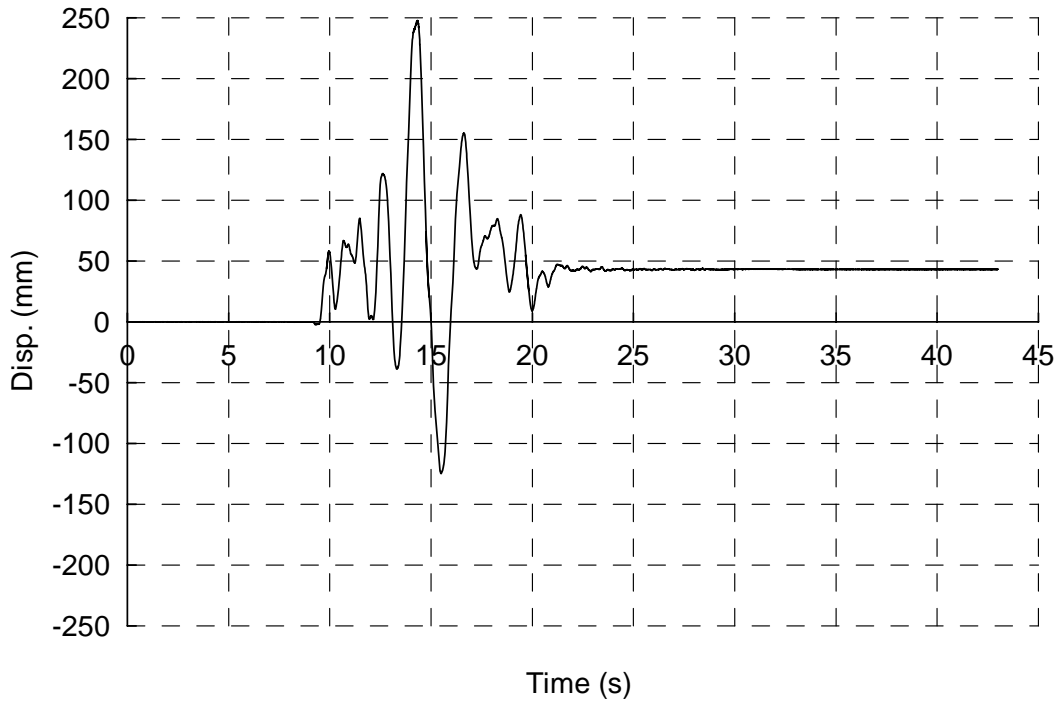


Figure 4.12 Seismic Floor Displacement Record of 3Acc31wo

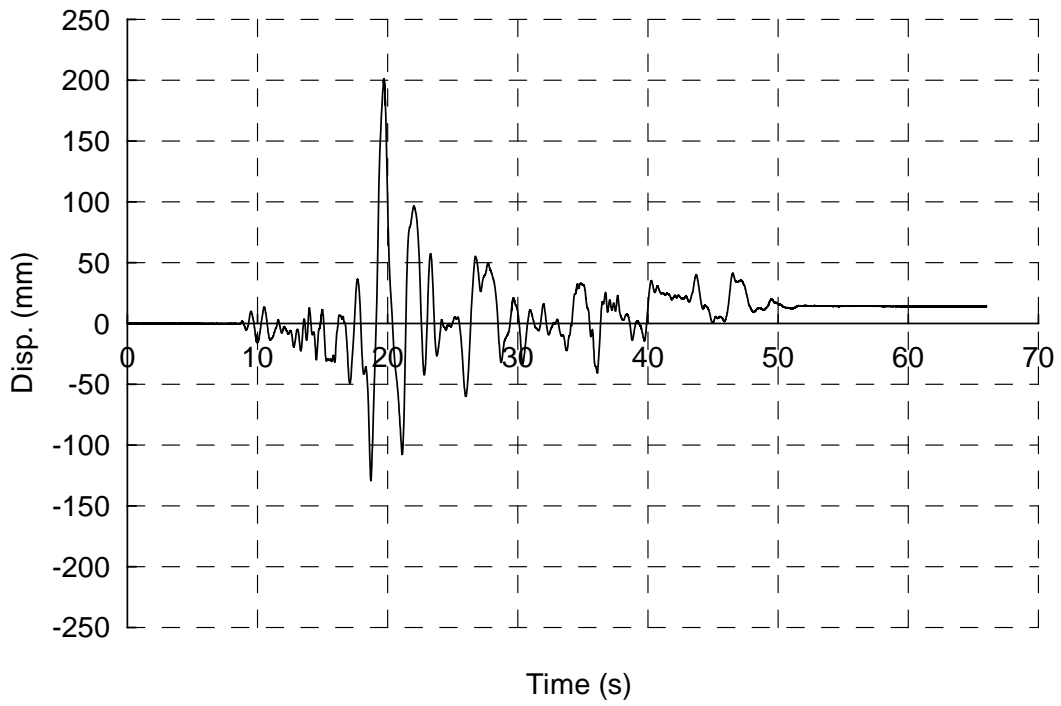


Figure 4.13 Seismic Displacement Record of B107050

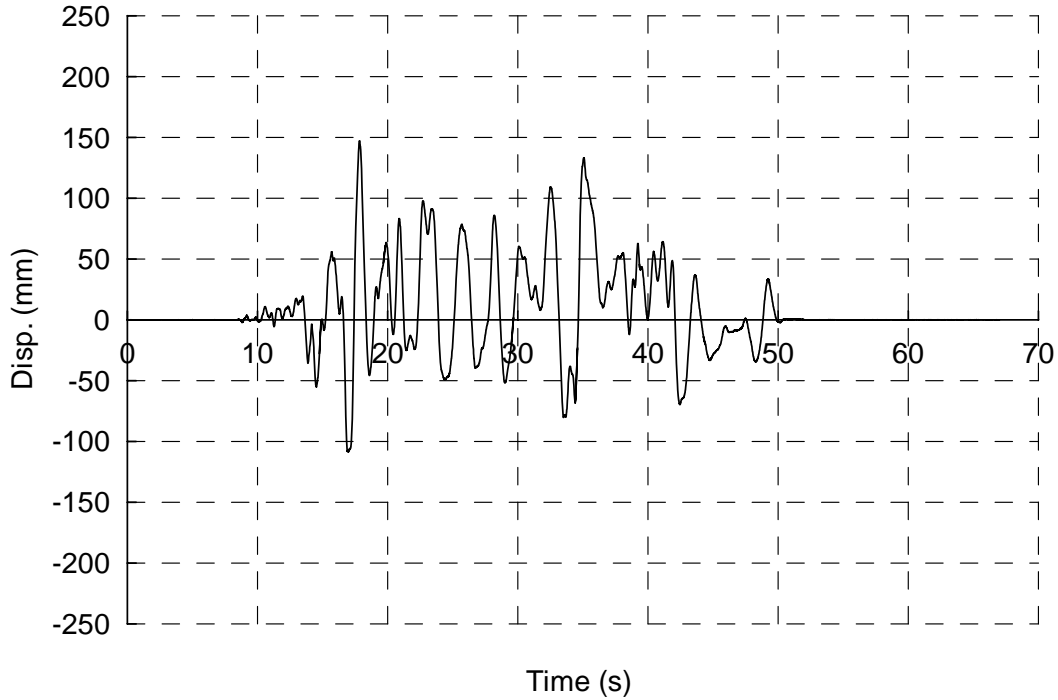


Figure 4.14 Seismic Floor Displacement Record of B207050

4.3.3 Test Protocol

Different multi-directional spring units, built with internal springs having different stiffnesses, can be manufactured and used in the isolated floor systems. Under relatively small floor gravity loads, the manufacturer recommended to use multi-directional spring units with relatively low nominal stiffness, and vice versa. Therefore, to obtain the mechanical behavior (such as force-displacement relationship) of each type of spring unit used in the complete isolated systems tested later, springs with two different nominal stiffnesses were considered as part of the current test program. Also, to investigate consistency between nominal (specified) and actual stiffnesses, two springs with nominal stiffness of 2627 N/m (15 lb/in), and two springs with nominal stiffness of 1313 N/m (7.5 lb/in) were tested. The test sequence is shown in Table 4.1, where the names of tests were chosen per the following nomenclature:

- Names for sinusoidal inputs are denoted in series from the beginning as signal frequency

(0.05 Hz is expressed as “05”, and 0.2 Hz as “2”), nominal spring stiffness (15 lb/in is expressed as “15” and 7.5 lb/in as “07”), null (“0”) or 51 mm (2 in expressed as “2”) pretension, with (“w”) or without (“wo”) tube, and with (“w”) or without (“wo”) bushing. For example, “05150wowo” means test for a 0.05 Hz sinusoidal input signal, for a spring of 2627 N/m (15 lb/in) nominal stiffness spring, without pretension, and without tube and bushing on (i.e. Test Series 2). For Test Series 1 and 2, only one spring of each nominal stiffness was tested. For Test Series 3, both springs of each nominal stiffness were assembled and tested sequentially to check the repeatability of the behavior of the spring units. In Test Series 3, there is an extra “2” at the end of the names of the tests for which the second spring of same nominal stiffness was used.

- Names of tests using seismic floor displacement record inputs are constructed using seismic displacement record input name, followed by the same conversion indicated above for the nominal spring stiffness, the pretension condition (null or 51 mm), and whether the tests was conducted with or without tube, and with or without bushing.

4.4 Test Results

4.4.1 Results of Test Series 1 and 2

It was found that during all the tests in Test Series 2, the springs remained in contact with the top surface of the steel channel due to its sag under its self-weight. The springs were not seen to deform or vibrate transversely. This suggests the rumbling sound heard in Test Series 1 was caused by the friction between the spring and the bottom surface of the tube. Results also confirm that that the configurations of Test Series 1 and 2 are actually identical in terms of behavior.

Table 4.1 Test Sequence

Test Series # (1)	Test Name (2)	Input Frequency* (Hz) (3)	Spring Stiffness (N/m) (4)	Pretension (mm) (5)	Spring Location (6)	Bushing (7)	Amplitude (mm) (8)	Number of Cycles (9)
1	05150ww	0.05	2627	Null	in Tube	without	254	10
	2150ww	0.2	2627	Null	in Tube	without	203	10
	05152ww	0.05	2627	51	in Tube	without	254	10
	2152ww	0.2	2627	51	in Tube	without	203	10
	05070ww	0.05	1313	Null	in Tube	without	254	10
	2070ww	0.2	1313	Null	in Tube	without	203	10
	05072ww	0.05	1313	51	in Tube	without	254	10
	2072ww	0.2	1313	51	in Tube	without	203	10
2	05150wowo	0.05	2627	Null	on Plate	without	254	10
	2150wowo	0.2	2627	Null	on Plate	without	203	10
	05152wowo	0.05	2627	51	on Plate	without	254	10
	2152wowo	0.2	2627	51	on Plate	without	203	10
	05070wowo	0.05	1313	Null	on Plate	without	254	10
	2070wowo	0.2	1313	Null	on Plate	without	203	10
	05072wowo	0.05	1313	51	on Plate	without	254	10
	2072wowo	0.2	1313	51	on Plate	without	203	10
3	05150ww	0.05	2627	Null	in Tube	with	254	10
	2150ww	0.2	2627	Null	in Tube	with	203	10
	05152ww	0.05	2627	51	in Tube	with	254	10
	2152ww	0.2	2627	51	in Tube	with	203	10
	2Acc31wo152ww	2Acc31wo	2627	51	in Tube	with	141	1
	3Acc31wo152ww	3Acc31wo	2627	51	in Tube	with	162	1
	05070ww	0.05	1313	Null	in Tube	with	254	10
	2070ww	0.2	1313	Null	in Tube	with	203	10
	05072ww	0.05	1313	51	in Tube	with	254	10
	2072ww	0.2	1313	51	in Tube	with	203	10
	b107050072ww	b107050	1313	51	in Tube	with	201	1
	b207050072ww	b207050	1313	51	in Tube	with	189	1
	05150ww2	0.05	2627	Null	in Tube	with	254	10
	2150ww2	0.2	2627	Null	in Tube	with	203	10
	05152ww2	0.05	2627	51	in Tube	with	254	10
	2152ww2	0.2	2627	51	in Tube	with	203	10
	05070ww2	0.05	1313	Null	in Tube	with	254	10
	2070ww2	0.2	1313	Null	in Tube	with	203	10
	05072ww2	0.05	1313	51	in Tube	with	254	10
	2072ww2	0.2	1313	51	in Tube	with	203	10

* Only the frequencies of the sinusoidal signals are shown, either 0.05 Hz or 0.2 Hz; For seismic floor displacement record inputs, the name of the record is shown for the corresponding test.

To check whether the behavior of the spring is sensitive to motion velocity, which is directly related to frequency of the sinusoidal motion, the force-displacement history results for each spring from different frequency sinusoidal signals are plotted together for comparison. Figs. 4.15 and 4.16 show the results of the tests without pretension when subjected to different frequency sinusoidal motions. The results of the spring tests with 51 mm (2 in) pretension are illustrated in Figs. 4.17 and 4.18.

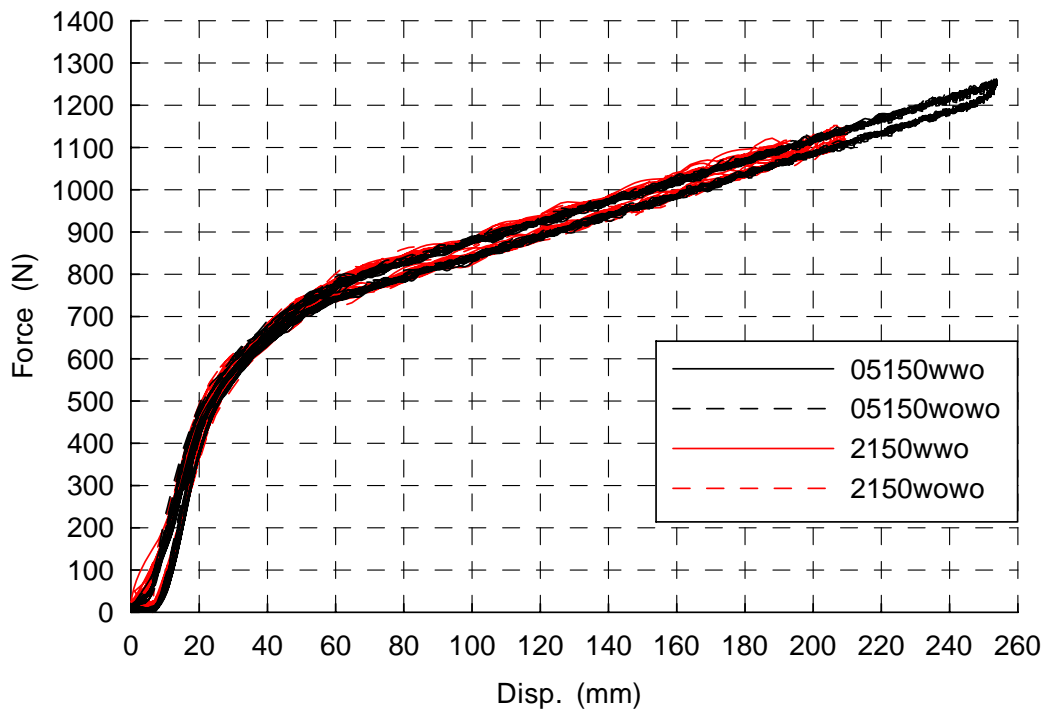


Figure 4.15 Test Results of 2627 N/m (15 lb/in) Spring without Pretension

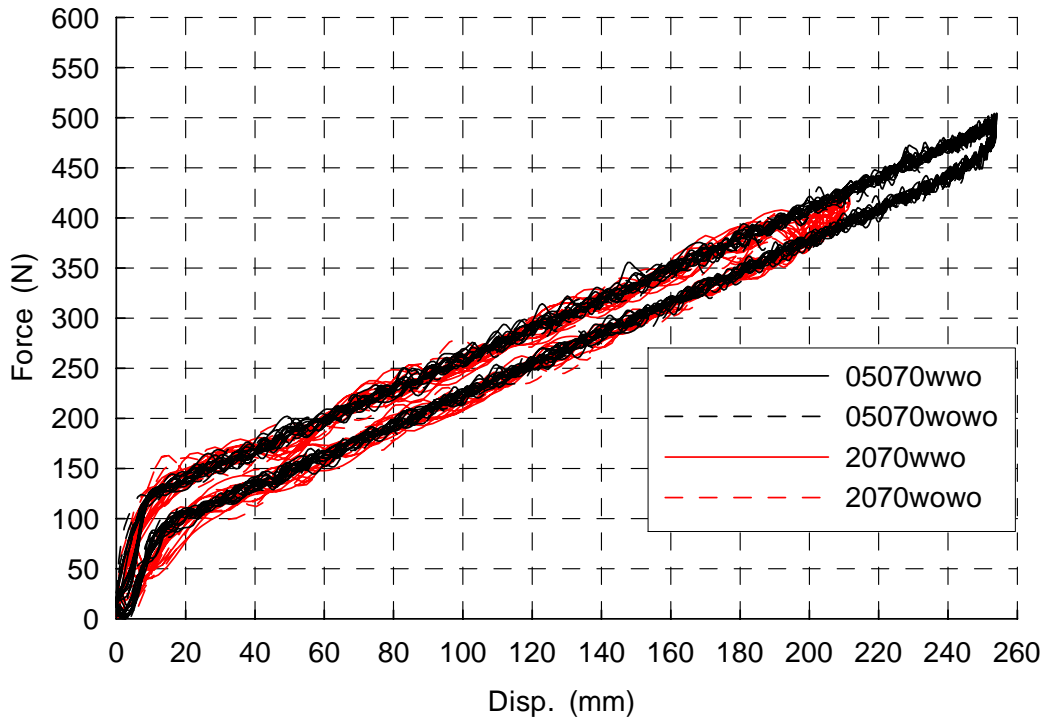


Figure 4.16 Test Results of 1313 N/m (7.5 lb/in) Spring without Pretension

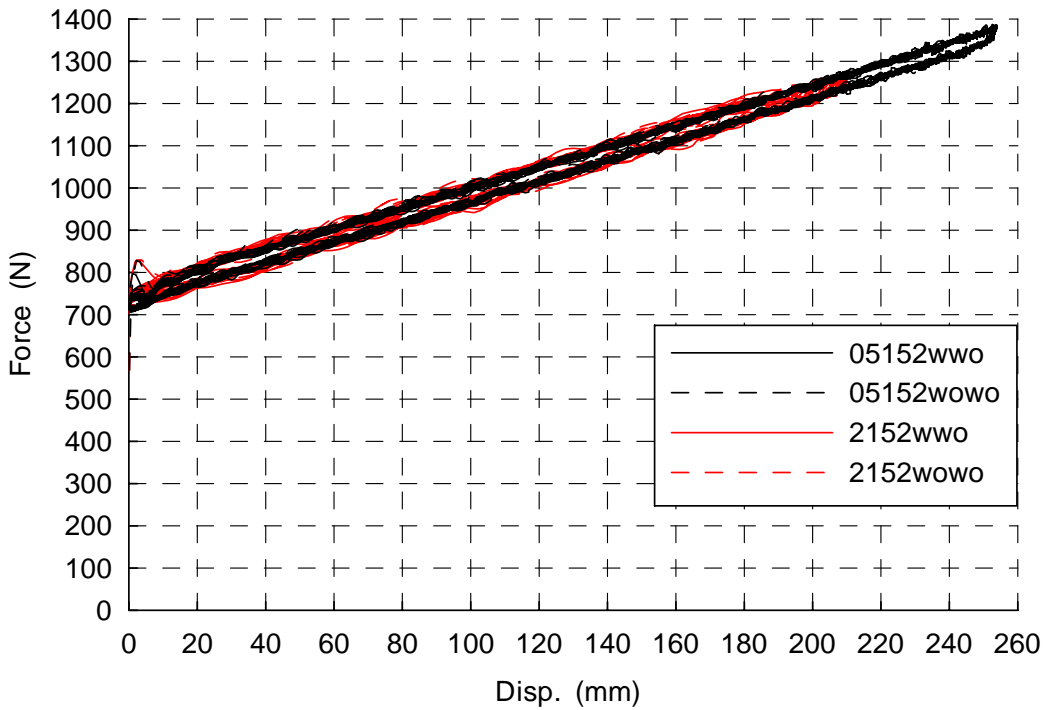


Figure 4.17 Test Results of 2627 N/m (15 lb/in) Spring with 51 mm (2 in) Pretension

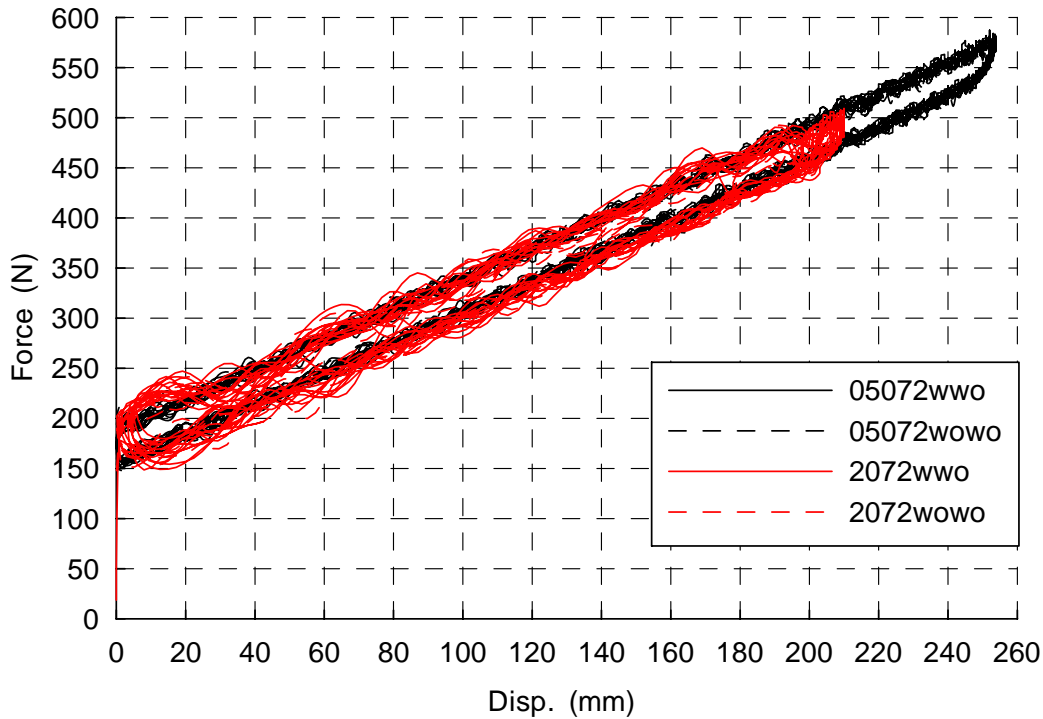


Figure 4.18 Test Results of 1313 N/m (7.5 lb/in) Spring with 51mm (2 in) Pretension

As shown in these figures, the force-displacement loop corresponding to each cycle of the 10-cycle half sinusoidal signals agrees with each other well. This means that the behavior of the pure spring is stable with respect to the number of the cycles of motions. Also, from any of these figures, it may be noted that the force-displacement loops of the springs when subjected to different frequency sinusoidal motions agree well with each other, demonstrating that the behavior of the springs is not sensitive to motion frequency/velocity. In addition, from any of these figures, note that the results from Test Series 1 and the corresponding ones from Test Series 2 coincide with each other, which again confirms that there is no effect on the behavior from the spring and the vertical surfaces and top surface of the tube in Test Series 1 and the configurations of Test Series 1 and 2 are actually identical.

From Fig. 4.15, for the 2627 N/m nominal stiffness spring without any pretension, note that the behavior is bilinear with a small offset at the beginning, or trilinear if a small linear segment is

used at the beginning to model the offset: a first phase of behavior is relatively soft when the displacement is less than about 6 mm (0.25 in), then much stiffer until a displacement of about 50mm (2 in), after which elongation proceeds per a lower linear stiffness of about 2428 N/m (13.866 lb/in). From Fig. 4.16, it is found for the 1313 N/m (7.5 lb/in) nominal stiffness spring without any pretension that the behavior is bilinear (without an offset in this case): after a displacement of about 10 mm (0.4 in), the spring continues to elongate with a lower linear stiffness of about 1525 N/m (8.708 lb/in). Note that the actual stiffnesses of 2428 N/m (13.866 lb/in) and 1525 N/m (8.708 lb/in) were respectively 7.6% and 16.1% below and above their specified nominal values. The expected manufacture's tolerance for the nominal stiffness is 15%. For the 1313 N/m spring, the obtained difference percentage (i.e. 16.1%) is slightly over the expected value. The behavior of these springs is different from the normal behavior of springs which typically exhibit a linear stiffness over the entire range of response. When the springs were pre-tensioned by elongating them by 51 mm (2 in) before starting the tests, as shown in Figs. 4.17 and 4.18, the curves plotted starting from zero displacement were linear and corresponded to the data that would be read from the curves for the cases without any pretension (shown in Figs. 4.15 and 4.16) if starting to read the curves from a point that is 51 mm (2 in) right to the original vertical axis.. Figs. 4.15 to 4.18 also show that each of the force-displacement curves obtained for the spring components exhibit some small hysteresis around the mean force line, likely attributed to the friction between the spring and the tube in Test Series 1 and between the spring and the steel channel in Test Series 2.

4.4.2 Results of Test Series 3

Figs. 4.19 through 4.22 compare the achieved signals (from tests of 2Acc31wo152ww, 3Acc31wo152ww, B107050072ww, and B207050072ww, respectively) versus the corresponding target signals, plotted together for comparison. Note that although the peak amplitudes of the seismic displacement records were slightly less than desired because of the velocity limitation of

the actuator, however, the realization and the corresponding target signals were almost in phase. This was deemed to be a satisfactory accuracy for the current purpose, which was to investigate, using seismic floor displacement histories, whether the behavior of the multi-directional spring units is sensitive to motion frequencies, which is directly related to the motion velocity. In addition, the fidelity of all the realized sinusoidal signals, including those in Test Series 1 and 2, was excellent. Although not shown here, comparison of the target sinusoidal signal and the corresponding motion shows that the difference is less than 2 percent for both frequency and amplitude in those cases.

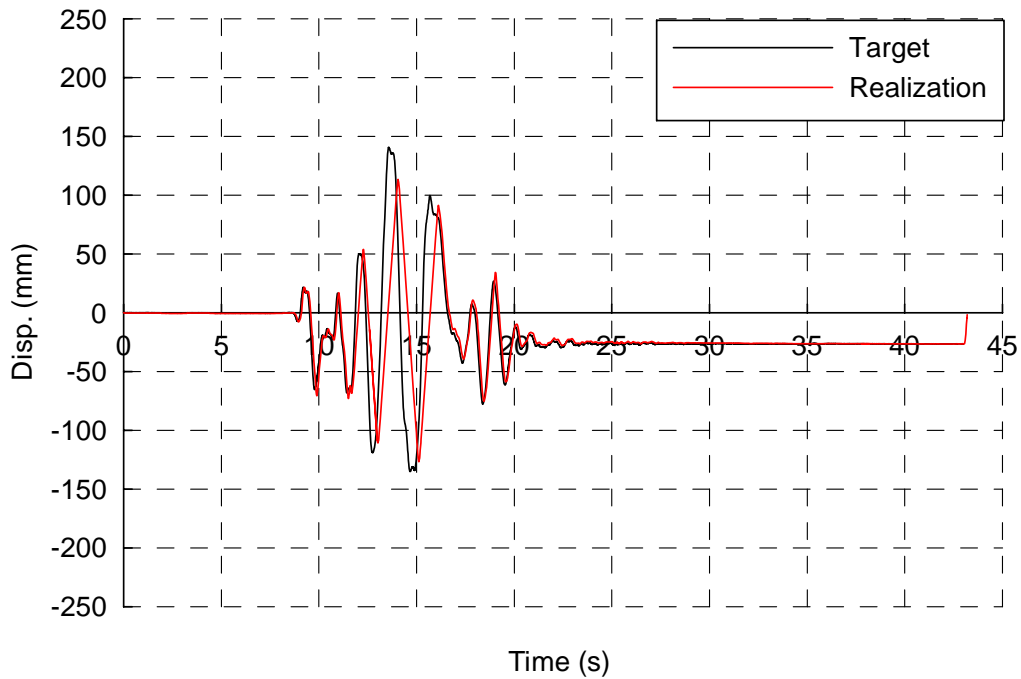


**Figure 4.19 Comparison of Realization and Target of Seismic Displacement Record
2Acc31wo (from Test of 2Acc31wo152ww)**

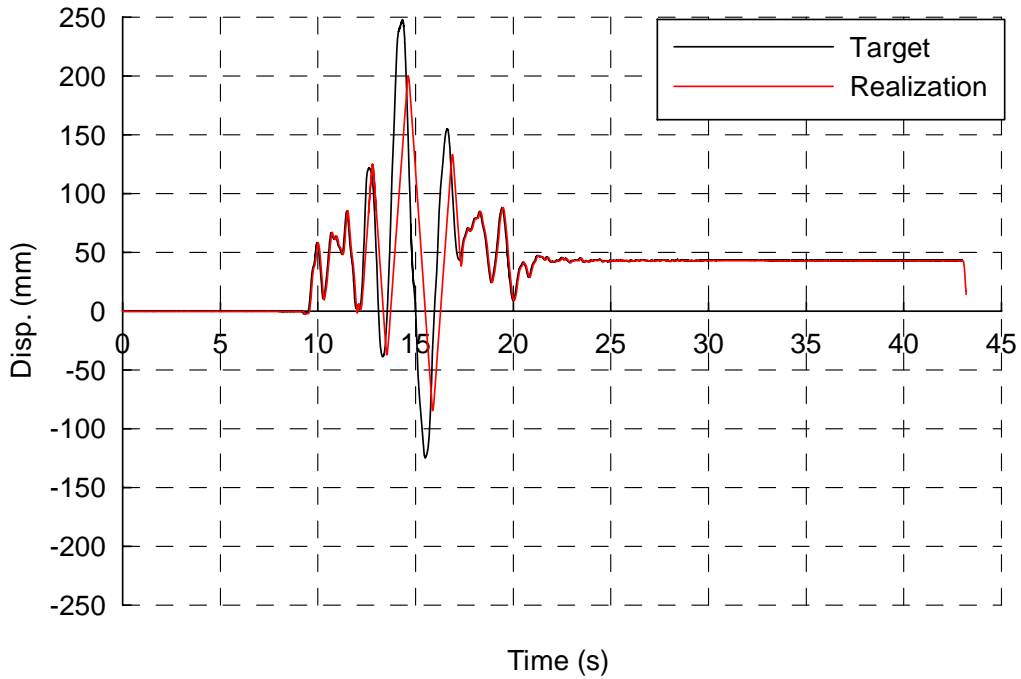


**Figure 4.20 Comparison of Realization and Target of Seismic Displacement Record
3Acc31wo (from Test of 3Acc31wo152ww)**

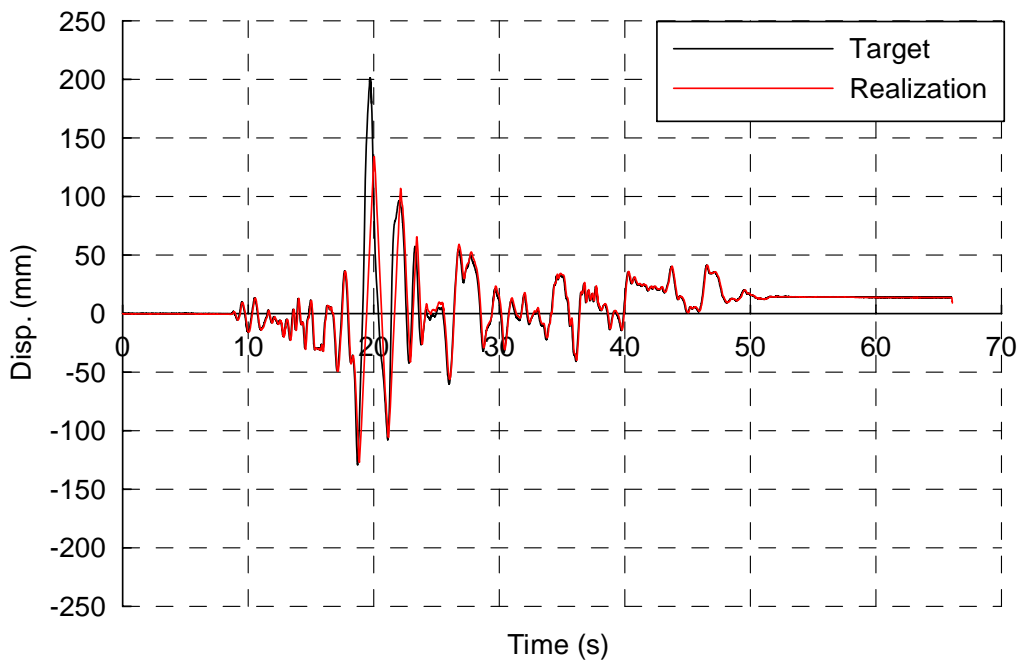


**Figure 4.21 Comparison of Realization and Target of Seismic Displacement Record
B107050 (from Test of B107050072ww)**

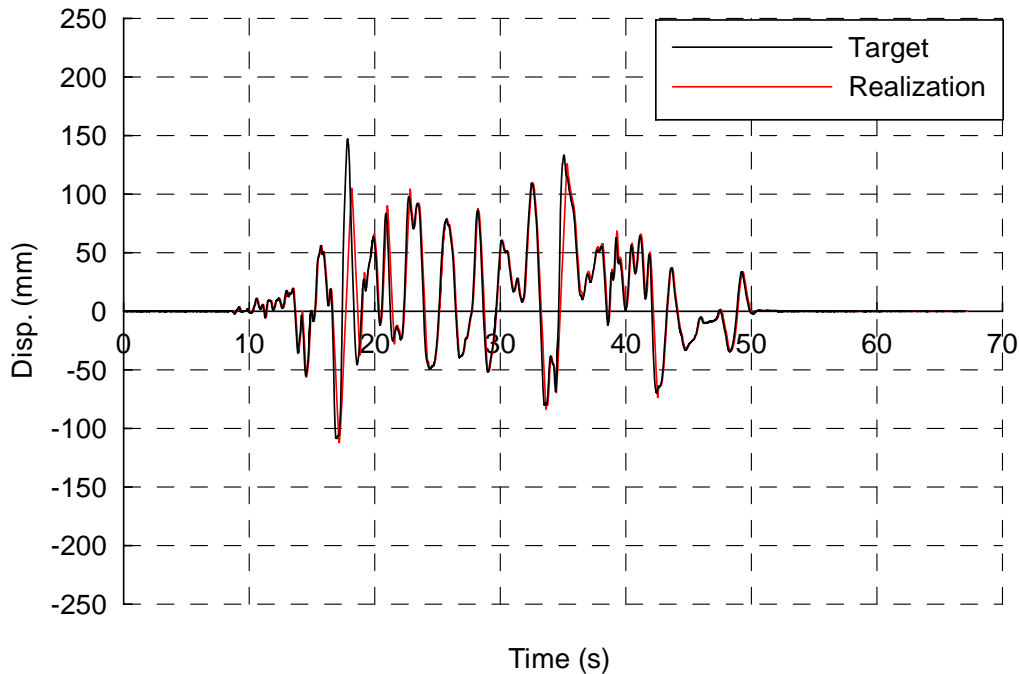


**Figure 4.22 Comparison of Realization and Target of Seismic Displacement Record
B207050 (from Test of B207050072ww)**

Figs. 4.23 and 4.24 show the results of spring unit tests without any pretension. The test results of spring units with 51 mm (2 in) are illustrated in Figs. 4.25 and 4.26.

Figs. 4.23 to 4.26 show that the force-displacement loops of the spring units, when subjected to cyclic sinusoidal motions, agree well with each other from test to test and that the behavior of the spring unit is stable with respect to the number of cycles of cyclic motion. Note that the behavior of the spring units is also stable with respect to the frequencies of motions (i.e. the behavior of the spring unit is not sensitive to motion velocity). Figs. 4.25 and 4.26 also demonstrate that the behavior of the spring units subjected to seismic displacement records coincide well with the corresponding ones subjected to sinusoidal signals, which again confirms that the hysteretic behavior of the spring units is stable and not sensitive to displacement history. In addition, in this series of tests, both spring units having the same nominal stiffness were tested. Figs. 4.23 through 4.36 also show consistency in the force-displacement loops for both spring units with

same nominal stiffness. However, the shape of the hysteretic loops themselves is unconventional and deserves further study. The physics of this behavior is described in Section 4.5. Note that the curve goes up bilinearly when loading, and drops vertically on load reversal, and goes down bilinearly when unloading. For the spring unit with a nominal stiffness of 2627 N/m (15 lb/in), the curve has a linear stiffness when the displacement is bigger than about 76 mm (3 in) under both loading or unloading. For spring unit with nominal stiffness of 1313 N/m (7.5 lb/in), the curve also has a linear stiffness when the displacement is bigger than about 30 mm (1.2 in) under both loading or unloading. However, the unloading slopes are different from the loading slopes. The reasons for this will be explained in the next section.

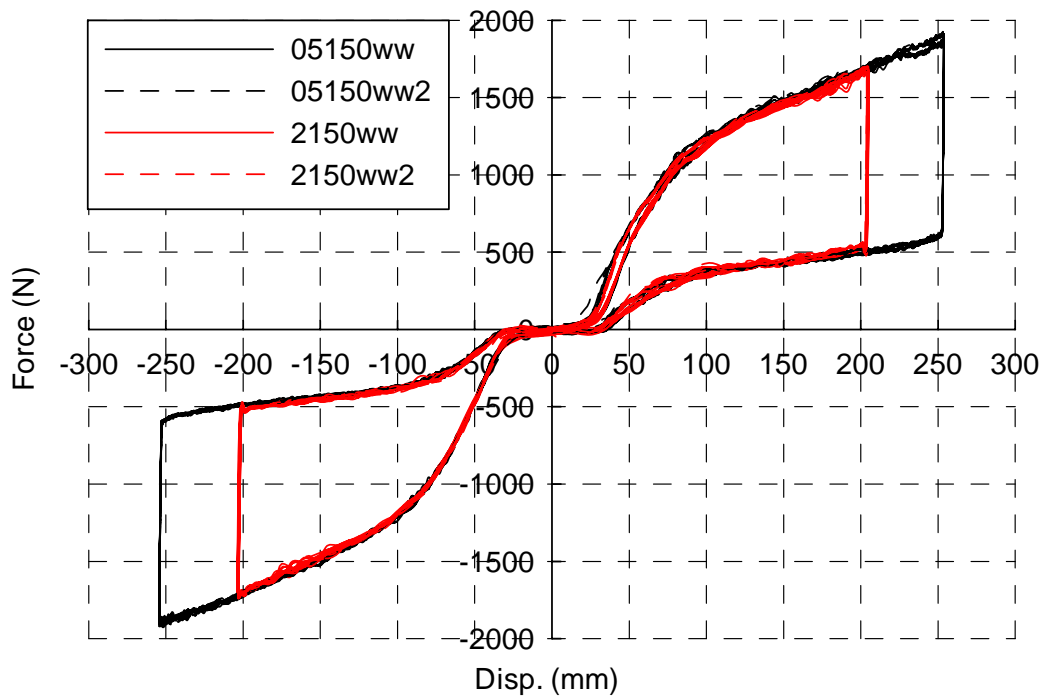


Figure 4.23 Test Results of 2627 N/m (15 lb/in) Spring Units without Pretension

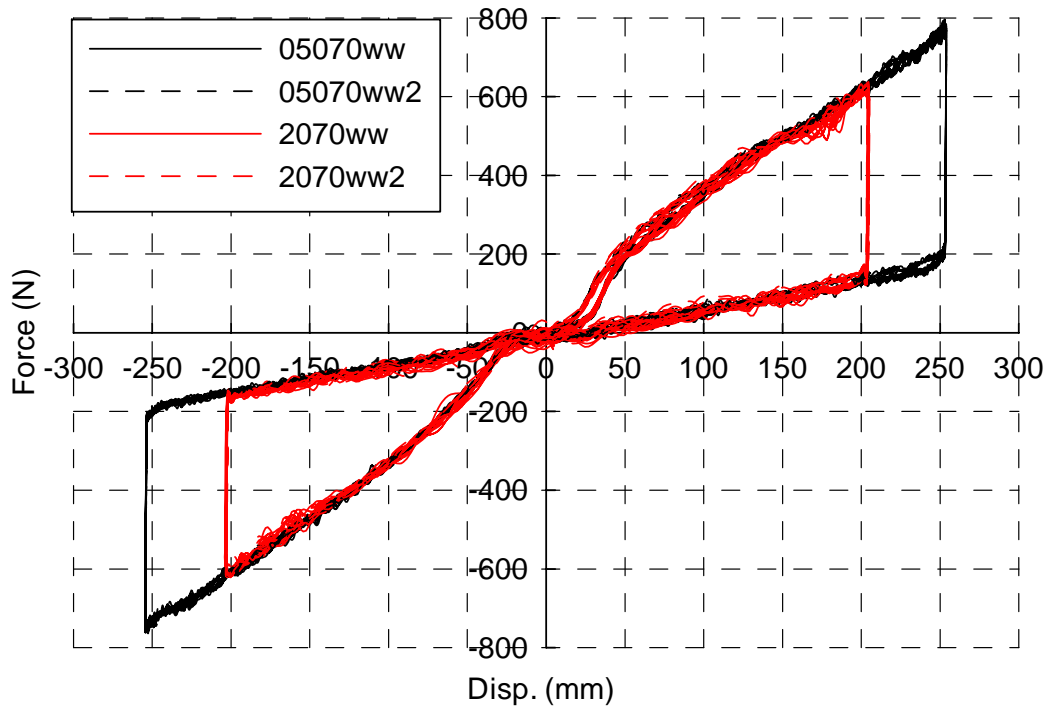


Figure 4.24 Test Results of 1313 N/m (7.5 lb/in) Spring Units without Pretension

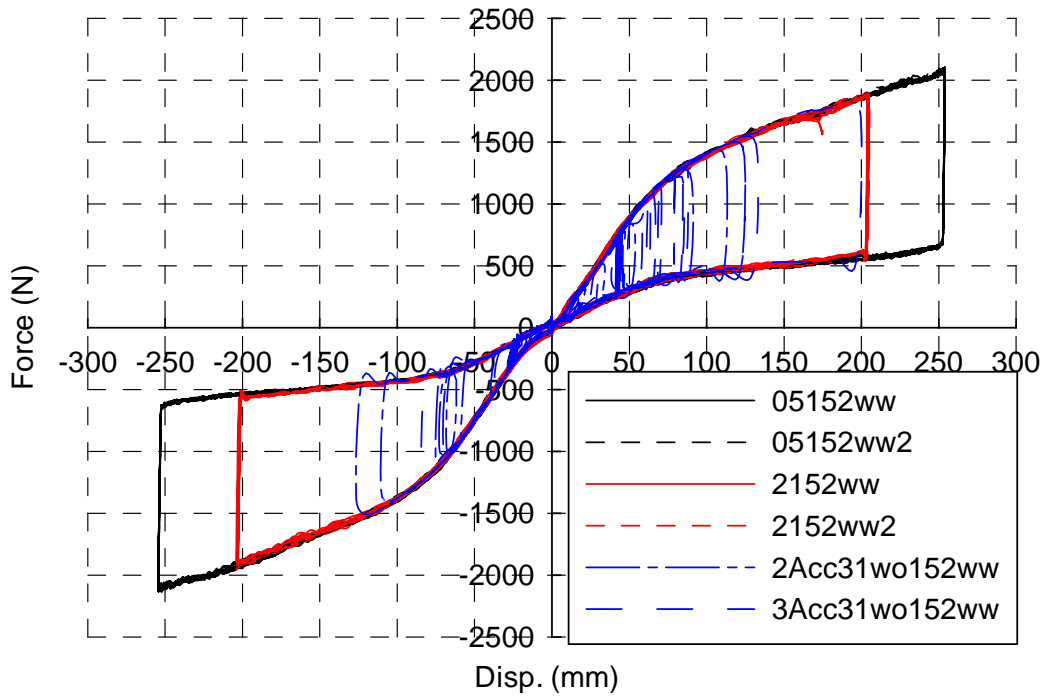


Figure 4.25 Test Results of 2627 N/m (15 lb/in) Spring Units with 51mm (2 in) Pretension

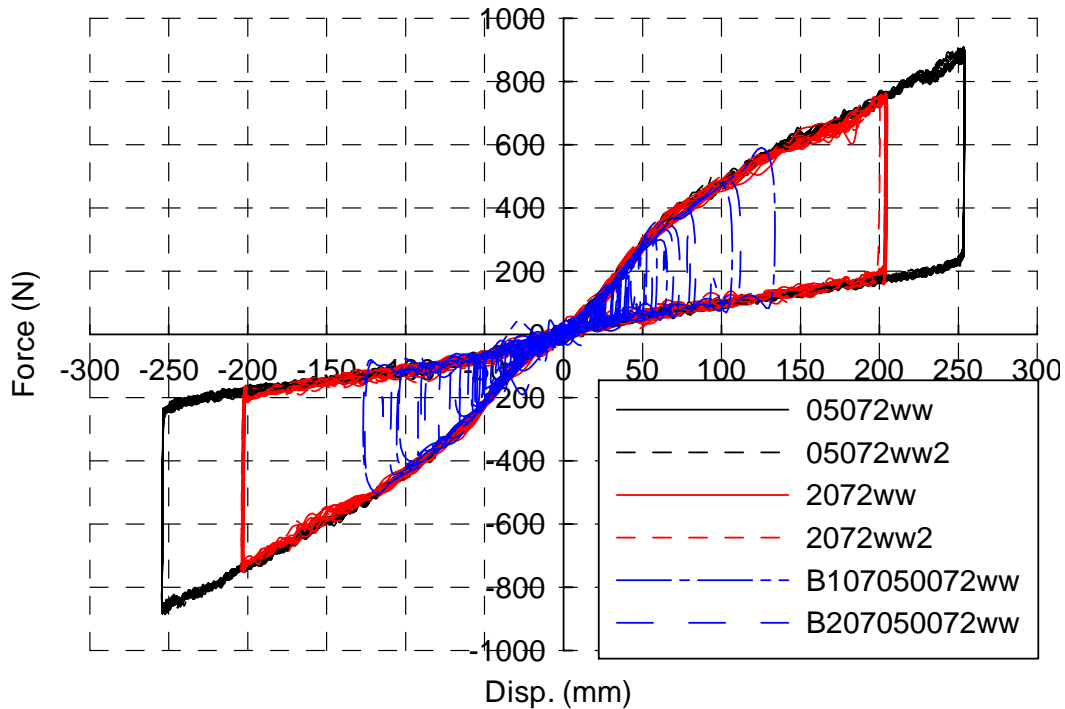


Figure 4.26 Test Results of 1313 N/m (7.5 lb/in) Spring Units with 51 mm (2 in) Pretension

Note that some minor data correction had to be applied to the results of Test Series 3, especially for the cases of springs with pretension applied. For the test setup and assembly shown in Section 4.3.1, even though at the start of the test, the initial condition of the steel cable is vertical for the tests with 51 mm (2 in) pretension in Test Series 3, the load cell read a force value, which is about 85 N (19 lb) for 2627 N/m (15 lb/in) nominal stiffness spring unit and about 18 N (4 lb) for 1313 N/m (7.5 lb/in) nominal stiffness spring unit, respectively. By geometry, no horizontal axial force could be present in this system. Upon further investigation, it was found that, because of the distance between the cable and the load cell, some moment was induced on the load cell during these tests even at the initial state, which affected the reading data of the load cell. This means that even under pure bending, for which no axial force should have been recorded by the load cell, there was a nonzero value recorded by the load cell, presumably because the strain gages inside the load cell were not perfectly symmetrically deployed and the data read from different strain gages did not perfectly cancel each other. This phenomenon is denoted here as

“moment effect” on the load cell and was verified to exist by conducting simple pure-bending tests on the load cell. This moment effect was present at the beginning of the tests with pretension, as the cable was vertical and perpendicular to the actuator and axis of the load cell and the vertical force induces a moment on the load cell. When the tests started, the steel cable became inclined, and applied moments to the load cell. Both horizontal and vertical force components of the cable force causes moments on the load cell. For those spring unit tests without pretension, although the initial load cell reading is about 0, the moment effect from the cable force also existed during motion as mentioned just now. Fig. 4.27 shows an example comparison of the original results and the modified results obtained by eliminating the “moment effect”. Note that the original results are not symmetric and the modified results are almost symmetric. Theoretically speaking as will be demonstrated in the next section, the behavior of the spring units is same in any direction. The modified results correctly reproduce this behavior. Note that a number of other approaches had been used to modify the original results before the moment effect was understood. However, the “moment effect” correction method provides the best results (as shown in Figs. 4.23 to 4.26) which are the most symmetric and best agree with the physical model presented in Section 4.5.

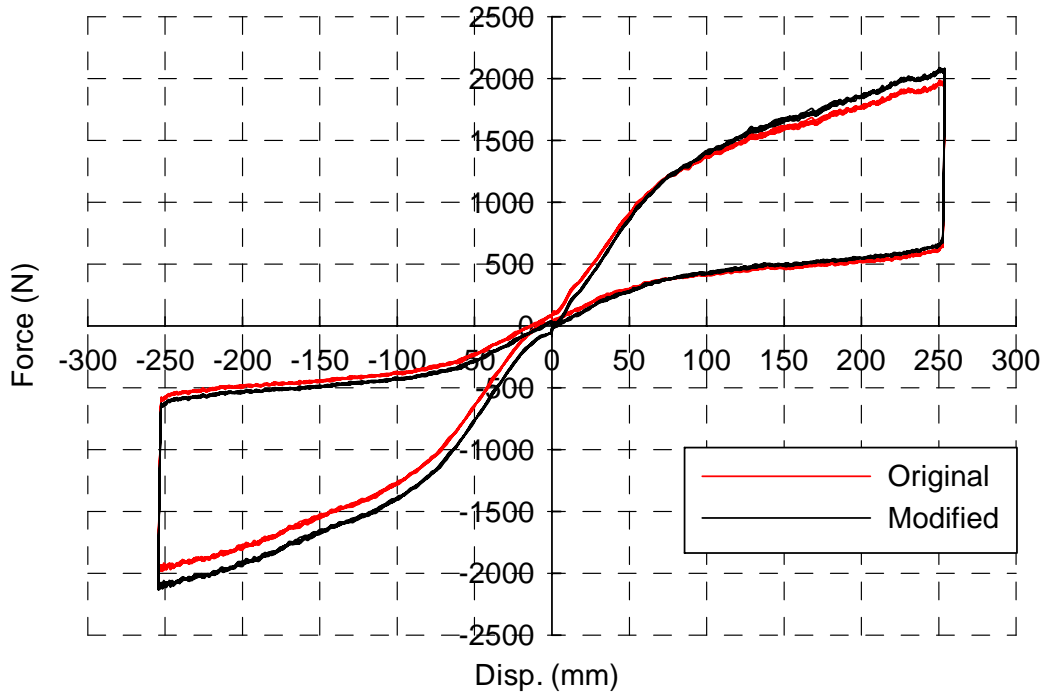


Figure 4.27 Comparison of Original and Modified Results of Test 05152ww

4.5 Physical Model of Multi-directional Spring Unit

4.5.1 General System Geometry

To simulate the behavior of the multi-directional spring units in computer program, a physical model was developed. The detailed geometry relationships, needed to develop this model for the bushings during unidirectional motions, consider both the bushing in spring unit and the bushing fixed on the underside of the isolated floor, and are shown in Fig. 4.28. In this figure, “ $F_1 \pm f$ ” means the force in the spring cable at the end which connects to the internal spring in the spring unit and the meaning of F_1 and f in this expression will be presented in Section 4.5.2. Also, “ r ” represents the radius of each of the two bushings, which is 31 mm (1.218 in) for the case at hand, “ θ ” is the angle from the horizontal of the cable between the two bushings, which also corresponds by geometry to the angle over which the spring cable is not in contact with the

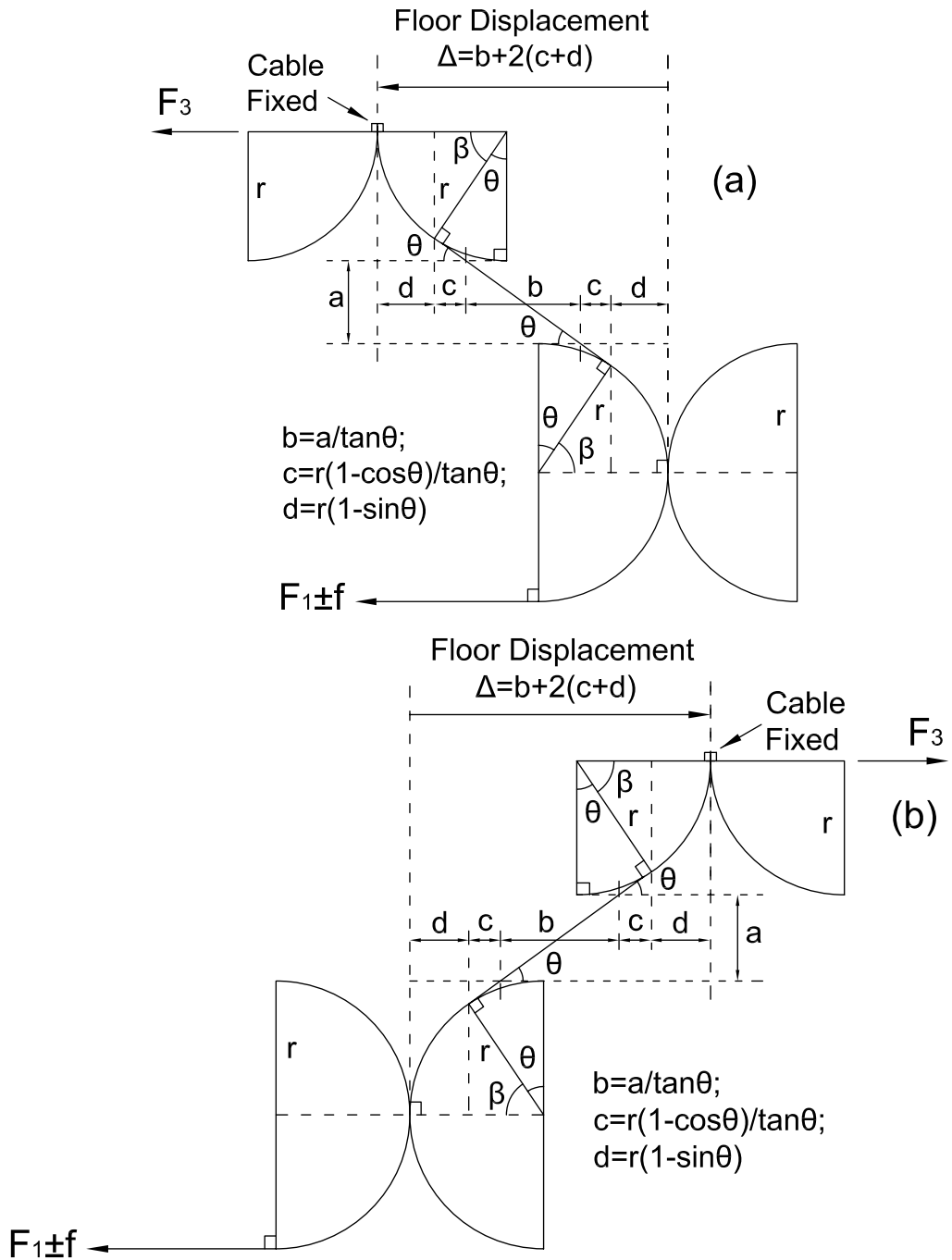


Figure 4.28 Geometry of Bushing and Cable System under Isolated Floor Displacement: (a) Floor Motion towards the Spring Unit, and; (b) Floor Motion away from the Spring Unit

bushing over its quarter circle surface and “ β ” is the complementary angle of “ θ ”, “ Δ ” is the horizontal relative displacement between the isolated floor and the spring unit underneath, and “ a ” is the clear distance between the bushings (which is about 20 mm (0.783 in) as mentioned in Section 4.3.1). The terms, “ b ”, “ c ”, and “ d ”, are geometric dimensions, shown in Fig. 4.28. Adding up to give the total floor displacement, Δ , in this figure, “ $b + 2c$ ” and “ $2d$ ” are the horizontal projections of the cable segments between the bushings that are, respectively, not in contact, and in contact, with the quarter circle segments of the bushings. “ F_3 ” is the horizontal restoring force of the spring unit corresponding to the isolated floor displacement (Δ). Note that here, the spring cable is simplified as a line without thickness for simplicity.

For the horizontal travel distance Δ , shown on Fig. 4.28 as equal to $b + 2(c + d)$, the following geometric relationship during motion can be obtained, knowing that $b = a / \tan \theta$, $c = r(1 - \cos \theta) / \tan \theta$, and $d = r(1 - \sin \theta)$.

$$\Delta = a / \tan \theta + 2r[1 - \sin \theta + (1 - \cos \theta) / \tan \theta] \quad (4.1)$$

As shown in Fig. 4.28, $\beta = \pi / 2 - \theta$. Substituting, the above relationship may be expressed as,

$$\Delta = a \tan \beta + 2r[1 - \cos \beta + (1 - \sin \beta) \tan \beta] \quad (4.2)$$

Substituting $\beta = 2\varphi$ allows to simplify the resulting expression knowing that,

$$\sin \beta = \frac{2 \tan \varphi}{1 + \tan^2 \varphi} \quad (4.3)$$

$$\cos \beta = \frac{1 - \tan^2 \varphi}{1 + \tan^2 \varphi} \quad (4.4)$$

$$\tan \beta = \frac{2 \tan \varphi}{1 - \tan^2 \varphi} \quad (4.5)$$

Substituting Eqs. 4.3, 4.4 and 4.5 into Eq. 4.2, and substituting $\tan \varphi$ by x (to simplify the

resulting expression) gives the following equation,

$$(\Delta - 4r)x^2 + 2(a + 2r)x - \Delta = 0 \quad (4.6)$$

Solving Eq. 4.6 gives,

$$x = \frac{-(a + 2r) \pm \sqrt{(a + 2r)^2 + \Delta(\Delta - 4r)}}{\Delta - 4r} \quad (\text{when } \Delta \neq 4r) \quad (4.7)$$

From calculation and comparison with bushing motion geometry, choose the positive value of x ,

$$x = \frac{-(a + 2r) + \sqrt{(a + 2r)^2 + \Delta(\Delta - 4r)}}{\Delta - 4r} \quad (\text{when } \Delta \neq 4r) \quad (4.8)$$

Because $\beta = 2\varphi$ and $x = \tan \varphi$, then,

$$\beta = 2a \tan \left[\frac{-(a + 2r) + \sqrt{(a + 2r)^2 + \Delta(\Delta - 4r)}}{\Delta - 4r} \right] \quad (\text{when } \Delta \neq 4r) \quad (4.9)$$

Note that when $\Delta = 4r$, Eq. 4.9 converges to $\beta = 1.296$. (4.10)

From Fig. 4.28, the elongation of the internal spring of the multi-directional spring unit, denoted as Δ_s here, corresponding to the isolated floor horizontal displacement, Δ , can be expressed as,

$$\Delta_s = a / \cos \beta + 2r\beta + 2r(1 - \sin \beta) / \cos \beta - 2r - a \quad (4.11)$$

4.5.2 Hysteretic Behavior Model for Pre-tensioned Multi-directional Spring Units

Considering that multi-directional spring units in isolated floor system will be pre-tensioned by pre-pulling the cable by 51 mm (2 in) to facilitate self-centering of the system, here, the physical model of multi-directional spring units considering pretension was first developed. The linear force-displacement relationships of pure springs (within tube) with 51 mm (2 in) pretension, shown in Section 4.4.1, can be simulated with straight lines for the average force (“ F_1 ” in Fig. 4.28) and a small hysteretic friction (“ f ” in Fig.4.28) to capture the observed friction effect.

For the 2627 N/m (15 lb/in) spring with 51 mm (2 in) pretension case, the equation of the straight line used to simulate the internal spring force (F_1)-displacement (Δ_s) relationship, in units of N and mm respectively, is,

$$F_1 = 2.428\Delta_s + 745.841 \quad (4.12)$$

or, in units of lb and in respectively,

$$F_1 = 13.866\Delta_s + 167.68 \quad (4.13)$$

For the 1313 N/m (7.5 lb/in) spring with 51 mm (2 in) pretension case, the equation of the line used to model the pure spring force (F_1)-displacement (Δ_s) relationship, in units of N and mm respectively, is,

$$F_1 = 1.525\Delta_s + 169.198 \quad (4.14)$$

or, in units of lb and in respectively,

$$F_1 = 8.708\Delta_s + 38.039 \quad (4.15)$$

The comparisons between the straight lines and the results from test cases 05152wowo and 05072wowo are shown in Figs. 4.29 and 4.30, respectively. Note that the friction is around 18 N (4 lb) from these two figures. Therefore, the force-displacement relationships of springs (in tube) with 51 mm (2 in) pretension are equal to the corresponding straight lines plus and minus the friction effect when the cable is extending out and retracting in, respectively.

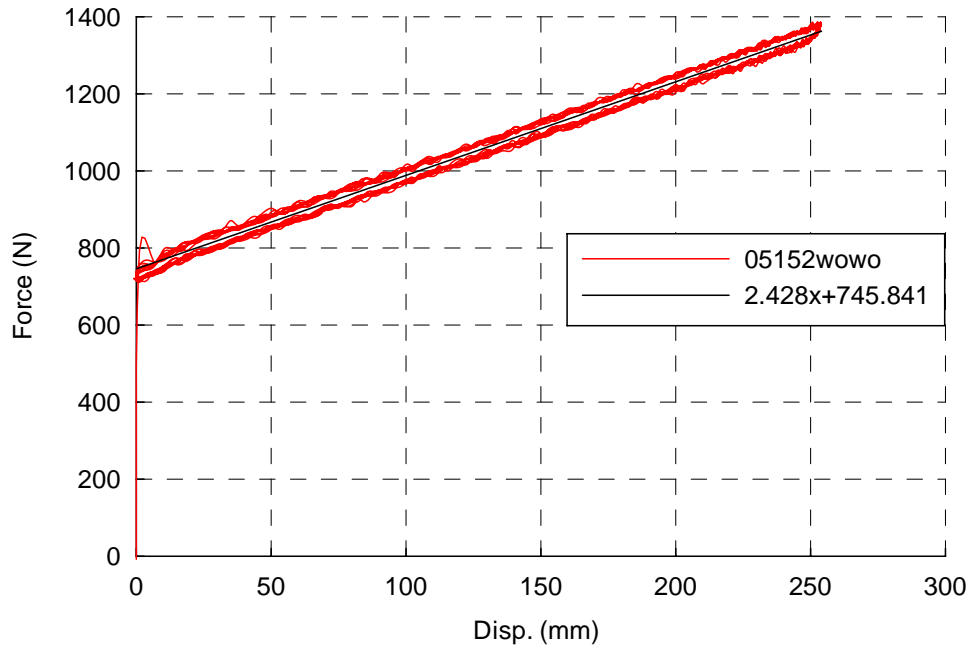


Figure 4.29 Comparison of Model Straight Line for 2627 N/m (15 lb/in) Spring and Test Results of 05152wowo

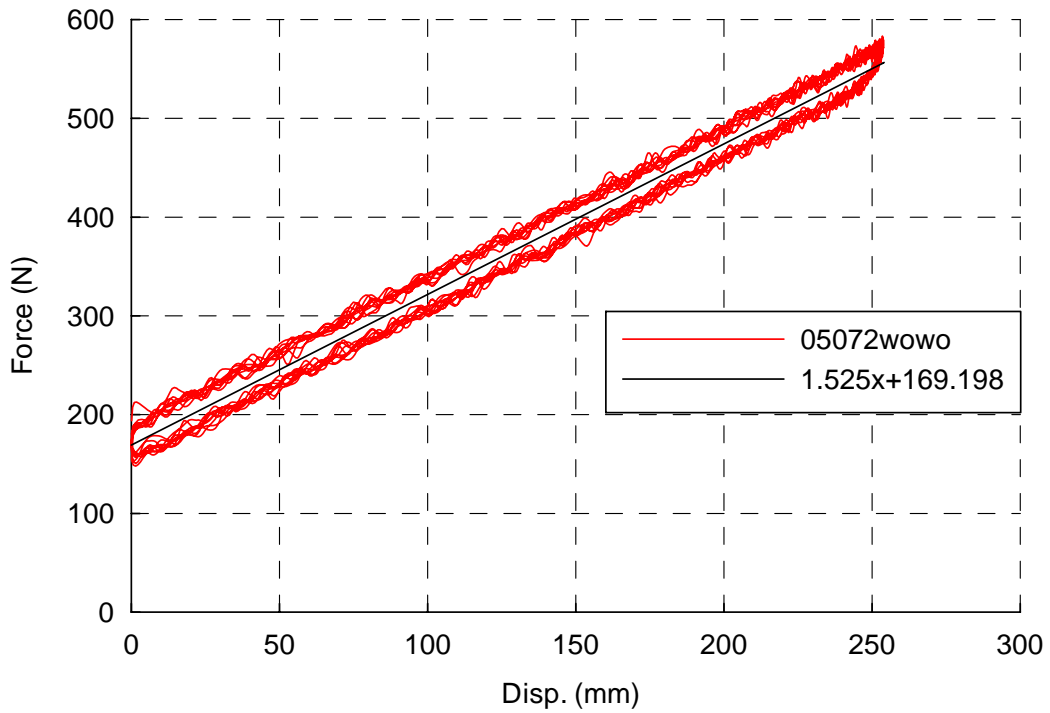


Figure 4.30 Comparison of Model Straight Lines for 1313 N/m (7.5 lb/in) Spring and Test Results of 05072wowo

Then, based on the belt friction formula (Bedford and Fowler, 2005), the force in the spring cable segment outside the bushing, denoted as F_2 , can be expressed as,

$$F_2 = (F_1 + f)e^{\mu_k(\pi/2+\beta)} \quad (\text{when the cable is extending out}) \quad (4.16)$$

$$F_2 = (F_1 - f)/e^{\mu_k(\pi/2+\beta)} \quad (\text{when the cable is retracting in}) \quad (4.17)$$

The horizontal restoring force F_3 , equal to the horizontal component of F_2 , can be obtained as following,

$$F_3 = (F_1 + f)e^{\mu_k(\pi/2+\beta)} \cos \theta \quad (\text{when the cable is extending out}) \quad (4.18)$$

$$F_3 = (F_1 - f)/e^{\mu_k(\pi/2+\beta)} \cos \theta \quad (\text{when the cable is retracting in}) \quad (4.19)$$

Because $\beta = \pi/2 - \theta$, Eqs. 4.18 and 4.19 can be alternatively expressed as,

$$F_3 = (F_1 + f)e^{\mu_k(\pi/2+\beta)} \sin \beta \quad (\text{when the cable is extending out}) \quad (4.20)$$

$$F_3 = (F_1 - f)/e^{\mu_k(\pi/2+\beta)} \sin \beta \quad (\text{when the cable is retracting in}) \quad (4.21)$$

where, f is the friction between the spring and the tube, taken as 18 N (4 lb), and μ_k is the sliding friction coefficient (which is a kinetic friction coefficient) between the steel cable and the brass bushing of the multi-directional spring unit. The static coefficient of friction between these two materials is typically given as 0.19 for greasy contacting surface condition (http://www.roymech.co.uk/Useful_Tables/Tribology/co_of_friect.htm). However, no values of kinetic friction coefficient could be found for these two surfaces. Here, to best simulate the behavior of the multi-directional spring units, sliding friction coefficient values of μ_k of 0.171 and 0.190 were found to be adequate for the 2627 N/m (15 lb/in) and 1313 N/m (7.5 lb/in) nominal stiffness spring units, respectively. These selected values of the sliding coefficient of friction are those which gave the minimum sum of square error (SSE) by statistically comparing the model prediction and the corresponding test result.

From Section 4.4, note that the behavior of both the pure spring and the spring units is stable when subjected to different inputs. Hence, as examples, the comparisons of the model prediction results and the corresponding test results presented in Section 4.4.2 for tests of 05152ww and 05072ww are shown in Figs. 4.31 and 4.32, respectively. Note that the “Force” and “Disp.” in these figures are the lateral restoring force from the spring units, “ F_3 ”, and the displacement of the isolated floor system, “ Δ ”, as shown in Fig. 4.28. Good agreement may be found between the results from the physical model and the corresponding test results.

Note that in all the equations shown above, the displacement and force parameters are treated as scalars, which means that these parameters have no vector directional meaning. Therefore, in computations, if the force and displacement are defined as positive in one motion direction, then the force and displacement in the opposite direction should be considered with a negative sign when using the above equations. Furthermore, note that four key physical terms were used in developing this model: r , a , f , and μ_k , which are denoted as primary parameters here. All the other quantities (i.e., β , Δ_s , F_1 , F_2 , and F_3) used in this model can directly or indirectly be expressed by using these four independent parameters, which are the physical properties of the spring unit itself.

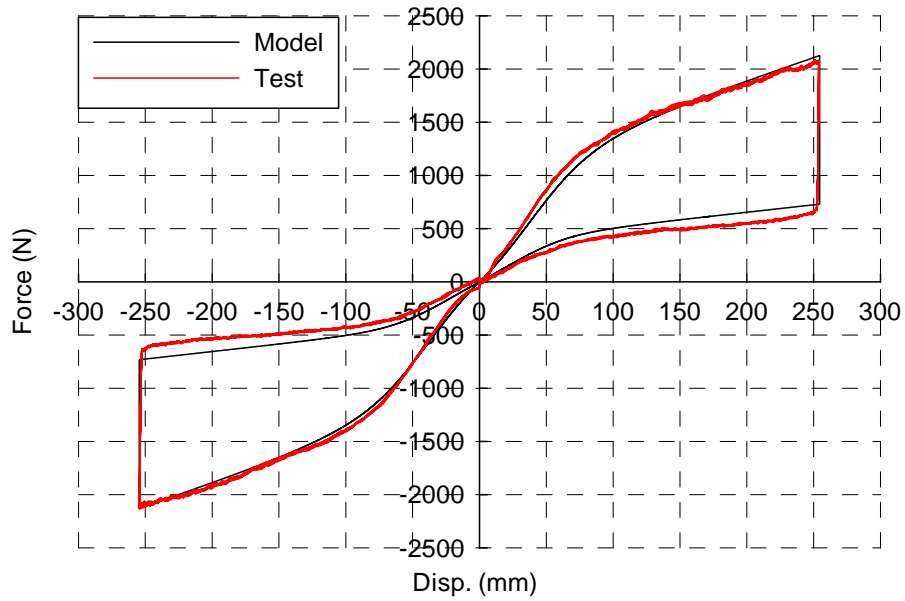


Figure 4.31 Comparison of Model Prediction for 2627 N/m (15 lb/in) Spring Unit and 05152ww Test Results

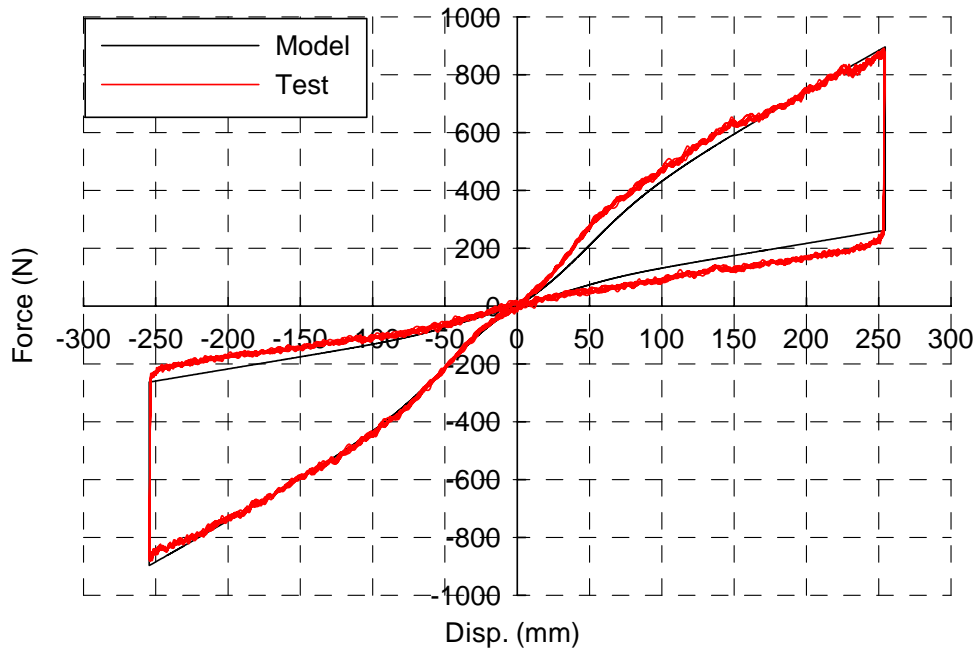


Figure 4.32 Comparison of Model Prediction for 1313 N/m (7.5 lb/in) Spring Unit and 05072ww Test Results

4.5.3 Hysteretic Behavior Model for Non-pre-tensioned Multi-directional Spring Units

The process and all the equations for building up the physical model for multi-directional spring units with pretension shown above can also be used for the development of the physical analytical model for multi-directional spring units without any pretension and with other amount of pretension as long as the corresponding values of the four primary parameters and the force-displacement relationship of spring components are known. As an example, the following will show the development of the physical model for multi-directional spring units without pretension using these equations shown above. The only difference of this process is that the force-displacement relationships (i.e. Eqs. 4.12 to 4.15) must be replaced by the corresponding force-displacement relationship of springs without any pretension. The values of the four primary parameters (r , a , f , and μ_k) are kept same as those used in model for pretension cases.

For the 2627 N/m (15 lb/in) spring without any pretension case, trilinear model was adopted here. The equations of the lines in different displacement phases used to simulate the pure spring force (F_1)-displacement (Δ_s) relationship, in units of N and mm respectively, are,

$$F_1 = 2.643\Delta_s + 2.802 \quad (\text{when } \Delta_s \leq 6.3 \text{ mm}) \quad (4.22)$$

$$F_1 = 31.363\Delta_s + 179.117 \quad (\text{when } 6.3 \text{ mm} < \Delta_s \leq 27.6 \text{ mm}) \quad (4.23)$$

$$F_1 = 2.429\Delta_s + 618.606 \quad (\text{when } \Delta_s > 27.6 \text{ mm}) \quad (4.24)$$

or, in units of lb and in respectively,

$$F_1 = 15.093\Delta_s + 0.63 \quad (\text{when } \Delta_s \leq 0.249 \text{ in}) \quad (4.25)$$

$$F_1 = 179.095\Delta_s - 40.269 \quad (\text{when } 0.249 \text{ in} < \Delta_s \leq 1.086 \text{ in}) \quad (4.26)$$

$$F_1 = 13.872\Delta_s + 139.075 \quad (\text{when } \Delta_s > 1.086 \text{ in}) \quad (4.27)$$

For the 1313 N/m (7.5 lb/in) spring without any pretension case, bilinear model was adopted here. The equations of the lines in different displacement phases used to simulate the pure spring

force (F_1)-displacement (Δ_s) relationship, in units of N and mm respectively, are,

$$F_1 = 9.598\Delta_s + 7.704 \quad (\text{when } \Delta_s \leq 10.1 \text{ mm}) \quad (4.28)$$

$$F_1 = 1.514\Delta_s + 88.947 \quad (\text{when } \Delta_s > 10.1 \text{ mm}) \quad (4.29)$$

or in units of lb and in respectively,

$$F_1 = 54.806\Delta_s + 1.732 \quad (\text{when } \Delta_s \leq 0.396 \text{ in}) \quad (4.30)$$

$$F_1 = 8.647\Delta_s + 19.997 \quad (\text{when } \Delta_s > 0.396 \text{ in}) \quad (4.31)$$

The comparisons between the straight lines and the results from test cases 05150wowo and 05070wowo are shown in Figs. 4.33 and 4.34, respectively. From these two figures, the same value of friction is found as that obtained for pretension cases which is around 18 N (4 lb). Therefore, the force-displacement relationships of springs without any pretension are equal to the corresponding straight lines plus and minus the friction effect when the cable is extending out and retracting in, respectively.

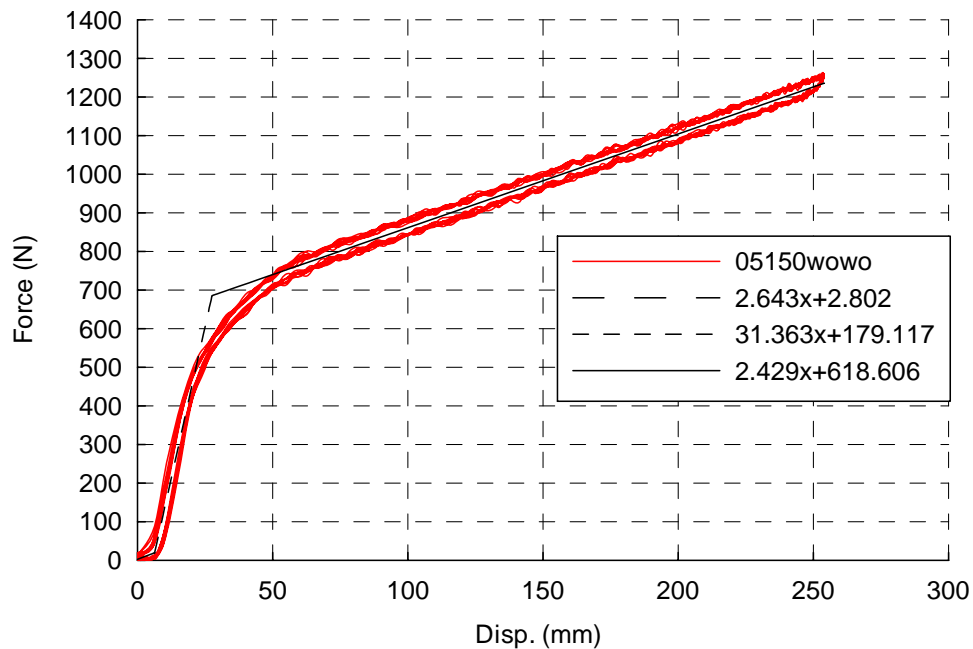


Figure 4.33 Comparison of Model Straight Lines for 2627 N/m (15 lb/in) Spring and Test Results of 05150wowo

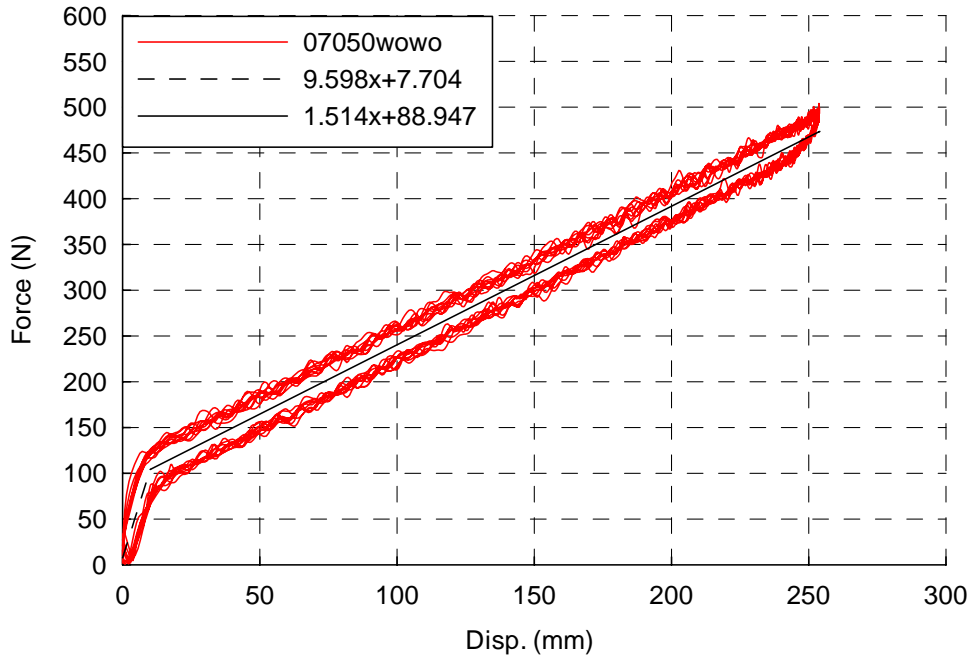


Figure 4.34 Comparison of Model Straight Lines for 1313 N/m (7.5 lb/in) Spring and Test Results of 05070wowo

As in Section 4.5.2, the comparisons of the model prediction results and the corresponding test results from test cases 05150ww and 05070ww are shown in Figs. 4.35 and 4.36 as examples, respectively. It can be found that the results from the physical model and the corresponding test results agree well with each other.

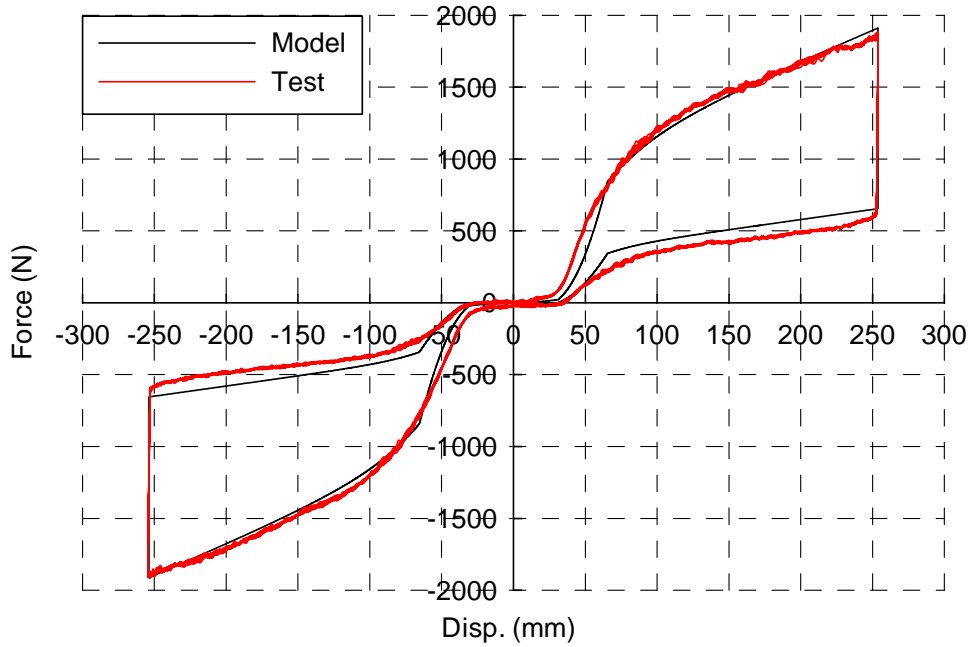


Figure 4.35 Comparison of Model Prediction for 2627 N/m (15 lb/in) Spring Unit and 05150ww Test Results

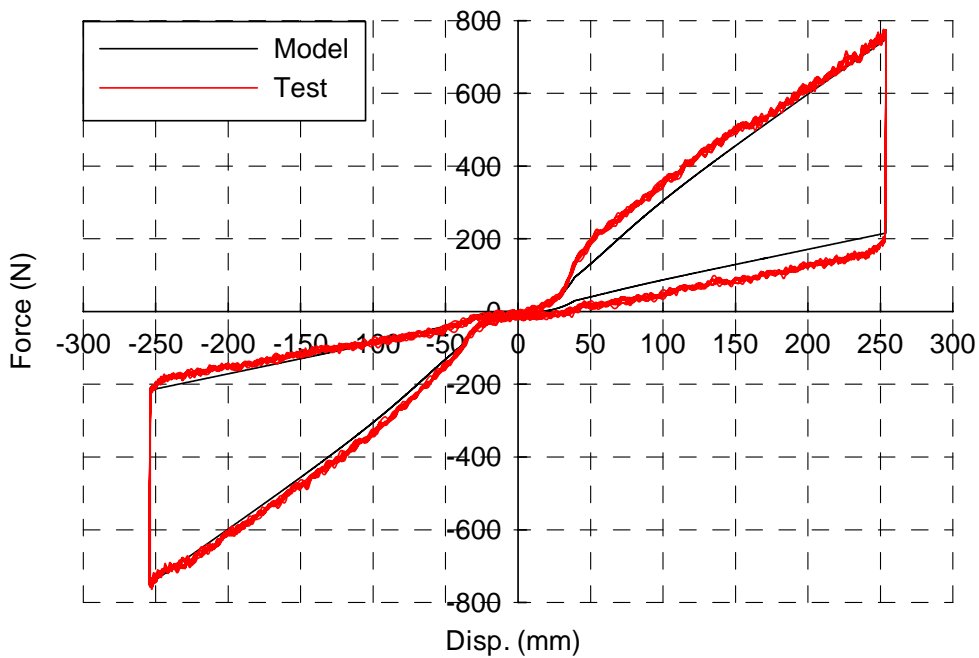


Figure 4.36 Comparison of Model Prediction for 1313 N/m (7.5 lb/in) Spring Unit and 05070ww Test Results

4.6 Sensitivity Study

For a given spring stiffness and pretension, the physical model developed in Section 4.5.2 was defined in terms of four primary parameters: the radius of the bushings around which spring cable was wrapped (r), the clear gap between the bushings (a), the friction between the internal spring and the spring unit tube (f), and the sliding coefficient of friction between the spring cable and the brass bushing in the spring unit (μ_k). To instigate how variation in the value of these parameters impact this physical model's ability to capture the behavior of the spring units, a sensitivity study was conducted.

Analyses were sequentially conducted on the four primary parameters mentioned above by separately using values 30 percent bigger and smaller than that of each parameter in the physical model. This sensitivity study was conducted using the physical model for pre-tensioned multi-directional spring units. The resulting multi-directional spring unit hysteretic behavior obtained from this sensitivity study are shown in Figs. 4.37 to 4.44 for the spring unit with a 2627 N/m nominal stiffness (i.e. Figs 4.37 to 4.40) and the spring unit with a 1313 N/m nominal stiffness (i.e. Figs. 4.41 to 4.44), respectively.

Figs. 4.37, 4.38, 4.41, and 4.42 show that a 30 percent change of radius of the bushings around which the spring cable bends, or a 30 percent change in the clear distance between the bushings, do not result in a significant difference in behavior. For a \mp 30 percent variation in the radius of the bushings, the initial stiffness (for both loading and unloading branches) of the hysteretic curve increases and decreases by 15 percent on average. However, the secondary stiffness practically remains unchanged. The transition point between these two stiffnesses correspondingly occurs earlier and later than in the original reference system for both the loading and unloading branches of the curve. For a \mp 30 percent change in the clear distance between the bushings, the same trends observed above are found, except that the change in magnitude of

initial stiffness, compared to the original system, is on average 9 percent. Figs. 4.39 and 4.43 show the physical model is not sensitive to a 30 percent variation of the friction coefficient between the internal spring and the spring unit tube, as the corresponding hysteretic curves practically coincide with each other. The physical model is, however, more sensitive to variations in the sliding coefficient of friction between the spring cable and the brass bushing in the spring unit. Significant difference in behavior (i.e., force value difference at same displacement) can be found from Figs. 4.40 and 4.44 for the spring units having 2627 N/m and 1313 N/m nominal stiffness spring units, respectively. Note that the hysteretic curve will expand when the sliding friction coefficient increases, which means the loading branch goes further away from the abscissa axis and the unloading branch will come closer to the abscissa axis. It can be found that for the loading branch of the curve, for a ± 30 percent variation of the sliding coefficient, the initial stiffness and the secondary stiffness both correspondingly either increase or decrease, respectively. The change magnitude is 13 percent and 18 percent on average for the initial and secondary stiffnesses under this case, respectively. In addition, the maximum force developed is on average ± 17 percent of that of the original system, respectively. For the unloading branch of the hysteretic curve, the trend observed above is reversed. However, the transition point between the two different stiffnesses in each branch practically remains at the same displacement in this case.

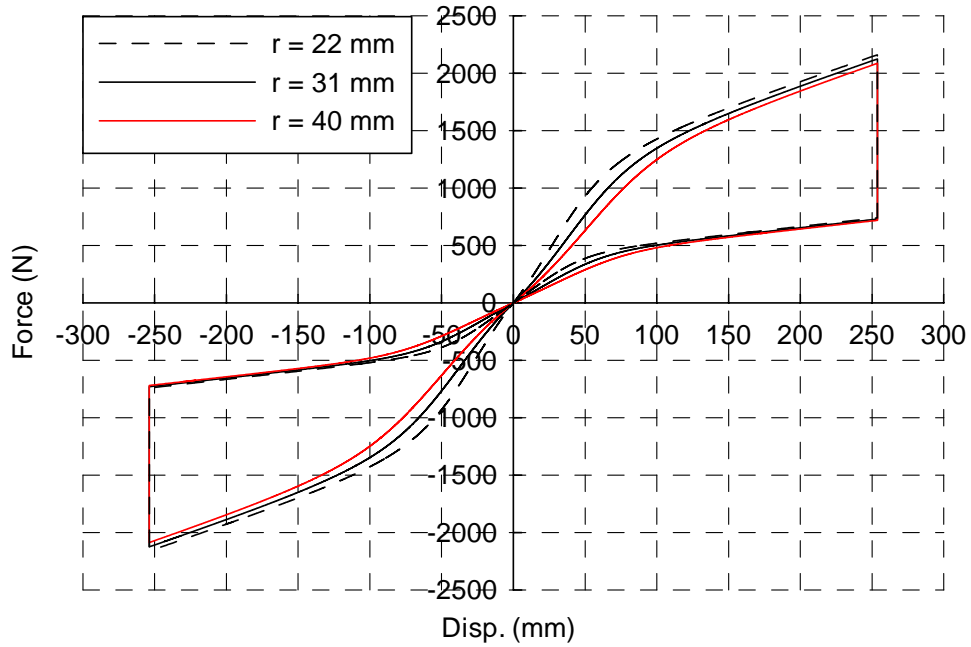


Figure 4.37 Comparison of Behaviors of 2627 N/m Spring Unit under Different r Values

$(a = 20 \text{ mm}, f = 18 \text{ N}, \mu_k = 0.171)$

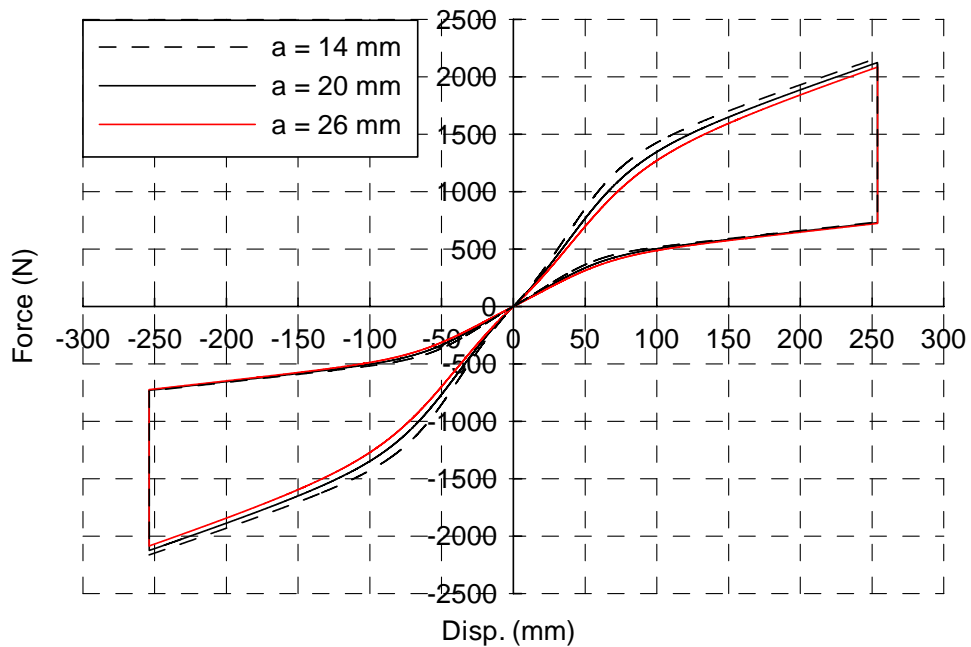


Figure 4.38 Comparison of Behaviors of 2627 N/m Spring Unit under Different a Values

$(r = 31 \text{ mm}, f = 18 \text{ N}, \mu_k = 0.171)$

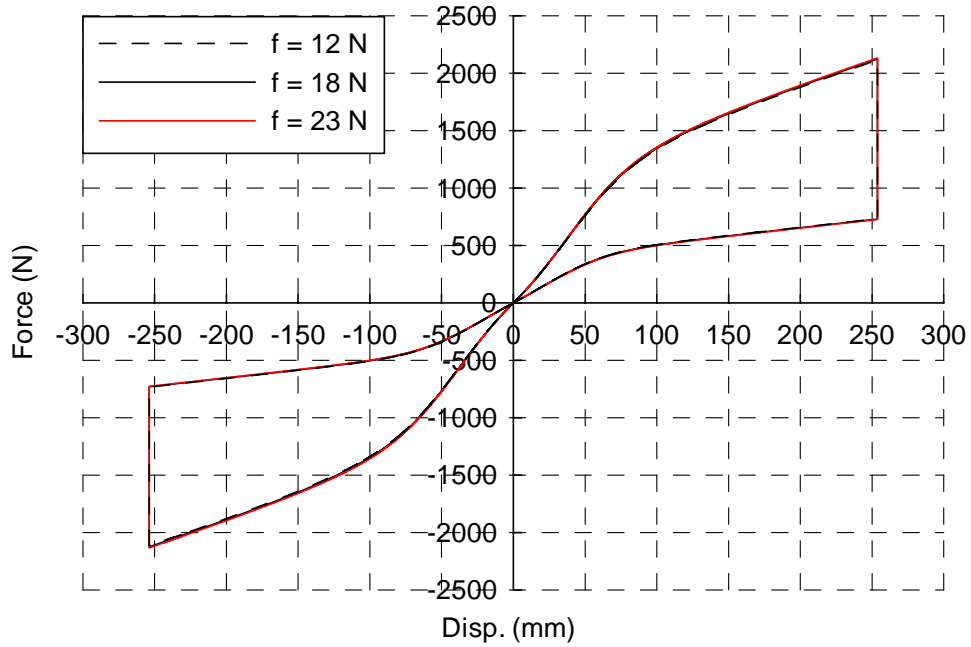


Figure 4.39 Comparison of Behaviors of 2627 N/m Spring Unit under Different f Values
 ($r=31$ mm, $a=20$ mm, $\mu_k = 0.171$)

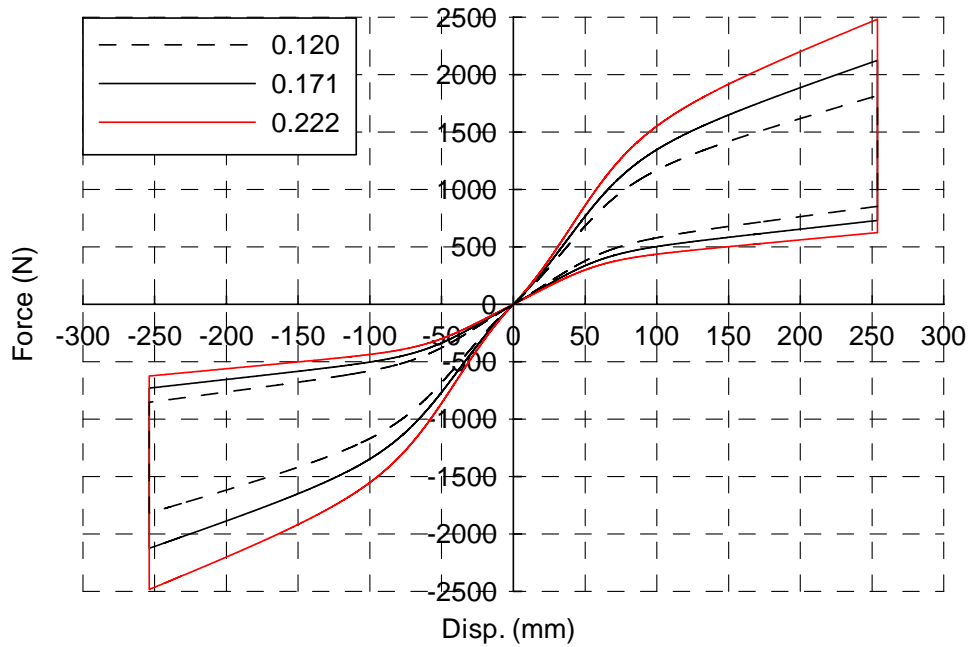


Figure 4.40 Comparison of Behaviors of 2627 N/m Spring Unit under Different μ_k Values
 ($r=31$ mm, $a=20$ mm, $f=18$ N)

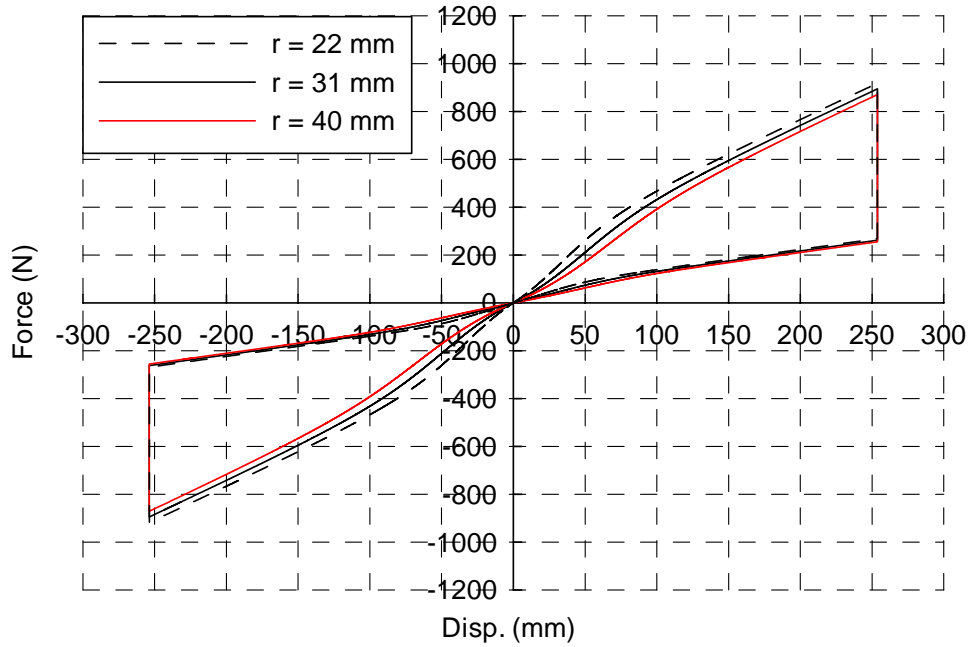


Figure 4.41 Comparison of Behaviors of 1313 N/m Spring Unit under Different r Values

$(a = 20 \text{ mm}, f = 18 \text{ N}, \mu_k = 0.190)$

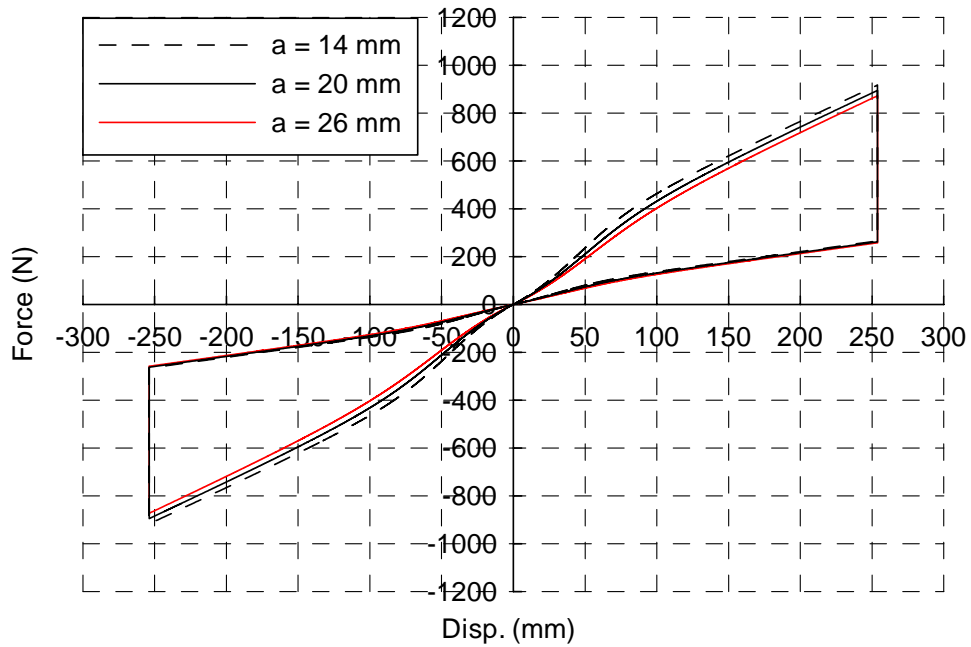


Figure 4.42 Comparison of Behaviors of 1313 N/m Spring Unit under Different a Values

$(r = 31 \text{ mm}, \mu_k = 0.190, f = 18 \text{ N})$

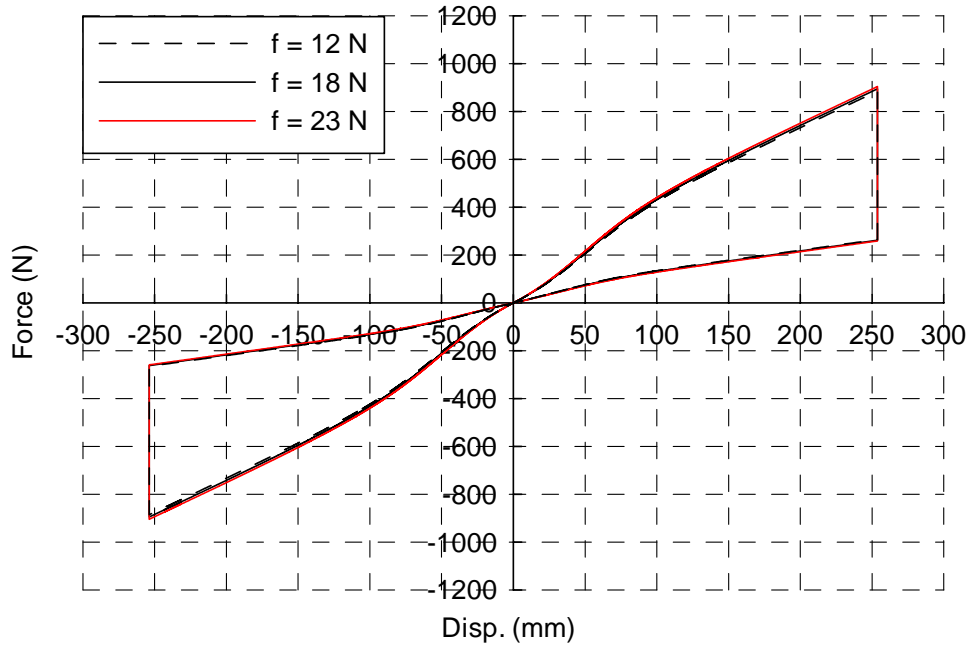


Figure 4.43 Comparison of Behaviors of 1313 N/m Spring Unit under Different f Values
 ($r=31$ mm, $a=20$ mm, $\mu_k = 0.171$)

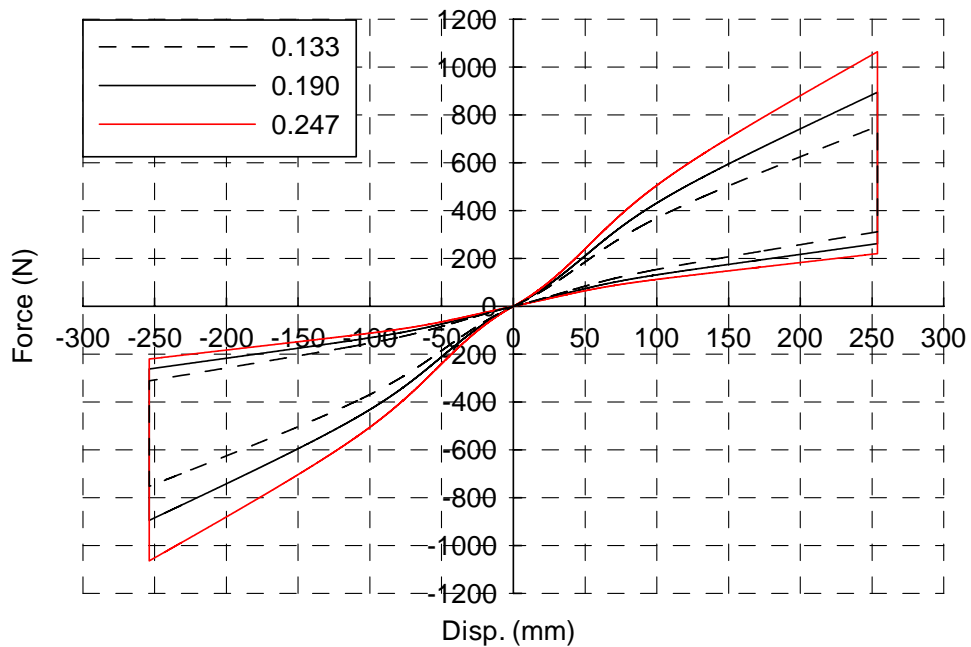


Figure 4.44 Comparison of Behaviors of 1313 N/m Spring Unit under Different μ_k Values
 ($r=31$ mm, $a=20$ mm, $f=18$ N)

4.7 Observations

This chapter presented research conducted to characterize the behavior of multi-directional spring units used in an isolated floor system. From the tests, it can be found that the behavior of the spring units is stable under repeated cyclic motion and independent of velocity of motion. The test results also show that the behavior of both the springs used in spring units and the complete spring units is unusual. The force-displacement curves of the springs alone without any pretension are mostly bilinear for 2627 N/m and 1313 N/m nominal stiffness springs, respectively. The behavior of the springs with pretension is almost linear and agrees with the corresponding linear part of the behavior of the corresponding springs from a displacement corresponding to the pretension value. The force-displacement relationships of the complete spring units, with and without pretension, are near bilinear and characterized by loading and unloading segments of different slopes. A physical model was developed to capture the unique behavior of these multi-directional spring units with and without pretension. Comparison of the results between the physical analytical model and the spring unit tests shows good agreement. A sensitivity study showed that this model is more sensitive to the sliding coefficient of friction between the spring cable and the brass bushing in the spring unit, and not so sensitive to change in the radius of the bushings around which the spring cable was bent, the clear distance between the bushings, and the friction effect between the internal spring and the spring unit tube. The physical model of multi-directional spring units provides a foundation to model the behavior of the isolated floor system studied in Chapter 5 using this kind of multi-directional spring units as isolators (which is the subject of Chapter 7).

CHAPTER 5

ISOLATED FLOOR SYSTEM II CHARACTERIZATION TEST

5.1 Introduction

As mentioned in Chapter 1, when this project started, a number of manufacturers were developing their own isolated floor system and were not in a position to release details on their systems until their patents were issued. For this reason, a special kind of concrete ball-in-cone (BNC) isolators and a corresponding isolated floor system using this kind of concrete isolators, which was named Isolated Floor System I, were designed. Characterization tests were designed to investigate their respective behaviors. After the characterization tests of the single concrete BNC isolator were completed, and just before the characterization tests of Isolated Floor System I started, an isolated floor system by Dynamic Isolation Systems (DIS) became available. This research project was therefore expanded to include this recently developed system, and to investigate its behavior. This DIS product was called Isolated Floor System II, since it was obtained after Isolated Floor System I was developed. Considering the sudden immediate availability of Isolated Floor System II, it was first tested using the shake table facilities in the Structural Engineering and Earthquake Simulation Laboratory (SEESL) at the University at Buffalo. After the tests of the Isolated Floor System II, characterization tests were conducted on the originally developed isolated floor system-Isolated Floor System I.

Chapter 4 presented the characterization tests of the multi-directional spring units from Dynamic Isolation Systems (DIS). This chapter presents the characterization tests of Isolated Floor System

II, which used this special kind of spring units as isolators. The contents of the characterization tests of Isolated Floor System I will be presented in the next chapter.

The objective of the characterization tests is to obtain the mechanical properties (such as force-displacement relationship) of Isolated Floor System II to be able to simulate its dynamic response in computer programs. In these characterization tests, to simulate the realistic conditions to be encountered when a floor isolation system is installed in an existing room, a surrounding masonry wall was built and some steel edge plates were used to cover the space between the isolated floor system and the wall. Two sets of 2627 N/m nominal stiffness spring units were investigated for this isolated floor system. Both synthetic ground motions and the analytical floor response of both single-degree-of-freedom (SDOF) and multi-degree-of-freedom (MDOF) structural fuse frames were used as seismic inputs. Besides unidirectional tests, some bidirectional tests were also conducted. Different load cases, both with symmetric and eccentric configurations of gravity loads, were considered. The mechanical properties of this system were presented in terms of acceleration-displacement relationship. Finally, several additional tests conducted on the isolated floor system using two sets of 1313 N/m nominal stiffness spring units were presented.

Combined, these tests allowed to investigate the behavior of Isolated Floor System II under different seismic inputs and different load cases. The test results were also compared from different points of view as described in Section 5.4.3, including comparison of behavior between the multi-directional spring units and the corresponding complete isolated floor system.

5.2 Isolated Floor System II Description

Isolated Floor System II is a proprietary system by DIS. To better see the details, a photo of the isolated platform of Isolated Floor System II (without the surrounding wall and steel edge plates) is shown in Fig. 5.1. Isolated Floor System II uses two sets of multi-directional spring units as described in Chapter 4, which are connected to a raised steel floor frame, to decouple the response of the nonstructural components on the isolated floor from the motion of the floor itself. The multi-directional spring units can be easily changed even after the system has been set up. Casters with a wheel diameter of about 152mm (6 in) are bolted to the steel floor frame to vertically support the loads. The steel cable of each spring unit passes through the steel bushing welded on the steel floor frame as shown in Fig. 5.2 and is then fixed to the floor frame with clamps, where the clamps tighten the cable to the vertical side of the steel channel of the floor frame. Floor panels (i.e., tiles) with a steel surface are bolted down to the floor frame and provide the walking surface. The total height of this isolated floor system is about 324 mm (12.75 in). Although it is taller than Isolated Floor System I which is only 193 mm high, it is still attractive for isolated floor system applications. The total weight of this isolated floor is about 8522 N (1916 lb).



Figure 5.1 Overview of Isolated Floor System II (without Wall and Steel Edge Plates)

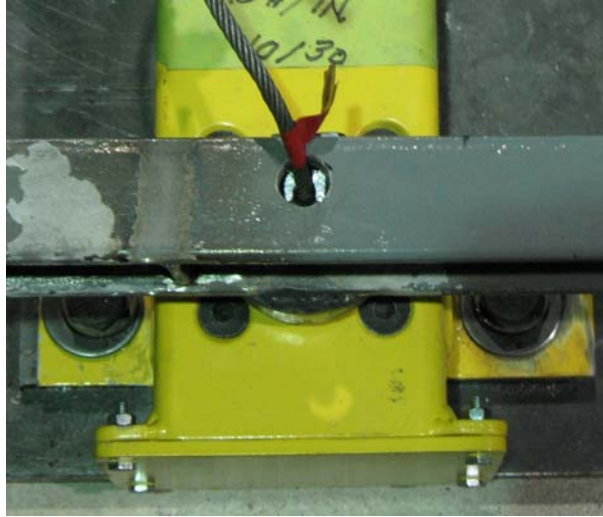


Figure 5.2 Cable Fixture of the Spring Units

5.3 Test Setup

5.3.1 Specimen Assembly and Setup

A 102 mm (4 in) thick concrete slab was designed and cast to simulate the structural floor surface on which isolated floors would be installed in a typical application. The surface of this concrete slab was finished by hand to a smoothness similar to concrete floor surfaces in buildings. No special finish was applied on the surface of this concrete slab. Furthermore, to simulate the constraints of installing such an isolated floor systems in building rooms, a 610 mm (24 in) tall masonry wall was built on the concrete slab, as shown in Fig. 5.3. Note that the space equivalent to a door opening was also included in the wall (as shown in Fig. 5.3). The inside area bounded by the wall was 3454 mm x 3454 mm (136 in x 136 in), which corresponds to the size of a small room. The concrete slab was fixed onto the shake table platform by steel angles (L4x6) and anchors bolted on the four sides of the footing slab as shown in Fig. 5.3. Note that some threaded rods were pre-cast into the slab at the corresponding positions of the anchors.

Two multi-directional spring units with 2627 N/m (15 lb/in) nominal stiffness were bolted down to steel plates which were themselves connected to the shake table by bolts running through holes in the concrete footing slab, as shown in Fig. 5.4. Two modules were assembled together above the multi-directional spring units to create the Isolated Floor System II surface, as shown in Fig. 5.5. During their installation, the cables of the two spring units underneath were pulled out 51 mm (2 in) and attached to the steel floor frame as mentioned in Section 5.2. This means that the multi-directional spring units were in pretension before tests. Finally, 8 pieces of steel edge plates, each being 1727 mm (half of the inner length of each side of the surrounding wall, 68 in) long, 610 mm (24 in) wide, and 4.8 mm (3/16 in) thick, were directly screwed down to the top surface of the “2x6” wood boards which were fixed onto the surrounding masonry wall. The bottom surface of the edge plates and the walking surface of the isolated floor were at the same level. These steel edge plates were used to cover the space between the surrounding concrete masonry wall and the isolated floor. One end of each edge plate was cut at an angle to form symmetric edges at the wall corners, as shown in Fig. 5.6. An overview of Isolated Floor System II specimen is shown in Fig. 5.7.



Figure 5.3 Concrete Footing Slab with Masonry Wall



Figure 5.4 Fixture of Spring Units



Figure 5.5 Assembly of Two Modules of the Isolated Floor System

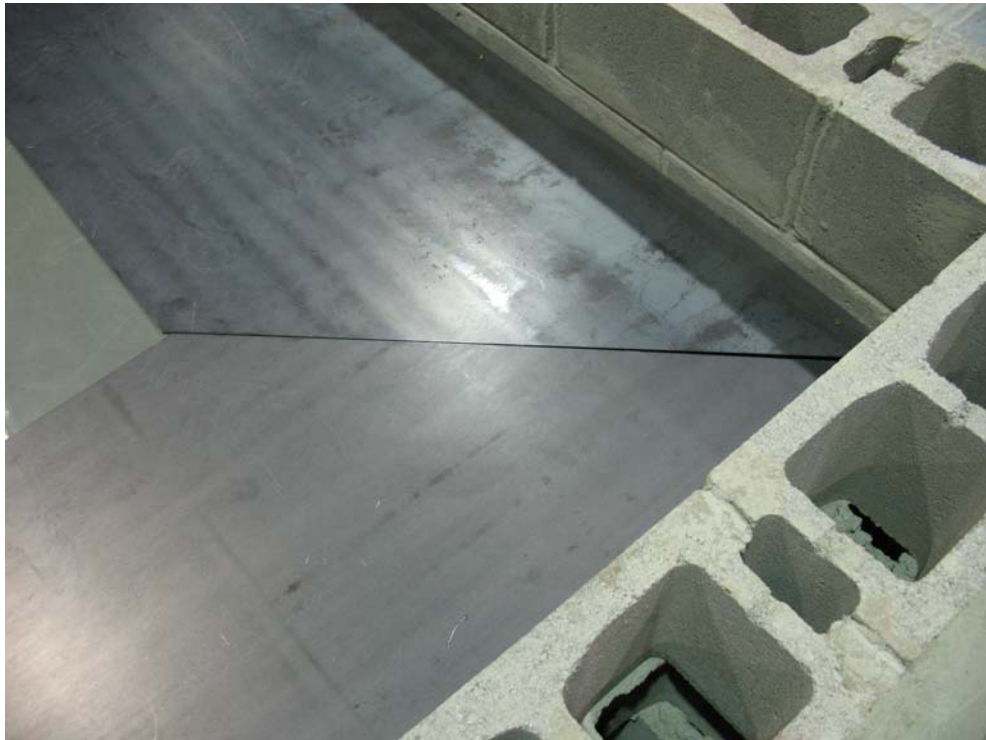


Figure 5.6 Corner Configuration of Edge Plates in Isolated Floor System II



Figure 5.7 Overview of Isolated Floor System II Specimen

5.3.2 Load Program

Two load criteria are used for the gravity load design of the isolated floor system. First, the floor has to be able to resist 0.012 MPa (250 psf) over a small area at any point over the floor system. This is referred to as the walking surface load carrying capacity. Second, the floor has to be able to resist a specified uniformly distributed load over its entire area, which is defined as the uniformly distributed load carrying capacity.

Cases with symmetric and eccentric distribution of gravity load were considered for the tests of Isolated Floor System II. Steel plates and lead bricks were placed at various locations on the isolated floor to create the different load cases. The sizes and weights of these steel plates are presented in Table 5.1. In addition, each piece of lead brick weighs around 111 N (25 lb). Based on the weights and sizes of these available steel plates, ten different load cases in total were

considered to test this isolated floor system to achieve the various conditions summarized in Table 5.2. In this table, Columns 2 and 3 respectively mean the target uniformly distributed gravity load in each load case and the corresponding realized value using the available steel plates, both of which calculated using the entire area of the isolated floor system (i.e., the area enclosed by the wall). Note that, Load Cases 1 to 3 investigate the behavior of this isolated floor system under different symmetric load cases, the only difference between these load cases being that uniformly distributed gravity loads of 0 psf, 25 psf, and 50 psf over the entire area of the isolated floor system were considered. Also, to compare the behavior of this isolated floor system under symmetric and eccentric loads and between different magnitudes of eccentricity, tests with Load Cases 5 to 8 were conducted. Load Cases 5 and 7 corresponded to floor subjected to the same gravity load magnitude as Load Case 2, but with two different values of eccentricity with respect to the X direction. For Load Cases 6 and 8, although the intent was to create a load magnitude as in Load Case 2, when attempting to locate the steel plates to create the eccentricities needed in the X and Y direction, it was found the local load value calculated based on the footprint of the steel plate on the floor exceeded the maximum permitted for the floor walking surface. Because creating large eccentricities had priority over maintaining the load magnitude, Load Cases 6 and 8, therefore, ended up being designed with a load magnitude of 14 psf instead of 25 psf, but with the correct desired eccentricities. To be able to compare the behavior of the system with symmetric layout of masses and eccentric layout of masses, Load Case 4 was created with a load magnitude of 14 psf, which is same as Load Cases 6 and 8, but with symmetric load layout.

The detailed description of how these load cases were achieved follows. The layout of the steel plates used to achieve each load case is also illustrated in Figs. 5.8 to 5.17 for each of these ten load cases considered for Isolated Floor System II, respectively, where the steel plates' dimensions are shown in inches. The layout order of the steel plates for each load case is also shown in the corresponding figures. For example, in Fig. 5.9 for Load Case 2, the layout order

means that from bottom to top, two 60" x 60" x 1.5" steel plates are stacked on top of each other under a 16-3/16" (16.2") x 16-1/16" (16.1") x 2" steel plate, itself under 2 lead bricks on top. In some instances, there are more than one steel plate on a given layer. For example, in Fig. 5.12 for Load Case 5, two 33.5" x 31" x 2" plates are laid next to each other on the bottom layer, on top of which is a 48" x 38" x 2" steel plate, itself under two 33.5" x 31" x 2" steel plates adjacent to each other. Note that in all cases, although the uniformly distributed loads were calculated and reported as if applied over the entire floor area, the steel plates could only be applied to the part of the isolated floor system that would not touch the edge plates during earthquake motions.

Table 5.1 Summary of Steel Plates

Size (1)			Quantity (pieces) (2)	Weight (N) (3)
Length (mm)	Width (mm)	Thickness (mm)		
851 (33.5)*	787 (31)	51 (2)	4	2575 (579)
1524 (60)	1524 (60)	38 (1.5)	4	6716 (1510)
1219 (48)	838 (33)	51 (2)	1	3945 (887)
411 (16.2)	408 (16.1)	51 (2)	1	623 (140)

* the numbers in paratheses are the corresponding values in U.S. customary units, i.e. in and lb.

Table 5.2 Summary of Load Cases

Load Case # (1)	Load*		Symmetric (4)	Eccentric with Respect to		EP** with Respect to	
	Target (Pa) (2)	Realization (Pa) (3)		X Direction (5)	Y Direction (6)	X Direction (%) (7)	Y Direction (%) (8)
1	0 (0)	0 (0)	√ [^]	—	—	—	—
2	1200 (25)	1200 (25)	√	—	—	—	—
3	2400 (50)	2304 (48)	√	—	—	—	—
4	1200 (25)	647 (14)	√	—	—	—	—
5	1200 (25)	1194 (25)	—	√	—	12	—
6	1200 (25)	647 (14)	—	√	√	12	12
7	1200 (25)	1194 (25)	—	√	—	19	—
8	1200 (25)	647 (14)	—	√	√	19	19
9***	Cabinet	Cabinet	—	—	—	—	—
10	Cabinet	Cabinet	—	—	—	—	—

* Load here means the uniformly distributed load value, calculated based on the area enclosed by the surrounding wall;

** For Load Cases 9 and 10, the load is referred as "Cabinet" here, and no definition of "symmetric" or "eccentric" in Columns (4) to (8) for these two load cases;

*** EP represents eccentricity percentage, calculated as the eccentricity divided by the length of each side of the inner area bounded by the wall;

^ If the term applicable for current load case, then use symbole "√", otherwise "—".

Load Case 1

In this case, no live load (i.e., steel plate) was applied on top of the isolated floor, as shown in Fig. 5.8.

Load Case 2

The target load corresponded to a uniformly distributed live load over the system's entire area of 1.2 kPa (25 psf), symmetrically applied with respect to both axes of the isolated floor. This load case, with half of the gravity load of Load Case 3 (2.4 kPa), was added to get more information about the behavior of the system under different gravity load values. The corresponding total load required was 14283 N ($25 \times 136 \times 136 / 12 / 12 = 3211$ lb), and 14278 N ($1510 + 1510 + 140 + 2 \times 25 = 3210$ lb) was actually applied (using the available steel plates) as shown in Fig. 5.9. The local walking surface load (which is the actual applied load over the footprint of the steel plate(s) on the isolated floor) was 6.1 kPa ($3210 \text{ lb} / 5 \text{ ft} / 5 \text{ ft} = 128$ psf), which was smaller than the walking surface load carrying capacity, 12 kPa (250 psf);

Load Case 3

This case corresponds to the office floor uniformly distributed design live load requirements of 2.4 kPa (50 psf) per various building codes, including the Minimum Design Loads for Buildings and Other Structures (ASCE7-05) (ASCE 2005). The corresponding total load required was 28565 N ($50 \times 136 \times 136 / 12 / 12 = 6422$ lb), and 27489 N ($1510 \times 4 + 140 = 6180$ lb) was actually applied (using the available steel plates) as shown in Fig. 5.10. The local walking surface load was 11.8 kPa ($6180 \text{ lb} / 60 \text{ in} / 60 \text{ in} = 247$ psf), which was almost equal to the walking surface load carrying capacity 12 kPa (250 psf);

Load Case 4

The target was a symmetrical uniformly distributed live load of 1.2 kPa (25 psf). The corresponding total load required was 14283 N ($25 \times 136 \times 136 / 12 / 12 = 3211$ lb), but only 7726 N ($579 \times 3 = 1737$ lb) was actually applied (using the available steel plates) as shown in Fig. 5.11 for the reason described earlier. The local walking surface load was 11.5 kPa ($1737 \text{ lb} / 33.5 \text{ in} / 31 \text{ in} = 241$ psf), which was almost equal to the walking surface load carrying capacity 12 kPa (250 psf);

Load Case 5

The case corresponds to a uniformly distributed live load of 1.2 kPa (25 psf), symmetrically applied with respect to only one axis of the isolated floor. The corresponding total load required is 14283 N ($25 \times 136 \times 136 / 12 / 12 = 3211$ lb), and 14247 N ($2316 + 887 = 3203$ lb) was actually applied as shown in Fig. 5.12. This load case had an eccentricity $e = 425$ mm (16.75 in) that corresponded to a ratio e/D of 12%, where D is the width of the isolated floor system (i.e. the length of each side of the square area surrounded by the masonry wall). The local walking surface load was 10.6 kPa ($3203 \text{ lb} / 33.5 \text{ in} / 31 \text{ in} / 2 = 222$ psf), which was 11% smaller than the walking surface load carrying capacity 12 kPa (250 psf);

Load Case 6

The target of this case was a uniformly distributed live load of 1.2 kPa (25 psf), eccentric to both axes of the isolated floor. The corresponding total load required was 14283 N ($25 \times 136 \times 136 / 12 / 12 = 3211$ lb), but only 7726 N ($579 \times 3 = 1737$ lb) was actually applied as shown in Fig. 5.13 for the reason described earlier. This load case had an eccentricity $e = 425$ mm (16.75 in) in both directions that corresponded to a ratio e/D of 12%. The local walking surface load was 11.5 kPa (1737 lb/ 33.5 in/ 31 in= 241 psf), which was almost equal to the walking surface load carrying capacity 12 kPa (250 psf);

Load Case 7

The target live load of 1.2 kPa (25 psf) for this case was only symmetrical with respect to one axis of the isolated floor. The corresponding total load requirement was 14283 N ($25 \times 136 \times 136 / 12 / 12 = 3211$ lb), and 14247 N ($2316 + 887 = 3203$ lb) was actually applied as shown in Fig. 5.14. Note that the bottom layer of steel plates was put 19 mm (0.75 in) away from the central line of the isolated floor and each layer of steel plate makes an offset of 229 mm (9 in) with respect to the adjacent bottom one to obtain large eccentricity. This case had an eccentricity $e = 671$ mm (26.43 in) that corresponded to a ratio e/D 19%. The local walking surface load was 10.6 kPa (3203 lb/ 33.5 in/ 31 in/ $2 = 222$ psf), which was 11% smaller than the walking surface load carrying capacity 12 kPa (250 psf);

Load Case 8

The target live load of 1.2 kPa (25 psf) for this case was eccentric with respect to both axes of the isolated floor. The corresponding total load requirement was 14283 N ($25 \times 136 \times 136 / 12 / 12 = 3211$ lb), but only 7726 N ($579 \times 3 = 1737$ lb) was actually applied as shown in Fig. 5.15 for the reason described earlier. Note that the bottom layer of steel plates was put 19 mm (0.75 in) and 83 mm (3.25 in), respectively, away from the central lines of the isolated floor and each layer of steel plate makes an offset of 229 mm (9 in) and 203 mm (8 in), respectively, with respect to the

adjacent bottom one in two directions to obtain bigger eccentricity. This load case had an eccentricity $e = 673 \text{ mm}$ (26.5 in) in both directions that corresponds to a ratio e/D of 19%. The local walking surface load was 11.5 kPa ($1737 \text{ lb}/33.5 \text{ in}/31 \text{ in}=241 \text{ psf}$), which was almost equal to the walking surface load carrying capacity 12 kPa (250 psf);

Load Case 9

The objective of this load case was to simulate the consequence on behavior of heavy furniture placed on the edge cover plates against the design intent, such as a heavy file cabinet sitting both on the steel edge plate and on the isolated floor. One small cabinet $381 \text{ mm} \times 673 \text{ mm} \times 737 \text{ mm}$ (15 in x 26.5 in x 29 in) in size was filled with 27 lead bricks, totally 3002 N (675 lb), and placed as shown in Fig. 5.16. The local walking surface load was 11.7 kPa ($675 \text{ lb}/15 \text{ in}/26.5 \text{ in}=245 \text{ psf}$), which was almost equal to the walking surface load capacity 12 kPa (250 psf);

Load Case 10

The objective of this load case was the same as in Load Case 9, but considering heavy furniture entirely on the edge cover plate instead of partly resting on it. The same cabinet as in Load Case 9, with 27 lead bricks inside and total weight of 3002 N (675 lb), was located as shown in Fig. 5.17. The local walking surface load was 11.7 kPa ($675 \text{ lb}/15 \text{ in}/26.5 \text{ in}=245 \text{ psf}$), which was almost equal to the walking surface load capacity 12 kPa (250 psf).

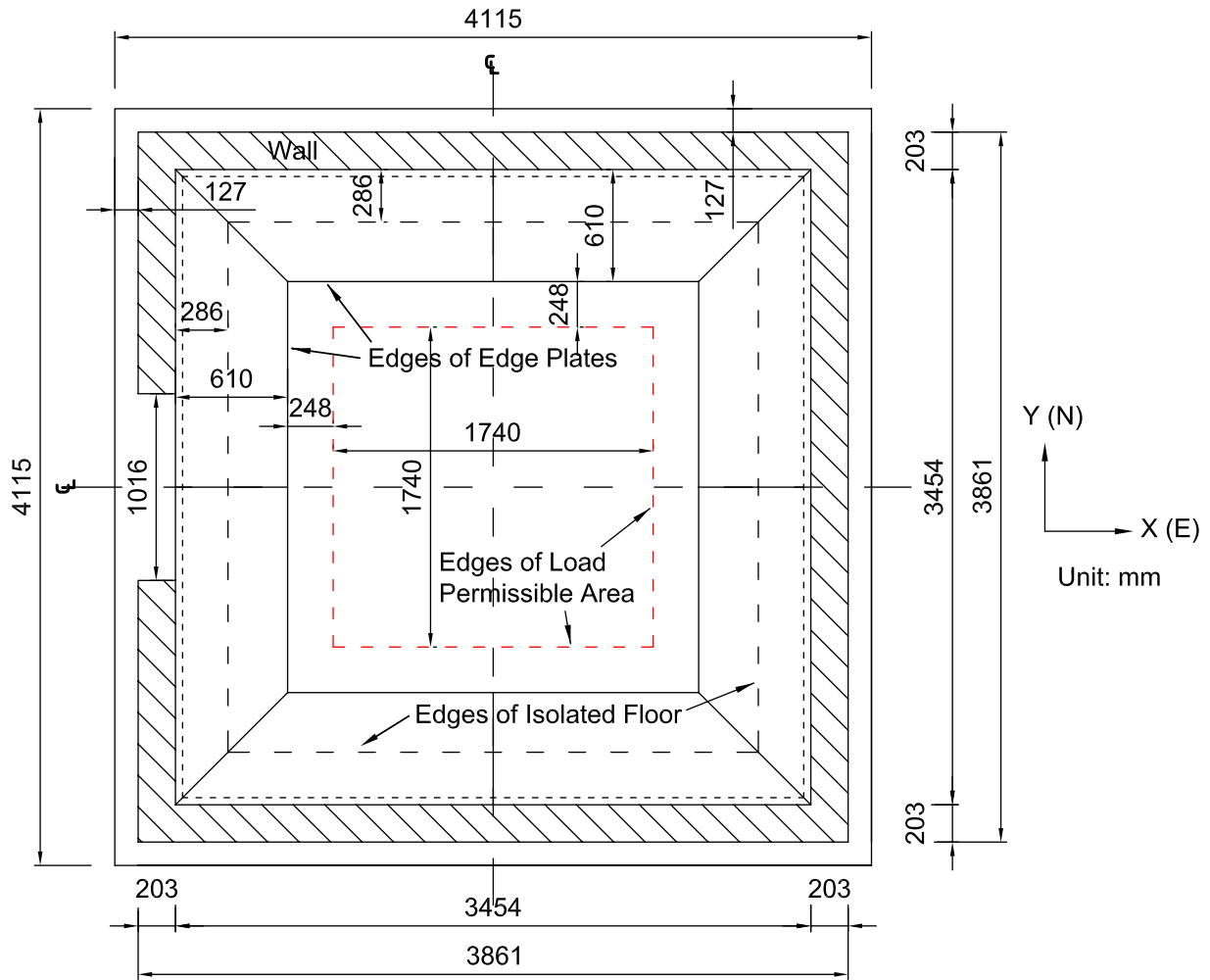


Figure 5.8 Top View of Load Case 1

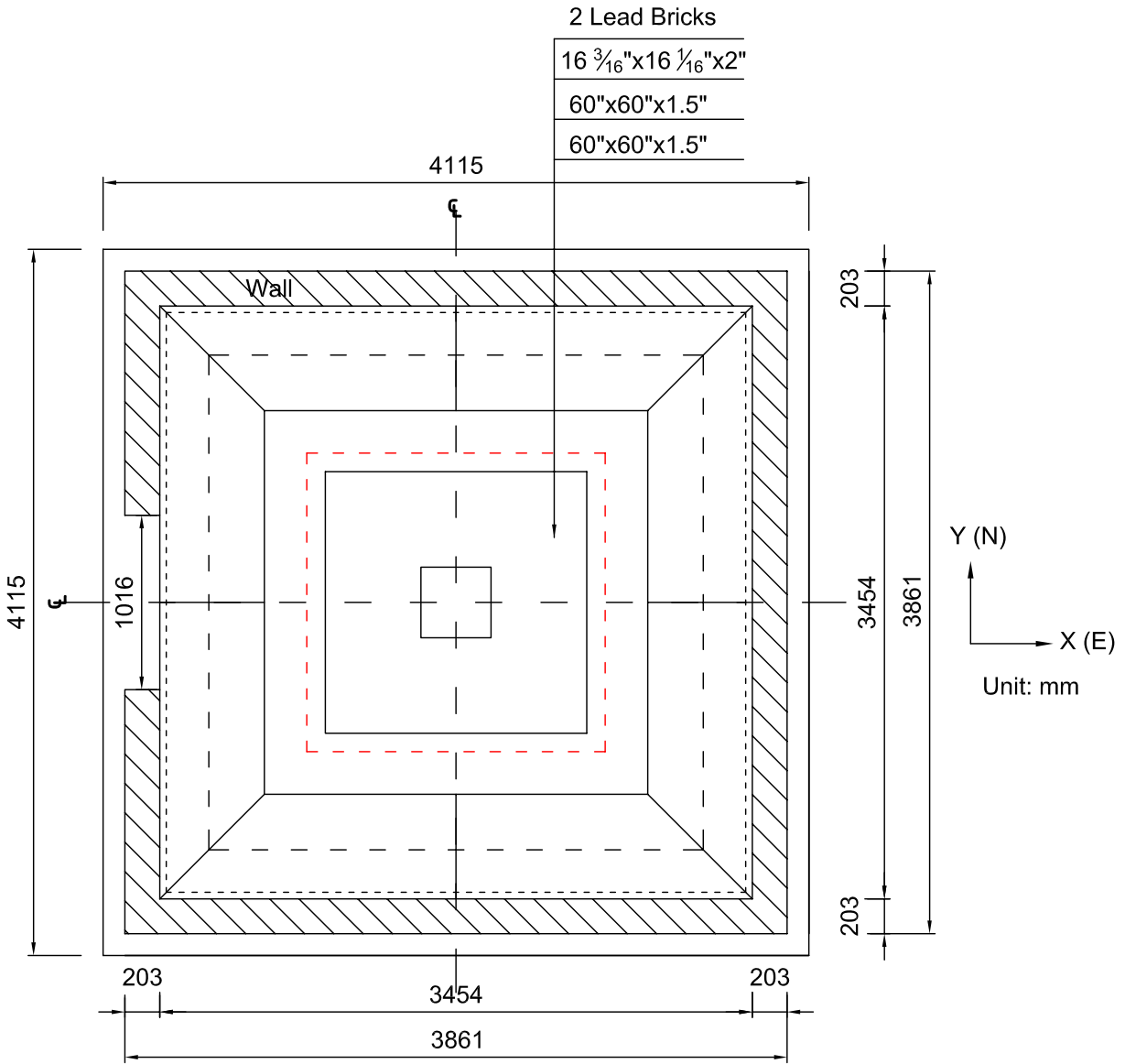


Figure 5.9 Top View of Load Case 2

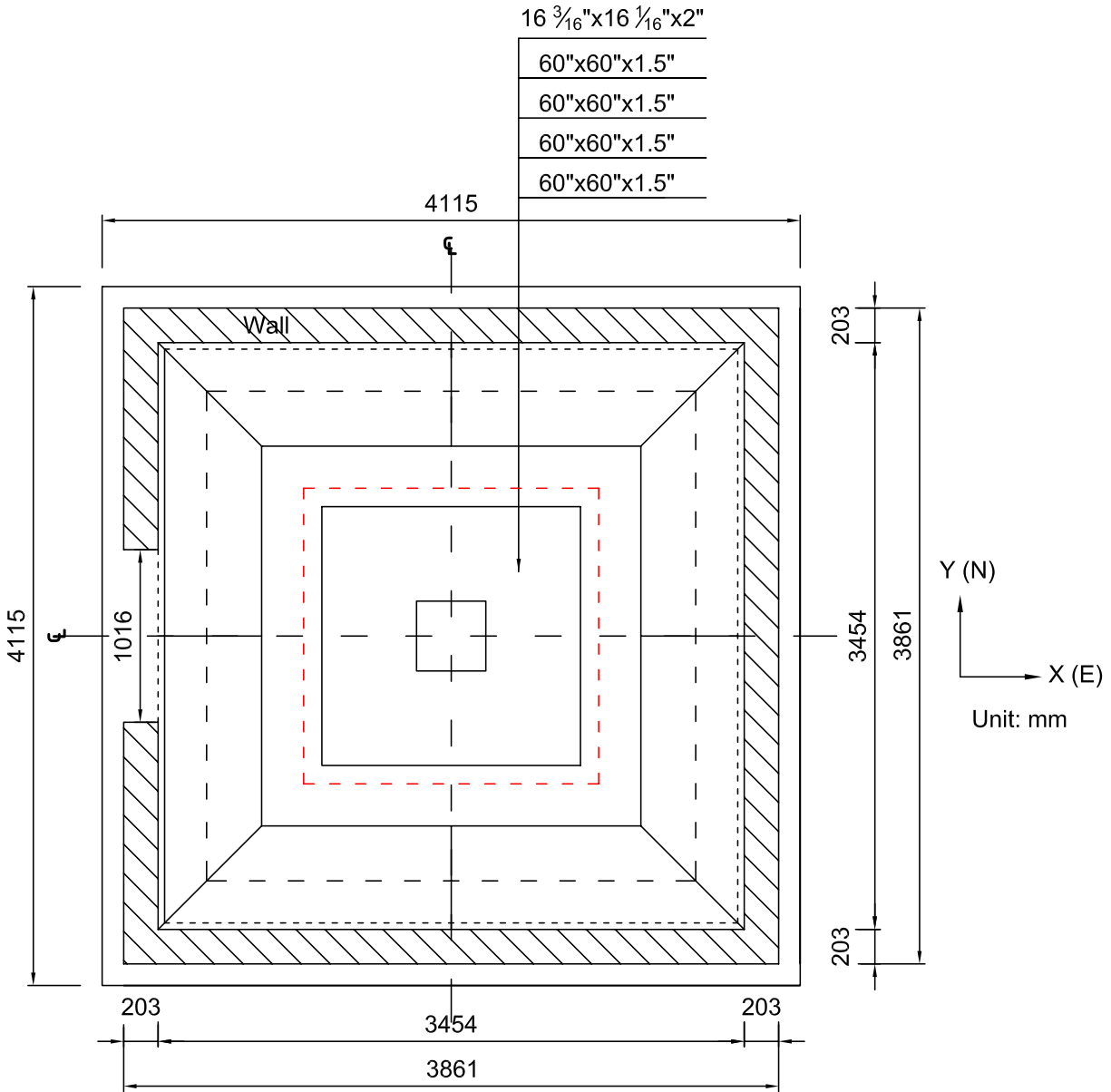


Figure 5.10 Top View of Load Case 3

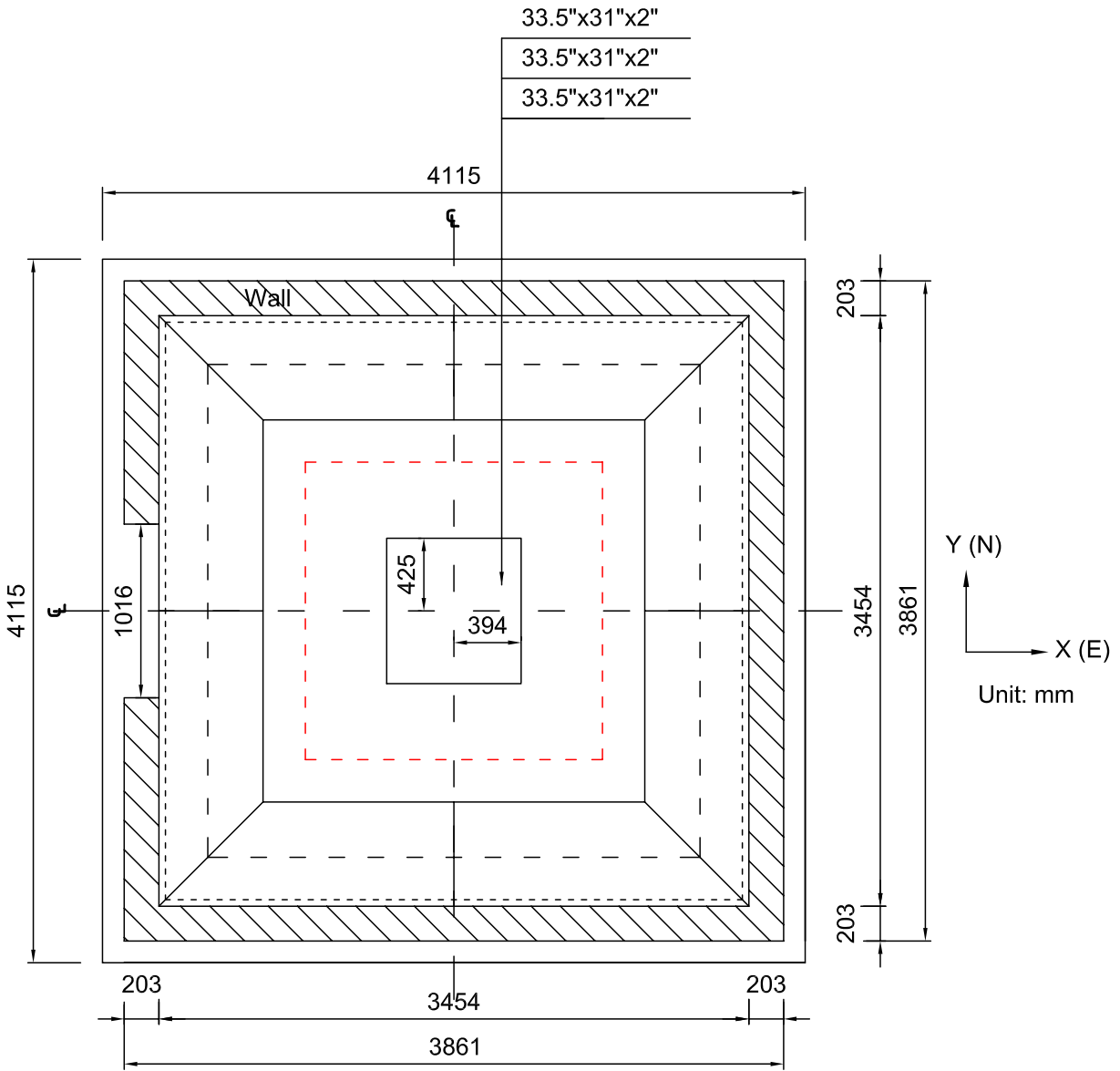


Figure 5.11 Top View of Load Case 4

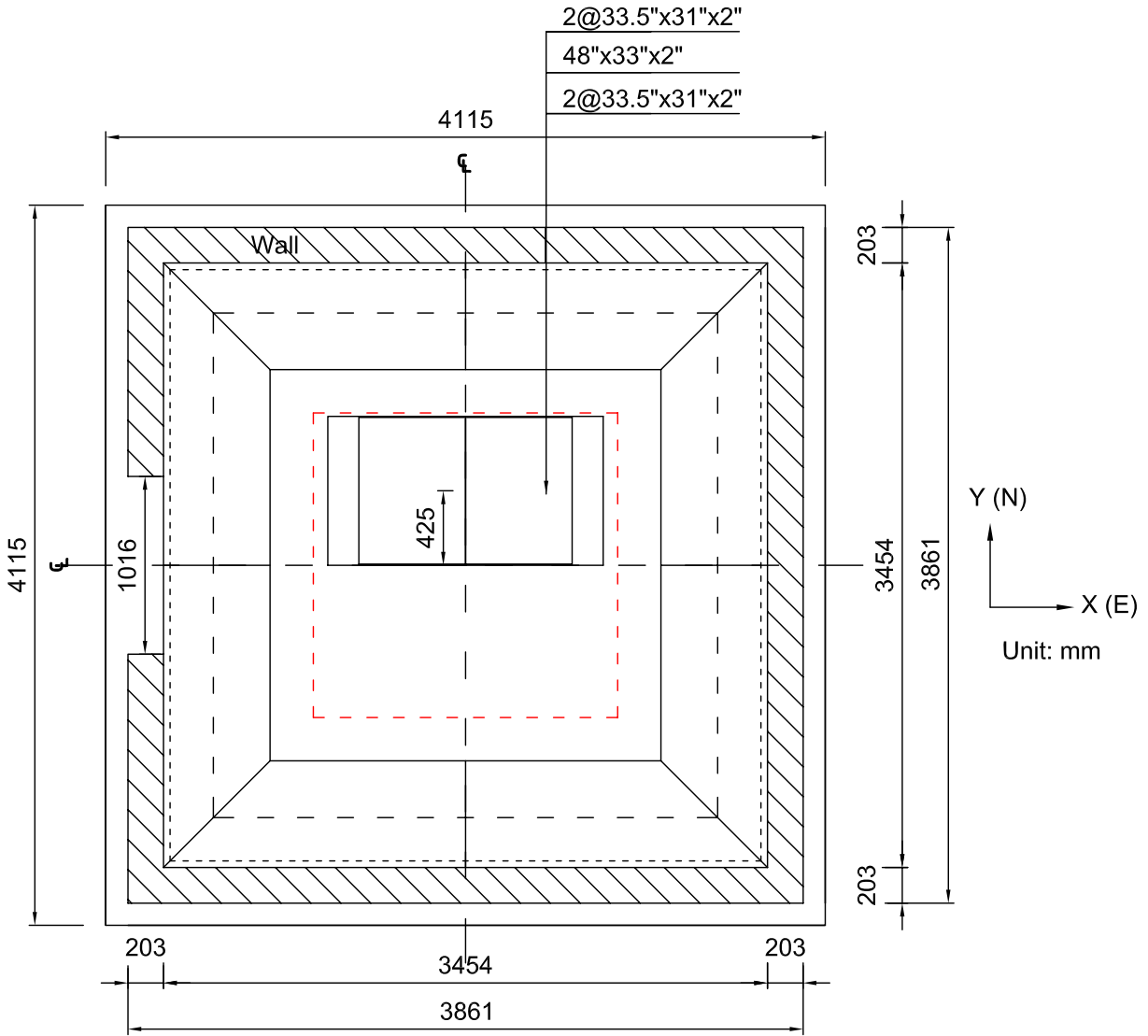


Figure 5.12 Top View of Load Case 5

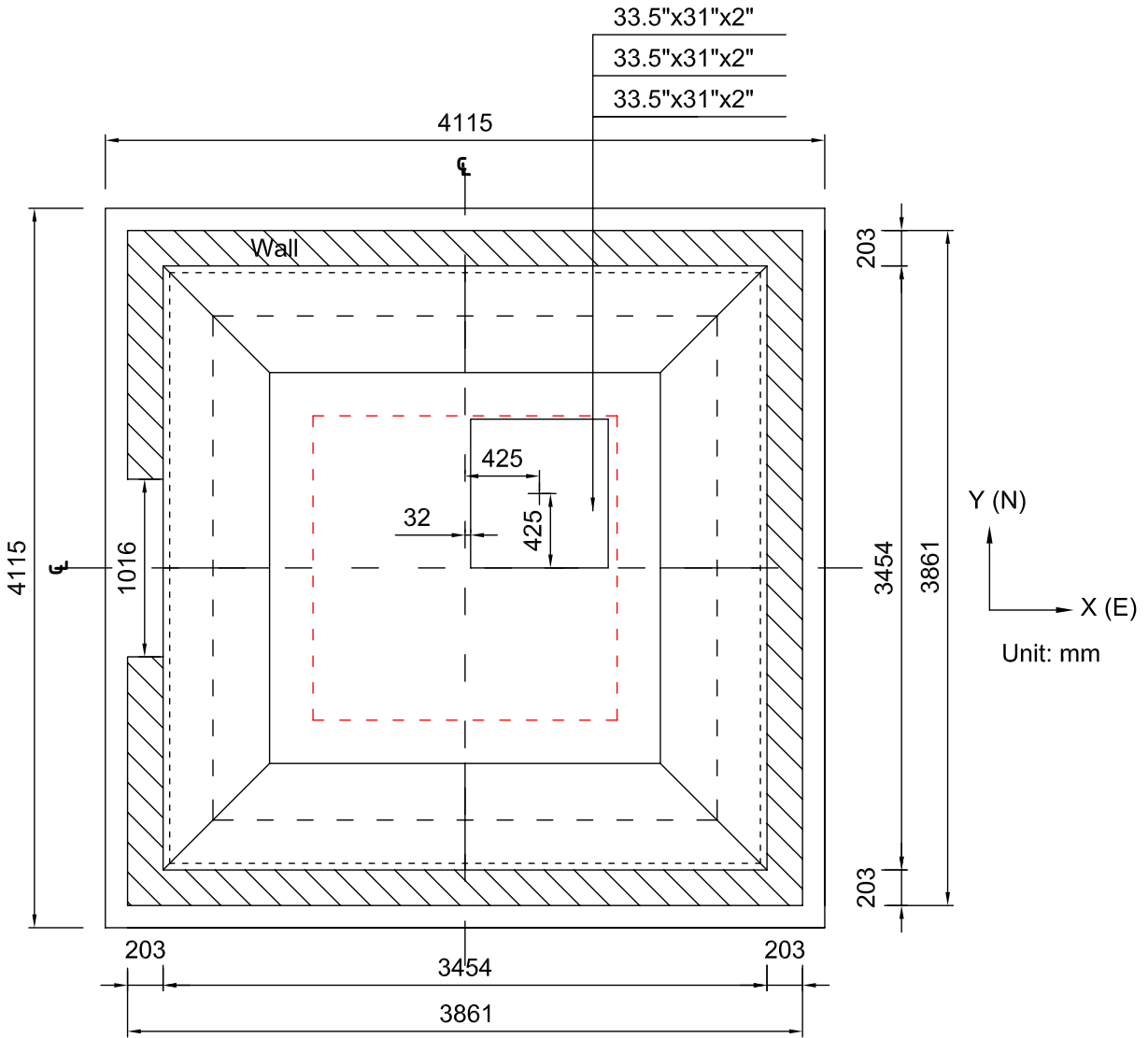


Figure 5.13 Top View of Load Case 6

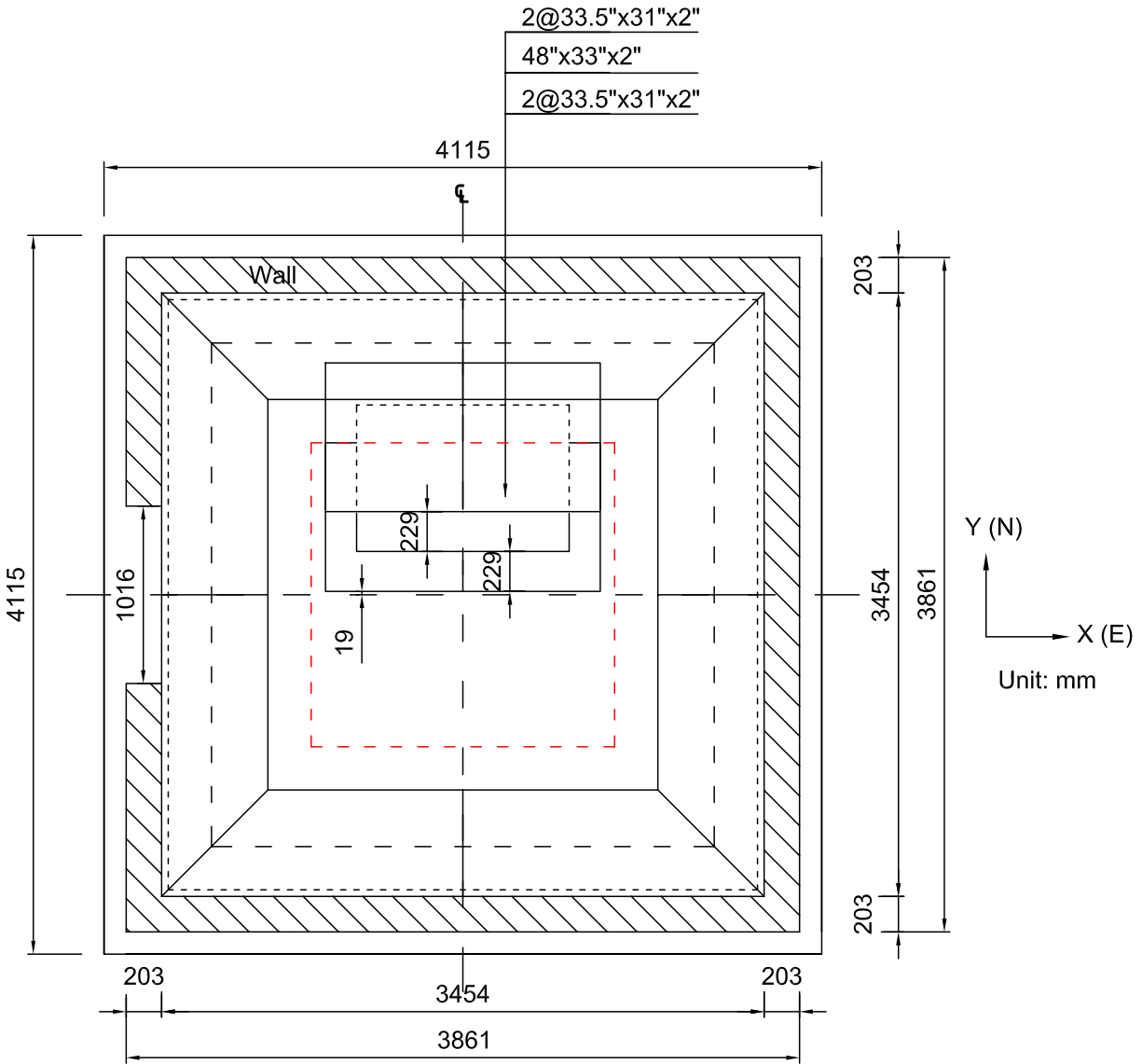


Figure 5.14 Top View of Load Case 7

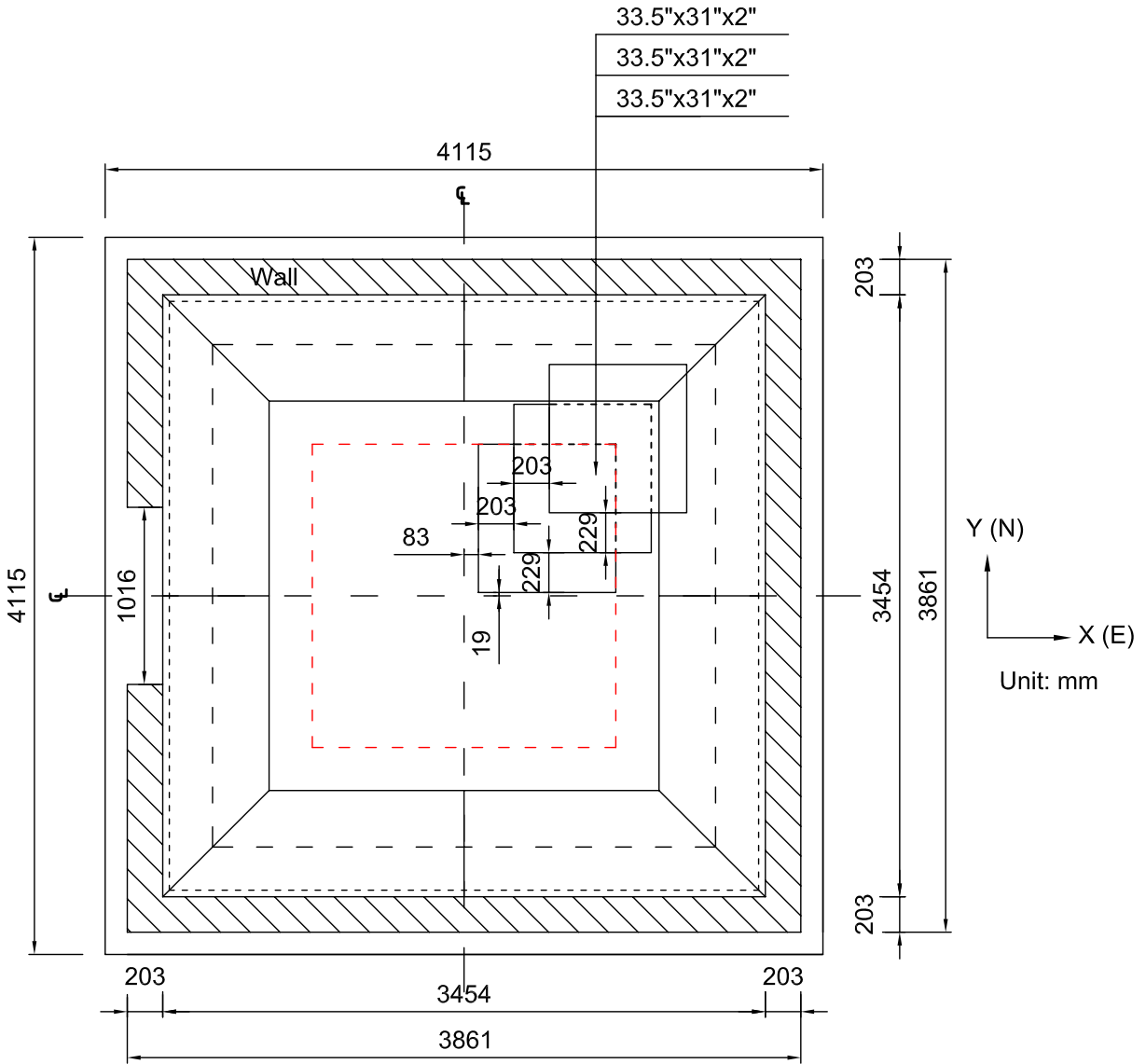


Figure 5.15 Top View of Load Case 8

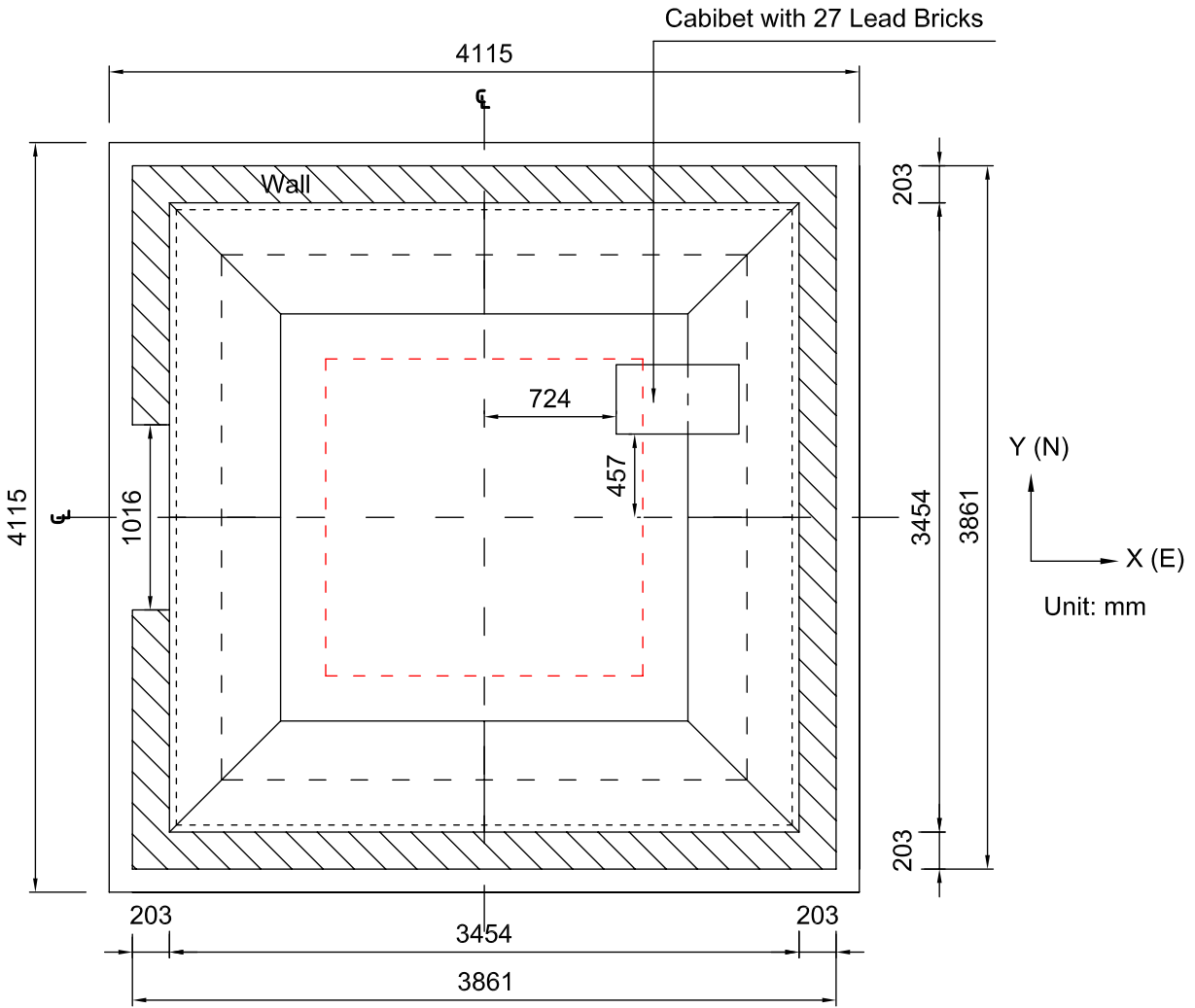


Figure 5.16 Top View of Load Case 9

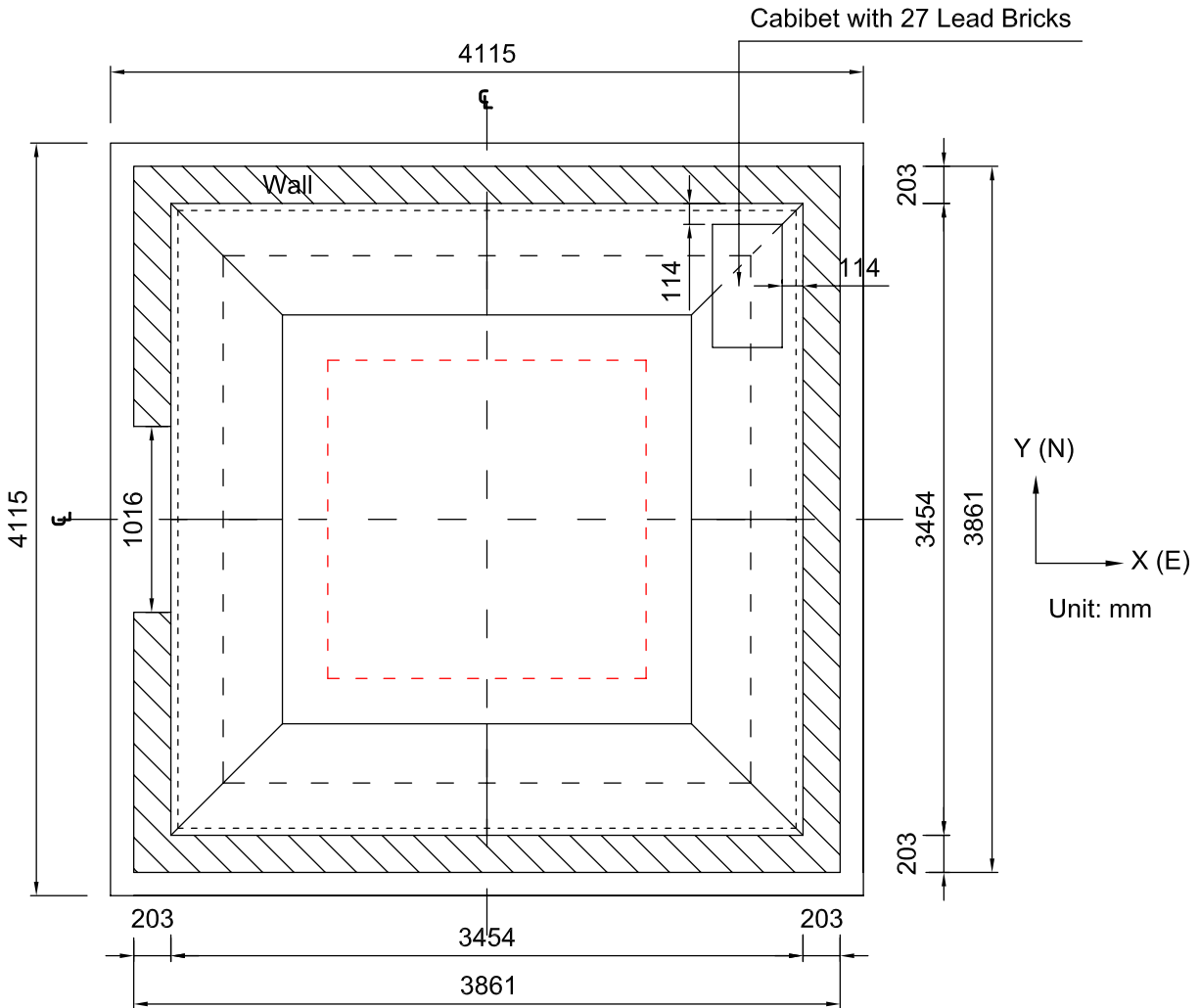


Figure 5.17 Top View of Load Case 10

5.3.3 Input Program

The characterization tests of Isolated Floor System II included both unidirectional and bidirectional tests. For unidirectional tests, spectra compatible acceleration time histories were generated and used as seismic inputs as mentioned in Section 3.3.3. Here, Acc01 and Acc02, generated in Section 3.4.3 and shown in Figs. 5.18 and 5.19, respectively, were used to either test the isolated floor system directly, or to generate floor response time histories for this purpose. The resulting analytical floor absolute acceleration response records of three structural fuse

frames obtained from analysis in SAP2000 (Computers and Structures Inc. 2004) were used as seismic inputs to test Isolated Floor System II. First, as in Section 3.3.3, the same single-degree-of-freedom (SODF) structural fuse frame with natural vibration period of 0.53 s, and designed by Vargas and Bruneau (2006a), was modeled and analyzed to obtain the floor absolute acceleration records corresponding to synthetic ground acceleration time history Acc01. The resulting motion is denoted as Acc11 and shown in Fig. 5.20. Second, a 4-story, 3-bay structural fuse frame, also designed in Vargas and Bruneau (2006a) was also modeled and analyzed by using Acc01 as ground motion, which used buckling resistant braces (BRBs) as energy dissipation devices in each story. The dimensions of this frame and its structural members are summarized in Table 5.3. The absolute acceleration records of the third story was used as seismic input to test Isolated Floor System II. It is shown in Fig. 5.21 and denoted as Acc31. Third, the actual structural fuse frame specimen tested by Vargas and Bruneau (2006b) was analyzed using the shake table motion recorded during the test at 0.75g amplitude. It is a 3-story 1-bay frame. The properties and dimensions of this frame are summarized in Table 5.4. The second floor absolute acceleration response (shown in Fig. 5.22) was recorded and used as a seismic input to test Isolated Floor System II, which was denoted as Acc002.

Besides the unidirectional tests mentioned above, some bidirectional tests were also conducted on Isolated Floor System II. Two sets of combined bidirectional inputs were used. One is the combination of Acc01 and Acc02 as inputs in the E-W and N-S directions, respectively, which was denoted as C1. The second set is the combination of Acc11 and Acc31 as inputs in the E-W and N-S directions, respectively, which was denoted as C2.

Although some preliminary analysis about the response of the isolated floor system was done before the tests, this data alone was conservatively judged insufficient to accurately predict the system behavior. Therefore, to protect the specimen, each variant of the isolated floor system was first tested using a low level of seismic excitations by scaling down the above seismic inputs.

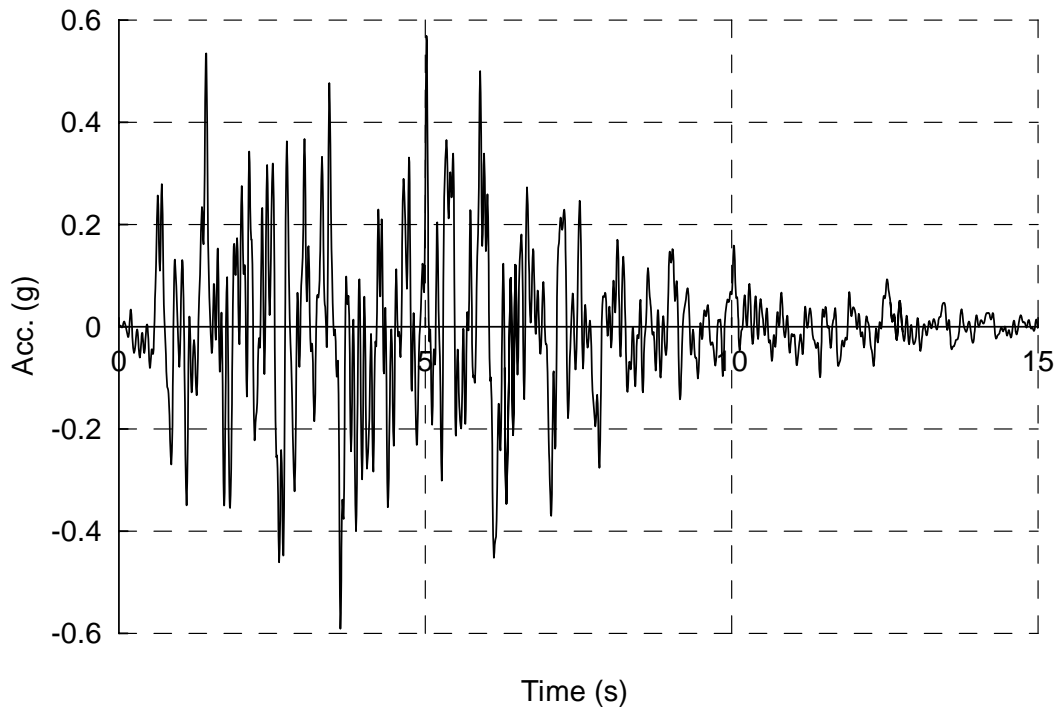


Figure 5.18 Input of Acc01

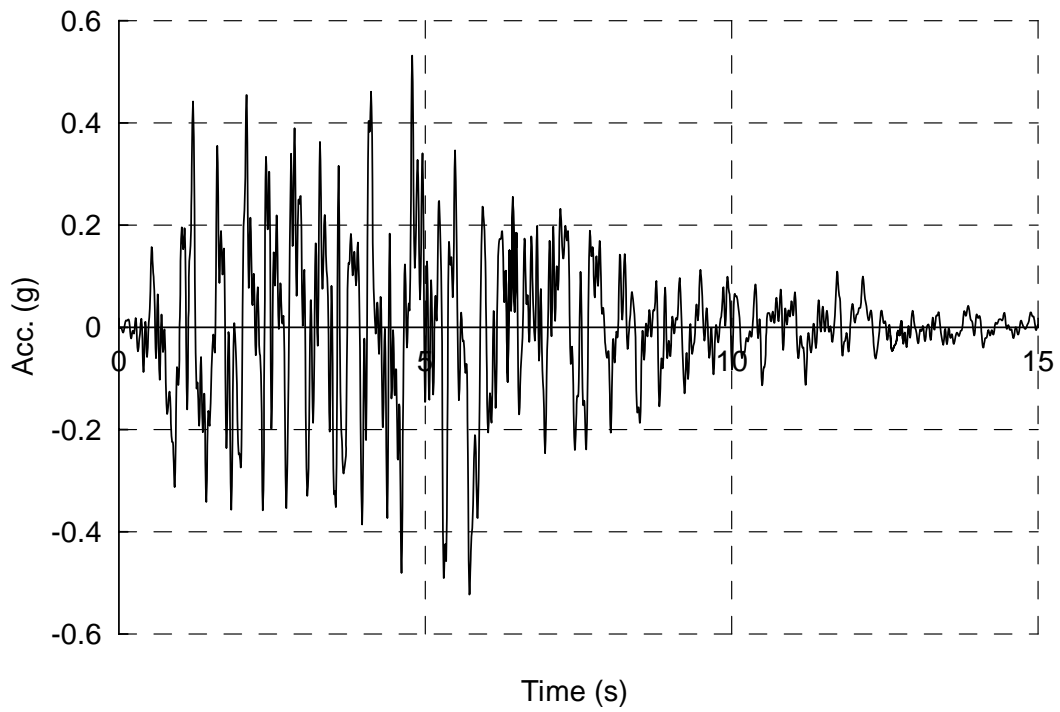


Figure 5.19 Input of Acc02

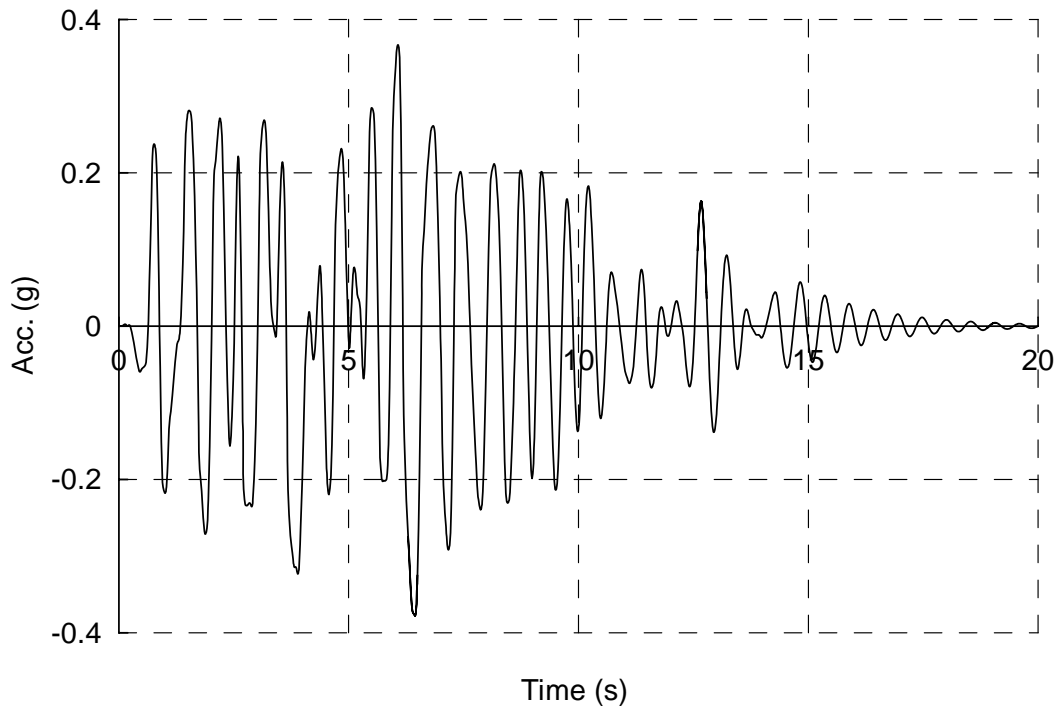


Figure 5.20 Input of Acc11

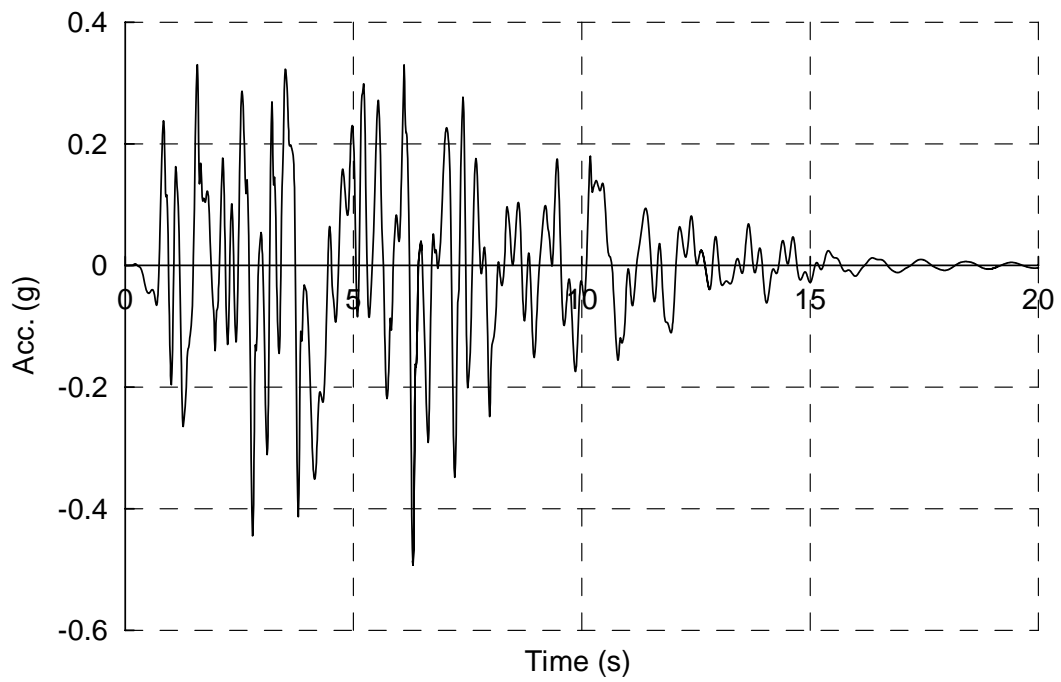


Figure 5.21 Input of Acc31

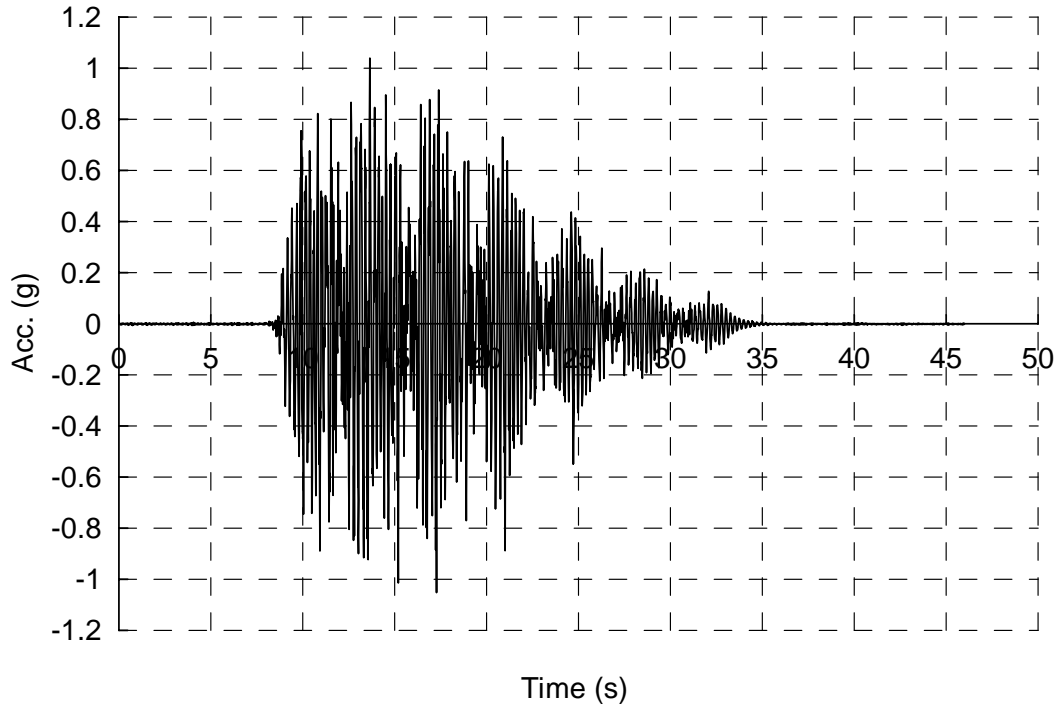


Figure 5.22 Input of Acc002

**Table 5.3 Summary of Dimensions and Elements of Structural Fuse Frame
(4-Story 3-Bay)**

Story (1)	Story Height (mm) (2)	Bay Width (mm) (3)		Beam (4)	External Column (5)	Internal Column (6)	BRB (mm) (7)
		Internal	External				
4	3810	7468	4877	w12x22	w14x34	w14x68	51x19
3	3810	7468	4877	w16x45	w14x34	w14x68	89x19
2	3810	7468	4877	w21x57	w14x61	w14x99	114x19
1	4115	7468	4877	w21x68	w14x61	w14x99	140x19

**Table 5.4 Summary of Dimensions and Elements of Structural Fuse Frame Specimen
(3-Story 1-Bay)**

Story (1)	Story Height (mm) (2)	Bay Width (mm) (3)	Beam (4)	Column (5)	BRB (mm) (6)
3	1289	2032	w6x9	w5x16	25x16
2	1289	2032	w6x9	w5x16	25x16
1	1340	2032	w6x9	w5x16	25x16

These seismic inputs were then gradually scaled up to different amplitudes to make the isolated floor system reach a displacement response of around 127 mm (5 in) in unidirectional tests and 102 (4 in) in bidirectional tests unless such displacements could not be reached due to the limits in the displacement capacity of 152 mm (6 in) of the shake table in SEESL.

5.3.4 Instrumentation

The objective of these characterization tests is to capture the force-displacement behavior of Isolated Floor System II and compare the resulting performance to that of the non-isolated floor. Here, “force” means the restoring force of the isolated floor system, and “displacement” is the relative displacement of the isolated floor with respect to the base. The restoring force of this system was to be calculated from the acceleration response of the isolated floor. Displacement and acceleration response of both the shake table and the isolated floor were measured. Furthermore, to instigate the rotation motion of the isolated floor, it was decided to measure the displacement response at both ends of each side of the isolated floor.

Twenty-four instrumentation channels in total were used to record the response of the specimen, namely, twelve accelerometers and twelve “string pots” displacement transducers. The positions of the twelve instrumentations are shown in Fig. 5.23, where the bold numbers from “1” to “12” represent the points where displacements and accelerations were measured. The description of

each channel is presented in Table 5.5 along the direction of motion recorded by each instrument. Because the surrounding wall was higher than the walking surface of the isolated floor, for the instrumentation on the walking surface, five steel rising bars were used to elevate the connecting points for the string pots so that they could be deployed straight, above the height of the wall, as shown in Fig. 5.24.

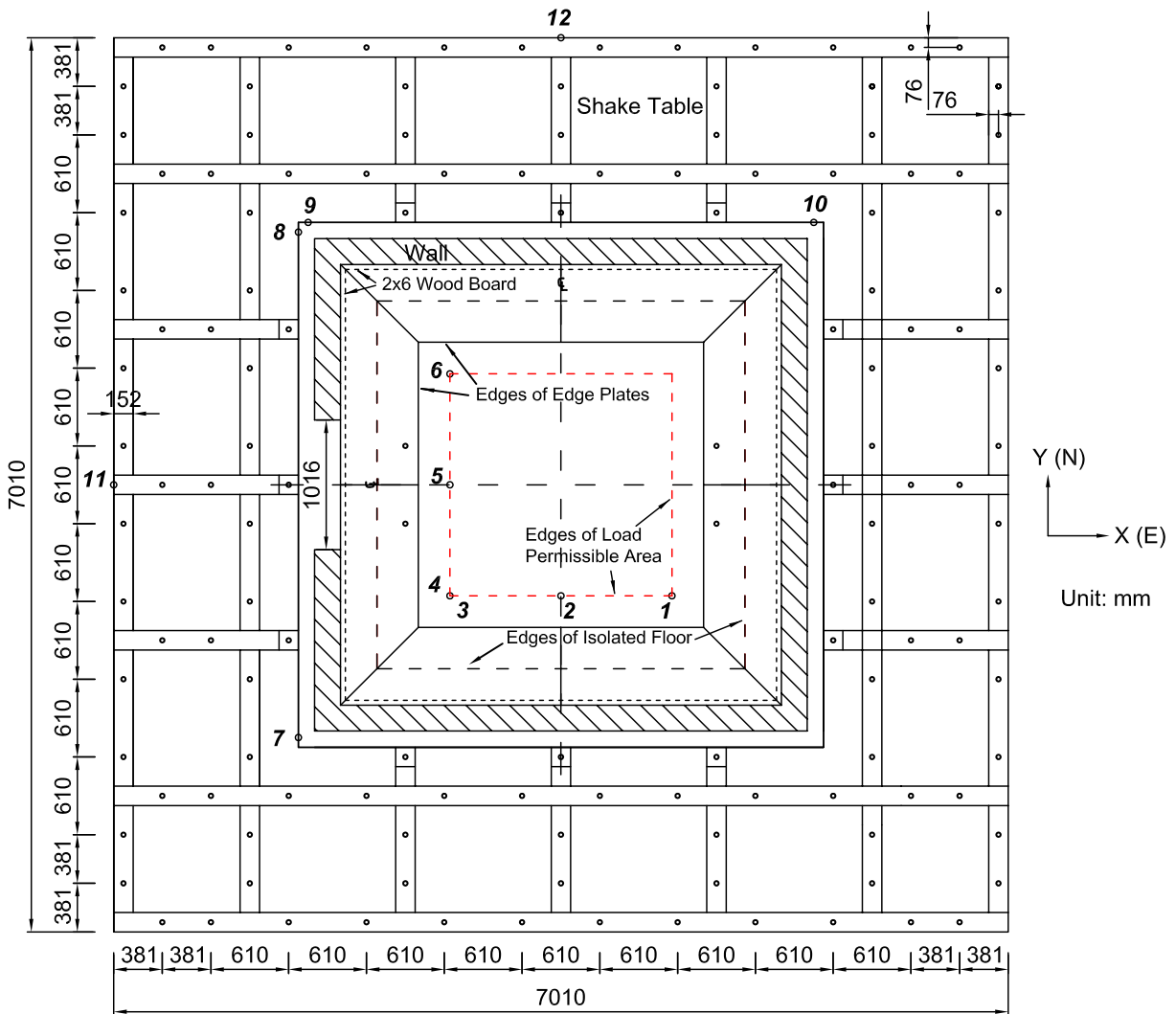


Figure 5.23 Top View of Instrumentation Positions

Table 5.5 Summary of Instrumentation Channels

Channel # (1)	Name (2)	Position* (3)	Type of Sensor (4)	Measure Direction (5)	Note (6)
1	Acc1	1	Accelerometer	N-S	Isolated floor surface**, East, South
2	Acc2	2	Accelerometer	N-S	Isolated floor surface, Middle, South
3	Acc3	3	Accelerometer	N-S	Isolated floor surface, West, South
4	Acc4	4	Accelerometer	E-W	Isolated floor surface, South,West
5	Acc5	5	Accelerometer	E-W	Isolated floor surface, Middel, West
6	Acc6	6	Accelerometer	E-W	Isolated floor surface, North, West
7	Acc7	7	Accelerometer	E-W	Footing slab, South, West
8	Acc8	8	Accelerometer	E-W	Footing slab, North, West
9	Acc9	9	Accelerometer	N-S	Footing slab, West, North
10	Acc10	10	Accelerometer	N-S	Footing slab, East, North
11	Acc11	11	Accelerometer	E-W	Shake Table,Middle, West
12	Acc12	12	Accelerometer	N-S	Shake Table,Middle, North
13	Sp1	1	String Pot	N-S	Isolated floor surface, East, South
14	Sp2	2	String Pot	N-S	Isolated floor surface, Middle, South
15	Sp3	3	String Pot	N-S	Isolated floor surface, West, South
16	Sp4	4	String Pot	E-W	Isolated floor surface, South,West
17	Sp5	5	String Pot	E-W	Isolated floor surface, Middle, West
18	Sp6	6	String Pot	E-W	Isolated floor surface, North, West
19	Sp7	7	String Pot	E-W	Footing slab, South, West
20	Sp8	8	String Pot	E-W	Footing slab, North, West
21	Sp9	9	String Pot	N-S	Footing slab, West, North
22	Sp10	10	String Pot	N-S	Footing slab, East, North
23	Sp11	11	String Pot	E-W	Shake Table,Middle, West
24	Sp12	12	String Pot	N-S	Shake Table,Middle, North

* Position means the instrumentation position in Fig. 5.23;

** Isolated floor surface actually means the rising bars fixed on the isolated floor walking surface.



Figure 5.24 Rising Bars Fixed on Walking Surface

5.3.5 Test Protocol

As mentioned in Section 5.3.2, different load cases, including symmetric and eccentric in one or two directions, were considered for these tests. The objectives of these tests are to capture the behavior of the Isolated Floor System II under each load case, instigate whether the behavior of this system is stable under each load case when subjected to different seismic input, compare the behavior of the isolated floor system under different load cases (i.e., between different symmetric load cases and between symmetric and corresponding eccentric load cases having same magnitude of gravity loads). Therefore, under each load case, especially for symmetric load cases (i.e., Load Cases 1 to 3) and the eccentric load case having relative large magnitude of gravity load (i.e., Load Case 7), tests subjected to different seismic inputs were conducted, including bidirectional inputs. Furthermore, to compare the behavior of the isolated floor system between cases with and without edge plates, several tests without edge plates and without the

surrounding concrete masonry wall were also conducted to allow comparison of the behavior of the system between with and without edge plates. Also, doing these tests without the surrounding wall allowed to test the isolated floor system to larger displacements and to see performance of the spring units as part of the isolated floor system under those larger displacements.

The sequences of the characterization tests are tabulated in Table 5.6, where the nomenclature of the test name is constructed by sequentially referring to load case number first, and the input motion name second. For example, “1Acc002” means the test of the floor under Load Case 1 when subjected to input Acc002. Also, the letters “wo” have been added at the end of the name for the tests conducted on the isolation system.

Table 5.6 Test Sequences of Isolated Floor System II

Test # (1)	Test Name (2)	Input Name (3)	Load Case # (4)	Edge Plates (5)
1	1Acc002	Acc002	1	with
2	1Acc01	Acc01	1	with
3	1Acc11	Acc11	1	with
4	1Acc31	Acc31	1	with
5	1C1	C1	1	with
6	1C2	C2	1	with
7	2Acc002	Acc002	2	with
8	2Acc01	Acc01	2	with
9	2Acc11	Acc11	2	with
10	2Acc31	Acc31	2	with
11	2C1	C1	2	with
12	2C2	C2	2	with
13	3Acc11	Acc11	3	with
14	3Acc31	Acc31	3	with
15	3C2	C2	3	with
16	4C2	C2	4	with
17	5C2	C2	5	with
18	6C2	C2	6	with
19	7Acc002	Acc002	7	with
20	7Acc01	Acc01	7	with
21	7Acc11	Acc11	7	with
22	7Acc31	Acc31	7	with
23	7C2	C2	7	with
24	8Acc31	Acc31	8	with
25	8C1	C1	8	with
26	8C2	C2	8	with
27	9Acc31	Acc31	9	with
28	9C2	C2	9	with
29	10Acc31	Acc31	10	with
30	10C1	C1	10	with
31	10C2	C2	10	with
32	2Acc31wo	Acc31	2	without
33	2C2wo	C2	2	without
34	3Acc31wo	Acc31	3	without
35	3C2wo	C2	3	without

5.4 Test Results

5.4.1 General

As mentioned in Section 5.3.3, the shake table excitations were first run at a low level of peak accelerations and then gradually scaled up. Hence, many trial tests were conducted to get the appropriate scaling factors for the inputs to reach the isolated floor's target amplitudes of displacement response. For all the tests that gave the target floor response for a given load and input condition, the peak values of the measured response quantities, including peak displacement of shake table (PTD), peak displacement of isolated floor (PFD), peak acceleration of shake table (PTA), peak acceleration of isolated floor (PFA), maximum rotation angle of the isolated floor, and peak relative displacement of isolated floor with respect to shake table, are tabulated in Table 5.7. For the E-W direction, the rotation angle is the difference in displacements measured by Sp6 and Sp4, divided by the distance between these two string pots. It is also the ratio of the displacement difference between Sp3 and Sp1 for N-S direction to the distance between these two string pots. Note that the maximum rotation angles in the E-W and N-S directions for each test are not exactly the same. The observed small differences are because the large displacement theory was not used to correct back the data. In other words, change of the axis angle of the string pots in both directions were not taken into account when creating the data as above. Note that the rotation angle is small in all cases, and not significant enough to warrant further precision. Selected typical results of the tests, listed in Table 5.7, are presented in Figs. 5.25 to 5.34. The rest of the test results summarized in Table 5.7 are presented in Appendix C. All these tests are for isolated floor systems using spring units having a nominal stiffness of 2627 N/m (15 lb/in).

Each of Figs. 5.25 to 5.34 contains four plots labeled from (a) to (d). A first plot (a) illustrates the displacement of both the shake table and the isolated floor as a function of time, for comparison

purpose. The second plot (b) presents the acceleration of both the shake table and the isolated floor as a function of time. The third plot (c) illustrates the rotation of the isolated floor as a function of time. The fourth plot (d) most importantly describes the mechanical behavior of the isolated floor system. This could be expressed in terms of a force-displacement relationship. Here, the displacement used is the relative displacement of the isolated floor with respect to the shake table, as the restoring force of the isolated floor system is a function of this displacement. However, because the restoring force of the isolated floor is equal to the isolated mass times the absolute acceleration of the isolated floor, the acceleration-displacement relationship of the isolated floor system for each test is plotted instead in part (d) of each figure. Even though it is understood that acceleration and displacement are typically out of phase, here, the sign of acceleration has been reversed when the acceleration-displacement relationship is plotted as part (d) of each figure, to make the curve resemble the restoring force-displacement relationship of the system. To be consistent, this has been done in both the acceleration-displacement curves as well as in the plots of the acceleration time histories of the system (i.e., part (b) of each figure).

5.4.2 Typical Results

Throughout all these characterization tests, no damage occurred to the isolated floor system itself. Although comparisons between the performances of various systems are done in the next section, some typical responses of the system are shown in Figs. 5.25 to 5.34. Fig. 5.25 shows the typical response of Isolated Floor System II (with edge plates) for a unidirectional earthquake floor excitation. Note from 5.25a that the floor displacement response generally follows the shake table excitation, but, the relative displacement between the isolated floor and the shake table is significant enough to produce the isolation effect. Also, note from 5.25c that the rotation of the system is not significant, which is less than 0.014 rad (i.e., 0.8 degrees). It can also be observed from the part (c) of other figures that the rotation angle of the isolated floor is not significant. Figs. 5.26 and 5.27 illustrate the case, where bidirectional earthquake excitation was used. Note

that the displacement response of the isolated floor and the shake table excitation are still generally in phase as observed before. The acceleration-displacement hysteretic curve is slightly more erratic. This may be due to the fact that the cable of the spring unit circles around the brass bushing surface in a horizontal plane during bidirectional motion.

Figs. 5.28 to 5.29 and Figs. 5.30 to 5.31 show the typical cases for Load Cases 9 and 10, respectively. Note that during the tests under Load Cases 9 and 10, where a small file cabinet filled with lead bricks was located on top and/or across of the edge plates, the isolated floor only moved slightly relatively with respect to the shake table. This is logical since it is much harder for the isolated floor to be effective for these two load cases. The file cabinet impeded the movement of the floor by creating significant friction between the walking surface and the cabinet in Load Case 9 and between the walking surface and the steel cover plates in Load Case 10. The cabinet did vibrate and slide a little bit during the tests. However, it did not overturn or hit against the wall.

Some typical responses of the isolated floor system without edge plates are shown in Figs. 5.32 to 5.34. Again, for both unidirectional and bidirectional tests under these cases, it can be observed that rotation of the isolated floor is not significant, and the displacement response of the isolated floor and the shake table are generally in phase although the relative displacement between them is significant enough to achieve the intended isolation effect. Again, the acceleration-displacement hysteretic curves are slightly more erratic in bidirectional tests than those in unidirectional cases.

From Columns (2) to (5) of Table 5.7, note that the peak displacement response of the isolated floor is typically bigger than the corresponding displacement of the shake table. Columns (6) to (9) of Table 5.7 show that the peak acceleration response of the isolated floor is reduced more or less compared to the corresponding acceleration response of the shake table, except for test of

1Acc11 where the two peak response values are almost the same. It might be because the isolated mass was small and the friction from the edge plates prevented relative displacements (a similar observation will be made in Chapter 6 for Isolated Floor System I). Also note from Columns (10) and (11) of Table 5.7 that the rotation of the isolated floor is generally not significant, even for bidirectional tests with large mass eccentricities (i.e. Load Case 7 and 8). The maximum value of the peak rotation angle for all these characterization tests is 0.071 rad (i.e., only 4.1 degrees). However, the rotation can cause an increase in the displacement response (relative to the shake table) of the isolated floor corner, which is equal to the rotation angle (in rads) times half length of the isolated floor side perpendicular to the seismic direction under consideration. This effect should be considered in the design of Isolated Floor System II. This rotation effect will be further discussed in the following section.

As shown in the typical Figs. 5.25d to 5.34d, the acceleration-displacement relationships of Isolated Floor System II exhibit hysteretic loops. As mentioned in Chapter 4, this is because of the friction between the cable and the brass bushing of the spring units. Since the acceleration of the isolated floor is directly related to the restoring force, then, the enclosed area is proportional to energy dissipation. Furthermore, the loops for each unidirectional test seem to agree with each other well, which means the behavior of the isolated floor system is stable under repeated motions. In addition, as mentioned in Chapter 4, the rising rate of the restoring force with respect to displacement significantly drops down to the system's second stiffness at displacement larger than about 76 mm (3 in) at a rate of 4.7 N/mm (27 lb/in). For the two 2627 N/m (15 lb/in) nominal stiffness multi-directional spring units used in Isolated Floor System II under given isolated weight of 8522 N (1916 lb) (i.e., Load Case 1), the slope of the system second stiffness will be $(27 \text{ lb/in} \times 2)/(1916 \text{ lb/g})=0.028 \text{ g/in}$ (where g is the acceleration of gravity), which is equivalent to a maximum acceleration plateau. Therefore, the acceleration-displacement relationship of the isolated floor system is almost flat at relatively large displacement as shown in each part (d) of Figs. 5.25 to 5.27 (for cases with edge plates) and Figs. 5.32 to 5.34 (for cases

without edge plates), which are results for tests under Load Case 2. Furthermore, when the isolated mass became larger, the maximum acceleration response of the isolated floor system will decrease when the second stiffness of the given spring units, which is a constant value, divided by the isolated mass, which will be investigated in the following section.

Finally, it is observed from the data in Columns (8) and (9) that the peak acceleration response of the isolated floor in bidirectional tests is almost the same as in unidirectional tests for each load case (i.e., for a given value of gravity load and load configuration). For example, the peak acceleration response of the isolated floor in tests of 3Acc11, 3Acc31, and 3C2 is 0.14g, 0.15g unidirectionally, and 0.14g in both directions, respectively. This is reasonable because as described before, at relatively large displacement (larger than about 76 mm (3 in)), the slope of the system second stiffness in the acceleration-displacement is a maximum acceleration plateau and the displacements in the above cases were all over 76 mm. Also, it can be observed from Table 5.7 that the peak relative displacement of the isolated floor in both directions (198.0 mm and 152.5 mm, respectively) of 3C2 are different from the corresponding values in the corresponding unidirectional tests (169.0 mm in 3Acc11 and 239.5 mm in 3Acc31, respectively). If the isolated weight became larger as in other load cases with steel plates, the system second slope in the acceleration-displacement relationship would be more equivalent to a maximum acceleration plateau.

5.4.3 Comparisons

To investigate whether the behavior of Isolated Floor System II is stable when subjected to different unidirectional seismic inputs, the comparison of the acceleration-displacement relationships for the symmetric load cases (Load Cases 1 to 3) is plotted in Figs. 5.35 to 5.37, respectively. It is observed from these figures that the acceleration-displacement loops, under the same load case, when subjected to different seismic inputs agree well with each other,

confirming the behavior of this isolated floor system is stable when subjected to different seismic excitations.

To investigate how the behavior of Isolated Floor System II (with edge plates on) changes under unidirectional seismic inputs and different applied gravity loads, the test results for Load Cases 1 to 3 under shake table excitation inputs Acc11 and Acc31, in terms of acceleration-displacement relationship, are shown together in Figs. 5.38 5.39, respectively. Note that the observed differences in the behavior of the isolated floor system in these figures are due to the differences in gravity loads. The same comparison is also made for Isolated Floor System II without edge plates (i.e., unidirectional seismic inputs and different load cases), for Load Cases 2 and 3 under shake table excitation input Acc31, in Fig. 5.40. From these figures, consistently, the floors subjected to greater gravity loads undergo lower peak accelerations. As shown in Chapter 4, the behavior of the multi-directional spring units is stable. Given that it provides the restoring force in this isolated floor system, when the mass supported by the floor is larger, for a constant restoring force, the maximum acceleration response of the isolated floor will be proportionally less.

To investigate the difference in behavior between symmetric and eccentric load cases for this isolated floor system, the test results for 2Acc31 and 7Acc31 are compared in Fig 5.41. It is observed that the behavior of the isolated floor system from each test agrees with each other well, which is consistent with the observation that the rotation effect of the isolated floor is not significant as mentioned before.

As mentioned in Section 5.3, some steel edge plates were used to cover the space between the isolated floor and the surrounding wall. This may introduce friction between the steel cover plates and the walking surface of the isolated floor. To investigate the effect of this friction, the tests results for cases with and without these edge plates for Load Cases 2 and 3 under both

unidirectional and bidirectional tests, in terms of acceleration-displacement relationships, are shown together for comparison in Figs. 5.42 and 5.47, respectively. Note that because the acceleration-displacement relationship of Isolated Floor System II in bidirectional tests is similar to that in unidirectional tests at relatively large displacement, the results for bidirectional tests were also included in this comparison. From these figures, note that there is no significant difference in the amplitude of the acceleration attained by the isolated floor under both unidirectional and bidirectional tests. This is reasonable because although there might be some friction effect introduced between the edge plates and the isolated floor walking surface, the friction effect on the acceleration response of the isolated floor is almost negligible when compared to the total weight of the isolated floor system and the loads (i.e., steel plates) applied on the floor in Load Cases 2 and 3. This friction effect will be further investigated in this section.

To better model the behavior of the isolated floor system in computer programs, it is necessary to compare the behavior of the multi-directional spring unit as a component versus that of the whole isolated floor system. As mentioned in Chapter 4, some tests (i.e., 2Acc31wo152ww and 3Acc31wo152ww) were conducted on the spring units having a nominal stiffness of 2627 N/m (15 lb/in) by using the seismic displacement histories recorded during the tests for the full isolation floor system (i.e., results of in this chapter). Note that in those cases, there were no edge plates on the isolated floor system. To enable such a comparison, the test results of the spring units with nominal stiffness of 2627 N/m (15 lb/in) in Chapter 4 were first doubled because two spring units were used in the complete floor system. Then, the spring force-displacement relationship was divided by the total mass of the isolated floor and the corresponding load (i.e., steel plates) on top of the walking surface of the isolated floor to get an equivalent acceleration response for the corresponding isolated floor that uses these spring units. Finally, the obtained behavior of the spring units, in terms of acceleration-displacement relationship, is compared with the system behavior from the corresponding system test results. The comparison is shown in Figs. 5.48 and 5.49, respectively. From these two figures, note that the acceleration response from the

spring units is almost zero when the displacement is near zero. However, it is not the case for the whole isolated floor system where the acceleration response is about 0.035g when the displacement is near zero. Furthermore, the acceleration-displacement loops for whole system tests are fatter than the corresponding ones for the spring units. The difference between these two groups of loops is about a constant as 0.035g. This suggests that there exists a constant friction in the system, presumably between the casters and the concrete footing slab.

Furthermore, as mentioned before, there might be some friction between the edge plates and the walking surface of the isolated floor. Fig. 5.50 shows the results for test 1Acc31 which was conducted with the edge plates. It can be observed from the (d) plot that when the displacement is near zero, the system acceleration response is near 0.07g. As expected, this is greater than the value of 0.035g obtained above for the cases without edge plates. This confirms that the friction between the edge plates and the isolated floor is also about 0.035g by itself, which is $(0.07g - 0.035g) \times 1916 \text{ lb/g} = 67 \text{ lb}$ (298 N). Therefore, when simulating the behavior of this complete system based on the behavior of the spring units, these extra frictions shall be considered. The comparison of behavior between multi-directional spring units having nominal stiffness of 1313 N/m (7.5 lb/in) and the corresponding whole system will be shown later in this chapter.

**Table 5.7 Summary of Peak Values of Response Quantities for Isolated Floor System II
Having 2627 N/m Multi-directional Spring Units**

Test Name (1)	PTD* (mm)		PFD** (mm)		PTA*** (g)		PFA**** (g)		Maximum Rotation (10 ⁻³ rad)		Peak Relative Disp. (mm)	
	E-W (2)	N-S (3)	E-W (4)	N-S (5)	E-W (6)	N-S (7)	E-W (8)	N-S (9)	E-W (10)	N-S (11)	E-W (12)	N-S (13)
1Acc002	47.1	—	71.2	—	1.24	—	0.29	—	4.7	4.3	57.8	—
1Acc01	152.2	—	160.4	—	0.74	—	0.31	—	2.8	4.7	66.0	—
1Acc11	151.3	—	187.4	—	0.40	—	0.43	—	4.2	4.9	124.0	—
1Acc31	152.4	—	206.9	—	0.46	—	0.39	—	4.0	4.9	77.4	—
1C1	153.1	152.5	203.9	226.8	0.76	0.98	0.33	0.40	8.4	10.9	76.6	98.8
1C2	155.7	155.1	260.7	225.5	0.40	0.45	0.38	0.39	14.9	13.9	128.5	146.0
2Acc002	46.3	—	60.1	—	1.20	—	0.15	—	9.8	7.5	72.5	—
2Acc01	125.3	—	144.8	—	0.60	—	0.18	—	6.0	6.5	64.4	—
2Acc11	156.5	—	215.4	—	0.42	—	0.19	—	8.4	8.1	153.7	—
2Acc31	153.4	—	185.3	—	0.46	—	0.18	—	9.7	11.6	130.5	—
2C1	151.4	151.9	223.7	214.3	0.75	0.97	0.16	0.20	19.3	20.0	177.6	189.9
2C2	155.1	155.0	238.5	196.2	0.41	0.46	0.19	0.17	12.6	13.8	210.2	132.1
3Acc11	143.1	—	197.4	—	0.30	—	0.14	—	11.4	10.5	169.0	—
3Acc31	208.7	—	256.4	—	0.50	—	0.15	—	10.7	11.6	239.5	—
3C2	117.4	116.7	180.8	154.8	0.34	0.34	0.14	0.14	18.4	18.8	198.0	152.5
4C2	154.7	155.7	222.1	204.7	0.41	0.46	0.25	0.21	14.8	15.5	146.4	148.1
5C2	152.1	155.5	238.2	206.0	0.40	0.45	0.30	0.24	50.3	50.8	219.7	142.4
6C2	152.5	152.0	223.0	200.1	0.41	0.45	0.25	0.21	36.5	36.5	155.7	149.5
7Acc01	149.7	—	200.8	—	0.75	—	0.20	—	25.5	27.4	119.1	—
7Acc11	154.8	—	194.7	—	0.41	—	0.20	—	38.5	42.2	152.2	—
7Acc31	156.5	—	172.8	—	0.46	—	0.19	—	21.5	21.8	107.0	—
7C2	152.7	156.8	214.5	209.7	0.41	0.45	0.21	0.18	68.0	71.2	191.5	156.3
8Acc31	156.7	—	188.1	—	0.47	—	0.22	—	19.3	20.6	92.0	—
8C1	150.1	153.3	206.2	227.1	0.76	1.01	0.22	0.23	56.6	63.6	132.6	180.8
8C2	154.0	157.7	209.1	204.5	0.42	0.45	0.25	0.22	39.5	41.2	155.4	132.0
9Acc31	156.9	—	159.1	—	0.47	—	0.29	—	15.2	34.8	30.0	—
9C2	152.8	157.3	154.6	178.6	0.41	0.45	0.38	0.27	22.6	24.3	86.9	70.7
10Acc31	156.7	—	165.0	—	0.47	—	0.28	—	10.4	12.2	55.9	—
10C1	150.6	153.6	176.1	200.6	0.77	1.02	0.33	0.37	24.7	28.4	70.0	76.6
10C2	152.9	156.6	213.8	187.4	0.41	0.45	0.41	0.28	25.1	25.0	117.6	97.5
2Acc31wo	152.7	—	218.6	—	0.44	—	0.19	—	12.2	30.7	150.7	—
2C2wo	157.5	154.5	253.2	196.3	0.40	0.44	0.19	0.17	19.2	35.1	235.8	162.1
3Acc31wo	152.0	—	222.1	—	0.43	—	0.14	—	17.4	18.6	185.8	—
3C2wo	118.9	115.3	192.2	149.6	0.29	0.33	0.13	0.12	26.5	28.8	191.8	121.6

* PTD is the peak absolute displacement response of the shake table;
 **PFD is the peak absolute displacement response of the isolated floor;
 ***PTA is the peak absolute acceleration response of the shake table;
 ****PFA is the peak absolute acceleration response of the isolated floor.

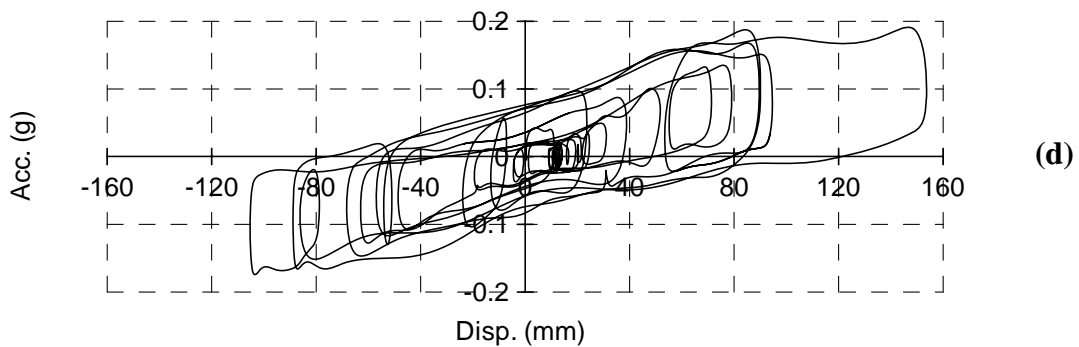
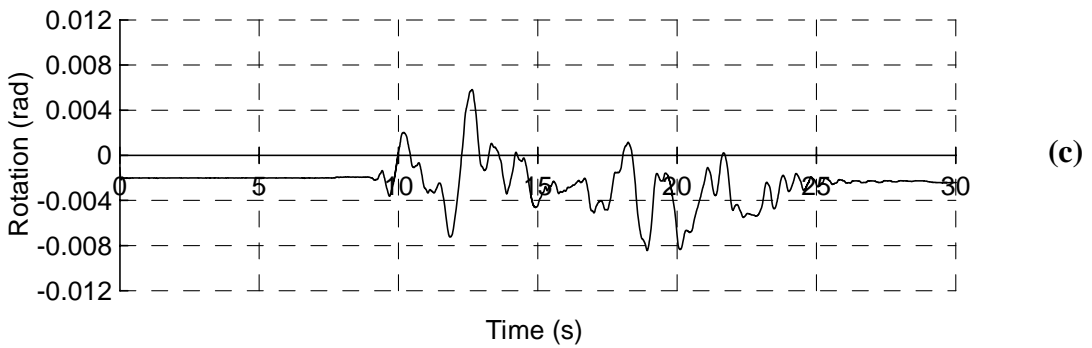
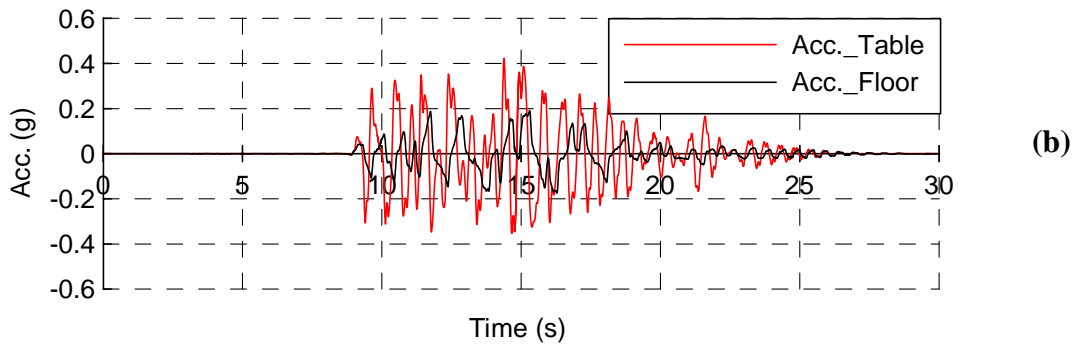
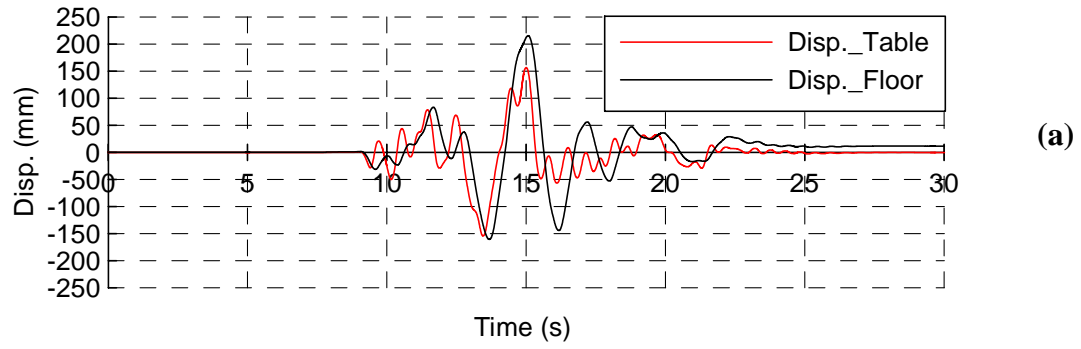


Figure 5.25 Results of Test 2Acc11: (a) and (b) Displacement and Acceleration of Shake Table and Isolated Floor, Respectively; (c) Rotation; (d) Acceleration-Displacement Relationship of Isolated Floor System II

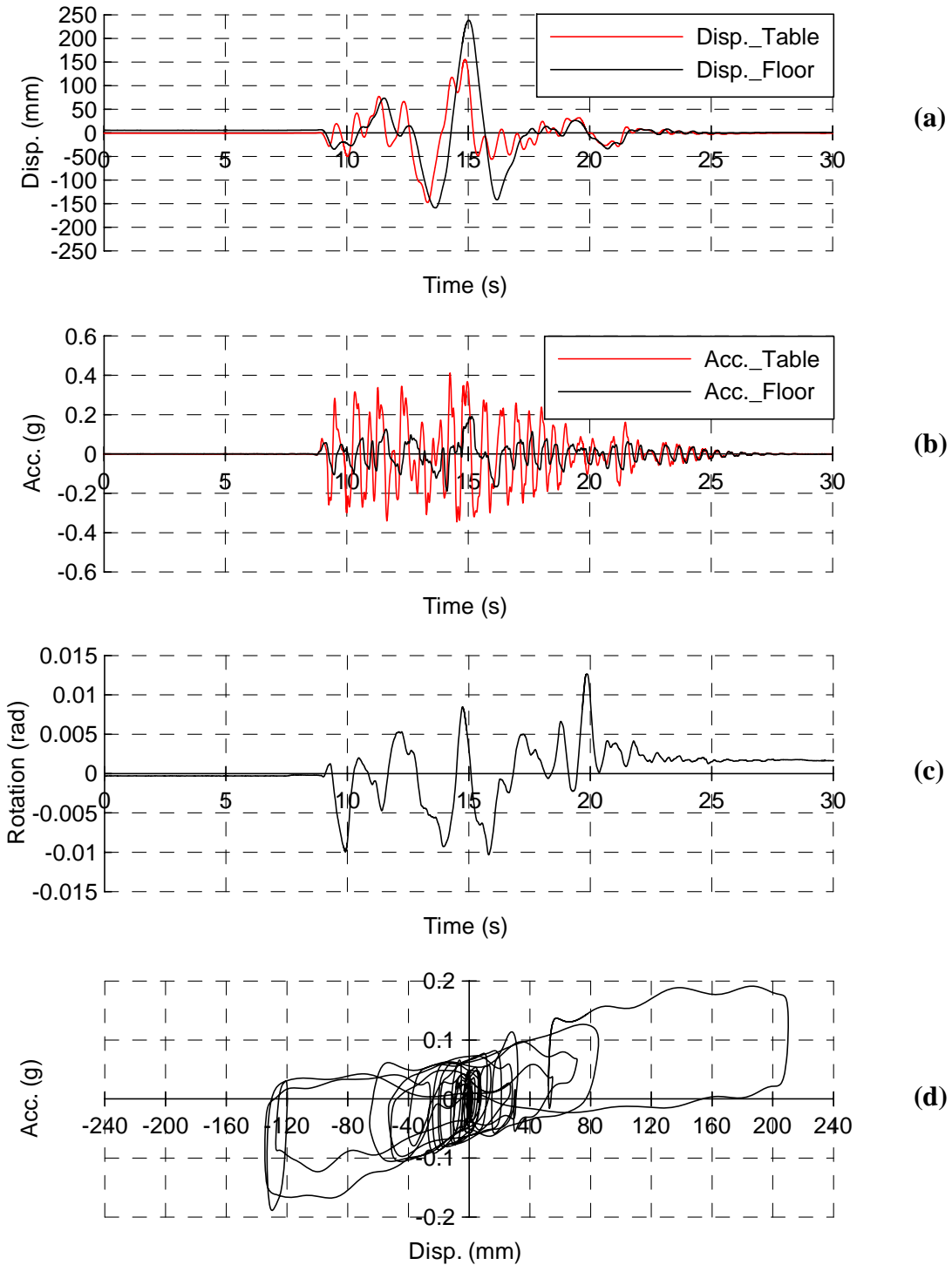


Figure 5.26 Results of Test 2C2 in E-W Direction: (a) and (b) Displacement and Acceleration of Shake Table and Isolated Floor, Respectively; (c) Rotation ; (d) Acceleration-Displacement Relationship of Isolated Floor System II

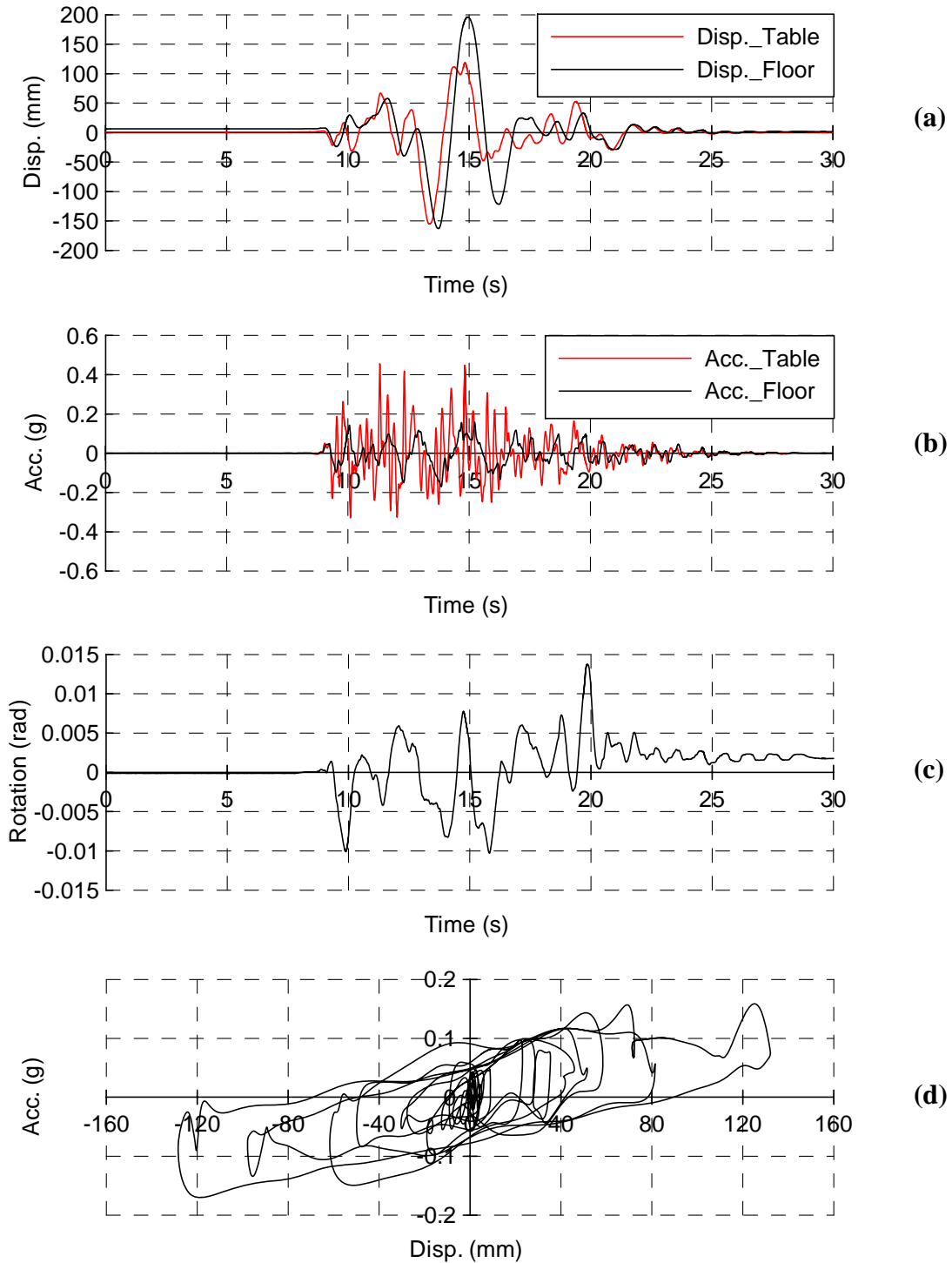


Figure 5.27 Results of Test 2C2 in N-S Direction: (a) and (b) Displacement and Acceleration of Shake Table and Isolated Floor, Respectively; (c) Rotation ; (d) Acceleration-Displacement Relationship of Isolated Floor System II

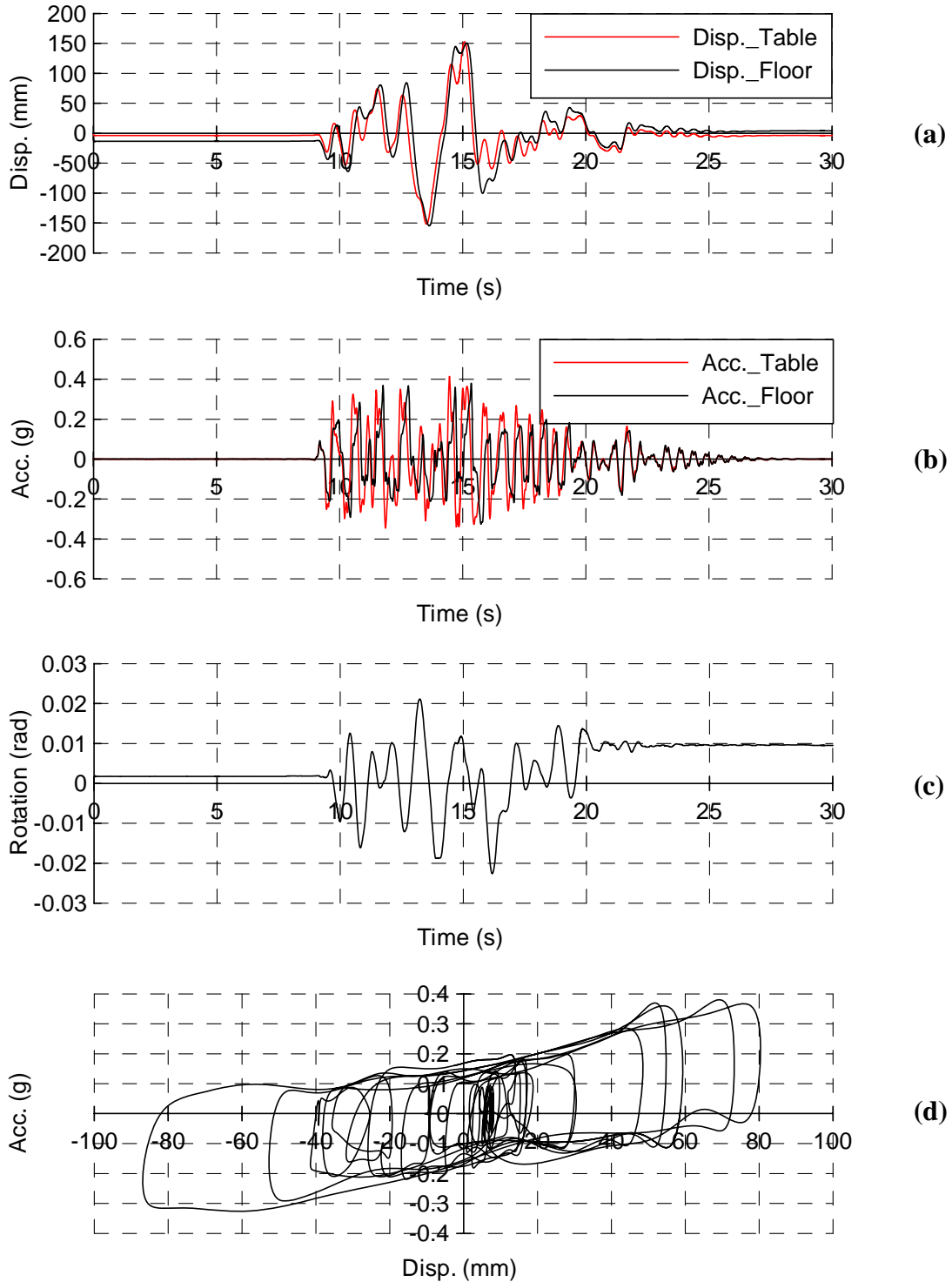


Figure 5.28 Results of Test 9C2 in E-W Direction: (a) and (b) Displacement and Acceleration of Shake Table and Isolated Floor, Respectively; (c) Rotation ; (d) Acceleration-Displacement Relationship of Isolated Floor System II

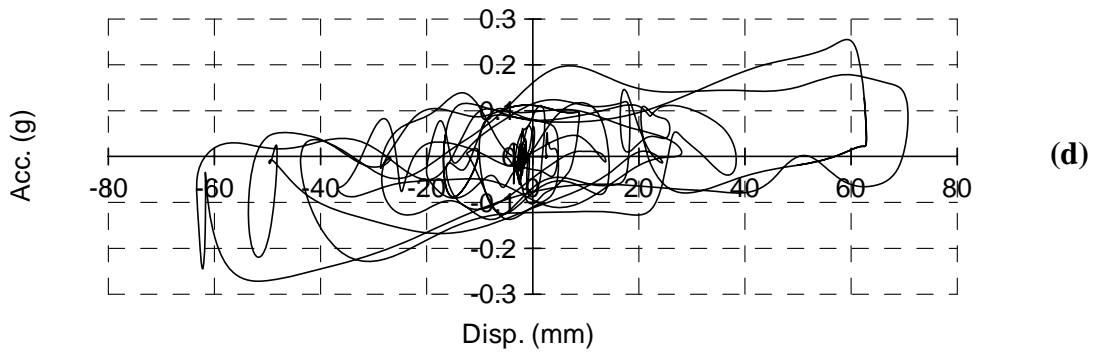
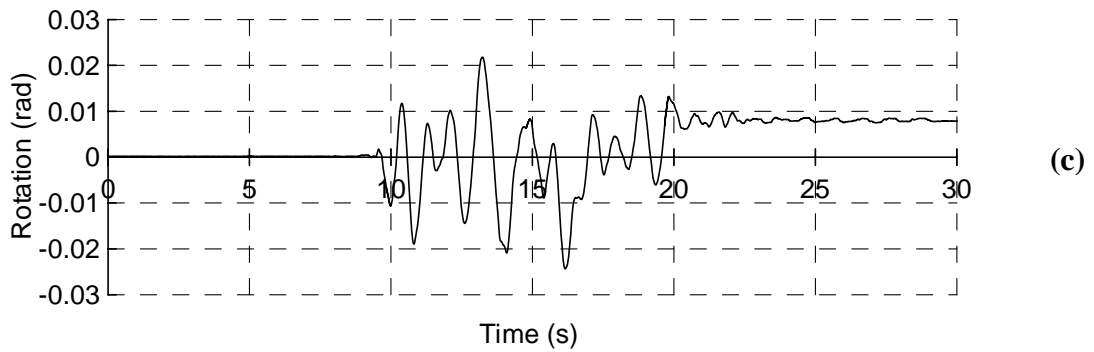
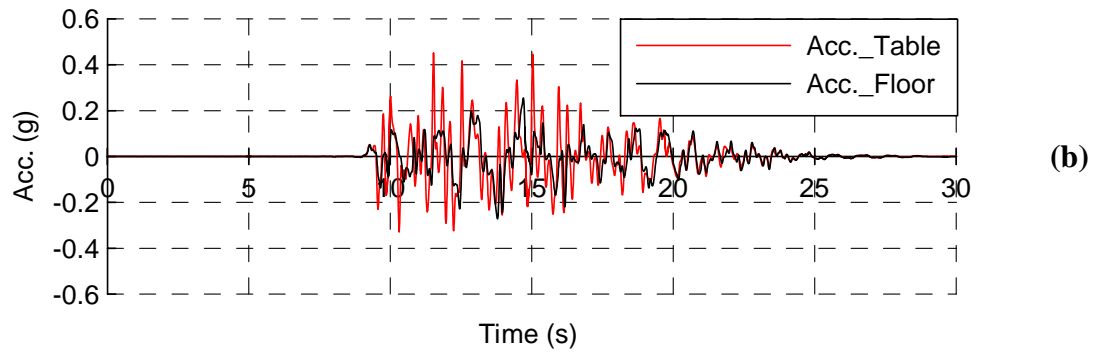
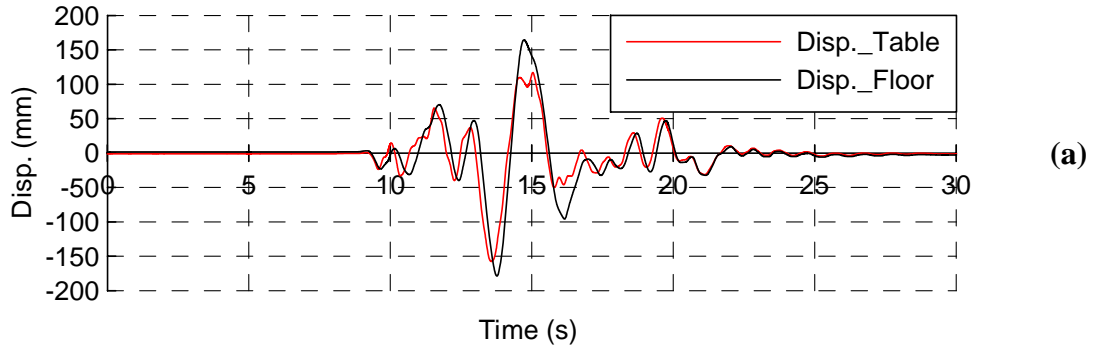


Figure 5.29 Results of Test 9C2 in N-S Direction: (a) and (b) Displacement and Acceleration of Shake Table and Isolated Floor, Respectively; (c) Rotation ; (d) Acceleration-Displacement Relationship of Isolated Floor System II

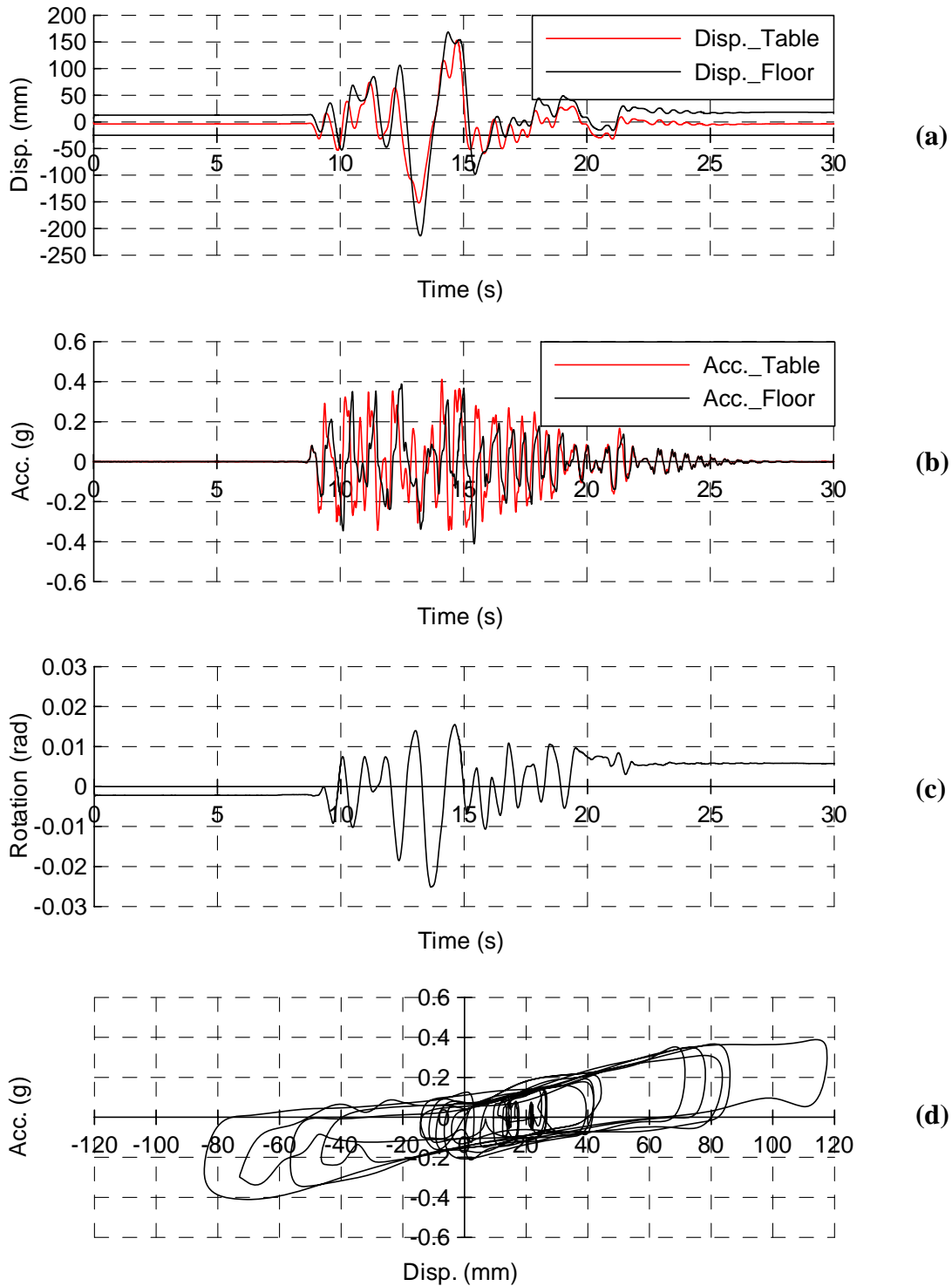


Figure 5.30 Results of Test 10C2 in E-W Direction: (a) and (b) Displacement and Acceleration of Shake Table and Isolated Floor, Respectively; (c) Rotation ; (d) Acceleration-Displacement Relationship of Isolated Floor System II

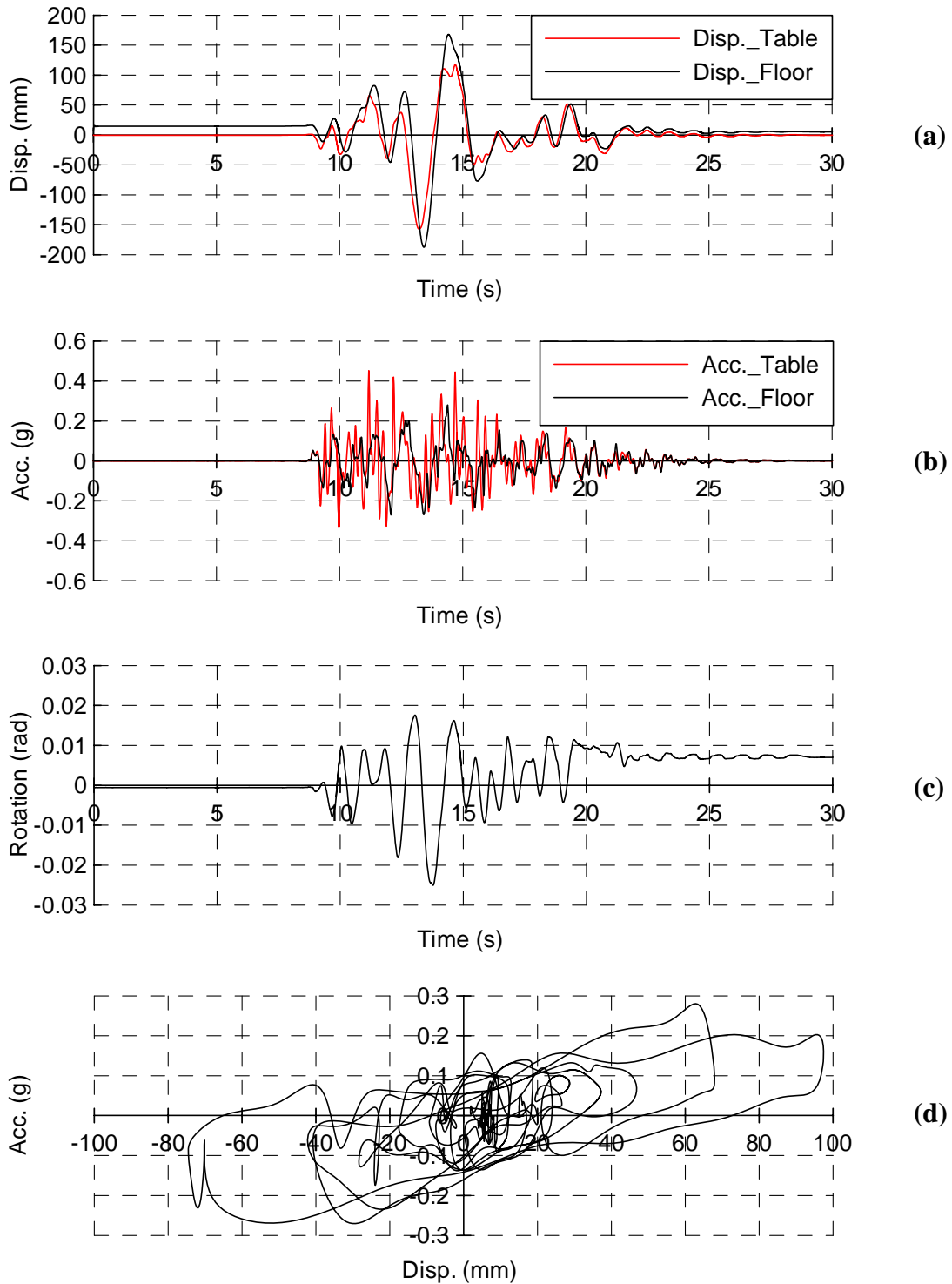


Figure 5.31 Results of Test 10C2 in N-S Direction: (a) and (b) Displacement and Acceleration of Shake Table and Isolated Floor, Respectively; (c) Rotation; (d) Acceleration-Displacement Relationship of Isolated Floor System II

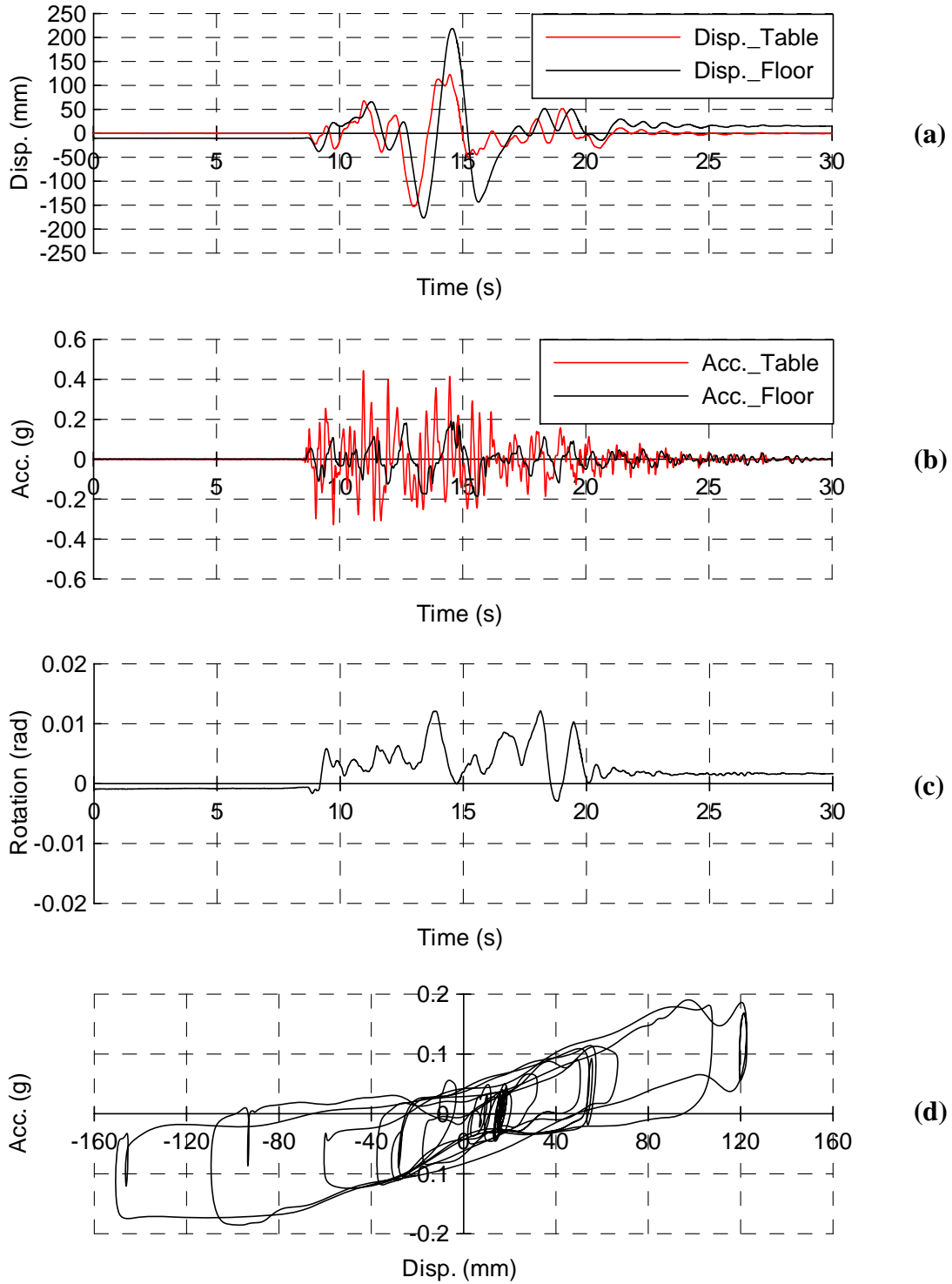


Figure 5.32 Results of Test 2Acc31wo: (a) and (b) Displacement and Acceleration of Shake Table and Isolated Floor, Respectively; (c) Rotation; (d) Acceleration-Displacement Relationship of Isolated Floor System II

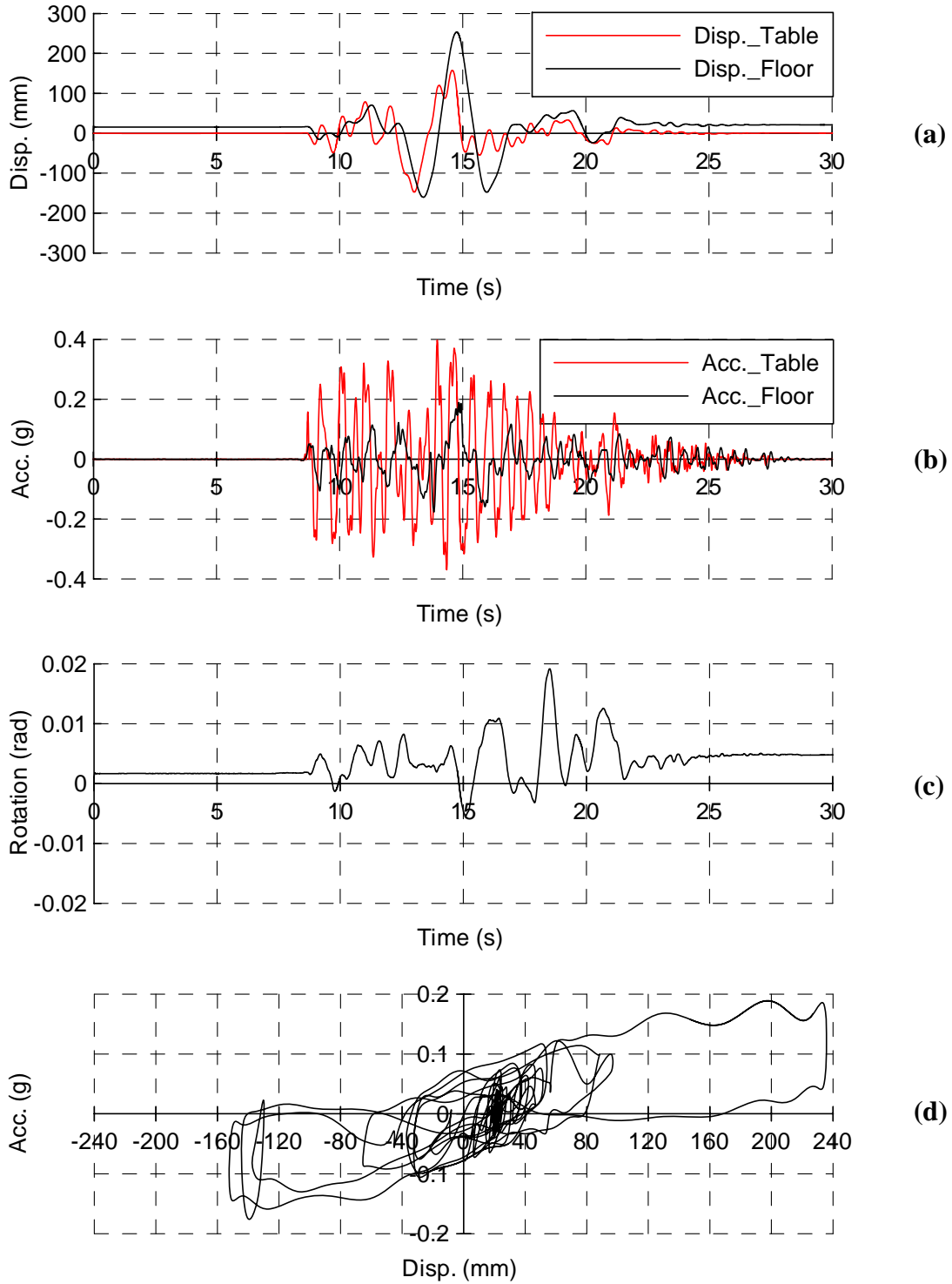


Figure 5.33 Results of Test 2C2wo in E-W Direction: (a) and (b) Displacement and Acceleration of Shake Table and Isolated Floor, Respectively; (c) Rotation; (d) Acceleration-Displacement Relationship of Isolated Floor System II

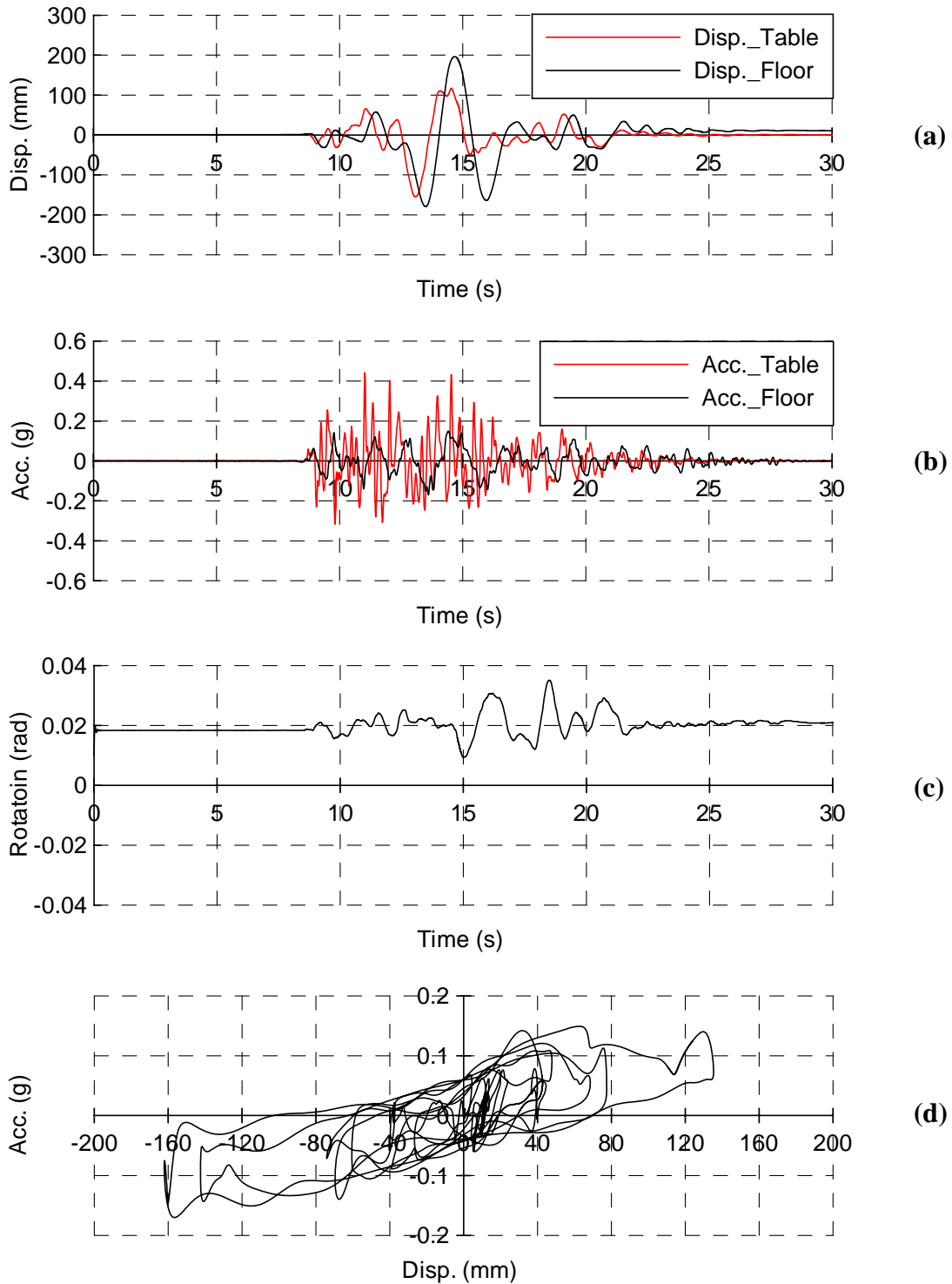


Figure 5.34 Results of Test 2C2wo in N-S Direction: (a) and (b) Displacement and Acceleration of Shake Table and Isolated Floor, Respectively; (c) Rotation; (d) Acceleration-Displacement Relationship of Isolated Floor System II

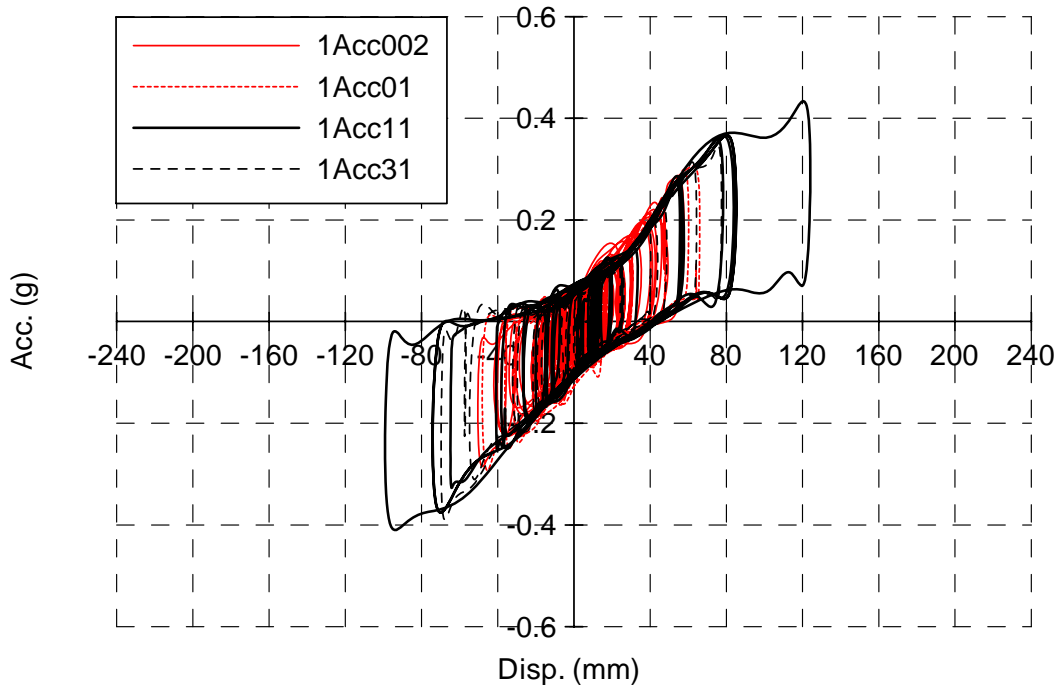


Figure 5.35 Comparison of Acceleration-Displacement Relationships under Different Inputs and Load Case 1

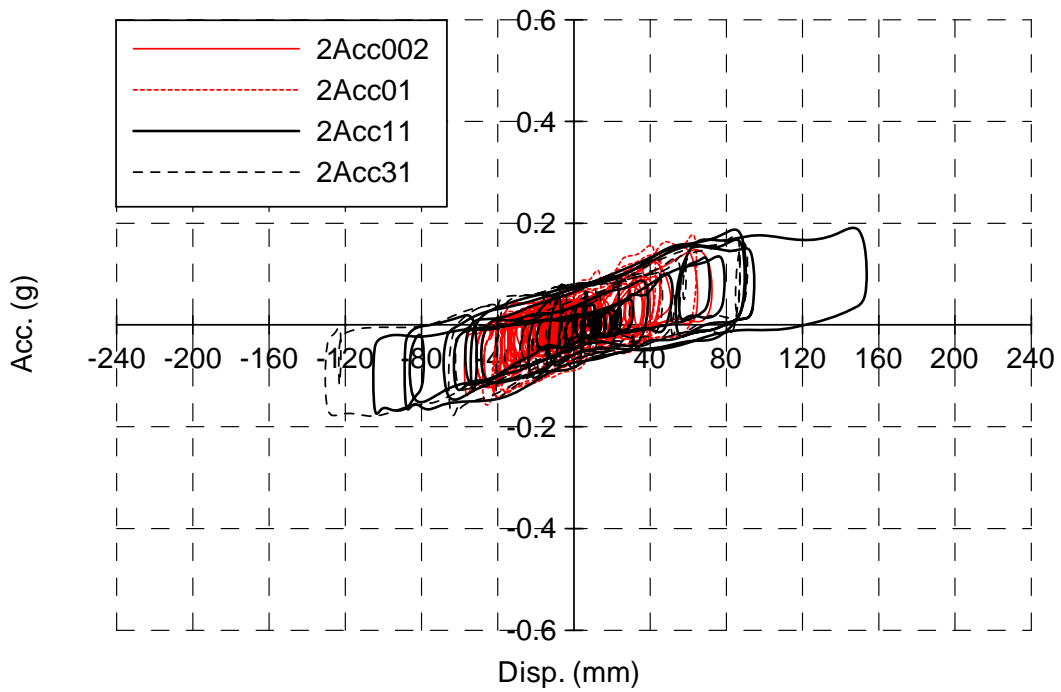


Figure 5.36 Comparison of Acceleration-Displacement Relationships under Different Inputs and Load Case 2

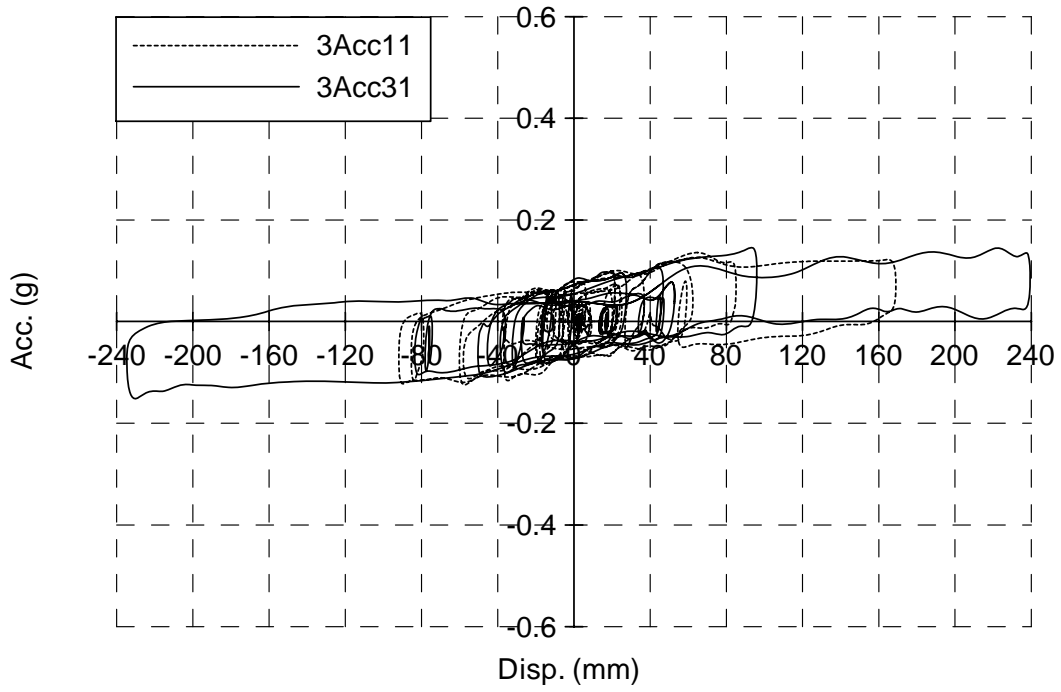


Figure 5.37 Comparison of Acceleration-Displacement Relationships under Different Inputs and Load Case 3

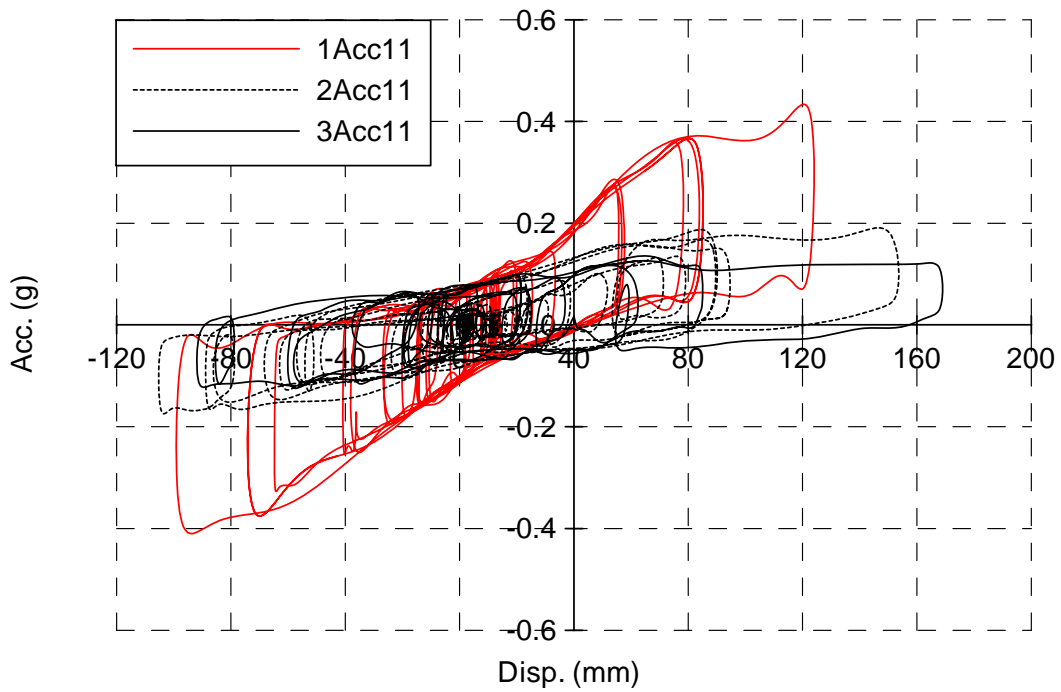


Figure 5.38 Comparison of Acceleration-Displacement Relationships under Different Symmetric Load Cases and Same Input of Acc11 (with edge plates)

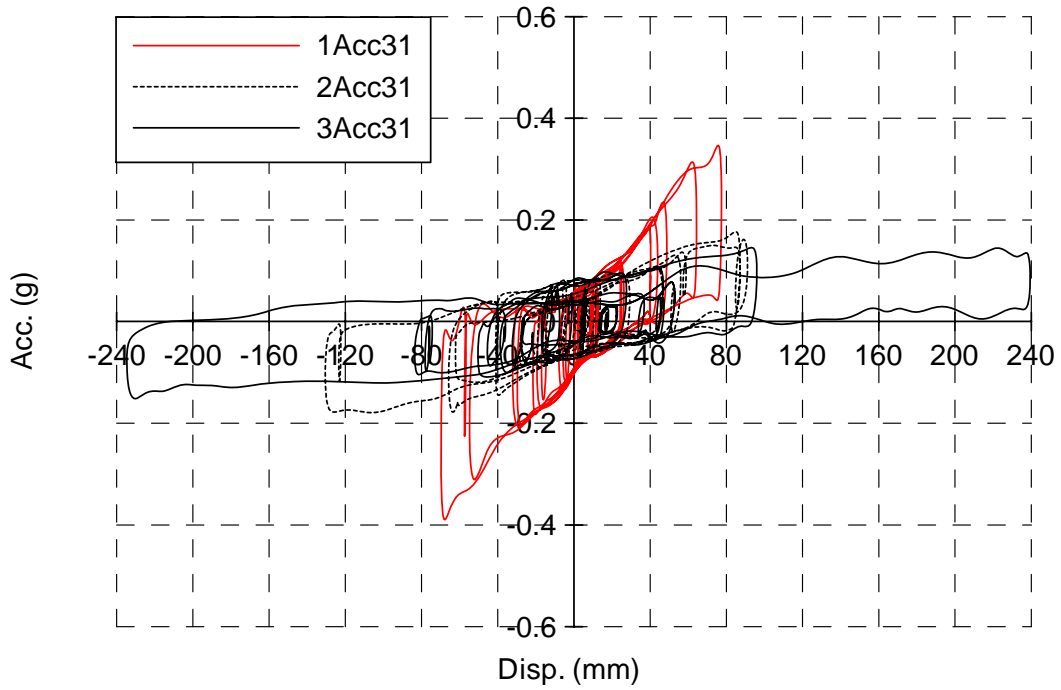


Figure 5.39 Comparison of Acceleration-Displacement Relationships under Different Symmetric Load Cases and Same Input of Acc31 (with edge plates)

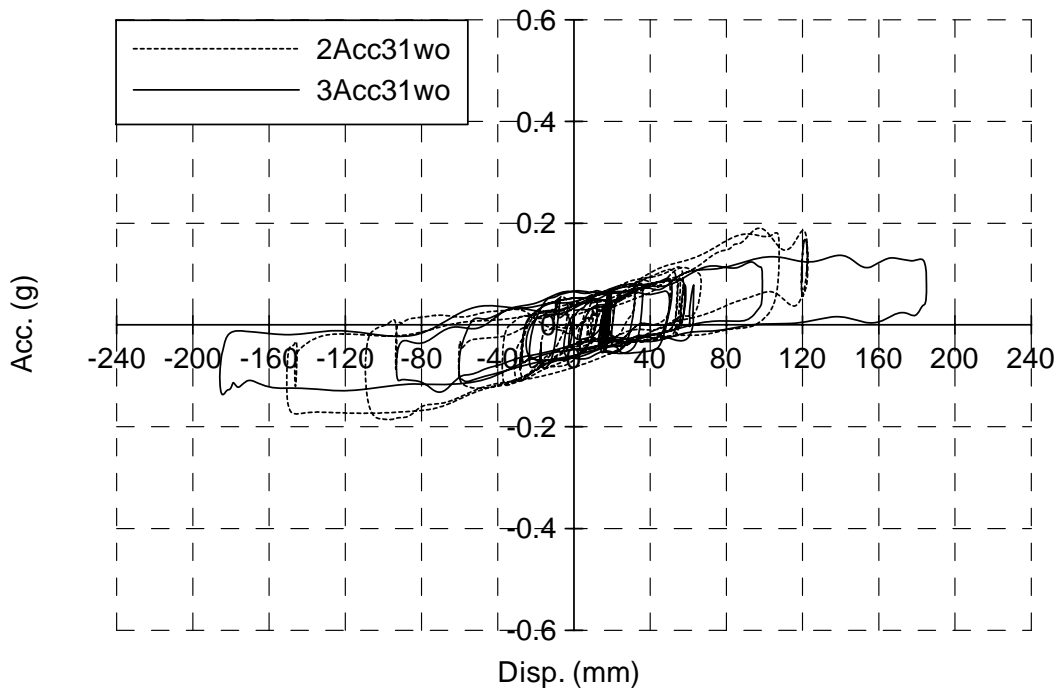


Figure 5.40 Comparison of Acceleration-Displacement Relationships under Different Symmetric Load Cases and Same Input of Acc31 (without edge plates)

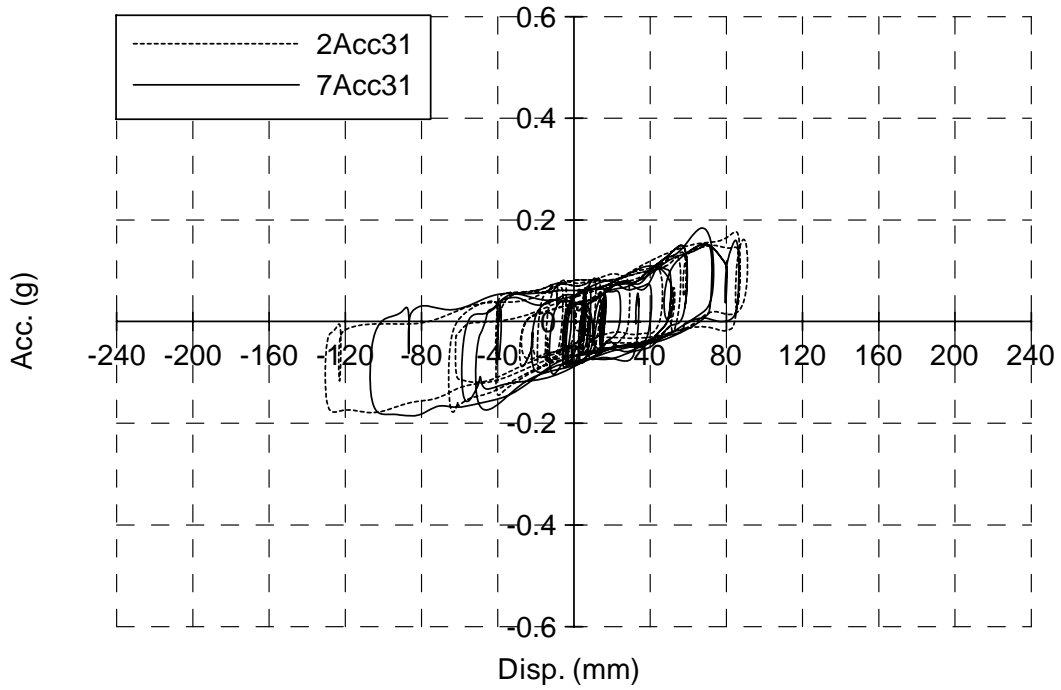


Figure 5.41 Comparison of Acceleration-Displacement Relationships Between Symmetric and Eccentric Load Cases under Input of Acc31

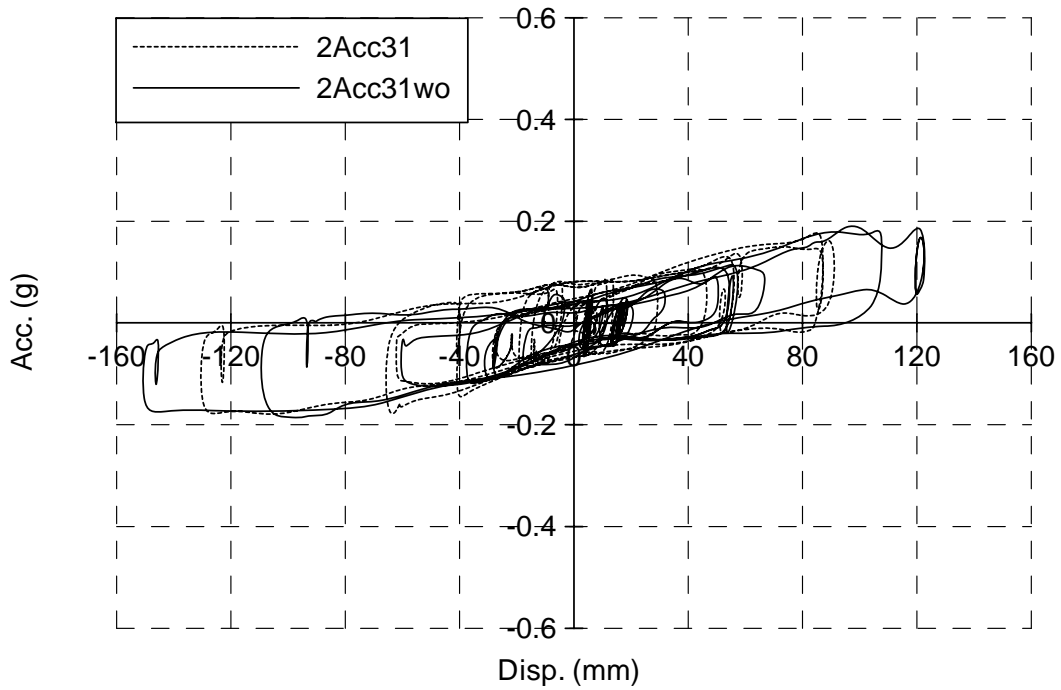


Figure 5.42 Comparison of Acceleration-Displacement Relationships Between With and Without Cover Plates under Load Case 2 When Subjected to Acc31

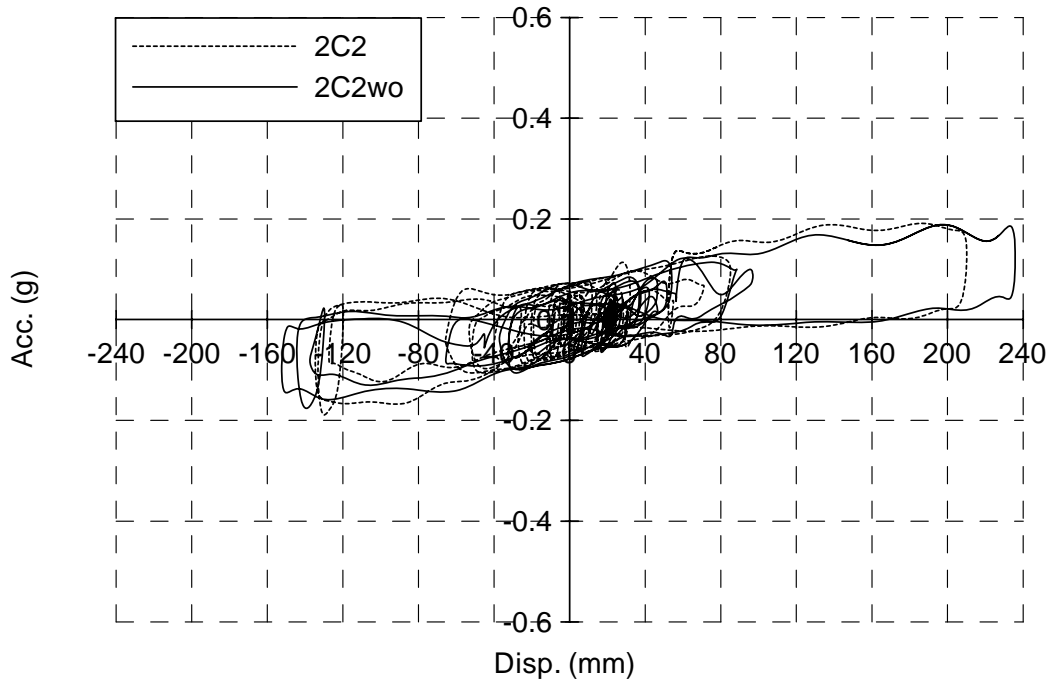


Figure 5.43 Comparison of Acceleration-Displacement Relationships in E-W Direction Between With and Without Cover Plates under Load Case 2 When Subjected to C2

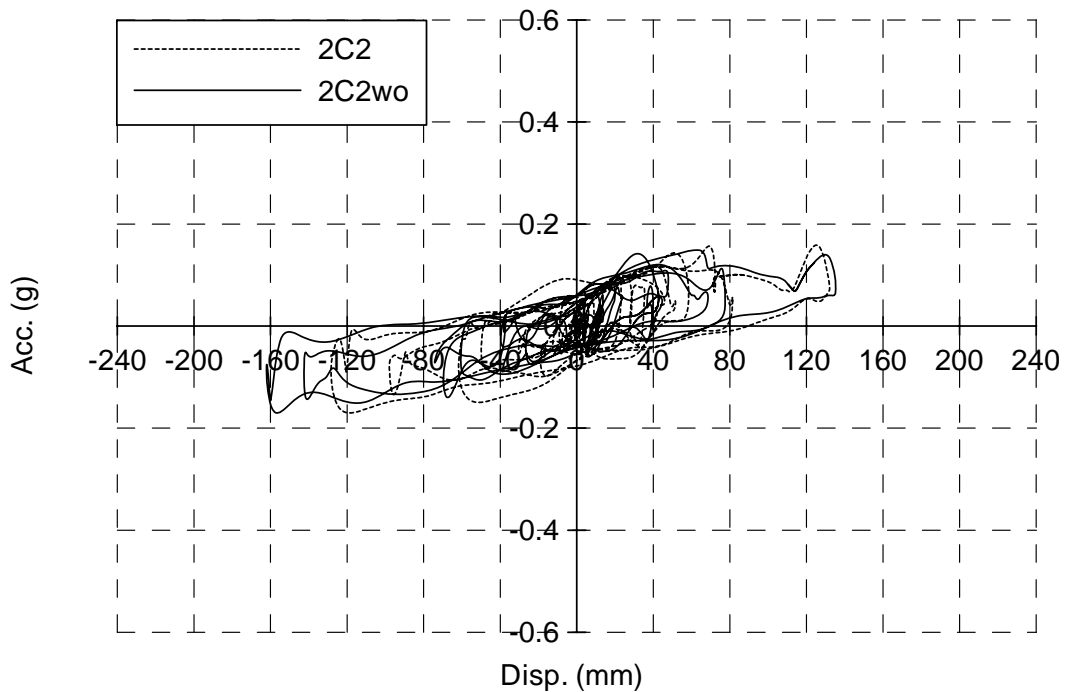


Figure 5.44 Comparison of Acceleration-Displacement Relationships in N-S Direction Between With and Without Cover Plates under Load Case 2 When Subjected to C2

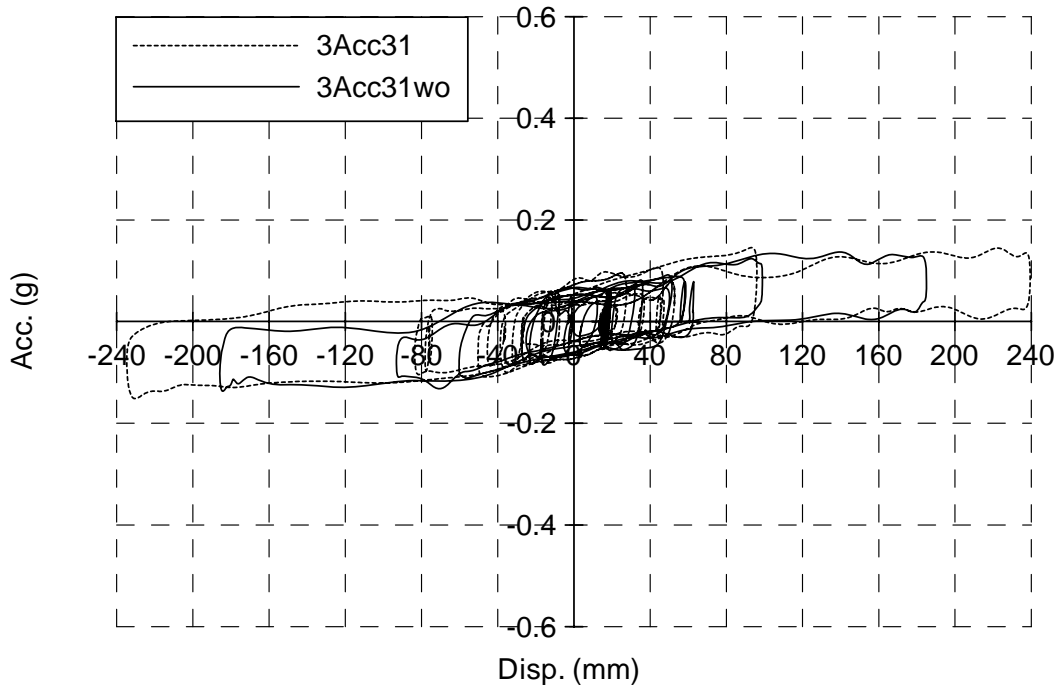


Figure 5.45 Comparison of Acceleration-Displacement Relationships Between With and Without Cover Plates under Load Case 3 When Subjected to Acc31

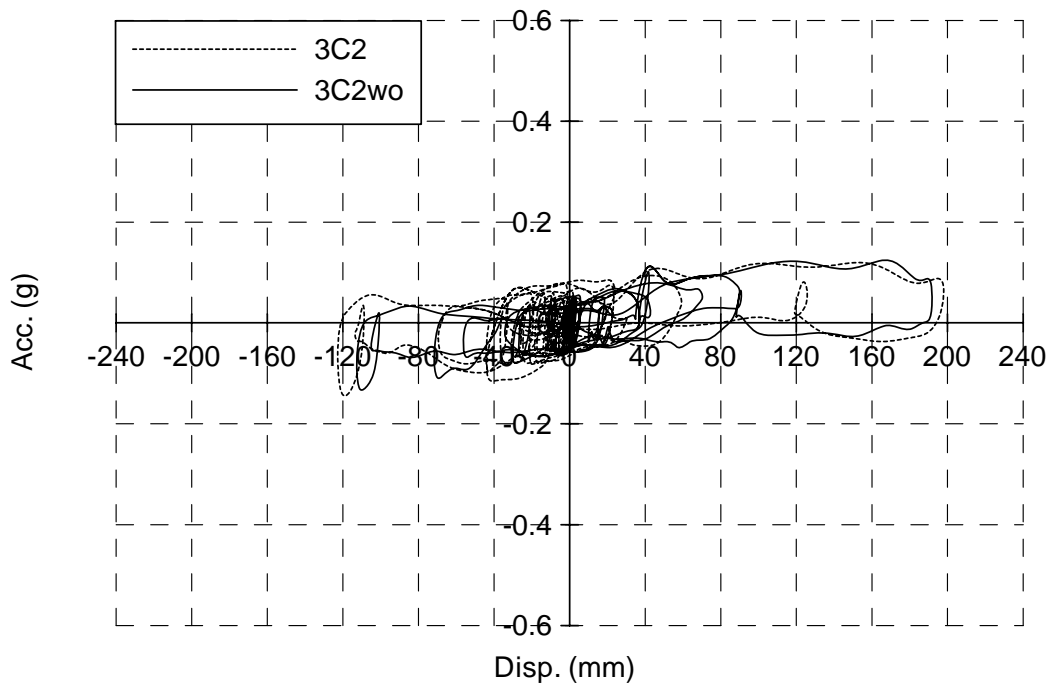


Figure 5.46 Comparison of Acceleration-Displacement Relationships in E-W Direction Between With and Without Cover Plates under Load Case 3 When Subjected to C2

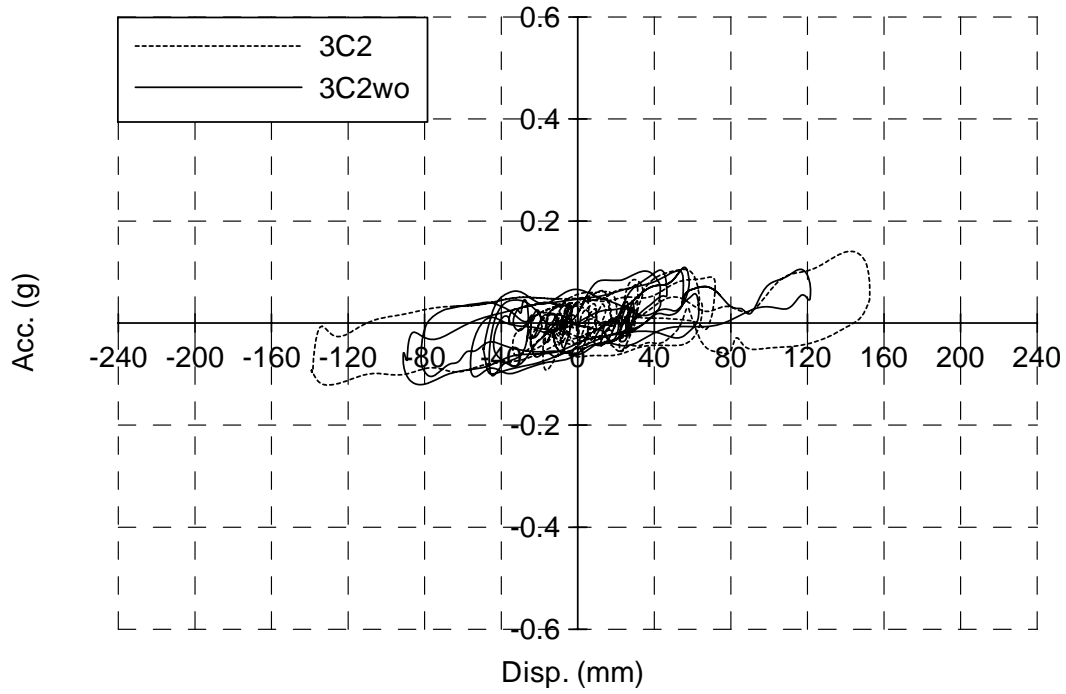


Figure 5.47 Comparison of Acceleration-Displacement Relationships in N-S Direction Between With and Without Cover Plates under Load Case 3 When Subjected to C2

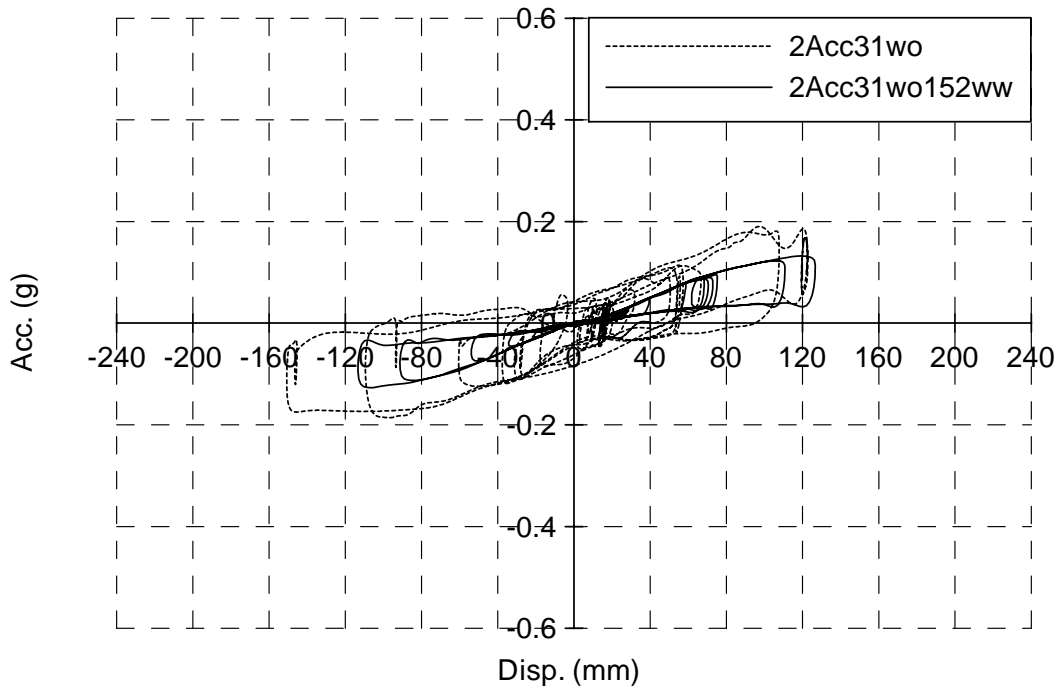


Figure 5.48 Comparison of Acceleration-Displacement Relationships Between Spring Units and Whole System under Load Case 2

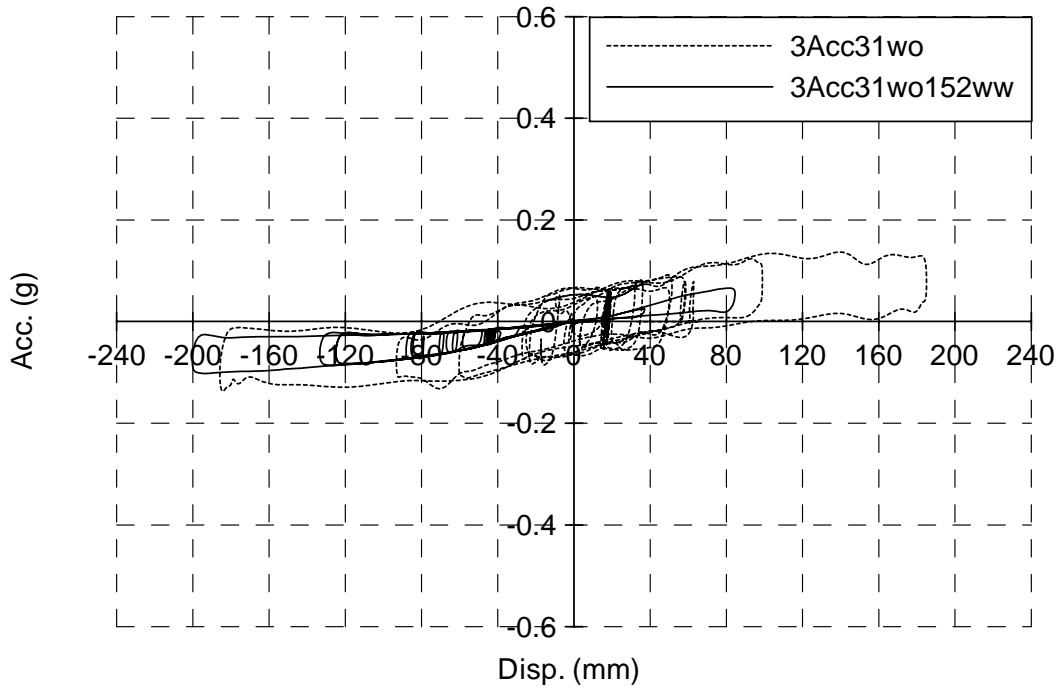


Figure 5.49 Comparison of Acceleration-Displacement Relationships Between Spring Units and Whole System under Load Case 3

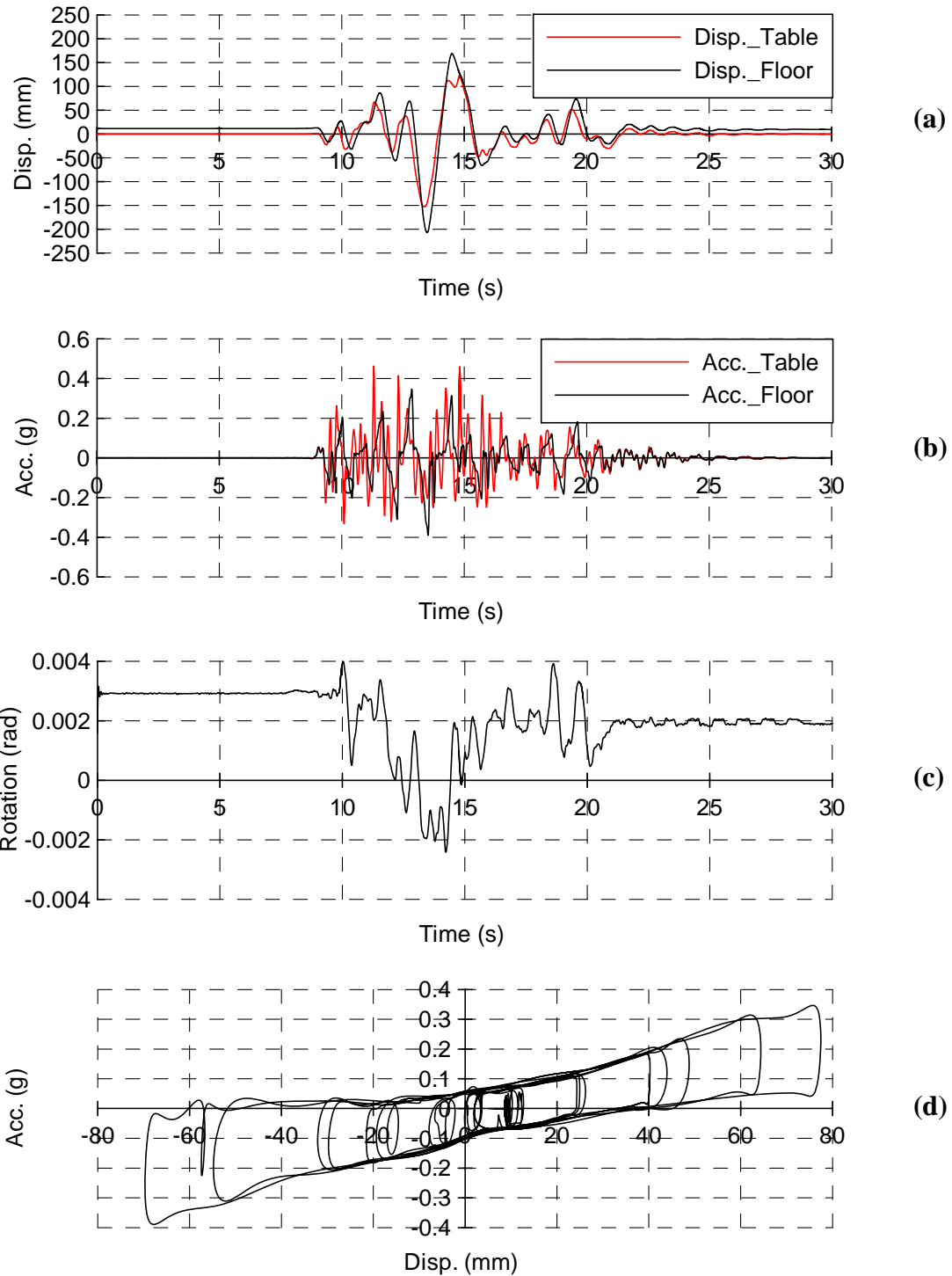


Figure 5.50 Results of Test 1Acc31: (a) and (b) Displacement and Acceleration of Shake Table and Isolated Floor, Respectively; (c) Rotation; (d) Acceleration-Displacement Relationship of Isolated Floor System II

5.5 Additional Tests

As mentioned in Chapter 4, two groups of spring units were tested. One group had nominal stiffness of 2627 N/m (15 lb/in) and the other having a 1313 N/m (7.5 lb/in) nominal stiffness. Here, after the tests of the isolated floor system with 2 sets of 2627 N/m (15 lb/in) nominal stiffness spring units were done (for which results have been reported in the preceding sections), some additional tests (not listed in Table 5.7) were also conducted on Isolated Floor System II using other spring units having nominal stiffnesses of 5254 N/m (30 lb/in) and 1313 N/m (7.5 lb/in), and different floor time history inputs provided by DIS. Here, only a couple of the tests in which 1313 N/m nominal stiffness spring units were used are shown to compare the behavior of the spring units introduced in Chapter 4 with that of the corresponding isolated floor system.

These additional tests were run without edge plates and without the surrounding wall. The inputs used in these tests were generically called B1, and B2. They are shown in Figs. 5.51 and 5.52, respectively.

Here, load of about 12386 N (2785 lb) was used to create the load cases of 2.4 kPa (50 psf) uniformly distributed only over the area of the isolated floor (not the entire area surrounding by the concrete wall). For these tests, since there was no edge plates and surrounding wall anymore, the load were placed more symmetrically over the walking surface of the isolated floor even though recognizing that not all of the isolated floor walking surface will be available as mentioned before. The tests were denoted as B107050 and B207050, respectively, which is consistent with the nomenclature followed throughout, using the input name (“B1” or “B2”), the nominal stiffness of the spring units (7.5 lb/in expressed as “07”), the uniformly distributed load value (50 psf expressed as “050), and without edge plates (“wo”). The test results are shown in Figs. 5.53 and 5.54, respectively. Again, there was no damage to the isolated floor system during

these tests. The (b) plot of each figure shows that the acceleration response on top of the isolated floor is less than the corresponding acceleration of the shake table.

To investigate whether the behavior of this group of spring units is stable when subjected to different seismic inputs, test results are compared in terms of acceleration-displacement relationship, as shown in Fig. 5.55. From this figure, note that the acceleration-displacement loops under different seismic inputs (i.e. B1 and B2) coincide with each other well, which indicates that the behavior is stable when subjected to different seismic inputs. Also, the envelopes of the loops from each test almost keep the same and enclose some area, which shows that the behavior of the isolated floor system is stable and dissipate some energy during motion.

As in Section 5.4, to investigate the difference in behavior between the multi-directional spring units and the complete system, responses are compared in Figs. 5.56 and 5.57 in the same way following the same procedure outlined previously. Again, a constant friction is observed as reported in Section 5.4 is also observed here. The magnitude of this friction about 0.035g, which is the same as the value found in Section 5.4.

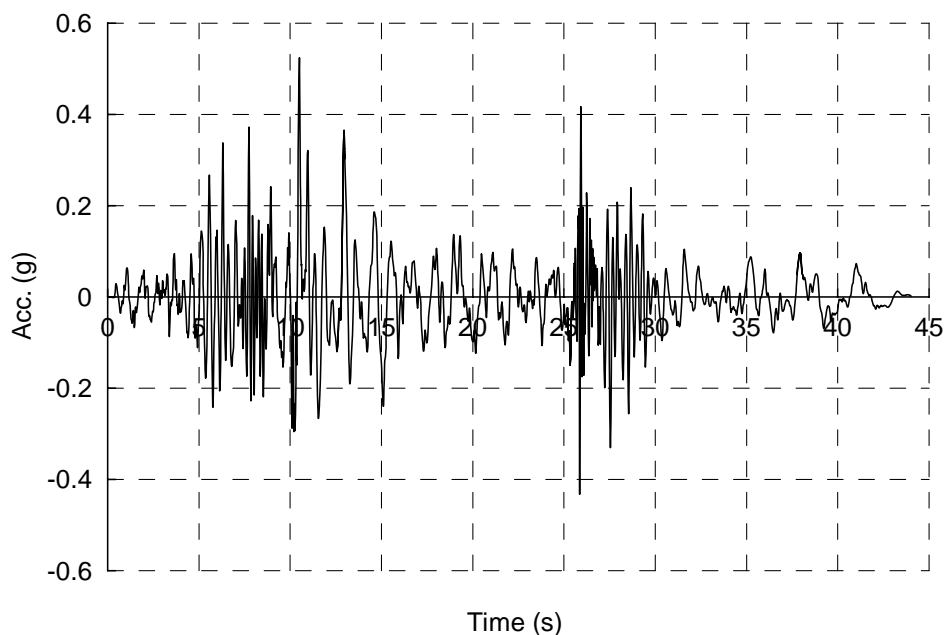


Figure 5.51 Input of B1

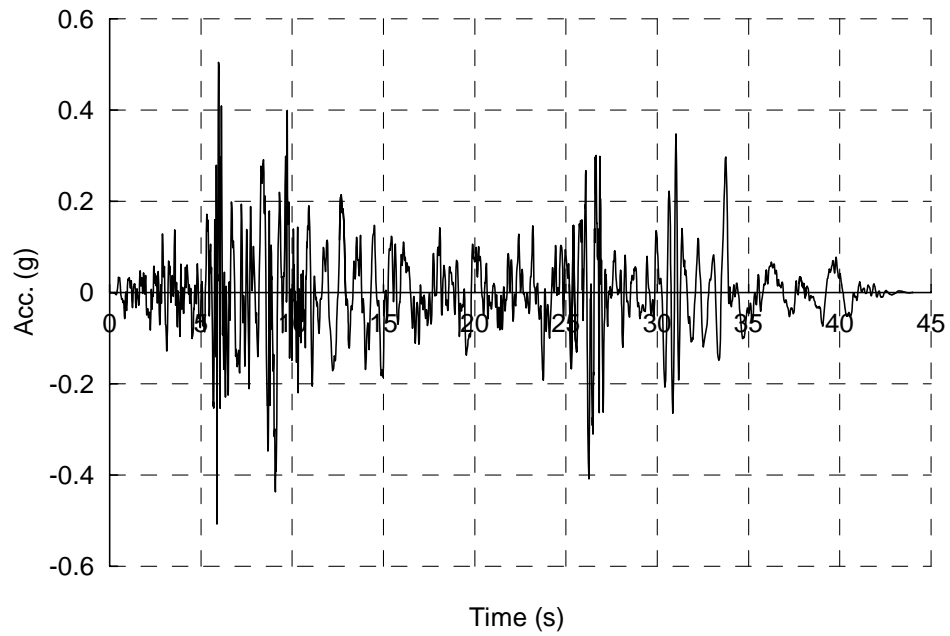


Figure 5.52 Input of B2

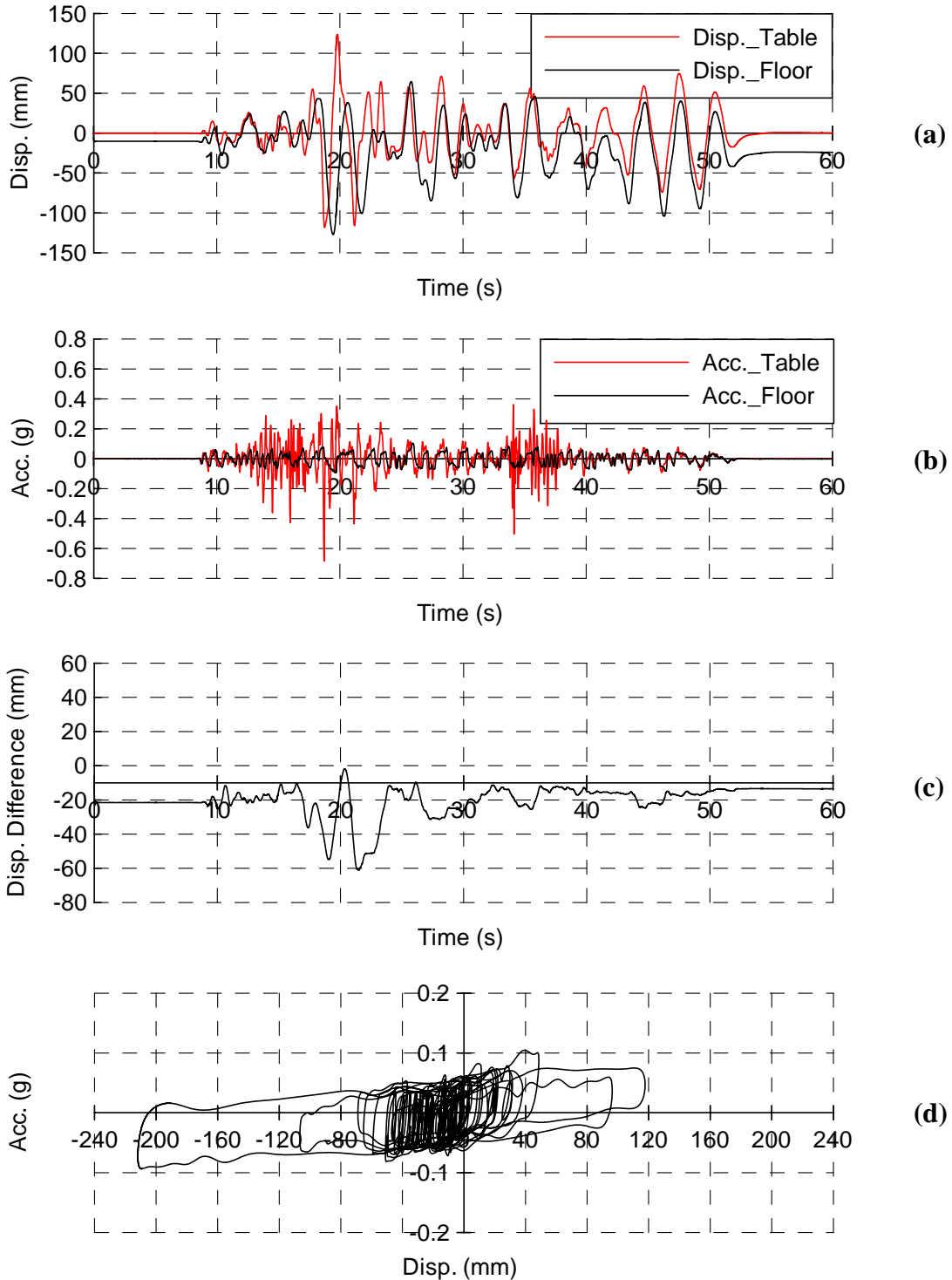


Figure 5.53 Results of Test B107050wo: (a) and (b) are Displacement and Acceleration of Shake Table and Isolated Floor, Respectively; (c) Rotation; (d) Acceleration-Displacement Relationship of Isolated Floor System II

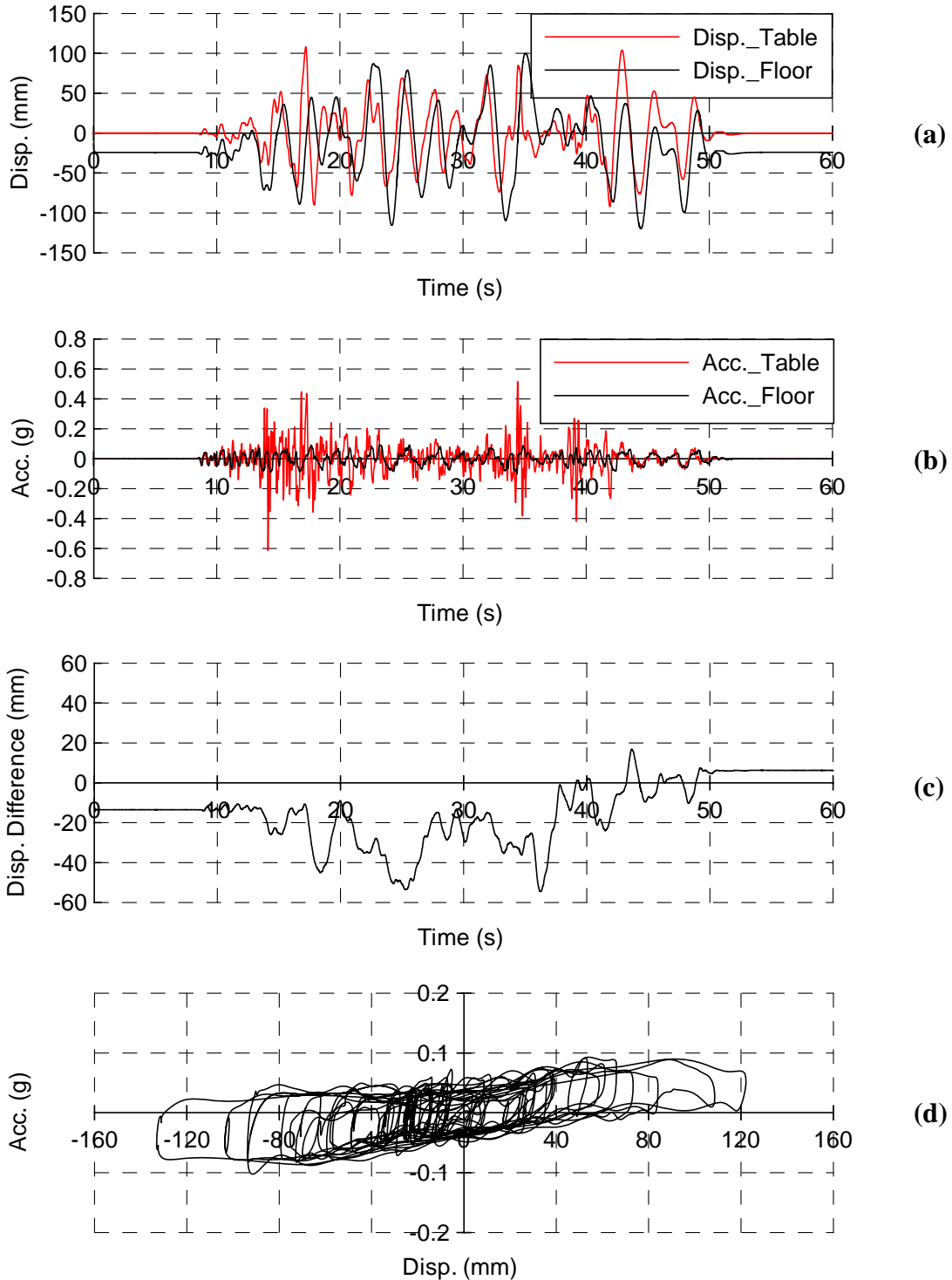


Figure 5.54 Results of Test B207050wo: (a) and (b) Displacement and Acceleration of Shake Table and Isolated Floor, Respectively; (c) Rotation; (d) Acceleration-Displacement Relationship of Isolated Floor System II

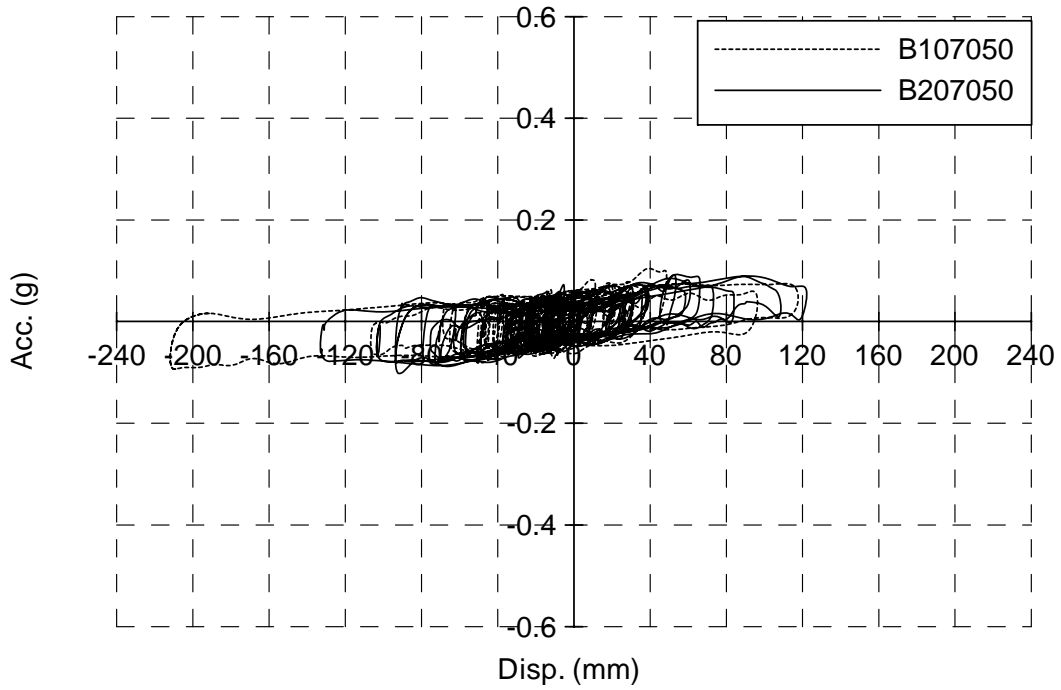


Figure 5.55 Comparison of Acceleration-Displacement Relationships under Different Inputs (1313 N/m Spring Units)

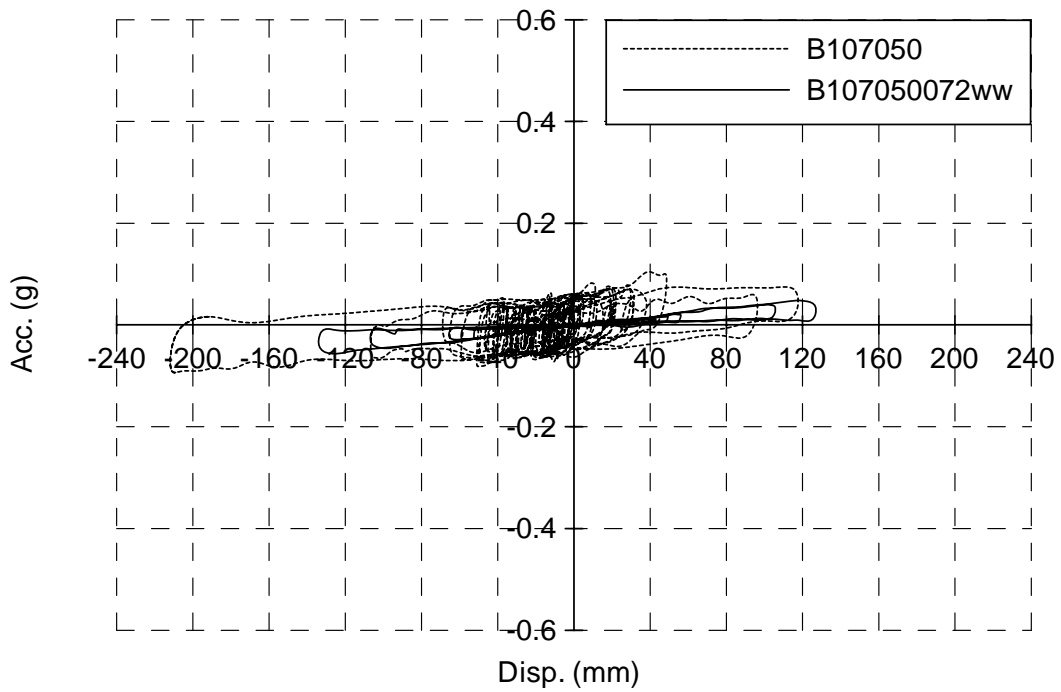


Figure 5.56 Comparison of Acceleration-Displacement Relationships Between Spring Units and Entire System under Input of B1

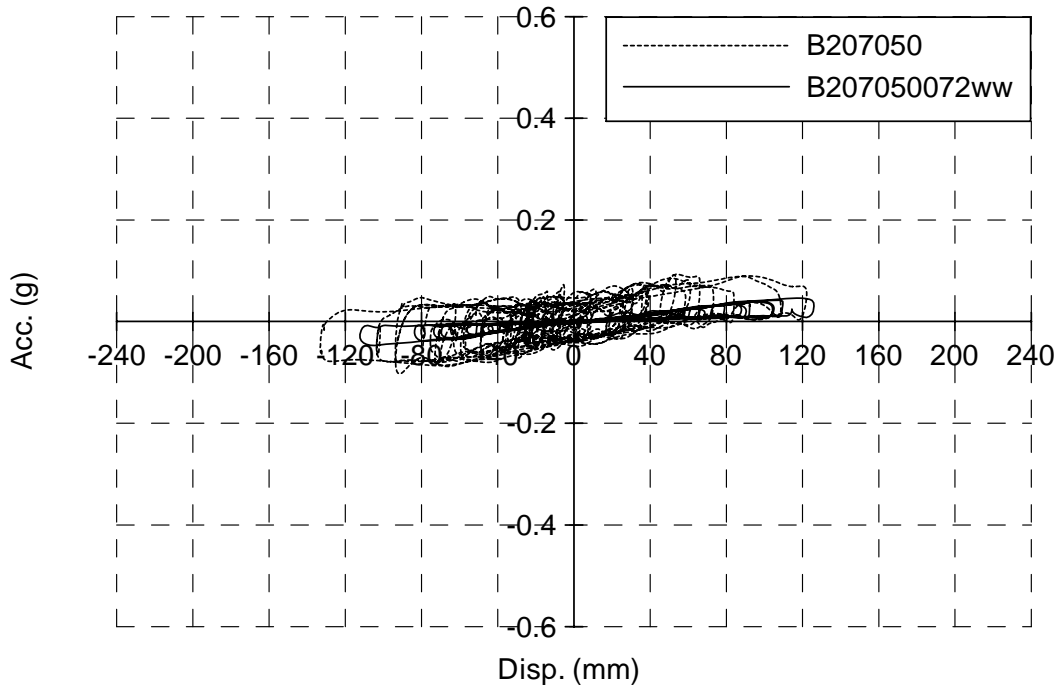


Figure 5.57 Comparison of Acceleration-Displacement Relationships Between Spring Units and Entire System under Input of B2

5.6 Further Investigation of Rotation Effect

It is observed in Section 5.4 that during all the tests, the rotation angle of Isolated Floor System II is not significant. However, the rotation can cause an increase in the displacement response (relative to the shake table) of the isolated floor corner, which is equal to the rotation angle times half length of the isolated floor side perpendicular to the seismic direction under consideration. This effect should be considered in the design of Isolated Floor System II.

The ratios of the corner displacement (relative to the shake table) due to the rotation of the isolated floor over the isolated floor displacement at the middle point of the side perpendicular to the seismic direction under consideration are summarized in Table 5.8 for cases using the 2 sets of 2627 N/m (15 lb/in) nominal stiffness spring. The responses in both X and Y directions are collected for bidirectional tests. In this table, “e” represents eccentricity; “t” means time; D_{ris} is

displacement (relative to the shake table) of the middle point of the side perpendicular to the seismic direction under consideration; R_c is the displacement of the isolated floor corner due to rotation. Note that there are three rows listed for each test: the first row is the results at the time when the maximum D_{ris} occurs; the second row is for the responses at the time when the maximum R_c occurs, and; the third row means the responses when $D_{ris}+R_c$ (i.e., the total displacement of the isolated floor corner relative to the shake table) reaches its maximum value during the test.

From this table, it can be found that the maximum value of D_{ris} and the maximum value of R_c occur at different times. Also it can be observed that the total displacement (i.e., $D_{ris}+R_c$) at the corner of the isolated floor system when the maximum value of D_{ris} occurs is bigger than that when the maximum R_c occurs, and is equal to/almost same as that when the maximum ($D_{ris}+R_c$) happens (at almost the same time as when the maximum D_{ris} occurs). The averaged value of the ratios of R_c/D_{ris} when the maximum D_{ris} occurs is obtained as 5.2%, 18.8%, and 23.9% for the cases with symmetric gravity loads, eccentric loads at an eccentricity of 425 mm, and eccentric loads at an eccentricity of 671 mm, respectively.

The comparison between these values obtained from tests with those obtained by using Eq. 13.3-5 for total displacement calculation in NEHRP 2003 show that the formula in NEHRP 2003 is too conservative for the eccentric load cases, which gives a value of higher than 40% for the 425 mm eccentric load case, and 70% for the 671 mm eccentric load case, respectively. At the current stage of this project, the R_c/D_{ris} values obtained from tests will be used in the development of the design methodology for Isolated Floor System II, which is part of the topic of Chapter 9. Because the data obtained from the tests shown in this chapter is limited, future research could further investigate the rotation effects of Isolated Floor System II (for example, to better determine the factors that impact the rotation effect, and to develop a closed-form formula to predict this rotation effect under different cases of floor excitations).

Table 5.8 Rotation Effects_2627 N/m Spring Units

Load Case	e (mm)	Test	X Direction					Y Direction						
			t (s)	D _{ris} (mm)	R _c (mm)	D _{ris} +R _c (mm)	R _c /D _{ris} (%)	t (s)	D _{ris} (mm)	R _c (mm)	D _{ris} +R _c (mm)	R _c /D _{ris} (%)		
1	0	1Acc002	11.914	57.8	1.4	59.2	2.5	12.695	7.1	1.7	8.9	24.4		
			0.043	7.5	6.8	14.3	91.2	24.438	1.8	6.2	8.0	333.3		
			11.914	57.8	1.4	59.2	2.5	0.043	4.4	5.6	10.0	128.6		
		1Acc11	12.297	124.0	1.4	125.4	1.1	11.355	5.8	5.2	11.0	88.7		
			11.672	61.1	6.0	67.1	9.8	36.953	0.9	7.0	7.9	775.4		
			12.301	124.0	1.4	125.4	1.1	11.344	5.8	5.2	11.0	89.4		
		1Acc31	12.898	77.4	2.1	79.6	2.7	12.379	7.2	3.2	10.4	44.2		
			10.035	42.5	5.8	48.2	13.5	0.043	0.8	7.0	7.9	827.5		
			12.902	77.4	2.2	79.6	2.8	12.336	7.0	3.6	10.6	51.6		
		1C1	13.520	76.6	10.0	86.7	13.1	15.266	98.8	9.0	107.7	9.1		
			13.605	66.2	12.0	78.3	18.2	13.602	27.8	15.7	43.4	56.4		
			13.527	76.5	10.3	86.9	13.5	15.266	98.8	9.0	107.7	9.1		
		1C2	12.395	128.5	4.7	133.2	3.7	13.566	146.0	16.1	162.2	11.0		
			13.363	83.8	21.5	105.3	25.7	13.355	115.9	20.1	135.9	17.3		
			13.199	123.2	15.6	138.8	12.7	13.563	146.0	16.2	162.2	11.1		
		2	0	2Acc002	13.293	72.5	6.4	78.9	8.8	11.613	9.4	0.7	10.1	7.1
					12.109	13.5	14.2	27.7	104.7	12.086	0.2	10.8	11.1	4837.9
					13.293	72.5	6.4	78.9	8.8	13.066	8.4	7.6	15.9	90.3
2Acc01	14.609			64.4	4.5	68.9	7.0	12.414	11.6	2.3	13.9	20.1		
	15.141			38.8	8.7	47.5	22.4	15.164	3.1	9.4	12.5	302.4		
	14.609			64.4	4.5	68.9	7.0	12.410	11.6	2.3	13.9	20.1		
2Acc11	15.359			153.7	4.4	158.1	2.9	15.496	20.2	1.7	21.9	8.5		
	18.926			43.0	12.2	55.2	28.3	18.891	1.2	11.6	12.8	992.4		
	15.359			153.7	4.4	158.1	2.9	12.520	20.1	9.6	29.7	47.7		
2Acc31	14.191			130.5	4.7	135.2	3.6	14.289	31.1	1.8	32.9	5.9		
	20.016			27.7	14.0	41.8	50.6	16.230	4.2	16.8	20.9	403.0		
	14.195			130.4	4.8	135.2	3.7	14.582	29.9	6.6	36.5	22.2		
2C1	15.125			177.6	3.2	180.8	1.8	15.488	189.9	9.4	199.3	4.9		
	18.766			7.1	27.8	34.9	390.3	18.762	35.6	28.8	64.4	80.9		
	15.152			177.2	4.2	181.5	2.4	15.473	189.4	10.5	199.9	5.6		
2C2	15.246			210.2	6.8	217.0	3.2	15.305	132.1	10.0	142.1	7.6		
	19.859			0.2	18.2	18.4	9106.4	19.852	23.1	19.8	42.9	86.0		
	15.250			210.2	6.9	217.1	3.3	15.305	132.1	10.0	142.1	7.6		

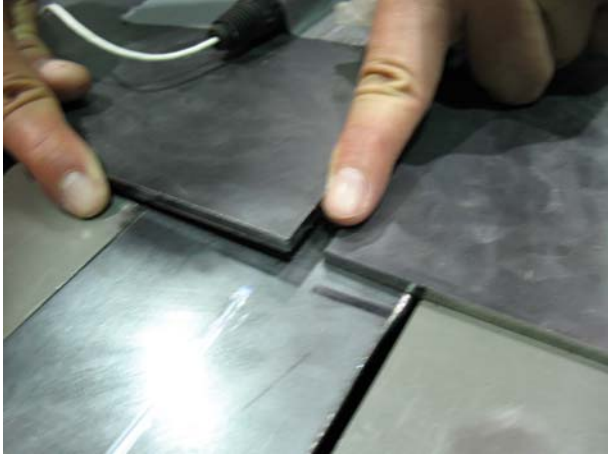
Table 5.8 Rotation Effects_2627 N/m Spring Units (Contd.)

Load Case	e (mm)	Test	X Direction					Y Direction				
			t (s)	D _{ris} (mm)	R _c (mm)	D _{ris} +R _c (mm)	R _c /D _{ris} (%)	t (s)	D _{ris} (mm)	R _c (mm)	D _{ris} +R _c (mm)	R _c /D _{ris} (%)
3	0	3Acc11	15.230	169.0	16.3	185.3	9.6	-	-	-	-	-
			15.207	168.3	16.4	184.7	9.7	-	-	-	-	-
			15.227	169.0	16.3	185.3	9.7	-	-	-	-	-
		3Acc31	15.414	239.5	5.3	244.7	2.2	-	-	-	-	-
			18.664	36.8	15.4	52.2	41.8	-	-	-	-	-
			15.418	239.4	5.3	244.8	2.2	-	-	-	-	-
		3C2	15.625	198.0	1.2	199.2	0.6	15.711	152.5	0.2	152.7	0.1
			10.922	17.6	26.5	44.1	150.4	10.918	8.6	27.1	35.8	315.0
			15.621	198.0	1.3	199.2	0.6	15.734	152.4	0.5	152.9	0.3
4	0	4C2	15.516	146.4	4.6	151.0	3.2	14.270	148.1	15.8	164.0	10.7
			20.664	3.6	21.4	25.0	599.5	20.625	2.5	22.3	24.8	907.9
			15.520	146.4	4.7	151.1	3.2	14.434	147.4	17.3	164.7	11.8
5	425	5C2	15.109	219.7	46.7	266.4	21.3	15.156	142.4	50.5	192.9	35.5
			16.262	104.8	72.5	177.3	69.2	16.281	115.7	73.2	189.0	63.2
			15.113	219.7	46.9	266.5	21.3	13.828	137.9	56.5	194.4	40.9
6	425	6C2	15.613	155.7	0.1	155.8	0.1	14.332	149.5	52.5	202.0	35.1
			14.324	87.8	52.6	140.4	59.9	14.344	149.3	52.6	201.9	35.2
			15.621	155.6	0.5	156.0	0.3	14.332	149.5	52.5	202.0	35.1
7	671	7Acc11	15.125	152.2	42.1	194.3	27.6	-	-	-	-	-
			15.387	49.6	55.4	105.1	111.6	-	-	-	-	-
			15.145	151.5	43.9	195.4	28.9	-	-	-	-	-
		7Acc31	13.754	107.0	21.0	128.0	19.6	-	-	-	-	-
			13.996	86.7	31.0	117.6	35.7	-	-	-	-	-
			13.773	106.4	22.7	129.1	21.3	-	-	-	-	-
		7C2	14.965	191.5	76.0	267.4	39.7	15.020	156.3	83.8	240.1	53.6
			16.250	47.1	98.1	145.1	208.4	16.238	90.8	102.6	193.4	113.0
			14.977	191.0	77.0	268.0	40.3	15.035	156.1	84.3	240.4	54.0
8	671	8Acc31	15.004	92.0	12.5	104.6	13.6	-	-	-	-	-
			20.207	59.8	27.8	87.5	46.5	-	-	-	-	-
			14.230	89.1	24.7	113.7	27.7	-	-	-	-	-
		8C1	15.512	132.6	15.3	147.9	11.5	15.906	180.8	66.1	246.9	36.5
			16.238	103.8	81.5	185.3	78.5	16.238	120.8	91.6	212.3	75.8
			16.355	119.4	78.0	197.4	65.3	15.930	179.5	69.3	248.8	38.6
		8C2	15.328	155.4	4.5	159.9	2.9	14.016	132.0	52.2	184.2	39.6
			14.176	68.0	57.0	125.0	83.7	14.207	118.9	59.3	178.2	49.9
			15.328	155.4	4.5	159.9	2.9	14.039	131.3	54.0	185.3	41.1

5.7 Importance of Quality Control

While the previous sections illustrate that the isolated floor system worked well. It is important to emphasize here that before all these results were obtained, the isolated floor system was installed in a faulty manner that created unevenness on the floor surface. During the first tests, as the isolated floor moved, a tile of the walking surface protruded slight above the adjacent ones and hit edge of an edge plate during motion, as shown in Fig. 5.58, and the isolated floor abruptly stopped moving when it happened, which caused high accelerations on the isolated floor because of the sudden discontinuous jerky motion. The results of a of 2Acc11 during which this problem happed are shown in Fig. 5.59 as an example to illustrate this problem, which is denoted as 2Acc111 to distinguish it from test 2Acc11 (presented earlier) in which the problem was corrected. High spikes of acceleration up to 1.5g can be seen in Fig. 5.59. Close inspection of the specimen allowed to discover this construction error. Since there was no time during the test program to fix this discontinuity issue, the two edge plates that were creating this problem were removed as shown in Fig. 5.60. Advantage was taken of the fact that the wheels under the isolated floor became visible by removing these two edge plates and cameras were installed such that the motion of the isolated floor could be better documented. All the results shown in preceding sections were obtained after this modification.

In an actual implementation, it is recommend that a quality control program is implemented to prevent such a problem. The walking surface of the isolated floor consisting of tiles should be closely inspected such that the isolated floor can actually slide unhampered. Another solution to this problem is that the edge plates should be made continuous over the seams of the tiles such that such problem will not rise.



(a)



(b)

Figure 5.58 Impact between the Edges of the Edge Plate and the Tile: (a) Edge of the Edge Plate after Impact, and; (b) Edge of the Tile after Impact

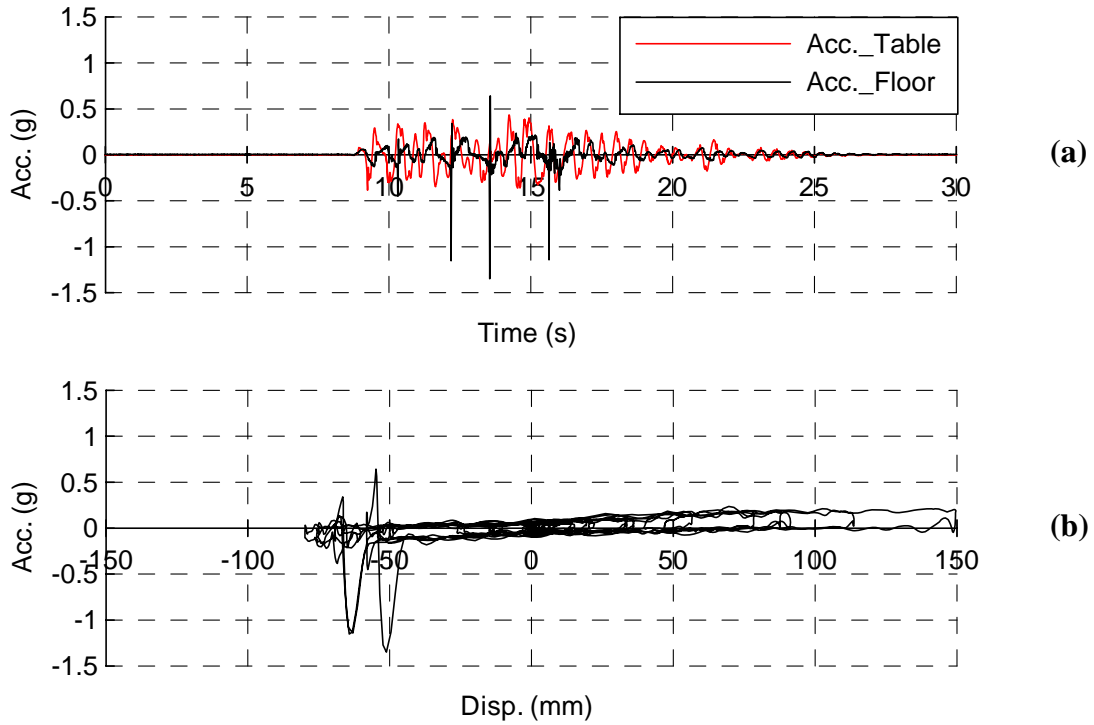


Figure 5.59 Results of Test 2Acc111: (a) Acceleration of Shake Table and Isolated Floor, and; (b) Acceleration-Displacement Relationship of Isolated Floor System II

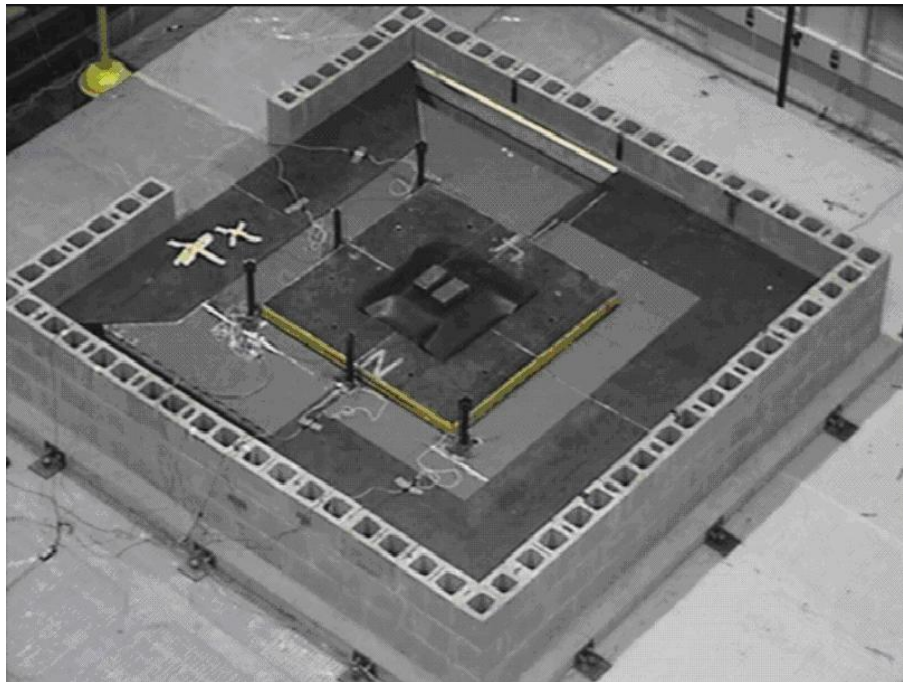


Figure 5.60 Removal of Edge Plates

5.8 Observations

This chapter presented the details of the characterization tests conducted on Isolated Floor System II. Throughout all these characterization tests, the isolated floor system remained undamaged. The test results show that the isolated floor system worked well in reducing the acceleration response on top of the isolated floor. The behavior of this isolated floor system, regardless of the nominal stiffness of the multi-directional spring units used as isolators, is stable when subjected to different seismic inputs for a given gravity load configuration and when subjected to repeated motions. Furthermore, the peak acceleration of the isolated floor was found to reduce when it supported greater gravity load.

It was found that at relatively large displacements (larger than 76 mm), the acceleration response of the isolated floor reaches a plateau. The system maximum acceleration response in bidirectional tests was found to be the same as in corresponding unidirectional tests as long as the displacement in both directions exceeded than 76 mm, although their displacement response may be different.

The behavior of the entire isolated floor system was also compared with that of its multi-directional spring units, i.e., as individual components. A difference in behavior was observed, and amounted to a constant friction value of 0.035g, which is attributed to the friction between the floor casters and the concrete base. Another friction, which is between the edge plates and the walking surface, was also found. These frictions, together with the model proposed in Chapter 7 for multi-directional spring units, will provide the foundation for better simulating the behavior of Isolated Floor System II in computer programs.

CHAPTER 6

ISOLATED FLOOR SYSTEM I CHARACTERIZATION TEST

6.1 Introduction

The mechanical properties of a special kind of concrete ball-in-cone (BNC) isolator, in terms of acceleration-displacement relationship, were obtained by characterization tests and presented in Chapter 3. This chapter presents the characterization tests of an entire isolated floor system built using this kind of concrete BNC isolators, which is denoted here as Isolated Floor System I to distinguish it from the other isolated floor system manufactured by Dynamic Isolation Systems (DIS) presented in Chapter 5 (which is denoted as Isolated Floor System II). As mentioned in Chapter 5, Isolated Floor System I was designed first, although Isolated Floor System II was tested first.

To characterize the mechanical properties (such as force-displacement relationship) of Isolated Floor System I to be able to simulate its dynamic response in computer programs, some characterization tests were conducted using the shake table facilities located in the Structural Engineering and Earthquake Simulation Laboratory (SEESL) at the University at Buffalo. In these characterization tests, to simulate realistic conditions to be encountered when a floor isolation system is installed in an existing room, the isolated floor system was surrounded by a masonry wall and steel edge plates were used to cover the space between the isolated floor and the wall. As considered in the single isolator tests (reported in Chapter 3), both polyurethane balls and rubber balls were adopted as the rolling balls of the concrete BNC isolators. For the

tested complete floor system, both synthetic ground motions and analytically obtained floor responses from both SDOF and MDOF structural fuse frames were adopted as seismic inputs. Unidirectional tests, as well as bidirectional tests, were conducted. Both symmetric and eccentric placements of gravity load were considered. In addition, some tests of the isolated floor without the edge plates were conducted to compare behavior with that of the floor with its edge plates in place. The mechanical properties of the system studied were presented in terms of acceleration-displacement relationships in this chapter.

The objectives of these tests are to investigate the behavior of Isolated Floor System I under different seismic inputs, different load cases, and under repeated motions. Therefore, the test results are compared from these different points of view. Furthermore, comparison of behavior between single concrete BNC isolator and the corresponding entire isolated floor system was presented. Observations from the above comparisons will be used to better model this isolated floor system.

6.2 Isolated Floor System I Description

Some schematic drawings of the Isolated Floor System I concept are shown in Fig. 6.1. The detailed design of Isolated Floor System I is presented in Appendix A. It is proposed as a solution to decouple the response of the nonstructural components on the isolated floor from the motion of the floor itself. The Isolated Floor System I was designed as a modular system to satisfy a number of practical constraints of this system, including ease of inspection, repair or replacement after seismic events in case damage occurs to any component of this system, small weight for each part for manual assembly, small height of the isolated floor system to minimize size of the step to access the isolated floor and minimize loss of usable room clearance. The prototype used for the current test program consisted of three rows of concrete BNC isolators to decouple the response as shown in Fig. 6.1a. There were 12 sets of isolators, 24 bearing plates

(including 12 bottom bearing plates and 12 top ones) in total, in these three rows. Each row included four sets of isolators. The top and bottom concrete bearing plates in each row were connected by steel flat bars, 38 mm (1.5 in) deep and 6 mm (0.25 in) thick, respectively. These flat bars were bolted down to the 6 mm (1/4 in) diameter threaded rods pre-cast into the concrete bearing plates. As mentioned in Chapter 3, either polyurethane balls or rubber balls can be used as rolling balls between the top and bottom bearing plates of these concrete BNC isolators. A steel frame consisting of L2x2x1/4 angles was bolted onto the 6 mm (0.25 in) diameter threaded rods pre-cast into the top bearing plates of the concrete BNC isolators. The walking surface adopted for this system was a fiber reinforced polymer (FRP) product called SAFPLANK (which is a commercially available interlocking decking system) which was cut to size to sit into the steel frame. The FRP decking system used here is produced in 610 mm (24 in) wide units which were cut into 914 mm (36 in) long pieces to fit into the frame formed by the steel angles. The total weight of the moving parts of Isolated Floor System I (i.e., excluding the 12 bottom bearing plates of the concrete BNC isolators resting directly on the supporting floor) is about 5186 N (1166 lb).

Steel edge plates were used here to cover the space between the isolated floor and the wall, as shown in Fig. 6.1. Continuous “2x6” wood boards bolted onto the wall served to connect and support these edge plates using piano hinges as shown in Fig. 6.2. As demonstrated in Chapter 3, when the top bearing plates of the concrete BNC isolator move relative to the bottom ones, they will rise by about 1/10 times the horizontal relative displacement amount. Therefore, the top surface of the “2x6” wood boards was set about 25 mm (1 in) higher than the walking surface of the isolated floor to ensure that the edge plates remained inclined downward and in contact with the isolated floor’s walking surface during motion of the isolated floor system, as shown in Fig. 6.2. The steel edge plates used in Isolated Floor System I were rectangular. The resulting corner configuration of Isolated Floor System I is shown in Fig. 6.3. Note that this created a small gap in height between the edges of two adjacent edge plates. An alternative corner

configuration which avoids this gap is the corner configuration that was used in Isolated Floor System II, as shown in Fig. 6.4 (and as previously reported in Chapter 5), where the edge plates were cut off at an angle in the corners to better match adjacent edge plates at those locations. Note that floor area that can be loaded without obstructing sliding of the system is the central 2032 mm x 1829 mm (80 in x 72 in) rectangular area, which is bigger than the corresponding 1740 mm x 1740 mm (68.5 in x 68.5 in) one in Isolated Floor System II.

Also note that the resulting Isolated Floor System I concept meets the design constraints that have been outlined earlier. In particular, the components of this system are of small weight and easy to be inspected, removed, or replaced. The total height of this isolated floor system, from the bottom surface of the bottom concrete bearing plates to the walking surface, is only about 193 mm (7.6 in).

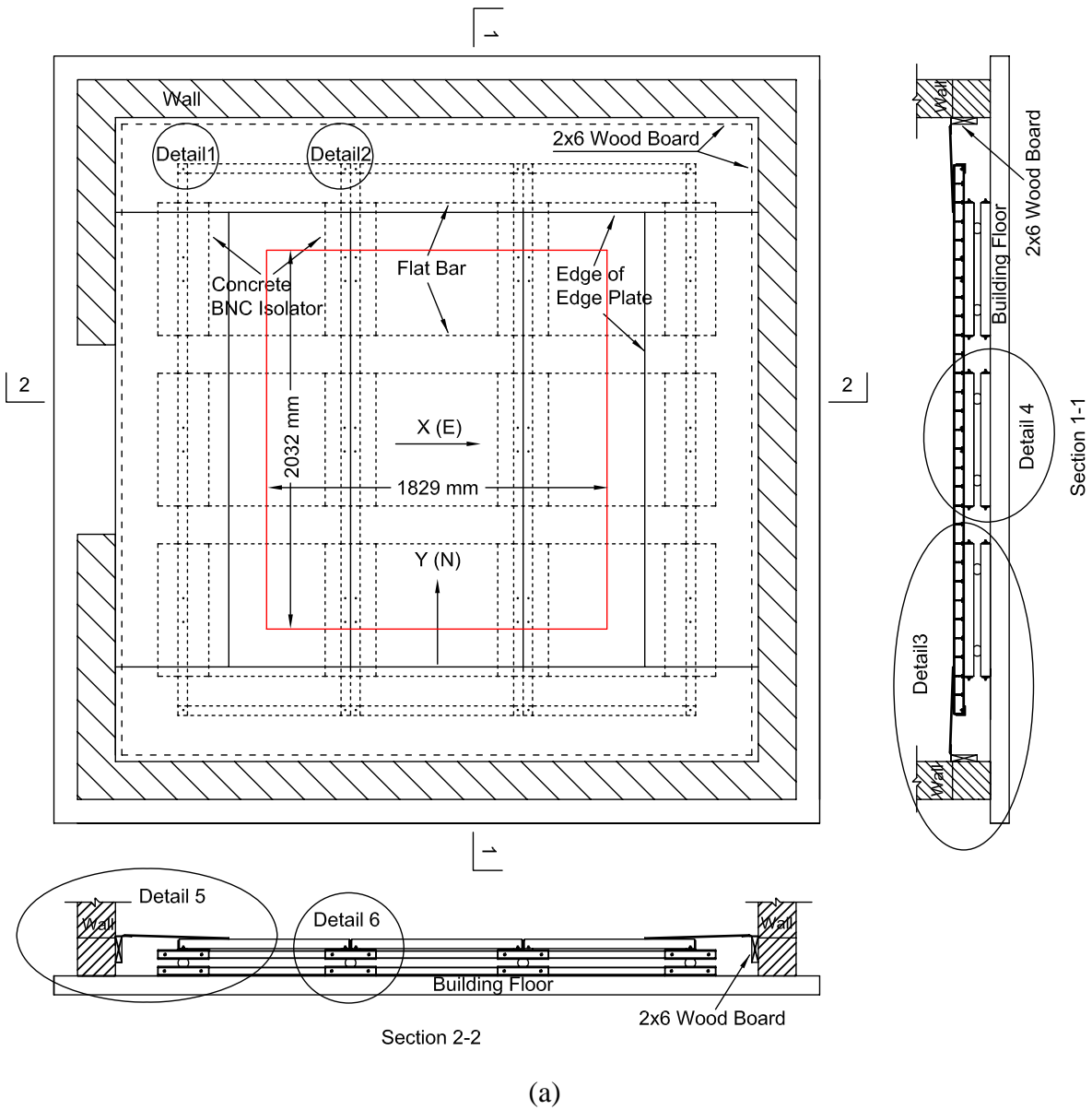


Figure 6.1 Isolated Floor System I: (a) Plan and Cross Section Views of Isolated Floor System I, and; (b) and (c) Details 1 and 2 indicated in (a)

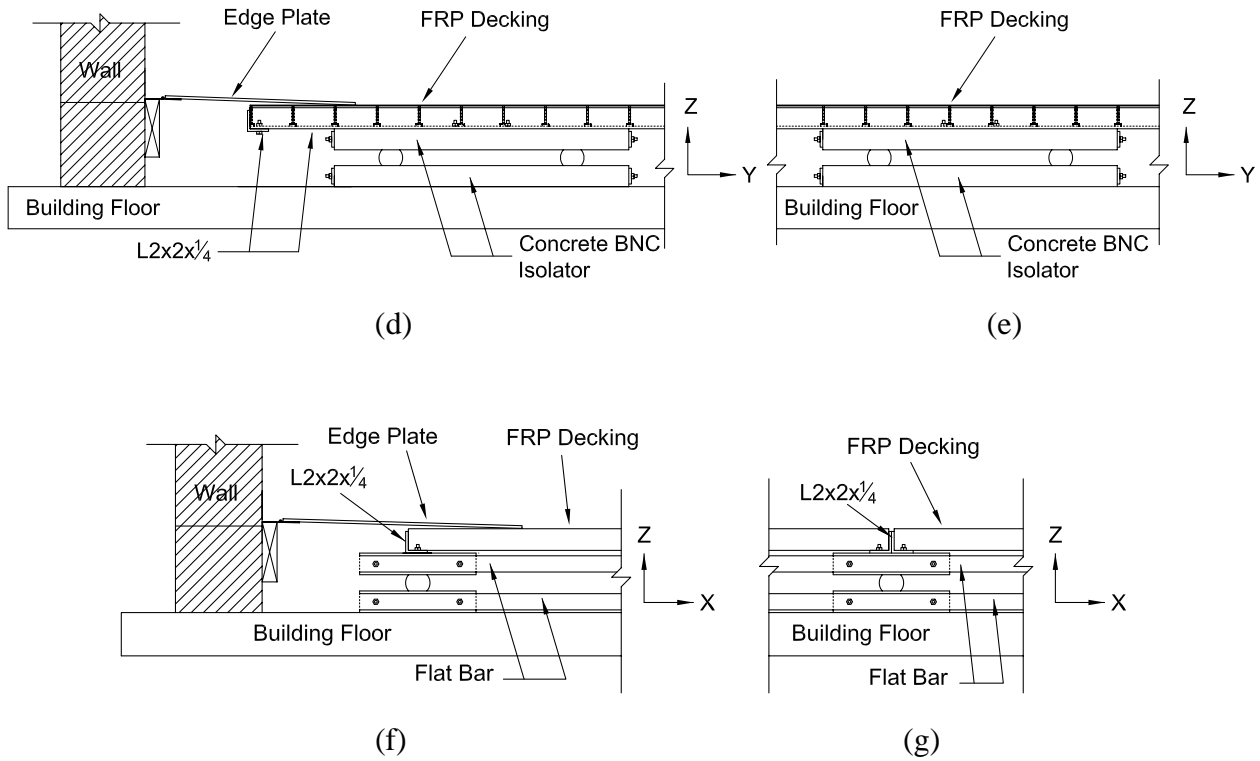


Figure 6.1 Isolated Floor System I: (d) to (g) Details 3 to 6 Indicated in (a)

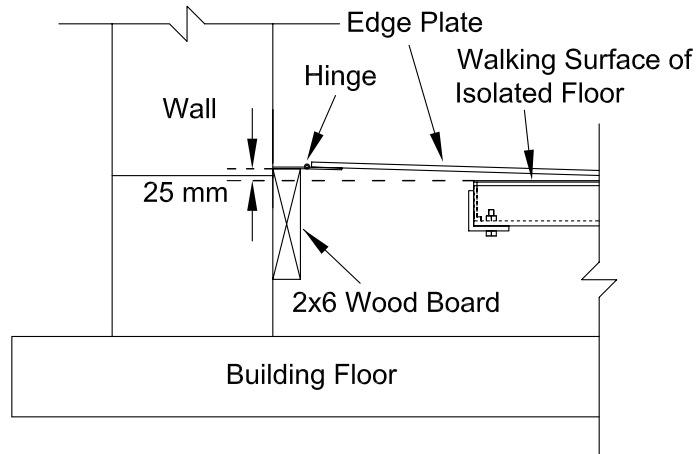


Figure 6.2 Configuration of Edge Plate in Isolated Floor System I



Figure 6.3 Corner Configuration of Edge plates in Isolated Floor System I

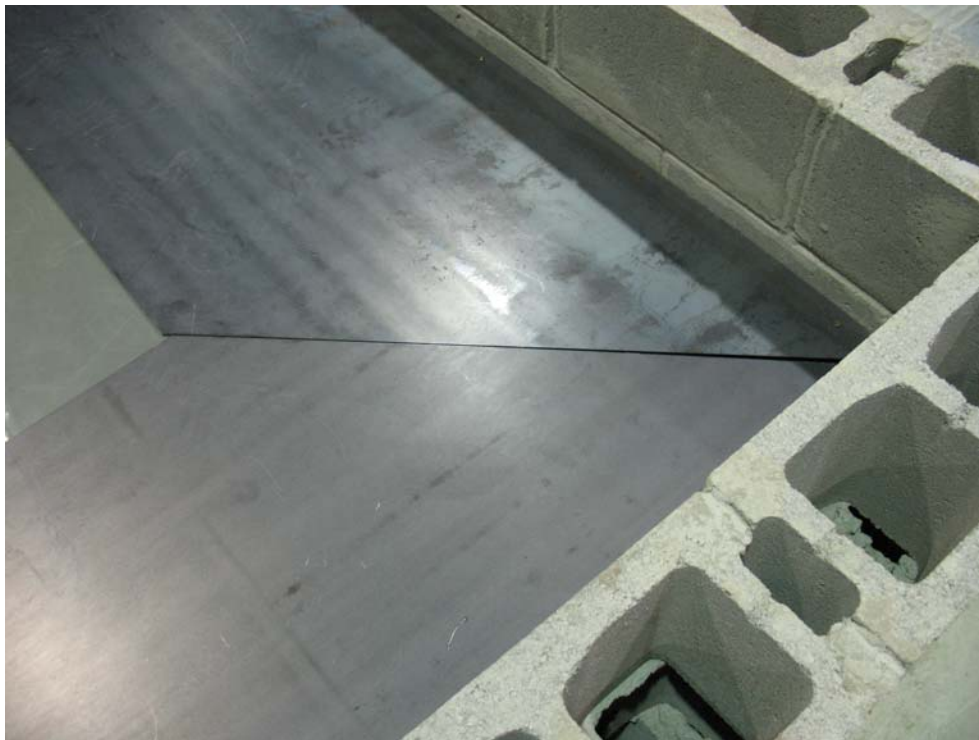


Figure 6.4 Corner Configuration of Edge Plates in Isolated Floor System II

6.3 Test Setup

6.3.1 Specimen Assembly and Setup

The same concrete slab used for the tests of Isolated Floor System II (presented in Chapter 5) was used here to simulate the structural floor surface on which isolated floors would be installed in a typical application. Again, to simulate the constraints of installing such an isolated floor systems in building rooms, a 610 mm (24 in) tall masonry wall, identical to that used in tests of Isolated Floor System II, was also built on the concrete slab. The inside area bounded by the wall was 3464 mm x 3464 mm (136 in x 136 in), which was same as that in Isolated Floor System II and corresponded to the size of a small room. The fixture of the concrete slab to the shake table was identical to that presented in Section 5.3.1.

Assembly of the isolated floor specimen proceeded as follows. Twelve sets of concrete isolators were set in position on the surface of the concrete slab. A 1.6 mm (1/16 in) thick rubber pad was placed between the bottom of the isolator bearing plate and the slab to improve friction between the two surfaces. The L2x2x1/4 steel angles were then bolted to the threaded rods that had been pre-cast into the top surface of the concrete top bearing plates, as shown in Fig. 6.5. Next, the 914 mm (36 in) long FRP decking pieces were dropped into the space formed by adjacent steel angles, as shown in Fig. 6.6, and interlocked together. Three rows of FRP decking formed the walking surface of this isolated floor system. To prevent slippage of the FRP decking pieces during the tests, these pieces were tightened down to the steel angles using a proprietary insert hold down systems from Strongwell (Strongwell, 2003), working as shown in Fig. 6.7. Finally, the 4 steel edge plates were tack welded onto one of the piano hinge leaves, and the other leaf of the piano hinges were screwed down to the top surface of “2x6” wood boards, themselves bolted onto the wall (as shown in Fig. 6.2). Two of these 4 pieces, 2438 mm (96 in) long, 610 mm (24 in) wide, and 4.8 mm (3/16 in) thick, were fixed along the east and west sides of the

surrounding wall. The other two pieces, 3464 mm (136 in) long, 608 mm (20 in) wide, and 6.4 mm (1/4 in) thick, were fixed along the north and south side of the surrounding wall. An overview of the resulting assembled Isolated Floor System I specimen is shown in Fig. 6.8.



Figure 6.5 Grid of Steel Angles on Top of Isolators



Figure 6.6 Inserting of FRP Decking Pieces

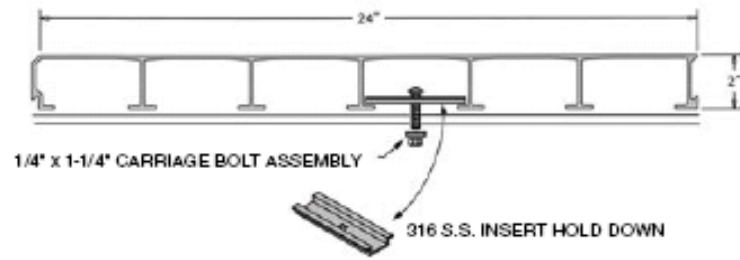


Figure 6.7 Insert Hold Down System (Strongwell, 2003)



Figure 6.8 Overview of Isolated Floor System I Specimen

6.3.2 Load Program

As mentioned in Chapter 5, the isolated floor system by DIS (i.e., Isolated Floor System II) was tested earlier than Isolated Floor I although Isolated Floor I was designed first. To compare the behavior of the two isolated floor systems considered, a consistent set of load cases was used with some minor modifications due to some system-specific constraints. As defined in Chapter 5, two load criteria are used for the gravity design of the isolated floor system. First, the floor has to be able to resist 0.012 MPa (250 psf) over a small area at any point over the floor system. This is referred to as walking surface load carrying capacity. Second, the floor has to be able to resist a specified uniformly distributed load over its entire area, which is defined as the uniformly distributed load carrying capacity. Here, the same walking surface load carrying capacity as in Isolated Floor System II of 0.012 MPa (250 psf) was adopted as the nominal load carrying capacity of the walking surface of Isolated Floor System I. Also, Isolated Floor System I was

designed for a 2400 Pa (50 psf) uniformly distributed load.

The same steel plates, file cabinet, and lead bricks as those used in tests of Isolated Floor System II were used here to create different load cases for tests of Isolated Floor System I. The ten load cases considered in Chapter 5 for tests of Isolated Floor System II, including both symmetric and eccentric cases, were also considered here for Isolated Floor System I except some minor modifications in some specific load cases due to the system itself specific constraints. Fig. 6.9 illustrates the dimensions of the different parts (i.e., the edge plates, the load permissible area) of the area enclosed by the surrounding masonry wall for the Load Case 1 for Isolated Floor System I. Note that in Isolated Floor System I, the edge plates had rectangular edges, which are different from the triangular ones used in Isolated Floor System II. Also, although the area enclosed by the surrounding masonry wall is the same in both isolated floor systems, namely 3454 mm x 3454 mm (136 in x 136 in), the area available for gravity loading in Isolated Floor System I is 2032 mm x 1829 mm (80 in x 72 in), bigger than the area of 1740 mm x 1740 mm (68.5 in x 68.5 in) in Isolated Floor System II. This is because the widths of the edge plates used were smaller in Isolated Floor System I because the gap between the wall and the edge of the isolated floor system was also smaller. Therefore, for the load cases with large eccentricities of applied load (i.e., Load Cases 7 and 8), there is some more space on the floor surface for the bottom layer of steel plates to be located offset from the perfectly symmetric case. However, the steel plates were used in the same configuration and at the same position as in Isolated Floor System II with respect to the center of the isolated floor, for consistency to allow possible comparison between the behavior of both isolated floor systems. As such, for all load cases, except Load Case 10, the load configuration used for Isolated Floor Systems I and II were identical. For Load Case 10, as shown in Figs. 6.10, the file cabinet was instead put on a whole piece of edge plate to avoid sitting on the uneven surfaces of two adjacent edge plates at the corner as mentioned in Section 6.2, to keep the cabinet more stable during the tests.

Preliminary analyses indicated that the Isolated Floor System I was conservatively designed to carry these ten load cases, even though sometimes locally loaded up to 0.012 MPa (250 psf). As such, these tests acted as “proof tests” to check whether this isolated floor system could carry these expected load cases.

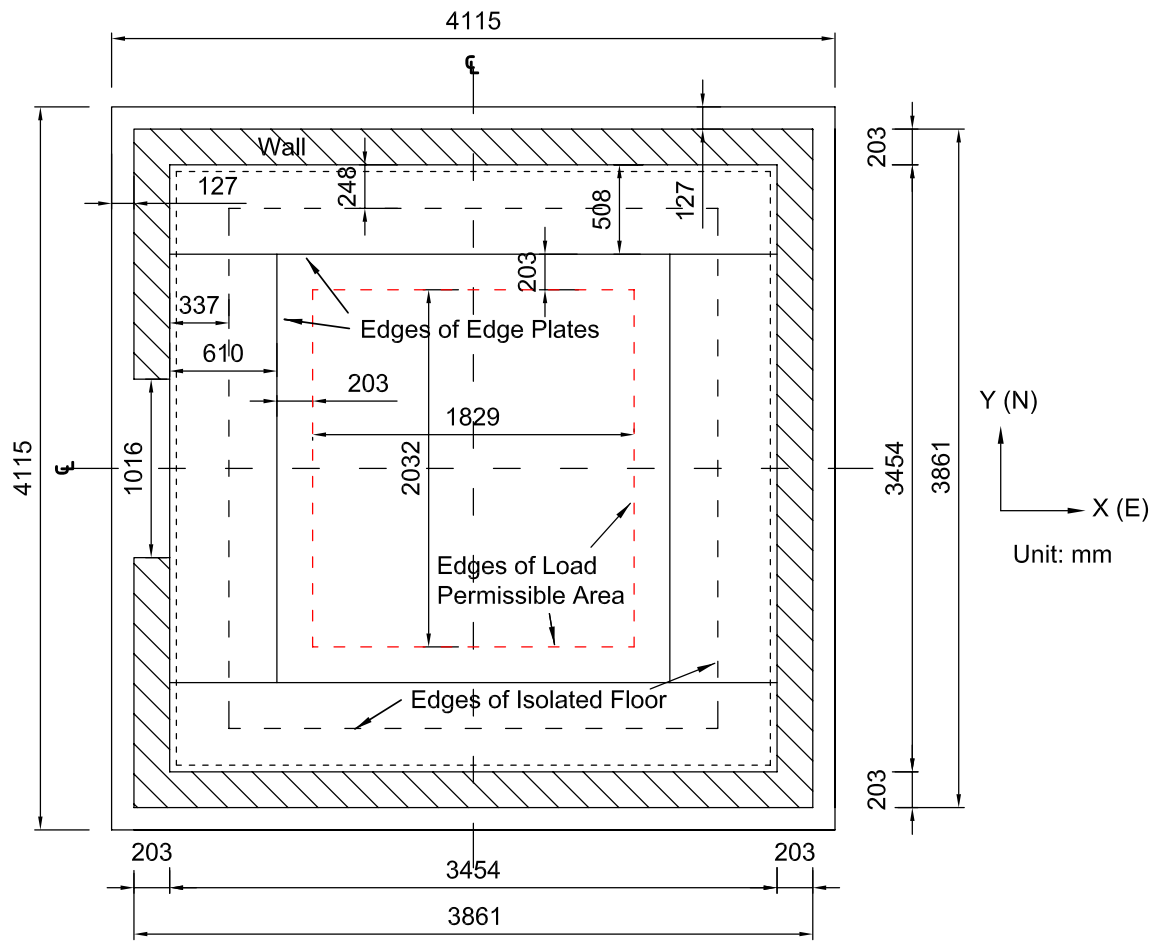


Figure 6.9 Top View of Load Case 1

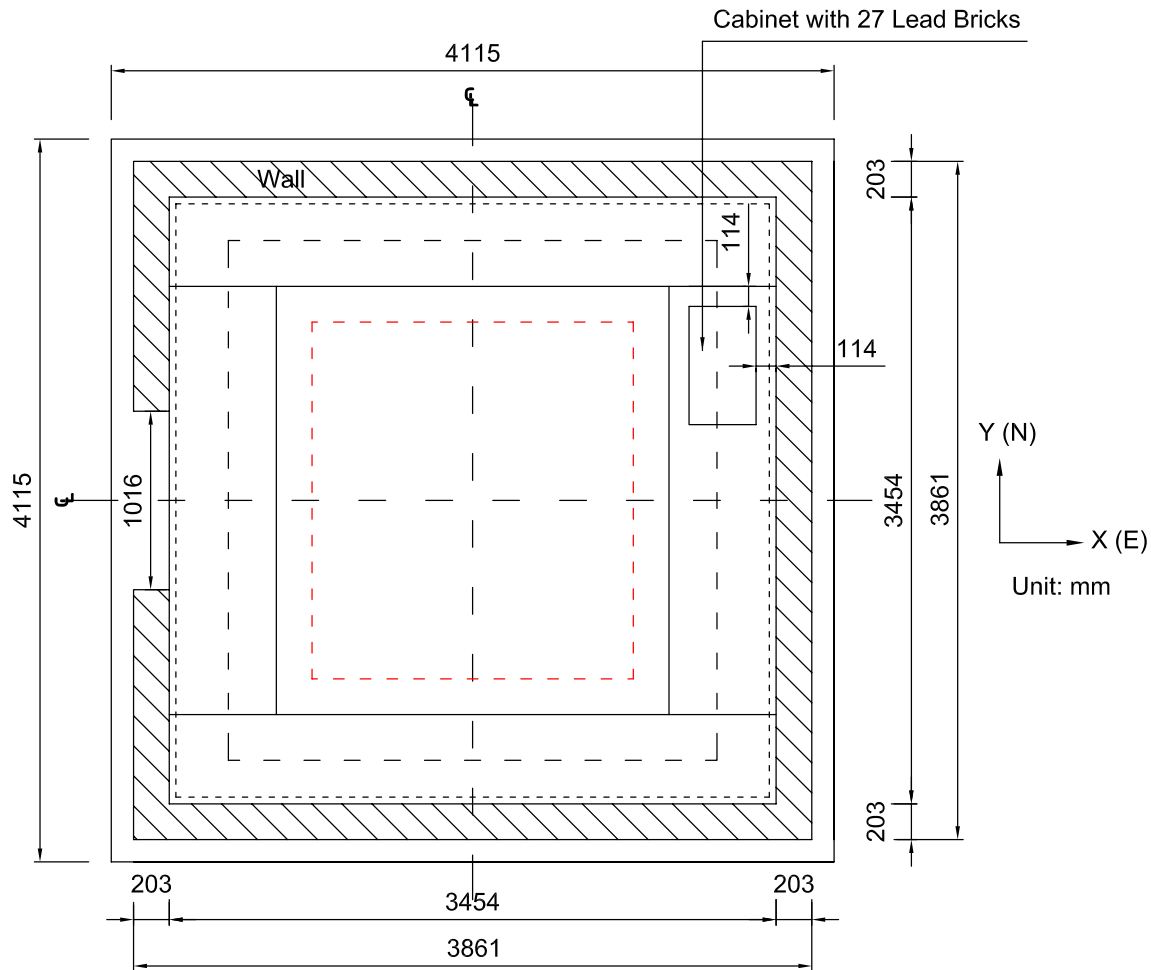


Figure 6.10 Top View of Load Case 10

6.3.3 Input Program

For the characterization tests of Isolated Floor System I, similar to those for Isolated Floor System II previously presented in Chapter 5, both unidirectional and bidirectional inputs were used. The seismic input, Acc01, Acc02, Acc11, Acc31, and B1, used in characterization tests of Isolated Floor System II presented in Section 5.3.3, were also used here to test Isolated Floor System I to allow comparing the behaviors of these two isolated floor system. In addition, sine sweep tests were conducted for several load cases by using constant acceleration control. The frequency range of sine sweep signal used varied from 0.5 Hz to 20 Hz. The acceleration

amplitude of the sine sweep signal was 0.15g and 0.20g for the floors having polyurethane and rubber balls, respectively, except that a value of 0.20g was used in one case with polyurethane balls as described later.

In addition to using the above input motions for unidirectional tests, some bidirectional tests were also conducted on Isolated Floor System I. The two sets of combined bidirectional inputs, C1 (combination of Acc01 and Acc02) and C2 (combination of Acc11 and Acc31), used in the characterization tests of Isolated Floor System II introduced in Section 5.3.3 were also adopted here to test Isolated Floor System I in two directions at the same time.

Although some mechanical properties of the concrete BNC isolators were obtained through characterization tests introduced in Chapter 3, this data alone was conservatively judged insufficient to predict the whole system behavior. Therefore, to protect the specimen, each variant of the isolated floor system was first tested using a low level of seismic excitations by scaling down the above seismic inputs. These seismic inputs were then gradually scaled up to different amplitudes such as to make the isolated floor system reach a displacement response of about 127 mm (5 in) in unidirectional tests and 102 mm (4 in) in bidirectional tests, unless such displacements could not be reached due to limit in the displacement capacity of 152 mm (6 in) of the shake table in SEESL, as done in Chapter 5.

6.3.4 Instrumentation

Again, the objective of these tests is to capture the force-displacement behavior of Isolated Floor System I and compare the resulting performance to that of the non-isolated floor. Here, “force” means the restoring force of the isolated floor system, and “displacement” is the relative displacement of the isolated floor with respect to the base. The restoring force of this system was to be calculated from the acceleration response of the isolated floor. Displacement and

acceleration response of both the shake table and the isolated floor were measured. Furthermore, to investigate the rotation motion of the isolated floor, it was decided to measure the displacement response at both ends of each side of the isolated floor, like in those tests for Isolated Floor System II.

The same twenty-four instrumentation channels as used previously (Chapter 5) were used to record the response of the specimen here, namely, twelve accelerometers and twelve “string pots” displacement transducers. The positions of the twelve instrumentations are shown in Fig. 6.11, where the bold numbers from “1” to “12” represent the points where displacements and accelerations were measured. The description of each channel is presented in Table 6.1 along the direction of motion recorded by each instrument. Again, similar to those in Chapter 5, because the surrounding wall was higher than the walking surface of the isolated floor, for the instrumentation on the walking surface, five steel rising bars were used to elevate the connecting points for the string pots so that they could be deployed straight, above the height of the wall, as shown in Fig. 6.12.

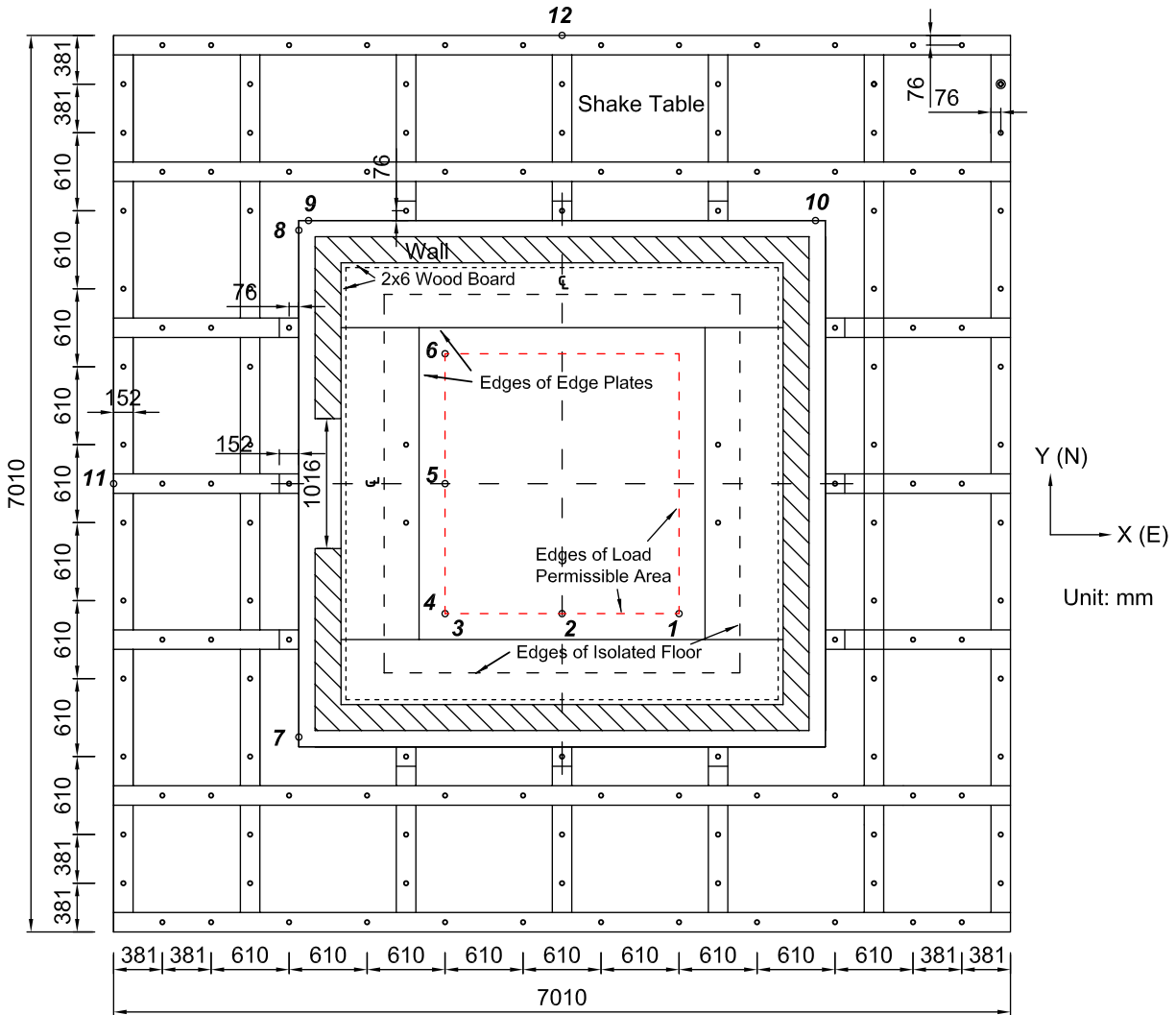


Figure 6.11 Top View of Instrumentation positions

Table 6.1 Summary of Instrumentation Channels

Channel # (1)	Name (2)	Position* (3)	Type of Sensor (4)	Measure Direction (5)	Note (6)
1	Acc1	1	Accelerometer	N-S	Isolated floor surface**, East, South
2	Acc2	2	Accelerometer	N-S	Isolated floor surface, Middle, South
3	Acc3	3	Accelerometer	N-S	Isolated floor surface, West, South
4	Acc4	4	Accelerometer	E-W	Isolated floor surface, South,West
5	Acc5	5	Accelerometer	E-W	Isolated floor surface, Middel, West
6	Acc6	6	Accelerometer	E-W	Isolated floor surface, North, West
7	Acc7	7	Accelerometer	E-W	Footing slab, South, West
8	Acc8	8	Accelerometer	E-W	Footing slab, North, West
9	Acc9	9	Accelerometer	N-S	Footing slab, West, North
10	Acc10	10	Accelerometer	N-S	Footing slab, East, North
11	Acc11	11	Accelerometer	E-W	Shake Table,Middle, West
12	Acc12	12	Accelerometer	N-S	Shake Table,Middle, North
13	Sp1	1	String Pot	N-S	Isolated floor surface, East, South
14	Sp2	2	String Pot	N-S	Isolated floor surface, Middle, South
15	Sp3	3	String Pot	N-S	Isolated floor surface, West, South
16	Sp4	4	String Pot	E-W	Isolated floor surface, South,West
17	Sp5	5	String Pot	E-W	Isolated floor surface, Middle, West
18	Sp6	6	String Pot	E-W	Isolated floor surface, North, West
19	Sp7	7	String Pot	E-W	Footing slab, South, West
20	Sp8	8	String Pot	E-W	Footing slab, North, West
21	Sp9	9	String Pot	N-S	Footing slab, West, North
22	Sp10	10	String Pot	N-S	Footing slab, East, North
23	Sp11	11	String Pot	E-W	Shake Table,Middle, West
24	Sp12	12	String Pot	N-S	Shake Table,Middle, North

* Position means the instrumentation position in Fig. 6.12;

** Isolated floor surface actually means the rising bars fixed on the isolated floor walking surface.



Figure 6.12 Rising Bars Fixed on Walking Surface

6.3.5 Test Protocol

As mentioned in Section 6.3.2, different load cases, including cases with mass eccentricity in one or two directions, were considered for these tests. The objectives of these tests were to capture the behavior of the Isolated Floor System I under each load case, to investigate whether the behavior of this system is stable under each load case when subjected to different seismic input, and to compare the behavior of the isolated floor system under different load cases (i.e., between different symmetric load cases, and between symmetric and corresponding eccentric load cases having the same magnitude of gravity loads). Therefore, as for those tests previously presented in Section 5.3.5, under each load case, especially for symmetric load cases (i.e., Load Cases 1 to 3) and the eccentric load case having relative large magnitude of gravity load (i.e., Load Case 7), tests subjected to different seismic inputs were conducted, including bidirectional inputs. Furthermore, to compare the behavior of the isolated floor system between cases with and without edge plates, some tests without edge plates were conducted for each load case (except

for Load Cases 9 and 10 where the file cabinet had to sit on the edge plates). These tests were conducted by lifting the edge plates about the pin axes of the piano hinges and fixing them to the surrounding wall with clamps, as shown in Fig. 6.13. Finally, as mentioned before, because either polyurethane balls or rubber balls can be used as rolling balls between bearing plates of the concrete isolators, floor having both kinds of balls were tested.

Both 51 mm (2 in) diameter polyurethane balls with hardness of 95A and 51 mm (2 in) diameter rubber balls with hardness of 70A were used, respectively, as the rolling balls between the bearing plates of the concrete BNC isolators to test Isolated Floor System I. The sequences of the characterization tests conducted for the floors having the different balls are in Tables 6.2 and 6.3, respectively, where the nomenclature of the test name is constructed by sequentially referring to the ball type first, load case number second, and the motion input name last. For this purpose, polyurethane balls were denoted as “1”, and rubber balls as “2”. For example, “11Acc01” means the test adopting polyurethane balls under Load Case 1 when subjected to input Acc01. The name for each test conducted for the isolated floor without edge plates, is constructed by adding “wo” at the end of the test name obtained per the above rule.

Table 6.2 Test Sequences of Isolated Floor System I with Polyurethane Balls

Test # (1)	Test Name (2)	Input Name (3)	Load Case # (4)	Edge Plates (5)
1	11ss*	Sine Sweep**	1	with
2	11B1	B1	1	with
3	11Acc01	Acc01	1	with
4	11Acc11	Acc11	1	with
5	11Acc31	Acc31	1	with
6	11C1	C1	1	with
7	11C2	C2	1	with
8	11B1wo	B1	1	without
9	11Acc11wo	Acc11	1	without
10	11C2wo	C2	1	without
11	12ss	Sine Sweep	2	with
12	12B1	B1	2	with
13	12Acc01	Acc01	2	with
14	12Acc11	Acc11	2	with
15	12Acc31	Acc31	2	with
16	12C1	C1	2	with
17	12C2	C2	2	with
18	12B1wo	B1	2	without
19	12Acc11wo	Acc11	2	without
20	12Acc31wo	Acc31	2	without
21	12C2wo	C2	2	without
22	13ss	Sine Sweep	3	with
23	13B1	B1	3	with
24	13Acc11	Acc11	3	with
25	13C2	C2	3	with
26	13B1wo	B1	3	without

* Sine sweep signal is denoted as "ss" in test name;

** Input of sine sweep test is denoted as "Sine Sweep".

Table 6.2 Test Sequences of Isolated Floor System I with Polyurethane Balls (Contd.)

Test # (1)	Test Name (2)	Input Name (3)	Load Case # (4)	Edge Plates (5)
27	13Acc11wo	Acc11	3	without
28	13C2wo	C2	3	without
29	14C2	C2	4	with
30	14C2wo	C2	4	without
31	15C2	C2	5	with
32	15C2wo	C2	5	without
33	16C2	C2	6	with
34	16C2wo	C2	6	without
35	17B1	B1	7	with
36	17Acc01	Acc01	7	with
37	17Acc11	Acc11	7	with
38	17Acc31	Acc31	7	with
39	17C2	C2	7	with
40	17B1wo	B1	7	without
41	17Acc11wo	Acc11	7	without
42	17Acc31wo	Acc31	7	without
43	17C2wo	C2	7	without
44	18Acc31	Acc31	8	with
45	18C1	C1	8	with
46	18C2	C2	8	with
47	18Acc31wo	Acc31	8	without
48	18C2wo	C2	8	without
49	19B1	Acc31	9	with
50	19C1	C2	9	with
51	110B1	Acc31	10	with
52	110C1	C1	10	with

Table 6.3 Test Sequences of Isolated Floor System I with Rubber Balls

Test # (1)	Test Name (2)	Input Name (3)	Load Case # (4)	Edge Plates (5)
1	21ss*	Sine Sweep**	1	with
2	21Acc11	Acc11	1	with
3	21C2	C2	1	with
4	21Acc11wo	Acc11	1	without
5	21C2wo	C2	1	without
6	22ss	Sine Sweep	2	with
7	22B1	B1	2	with
8	22Acc11	Acc11	2	with
9	22C2	C2	2	with
10	22B1wo	B1	2	without
11	22Acc11wo	Acc11	2	without
12	22C2wo	C2	2	without
13	23ss	Sine Sweep	3	with
14	23B1	B1	3	with
15	23Acc11	Acc11	3	with
16	23C2	C2	3	with
17	23B1wo	B1	3	without
18	23Acc11wo	Acc11	3	without
19	23C2wo	C2	3	without
20	27B1	B1	7	with
21	27Acc11	Acc11	7	with
22	27C2	C2	7	with
23	27B1wo	B1	7	without
24	27Acc11wo	Acc11	7	without
25	27C2wo	C2	7	without
26	28C2	C2	8	with
27	28C2wo	C2	8	without
28	29C1	C1	9	with
29	210C1	C1	10	with

* Sine sweep signal is denoted as "ss" in test name;

** Input of sine sweep test is denoted as "Sine Sweep".

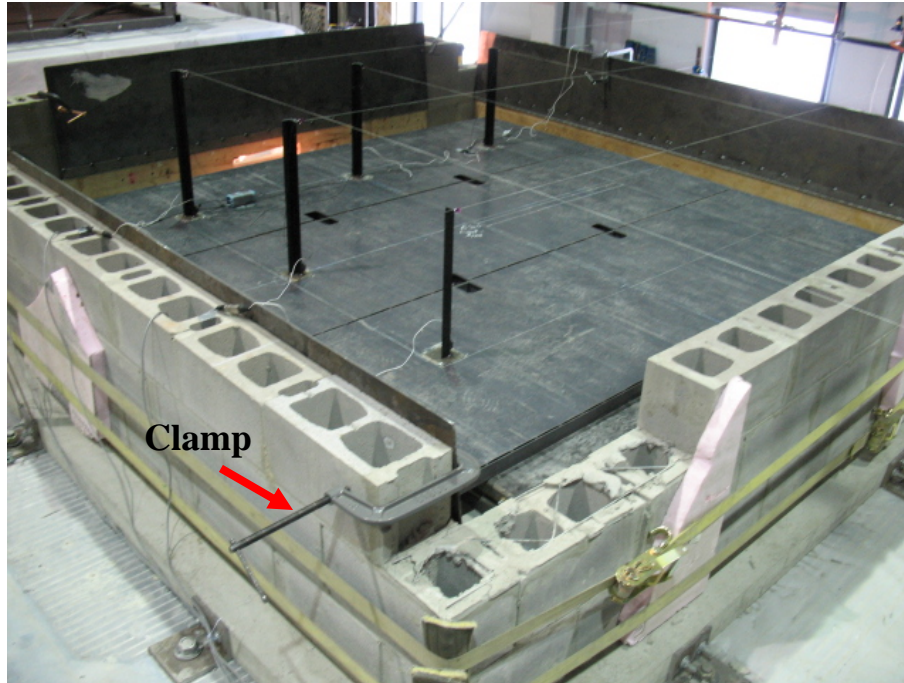


Figure 6.13 Lifting and Fixing of Edge Plates

6.4 Test Results

6.4.1 General

As mentioned in Section 6.3.3, the shake table excitations were first run at a low level of peak accelerations and then gradually scaled up. Hence, many trial tests were conducted to get the appropriate scaling factors for the inputs to reach the isolated floor's target amplitudes of displacement response. For all the tests that gave the target floor response for a given load and input condition, the peak values of the measured response quantities, including PTD, PFD, PTA, PFA, peak rotation angle of the isolated floor, and peak relative displacement of isolated floor with respect to shake table, are tabulated in Table 6.4 and Table 6.5 for tests on floors using polyurethane and rubber balls, respectively. The meaning of these abbreviated terms here are same as those defined in Section 5.4.1. Selected typical results for the tests conducted under corresponding appropriate input scaling factors are presented in Figs. 6.14 to 6.35, among which

Figs. 6.14 to 6.24 are for tests on floors using polyurethane balls and Figs. 6.25 to 6.35 are for tests on floors using rubber balls. The rest of the test results under corresponding appropriate input scaling factors are presented in Appendix D. Similar to those figures presented in Chapter 5, each of Figs. 6.14 through 6.35 contains four plots labeled from (a) to (d). The meaning of each of those plots is same as that described in Section 5.4.1.

6.4.2 Typical Results

During all these characterization tests, no damage occurred on the isolated floor system itself. Although the performance of various systems is compared in the next section, some typical responses of the system are shown in Figs. 6.14 to 6.35. Figs. 6.14 and 6.25 show response of the isolated floor typically obtained under a sine sweep type of excitation for isolated floors having polyurethane and rubber balls, respectively. As mentioned in Chapter 3, the sine sweep tests were not conducted to determine the period of this isolated floor system. Rather, they worked as tests to investigate the behavior of the system. This gives a good illustration of the type of acceleration-displacement relationship of the isolated floor system at various levels of displacement. Rotation of the system was small, typically less than 0.004 rad (i.e., 0.2 degrees). This can also be observed for all other cases later. Figs. 6.15 and 6.26 show the typical results for unidirectional earthquake excitation for polyurethane and rubber balls, respectively. Note from the plot (a) of each figure that the floor displacement response is generally in phase with the shake table excitation. But, the relative displacement between the isolated floor and the shake table is significant enough to produce the isolation effect. Also, note that the acceleration-displacement hysteretic curves are similar to those obtained in the sine sweep cases. Again, the rotation of the system is not significant. Figs. 6.16 to 6.17 and 6.27 to 6.28 illustrate cases, where bidirectional earthquake excitation was used, for polyurethane and rubber balls, respectively. Note under these cases, that the displacement response of the isolated floor and the shake table excitation are still generally in phase as observed before. The

acceleration-displacement hysteretic curves are much more erratic. This is because, in the BNC system, the rolling balls may start to circle on a plane at identical elevation inside the cone. This observation has also been made in prior tests of ball-in-cone systems (Andrei M. Reinhorn, University at Buffalo, The State University of New York, private communication, 2008).

Some typical responses of the isolated floor system without edge plates are shown (i.e., Figs. 6.18 to 6.20 for polyurethane balls, and Figs. 6.29 to 6.31 for rubber balls) following the figures for the corresponding cases with the edge plates. Again, for both unidirectional and bidirectional tests under these cases, it could be observed that rotation angle of the isolated floor is small, and the displacement response of the isolated floor and the shake table are generally in phase although the relative displacement between them is significant enough to illustrate the isolation effect. Again, the acceleration-displacement hysteretic curves are more erratic in bidirectional tests than those in unidirectional cases.

Figs. 6.21 to 6.24 and Figs. 6.32 to 6.35 show typical results for Load Cases 9 and 10 for polyurethane and rubber balls, respectively. Note that during the tests under Load Cases 9 and 10, where a small file cabinet filled with lead bricks was located on top and/or across of the edge plates, the isolated floor only moved slightly relatively to the shake table. This is logical since it was not possible for the isolated floor to be effective for these two load cases. The file cabinet impeded the movement of the floor by creating significant friction between the walking surface and the cabinet in Load Case 9 and between the walking surface and the steel cover plates in Load Case 10. The cabinet did vibrate and slide a little bit during the tests. However, it did not overturn or hit against the wall.

From the values in Columns (2) to (5) of Tables 6.4 and 6.5, note that the peak displacement response of the isolated floor is bigger than the corresponding displacement of the shake table. Results in Columns (6) to (9) of Tables 6.4 and 6.5 show that the peak acceleration response of

the isolated floor more or less reduced compared to the corresponding acceleration response of the shake table, except for tests of 11ss, 11Acc11, 21ss, and 21Acc11 where the peak response value of the floor was the same as or a little bit bigger than that of the shake table. In these cases, the isolated mass was small and the friction effect from the edge plates might have locked the systems partially. From the results in Columns (10) and (11) of Tables 6.4 and 6.5, note that the rotation of the isolated floor is not significant, even for bidirectional tests with large mass eccentricities (i.e. Load Case 7 and 8). The maximum value of the peak rotation angle for all these characterization tests is 0.034 rad in magnitude, which is only 1.9 degrees. However, the rotation can cause an increase in the displacement response (relative to the shake table) of the isolated floor corner, which is equal to the rotation angle times half length of the isolated floor side perpendicular to the seismic direction under consideration. Therefore, as done in Chapter 5, this effect should also be considered here in the design of the Isolated Floor System I. This rotation effect will be further discussed in the following section.

As shown in the typical Figs. 6.14d to 6.35d, the acceleration-displacement relationships of Isolated Floor System I form some hysteretic loops. As mentioned in Chapter 3, this is because of the friction between the rolling balls and the concrete bearing plates of the BNC isolators. Since the acceleration of the isolated floor is directly related to the restoring force, then, the enclosed area is proportional to energy dissipation. Furthermore, the loops for each unidirectional test seem to agree with each other well, which means the behavior of the isolated floor system is stable under repeated motions. In addition, as mentioned in Chapter 3, the peak acceleration response of the isolated floor should be constant at large relative displacements for each test (i.e. as long as the rolling balls are within the conical part of the working surface) based on the mechanical properties of this kind of isolator. This can be seen from the (d) plots of the figures for unidirectional tests among Figs. 6.14 to 6.35 where the acceleration-displacement loops are almost flat at large displacements. In all cases (either unidirectional or bidirectional tests), the restoring force is always radially applied towards the center of the isolator working

surface, in other words, the ball could go along a circular motion at a constant distance from the center of the isolator working surface as mentioned before, and as the result of this radial restoring force and friction, the ball will move spirally back to the center of the isolator. Per the same principles, then subjected to bidirectional excitation, when the ball is at any given X and Y position, the restoring force towards the center of the cone has X and Y components which will be smaller in magnitude than that of the restoring force acting in the radial direction, resulting in smaller maximum acceleration response in the X and Y directions than those observed during the corresponding unidirectional tests in each respective direction.

6.4.3 Comparisons

To investigate whether the behavior of Isolated Floor System I is stable when subjected to different unidirectional seismic inputs, the comparison of the acceleration-displacement relationships for the symmetric load cases (Load Cases 1 to 3) is plotted in Figs. 6.36 to 6.40 for polyurethane balls (Figs. 6.36 to 6.38) and rubber balls (Figs. 6.39 and 6.40). It is observed from these figures that the acceleration-displacement loops, under the same load case, when subjected to different seismic inputs agree well with each other, confirming that the behavior of this isolated floor system is stable when subjected to different seismic excitations.

To investigate how the behavior of Isolated Floor System I (with edge plates on) changes under unidirectional seismic inputs and different load cases, the test results for Load Cases 1 to 3 under shake table excitation inputs B1 and Acc11 respectively, in terms of acceleration-displacement relationship, are shown together in Figs. 6.41 to 6.44 for polyurethane balls and rubber balls, respectively. And to investigate how the behavior of Isolated Floor System I without edge plates changes under unidirectional seismic inputs and different load cases, the test results for Load Cases 1 to 3 under shake table excitation input Acc11, in terms of acceleration-displacement relationship, are shown together in Figs. 6.45 and 6.46 for polyurethane balls and rubber balls,

respectively. From Figs. 6.45 and 6.46, note that the loops become progressively fatter from Load Cases 1 to 3. However, in Figs. 6.41 to 6.44, this trend is not observed. The loops for Load Cases 2 and 3 almost agree with each other, and the loops for Load Case 1 are fatter than the corresponding ones for Load Cases 2 and 3. This is reasonable. The friction between the edge plates and the walking surface is a constant. When the total isolated mass (i.e., total mass of the isolated floor and the steel plates on top) increases from Load Case 1 to 3, the friction effect on the acceleration of the isolated floor (which is calculated as the ratio of the friction over the total isolated mass) will become less significant.

To investigate the difference in behavior between symmetric and eccentric load cases for this isolated floor system, for each kind of balls, the comparison of the test results of 12Acc11 and 17Acc11 and the comparison of the test results of 22Acc11 and 27Acc11 are shown in Figs. 6.47 and 6.48, respectively. It is observed that the behavior of the isolated floor system from each test agrees with each other well, which is because the rotation effect of the isolated floor is not significant as mentioned before.

As mentioned in Section 6.3, some steel edge plates were used to cover the space between the isolated floor and the surrounding wall. Consequently, friction between the steel cover plates and the walking surface of the isolated floor was introduced into this system. To investigate the effect of this friction, the test results for cases with and without these edge plates for Load Cases 1 to 3, and each kind of rolling balls, in terms of acceleration-displacement relationships, are shown together for comparison in Figs. 6.49 to 6.59, respectively. From these figures, a significant difference in the amplitude of the acceleration attained by the isolated floor can be observed. This difference between the acceleration-displacement loops from the cases with edge plates and the corresponding cases without edge plates confirms the presence of an additional friction effect. Furthermore, this difference becomes less significant going from Load Cases 1 to 3. In particular, for Load Case 3, as shown in Figs. 6.53 and 6.54 for polyurethane balls and Figs. 6.58 and 6.59

for rubber balls, the loops for cases with and without edge plates almost agree with each other and the friction effect is almost negligible. This is reasonable for the same reason described above regarding the lesser significance of the friction effect on the acceleration response of the isolated floor system when greater masses are applied on the floor. The difference between the loops in Figs. 6.49, 6.50, and 6.55 for Load Case 1, is about 0.085g, which when multiplied by the corresponding total isolated mass (of about 529 Kg (1166 lb)) corresponds to a friction of about 441 N (99.1 lb). This friction should be considered when simulating the behavior of Isolated Floor System I in computer programs, which is the subject of Chapter 7.

As shown above, the difference in the behavior of the isolated floor systems with and without edge plates has been observed. To better model the behavior of the isolated floor system in computer programs, it is necessary to compare the behavior of the concrete BNC isolator as a component versus that of the entire isolated floor system without edge plates. The gravity loads considered on each ball in Load Case 3 (i.e., 1350 N/ball (304 lb/ball), including the self-weight of the top concrete bearing plates) mentioned in Chapter 3 for concrete BNC isolator component tests almost perfectly corresponds to that in Load Case 3 (i.e., 1361 N/ball (306.1 lb/ball)) for the entire isolated floor system tests without edge plates here. Figs. 6.60 and 6.61 compare the seismic BNC isolator component test results under Load Case 3 from Chapter 3 with the corresponding system test results when subjected to Acc11 for the polyurethane ball and rubber ball cases, respectively. From these figures, note that the peak acceleration response of the isolated floor system is almost same as that of the isolator component alone. Also, the ordinate difference of the loops at given displacement (i.e., the “fatness” of the loops) in the acceleration-displacement loop for both component and system test is almost the same. As mentioned in Chapter 3, the magnitude of this range between the plateau of acceleration values on the loading and unloading parts of the loops is actually caused by the friction effect between the rolling balls and the concrete bearing plates. Therefore, the equivalent coefficient of rolling friction defined in Chapter 3, μ_e , for the system tests under Load Cases 3 is the same as the

values for the concrete BNC isolator component tests under corresponding load cases, which is about 0.044 and 0.1 for the cases using polyurethane balls and rubber balls respectively.

Recall from Chapter 3 that the magnitude of the coefficient of rolling friction, μ_e , depends on the value of the gravity load applied on the ball. For example, from Figs. 6.18 and 6.29, under Load Case 2 (i.e., 182 lb/ball corresponding to 25 psf), the μ_e is estimated to be 0.034 for polyurethane balls and 0.087 for rubber balls respectively. These data, together with the μ_e values estimated in Chapter 3, can be used for modeling the whole system behavior. This is the subject of Chapter 7.

Note here that the seismic inputs in the tests of Isolated Floor Systems I here and II (as shown in Chapter 5) were scaled differently in the tests of different floor systems. Detailed information on the shake table signals used for each test is available on the SEESL repository ([nas.nees.buffalo.edu/repository/allprojects/mceer/isolated raised floor](http://nas.nees.buffalo.edu/repository/allprojects/mceer/isolated%20raised%20floor)).

Table 6.4 Summary of Peak Values of Response Quantities (Polyurethane Balls)

Test Name (1)	PTD* (mm)		PFD** (mm)		PTA*** (g)		PFA**** (g)		Peak Rotation (x 10 ⁻³ rad)		Peak Relative Disp. (mm)	
	E-W (2)	N-S (3)	E-W (4)	N-S (5)	E-W (6)	N-S (7)	E-W (8)	N-S (9)	E-W (10)	N-S (11)	E-W (12)	N-S (13)
11ss	80.8	—	81.3	—	0.25	—	0.25	—	2.4	2.4	61.3	—
11B1	142.7	—	219.3	—	0.64	—	0.27	—	5.3	4	119.7	—
11Acc01	202.8	—	215.8	—	0.55	—	0.21	—	1.8	1.3	39.3	—
11Acc11	147.7	—	152.3	—	0.21	—	0.24	—	1.8	1.1	71.6	—
11Acc31	138.3	—	140.8	—	0.34	—	0.22	—	1.1	0.9	18.4	—
11C1	169.3	124.0	199.9	196.8	0.55	0.62	0.19	0.21	3.2	3.0	73.5	75.1
11C2	166.1	169.1	213.5	241.7	0.29	0.40	0.22	0.23	1.9	1.4	108	105.5
11B1wo	72.43	—	199.5	—	0.34	—	0.16	—	2.0	2.0	168.1	—
11Acc11wo	91.3	—	208.7	—	0.19	—	0.14	—	1.4	1.4	153.4	—
11C2wo	65.5	66.8	133.7	166.4	0.13	0.15	0.11	0.14	6.9	8.0	84.1	125.5
12ss	70.8	—	136.2	—	0.19	—	0.22	—	3.4	3.9	171.6	—
12B1	99.4	—	189.8	—	0.47	—	0.18	—	2.7	3.4	142.8	—
12Acc01	163.9	—	254.9	—	0.49	—	0.18	—	2.4	2.6	104.7	—
12Acc11	160.3	—	273.0	—	0.26	—	0.19	—	3.6	4.0	151.9	—
12Acc31	159.0	—	272.9	—	0.37	—	0.23	—	2.5	3.0	162.3	—
12C1	162.7	119.7	275.5	225.4	0.55	0.55	0.19	0.17	7.5	9.5	136.5	130.9
12C2	115.3	130.9	173.7	235.6	0.20	0.30	0.16	0.18	9.2	10.4	87.9	153.6
12B1wo	65.7	—	123.4	—	0.30	—	0.14	—	3.3	3.5	84.3	—
12Acc11wo	114.3	—	228.4	—	0.20	—	0.15	—	3.8	3.9	147.7	—
12Acc31wo	114.3	—	222.3	—	0.37	—	0.17	—	2.7	3.6	144.2	—
12C2wo	81.4	93.0	144.0	201.0	0.15	0.21	0.12	0.16	6.1	7.2	86.6	146.3
13ss	67.6	—	125.6	—	0.18	—	0.19	—	3.5	3.7	135	—
13B1	93.4	—	176.1	—	0.43	—	0.17	—	1.7	1.5	129.7	—
13Acc11	121.1	—	199.2	—	0.23	—	0.17	—	1.3	1.3	105.2	—
13C2	107.6	127.8	165.8	218.5	0.17	0.28	0.16	0.22	1.3	1.3	74.2	121.4
13B1wo	82.2	—	178.2	—	0.38	—	0.16	—	5.9	5.5	141.7	—

* PTD is the peak absolute displacement response of the shake table;

**PFD is the peak absolute displacement response of the isolated floor;

***PTA is the peak absolute acceleration response of the shake table;

****PFA is the peak absolute acceleration response of the isolated floor.

Table 6.4 Summary of Peak Values of Response Quantities (Polyurethane Balls) (Contd.)

Test Name (1)	PTD* (mm)		PFD** (mm)		PTA*** (g)		PFA**** (g)		Peak Rotation (x 10 ⁻³ rad)		Peak Relative Disp. (mm)	
	E-W (2)	N-S (3)	E-W (4)	N-S (5)	E-W (6)	N-S (7)	E-W (8)	N-S (9)	E-W (10)	N-S (11)	E-W (12)	N-S (13)
13Acc11wo	119.4	—	222.6	—	0.22	—	0.16	—	3.2	3.4	135.5	—
13C2wo	84.5	101.0	138.1	192.4	0.15	0.23	0.15	0.16	2.2	2.3	67.3	119.1
14C2	119.7	121.9	180.8	196.6	0.19	0.25	0.18	0.16	5.8	5.4	75.7	97.7
14C2wo	103.1	105.1	190.0	220.1	0.15	0.19	0.12	0.14	34.2	2.9	110.3	150.9
15C2	140.0	143.4	214.7	237.9	0.18	0.24	0.17	0.21	10.8	10.5	83.4	113.3
15C2wo	84.4	85.9	137.0	161.3	0.12	0.17	0.12	0.11	20.0	19.7	56.8	88.0
16C2	158.4	161.0	234.4	224.6	0.19	0.24	0.18	0.14	6.6	6.9	77.8	73.8
16C2wo	94.5	97.3	175.8	191.2	0.12	0.15	0.12	0.14	8.0	8.0	84.8	108.3
17B1	92.3	—	160.4	—	0.44	—	0.17	—	12.4	12.6	108.7	—
17Acc01	160.7	—	228.9	—	0.48	—	0.17	—	11.2	11.7	76.5	—
17Acc11	125.5	—	191.7	—	0.23	—	0.17	—	15.4	15.6	86.3	—
17Acc31	147.6	—	163.2	—	0.34	—	0.16	—	5.1	5.1	26.8	—
17C2	112.6	115.5	163.8	199.3	0.22	0.28	0.17	0.17	21.1	22.6	78.1	127.4
17B1wo	65.1	—	129.0	—	0.30	—	0.13	—	33.0	33.3	99.0	—
17Acc11wo	90.2	—	178.5	—	0.18	—	0.14	—	11.6	10.9	107.1	—
17Acc31wo	122.9	—	253.9	—	0.26	—	0.18	—	15.3	14.1	172.6	—
17C2wo	101.9	104.0	180.9	182.9	0.12	0.15	0.12	0.11	31.3	32.3	82.3	89.4
18Acc31	156.8	—	163.9	—	0.32	—	0.16	—	2.8	2.9	20.4	—
18C1	143.6	100.8	174.2	167.1	0.42	0.44	0.17	0.17	13.5	13.7	49.7	68.8
18C2	127.6	130.1	188.1	211.6	0.20	0.28	0.18	0.18	10.5	11.3	76.8	104.3
18Acc31wo	127.0	—	263.5	—	0.24	—	0.19	—	29.2	28.4	173.8	—
18C2wo	105.0	106.7	184.4	208.6	0.12	0.16	0.12	0.14	12.8	11.5	82.4	114.4
19B1	119.9	—	161.6	—	0.59	—	0.29	—	5.1	3.1	65.9	—
19C1	153.0	112.0	162.7	137.1	0.49	0.56	0.25	0.28	12.5	13.3	38.0	30.7
110B1	151.4	—	188.8	—	0.75	—	0.42	—	12.4	10.5	63.6	—
110C1	160.7	159.2	152.8	196.9	0.51	0.83	0.36	0.38	23.2	22.9	78.0	37.8

* PTD is the peak absolute displacement response of the shake table;

**PFD is the peak absolute displacement response of the isolated floor;

***PTA is the peak absolute acceleration response of the shake table;

****PFA is the peak absolute acceleration response of the isolated floor.

Table 6.5 Summary of Peak Values of Response Quantities (Rubber Balls)

Test Name (1)	PTD* (mm)		PFD** (mm)		PTA*** (g)		PFA**** (g)		Peak Rotation (x 10 ⁻³ rad)		Peak Relative Disp. (mm)	
	E-W (2)	N-S (3)	E-W (4)	N-S (5)	E-W (6)	N-S (7)	E-W (8)	N-S (9)	E-W (10)	N-S (11)	E-W (12)	N-S (13)
21ss	89.7	—	96.7	—	0.21	—	0.25	—	2.3	2.2	40.7	—
21Acc11	150.0	—	160.1	—	0.28	—	0.28	—	1.5	0.92	64.7	—
21C2	163.8	166.9	181.5	180.3	0.27	0.38	0.26	0.19	2.4	1.8	64.3	31.4
21Acc11wo	132.8	—	213.2	—	0.24	—	0.17	—	1.3	1.6	107.5	—
21C2wo	99.1	123.0	145.2	208.3	0.18	0.29	0.15	0.18	5.5	6.4	64.3	119.7
22ss	103.6	—	152.5	—	0.27	—	0.28	—	2.6	1.8	166.9	—
22B1	141.4	—	206.5	—	0.70	—	0.24	—	2.3	2.5	126.6	—
22Acc11	158.0	—	194.1	—	0.29	—	0.23	—	1.7	0.80	92.3	—
22C2	129.9	162.8	155.2	193.0	0.24	0.40	0.21	0.17	3.4	4.5	55.7	53.4
22B1wo	128.3	—	203.5	—	0.63	—	0.22	—	3.2	3.3	138.4	—
22Acc11wo	154.5	—	218.0	—	0.28	—	0.20	—	1.8	2.7	106.7	—
22C2wo	119.7	149.2	163.6	223.7	0.22	0.36	0.19	0.20	4.6	5.1	75.7	113.3
23ss	90.7	—	123.2	—	0.23	—	0.25	—	2.3	2.1	120.7	—
23B1	16.3	—	171.2	—	0.64	—	0.24	—	2.9	2.2	98.5	—
23Acc11	154.4	—	181.7	—	0.27	—	0.23	—	2.1	1.6	81.4	—
23C2	157.8	158.9	203.4	190.6	0.26	0.36	0.23	0.17	5.5	5.1	76.7	66.2
23B1wo	130.1	—	189.1	—	0.63	—	0.22	—	2.2	2.0	116.4	—
23Acc11wo	154.1	—	181.3	—	0.27	—	0.23	—	2.2	2.6	83.7	—
23C2wo	145.2	146.7	195.2	199.1	0.25	0.32	0.23	0.17	7.3	7.1	89.7	81.4
27B1	141.4	—	190.0	—	0.69	—	0.24	—	6.8	7.1	98.9	—
27Acc11	158.2	—	178.8	—	0.29	—	0.24	—	7.0	7.8	81.8	—
27C2	144.7	164.8	171.7	187.8	0.25	0.40	0.22	0.17	5.6	5.8	64.5	51.7
27B1wo	131.4	—	182.2	—	0.64	—	0.24	—	8.3	8.4	123.3	—
27Acc11wo	139.7	—	161.4	—	0.24	—	0.22	—	5.3	4.7	76.1	—
27C2wo	152.3	155.1	208.5	206.6	0.25	0.33	0.22	0.17	12.2	12.6	94.5	81.3
28C2	162.6	163.4	191.8	183.8	0.25	0.34	0.23	0.17	4.3	3.7	64.9	35.7
28C2wo	162.5	163.4	230.4	239.7	0.25	0.34	0.20	0.19	8.2	8.9	102.3	117.7
29C1	175.1	136.2	188.9	171.1	0.63	0.70	0.36	0.32	10.9	12.5	42.3	36.2
210C1	166.6	136.4	166.4	154.6	0.57	0.71	0.40	0.41	14.5	14.1	31.6	21.4

* PTD is the peak absolute displacement response of the shake table;

**PFD is the peak absolute displacement response of the isolated floor;

***PTA is the peak absolute acceleration response of the shake table;

****PFA is the peak absolute acceleration response of the isolated floor.

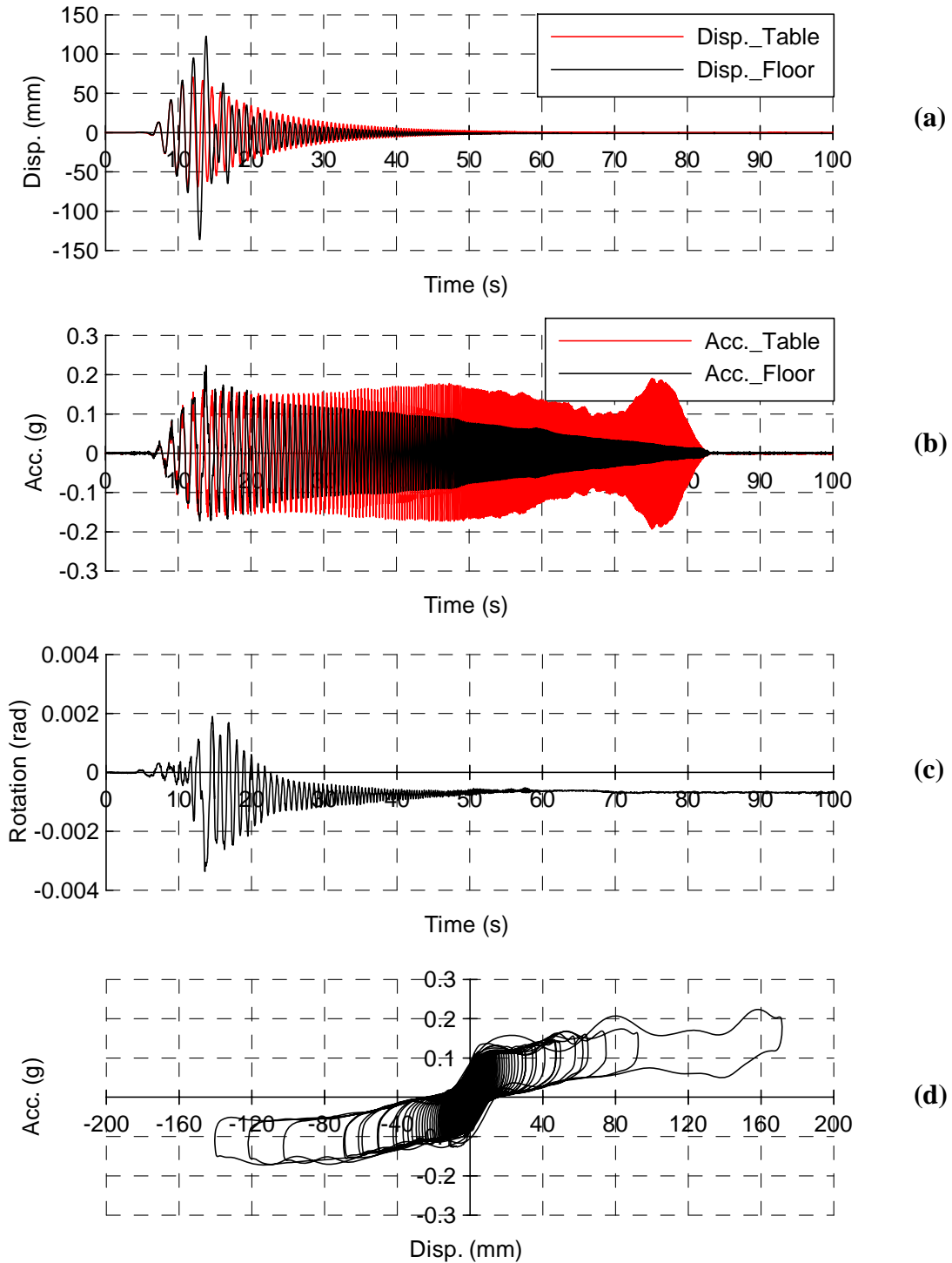


Figure 6.14 Results of Test 12ss: (a) and (b) Displacement and Acceleration of Shake Table and Isolated Floor, Respectively; (c) Rotation; (d) Acceleration-Displacement Relationship of Isolated Floor System I

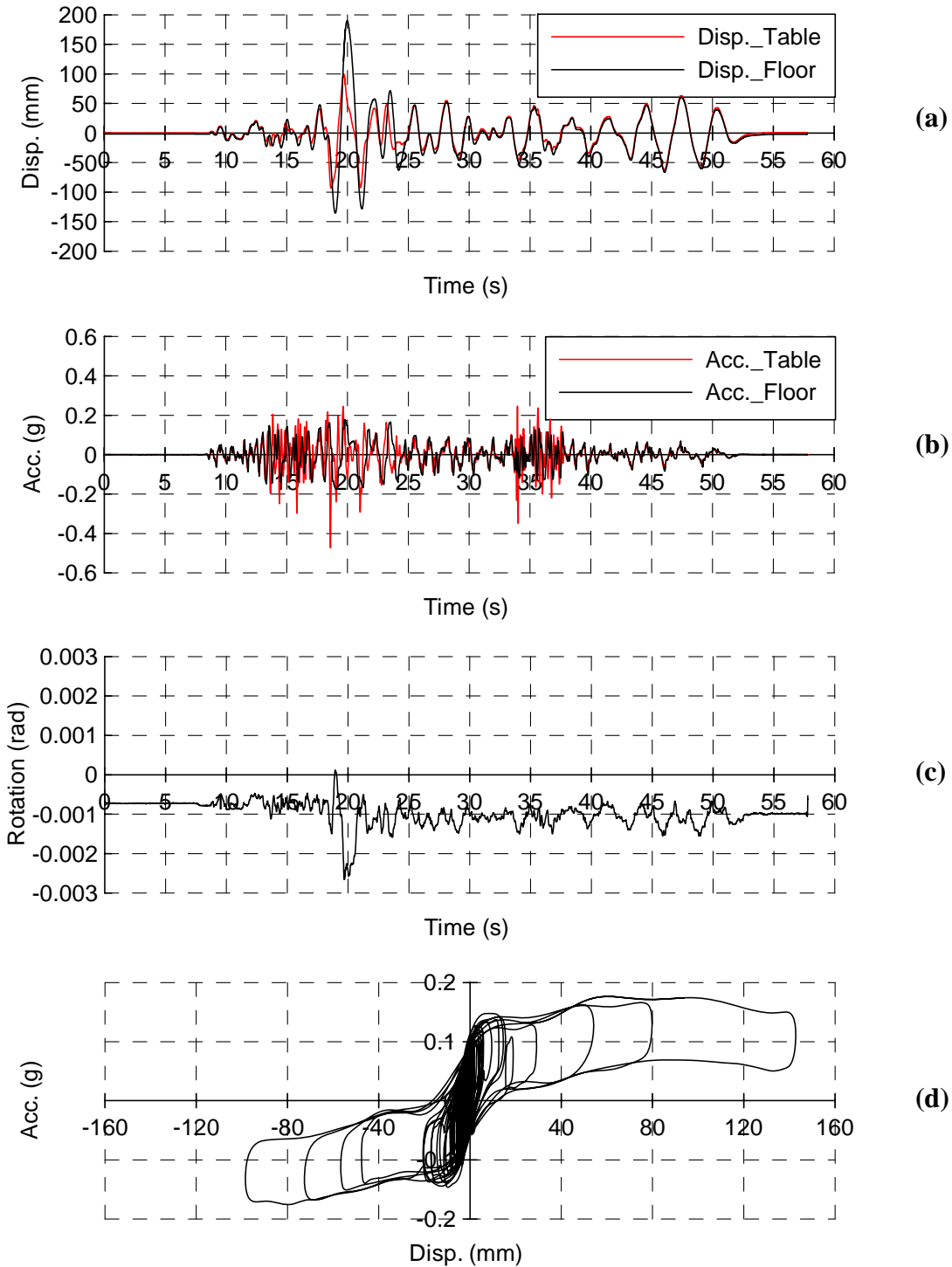


Figure 6.15 Results of Test 12B1: (a) and (b) Displacement and Acceleration of Shake Table and Isolated Floor, Respectively; (c) Rotation; (d) Acceleration-Displacement Relationship of Isolated Floor System I

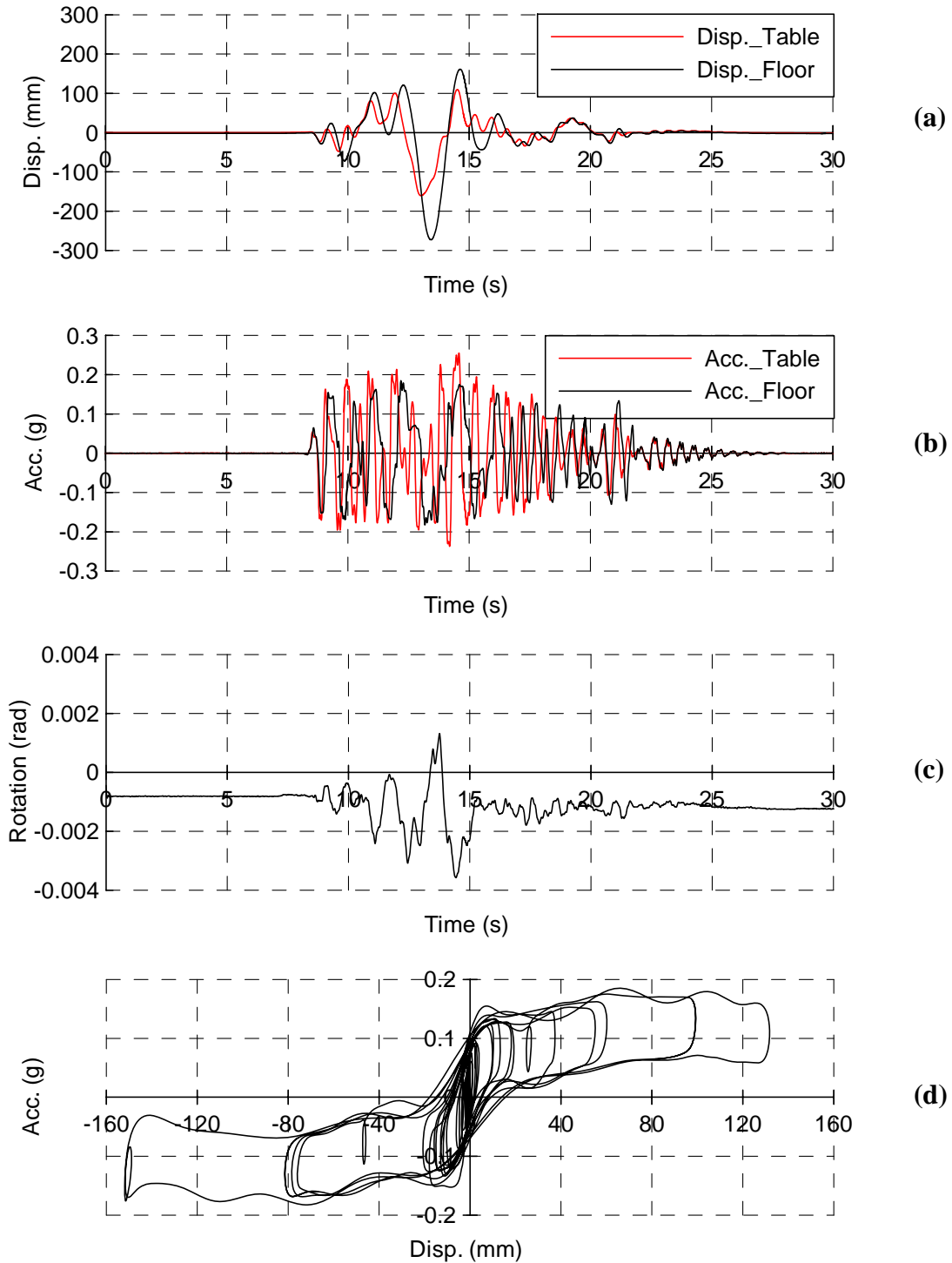


Figure 6.16 Results of Test 12C2 in E-W Direction: (a) and (b) Displacement and Acceleration of Shake Table and Isolated Floor, Respectively; (c) Rotation; (d) Acceleration-Displacement Relationship of Isolated Floor System I

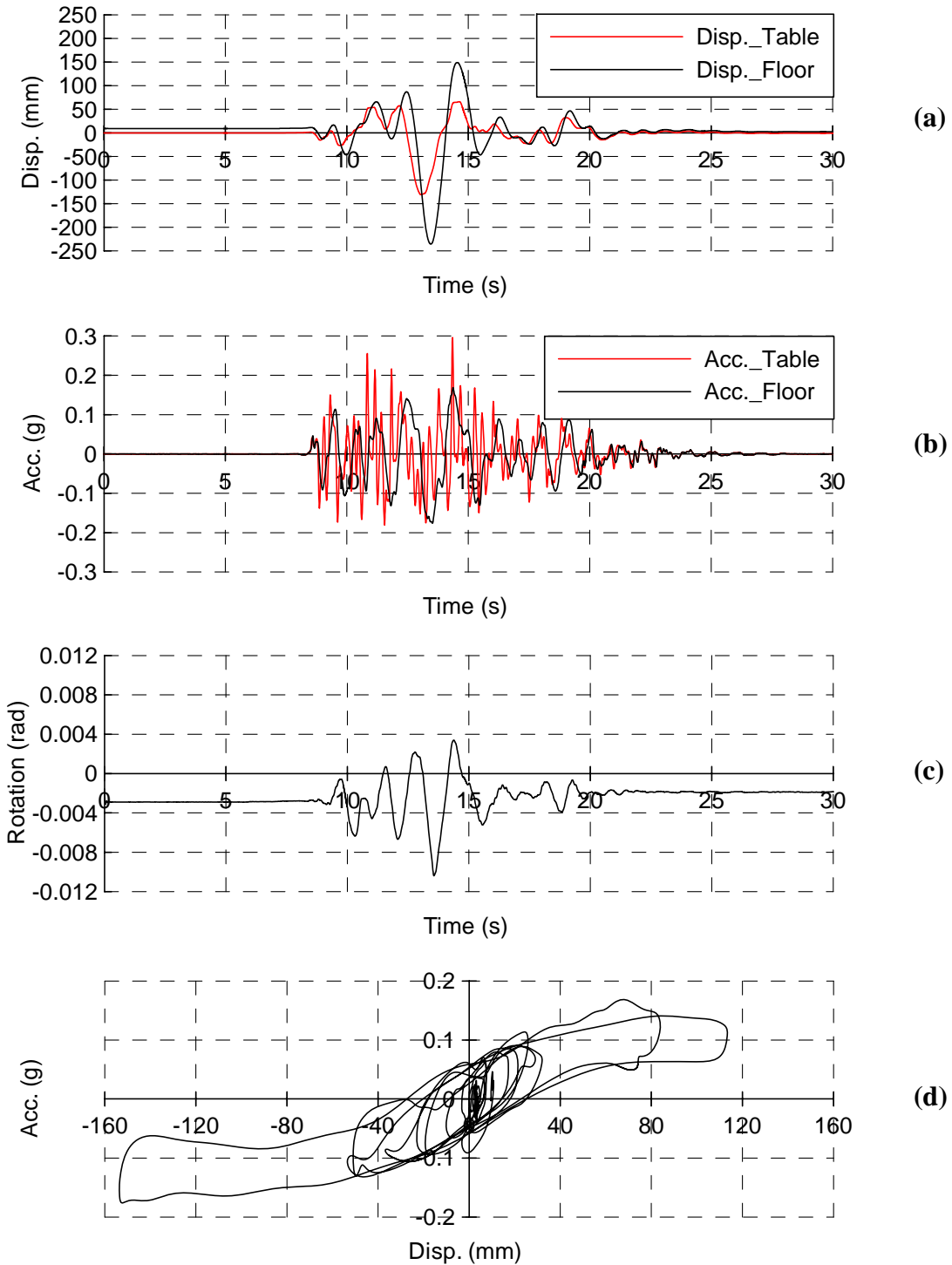


Figure 6.17 Results of Test 12C2 in N-S Direction: (a) and (b) Displacement and Acceleration of Shake Table and Isolated Floor, Respectively; (c) Rotation; (d) Acceleration-Displacement Relationship of Isolated Floor System I

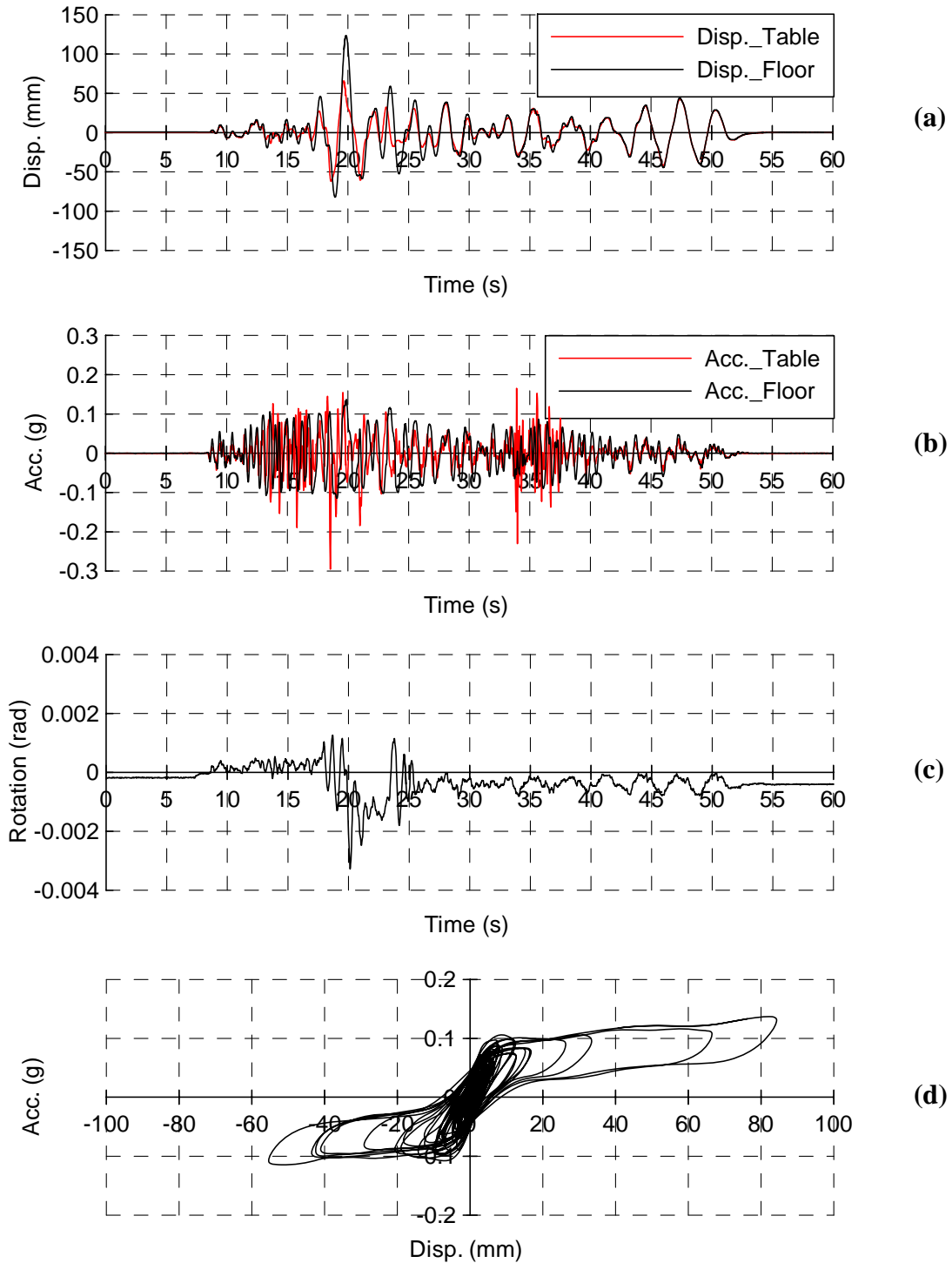


Figure 6.18 Results of Test 12B1wo: (a) and (b) Displacement and Acceleration of Shake Table and Isolated Floor, Respectively; (c) Rotation; (d) Acceleration-Displacement Relationship of Isolated Floor System I

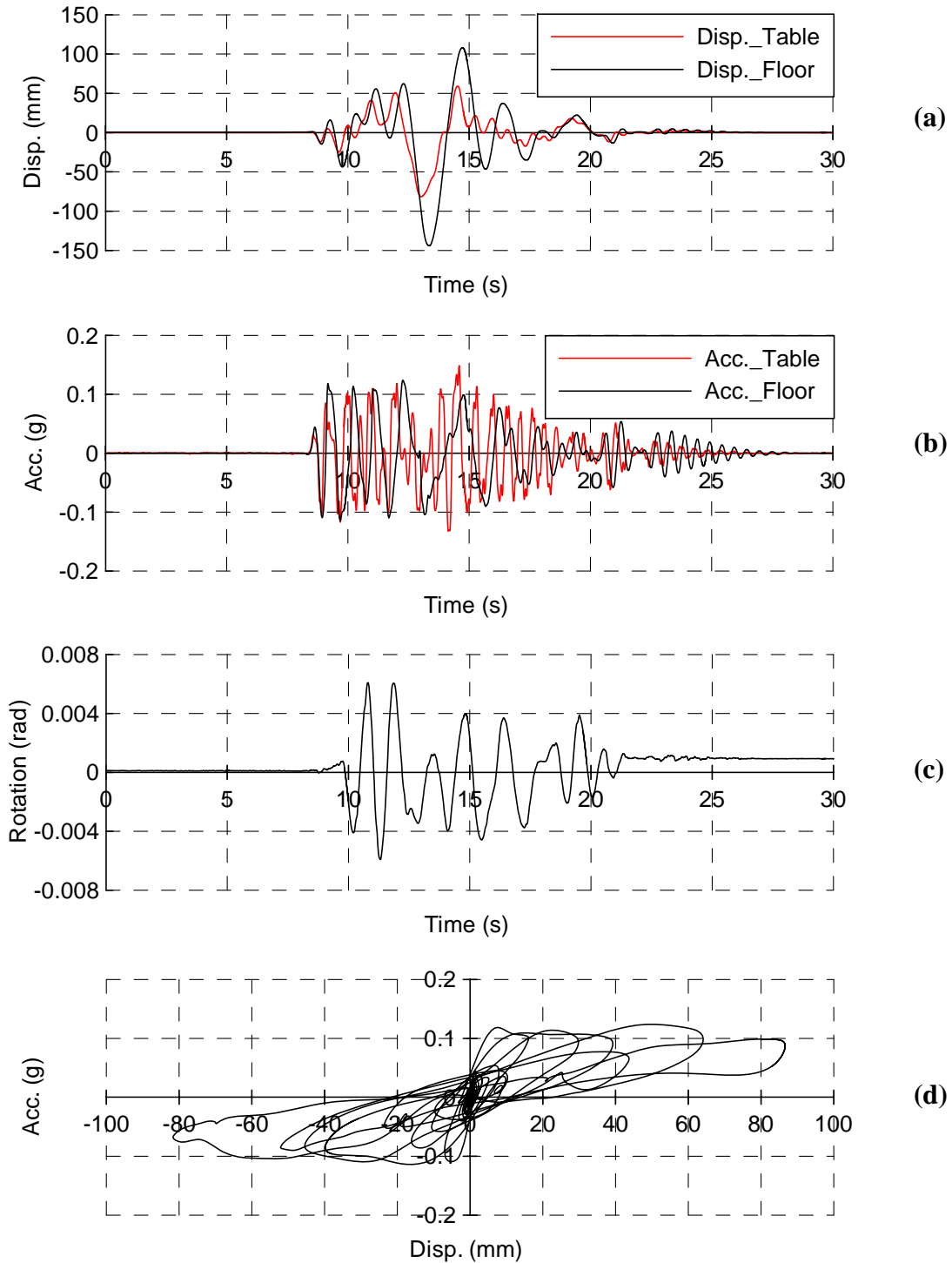


Figure 6.19 Results of Test 12C2wo in E-W Direction: (a) and (b) Displacement and Acceleration of Shake Table and Isolated Floor, Respectively; (c) Rotation; (d) Acceleration-Displacement Relationship of Isolated Floor System I

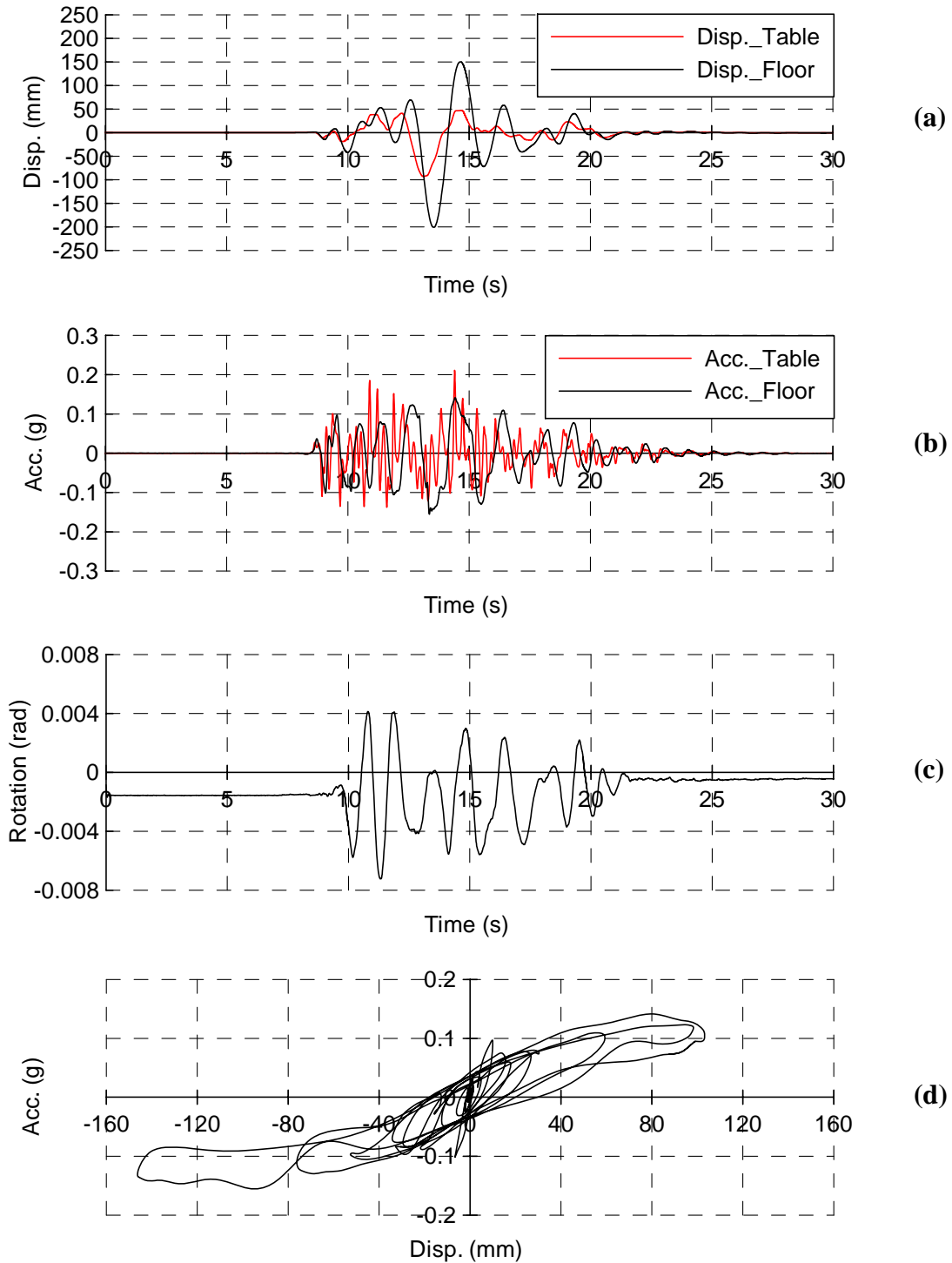


Figure 6.20 Results of Test 12C2wo in N-S Direction: (a) and (b) Displacement and Acceleration of Shake Table and Isolated Floor, Respectively; (c) Rotation; (d) Acceleration-Displacement Relationship of Isolated Floor System I

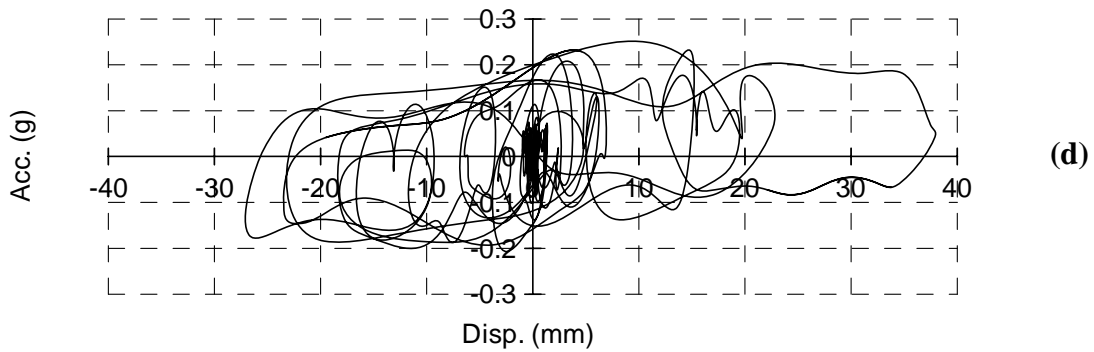
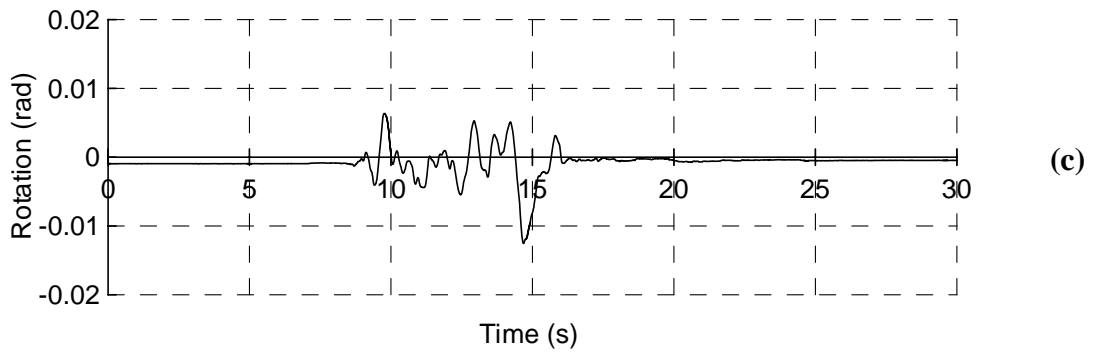
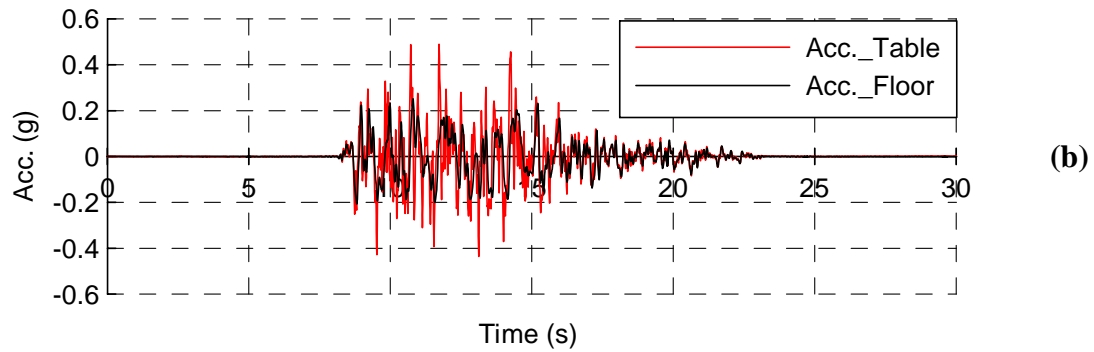
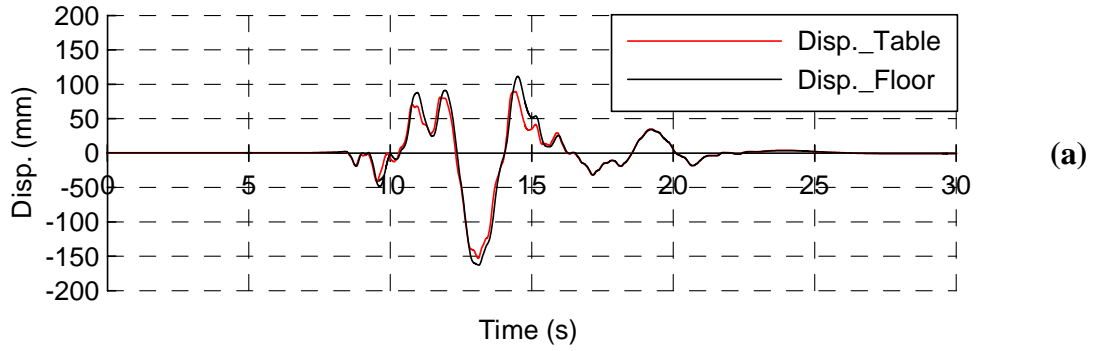


Figure 6.21 Results of Test 19C1 in E-W Direction: (a) and (b) Displacement and Acceleration of Shake Table and Isolated Floor, Respectively; (c) Rotation; (d) Acceleration-Displacement Relationship of Isolated Floor System I

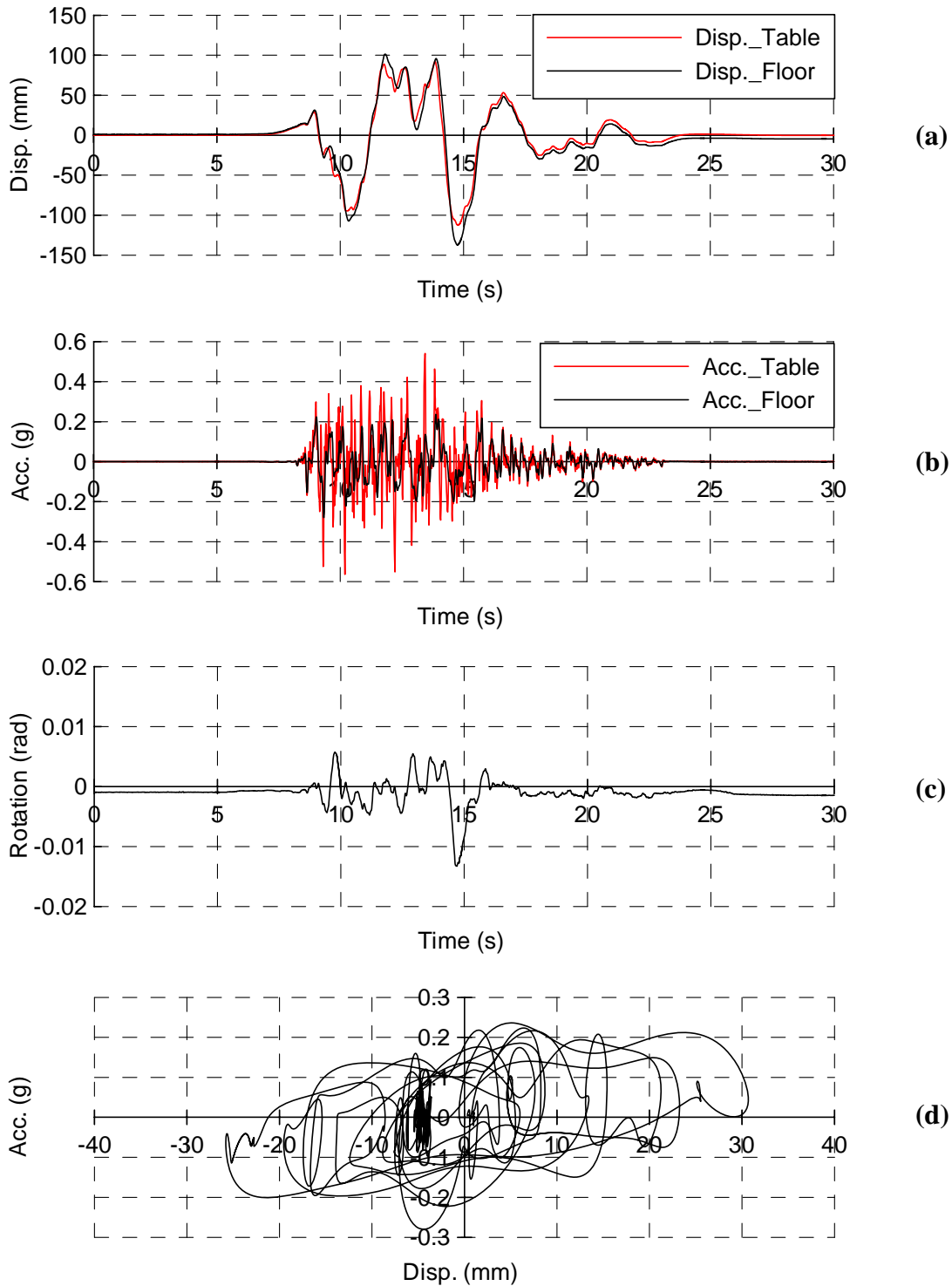


Figure 6.22 Results of Test 19C1 in N-S Direction: (a) and (b) Displacement and Acceleration of Shake Table and Isolated Floor, Respectively; (c) Rotation; (d) Acceleration-Displacement Relationship of Isolated Floor System I

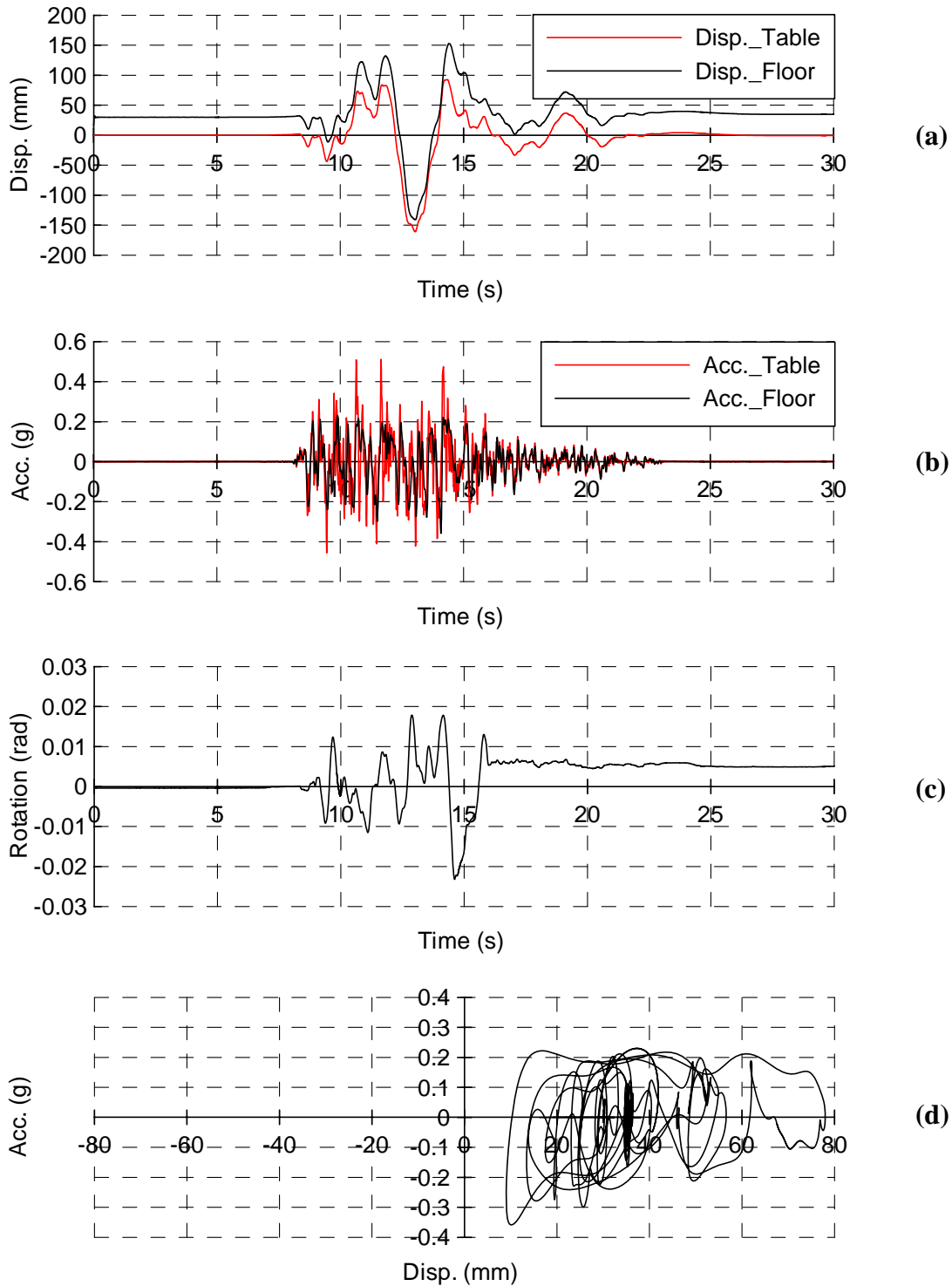


Figure 6.23 Results of Test 110C1 in E-W Direction: (a) and (b) Displacement and Acceleration of Shake Table and Isolated Floor, Respectively; (c) Rotation; (d) Acceleration-Displacement Relationship of Isolated Floor System I

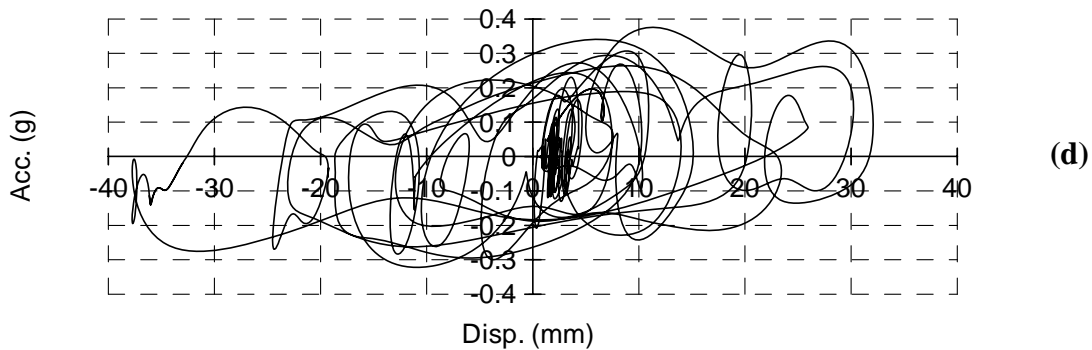
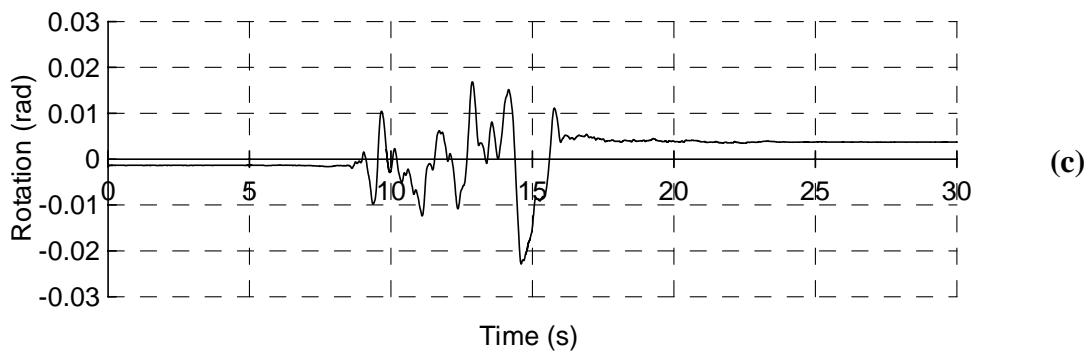
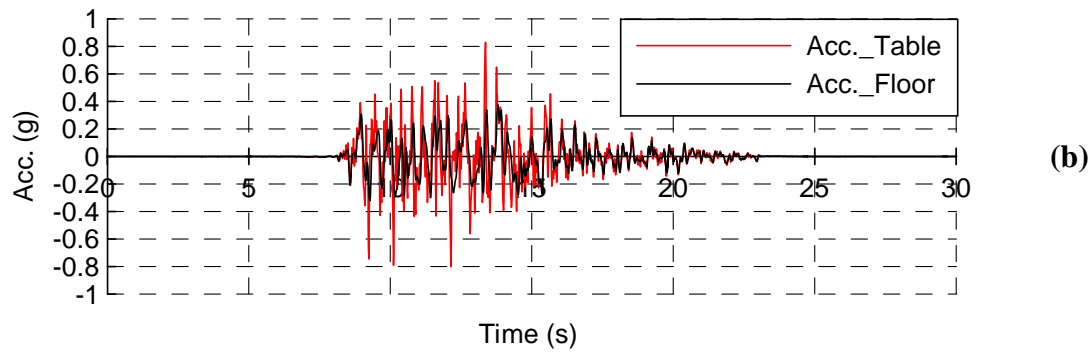
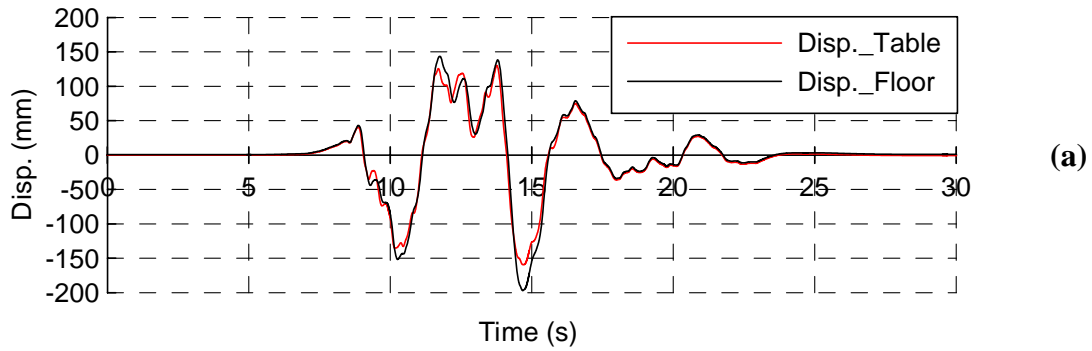


Figure 6.24 Results of Test 110C1 in N-S Direction: (a) and (b) Displacement and Acceleration of Shake Table and Isolated Floor, Respectively; (c) Rotation; (d) Acceleration-Displacement Relationship of Isolated Floor System I

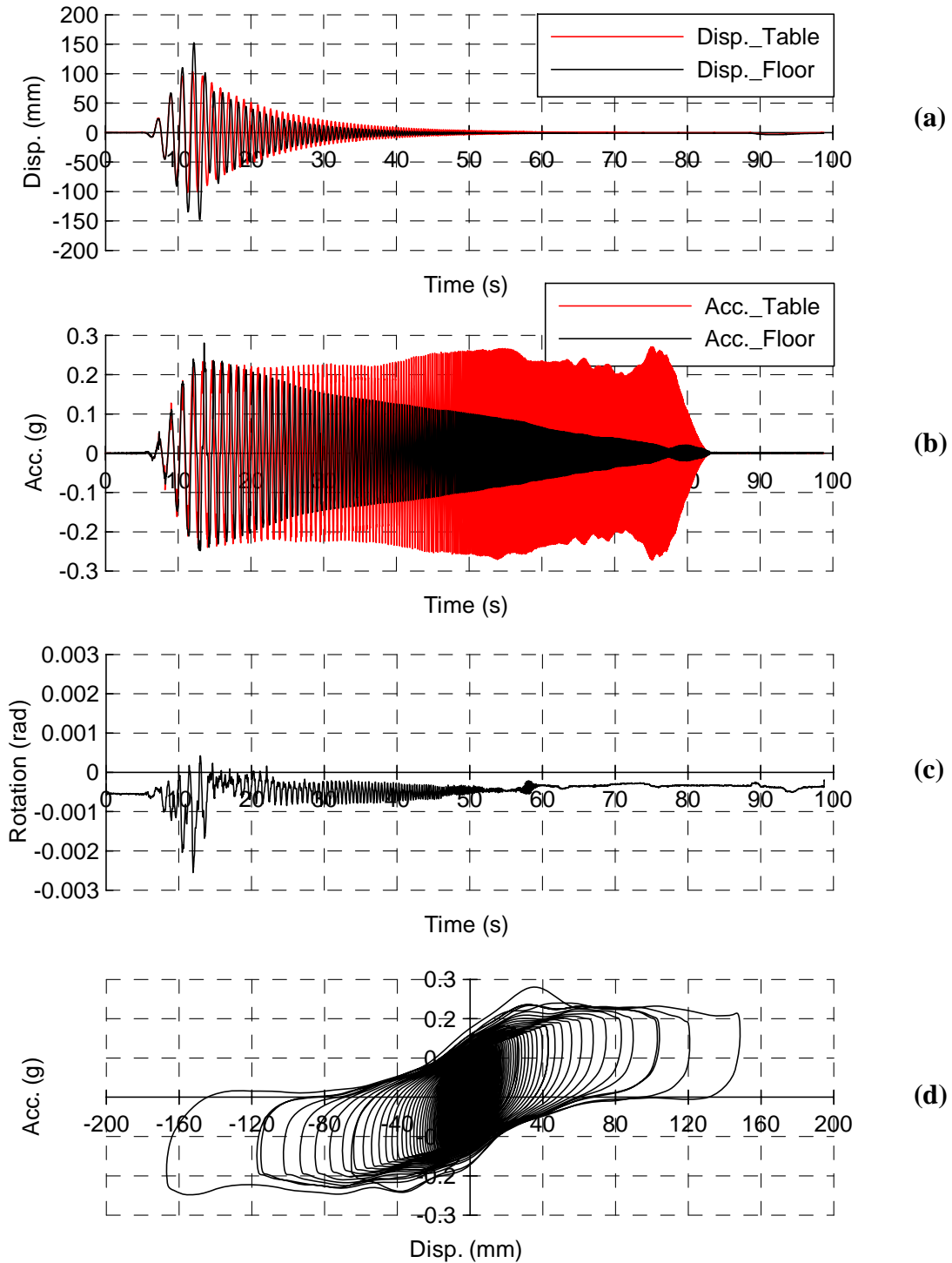


Figure 6.25 Results of Test 22ss: (a) and (b) Displacement and Acceleration of Shake Table and Isolated Floor, Respectively; (c) Rotation; (d) Acceleration-Displacement Relationship of Isolated Floor System I

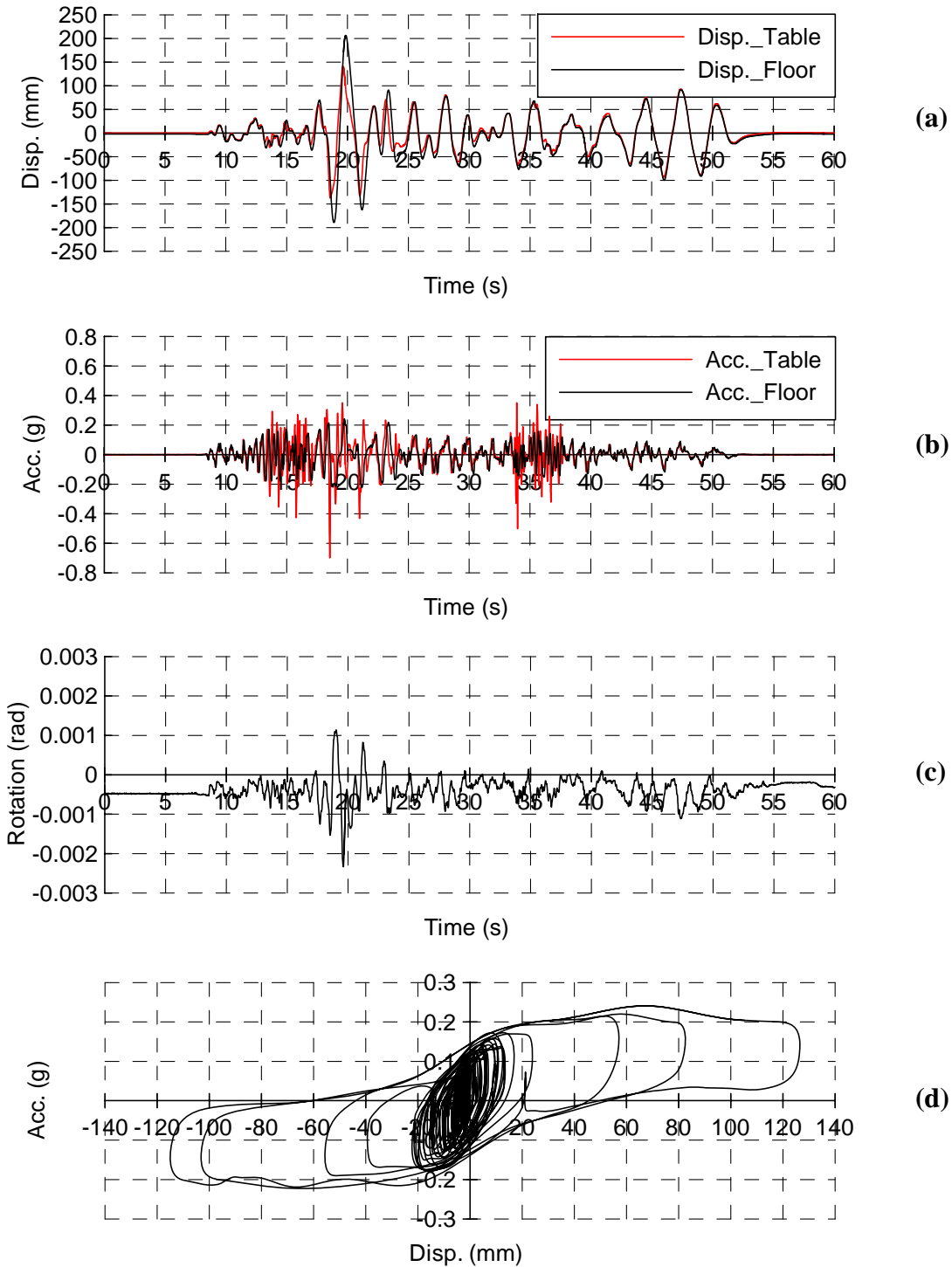


Figure 6.26 Results of Test 22B1: (a) and (b) Displacement and Acceleration of Shake Table and Isolated Floor, Respectively; (c) Rotation; (d) Acceleration-Displacement Relationship of Isolated Floor System I

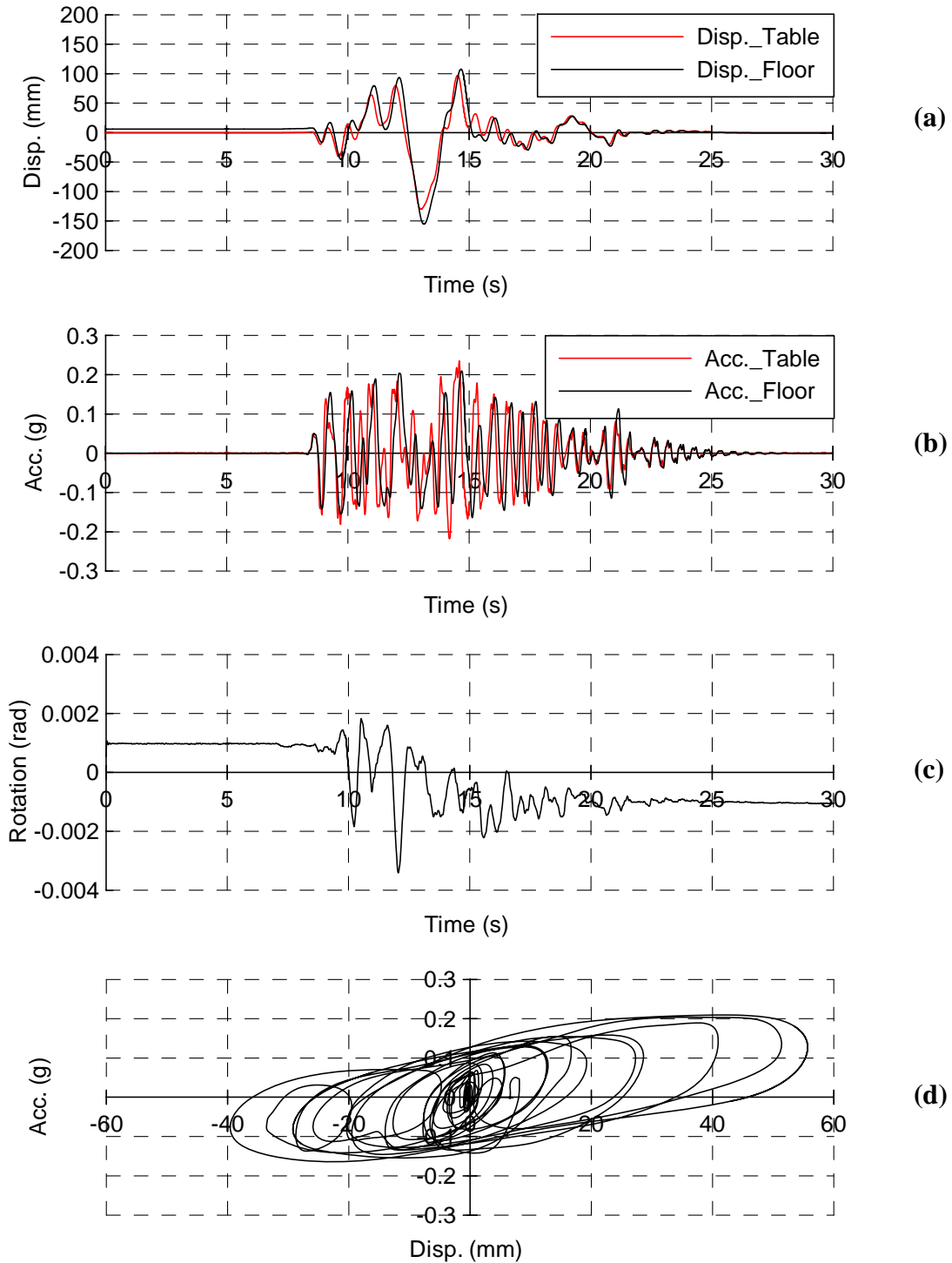


Figure 6.27 Results of Test 22C2 in E-W Direction: (a) and (b) Displacement and Acceleration of Shake Table and Isolated Floor, Respectively; (c) Rotation; (d) Acceleration-Displacement Relationship of Isolated Floor System I

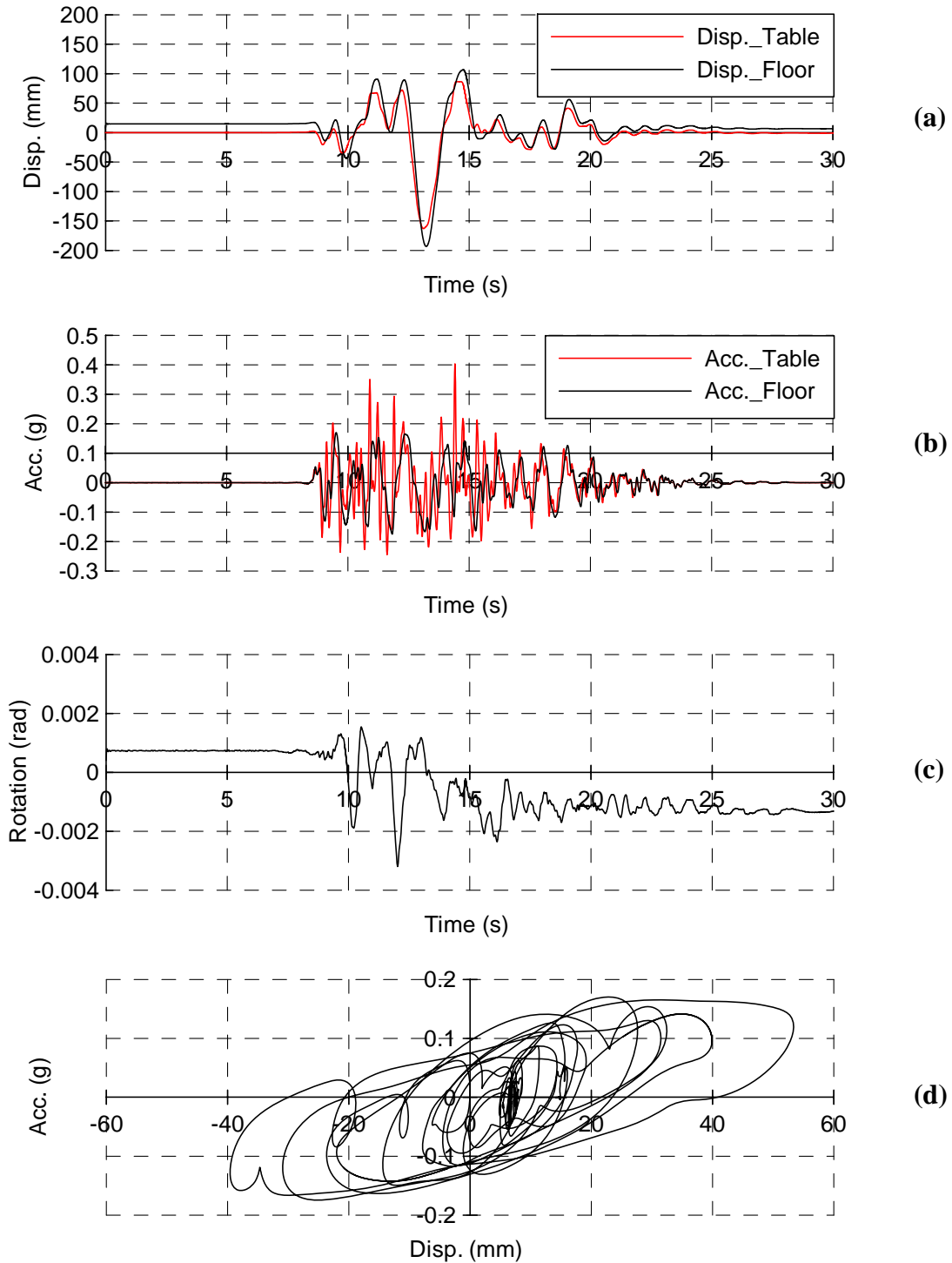


Figure 6.28 Results of Test 22C2 in N-S Direction: (a) and (b) Displacement and Acceleration of Shake Table and Isolated Floor, Respectively; (c) Rotation; (d) Acceleration-Displacement Relationship of Isolated Floor System I

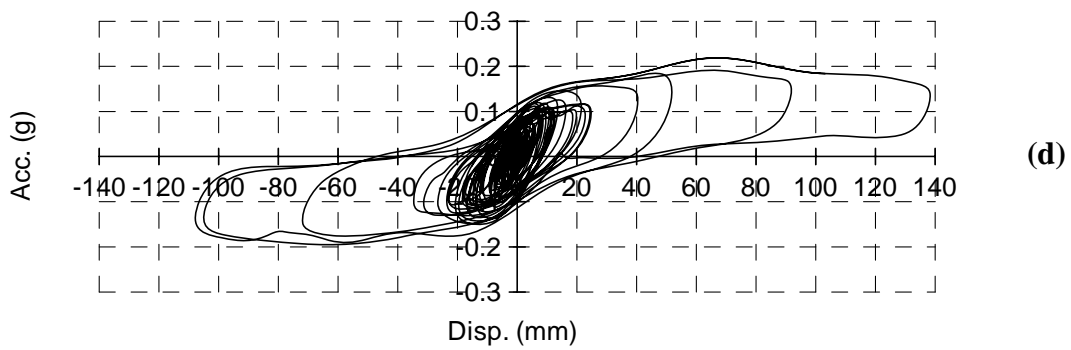
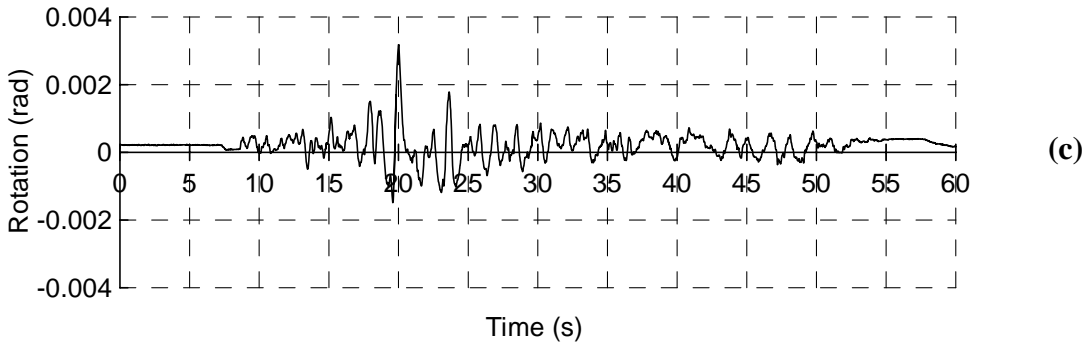
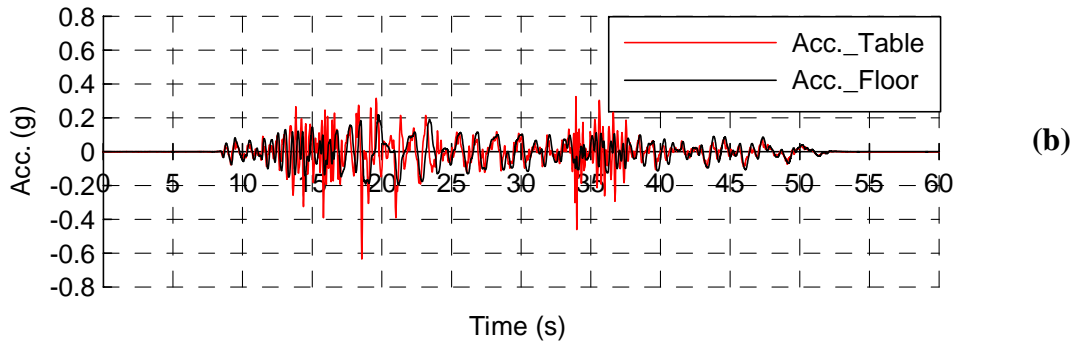
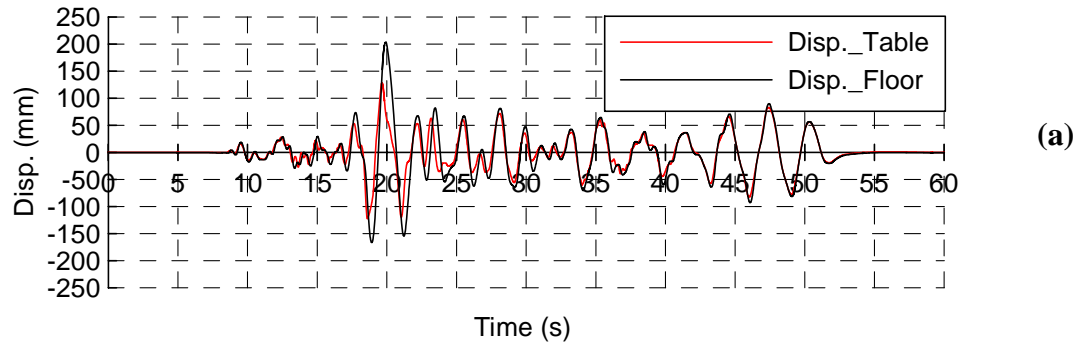


Figure 6.29 Results of Test 22B1wo: (a) and (b) Displacement and Acceleration of Shake Table and Isolated Floor, Respectively; (c) Rotation; (d) Acceleration-Displacement Relationship of Isolated Floor System I

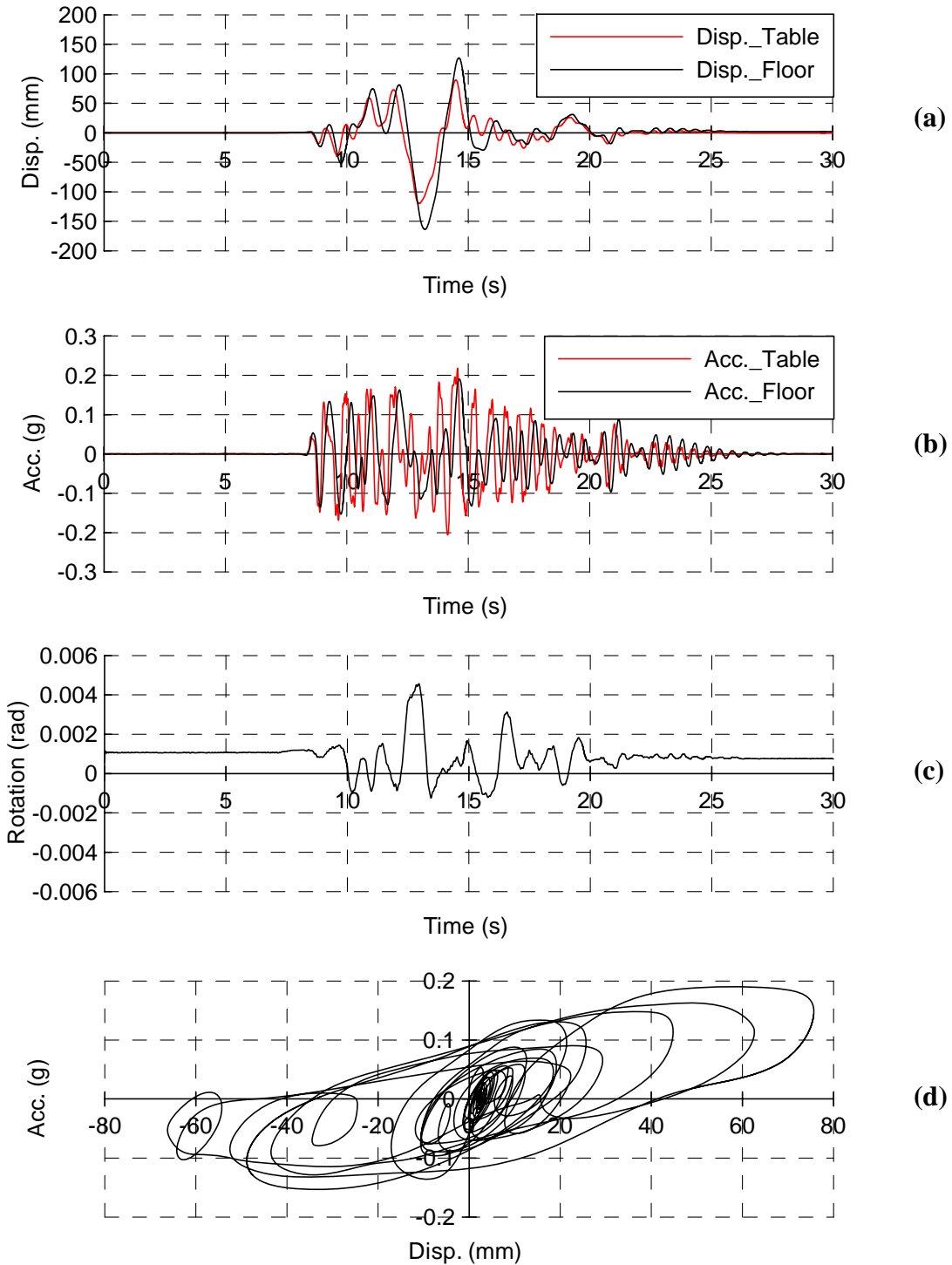


Figure 6.30 Results of Test 22C2wo in E-W Direction: (a) and (b) Displacement and Acceleration of Shake Table and Isolated Floor, Respectively; (c) Rotation; (d) Acceleration-Displacement Relationship of Isolated Floor System I

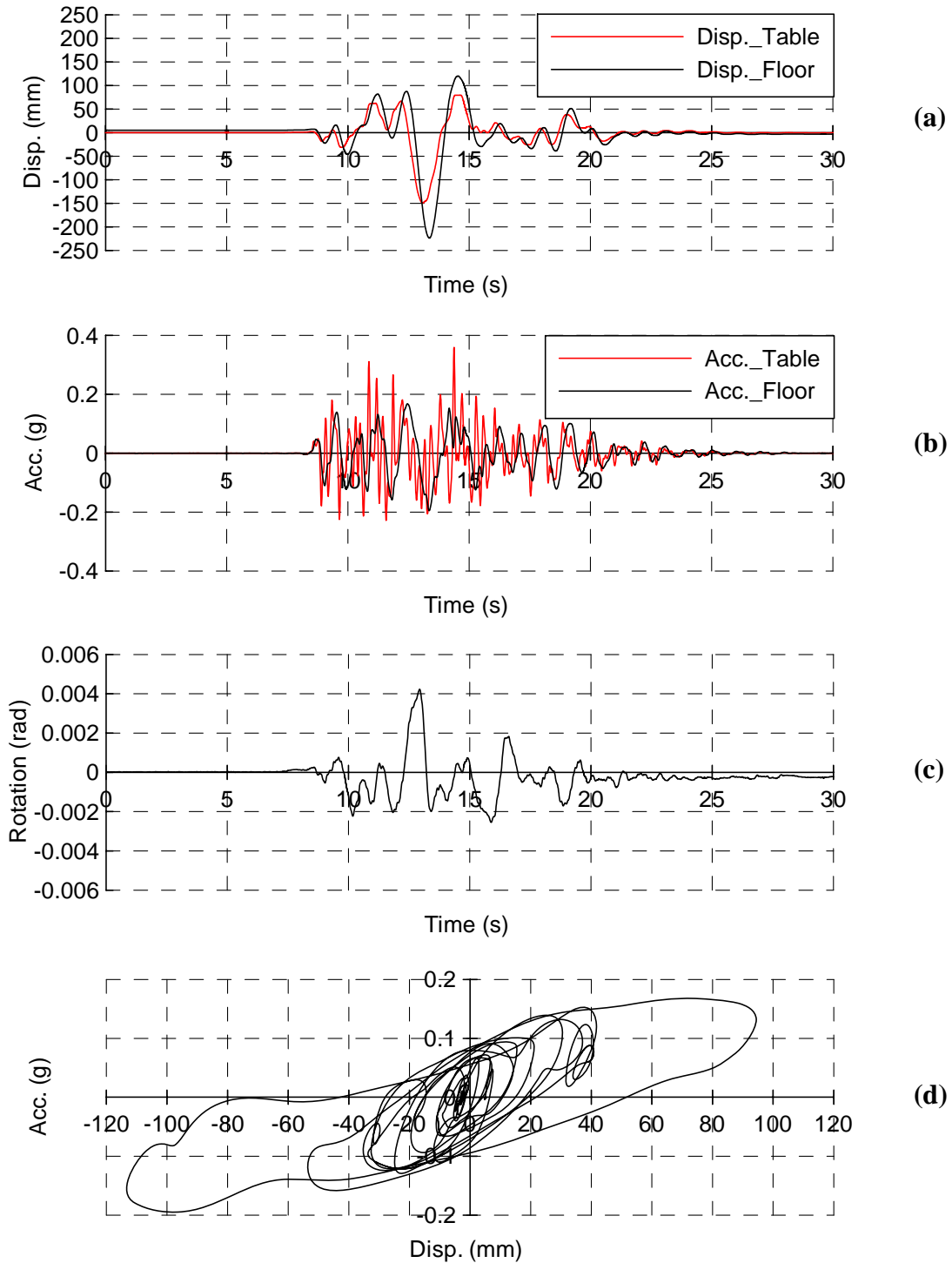


Figure 6.31 Results of Test 22C2wo in N-S Direction: (a) and (b) Displacement and Acceleration of Shake Table and Isolated Floor, Respectively; (c) Rotation; (d) Acceleration-Displacement Relationship of Isolated Floor System I

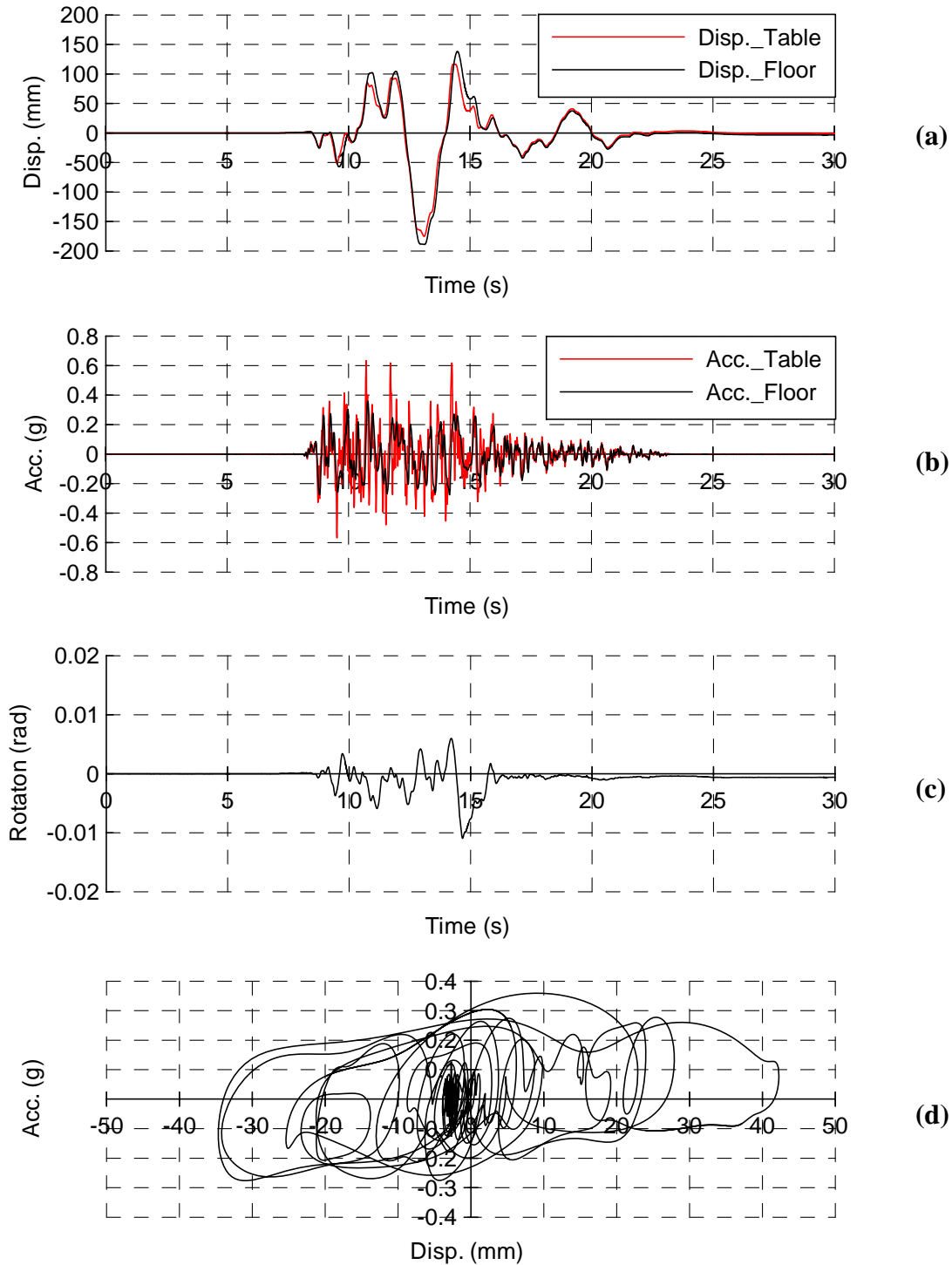


Figure 6.32 Results of Test 29C1 in E-W Direction: (a) and (b) Displacement and Acceleration of Shake Table and Isolated Floor, Respectively; (c) Rotation; (d) Acceleration-Displacement Relationship of Isolated Floor System I

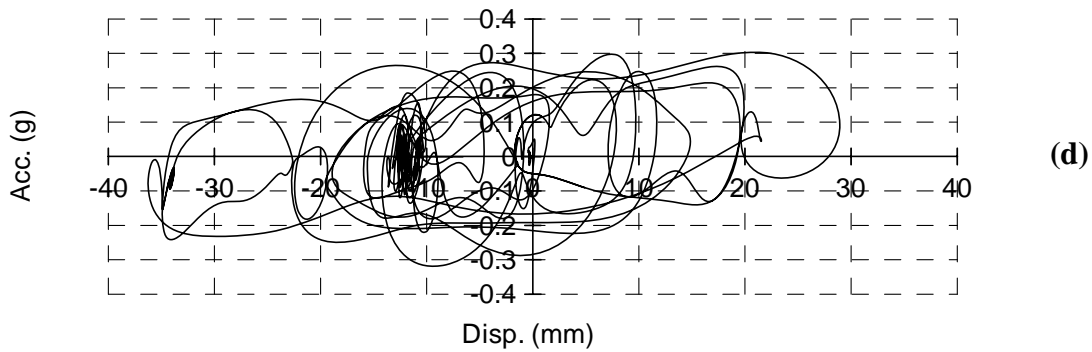
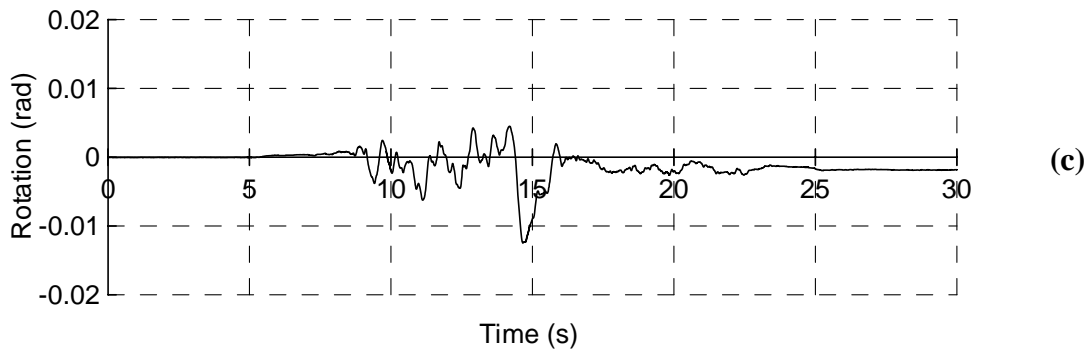
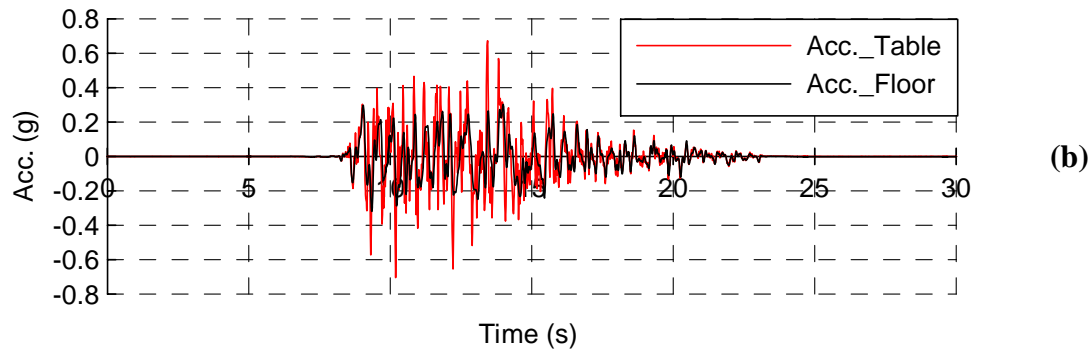
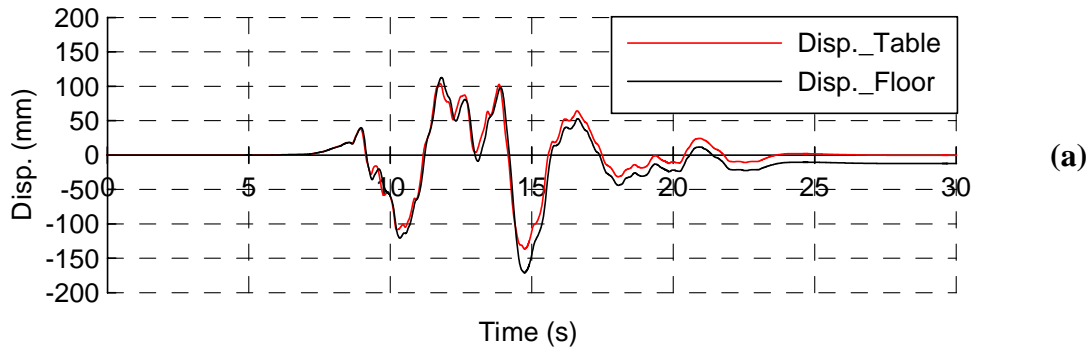


Figure 6.33 Results of Test 29C1 in N-S Direction: (a) and (b) Displacement and Acceleration of Shake Table and Isolated Floor, Respectively; (c) Rotation; (d) Acceleration-Displacement Relationship of Isolated Floor System I

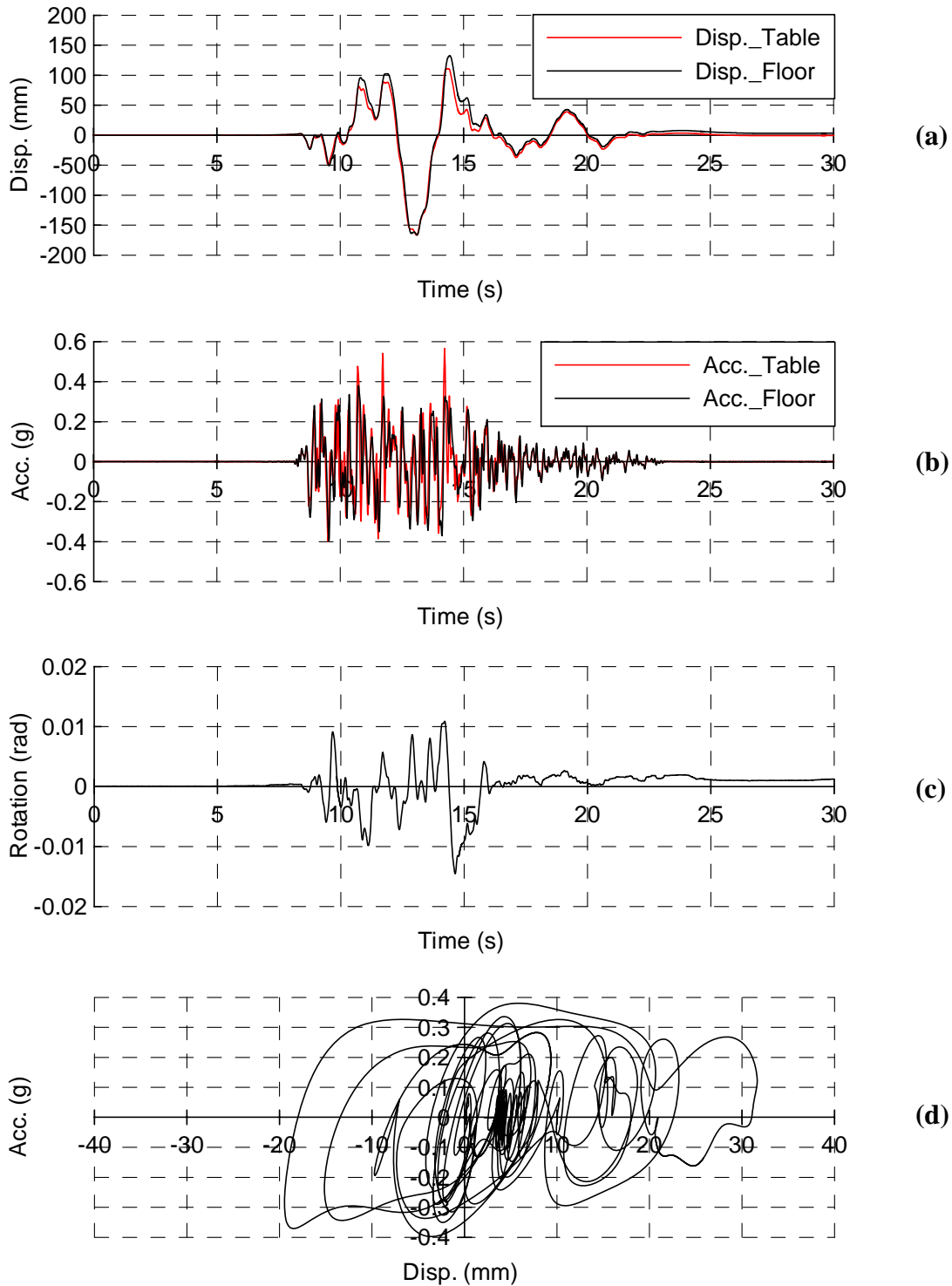


Figure 6.34 Results of Test 210C1 in E-W Direction: (a) and (b) Displacement and Acceleration of Shake Table and Isolated Floor, Respectively; (c) Rotation; (d) Acceleration-Displacement Relationship of Isolated Floor System I

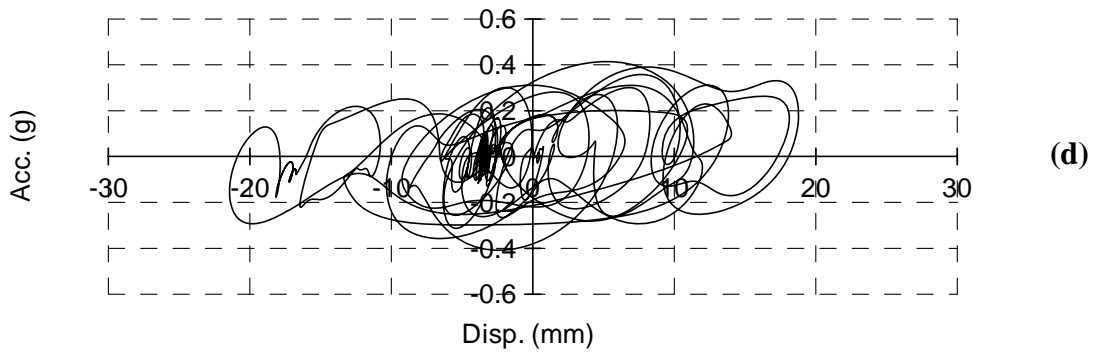
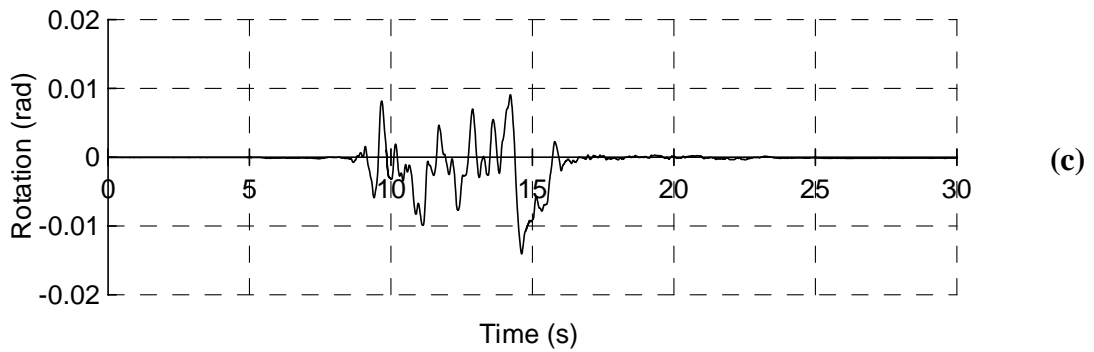
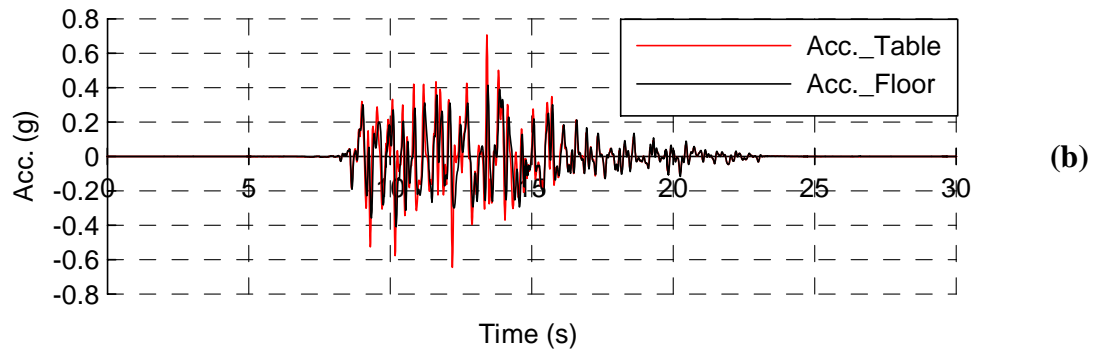
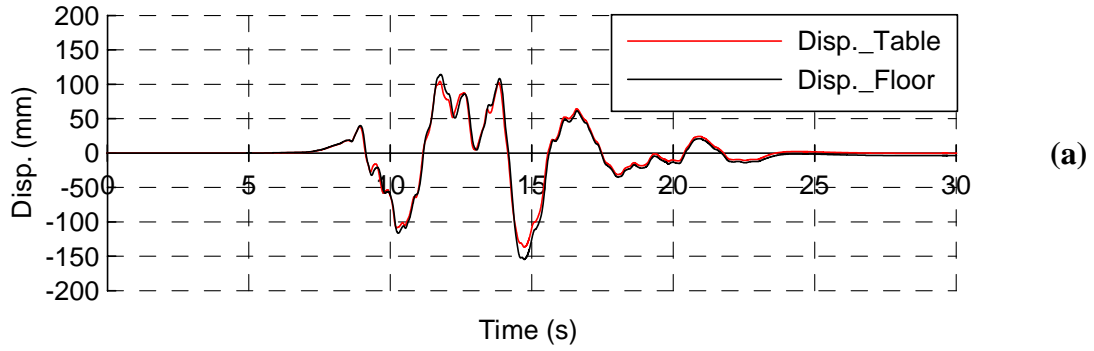


Figure 6.35 Results of Test 210C1 in N-S Direction: (a) and (b) Displacement and Acceleration of Shake Table and Isolated Floor, Respectively; (c) Rotation; (d) Acceleration-Displacement Relationship of Isolated Floor System I

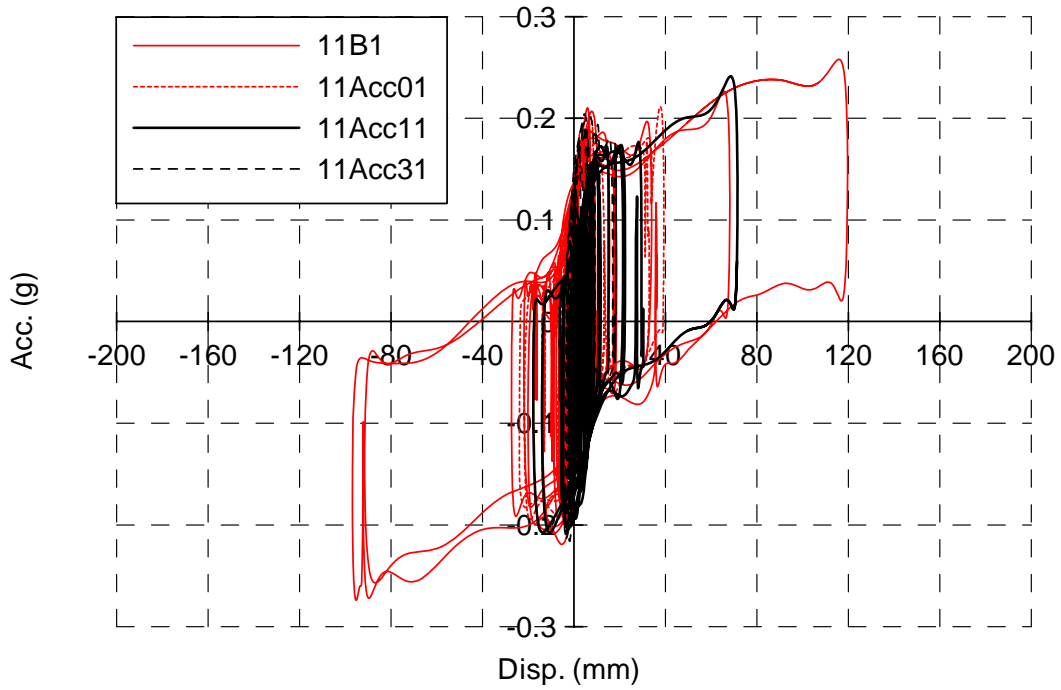


Fig. 6.36 Comparison of Acceleration-Displacement Relationships under Different Inputs and Load Case 1 (Polyurethane Balls)

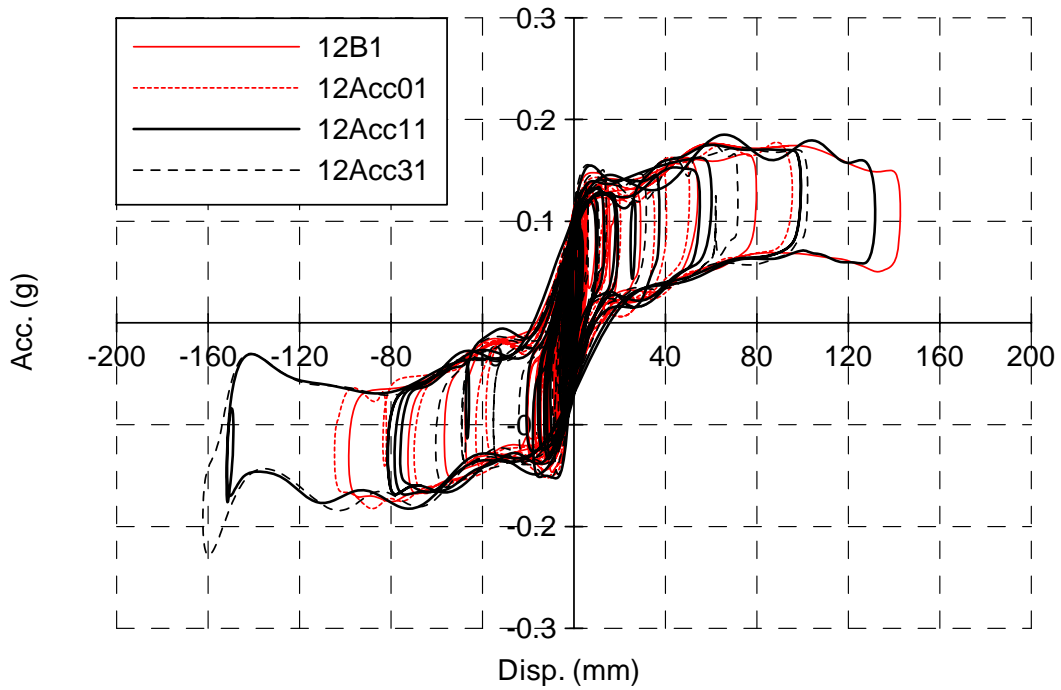


Fig. 6.37 Comparison of Acceleration-Displacement Relationships under Different Inputs and Load Case 2 (Polyurethane Balls)

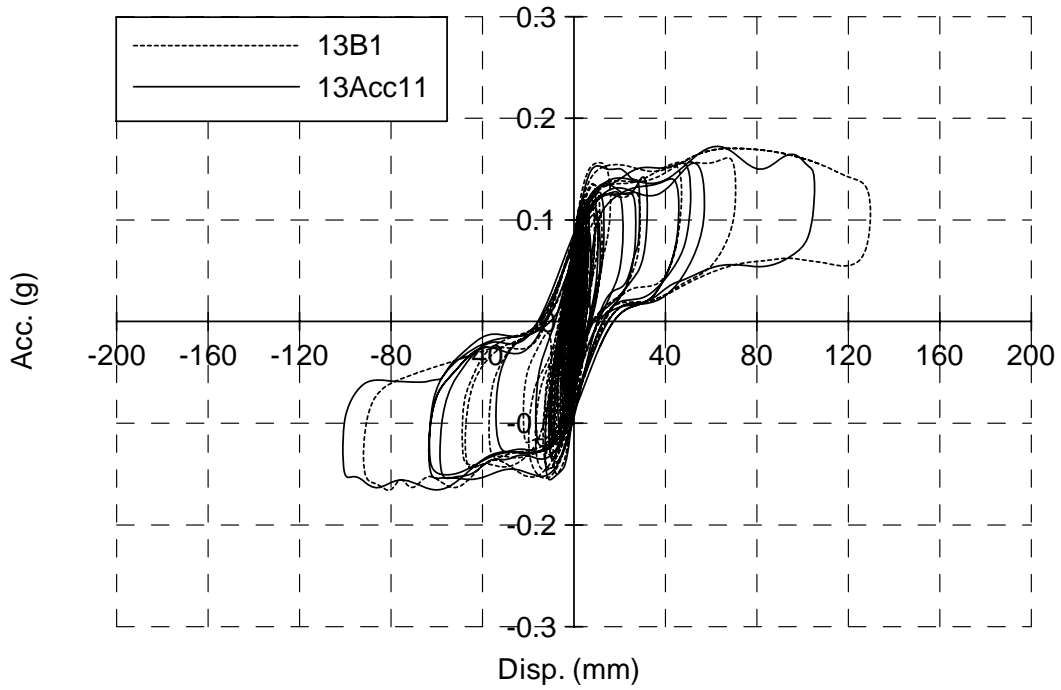


Fig. 6.38 Comparison of Acceleration-Displacement Relationships under Different Inputs and Load Case 3 (Polyurethane Balls)

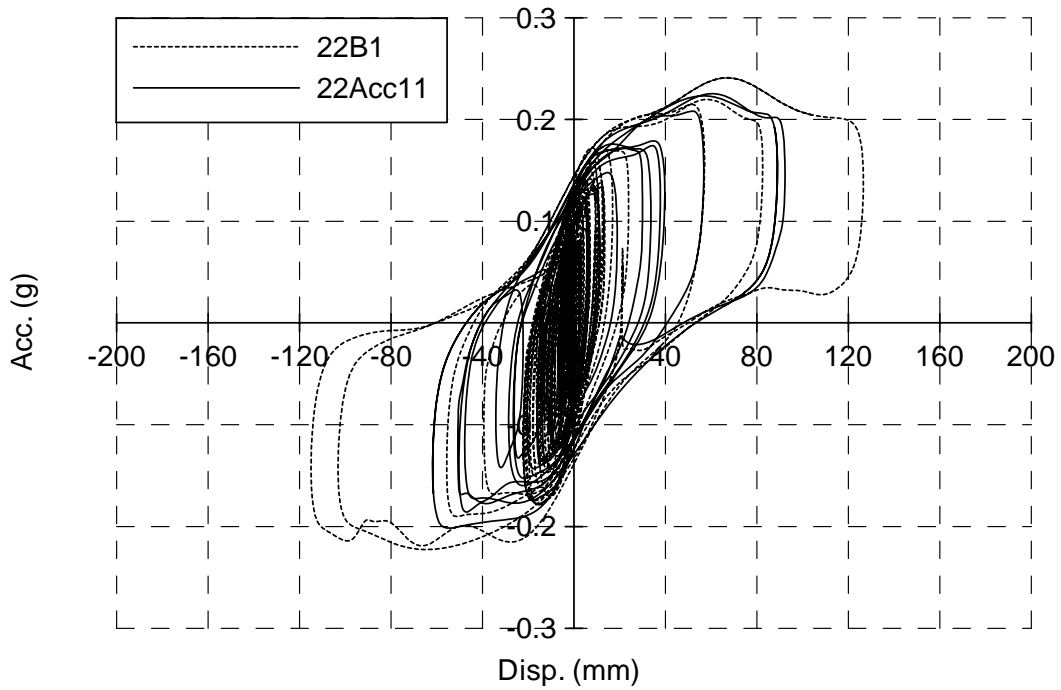


Fig. 6.39 Comparison of Acceleration-Displacement Relationships under Different Inputs and Load Case 2 (Rubber Balls)

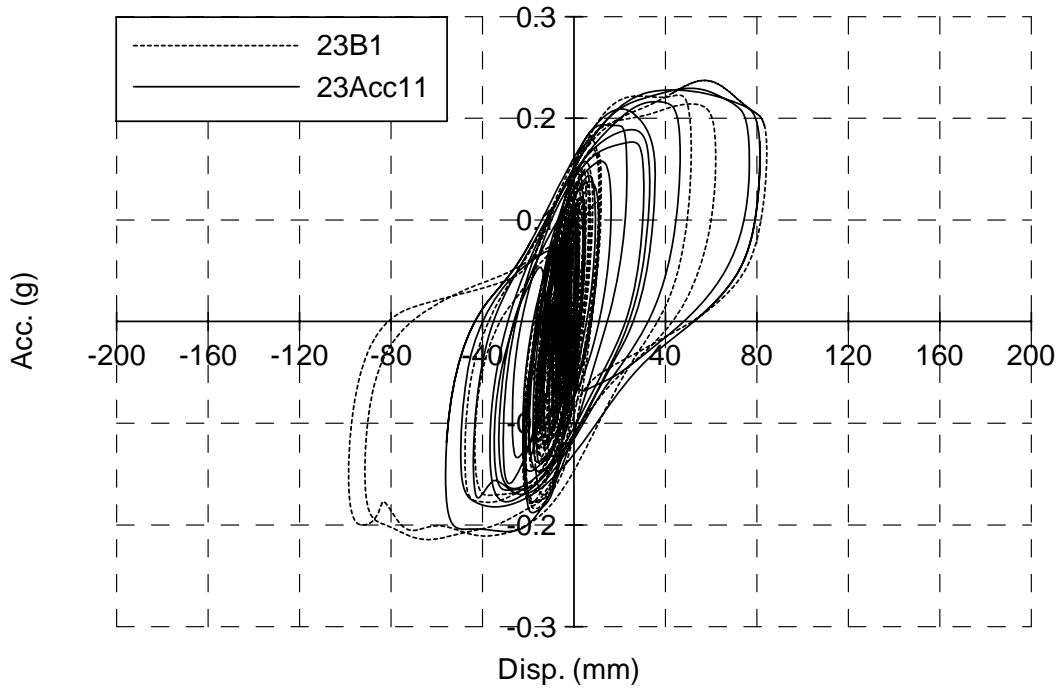


Fig. 6.40 Comparison of Acceleration-Displacement Relationships under Different Inputs and Load Case 3 (Rubber Balls)

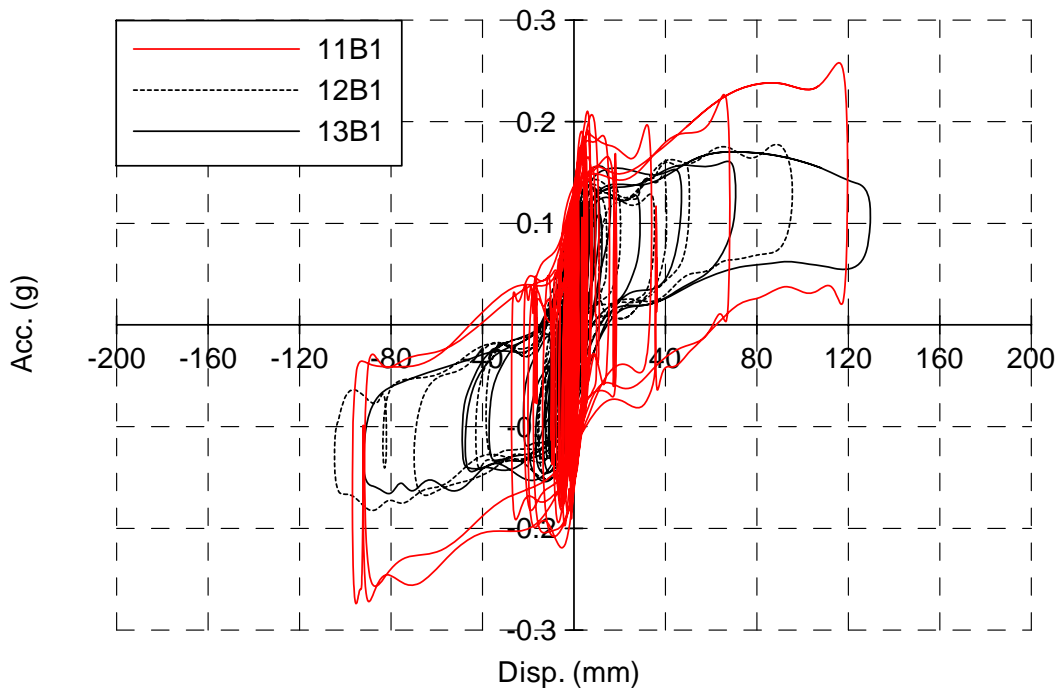


Figure 6.41 Comparison of Acceleration-Displacement Relationships under Different Symmetric Load Cases and Input of B1 (with Edge Plates, Polyurethane Balls)

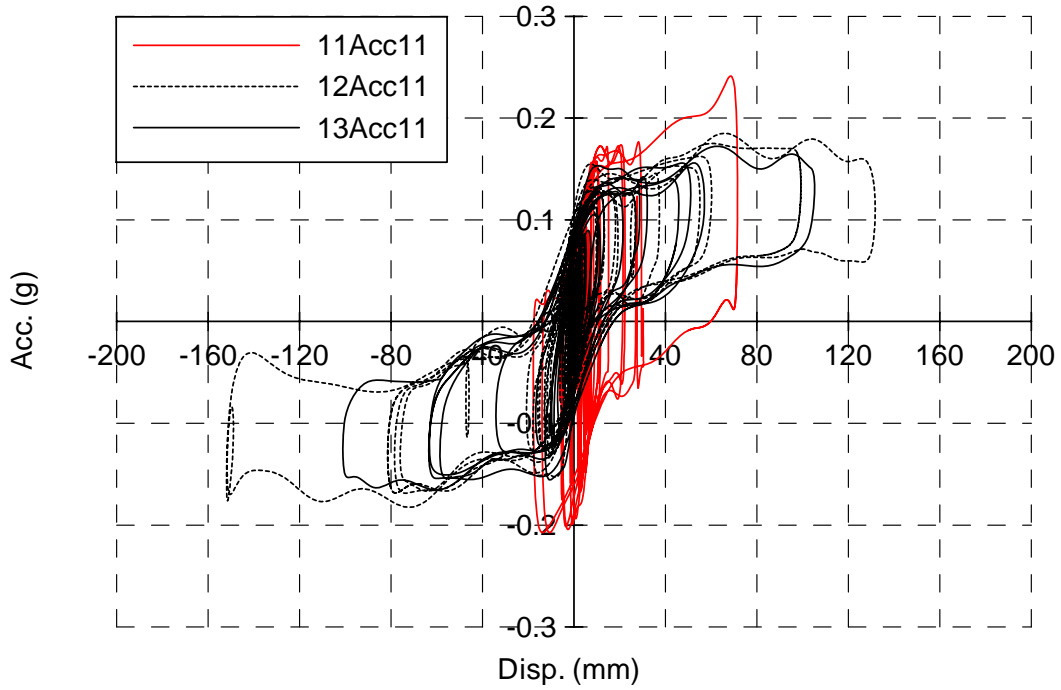


Figure 6.42 Comparison of Acceleration-Displacement Relationships under Different Symmetric Load Cases and Input of Acc11 (with Edge Plates, Polyurethane Balls)

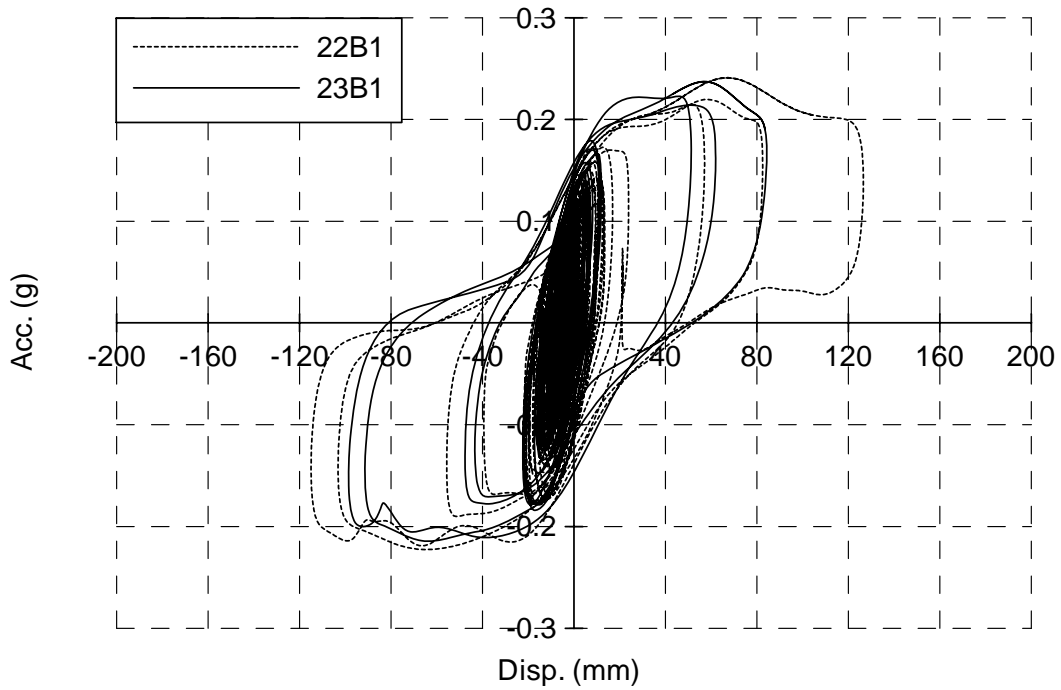


Figure 6.43 Comparison of Acceleration-Displacement Relationships under Different Symmetric Load Cases and Input of B1 (with Edge Plates, Rubber Balls)

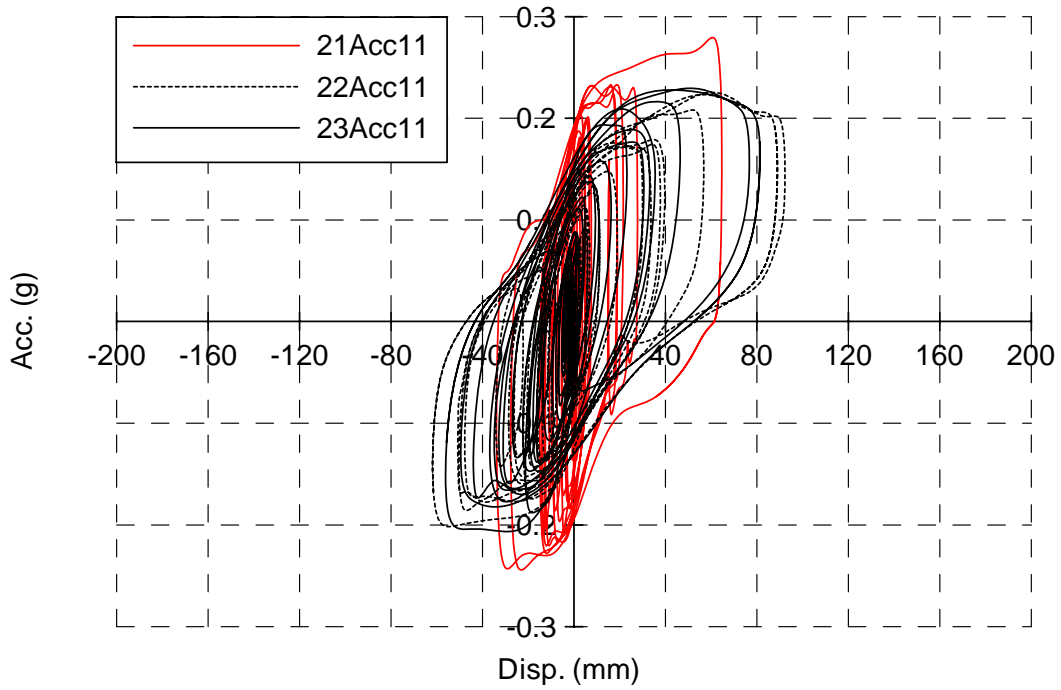


Figure 6.44 Comparison of Acceleration-Displacement Relationships under Different Symmetric Load Cases and Input of Acc11 (with Edge Plates, Rubber Balls)

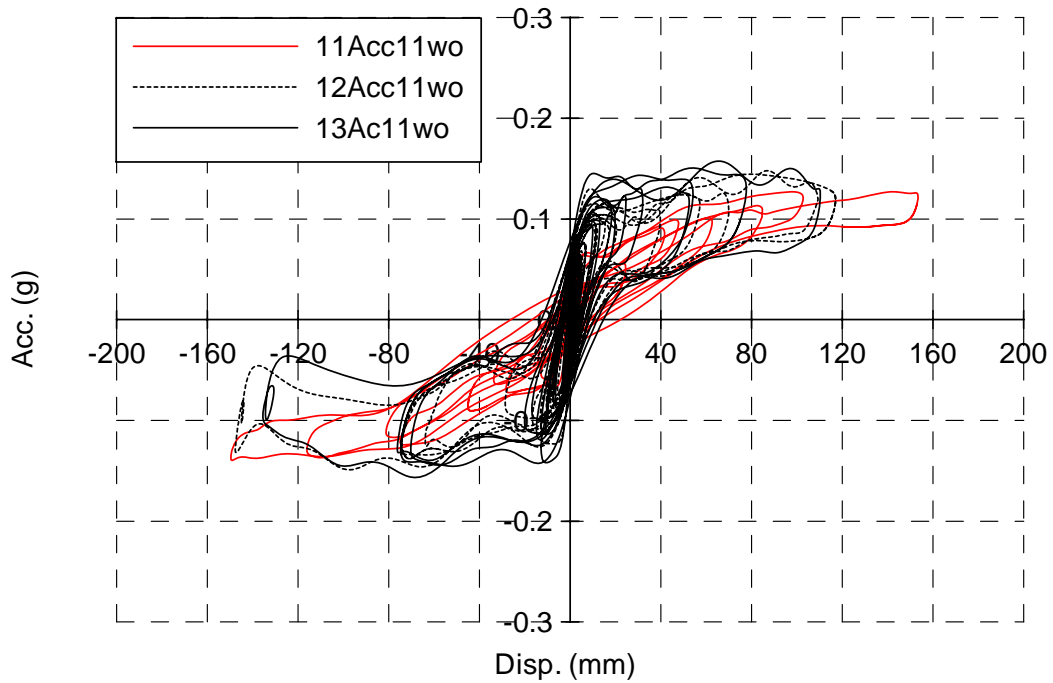


Figure 6.45 Comparison of Acceleration-Displacement Relationships under Different Symmetric Load Cases and Input of Acc11 (without Edge Plates, Polyurethane Balls)

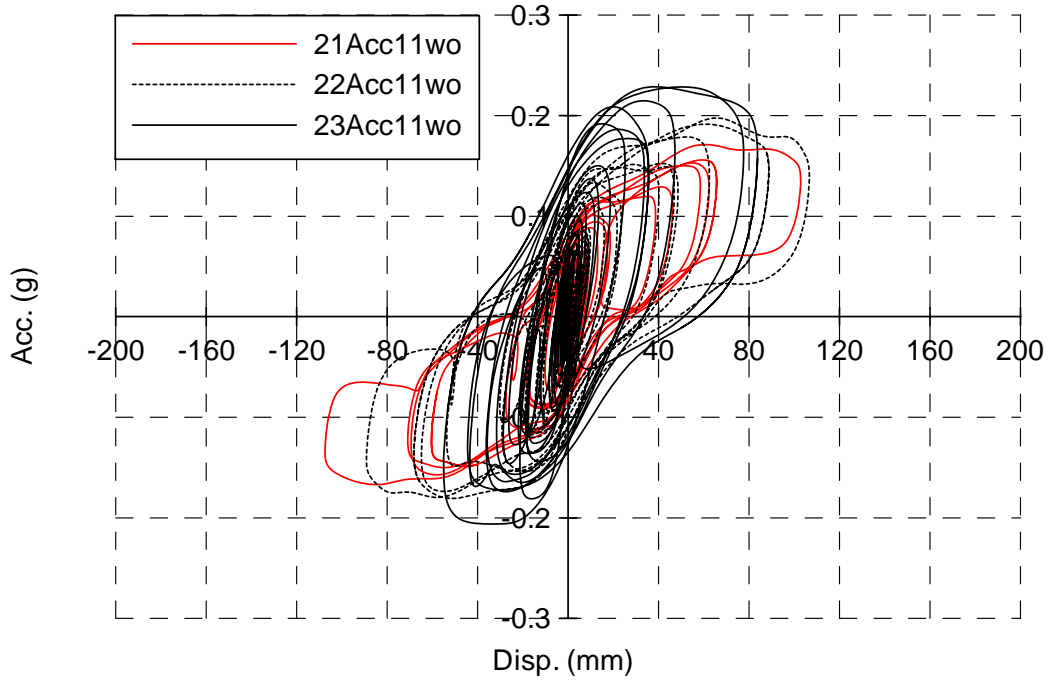


Figure 6.46 Comparison of Acceleration-Displacement Relationships under Different Symmetric Load Cases and Input of Acc11 (without Edge Plates, Rubber Balls)

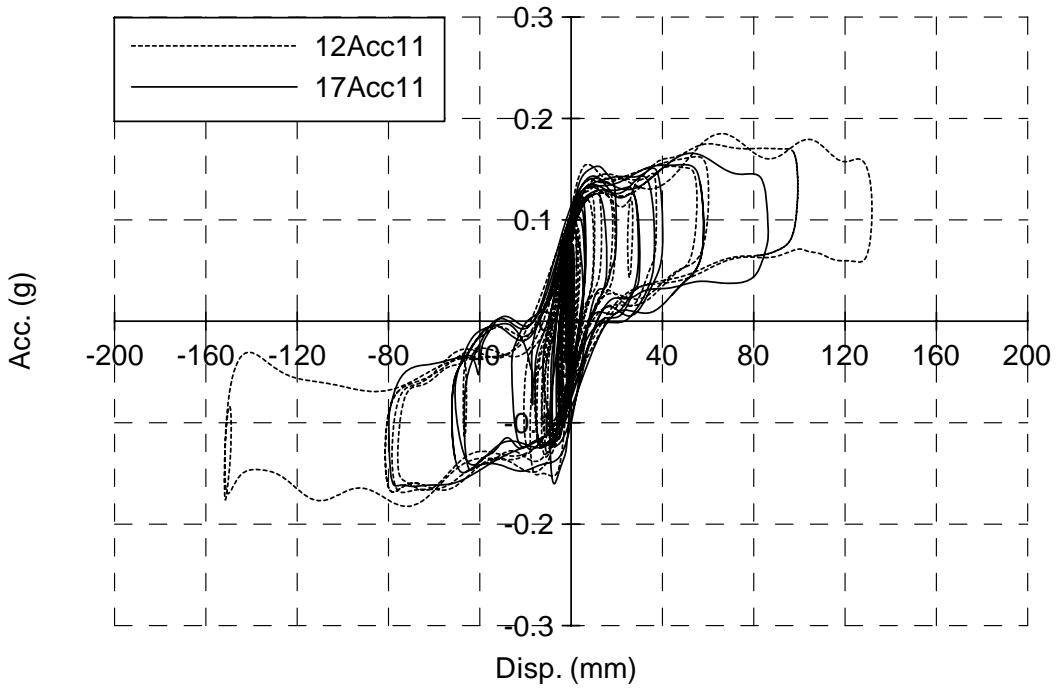


Figure 6.47 Comparison of Acceleration-Displacement Relationships Between Symmetric and Eccentric Load Cases under Input of Acc11 (Polyurethane Balls)

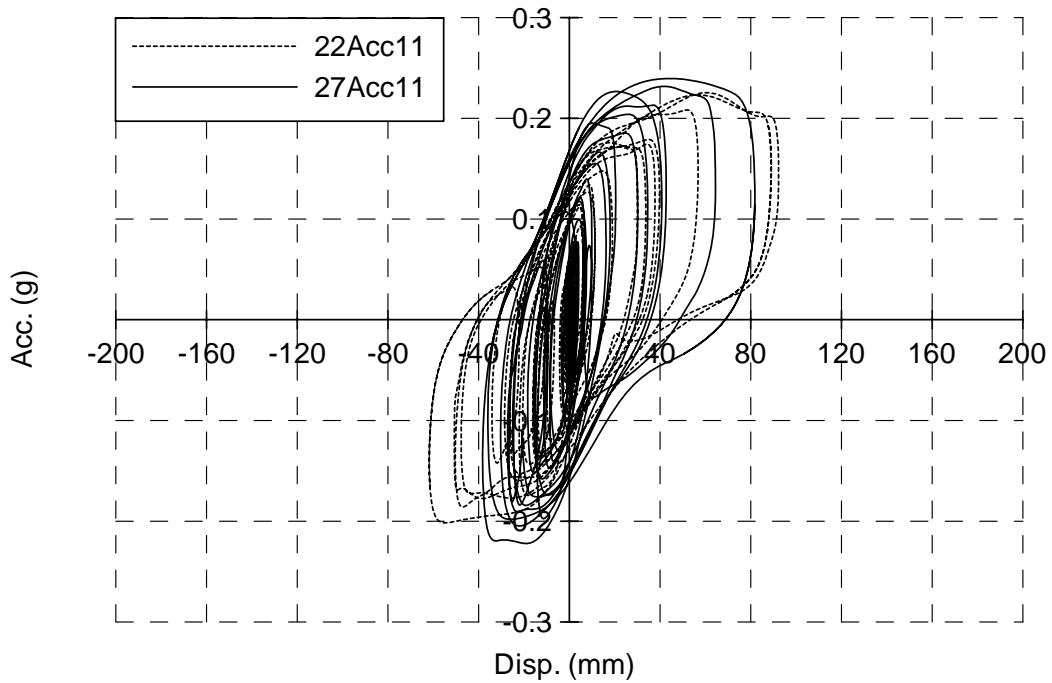


Figure 6.48 Comparison of Acceleration-Displacement Relationships Between Symmetric and Eccentric Load Cases under Input of Acc11 (Rubber Balls)

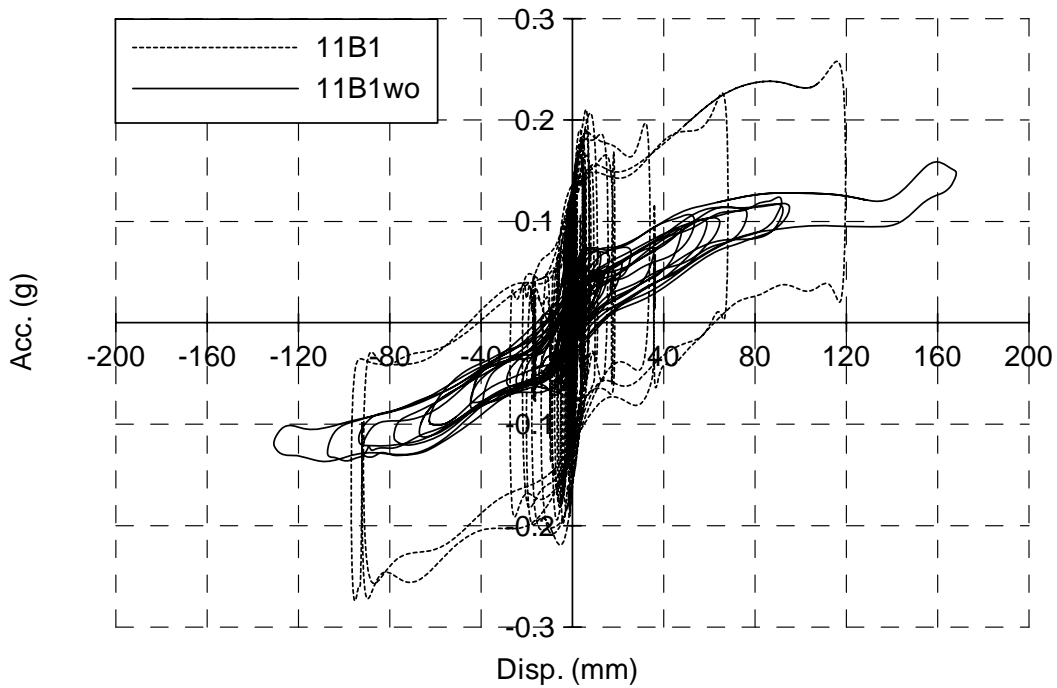


Figure 6.49 Comparison of Acceleration-Displacement Relationships Between With and Without Cover Plates under Load Case 1 When Subjected to B1 (Polyurethane Balls)

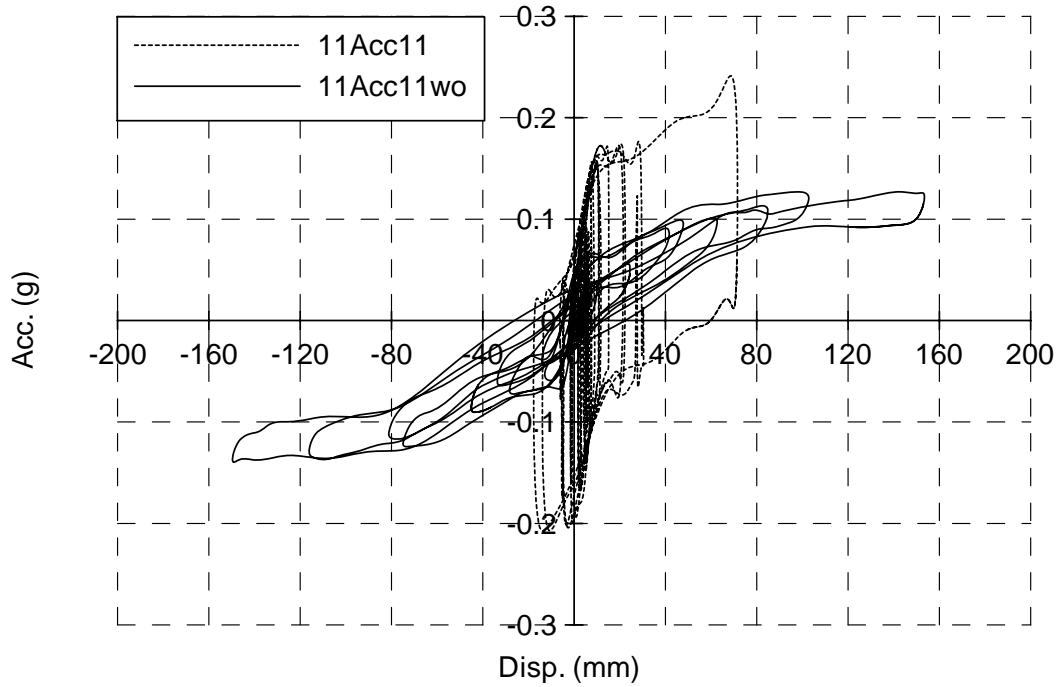


Figure 6.50 Comparison of Acceleration-Displacement Relationships Between With and Without Cover Plates under Load Case 1 When Subjected to Acc11 (Polyurethane Balls)

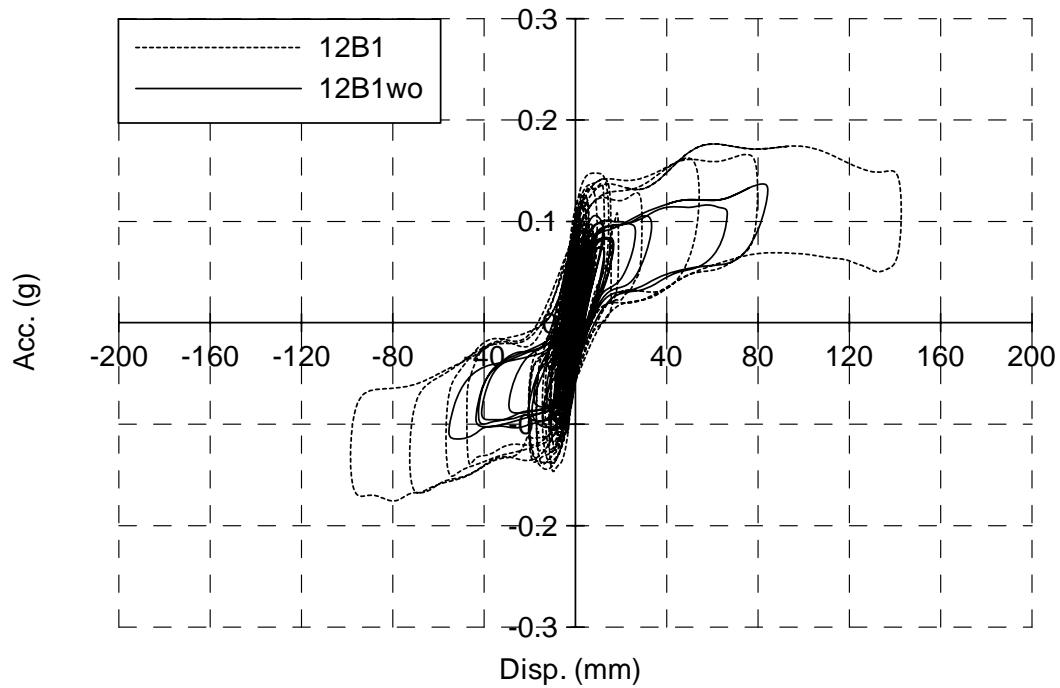


Figure 6.51 Comparison of Acceleration-Displacement Relationships Between With and Without Cover Plates under Load Case 2 When Subjected to B1 (Polyurethane Balls)

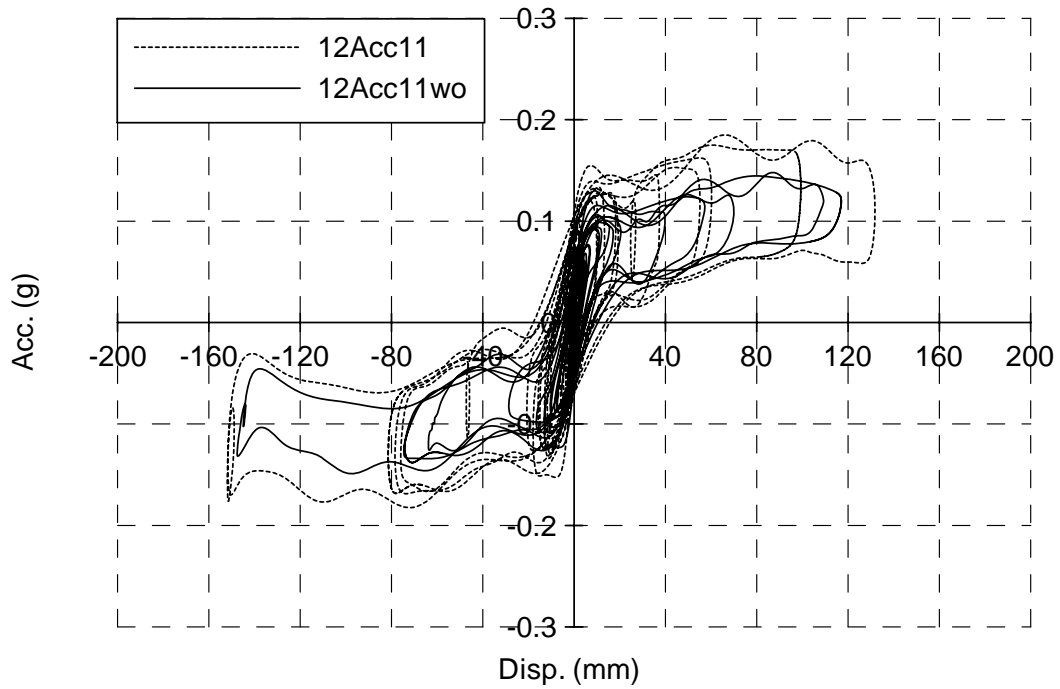


Figure 6.52 Comparison of Acceleration-Displacement Relationships Between With and Without Cover Plates under Load Case 2 When Subjected to Acc11 (Polyurethane Balls)

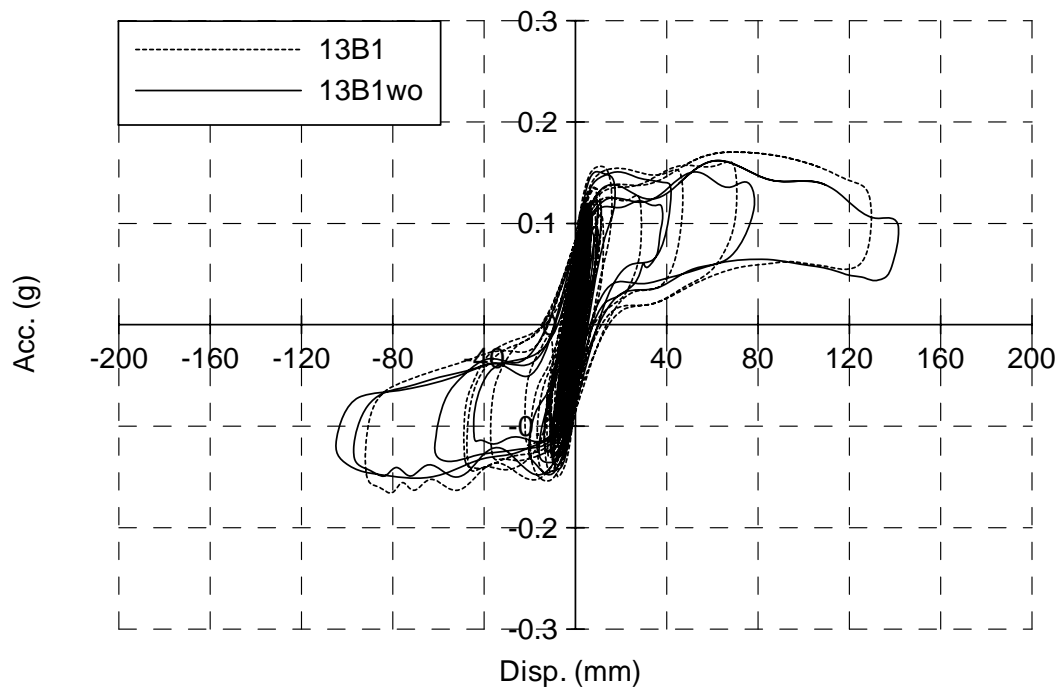


Figure 6.53 Comparison of Acceleration-Displacement Relationships Between With and Without Cover Plates under Load Case 3 When Subjected to B1 (Polyurethane Balls)

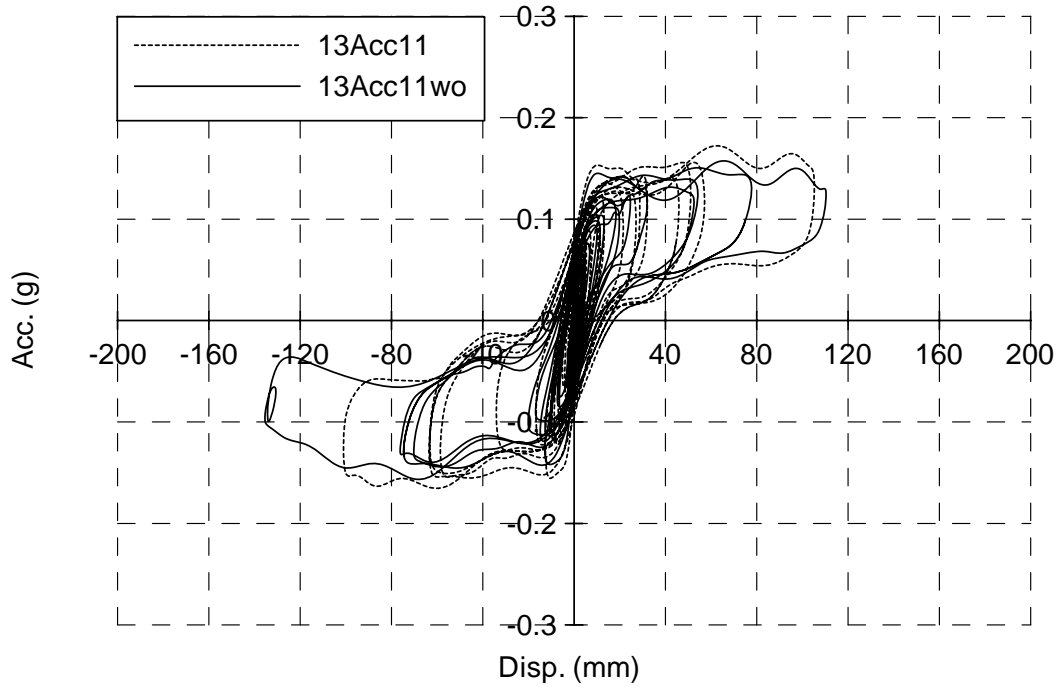


Figure 6.54 Comparison of Acceleration-Displacement Relationships Between With and Without Cover Plates under Load Case 3 When Subjected to Acc11 (Polyurethane Balls)

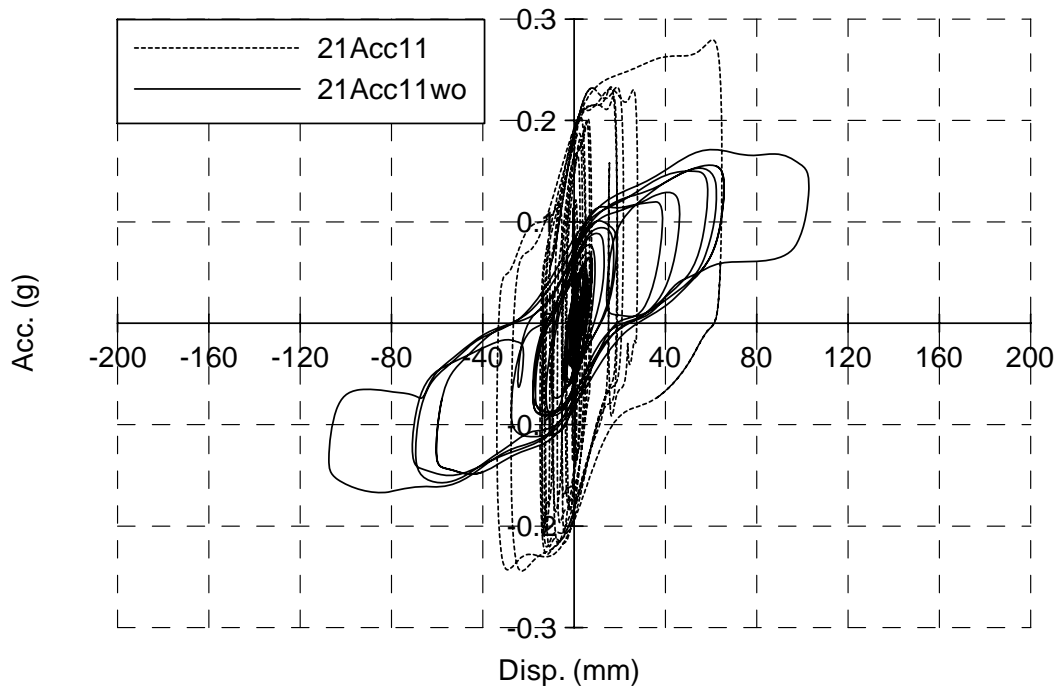


Figure 6.55 Comparison of Acceleration-Displacement Relationships Between With and Without Cover Plates under Load Case 1 When Subjected to Acc11 (Rubber Balls)

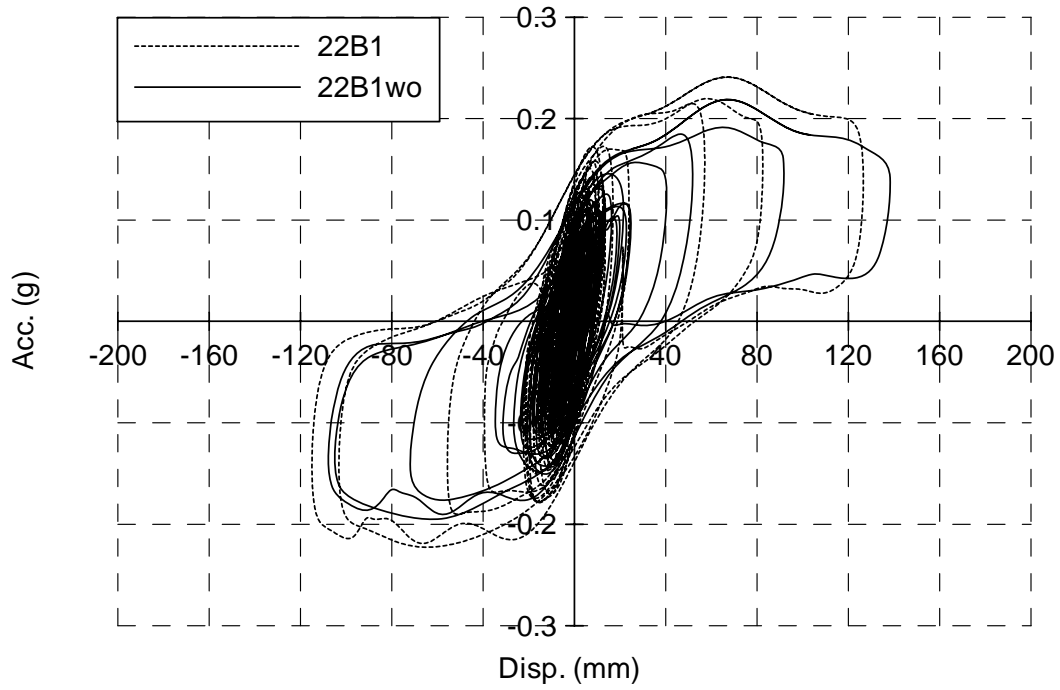


Figure 6.56 Comparison of Acceleration-Displacement Relationships Between With and Without Cover Plates under Load Case 2 When Subjected to B1 (Rubber Balls)

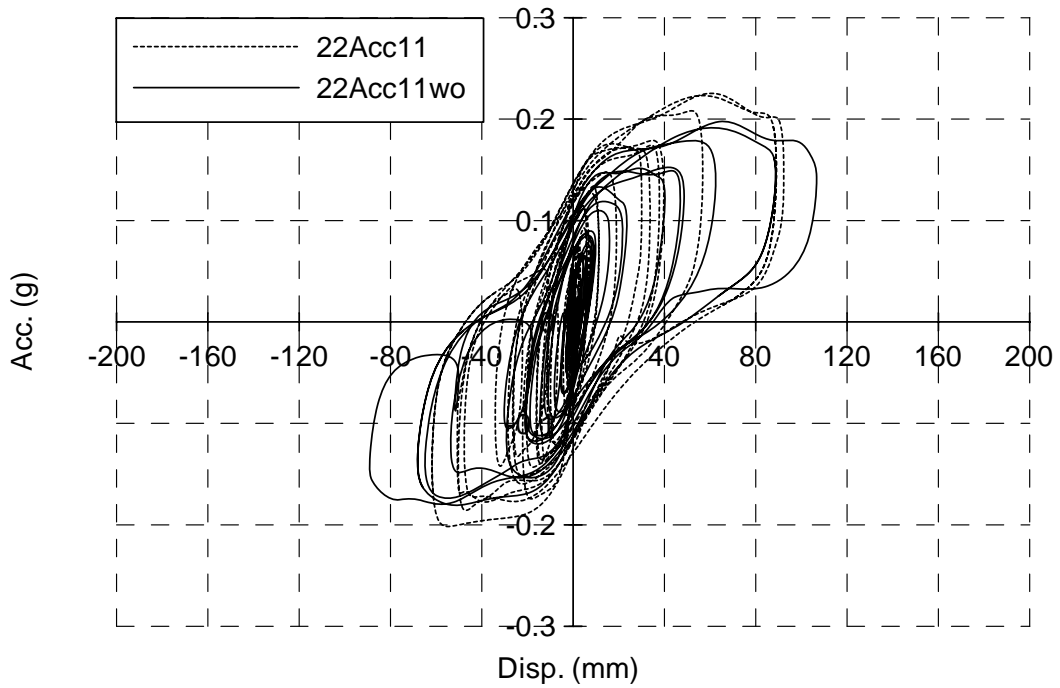


Figure 6.57 Comparison of Acceleration-Displacement Relationships Between With and Without Cover Plates under Load Case 2 When Subjected to Acc11 (Rubber Balls)

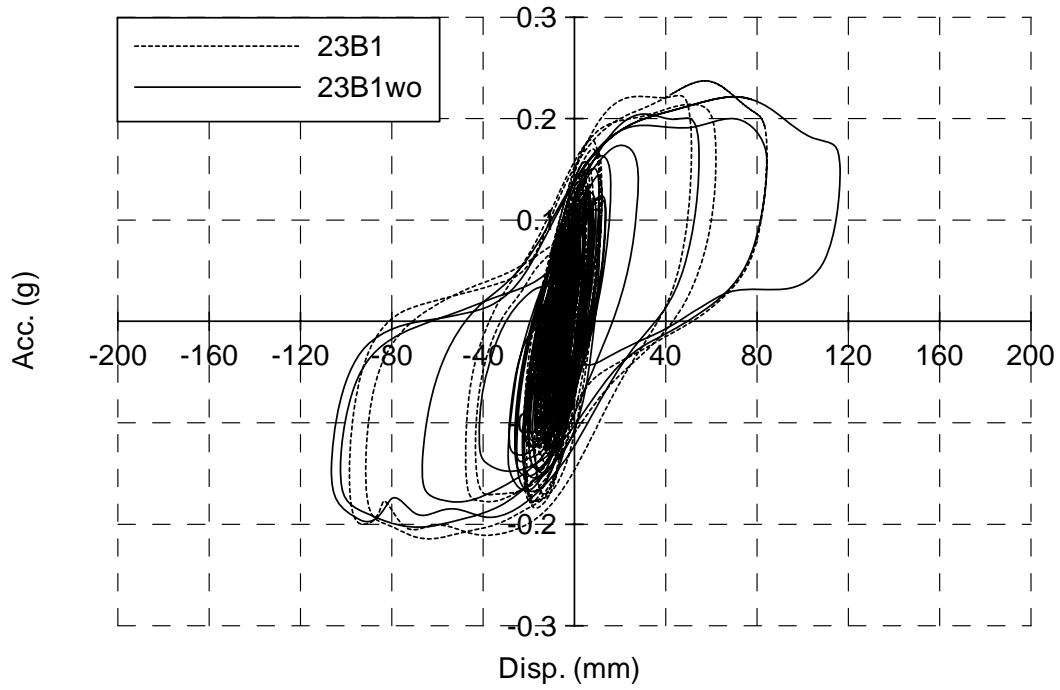


Figure 6.58 Comparison of Acceleration-Displacement Relationships Between With and Without Cover Plates under Load Case 3 When Subjected to B1 (Rubber Balls)

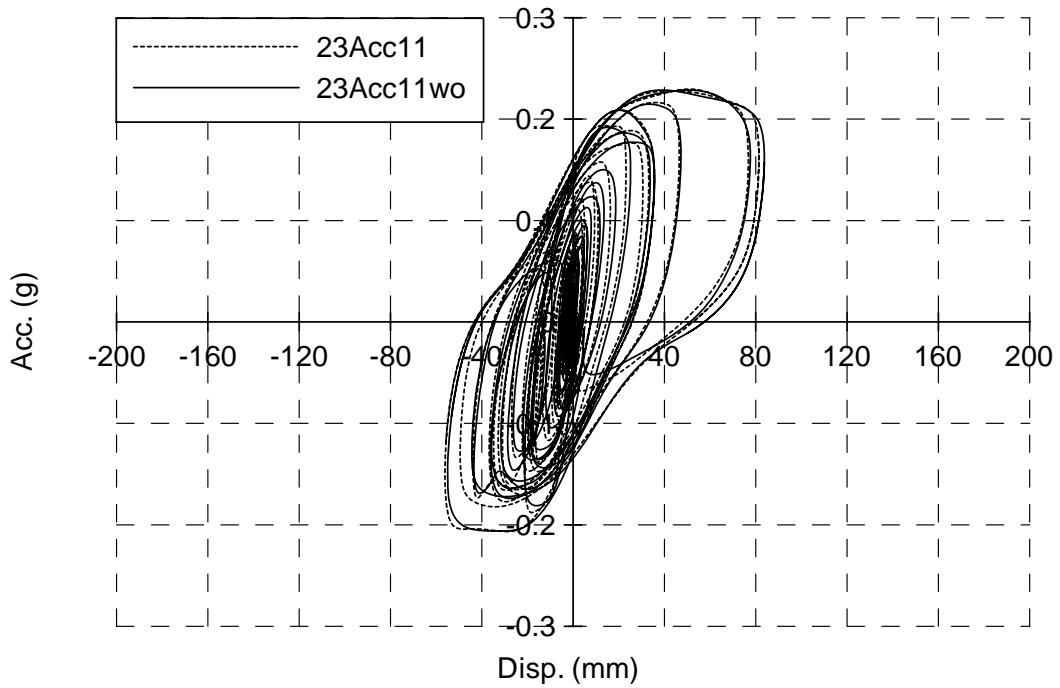


Figure 6.59 Comparison of Acceleration-Displacement Relationships Between With and Without Cover Plates under Load Case 3 When Subjected to Acc11 (Rubber Balls)

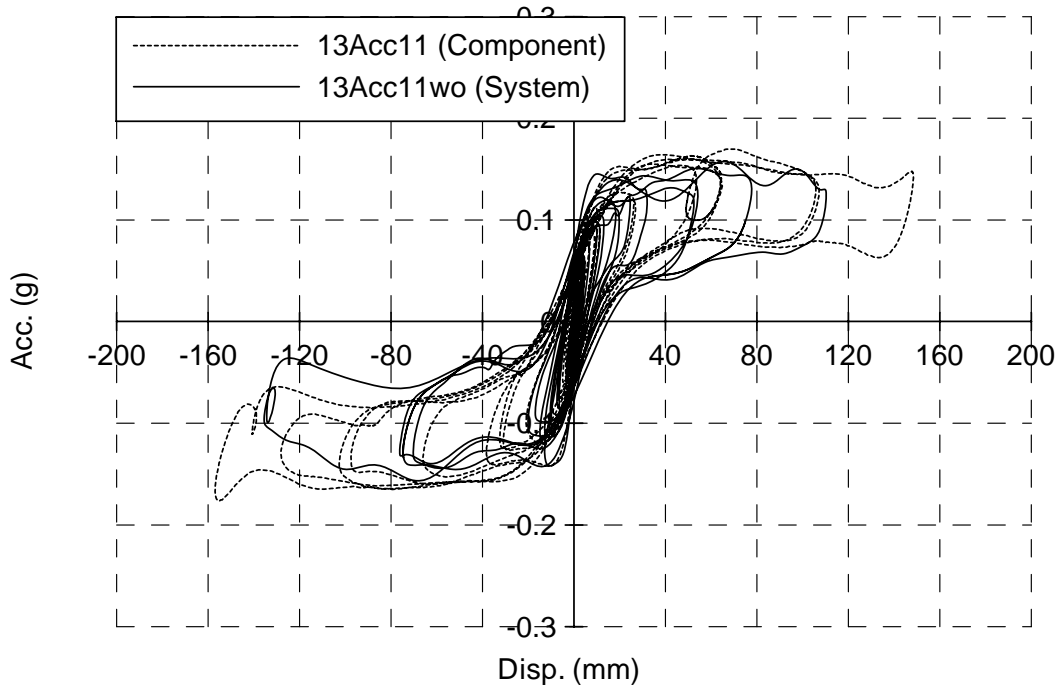


Figure 6.60 Comparison of Acceleration-Displacement Relationships between BNC Isolator Component and Whole System under Load Case 3 and Input of Acc11 (Polyurethane Balls)

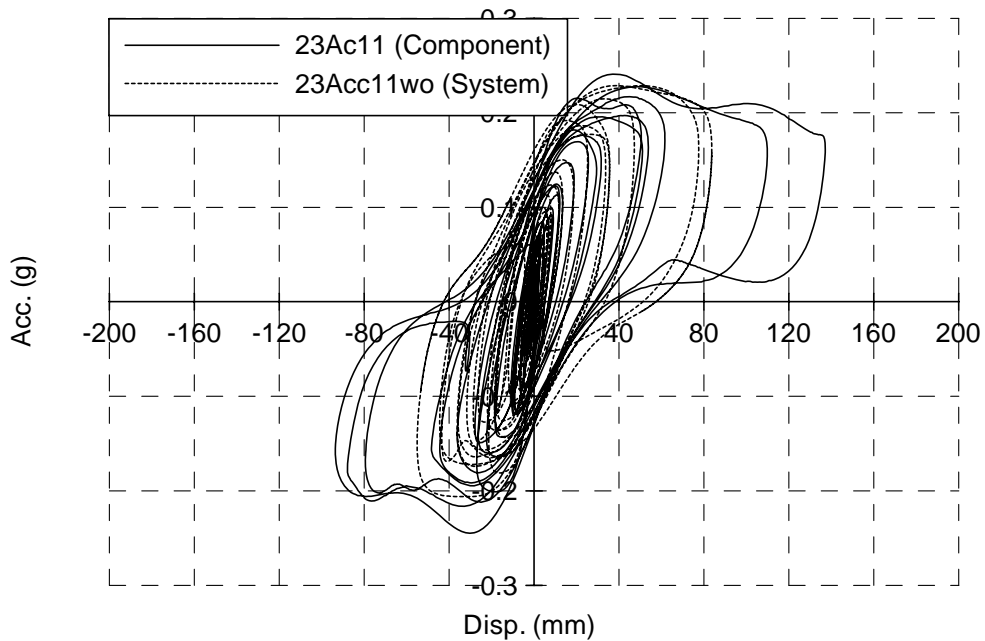


Figure 6.61 Comparison of Acceleration-Displacement Relationships Between BNC Isolator Component and Whole System under Load Case 1 and Input of Acc11 (Rubber Balls)

6.5 Response when Hitting the Wall

All above sections show that Isolated Floor System I worked well. However, one problem which occurred during one of the first tests, where the shake table controller experienced a failure and the shake table behaved in an erratic manner, provided interesting data. During that even, the displacement response of the isolated floor exceeded the capacity of its isolators underneath. The rolling balls of the isolators rolled out of the working surface at a displacement of about 200 mm and the isolated floor was projected towards the surrounding wall. The isolated floor hit against the wall at a displacement of about 220 mm and dropped down directly on the bottom bearing plates. The results of this test, denoted as 13ss1 to distinguish it from 13ss in above sections, are shown in Fig. 6.62. Note that a very high shake table impulse acceleration of approximately 5g was recorded. A very high acceleration response (as high as 4g) was recorded for the isolated floor when hitting against the wall. Incidentally, under the impact faces, the wall was damaged. The wall was repaired by running tension straps around it and filling grout into the hollow concrete block to keep its integrity. The test was then able to resume without any problem.

The above results show that the isolated floor hits the surrounding wall, high spikes of acceleration response will develop on the isolated floor. This underlines the importance of analysis to provide enough safety against the risk of sad impact.

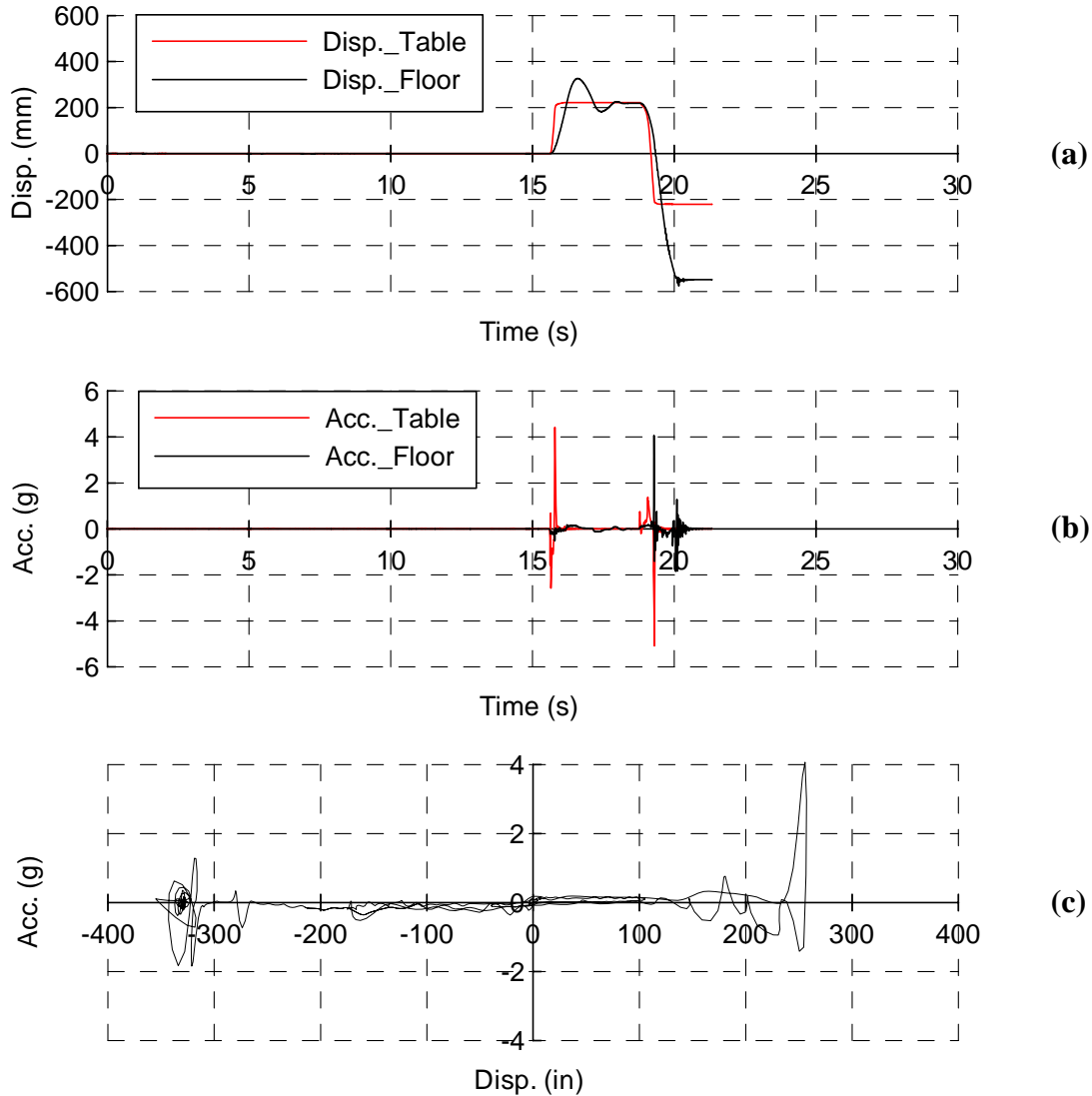


Figure 6.62 Results of Extra Test 13ss in N-S Direction: (a) and (b) Displacement and Acceleration of Shake Table and Isolated Floor, Respectively; (c) Acceleration-Displacement Relationship of Isolated Floor System I

6.6 Further Investigation of Rotation Effect

For the same reasons as described in Section 5.6, although it is observed from Section 6.4 that the rotation angle is small during all the tests, the displacement increase at the isolated floor corner due to the rotation should be considered in the design of Isolated Floor System I.

The ratios of the corner displacement (relative to the shake table) due to the rotation of the isolated floor over the isolated floor displacement at the middle point of the side perpendicular to the seismic direction under consideration are summarized in Tables 6.6 and 6.7 for cases using polyurethane and rubber balls, respectively. The terms/symbols used in these two tables have the same meaning as described in Section 5.6.

From these tables, it can be found that the maximum value of D_{ris} and the maximum value of R_c occur at different time moments. Also it can be observed that the total displacement (i.e., $D_{ris}+R_c$) at the corner of the isolated floor system when the maximum value of D_{ris} occurs is bigger than that when the maximum R_c occurs, and is equal to/almost same as that when the maximum ($D_{ris}+R_c$) happens (almost at the same time as when the maximum D_{ris} occurs). The averaged value of the ratios of R_c/D_{ris} when the maximum D_{ris} occurs is obtained as:

- For cases using polyurethane balls, 4.0%, 4.8%, and 13.6% for the cases with symmetric gravity loads, eccentric loads at an eccentricity of 425 mm, and eccentric loads at an eccentricity of 671 mm, respectively;
- For cases using rubber balls, 2.2% and 9.2% for the cases with symmetric gravity loads and eccentric loads at an eccentricity of 671 mm, respectively.

As done in Section 5.6, the comparison between these values obtained from tests with those obtained by using Eq. 13.3-5 for total displacement calculation in NEHRP 2003 was also conducted here. The results again show that the formula in NEHRP 2003 is too conservative for the eccentric load cases, which gives a value of higher than 40% for the 425 mm eccentric load case, and higher than 70% for the 671 mm eccentric load case, respectively. At the current stage of this project, the R_c/D_{ris} values obtained from tests will be used in the development of the design methodology for Isolated Floor System I, which is part of the topic of Chapter 9. Again, as mentioned in Section 5.6, because the data obtained here is limited, further research is

recommended to better quantify the rotation effects of Isolated Floor System i.

Table 6.6 Rotation Effects_Polyurethane Balls

Load Case	e (mm)	Test	X Direction					Y Direction				
			t (s)	D _{ris} (mm)	R _c (mm)	D _{ris} +R _c (mm)	R _c /D _{ris} (%)	t (s)	D _{ris} (mm)	R _c (mm)	D _{ris} +R _c (mm)	R _c /D _{ris} (%)
1	0	ss11	19.801	61.3	2.9	64.3	4.8	-	-	-	-	-
			20.309	58.3	3.1	61.4	5.3	-	-	-	-	-
			19.801	61.3	2.9	64.3	4.8	-	-	-	-	-
		11B1	19.910	119.7	2.4	122.1	2.0	-	-	-	-	-
			21.070	6.8	6.8	13.6	99.3	-	-	-	-	-
			19.914	119.7	2.5	122.1	2.0	-	-	-	-	-
		11Acc01	11.047	39.3	0.7	40.1	1.9	-	-	-	-	-
			13.660	13.1	2.3	15.3	17.5	-	-	-	-	-
			11.043	39.3	0.8	40.1	1.9	-	-	-	-	-
		11Acc11	14.738	71.6	2.1	73.6	2.9	-	-	-	-	-
			15.199	17.6	2.3	19.9	13.3	-	-	-	-	-
			14.734	71.6	2.1	73.7	2.9	-	-	-	-	-
		11Acc31	14.770	18.4	1.1	19.6	6.2	-	-	-	-	-
			14.516	16.0	1.4	17.4	8.7	-	-	-	-	-
			14.766	18.4	1.1	19.6	6.2	-	-	-	-	-
		11C1	14.648	73.5	0.1	73.6	0.2	14.879	75.1	0.3	75.3	0.3
			11.996	25.0	4.1	29.1	16.5	11.977	34.0	4.2	38.1	12.2
			14.652	73.5	0.1	73.6	0.2	14.898	75.1	0.4	75.4	0.5
		11C2	14.773	108.0	8.8	116.8	8.1	13.426	105.5	6.0	111.5	5.6
			14.375	20.6	24.0	44.6	116.8	14.348	20.1	19.5	39.6	97.1
			14.758	107.6	9.6	117.2	8.9	13.430	105.5	6.0	111.5	5.7
2	0	ss12	13.898	171.6	3.8	175.4	2.2	-	-	-	-	-
			13.590	43.9	4.3	48.2	9.7	-	-	-	-	-
			13.898	171.6	3.8	175.4	2.2	-	-	-	-	-
		12B1	20.031	142.8	3.2	146.0	2.3	-	-	-	-	-
			19.691	31.1	3.4	34.5	10.8	-	-	-	-	-
			20.035	142.8	3.2	146.0	2.3	-	-	-	-	-
		12Acc01	13.250	104.7	0.7	105.4	0.6	-	-	-	-	-
			14.469	34.9	3.0	37.9	8.7	-	-	-	-	-
			13.250	104.7	0.7	105.4	0.6	-	-	-	-	-
		12Acc11	13.719	151.9	1.5	153.4	1.0	-	-	-	-	-
			14.434	30.4	4.5	34.9	14.9	-	-	-	-	-
			13.727	151.9	1.5	153.4	1.0	-	-	-	-	-
		12Acc31	13.465	162.3	1.1	163.4	0.7	-	-	-	-	-
			14.258	50.8	3.2	53.9	6.2	-	-	-	-	-
			13.469	162.3	1.1	163.4	0.7	-	-	-	-	-
		12C1	13.258	136.5	4.9	141.4	3.6	15.000	130.9	1.4	132.3	1.0
			13.711	77.2	9.6	86.7	12.4	13.512	23.4	13.2	36.6	56.1
			13.270	136.3	5.2	141.5	3.9	15.000	130.9	1.4	132.3	1.0
		12C2	14.758	87.9	1.0	89.0	1.1	13.586	153.6	14.3	167.9	9.3
			13.586	76.1	11.7	87.8	15.3	13.563	153.5	14.4	167.9	9.4
			13.395	83.7	6.5	90.3	7.8	13.570	153.6	14.4	168.0	9.4

Table 6.6 Rotation Effects_Polyurethane Balls (Contd.)

Load Case	e (mm)	Test	X Direction					Y Direction				
			t (s)	D _{ris} (mm)	R _c (mm)	D _{ris} +R _c (mm)	R _c /D _{ris} (%)	t (s)	D _{ris} (mm)	R _c (mm)	D _{ris} +R _c (mm)	R _c /D _{ris} (%)
3	0	ss13	14.344	135.0	3.4	138.4	2.5	-	-	-	-	-
			14.992	120.1	4.4	124.5	3.7	-	-	-	-	-
			14.340	135.0	3.5	138.5	2.6	-	-	-	-	-
		13B1	19.961	129.7	1.1	130.8	0.9	-	-	-	-	-
			19.566	10.4	2.1	12.5	20.3	-	-	-	-	-
			19.961	129.7	1.1	130.8	0.9	-	-	-	-	-
		13Acc11	12.340	105.2	1.0	106.2	0.9	-	-	-	-	-
			14.422	7.1	1.7	8.8	23.6	-	-	-	-	-
			12.340	105.2	1.0	106.2	0.9	-	-	-	-	-
		13C2	13.355	74.2	14.9	89.1	20.1	13.477	121.4	17.2	138.6	14.2
			13.438	70.6	15.8	86.4	22.3	13.418	117.5	17.7	135.2	15.1
			13.371	74.1	15.2	89.2	20.5	13.469	121.3	17.4	138.7	14.3
4	0	14C2	13.344	75.7	2.7	78.5	3.6	13.457	97.7	4.8	102.5	4.9
			12.113	30.9	7.4	38.3	24.0	12.121	10.5	7.4	17.9	71.1
			13.359	75.7	2.9	78.6	3.9	13.457	97.7	4.8	102.5	4.9
5	425	15C2	13.418	83.4	11.2	94.6	13.4	13.512	113.3	13.1	126.4	11.6
			12.539	56.0	13.8	69.8	24.6	12.535	77.6	14.6	92.2	18.9
			13.422	83.4	11.2	94.6	13.4	13.508	113.3	13.2	126.4	11.6
6	425	16C2	13.277	77.8	0.3	78.1	0.4	12.469	73.8	0.5	74.3	0.7
			15.227	54.0	8.4	62.5	15.6	15.223	22.1	9.7	31.7	43.7
			13.262	77.7	0.5	78.2	0.6	12.449	73.5	1.1	74.6	1.5
7	671	17B1	19.977	108.7	15.5	124.2	14.2	-	-	-	-	-
			20.000	108.1	15.7	123.9	14.5	-	-	-	-	-
			19.984	108.6	15.6	124.3	14.4	-	-	-	-	-
		17Acc01	13.215	76.5	12.0	88.4	15.6	-	-	-	-	-
			12.344	75.8	14.2	90.0	18.8	-	-	-	-	-
			12.328	76.3	14.2	90.5	18.6	-	-	-	-	-
		17Acc11	12.355	86.3	19.5	105.8	22.6	-	-	-	-	-
			12.359	86.3	19.5	105.8	22.6	-	-	-	-	-
			12.355	86.3	19.5	105.8	22.6	-	-	-	-	-
		17Acc31	11.836	26.8	0.8	27.6	2.9	-	-	-	-	-
			12.473	22.4	6.4	28.9	28.7	-	-	-	-	-
			11.258	24.0	5.9	29.9	24.4	-	-	-	-	-
17C2	13.336	78.1	20.6	98.7	26.4	13.500	127.4	31.3	158.7	24.6		
	13.723	63.6	27.0	90.6	42.4	13.516	127.3	31.5	158.8	24.7		
	13.367	77.4	22.0	99.4	28.4	13.512	127.4	31.5	158.8	24.7		
8	671	18Acc31	11.207	20.4	2.5	23.0	12.3	-	-	-	-	-
			9.855	17.0	3.6	20.7	21.1	-	-	-	-	-
			11.211	20.4	2.5	23.0	12.3	-	-	-	-	-
		18C1	12.273	49.7	5.9	55.6	11.9	14.910	68.8	18.9	87.7	27.5
			14.883	16.1	17.1	33.2	106.6	14.891	68.7	19.0	87.7	27.7
			14.680	48.2	10.5	58.7	21.9	14.902	68.8	19.0	87.8	27.6
		18C2	13.328	76.8	0.4	77.2	0.5	13.422	104.3	1.9	106.3	1.8
			12.891	4.0	13.4	17.4	334.7	12.852	43.8	15.8	59.5	36.0
			13.352	76.4	1.1	77.5	1.5	13.438	104.1	2.3	106.4	2.3

Table 6.7 Rotation Effects_Rubber Balls

Load Case	e (mm)	Test	X Direction					Y Direction				
			t (s)	D _{ris} (mm)	R _c (mm)	D _{ris} +R _c (mm)	R _c /D _{ris} (%)	t (s)	D _{ris} (mm)	R _c (mm)	D _{ris} +R _c (mm)	R _c /D _{ris} (%)
1	0	ss21	16.082	40.7	2.8	43.6	7.0	-	-	-	-	-
			16.059	40.4	2.9	43.3	7.2	-	-	-	-	-
			16.078	40.7	2.9	43.6	7.0	-	-	-	-	-
		21Acc11	14.730	64.7	1.4	66.1	2.2	-	-	-	-	-
			12.012	18.9	1.8	20.7	9.8	-	-	-	-	-
			14.730	64.7	1.4	66.1	2.2	-	-	-	-	-
		21C2	14.762	64.3	1.9	66.2	3.0	14.844	31.4	1.1	32.5	3.5
			12.016	17.8	3.1	20.9	17.4	12.066	9.2	2.5	11.7	26.9
			14.758	64.3	1.9	66.2	3.0	14.836	31.3	1.1	32.5	3.7
2	0	ss22	13.129	166.9	0.3	167.1	0.2	-	-	-	-	-
			11.969	9.2	3.2	12.4	35.3	-	-	-	-	-
			13.133	166.9	0.3	167.1	0.2	-	-	-	-	-
		22Acc01	19.938	126.6	0.6	127.1	0.4	-	-	-	-	-
			19.613	3.8	3.0	6.8	77.1	-	-	-	-	-
			19.941	126.6	0.6	127.2	0.5	-	-	-	-	-
		22Acc11	12.270	92.3	1.6	93.9	1.7	-	-	-	-	-
			11.008	28.4	2.1	30.5	7.4	-	-	-	-	-
			12.270	92.3	1.6	93.9	1.7	-	-	-	-	-
		22C2	14.797	55.7	1.2	56.9	2.1	12.570	53.4	1.2	54.5	2.2
			12.051	17.9	4.3	22.3	24.2	12.023	11.6	4.4	16.0	38.3
			14.793	55.7	1.2	56.9	2.1	12.566	53.4	1.2	54.5	2.2
3	0	ss23	14.367	120.7	1.1	121.8	1.0	-	-	-	-	-
			13.313	2.3	3.0	5.2	130.6	-	-	-	-	-
			14.371	120.7	1.2	121.8	1.0	-	-	-	-	-
		23B1	19.105	98.5	0.6	99.2	0.6	-	-	-	-	-
			19.531	3.6	3.7	7.2	103.5	-	-	-	-	-
			19.105	98.5	0.6	99.2	0.6	-	-	-	-	-
		23Acc11	14.766	81.4	1.2	82.6	1.5	-	-	-	-	-
			11.941	7.1	2.7	9.8	38.0	-	-	-	-	-
			14.766	81.4	1.2	82.6	1.5	-	-	-	-	-
		23C2	14.762	76.7	0.5	77.2	0.6	12.527	66.2	3.2	69.4	4.9
			13.516	42.8	7.0	49.8	16.4	13.535	36.4	7.1	43.5	19.5
			14.766	76.7	0.6	77.2	0.7	12.527	66.2	3.2	69.4	4.9
7	671	27B1	19.906	98.9	8.7	107.5	8.8	-	-	-	-	-
			19.906	98.9	8.7	107.5	8.8	-	-	-	-	-
			19.906	98.9	8.7	107.5	8.8	-	-	-	-	-
		27Acc11	14.750	81.8	8.9	90.7	10.8	-	-	-	-	-
			14.762	81.6	8.9	90.5	10.9	-	-	-	-	-
			14.750	81.8	8.9	90.7	10.8	-	-	-	-	-
		27C2	14.770	64.5	6.0	70.4	9.3	12.527	51.7	1.2	52.9	2.4
			14.852	57.7	7.1	64.8	12.4	14.820	41.7	8.0	49.7	19.2
			14.777	64.4	6.2	70.5	9.6	12.508	51.5	1.7	53.2	3.4
8	671	28C2	14.754	64.9	2.0	66.9	3.1	12.492	35.7	5.0	40.7	14.1
			16.793	10.2	5.4	15.7	53.1	12.527	34.9	5.1	40.0	14.6
			14.758	64.8	2.0	66.9	3.1	12.496	35.7	5.0	40.7	14.1

6.7 Observations

Details of the characterization tests of Isolated Floor System I, from test setup to test results, were presented in this chapter. The results show that Isolated Floor System I is able to carry the expected load cases and behaved satisfactorily under both symmetric and eccentric load cases. Isolated Floor System I reduced the peak acceleration response of the isolated floor. The behavior of this isolated floor system, having either polyurethane balls or rubber balls, has a meaning that the peak acceleration of the isolated floor will remain a constant value at relatively large displacements (i.e. as long as the rolling balls are within the conical part of the working surface of the concrete bearing plates) and that the friction coefficient is also constant for a given magnitude of the gravity load. Although the rotation angle of the isolated floor system is small in spite of large load eccentricities on top of the isolated floor, the displacement at the corner of the isolated floor system due to rotation should be considered in Isolated Floor System I design. The behavior of the isolated floor system under bidirectional excitations is dependant on the motion properties in both directions.

The behavior of Isolated Floor System I was compared for cases with and without edge cover plates. This illustrated how friction between the rolling balls and the concrete working surface of isolator bearing plates affected the peak acceleration response of the isolated floors, and this effect became less significant with increases in the supported gravity load. The test results for Isolated Floor System I (without edge cover plates) was also compared with that of the isolator component tests presented in Chapter 3 for a given magnitude of gravity load, acting on each ball. The equivalent coefficient of friction, μ_e , was found to be almost same, regardless of whether it was tested in the whole isolated floor system or as a concrete BNC isolator component. The foundation provided in this chapter allows to better model the behavior of Isolated Floor System I in computing programs, which is the content of Chapter 7.

CHAPTER 7

ANALYTICAL MODELS OF BEHAVIOR OF ISOLATED FLOOR SYSTEMS

7.1 Introduction

The mechanical properties of individual isolators and complete isolated floor systems have been obtained from the characterization tests described in Chapters 3 to 6. Based on the experimentally obtained information, analytical models of isolated floor systems have been developed and are presented in this chapter. Section 7.2 presents modeling of the behaviors of both concrete Ball-in-Cone (BNC) isolators and the corresponding Isolated Floor System I, where the relationship between the equivalent friction coefficients and the load on each rolling ball (polyurethane ball or rubber ball) was simplified as linear. Cases of isolated floor systems with and without edge plates were considered. The model for cases with edge plates was set up by adding an extra friction effect from the edge plates to the model for the corresponding cases without edge plates (i.e., the model for individual isolators). Section 7.2 also includes results of a sensitivity study conducted to investigate whether the model is sensitive to the equivalent friction coefficient. In Section 7.3, the behavior of the multi-directional spring units is first simulated. A comparison of the results between the analytical model and the corresponding physical model is presented in this section. Based on the developed model for multi-directional spring units, the model for Isolated Floor System II is developed by considering the extra friction effects from the casters and the edge plates. Cases of isolated floor systems with and without edge plates were considered. As in Section 7.2, a similar sensitivity study is also conducted on the analytical

model of Isolated Floor System II. Note that analyses of BNC isolators and Isolated Floor System I (Sections 7.2) were conducted using SAP2000 (Computers and Structures Inc., 2004), while analyses of multi-directional spring units and Isolated Floor II on casters (Section 7.3) were conducted in IDARC2D (Reinhorn et al. 2009). Although it is easy to model the behavior of single BNC isolators and Isolated Floor System I by using link elements in SAP2000, there is no element in commercial structural analysis program readily available to model the unique behavior of the multi-directional spring units used as isolators in Isolated Floor System II. Therefore, for the modeling of Isolated Floor System II, a modified hysteretic element model implemented by Reinhorn and Roh in IDARC2D (Reinhorn et al. 2009) was found appropriate to replicate the behavior of the multi-directional spring units. In both of Sections 7.2 and 7.3, the results obtained from analytical models are compared with the corresponding test results. Reasonable agreements are observed. These computer models will be used in a parametric study of investigated systems consisting of structural fuse frames and isolated floor systems, which is the topic of Chapter 8.

7.2 Analytical Model of Isolated Floor System I Behavior

7.2.1 Equivalent Friction Coefficient

As defined in Chapter 3, an equivalent friction coefficient, μ_e , is used to represent the rolling friction effect between the rolling balls (polyurethane or rubber) and the working surface of the concrete BNC isolators. A number of equivalent friction coefficient values were estimated from the test results corresponding to load cases with different magnitudes of gravity load as described in Chapters 3 and 6. In Chapter 6, it was also established that when the average gravity load applied to each ball in Isolated Floor System I is the same as for individual isolators (even if all balls are not equally loaded over the entire floor), the corresponding equivalent friction coefficients are nearly identical.

The values of μ_e obtained from the tests on individual isolators (Chapter 3) and complete isolated floor systems (Chapter 6) are shown in Figs. 7.1 and 7.2 in terms of the equivalent friction coefficients for the corresponding average load for cases using polyurethane and rubber balls, respectively. In these two figures, the “triangular” marker points represent the values from isolated floor system results, and the “diamond” marker points correspond to the individual isolator tests.

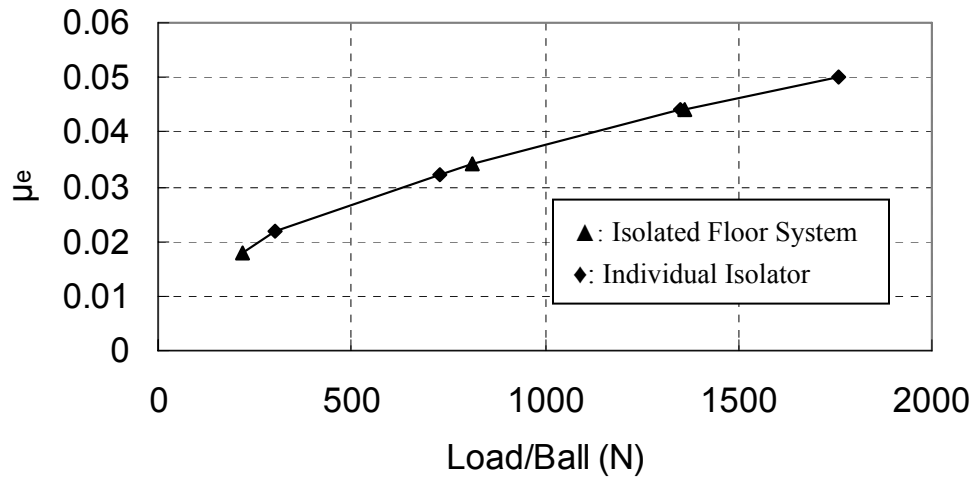


Figure 7.1 Relationship between Equivalent Friction Coefficient and Average Ball Load on Polyurethane Ball

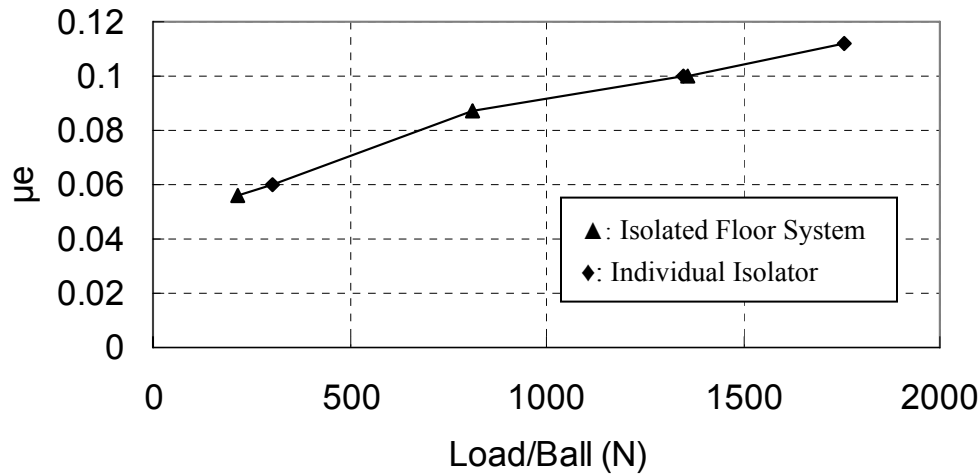


Figure 7.2 Relationship between Equivalent Friction Coefficient and Average Ball Load on Rubber Ball

Note from Figs. 7.1 and 7.2 that the equivalent friction coefficient increases with the average load on each ball, for both the polyurethane and rubber ball cases. In an effort to explain this, some tests were conducted on a single concrete BNC isolator, during which the isolator remained at its initial static-balance position and kept still, under different gravity load magnitude to investigate the relationship between the load magnitude and the “squash” of the rolling ball. The results are tabulated in Table 7.1, where the contacting area “ A_c ” was calculated based on the simplifying assumption that the “squashed” part of the rolling ball “disappears” without changing the otherwise perfect spherical shape of the remaining section of the ball. This is equivalent to neglecting deformations of the middle “un-squashed” part of the rolling ball.

Note from Table 7.1 that under higher load, a rolling ball will be “squashed” more, resulting in more contact area between the rolling ball and the working surface of the concrete BNC isolator. In investigating this problem, no reference was found quantifying the rolling friction of spherical rubber or polyurethane balls. Some research findings on the rolling friction of tires made of material similar to the isolator rolling balls was found, but only limited qualitative value

reference. For example, the U.S. department of transportation (1977) reports that under lower inflation pressure the rolling friction coefficient of tires increases. Lower inflation causes more flexing of a tire sidewalls (i.e., creating more contact area between the tire and the ground) and thus higher rolling resistance. By analogy, it is reasonable to postulate here that the increasing contact area between the rolling balls and the bearing plates of isolators consequently results in an increase in the equivalent friction coefficient. However, considering the difference in shape between tires and spherical balls, this reasonable proposition would need further study to better understand the physics and develop a quantitative model to predict the value of rolling friction for spherical balls.

Table 7.1 Squashing Ball Test Results

Load/Ball (N/ball) (1)	Polyurethane Balls		Rubber Balls	
	Squashed Amount (mm) (2)	Contact Area (mm ²) (3)	Squashed Amount (mm) (4)	Contact Area (mm ²) (5)
726.1	0.36	665.2	0.42	758.7
1321.1	0.40	730.1	0.54	951.2
1916.0	0.44	787.0	0.60	1026.6
2510.9	0.47	843.8	0.68	1138.2
3154.7	0.51	898.9	0.74	1223.7
3798.6	0.54	953.7	0.80	1299.0
4443.6	0.58	1001.1	0.85	1354.1
5086.3	0.62	1055.6	0.88	1394.6
6072.6	0.67	1124.4	0.95	1463.9
6746.5	0.70	1171.2	0.98	1504.6
7420.4	0.74	1216.0	1.01	1530.0

The values of the experimentally obtained data points in Figures 7.1 and 7.2 are tabulated in Table 7.2 and were used to model the behaviors of single isolators and complete isolated floor systems as described in the following sections. Based on these experimentally obtained values of μ_e , a closed-form expression of μ_e for the future parametric study and isolated floor system

design under any possible load magnitude is needed. Three different approaches were investigated to develop an expression to relate the experimentally obtained equivalent friction coefficients to the corresponding load on each ball, as shown in Figs. 7.3 to 7.8. Figs. 7.3 to 7.5 illustrate linear, polynomial, and power functions fit to the experimented data for polyurethane balls, respectively. Figs. 7.6 to 7.8 do the same for rubber balls. Good agreements can be observed in all of these figures. Therefore, for simplicity, the linear fit was retained here as an appropriate relationship between the equivalent friction coefficients and the corresponding average ball load. Note that the linear fit gives slightly lower values of the friction coefficient compared to the actual values over most of the middle part of the applied load range. However, it gives slightly higher values of the friction coefficient than the actual values near the two extreme ends (the maximum and the minimum values) of the applied load range. This will result in conservatism for analysis and design of isolated floor systems. This will be discussed more in the following sections of this chapter.

The resulting linear relationship between the equivalent friction coefficient and the averaged ball load is expressed as:

$$y = 0.00002x + 0.0157 \quad (\text{Polyurethane Ball}) \quad (7.1)$$

$$y = 0.00004x + 0.0507 \quad (\text{Rubber Ball}) \quad (7.2)$$

Note here that the purpose of generating the relationship between the equivalent friction coefficient and the average ball load is not to physically model the rolling friction between the rolling balls (polyurethane or rubber) and the concrete working surface. As will be demonstrated later in this chapter, the friction effects from the edge plates in the complete isolated floor system are a function of standard friction coefficient (which was empirically quantified from the tests shown in Chapter 6) and should be considered in the analytical model of the isolated floor system. One reasonable and simple method to consider all the friction effects in Isolated Floor System I is to lump all these friction effects together empirically as shown later, which is attractive to practicing engineers.

Table 7.2 Experimentally Obtained Values of Equivalent Friction Coefficients

Ball Typr (1)	Load/Ball (N/ball) (2)	μ_e (3)
Polyurethane	216.17	0.018
	303.58	0.022
	729.47	0.032
	811.02	0.034
	1349.97	0.044
	1361.46	0.044
	1759.18	0.050
Rubber	216.17	0.056
	303.58	0.060
	811.02	0.087
	1349.97	0.100
	1361.46	0.100
	1759.18	0.112

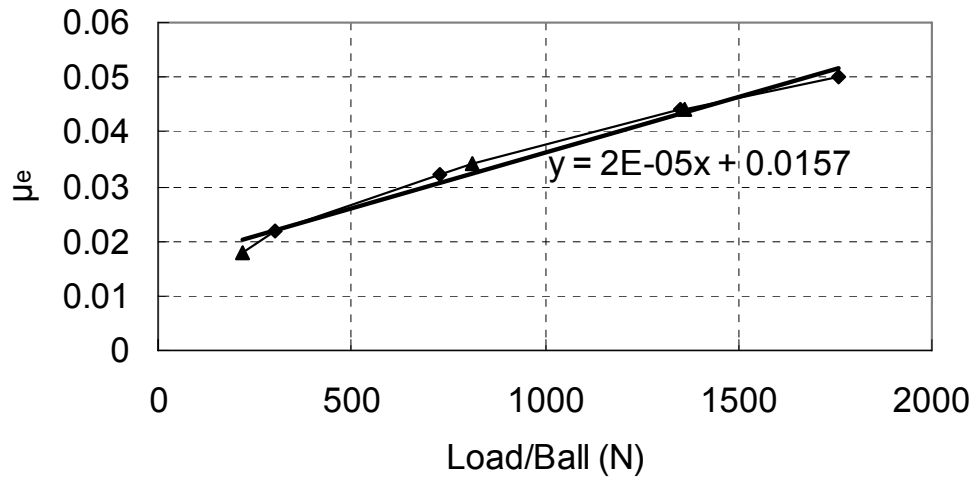


Figure 7.3 Linear Approximate Relationship between Equivalent Friction Coefficient and Average Ball Load on Polyurethane Ball

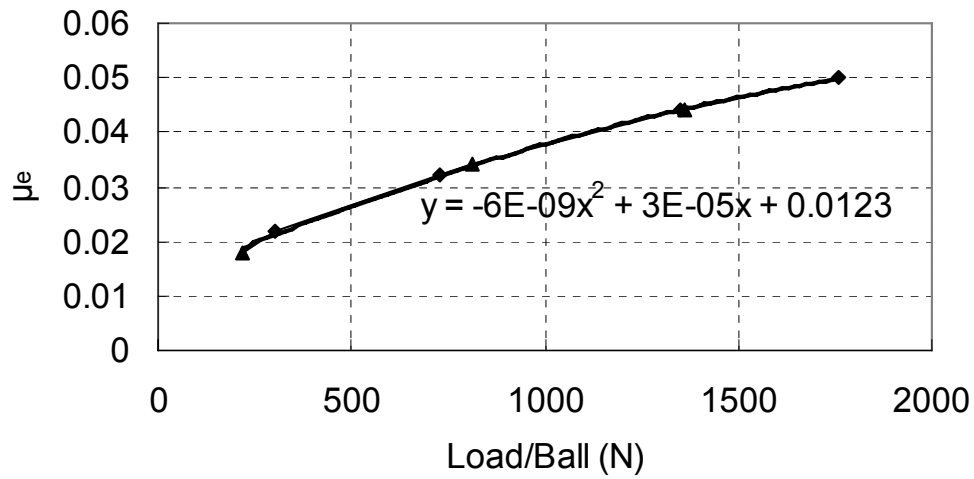


Figure 7.4 Polynomial Approximate Relationship between Equivalent Friction Coefficient and Average Ball Load on Polyurethane Ball

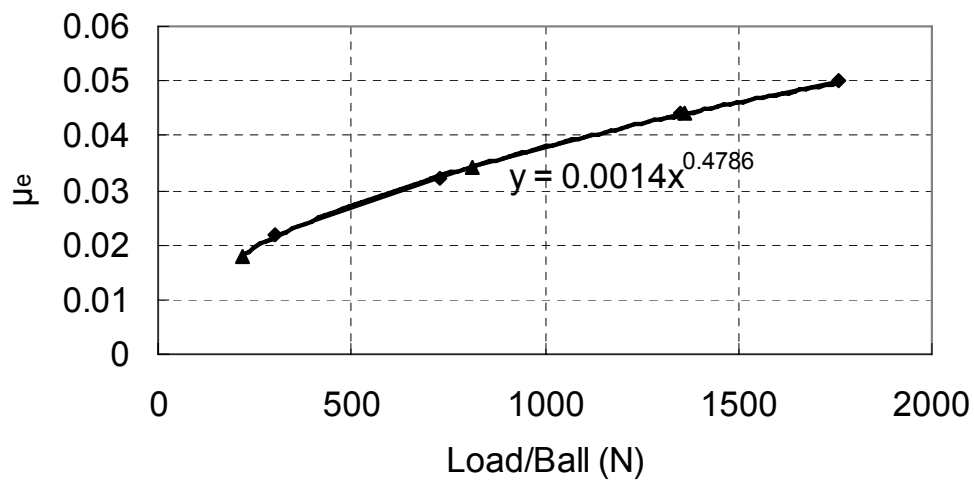


Figure 7.5 Power Approximate Relationship between Equivalent Friction Coefficient and Average Ball Load on Polyurethane Ball

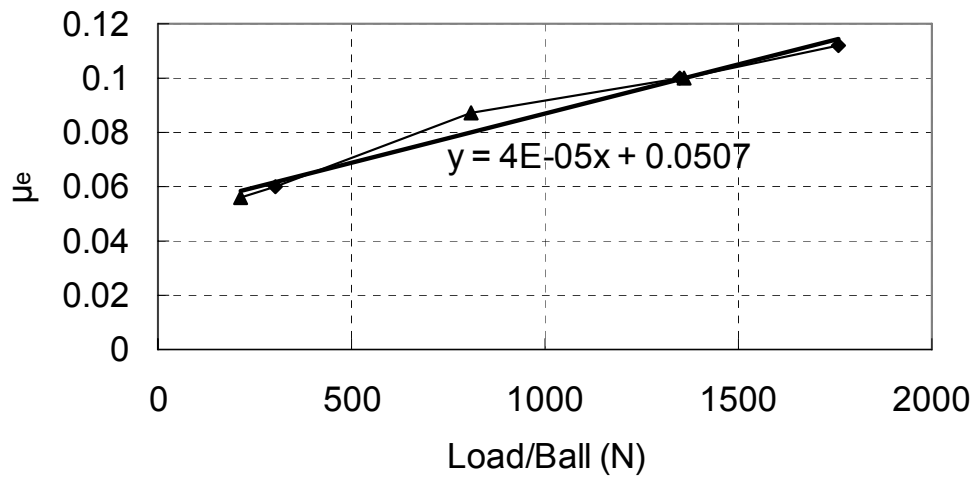


Figure 7.6 Linear Approximate Relationship between Equivalent Friction Coefficient and Average Ball Load on Rubber Ball

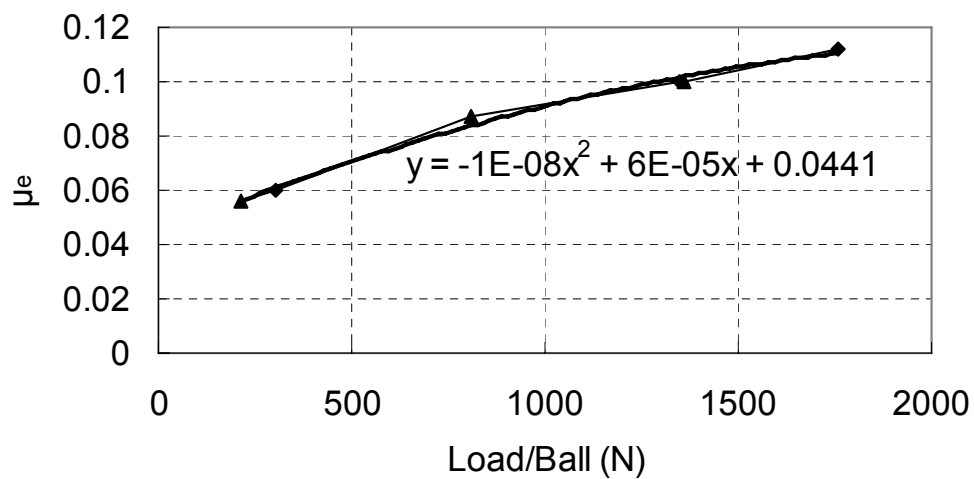


Figure 7.7 Polynomial Approximate Relationship between Equivalent Friction Coefficient and Average Ball Load on Rubber Ball

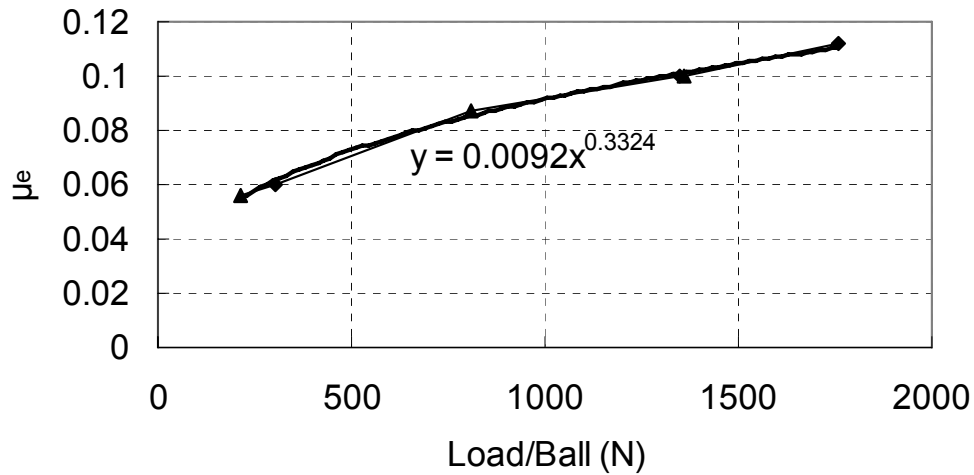


Figure 7.8 Power Approximate Relationship between Equivalent Friction Coefficient and Average Ball Load on Rubber Ball

7.2.2 Analytical Model

To develop the analytical model for Isolated Floor System I, it is necessary to first develop the model for the behavior of its concrete BNC isolators. For this purpose, as mentioned in Chapter 3, the behavior (Force-Displacement relationship) of a concrete BNC isolator is equivalent to the combination of a bilinear-elastic behavior and a frictional behavior, as shown in Fig. 7.9. Note in Fig. 7.9 that: “W” is the self-weight of the isolated objects including the self-weight of the top bearing plates of the isolator, “ γ ” is the inclined angle (with respect to a horizontal surface) of the conical part of the working surface of the BNC isolator, and “ μ_e ” is the equivalent friction coefficient described in Section 7.2.1. To model concrete BNC isolators in SAP2000, the bilinear elastic part was modeled by using a multilinear elastic element in parallel with a plastic-Wen element with almost rigid initial stiffness to model the friction energy dissipation. Note that the bilinear part corresponds to the elastic theoretical behavior of the BNC isolator without any friction.

For the analytical model of Isolated Floor System I with edge plates, the same model principle as shown in Fig. 7.9 and its realization in SAP2000 described above can also be used except that an extra friction effect from the edge plates (with a value of about 441N (99.11 lb) as mentioned in Chapter 6) should be considered. A simple way to realize this is that the frictional part in Fig. 7.9, modeled by using a plastic-Wen element, should also consider the friction effect between the edge plates and the isolated floor's walking surface in addition to the one between the rolling ball and the isolator's working surface.

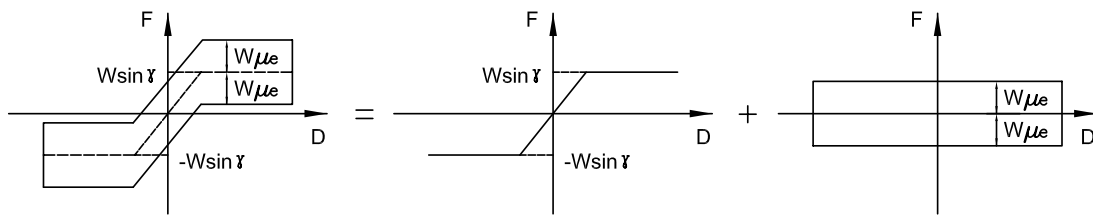


Figure 7.9 Principle for Concrete BNC Isolators Modeling

7.2.3 Comparison between Results from Analytical Model and Tests

Section 7.2.2 described the models used in SAP2000 to replicate the behaviors of concrete BNC isolators and the corresponding isolated floor systems. This section compares the analysis results obtained using these analytical models and the corresponding test results. For BNC isolators, the cases subjected to the input acceleration record Acc11 are presented. Figs. 7.10 to 7.12 show results for cases using polyurethane balls under the Load Cases 1, 3, and 4 described in Chapter 3, respectively, and Figs. 7.13 to 7.15 show results for cases using rubber balls. For complete isolated floor systems, comparisons of results between SAP2000 analysis and corresponding tests under Load Cases 1 to 3 described in Chapter 6 are presented in this section, as shown in Figs. 7.16 to 7.21 for cases without edge plates and Figs. 7.22 to 7.27 for cases with edge plates. Among these figures, Figs. 7.16 to 7.18 and Figs. 7.22 to 7.24 are for cases using polyurethane balls, and the rest are for cases using rubber balls.

In each of these figures, there are 3 plots. Parts (a) and (b) are the displacement and acceleration time-history responses of the isolated objects, respectively, and part (c) is the acceleration-displacement loops results from the analytical model and corresponding tests.

It is observed from parts (a) and (b) of each figure that although there is some discrepancy in magnitude for both displacement and acceleration responses between the analytical results and the corresponding test results, the analytical response results are well in phase with the corresponding test results. From part (c) of each figure, the discrepancy between the results from analytical model and the corresponding tests can also be found. It can also be noted from part (c) of each figure that the friction effect (i.e., the acceleration magnitude difference between the loading and unloading branch of the loops) is almost the same between the results from analytical model and the corresponding tests. That is to say the loading and unloading branches of the loops obtained from test results shift almost the same amount in the same direction (up or down), which actually is another observation from part (c) of each figure.

Based on the empirical model of BNC isolators described in Chapter 3, this discrepancy in the acceleration response (especially the peak value) is most likely attributed to the fact that manufacturing of the rolling surface of the isolators (done using foam molds was not perfectly accurate, as mentioned in Chapter 3. This resulted in bumps on the rolling surface and inaccuracy in the slope value of its conic part. Recall that the slope of the conical part will control the location (up or down) of the plateau of the bilinear elastic contribution of the empirical model. Actual measurements of the slope of the conical part of the concrete isolator specimen's rolling surfaces showed that the average slope of the conical surfaces of the isolator used in both individual isolator tests and complete isolated floor system tests was greater than the target value (see Chapter 3). Correspondingly, peak acceleration response from test results is higher than that from the corresponding analytical results, as observed in part (c) of each figure. This also explains the discrepancy in the acceleration response and displacement response between the

results from analytical model and the corresponding tests.

In addition, from part (b) of some figures, for the figure from analysis results, a long-duration high-frequency free vibration motion of constant magnitude is observed after the end of the seismic input, contrary to the damped free vibration motion observed from tests. This motion is attributed to the extremely high stiffness within the elastic range of both the multi-elastic element and the plastic-Wen element (there is no energy dissipation in this small amplitude residual vibration). Because the magnitude of this free vibration motion is significantly smaller than the peak response (the response quantity of interest in this research), no further efforts were made to eliminate this constant-magnitude free vibration and it remains as shown in part (b) of some figures here. For the same reason, in the modeling of Isolated Floor System II as will be shown in Section 7.3.1, such phenomenon can also be found for the friction damper brace element used there to simulate the friction effects. Finally, note that because designs of Isolated Floor System I in specific application may use edge plates with sizes differing from those used in the tests (in Chapter 6), the corresponding friction effect from such edge plates would also have different values considered in the analytical model.

The above show that reasonable agreement between the analytical results and the corresponding test results was found and that the corresponding analytical models can be used for future parametric studies.

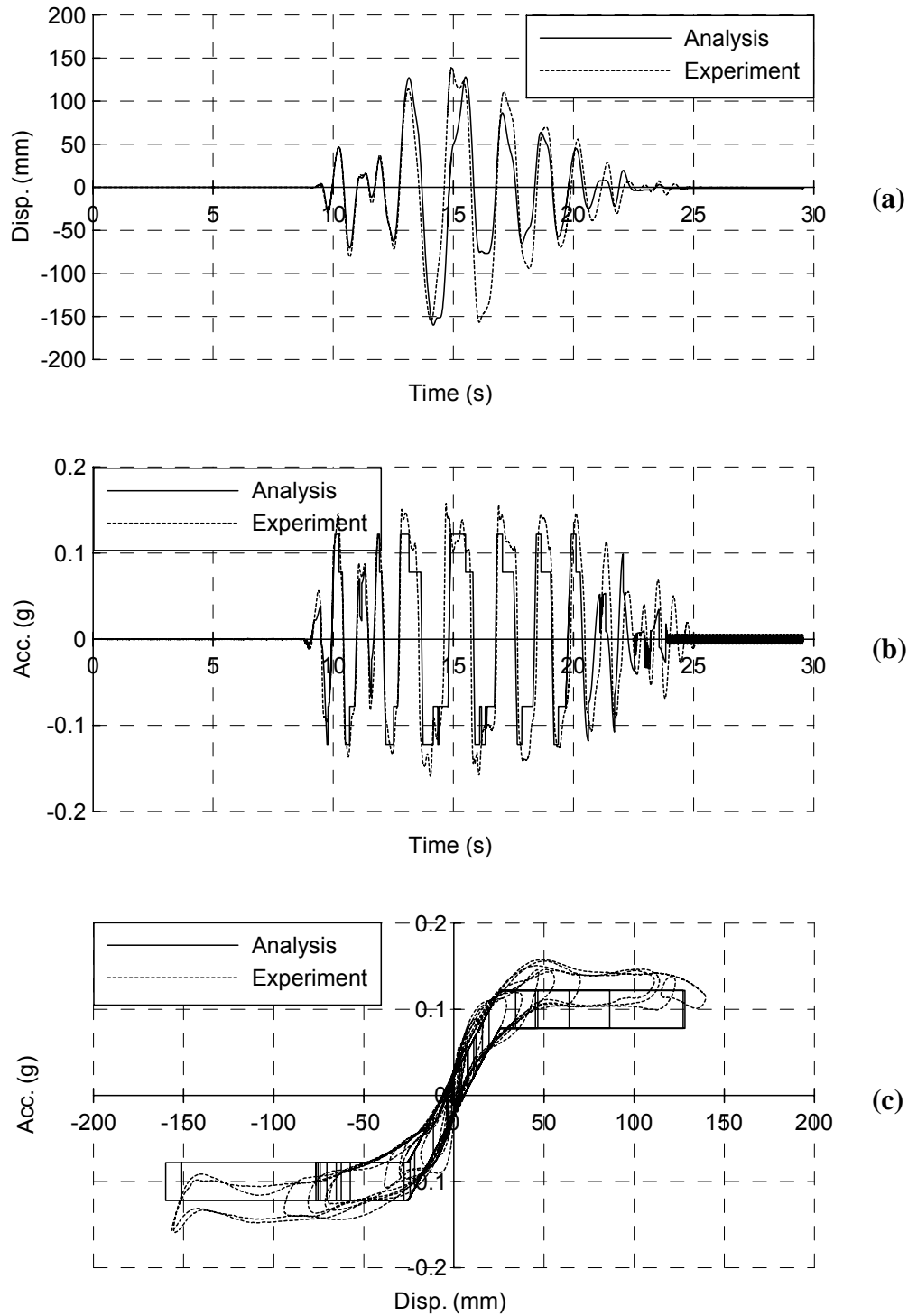


Figure 7.10 Comparison between Results from Analytical Model and Test for Concrete BNC Isolator Using Polyurethane Balls under Load Case 1: (a) Displacement; (b) Acceleration, and; (c) Acceleration-Displacement Relationship

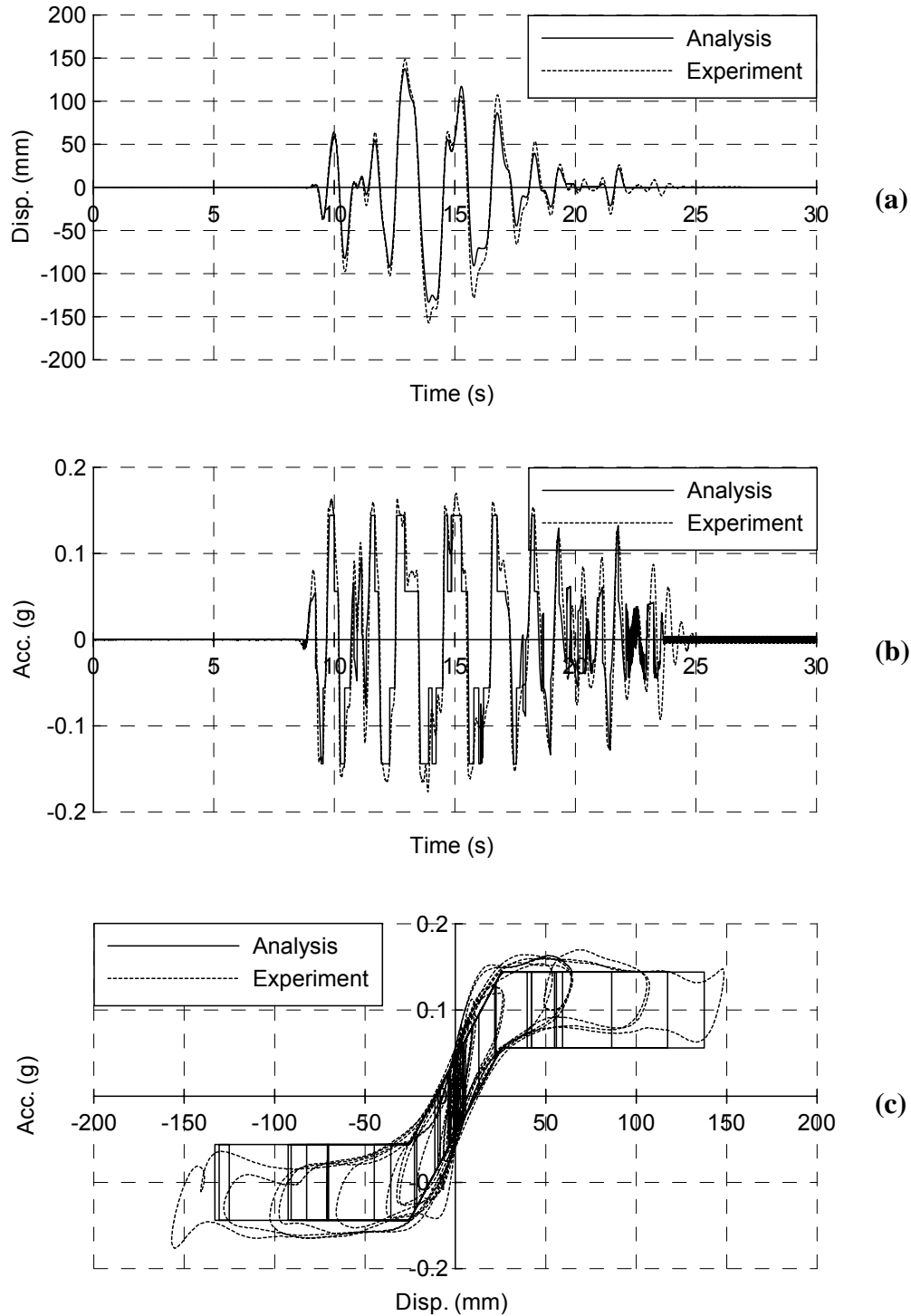


Figure 7.11 Comparison between Results from Analytical Model and Test for Concrete BNC Isolator Using Polyurethane Balls under Load Case 3: (a) Displacement; (b) Acceleration, and; (c) Acceleration-Displacement Relationship

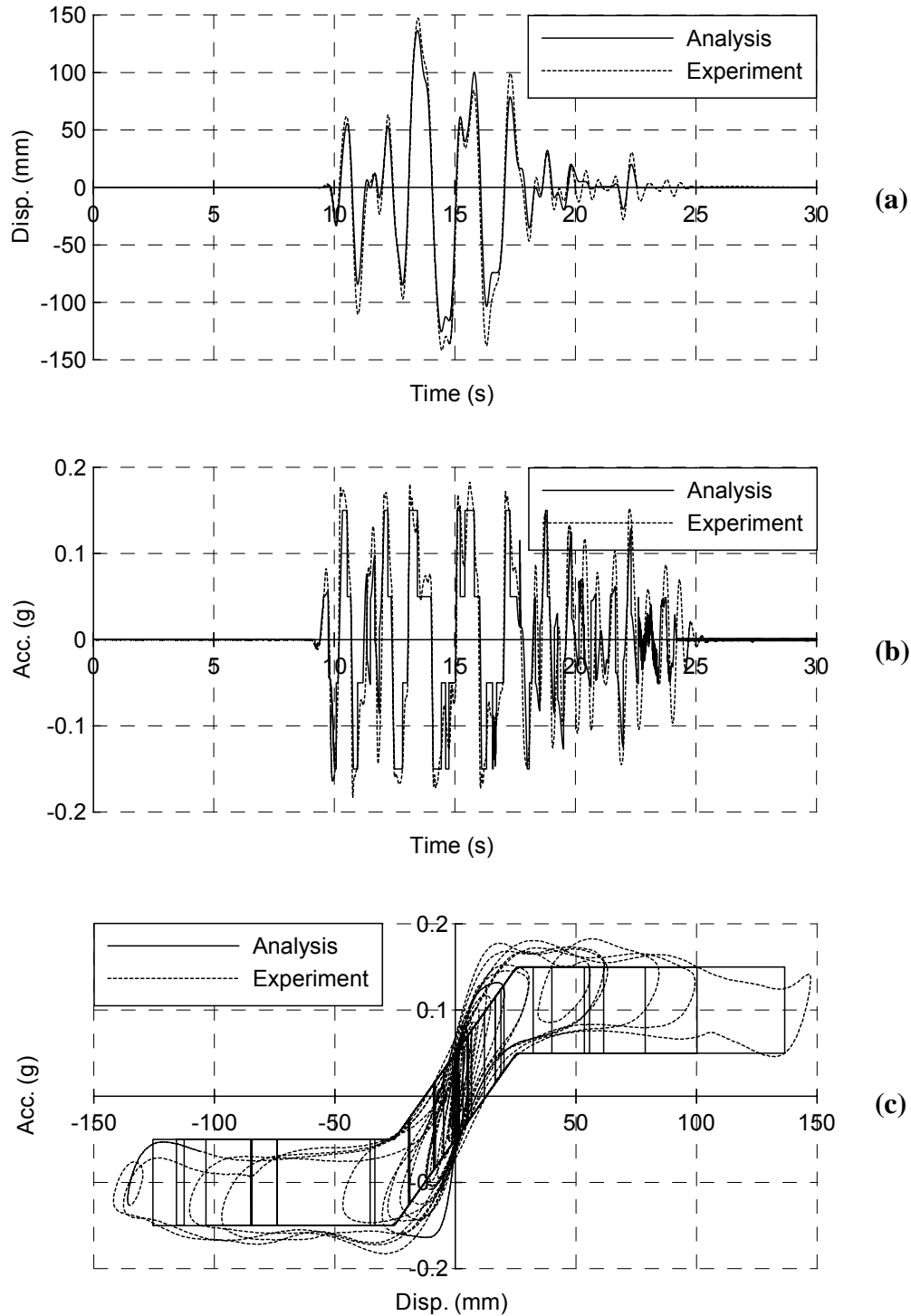


Figure 7.12 Comparison between Results from Analytical Model and Test for Concrete BNC Isolator Using Polyurethane Balls under Load Case 4: (a) Displacement; (b) Acceleration, and; (c) Acceleration-Displacement Relationship

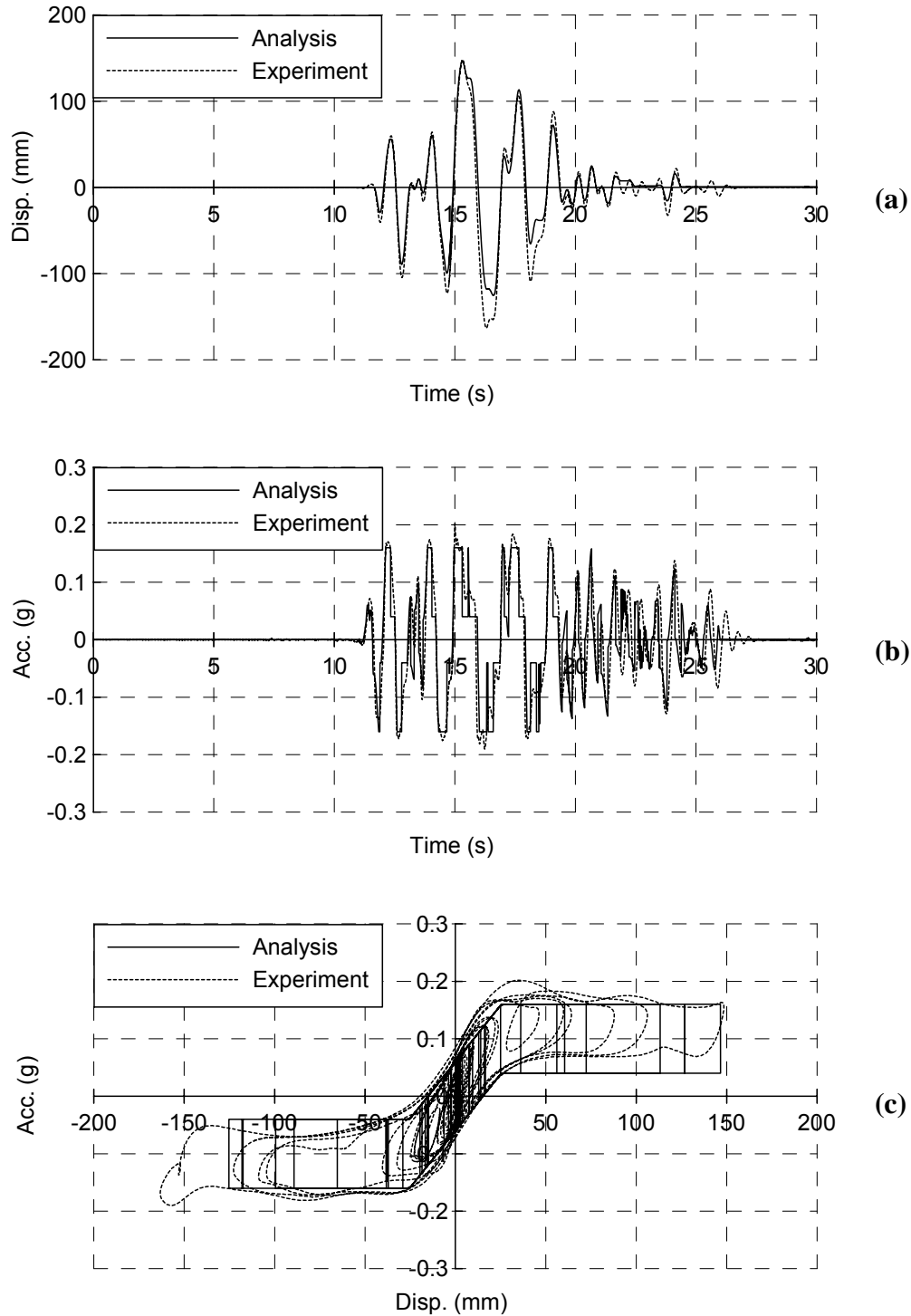


Figure 7.13 Comparison between Results from Analytical Model and Test for Concrete BNC Isolator Using Rubber Balls under Load Case 1: (a) Displacement; (b) Acceleration, and; (c) Acceleration-Displacement Relationship

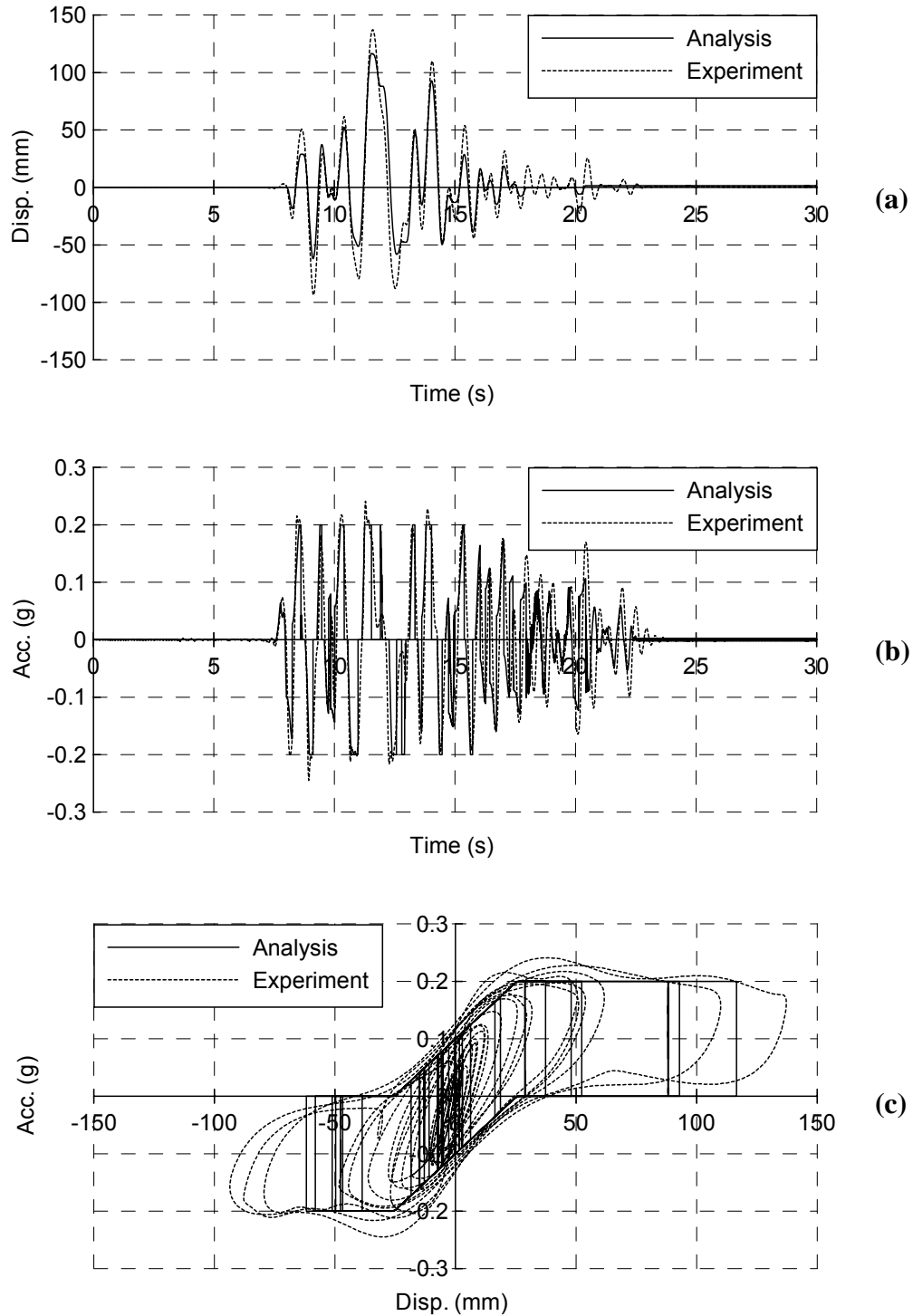


Figure 7.14 Comparison between Results from Analytical Model and Test for Concrete BNC Isolator Using Rubber Balls under Load Case 3: (a) Displacement; (b) Acceleration, and; (c) Acceleration-Displacement Relationship

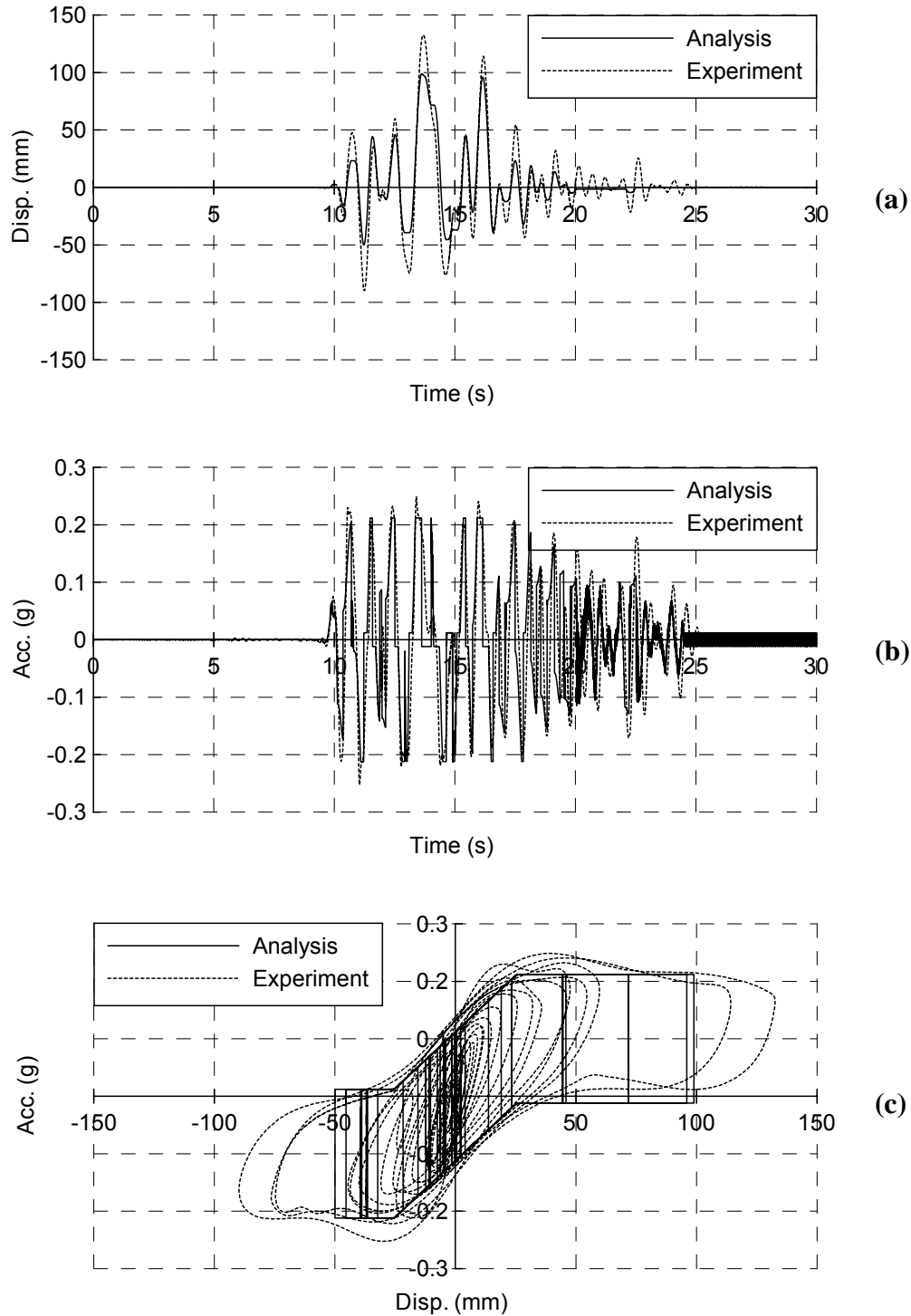


Figure 7.15 Comparison between Results from Analytical Model and Test for Concrete BNC Isolator Using Rubber Balls under Load Case 4: (a) Displacement; (b) Acceleration, and; (c) Acceleration-Displacement Relationship

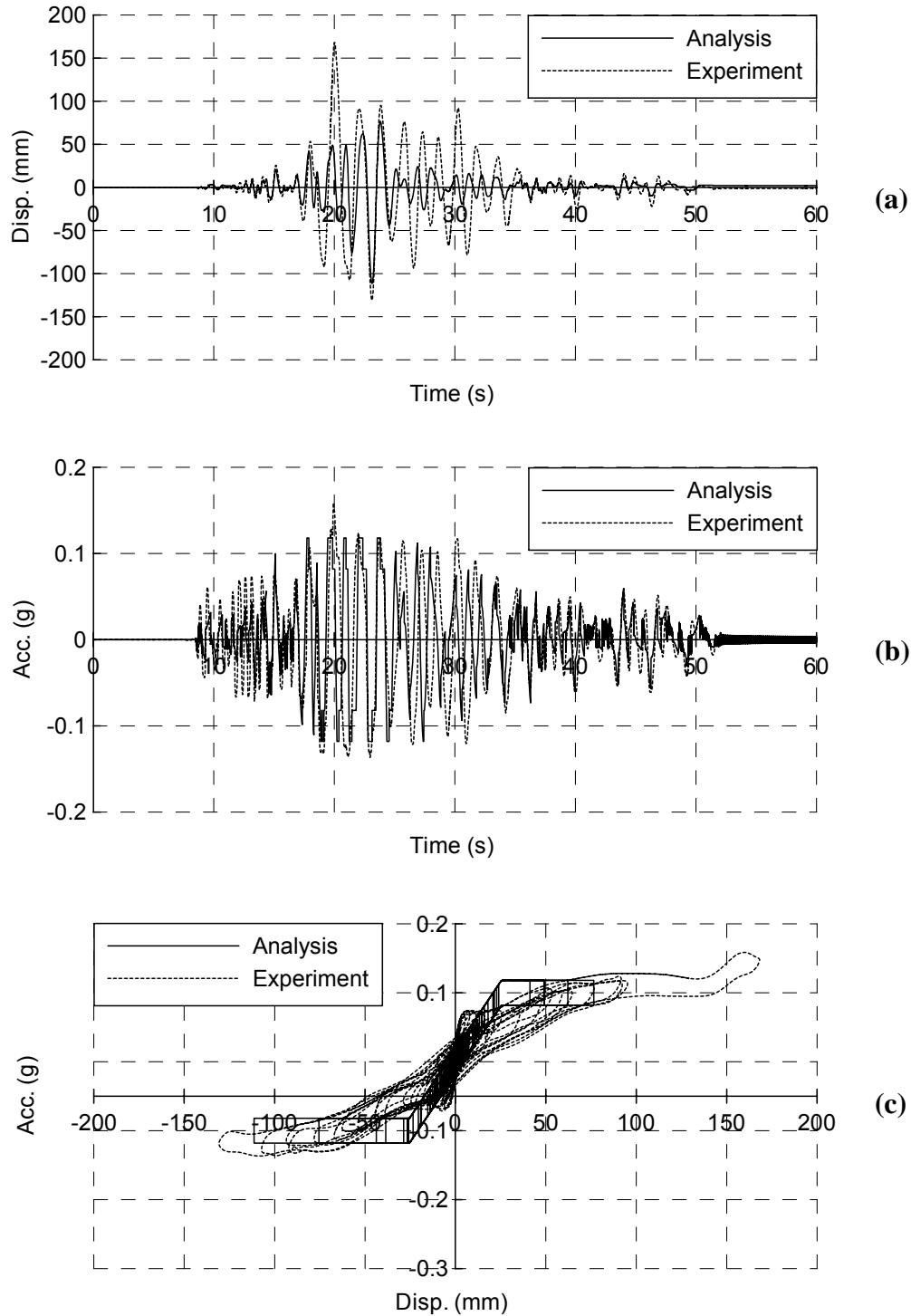


Figure 7.16 Comparison between Results from Analytical Model and Test for Isolated Floor System I without Edge Plates, Using Polyurethane Balls, under Load Case 1 and Input B1: (a) Displacement; (b) Acceleration, and; (c) Acceleration-Displacement Relationship

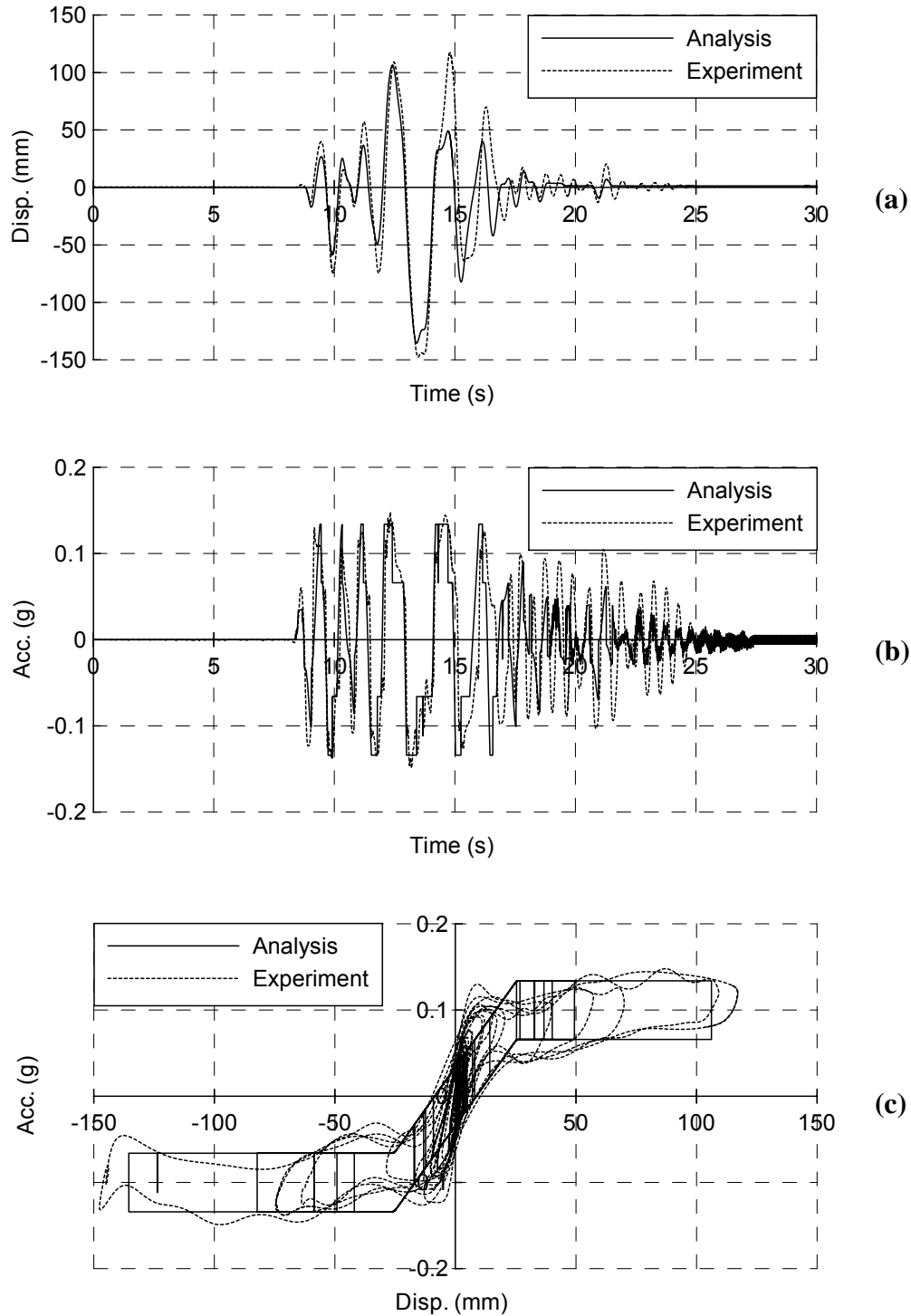


Figure 7.17 Comparison between Results from Analytical Model and Test for Isolated Floor System I without Edge Plates, Using Polyurethane Balls, under Load Case 2 and Input Acc11: (a) Displacement; (b) Acceleration, and; (c) Acceleration-Displacement Relationship

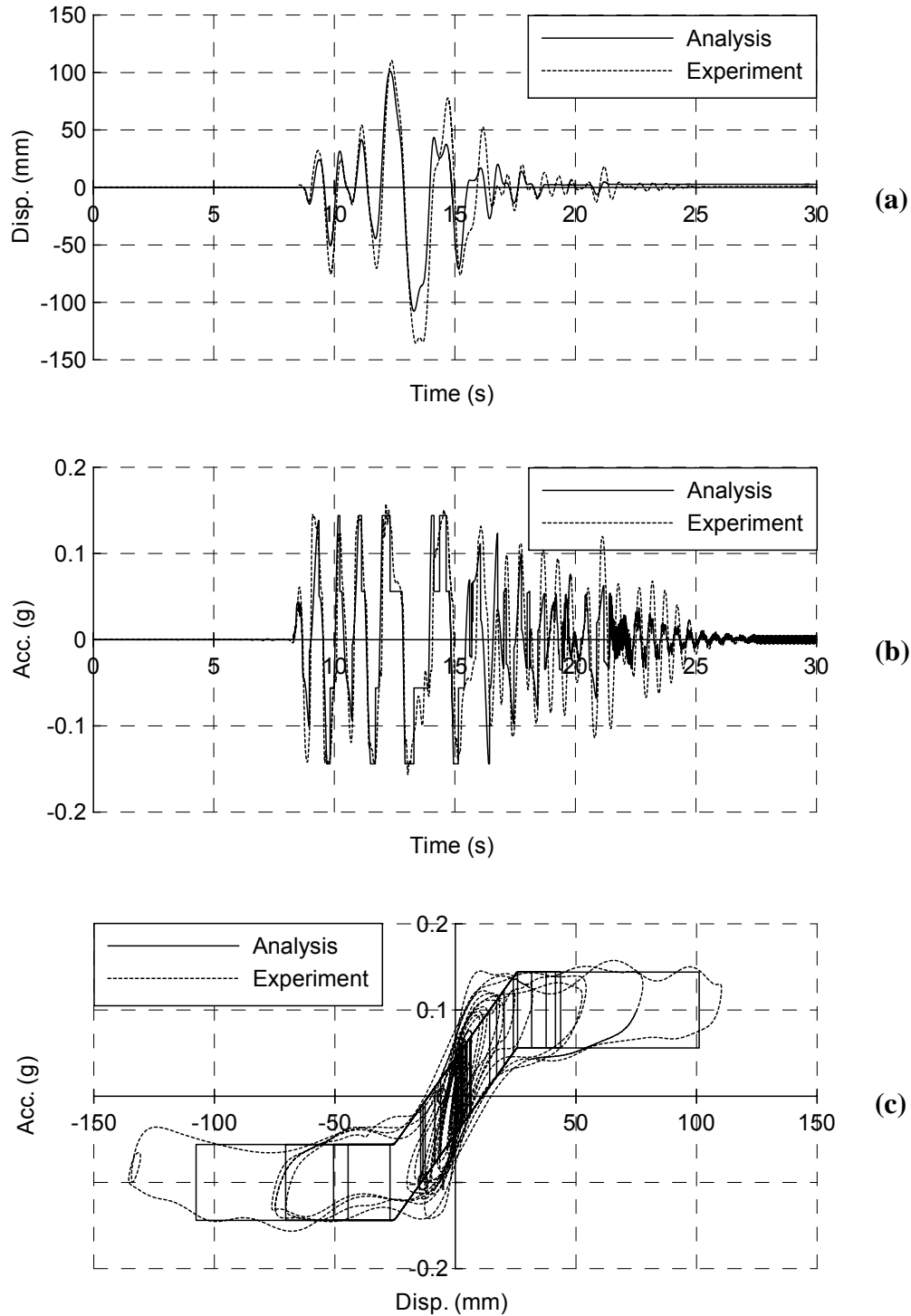


Figure 7.18 Comparison between Results from Analytical Model and Test for Isolated Floor System I without Edge Plates, Using Polyurethane Balls, under Load Case 3 and Input Acc11: (a) Displacement; (b) Acceleration, and; (c) Acceleration-Displacement Relationship

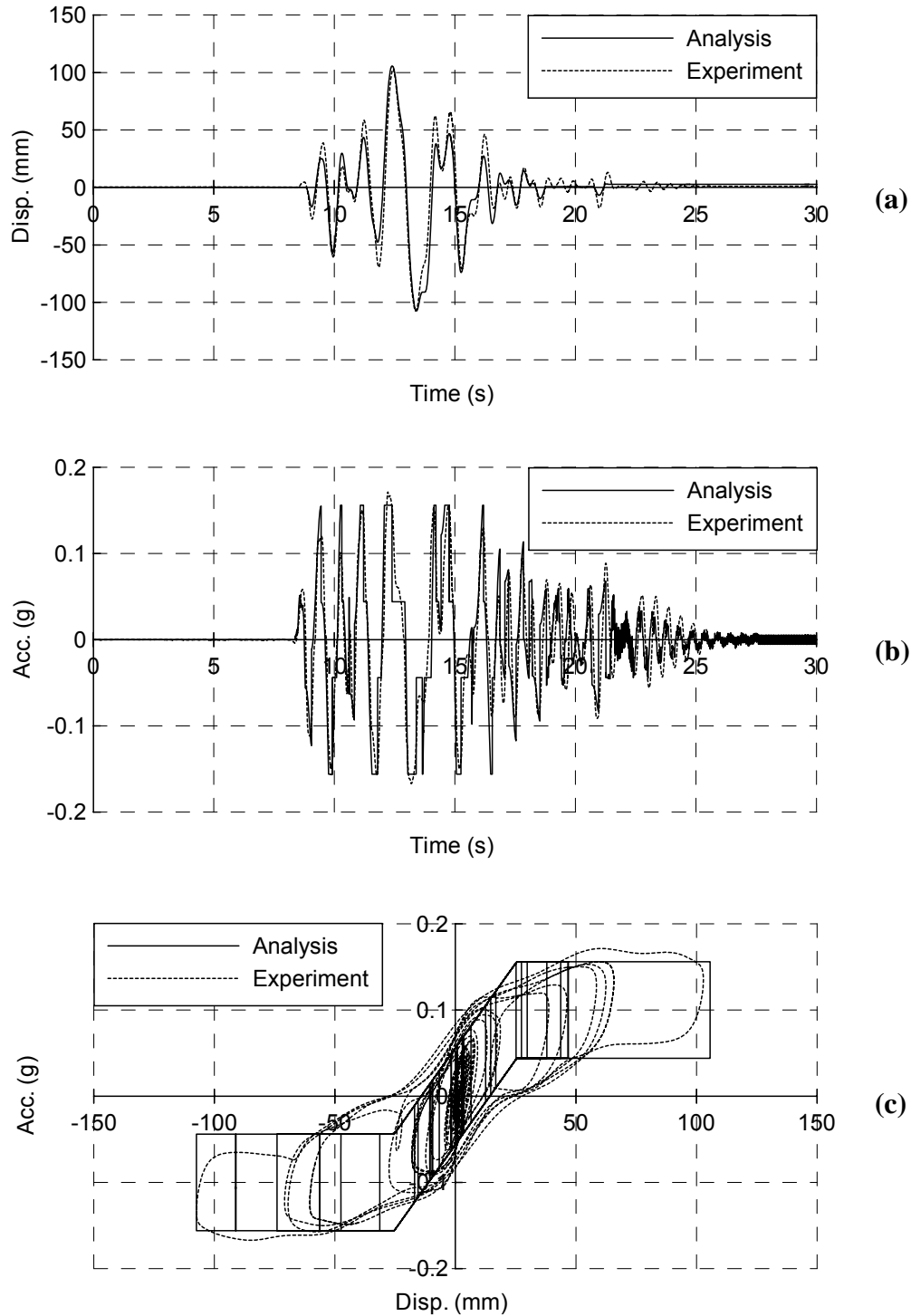


Figure 7.19 Comparison between Results from Analytical Model and Test for Isolated Floor System I without Edge Plates, Using Rubber Balls, under Load Case 1 and Input Acc11: (a) Displacement; (b) Acceleration, and; (c) Acceleration-Displacement Relationship

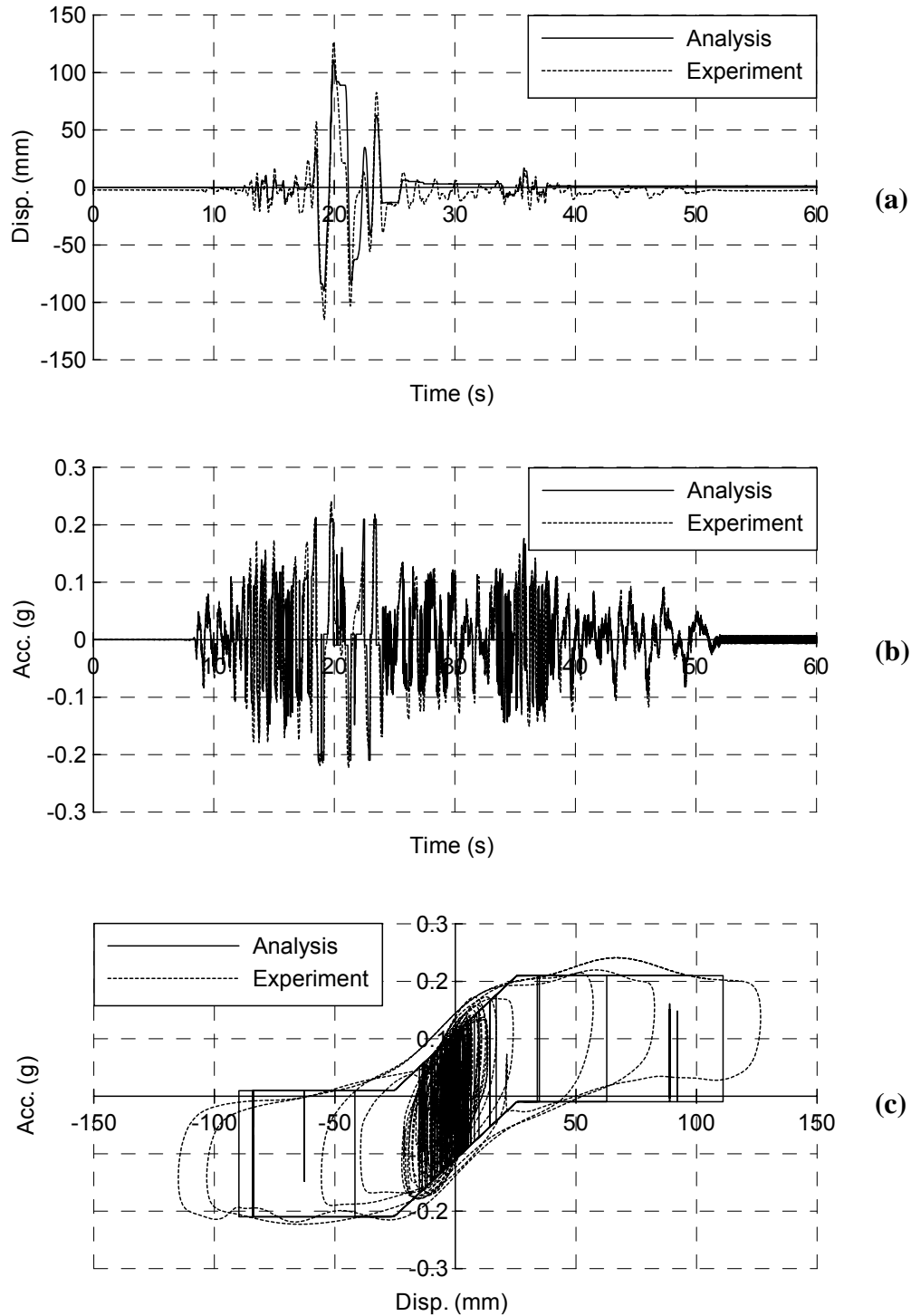


Figure 7.20 Comparison between Results from Analytical Model and Test for Isolated Floor System I without Edge Plates, Using Rubber Balls, under Load Case 2 and Input B1: (a) Displacement; (b) Acceleration, and; (c) Acceleration-Displacement Relationship

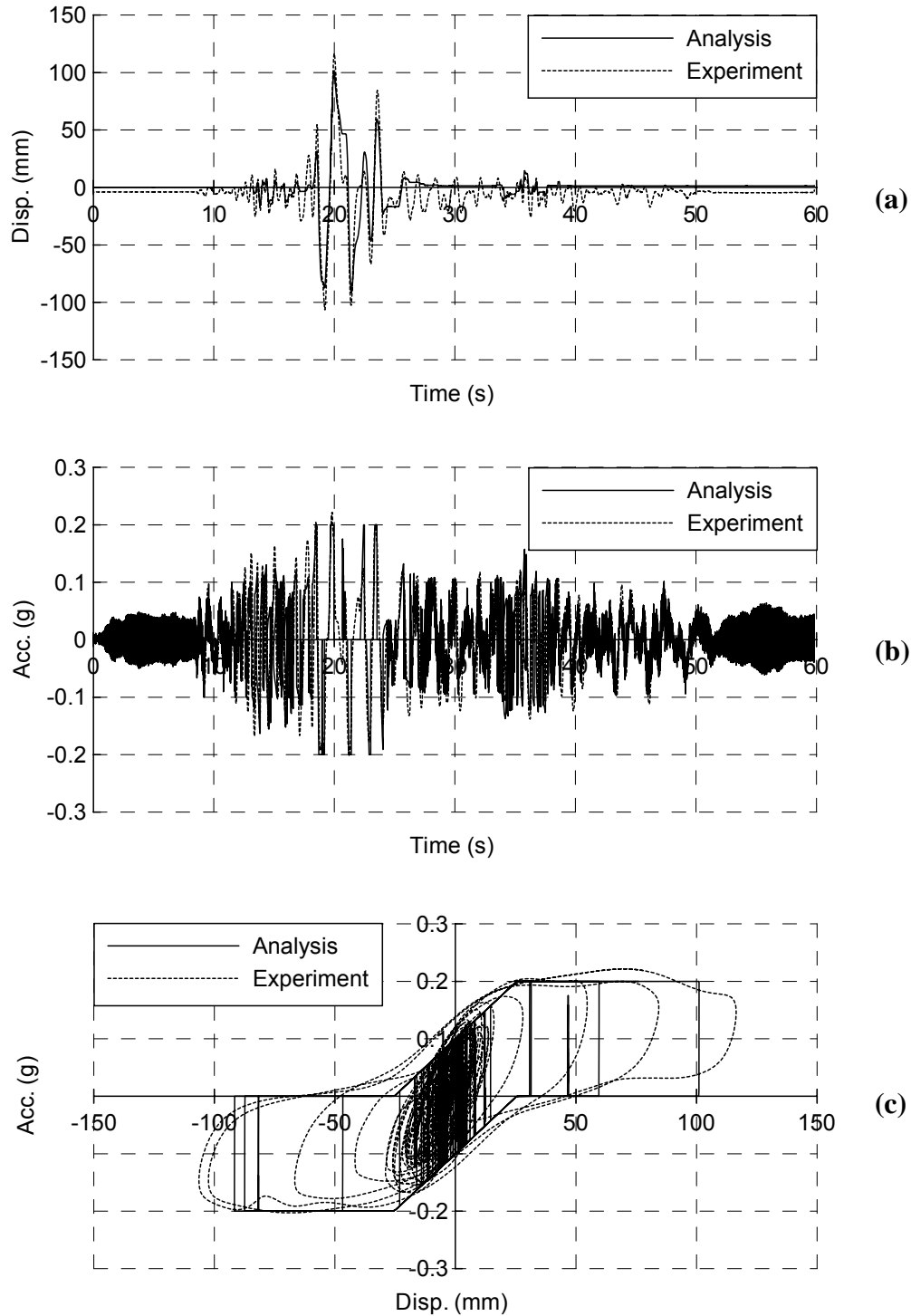


Figure 7.21 Comparison between Results from Analytical Model and Test for Isolated Floor System I without Edge Plates, Using Rubber Balls, under Load Case 3 and Input B1: (a) Displacement; (b) Acceleration, and; (c) Acceleration-Displacement Relationship

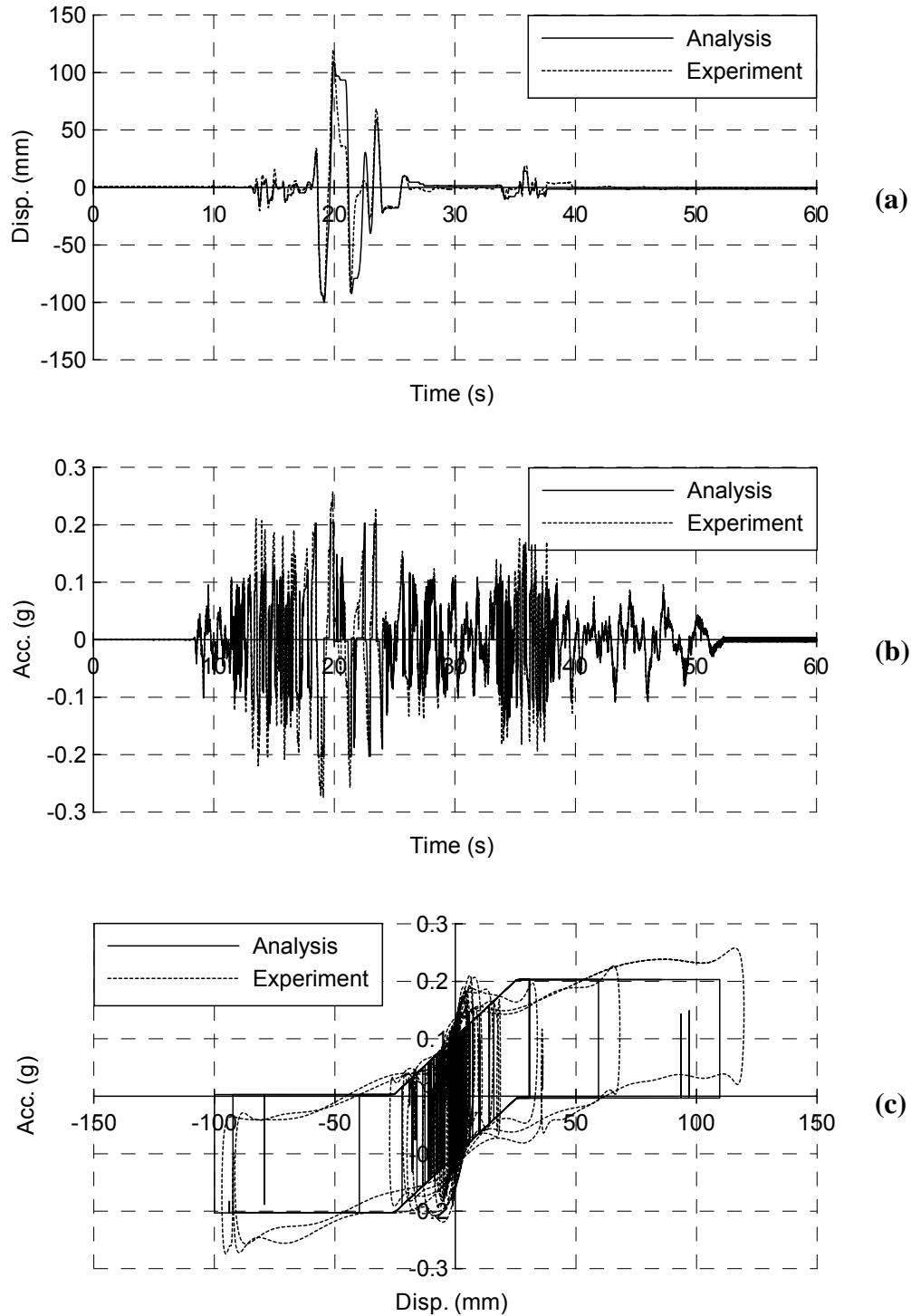


Figure 7.22 Comparison between Results from Analytical Model and Test for Isolated Floor System I with Edge Plates, Using Polyurethane Balls, under Load Case 1 and Input B1: (a) Displacement; (b) Acceleration, and; (c) Acceleration-Displacement Relationship

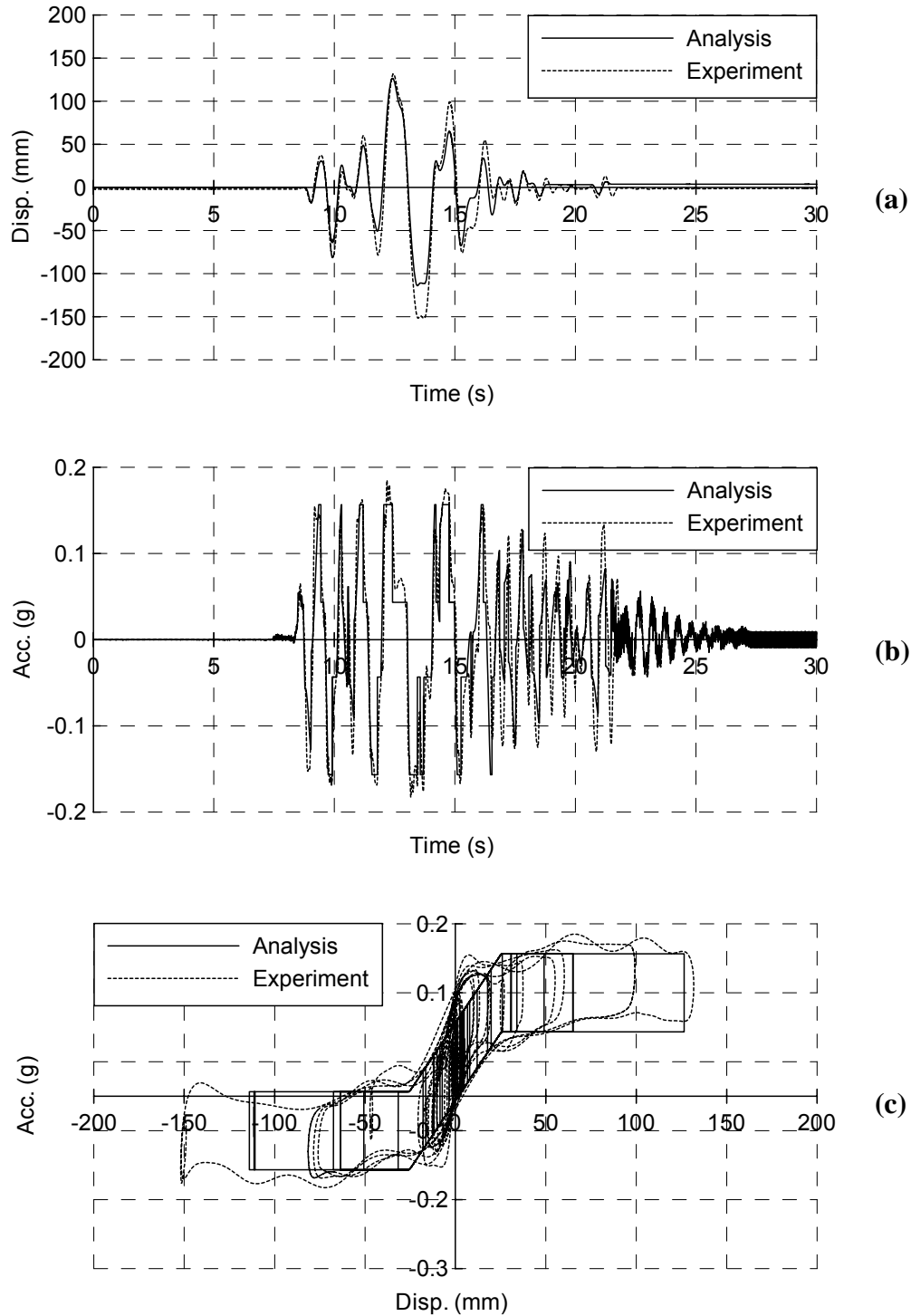


Figure 7.23 Comparison between Results from Analytical Model and Test for Isolated Floor System I with Edge Plates, Using Polyurethane Balls, under Load Case 2 and Input Acc11: (a) Displacement; (b) Acceleration, and; (c) Acceleration-Displacement Relationship

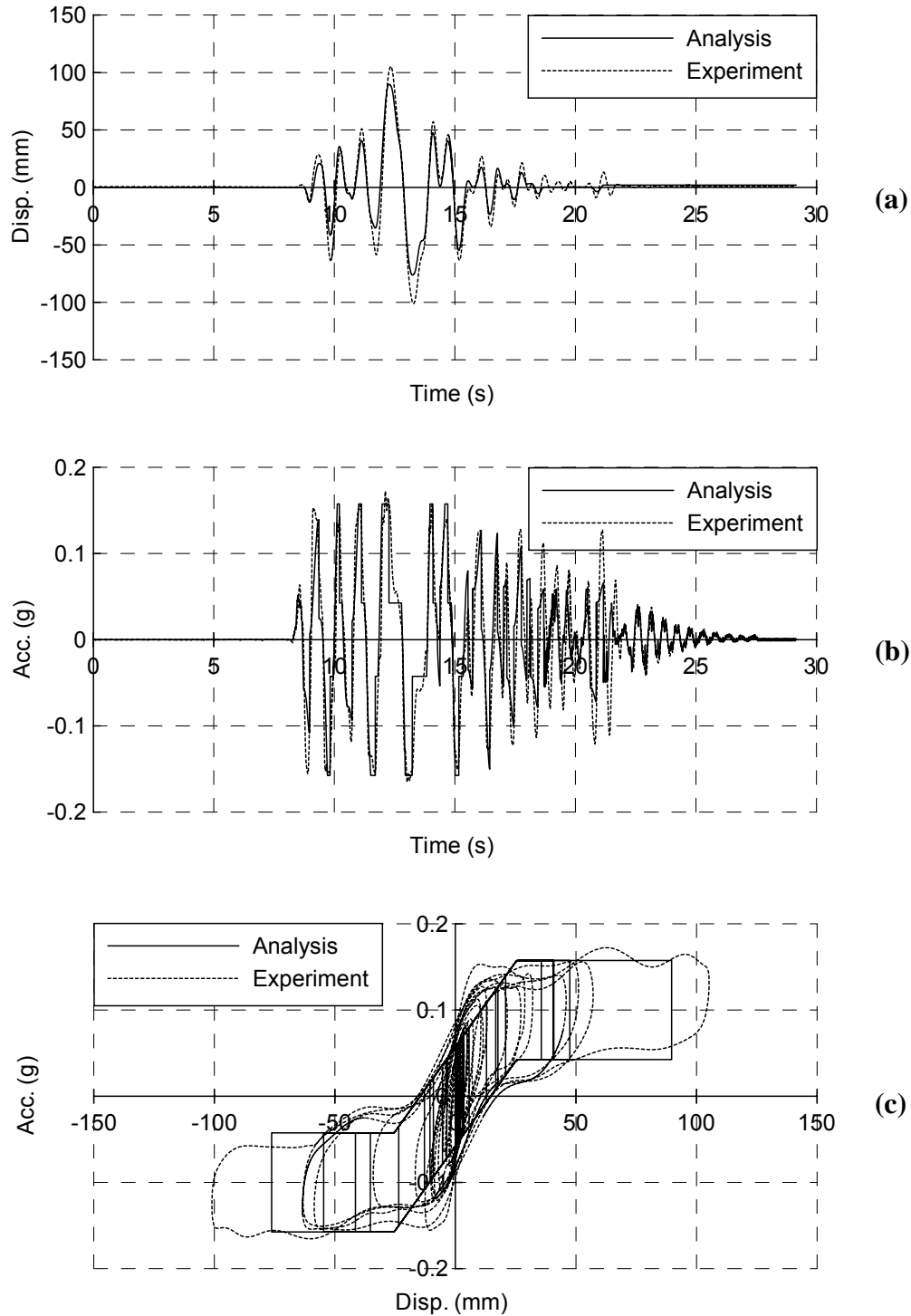


Figure 7.24 Comparison between Results from Analytical Model and Test for Isolated Floor System I with Edge Plates, Using Polyurethane Balls, under Load Case 3 and Input Acc11:
(a) Displacement; (b) Acceleration, and; (c) Acceleration-Displacement Relationship

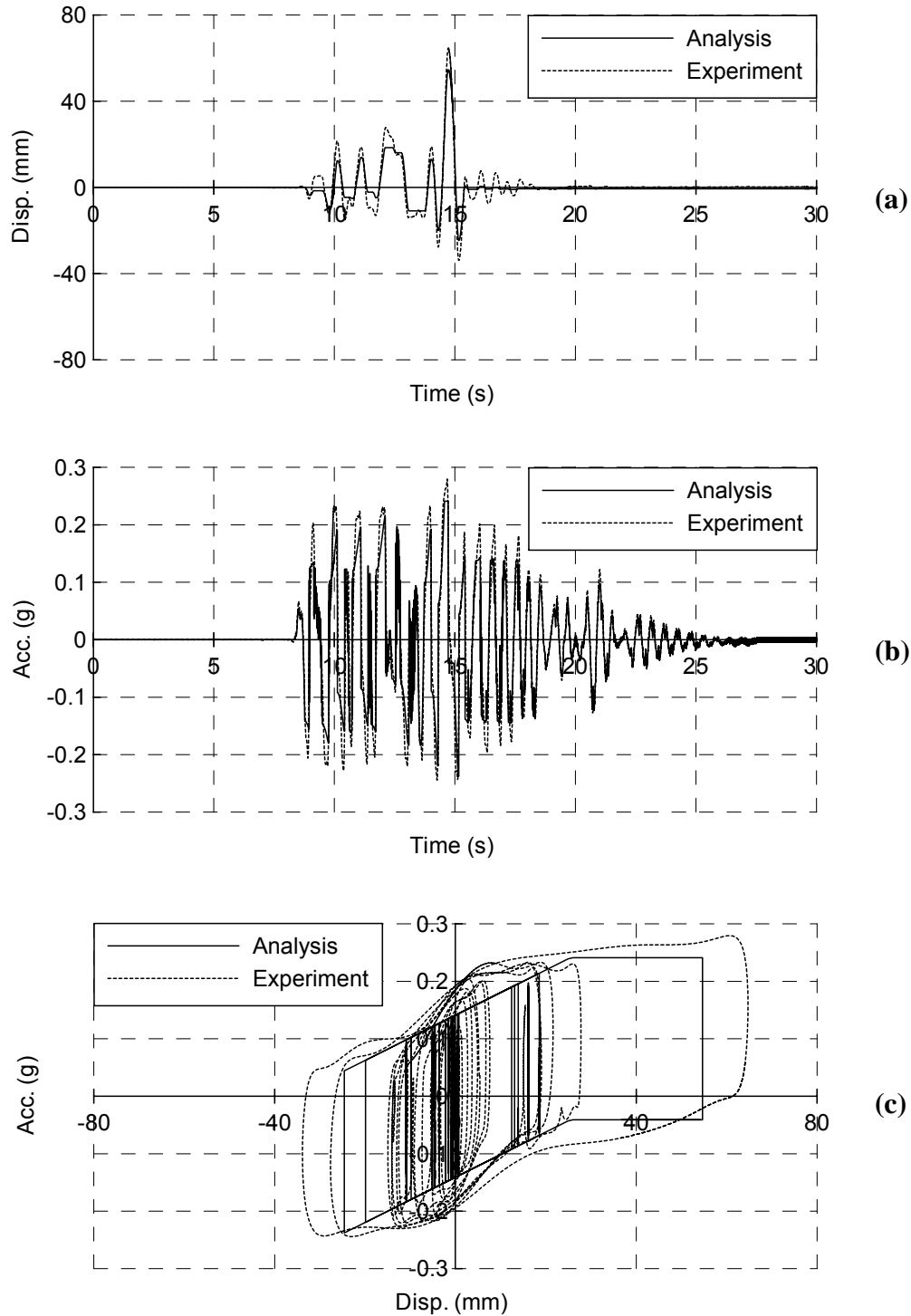


Figure 7.25 Comparison between Results from Analytical Model and Test for Isolated Floor System I with Edge Plates, Using Rubber Balls, under Load Case 1 and Input Acc11: (a) Displacement; (b) Acceleration, and; (c) Acceleration-Displacement Relationship

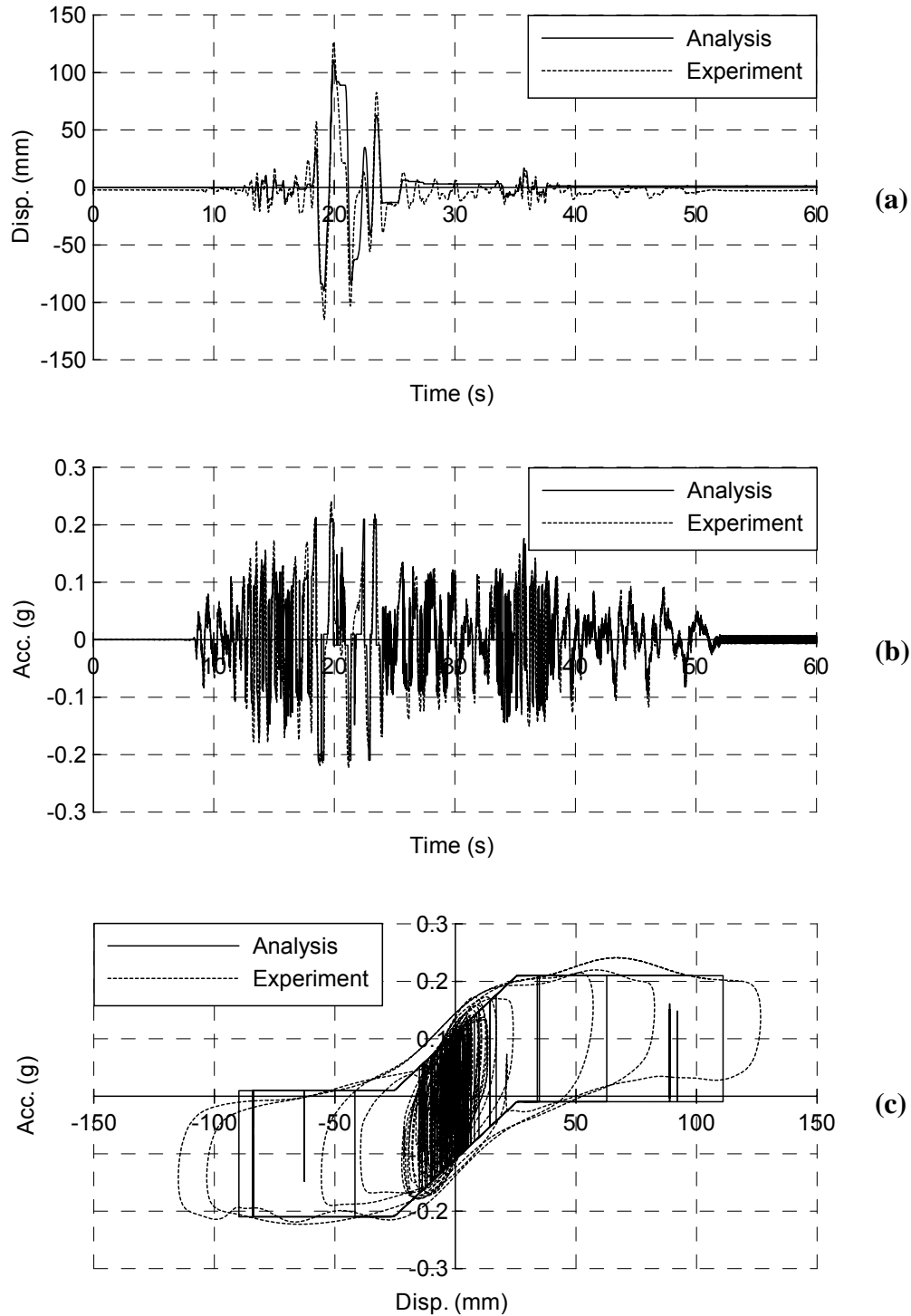


Figure 7.26 Comparison between Results from Analytical Model and Test for Isolated Floor System I with Edge Plates, Using Rubber Balls, under Load Case 2 and Input B1: (a) Displacement; (b) Acceleration, and; (c) Acceleration-Displacement Relationship

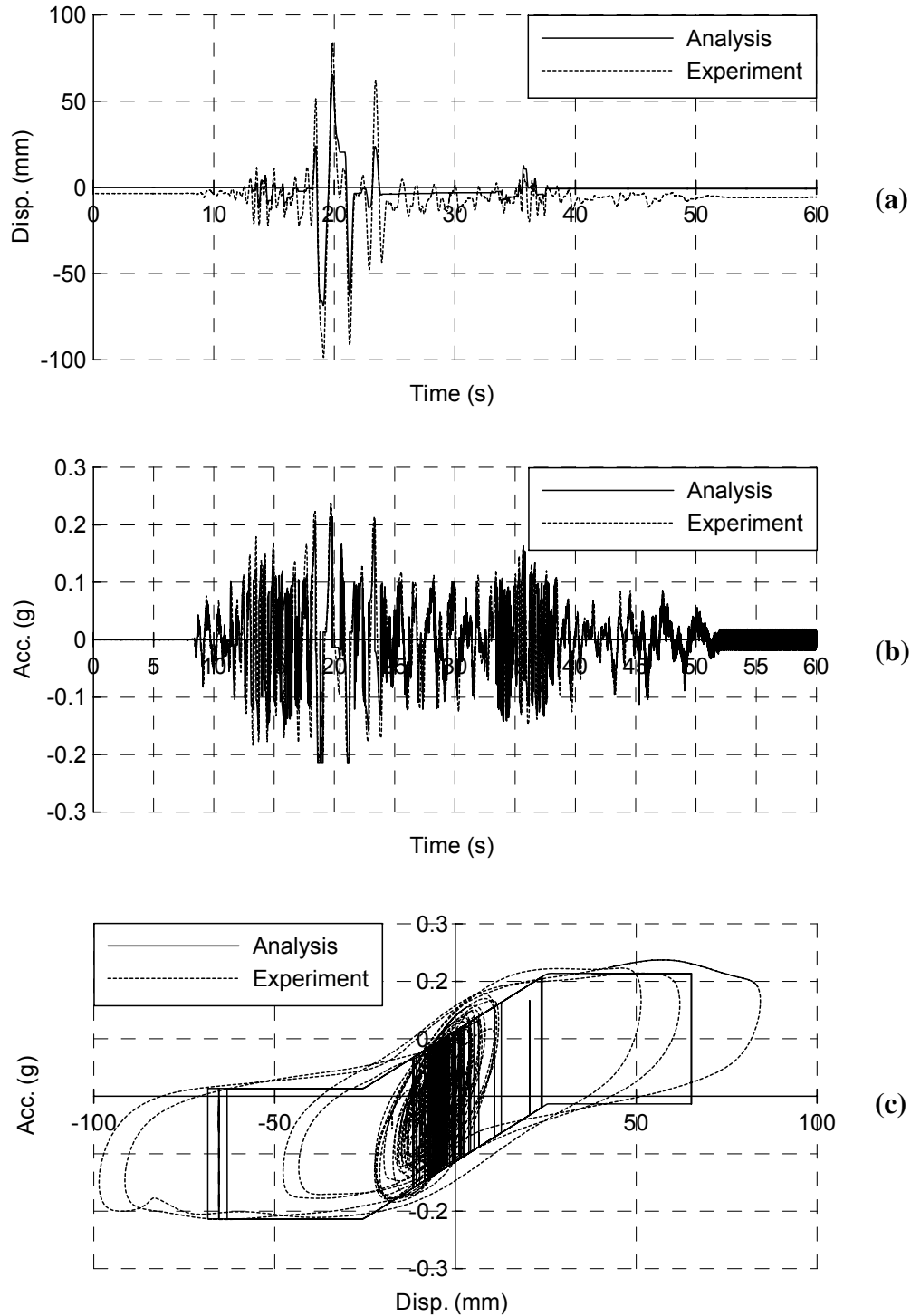


Figure 7.27 Comparison between Results from Analytical Model and Test for Isolated Floor System I with Edge Plates, Using Rubber Balls, under Load Case 3 and Input B1: (a) Displacement; (b) Acceleration, and; (c) Acceleration-Displacement Relationship

7.2.4 Sensitivity Study

To investigate whether the behavior of the analytical model for Isolated Floor System I is sensitive to the equivalent friction coefficient, a limited sensitivity study was conducted by changing the experimentally estimated equivalent friction coefficient by $\pm 10\%$. This was done using the isolated floor system without edge plates under Load Case 2 described in Chapter 6. Isolated floor systems using polyurethane and rubber balls were both considered. The results are shown in Figs. 7.28 and 7.29, respectively. Based on the model principle as shown in Figure 7.9, the friction effect, $W\mu_e$, will proportionally change along with the change in the equivalent friction coefficient (i.e., μ_e). Note from part (c) of each figure that with increasing of the equivalent friction coefficient, the loops corresponding to hysteretic behavior expands as expected and the peak displacement decreases. It is found that the acceleration due to the friction effect increases by 10% (as expected) along with the 10% increase in μ_e . It is also found that the peak displacement response decreases by an average of approximately 12% (maximum of 17%) for that same increase of 10% in the equivalent friction coefficient. This shows that response predicted using the analytical model is quite sensitive to the equivalent friction coefficient used in the model. It is therefore important not to over-estimate its value. In that perspective, it is appropriate that if the linear relationship is chosen to express the estimated equivalent friction coefficient as a function of average ball load, the predicted floor response will be conservative (as mentioned in Section 7.2.1).

Note that although this sensitivity study is conducted on the equivalent friction coefficient from the rolling balls, the observations described above are also valid for other friction effects in Isolated Floor System I (e.g., friction effect from the edge plates).

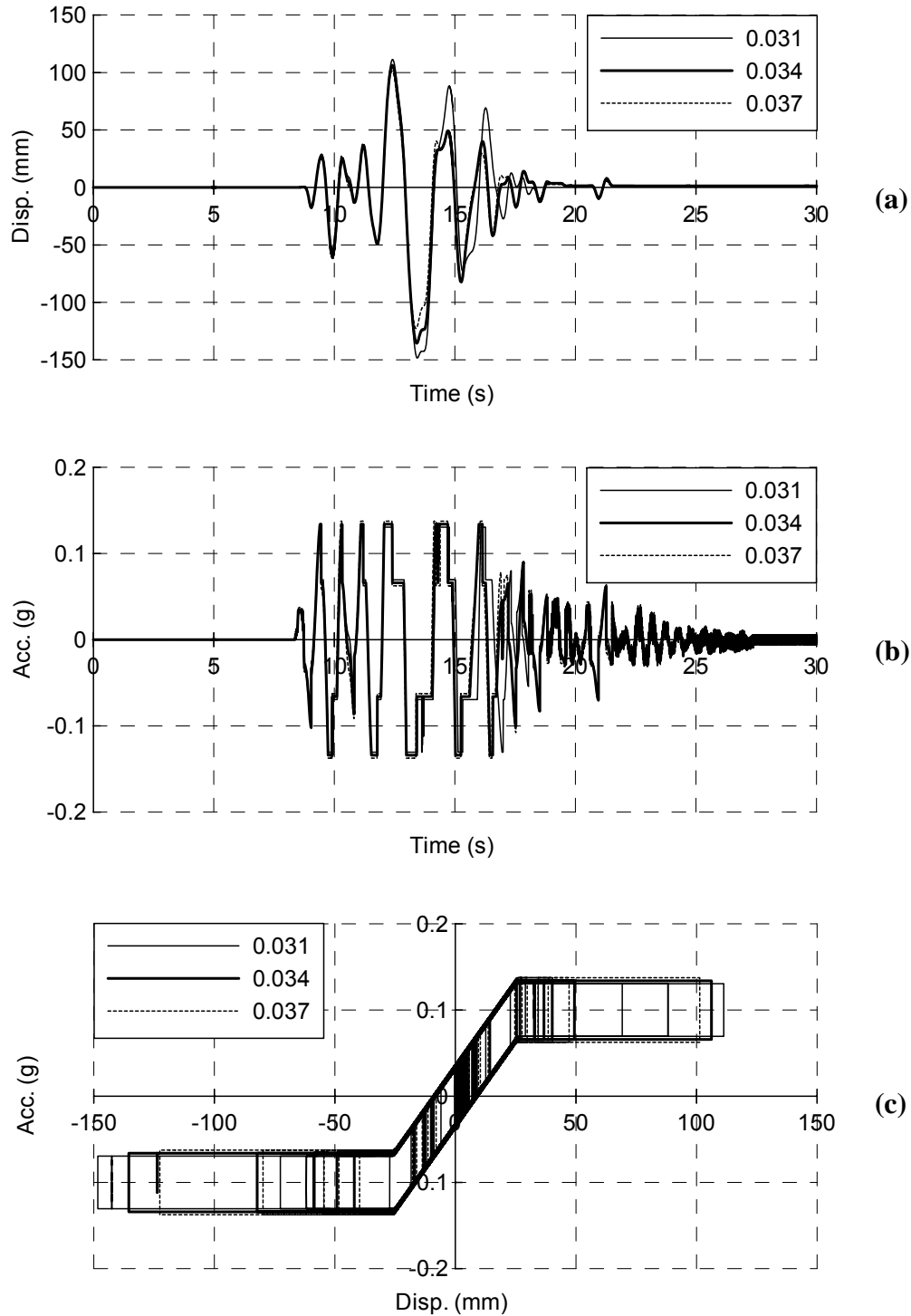


Figure 7.28 Results of Sensitivity Study for Isolated Floor System I without Edge Plates, Using Polyurethane Balls, under Load Case 2 and Input Acc11: (a) Displacement; (b) Acceleration, and; (c) Acceleration-Displacement Relationship

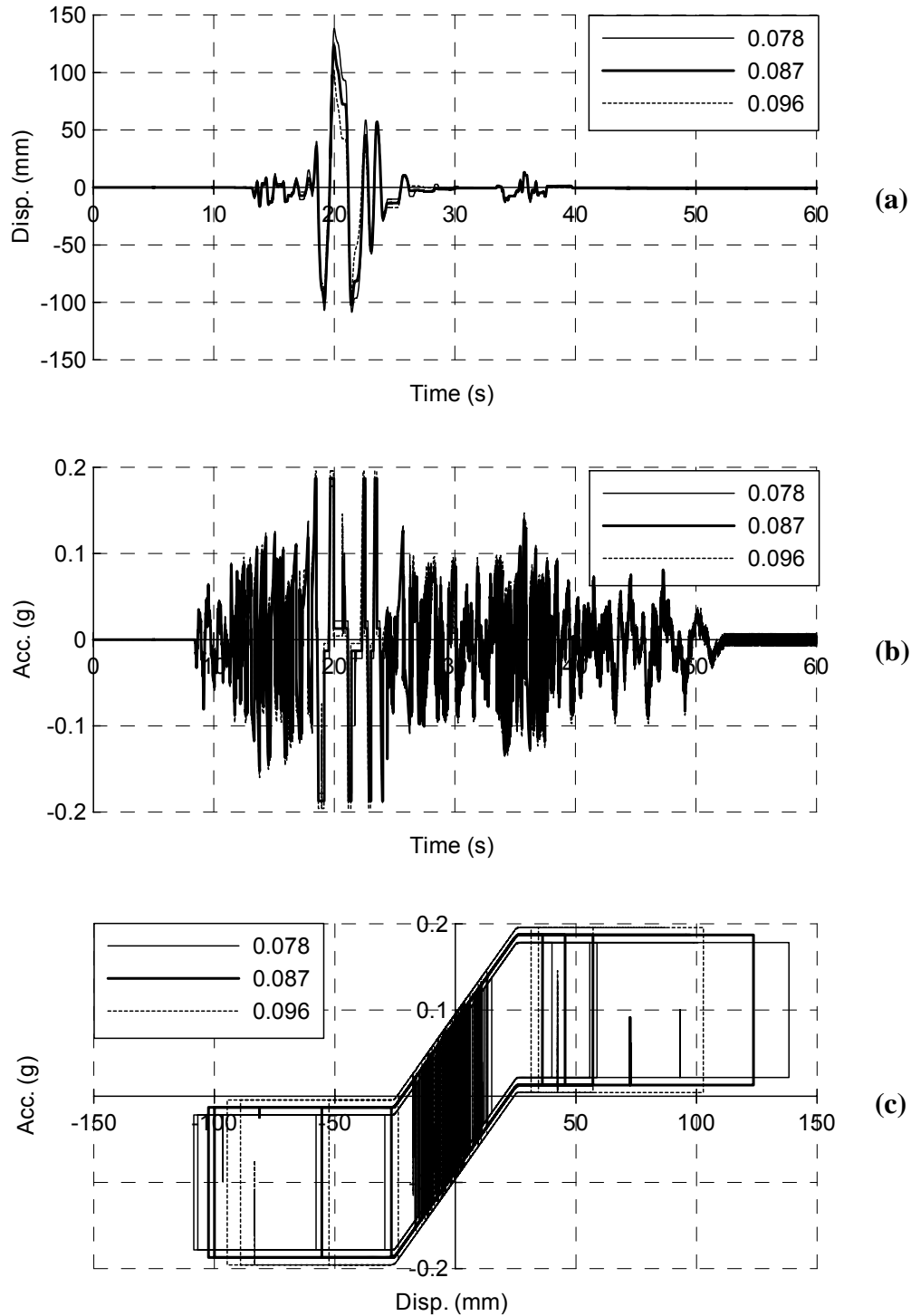


Figure 7.29 Results of Sensitivity Study for Isolated Floor System I without Edge Plates, Using Rubber Balls, under Load Case 2 and Input B1: (a) Displacement; (b) Acceleration, and; (c) Acceleration-Displacement Relationship

7.3 Analytical Model of Isolated Floor System II Behavior

7.3.1 Analytical Model

A physical model developed in Chapter 4 has been shown to accurately represent the behavior of the multi-directional spring units used in Isolated Floor System II. However, as mentioned in Section 7.1, such a physical model is not currently implemented in commercially available structural analysis programs. Therefore, a first step toward conducting analysis for Isolated Floor System II was to add such a hysteretic model to the element library of a non-linear inelastic analysis program. The program IDARC2D (Valles et al. 1996 and Reinhorn et al. 2009) was chosen for this purpose because it already contained a hysteretic damper brace element that could be modified to be appropriate to simulate the behavior of the physical model. Such modification to that hysteretic element was done by Reinhorn and Roh.

This modified hysteretic element model incorporated in IDARC2D Version 7.0 (Reinhorn et al., <http://civil.eng.buffalo.edu/idarc2d50/>) is illustrated in Fig. 7.30 and needs five input parameters: K_0 , F_y , α_1 , n , and η . As shown in Fig. 7.30, the two bilinear branches (upper loading and lower unloading branches) are the behavior target of this model, and the two smooth – curve branches are the behavior realization of this model. In this model, the force transition between these two bilinear branches is a fully vertical drop when velocity direction changes. The input parameter K_0 is the stiffness of the first part of the bilinear loading branch and is called initial stiffness; F_y corresponds to the force at the stiffness transition point of the bilinear loading branch and is defined as the yielding force; α_1 is the ratio of the second stiffness to the first stiffness (initial stiffness) and is called post-yielding stiffness ratio; n is the power of stiffness transition; and η is a proportionality factor that controls the steepness of the force dropping relating the unloading branch to the loading one, and is called force dropping factor here. Note

that the force on the unloading branch is $(1-2\eta)$ times the corresponding force value on the loading branch at any displacement value. In addition, the symbol “F1” in Figure 7.30 is an arbitrary force value on the target loading branch.

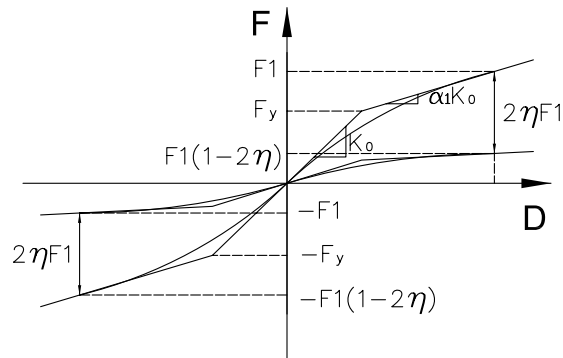


Figure 7.30 Sketch of Modified Hysteretic Damper Brace Element Model

To build the model, first, the loading branch of the physical model in the positive direction was simulated by using two straight lines, as shown in Figs. 7.31 and 7.32. For the multi-directional spring units having a nominal stiffness 2627 N/m (15 lb/in), the equations of the straight lines can be expressed, in units of N and mm, as:

$$y = 15.083x \quad (\text{when } x \leq 90.7 \text{ mm}) \quad (7.3)$$

$$y = 4.7139x + 940.34 \quad (\text{when } x > 90.7 \text{ mm}) \quad (7.4)$$

For the 1313 N/m (7.5 lb/in) nominal stiffness spring units, the equations of the straight lines can be expressed, in units of N and mm, as:

$$y = 4.2933x \quad (\text{when } x \leq 108.1 \text{ mm}) \quad (7.5)$$

$$y = 3.0217x + 137.41 \quad (\text{when } x > 108.1 \text{ mm}) \quad (7.6)$$

Therefore, for the IDARC2D model, the initial stiffness, K_0 , was selected as equal to the initial stiffness in the straight-line model described above (i.e., 15.083 kN/m and 4.2933 kN/m for the multi-directional spring units having nominal stiffnesses of 2627 N/m (15 lb/in) and 1313 N/m

(7.5 lb/in), respectively). The yielding force, F_y , was selected as the value at the stiffness transition points in the straight-line simulation model (i.e., 1368 N (307.56 lb) and 464 N (104.34 lb) for multi-directional spring units having nominal stiffnesses of 2627 N/m (15 lb/in) and 1313 N/m (7.5 lb/in), respectively). The post-yielding stiffness ratio, α_1 , was taken as the values in the straight-line simulation model (i.e., 0.3125 and 0.7038 for multi-directional spring units having nominal stiffnesses of 2627 N/m (15 lb/in) and 1313 N/m (7.5 lb/in), respectively). For the power of stiffness transition, n , a value of 20 was used. Finally, to determine the force-dropping factor, η , the values of η calculated based on the physical model are shown in Fig. 7.33. It can be noted that at relative large displacements (larger than 90 mm), the values of η is almost a constant, which corresponds to the plateau in Fig. 7.33. For the analytical model implemented in IDARC2D, the η value used is the average of the two η values at: (i) the point corresponding to the stiffness transition point in the straight-line simulation model as shown in Figs. 7.31 and 7.32 and; (ii) the point of maximum displacement for the spring unit in the specific floor implementation (i.e., 254mm (10 in)). For example, for multi-directional spring units having a nominal stiffness of 2627 N/m (15 lb/in), the values of η are 0.310 at displacement of 90.7 mm (the stiffness transition point in the straight-line simulation model) and 0.328 at displacement of 254 mm. Then, for a 2627 N/m (15 lb/in) spring unit, the η value was taken as the average of the two values, namely 0.319. In the same way, the value of η was selected as 0.351 for multi-directional spring unit having a nominal stiffness of 1313 N/m (7.5 lb/in).

For the analytical model for Isolated Floor System II without edge plates, as mentioned in Chapter 5, there is an extra friction effect from the casters rolling on the concrete slab. In parallel with the element used to model the multi-directional spring units' behavior within the complete isolated floor systems as described above, the model for such systems should also consider this extra friction effect by using a friction damper brace element with almost rigid initial stiffness in IDARC2D. For cases of Isolated Floor System with edge plates, the model should consists a

modified hysteretic damper brace element modeling the multi-directional spring units' behavior within the corresponding systems in parallel with a friction damper brace element with almost rigid initial stiffness which considers both the friction effect from the casters and the friction effect from edge plates. Note that the friction coefficient for the casters rolling on the concrete slab may keep a constant value (i.e., 0.035 as mentioned in Chapter 5). The friction effect from the edge plates (with a value of 298 N (67 lb) as mentioned in Chapter 5), however, can not be a constant value, as it depends on the edge plates' weight and different floor isolation system designs can adopt different sizes and weights for the edge plates.

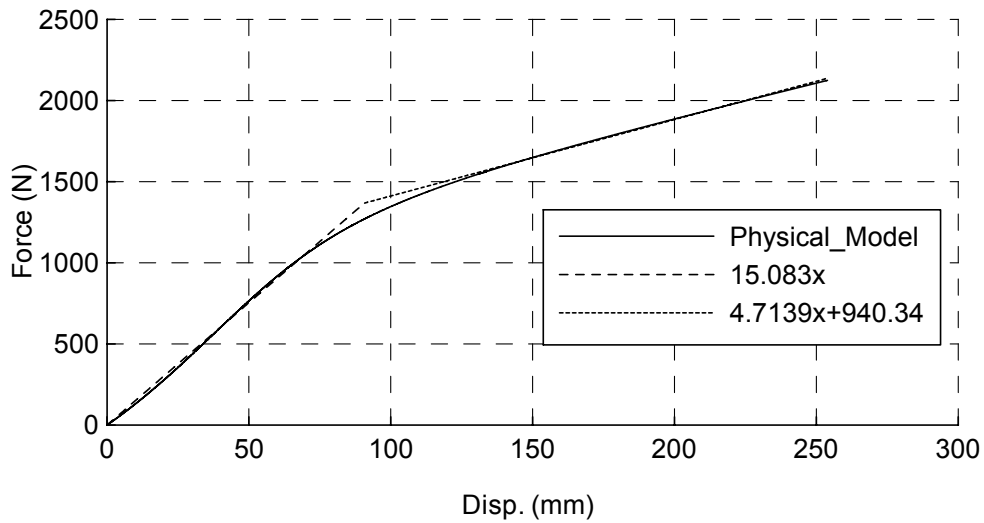


Figure 7.31 Straight Lines Used to Simulate Physical Model for 2627 N/m Multi-directional Spring Units

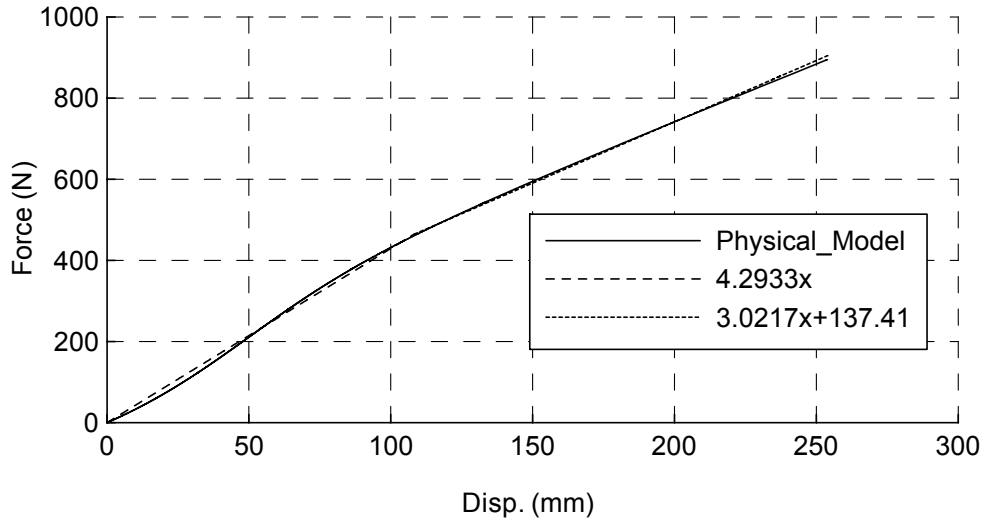


Figure 7.32 Straight Lines Used to Simulate Physical Model for 1313 N/m Multi-directional Spring Units

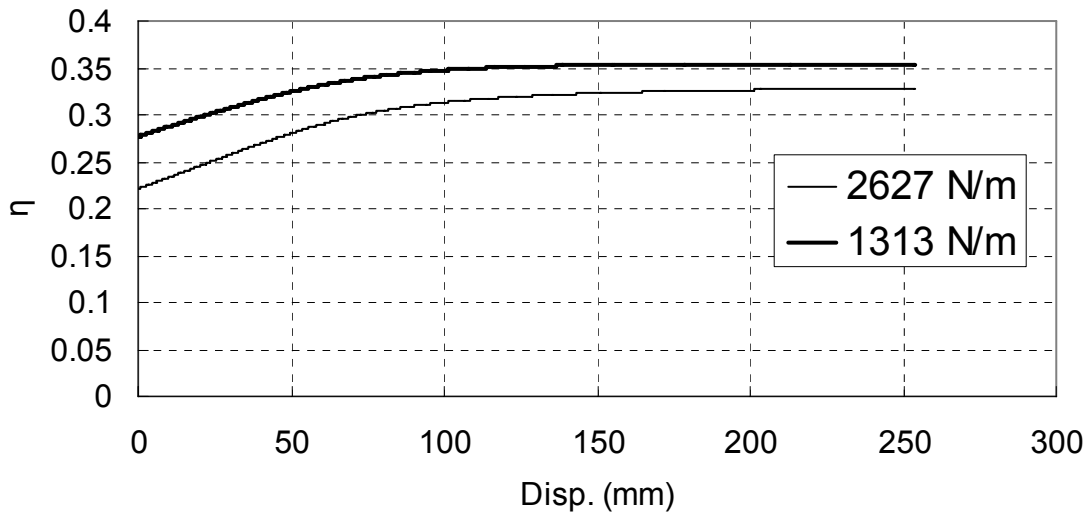


Figure 7.33 Values of Force Dropping Factor $-(\eta)$ from Physical Model

7.3.2 Comparison between Results from Analytical Model and Tests

To check the adequacy of the analytical model for multi-directional spring units built in Section 7.3.1, some quasi-static analyses were conducted using a single displacement cycle of sine wave

with 0.05 Hz frequency and 254 mm (10 in) amplitude. Comparison of results from the quasi-static analysis and the corresponding physical model described in Chapter 4 are shown in Fig. 7.34 and 7.35 for the two multi-directional spring units having nominal stiffnesses of 2627 N/m (15 lb/in) and 1313 N/m (7.5 lb/in), respectively. The results from IDARC2D quasi-static analysis and those from the physical model are almost identical.

To investigate the adequacy of the analytical model for Isolated Floor System II (cases with and without edge plates) as described in Section 7.3.1, some time-history analyses were conducted using: (i) the shake table accelerations recorded during the tests for systems without edge plates using multi-directional spring units having a nominal stiffness of 2627 N/m (15 lb/in) under Load Cases 2 and 3 and acceleration input Acc31; (ii) table accelerations obtained during the test of systems without edge plates using multi-directional spring units having a nominal stiffness of 1313 N/m (7.5 lb/in) under 50 psf load case and acceleration input of B2 (described in Chapter 5), and; (iii) table accelerations recorded during the tests for systems without edge plates using multi-directional spring units having a nominal stiffness of 2627 N/m (15 lb/in) under Load Cases 1 to 3 and acceleration input Acc31. Comparisons of the results from the IDARC2D analyses and the corresponding tests are shown in Figs. 7.36 to 7.41. Among these figures, Figs. 7.36 to 7.37 are for isolated floor systems using 2627 N/m (15 lb/in) spring units and without edge plates, Fig. 7.38 is for isolated floor system using 1313 N/m (7.5 lb/in) spring units and without edge plates, and Figs. 7.39 to 7.41 are for systems with 2627 N/m (15 lb/in) spring units and with edge plates. As in Section 7.2.3, there are three plots in each figure.

Reasonable agreement is observed between the results from analysis and those from the corresponding test. First of all, it can be noted that the completely vertical force dropping off is well realized by this model. Second, although the magnitude of displacement and acceleration responses from the analytical model are not the same as those from tests, they are almost always in phase with each other, as shown in parts (a) and (b) of each figure. This discrepancy can also

be found from part (c) of each figure. The observed discrepancy in magnitude of displacement and acceleration responses might be due to a combination of effects, namely the slight rotation of the isolated floors during the motion as mentioned in Chapter 5 and normal surface irregularity of the concrete slab. It is also noted that the shapes of the acceleration-displacement envelopes from analysis are similar to those from the tests. In addition, note from part (c) of each figure that the friction effect (i.e., acceleration difference between the loading and unloading branches, including the restoring force of multi-directional spring units due to friction in the isolator bushings, and friction effects from casters and edge plates) is near to that from the corresponding test, especially at relatively large displacement. The above observations comparing the behavior obtained from IDARC2D analyses and the corresponding test results suggest that the analytical model can be reliably used in the subsequent parametric analysis.

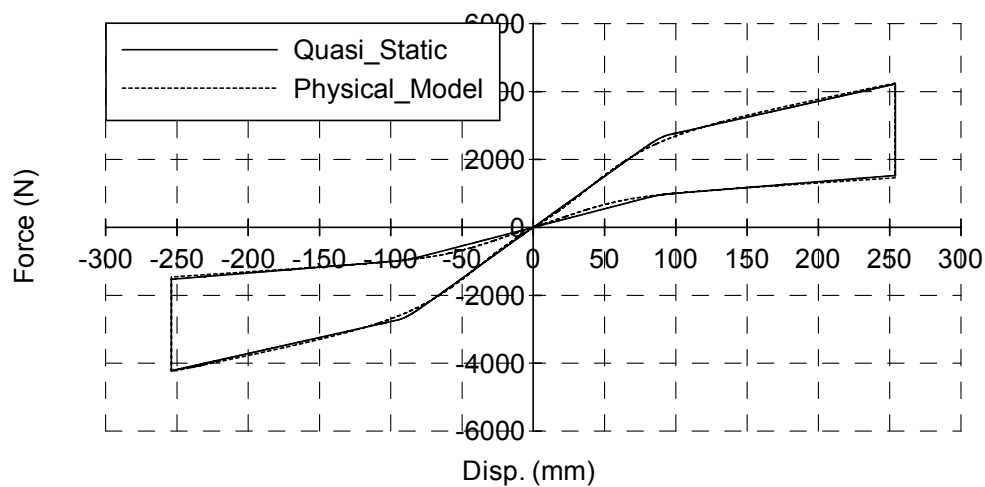


Figure 7.34 Comparison of Results between Quasi-static Analysis of Analytical Model and Physical Model for 2627 N/m Spring Unit

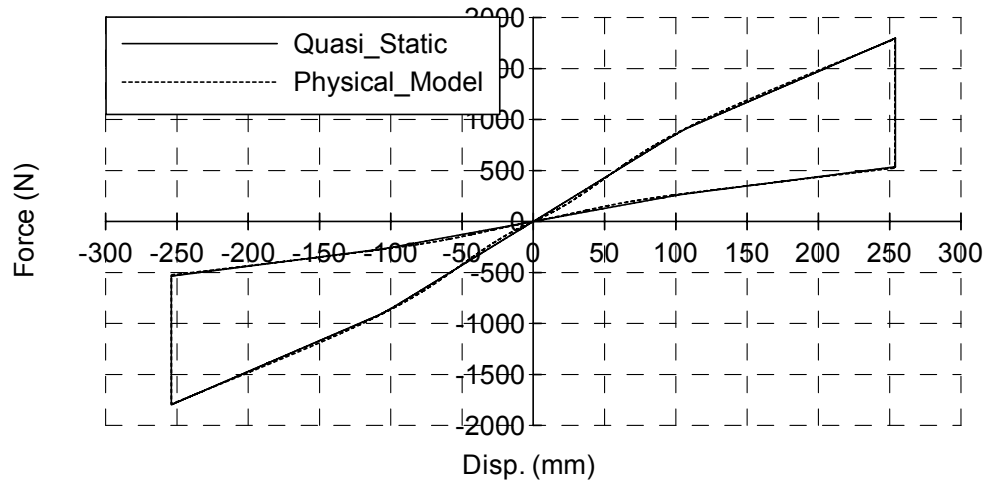


Figure 7.35 Comparison of Results between Quasi-static Analysis of Analytical Model and Physical Model for 1313 N/m Spring Unit

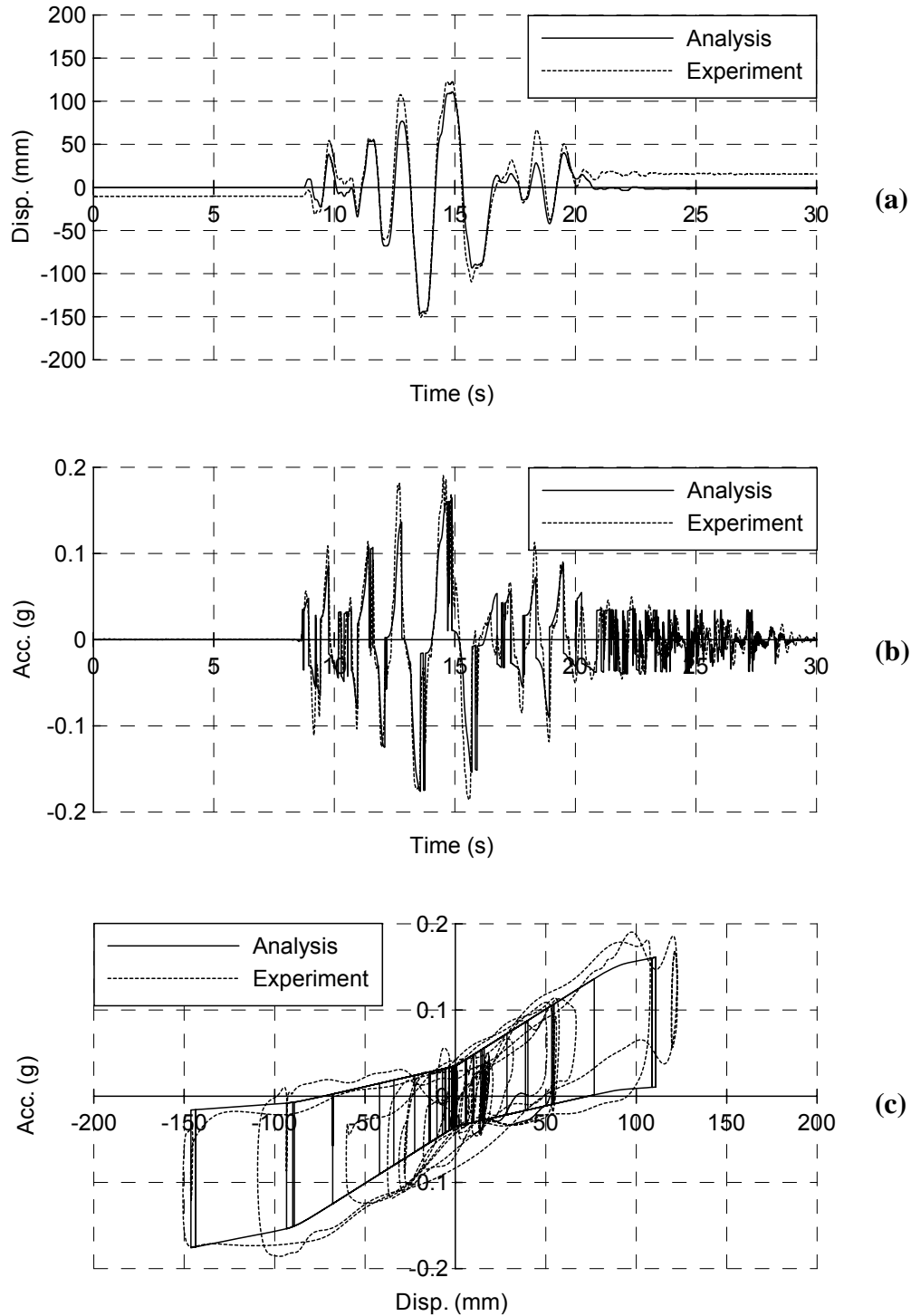


Figure 7.36 Comparison between Results from Analytical Model and Test for Isolated Floor System II Using 2627 N/m Spring Units, without Edge Plates, and under Load Case 2: (a) Displacement; (b) Acceleration, and; (c) Acceleration-Displacement Relationship

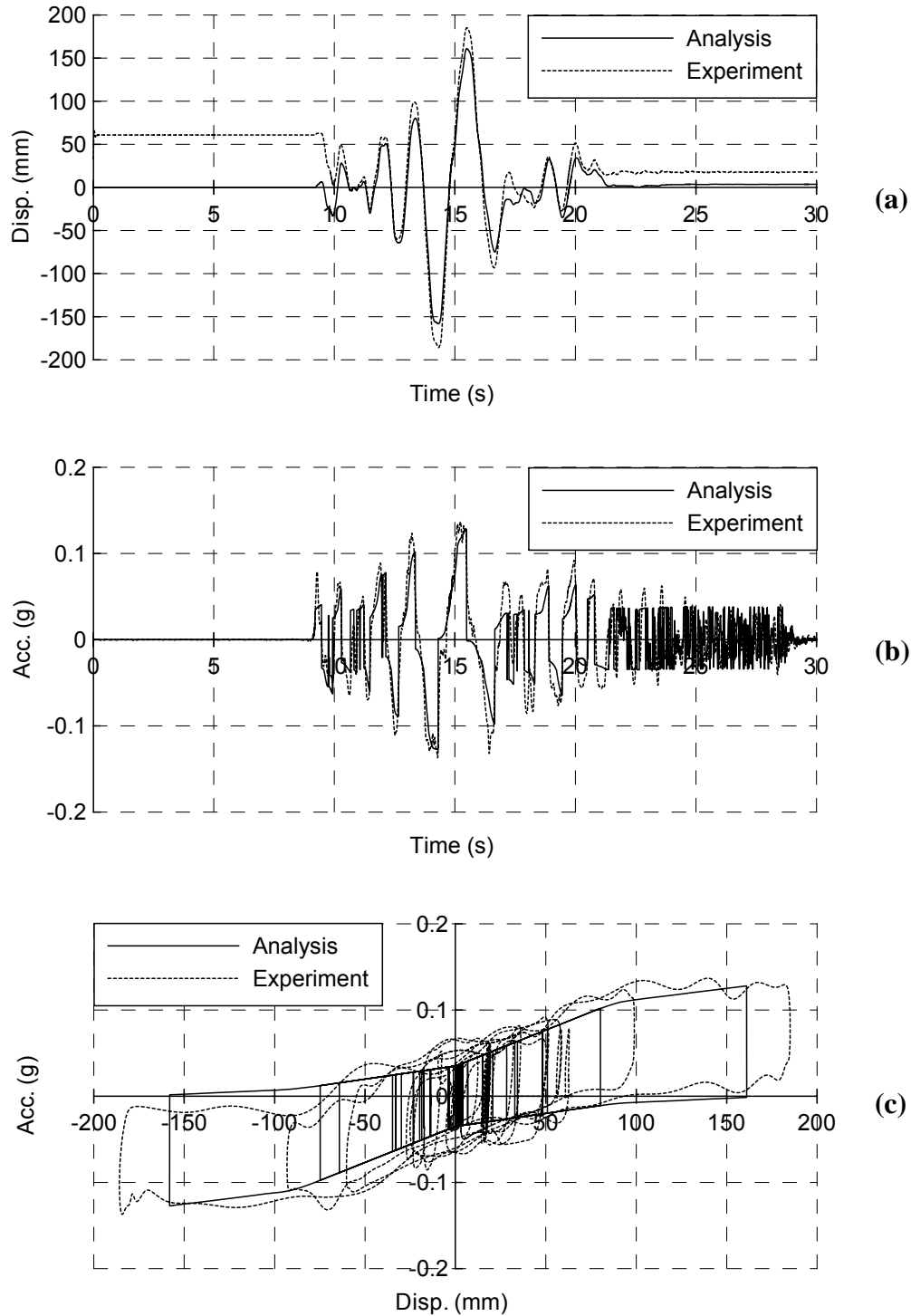


Figure 7.37 Comparison between Results from Analytical Model and Test for Isolated Floor System II Using 2627 N/m Spring Units, without Edge Plates, and under Load Case 3: (a) Displacement; (b) Acceleration, and; (c) Acceleration-Displacement Relationship

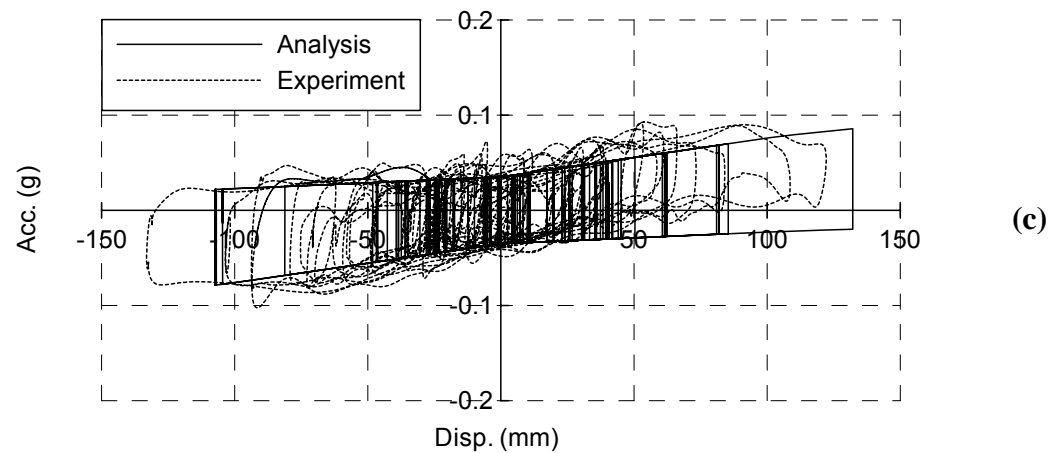
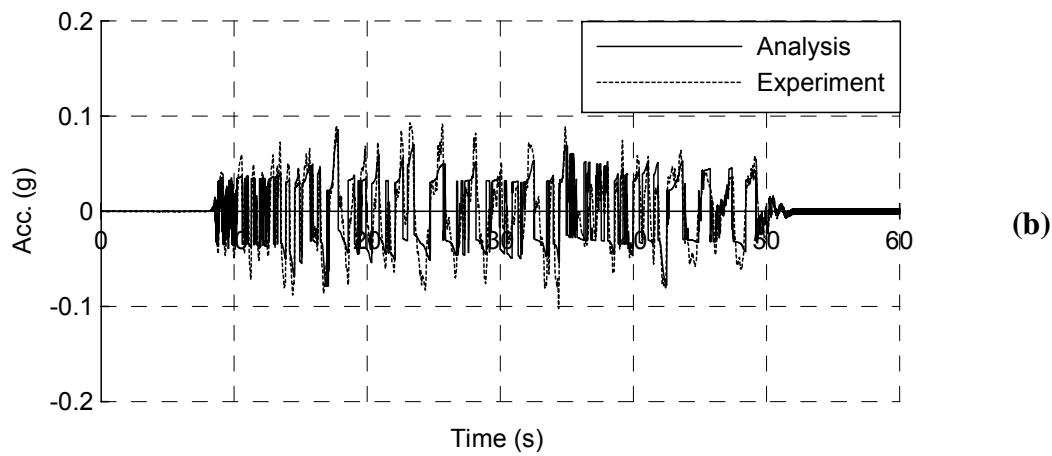
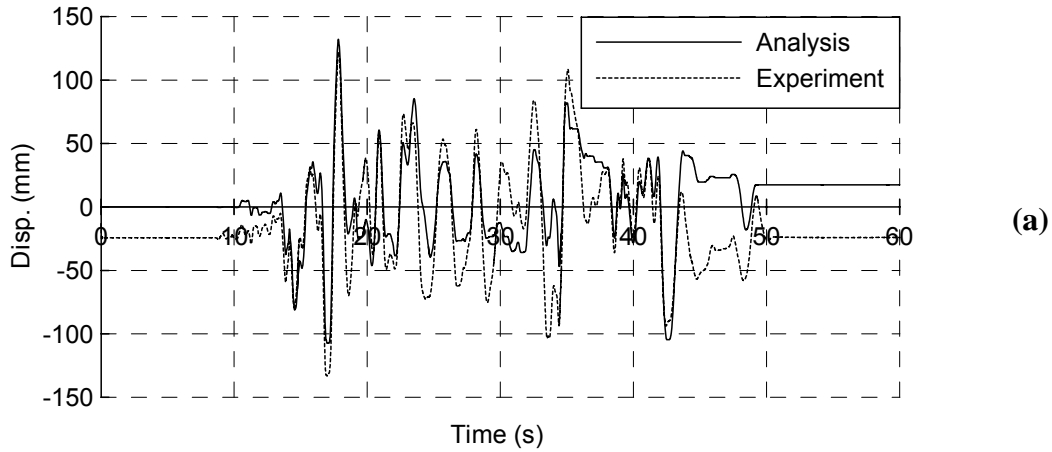


Figure 7.38 Comparison between Results from Analytical Model and Test for Isolated Floor System II Using 1313 N/m Spring Units, without Edge Plates, and under 50 psf Load: (a) Displacement; (b) Acceleration, and; (c) Acceleration-Displacement Relationship

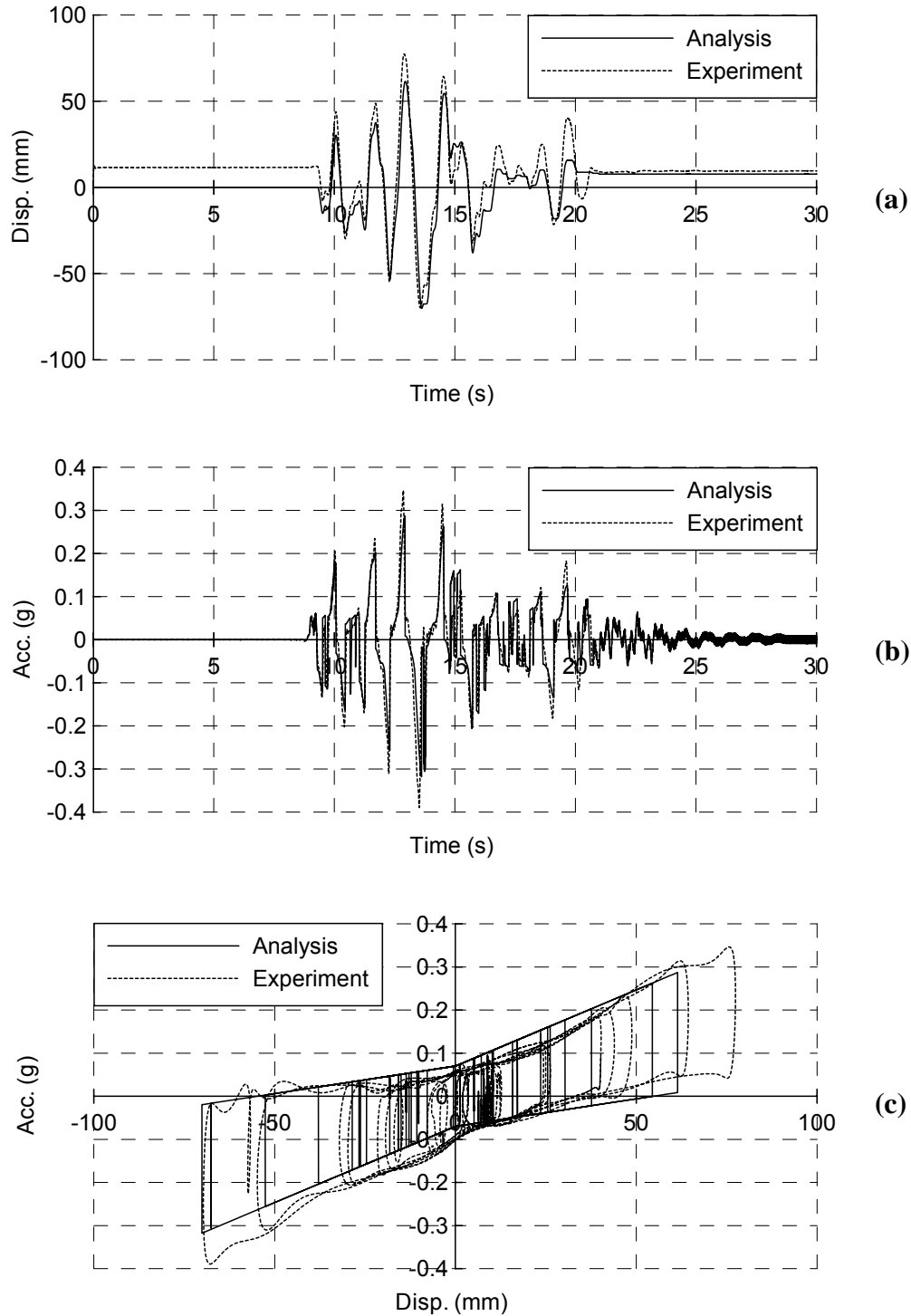


Figure 7.39 Comparison between Results from Analytical Model and Test for Isolated Floor System II Using 2627N/m Spring Units, with Edge Plates, and under Load Case 1: (a) Displacement; (b) Acceleration, and; (c) Acceleration-Displacement Relationship

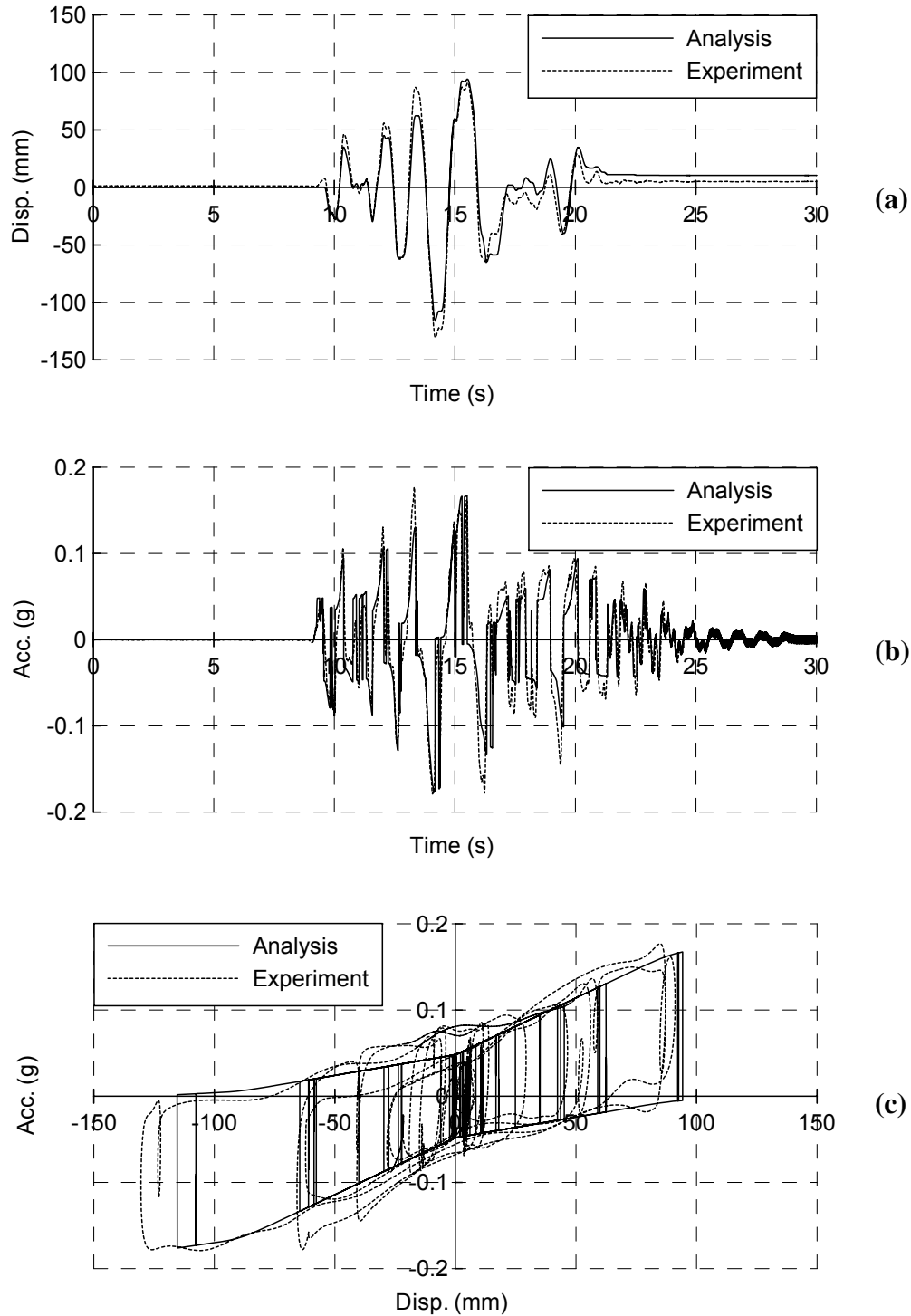


Figure 7.40 Comparison between Results from Analytical Model and Test for Isolated Floor System II Using 2627N/m Spring Units, with Edge Plates, and under Load Case 2: (a) Displacement; (b) Acceleration, and; (c) Acceleration-Displacement Relationship

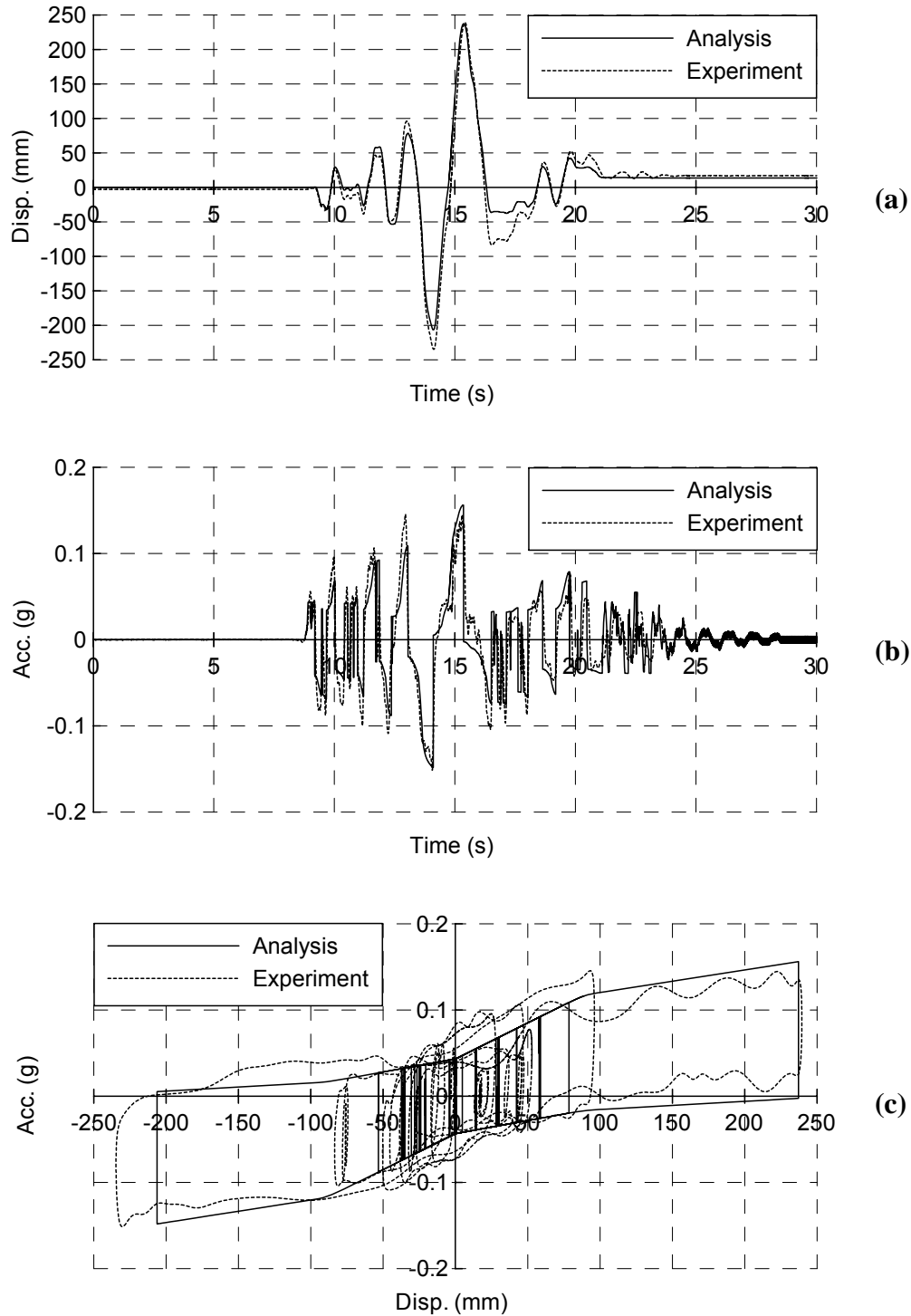


Figure 7.41 Comparison between Results from Analytical Model and Test for Isolated Floor System II Using 2627N/m Spring Units, with Edge Plates, and under Load Case 3: (a) Displacement; (b) Acceleration, and; (c) Acceleration-Displacement Relationship

7.3.3 Sensitivity Study

As done in the sensitivity study for the analytical model of Isolated Floor System I, a sensitivity study was also conducted on the analytical model for Isolated Floor System II to investigate whether the behavior of the analytical model for this Isolated Floor System II is sensitive to the friction effect between the casters and the concrete slab. As mentioned in Chapter 5, the friction from the casters for the tested Isolated Floor System II is 0.035 times of the weight of the isolated objects including the self-weight of the isolated floor. The value of 0.035 here is actually the friction coefficient between the casters and the concrete slab. The sensitivity study for Isolated Floor System II was conducted by changing this experimentally obtained friction coefficient for the casters by $\pm 30\%$. This was done using the isolated floor system without edge plates under Load Case 2 described in Chapter 5. The results are shown in Fig. 7.42. It is known that the friction effect for the casters will proportionally change along with the change in the friction coefficient between the casters and concrete slab. Note from part (c) of this figure that with increases in the friction coefficient, the acceleration-displacement loops of isolated Floor System II expands as expected and the peak displacement decreases. It is found that increasing the experimentally obtained friction coefficient between the casters and concrete slab by 30% increases the acceleration response due to this friction effect by 30%. It is also found that the peak displacement response decreases by an average of approximately 16% for the same increase of 30% in the friction coefficient. This shows that response predicted using the analytical model is sensitive to the equivalent friction coefficient used in the model. It is therefore important not to over-estimate its value.

In addition, it should be noted that the observations above on the sensitivity of friction effect from casters are also valid for other friction effects in Isolated Floor System II (e.g., friction effect from the edge plates).

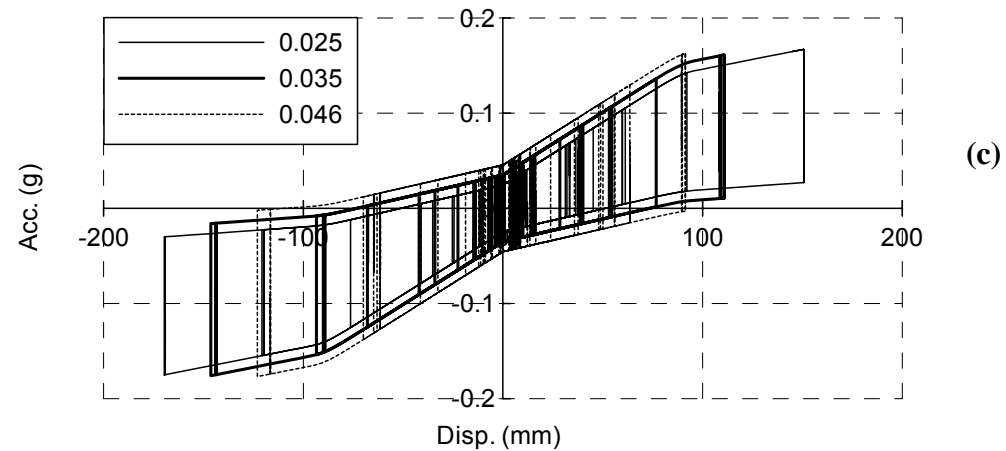
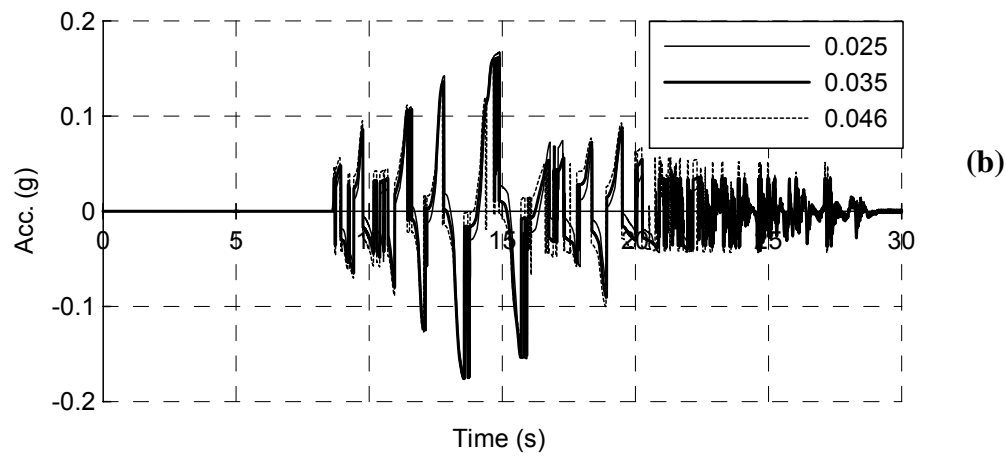
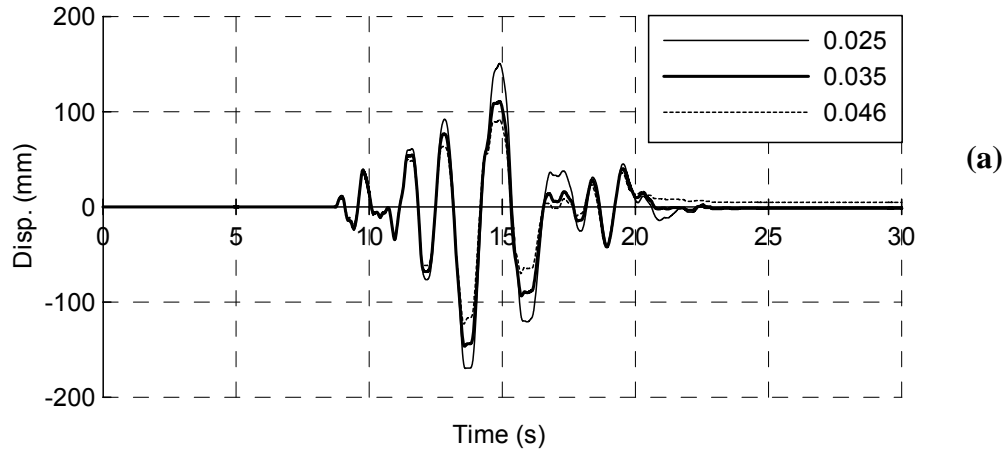


Figure 7.42 Results of Sensitivity Study for Isolated Floor System II without Edge Plates, Using 2627N/m Spring Units, under Load Case 2 and Input Acc31: (a) Displacement; (b) Acceleration, and; (c) Acceleration-Displacement Relationship

7.4 Observations

This chapter presented analytical models of the behavior for the two kinds of isolated floor systems considered in this research project, including both the individual isolator used in the isolated floor system and the corresponding complete isolated floor system. For Isolated Floor System I, the experimentally obtained equivalent friction coefficients described in Chapters 3 and 6 were simulated as being linearly related to the average ball gravity load. This information is necessary and used in parametric studies of isolated floor system and for design purpose. The linear relationship will induce conservative results based on the results of a sensitivity study on the equivalent friction coefficients.

Isolated Floor System I, as well as its isolators (concrete BNC isolators), was modeled in SAP2000 by combining a bilinear-elastic element and a plastic-Wen element in parallel. IDARC2D was used to model the behavior of Isolated Floor System II and its multi-directional spring unit isolators with a modified hysteretic damper brace element for spring units, and combined with a friction damper brace element in parallel for complete systems.

Reasonable agreements were observed in comparisons of results obtained from the analytical models and the corresponding tests. It was noted that although there was some difference in the amplitude of displacement and acceleration responses observed between the analytical models and the tests, the displacement and acceleration responses from analytical model are almost in phase with the corresponding ones recorded from the tests. The sensitivity studies conducted on these analytical models show that the hysteretic behaviors of these two isolated floor systems are both sensitive to variations in the magnitude of the friction effect considered in their corresponding models. It is therefore important not to overestimate friction in these two systems.

The models built in two computer programs used here for the two isolated floor systems considered will be used in the parametric study of the combined systems consisting of the structural fuse frames and isolated floor systems in Chapter 8.

CHAPTER 8

PARAMETRIC STUDY OF SYSTEMS CONSISTING OF SINGLE-DEGREE-OF-FREEDOM STRUCTURAL FUSE FRAMES AND ISOLATED FLOOR SYSTEMS

8.1 Introduction

The previous chapters (i.e., Chapters 3 to 6) have addressed the mechanical behaviors of two kinds of isolated floor systems, including characterization tests conducted on single isolators and corresponding complete isolated floor systems. In Chapter 7, analytical models duplicating these mechanical behaviors have been developed and used in structural analysis programs. This work makes it possible to conduct parametric studies on systems consisting of single-degree-of-freedom (SDOF) frames having structural fuse combined with isolated floor systems. The results of this parametric study can be used to develop an integrated methodology which considers the design of both parts. This chapter focuses on such parametric studies.

The following sections describe the various steps of that parametric study. First described are the seven new synthetic spectra compatible acceleration histories, corresponding to the NEHRP 2003 target spectrum, generated and used as ground seismic motions for the parametric studies. Then, the parameters required to define the SDOF structural fuse frame are introduced (note that they are slightly different from the four-parameter system used in Vargas and Bruneau (2006a)). Also, two ways to model the combined system used in the parametric studies, coupled and uncoupled

models, are presented. Details of the parametric studies follow. Note that parametric studies were first conducted to figure out the range of acceptable values for the three parameters defining the structural fuse frame. Systems consisting of SDOF structural fuse frames and Isolated Floor System I, as well as systems consisting of SDOF structural fuse frames and Isolated Floor System II, were considered. For the latter cases, the response of the system was investigated under both the lower and upper bound values of two load ranges considered for Isolated Floor System II (i.e., 0 psf to 50 psf and 25 psf to 50 psf). Based on the results of this first limited parametric study, a preferred range of the three parameters defining the structural fuse frame was recommended and further targeted parametric studies were conducted for the preferred range of the three parameters, using both uncoupled and coupled models to confirm that the interaction effect between these two SDOF parts in the combined system is insignificant for cases with low ratios of the isolated mass to that of the primary structural fuse SDOF frame, and to investigate the effect of that mass ratio on the response of the combined system (i.e., the effect of the interaction between these two parts in the combined system). The preferred values for the structural fuse frames' design were also found. Finally, the trends observed from these parametric study results are explained.

The results of the parametric studies presented in this chapter set up the foundation to develop the integrated design methodology that considers both the design of the SDOF structural fuse frames and isolated floor systems. That design methodology is the topic of Chapter 9.

8.2 Development of New Spectra Compatible Acceleration Time Histories

At the early stage of this project, three spectra compatible acceleration time histories with duration of 15 s were generated in Chapter 3, and were used as seismic inputs in the characterization tests of both single isolators and complete isolated floor systems, as shown in previous chapters (i.e., Chapters 3 to 6). The elastic response spectrum used to generate those

synthetic seismic motions was defined in accordance with the NEHRP Recommended Provisions for Seismic Regulations for New Buildings and other Structures (NEHRP 2003) for Sherman Oaks, California, and site soil-type class B, the site of the Multidisciplinary Center for Earthquake Engineering Research (MCEER) Demonstration Hospital (Yang and Whittaker 2002) chosen for this project. At that time, the design spectral accelerations for this site were $S_{DS}=1.3g$, and $S_{D1}=0.58g$ for 2% probability of exceedance in 50 years. When the project reaches the stage of conducting parametric study for the combined systems consisting of SDOF structural fuse frames and isolated floor system (i.e., the topic of this chapter), the design spectral accelerations for the same site and site soil-type class B were checked again from the USGS data for seismic design of buildings (USGS (2009): <http://earthquake.usgs.gov/hazards/design/buildings.php>) and found to have been updated to $S_{DS}=1.0g$, and $S_{D1}=0.4g$ for 2% probability of exceedance in 50 years, resulting in $T_s=0.4$ s and $T_0=0.08$ s. Therefore, a new elastic response spectrum was generated here following the same process as in Chapter 3, but according to these new values for design spectral accelerations, together with new spectra compatible acceleration time histories corresponding to this new target spectrum. Considering the requirements for nonlinear time history analysis in the NEHRP Recommended Provisions for Seismic Regulations for New Buildings and other Structure (NEHRP 2003) (i.e., for design values of structural response quantities to be taken as the average value of response values obtained from the analyses), seven new synthetic seismic motions were generated. Each has a duration of 40 s to ensure duration of strong motions long enough to capture possible long period effects on the response of the structural fuse frame (Vargas and Bruneau, 2006a). The comparison between the average of the elastic response spectra from the seven artificial accelerograms and the newly generated NEHRP 2003 target spectrum for 5% of critical damping is shown in Fig. 8.1. Good agreement can be found from this figure.

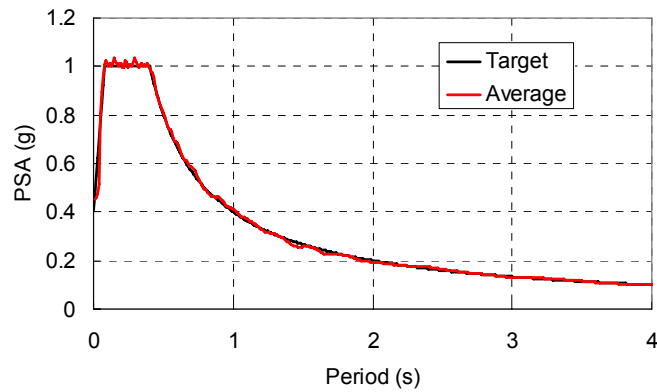


Figure 8.1 Comparison between the Average of Elastic Response Spectra from Synthetic Acceleration Time Histories and the Target NEHRP Spectrum (5% of Critical Damping)

8.3 Model Setup and Selection of Parameters

For the parametric study here, there are two ways to build the model of the combined systems consisting of SDOF structural fuse frames and isolated floor systems: coupled and uncoupled models. A combined system consisting of a base SDOF structural fuse frame and an isolated floor system is used for the parametric studies in this chapter to illustrate these two different modeling approaches.

The coupled model includes everything in the combined system as shown in Fig. 8.2. In this figure, M_{sf} is the mass of the base SDOF structural fuse frame, K_{sf} represents the stiffness (i.e., force-displacement relationship) of the structural fuse frame, C_{sf} is the damping coefficient for the structural fuse frame (which is taken to correspond to 5% of critical damping here), M_i is the mass supported by the isolated floor system, K_i represents the stiffness of the isolated floor system (which correspond to the elastic response part of the force-displacement relationship in Isolated Floor System I as shown in Fig. 7.9, or the force-displacement relationship of the multi-directional spring units used in Isolated Floor System II), and C_i is the damping coefficient for the isolated floor system (which corresponds to the sum of friction from edge plates and between the rolling

balls and working plates of the concrete BNC isolators used in Isolated Floor System I, or the sum of friction from edge plates and from the casters used in Isolated floor system II). Note that, because different structural analysis programs (i.e., SAP2000 (CSI, 2004) and IDARC2D (Valles et al. 1996 and Reinhorn et al. 2009)) were used to model the behaviors of different isolated floor systems as described in Chapter 7, different elements were used in each case to construct the model of the base frame in the corresponding different programs. In SAP2000, K_{sf} can be modeled with a link element with Wen plasticity property (Wen, 1976), and C_{sf} may be simulated using a linear viscous damping link element, as shown in Chapter 3. However, in IDARC2D, K_{sf} is modeled with column and beam elements by connecting the force-displacement relationship of the structural fuse frame into a corresponding moment-curvature relationship, and C_{sf} can be modeled with a visco-elastic brace element.

Fig. 8.3 illustrates the uncoupled model, which is also called a “system-in-cascade” in some references (e.g., Igusa and Der Kiureghian 1985b, and Villaverde 1997). It consists of two separate SDOF systems. First, the model of the base structural fuse frame is built using the same approach mentioned above, and nonlinear time history analyses are conducted on this SDOF model subjected to the artificial earthquake motions. The absolute acceleration response histories of the floor of the SDOF frame are recorded and used as inputs to analyze the second SDOF model corresponding to the isolated floor system, which can be built using the same approach as mentioned in Chapter 7.

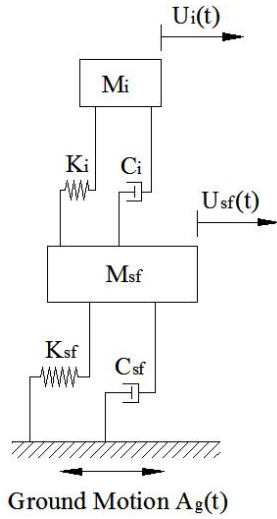


Figure 8.2 Coupled Model

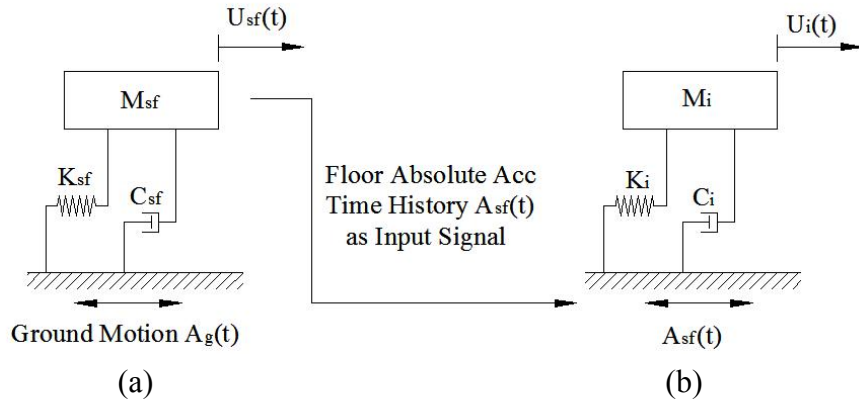


Figure 8.3 Uncoupled model: (a) Base SDOF Frame, and; (b) Isolated raised floor

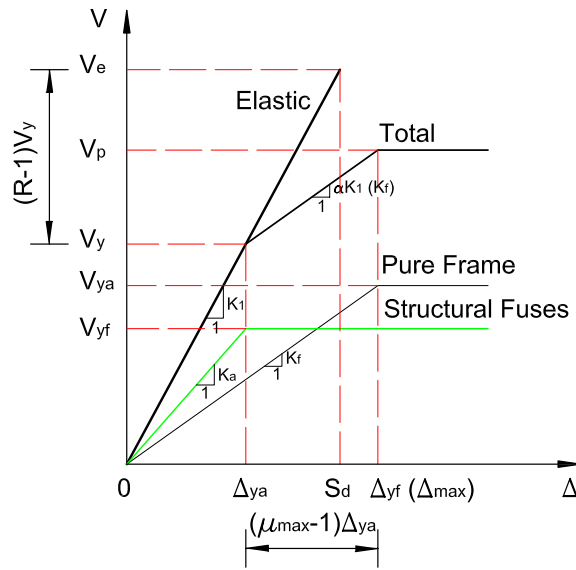


Figure 8.4 Pushover Curve of Structural Fuse Frame

The typical trilinear pushover behavior of a SDOF structural fuse frame is shown in Fig. 8.4, where, as defined in Vargas and Bruneau (2006a): K_1 is the initial stiffness which is equal to the sum of K_f (i.e., initial stiffness of the pure structural frame without structural fuses) and K_a (i.e., the initial stiffness of the structural fuse); V_y is the yield force of the complete structural fuse frame corresponding to the restoring force value of the complete structural fuse frame at the yield

displacement of the structural fuse, Δ_{ya} ; V_p is the load capacity of the complete structural fuse frame at the yield displacement of the pure frame, Δ_{yf} ; V_{yd} and V_{yf} are the yield force of the structural fuses and the yield force of the pure frame; R and μ_{max} are separately the response modification factor and maximum ductility that can be developed in the structural fuse when the rest of the structural fuse frame to remain elastic (Vargas and Bruneau, 2006a).

Note that only three parameters are used to define the structural fuse frame in this report, namely T , R , and α , which are respectively the natural vibration period, the response modification factor, and the post yielding stiffness ratio of the structural fuse frame. This approach differs somewhat from the four parameters (i.e., T , η , μ_{max} , and α) used in Vargas and Bruneau (2006a), although both sets of parameters can be related through some calculations as explained below. This demonstration proceeds starting from the expressions for spectral displacement, S_d , and maximum system displacement response, Δ_{max} , as expressed by Eqs. 8.1 and 8.2:

$$S_d = \frac{V_e}{K_1} = \frac{RV_y}{K_1} = R\Delta_{ya} \quad (8.1)$$

$$\Delta_{max} = \Delta_{yf} = \mu_{max}\Delta_{ya} \quad (8.2)$$

According to the provisions in NEHRP 2003, when the natural vibration period, T , lies in the constant velocity range (i.e., $T \geq T_s$), the equal displacement rule theory is valid, as expressed in Eq. 8.3.

$$S_d = \Delta_{max} \quad (8.3)$$

Substituting Eqs. 8.1 and 8.2 into Eq. 8.3 gives,

$$R = \mu_{max} \quad (8.4)$$

Therefore, for the three-parameter system, the relationship of the maximum ductility equals to the response modification factor is valid for cases with $T \geq T_s$.

For cases with T in the constant acceleration range of the NEHRP spectrum, as per the provisions in NEHRP 2003, the maximum nonlinear displacement of the structure can be obtained from the corresponding spectral displacement multiplied by a modification factor as shown in Eq. 8.5.

$$\Delta_{\max} = \frac{1}{R} \left(1 + \frac{(R-1)T_s}{T} \right) S_d \quad (8.5)$$

Substituting Eqs. 8.1 and 8.2 to Eq. 8.5 gives,

$$\mu_{\max} = 1 + \frac{(R-1)T_s}{T} \quad (8.6)$$

Although the structural fuse system is trilinear, because displacement response is limited to remain less than Δ_{yf} , only the first two linear segments of the system need to be modeled. This eliminates some modeling complexities. Note that if the results from nonlinear time history analysis exceed the maximum displacement (Δ_{yf}) determined from above relationships, the analysis results would have to be rejected since the use of a bilinear model of the first two segments of the trilinear curve would be insufficient to capture the proper inelastic response.

Under this three-parameter system, some of the parameters shown in Fig. 8.4 can be expressed per the following Equations 8.7 to 8.1, which can be used to calculate the values of the input parameters required in the modeling of the structural fuse frame for the parametric study here and for the design of the structural fuse frame in Chapter 9.

$$K_1 = \frac{4\pi^2 M_{sf}}{T^2} \quad (8.7)$$

$$V_y = \frac{M_{sf} \cdot S_{a,T}}{R} \quad (8.8)$$

$$K_f = \alpha \cdot K_1 \quad (8.9)$$

$$K_a = (1 - \alpha) \cdot K_1 \quad (8.10)$$

$$\Delta_{ya} = \frac{V_y}{K_1} = \frac{\Delta_{yf}}{R} \quad (8.11)$$

where, M_{sf} is the mass of the structural fuse frame; $S_{a,T}$ represents the spectral acceleration (in the generated NEHRP spectrum) at the natural vibration period of the structural fuse frame, T .

A first parametric study was conducted using the coupled model with a small mass ratio, M_r , of 1% (which is the ratio of the isolated mass over that of the base structural fuse frame). The intent of that parametric study was to identify the range of the three parameters under which the structural fuse concept works, which is here defined as “the acceptable range”. The reason selecting a small mass ratio for this parametric study is to minimize the effect of the interaction between the isolated floor system and the response of the base frame.

For this initial parametric study, the values of the three parameters defining the structural fuse frame were selected as: $T = 0.05s, 0.25s, 0.5s, 1.0s, 1.5s, 2.0s$; $\alpha = 0, 0.25, 0.5, 1.0$; and $R = 1, 5, 10$. Note that the periods chosen cover the initial ascending segment, the constant acceleration segment, and the constant velocity segment of the NEHRP spectrum. Also note that the cases of α equal to 0 and 1.0 respectively correspond to the perfectly elasto-plastic case and linear elastic case for the SDOF structural fuse frame. Finally, the chosen values of R encompass the range of values that would be used in design.

8.4 Initial Parametric Study on Coupled Models

8.4.1 Isolated Floor System I

As mentioned in Section 8.3, an initial parametric study was conducted using the selected parameter values and the low mass ratio of 1% to determine the acceptable range of the three parameters defining the SDOF structural fuse frames. This study was first conducted on the systems consisting of SDOF structural fuse frames and Isolated Floor System I with polyurethane balls for the concrete BNC isolators.

From the sensitivity study in Chapter 7, it was observed that the response of Isolated Floor System I is sensitive to the equivalent friction coefficient, with lower friction coefficients resulting in bigger displacement response (which is a key factor in the design of isolated floor systems). Therefore, for the parametric study here, the smallest friction coefficient obtained previously for the system with polyurethane balls was considered to get the worst displacement response. For the friction coefficient in the parametric study here, the friction effect from the edge plates in the tests shown in Chapter 6 was first averaged to each rolling ball. The value of this friction effect is about 441 N (99.11 lb), which, when averaged over the 24 balls in the tested isolated floor specimen, is 18.37 N/ball. This is a constant value regardless of the gravity load acting on each ball during the characterization tests in Chapter 6. However, note that it will change with the size of the edge plates as mentioned in Chapter 7. Under a certain value of gravity load per ball, denoted as x here, the total friction effect in terms of friction coefficient, considering both the rolling ball friction (i.e., the linear relationship between the equivalent rolling friction coefficient (i.e., μ_e) and the average load per rolling ball, as shown in chapter 7) and the friction coefficient from edge plates, can be expressed as,

$$\mu = 0.00002x + 0.0157 + \frac{18.37}{x} \quad (8.12)$$

From Equation 8.12, the smallest friction coefficient was determined to be 0.054 under the load per ball of 958.3 N (215.45 lb) for Isolated Floor System I using polyurethane balls. This friction coefficient value is used in all parametric studies for cases including Isolated Floor System I with polyurethane balls. The weight of the isolated floor system was back calculated as 24 times of the load value per ball of 958.3 N corresponding to the minimum friction coefficient, which is 23000 N (5170.91 lb). As mentioned in Section 8.3, the mass ratio chosen for the initial parametric study is 1%. Therefore, the weight of the primary structural fuse frame can be calculated as 100 times of the above weight of the isolated floor system (i.e., 23000 N). Note that other absolute values of the mass of the isolated floor system could have been chosen as long as

the minimum friction coefficient is used, the mass ratio between the isolated floor system and the base SDOF structural fuse frame remains 1%.

The average peak response of the structural fuse frame from this initial study is shown in Fig. 8.5, in terms of the ductility of the structural fuse frame, μ , which corresponds to the “global ductility” defined in Vargas and Bruneau (2006a). Here, the “average peak response” means the average of the peak responses obtained from the nonlinear time history analyses conducted separately using the seven synthetic acceleration time histories as ground motions.

From this figure, it can be noted that for cases with R value of 1.0 and cases with α value of 1.0 (i.e., cases where the structural fuse frame is elastic), the μ values obtained from nonlinear time history analyses in SAP2000 are almost the same as the target ones, regardless of the values of the natural vibration period of the structural fuse frame. This also confirms that the spectra compatible acceleration time histories work well. Although almost all these cases are “acceptable”, where the frames behave in its elastic range, these are not true examples of the structural fuse concept since the structural fuses have not yielded. Second, it can also be found from this figure that most acceptable cases which satisfy the structural fuse concept, except the elastic cases mentioned above, are the ones with α values of 0.25 and 0.5 and with R values of 5 and 10. So, the range of α values between 0.25 and 0.5 and the range of R values between 5 and 10 are selected as the preferred range of values for the parameters defining the structural fuse frame.

Note from Fig. 8.5 that most of the cases with natural vibration period of the structural fuse frame less than T_s (i.e., 0.4 s, over the range where the equal energy theory applies, and for which the modification factor for the nonlinear response of such cases is taken as per NEHRP 2003), except the elastic cases mentioned above, are not acceptable (i.e., the μ value obtained from analysis is bigger than the corresponding target). Chapter 9 will discuss this aspect further in the

perspective of the design of SDOF structural fuse frame in such cases. In addition, note that the response of the isolated floor system is not the focus at this stage of parametric study, and will instead be addressed in following sections.

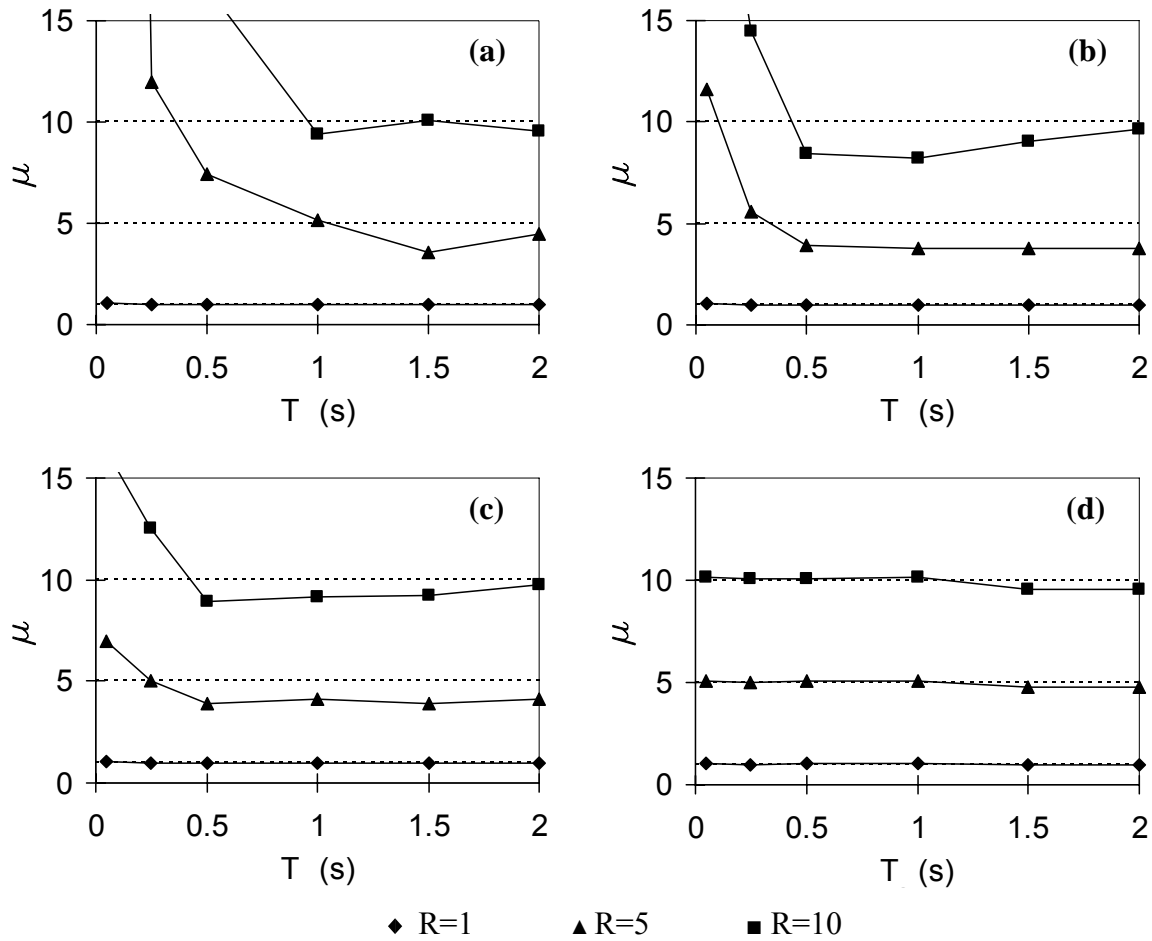


Figure 8.5 Average Peak Response of the SDOF Frame from Limited Parametric Study of Combined Systems Using Isolated Floor System I (Polyurethane Balls): (a) to (d) respectively correspond to α values of 0, 0.25, 0.5, and 1.0

8.4.2 Isolated Floor System II under Lower Bound Load

Following an approach similar to what was presented in Section 8.4.1 for Isolated Floor System I (using polyurethane balls), this section focuses on the initial parametric study for systems consisting of SDOF structural fuse frames and Isolated Floor System II. For this purpose, the stiffness of the spring in the multi-directional spring units first had to be determined in accordance with the following procedure.

As shown in Chapter 5, the maximum acceleration response of Isolated Floor System II is controlled by the restoring force from its multi-directional spring units and the friction effects from both the edge plates and the casters. If the values of all the friction effects in Isolated Floor System II are specifically given, then, the peak acceleration response of the isolated floor will be controlled by the restoring force provided by the multi-directional spring units used in this system. From the physical model of multi-directional spring units in Chapter 4, note that the restoring force is controlled by the force-displacement relationship of the pure spring inside the steel tube, the friction coefficient between the steel cable and the brass bushing, and the friction force between the pure spring and the steel tube. Further, the force-displacement relationship of the pure spring is controlled by its stiffness if the force-displacement relationship is assumed to be perfectly linear. Also, note that under same restoring force, the acceleration response of the isolated floor will decrease with an increase in the weight of the isolated floor based on Newton's second law.

Then, to choose a stiffness for the spring of the multi-directional spring units, an acceleration response limit (i.e., the peak acceleration response on top of the isolated floor) must first be specified for the isolated floor system. Here, 0.2g was arbitrarily chosen for this limit. Second, a gravity load range must be determined for the isolated floor system. For the parametric study here, the specimen from the characterization tests in Chapter 5 was used. Two different ranges of

the gravity loads applied on the isolated floor were selected: first, from 0 psf (corresponding to a total isolated weight of 1916 lb, i.e., the self-weight of Isolated Floor System II) to 50 psf (corresponding to total isolated weight of 8096 lb, i.e., the total weight of the self-weight of the isolated floor and the load on top) and second, from 25 psf (corresponding to a total isolated weight of 5126 lb) to 50 psf. The weight of the SDOF structural fuse frame was calculated as 100 times of the corresponding weight of the isolated floor system to match the selected mass ratio of 1%. Then, the values of the friction effects from edge plates and casters of Isolated Floor System II were taken as the same value as those found in the characterization tests of Chapter 5 (i.e., the friction coefficient between the casters and the base concrete slab was 0.035 and friction force from the edge plates was about 298 N (67 lb)).

After this, the maximum restoring force provided by the multi-spring units were determined by using the lower bound of the total isolated weight (including both the self-weight of the isolated floor specimen and the load applied on that floor) and the acceleration limit (i.e., 0.2g):

- 1) First, subtract the effect of the friction on the acceleration response of the isolated floor system out of the acceleration limit to get the acceleration contribution of the restoring force from the spring units;
- 2) Then, the maximum restoring force is taken as the total isolated mass multiplied by the acceleration contribution of the restoring force obtained in 1);
- 3) Finally, the stiffness of the springs of the multi-directional spring units were determined assuming that springs behave perfectly linearly and that two identical spring units were used in the isolated floor system being studied. The same geometry and parameters used in Chapter 4 are also used here for consistency. The resulting stiffness is given by Equation 8.13 (in units of lb and in), derived based on Eq. 4.16.

$$K_s = \frac{\frac{F_{2,\max}}{2 \cdot e^{\mu_k(\pi/2 + \beta_{\max})} \cdot \sin \beta_{\max}} - f}{\Delta_{s,\max} + 10}} \quad (8.13)$$

where, K_s is the spring stiffness to be determined; $F_{2,\max}$ is the maximum horizontal restoring force as mentioned above (corresponding to the force from the two spring units at the maximum displacement of the isolated floor, Δ_{\max}); β_{\max} is the maximum contact angle of the cable with the quarter-cycles of the bushing as shown in Fig. 4.28, which corresponds to the maximum displacement of the isolated floor, Δ_{\max} ; $\Delta_{s,\max}$ is the maximum spring extension corresponding to Δ_{\max} ; μ_k is the sliding friction coefficient between the steel cable and the brass bushing; f is the friction effect between the spring and the steel tube, value 2 means two pieces of spring units with same properties were used in such isolated floor system, and the value of 10 is obtained as follows.

As shown in Chapter 4, in cases with 51 mm (2 in) pretension applied, the springs tested there behaved linearly, except of course for the effect of friction between the spring and the tube. However, in cases without any pretension, they exhibited a high initial stiffness before they behaved per their nominal stiffness. This is because the springs were pre-twisted to a certain extent during their manufacturing process. Some deformation is needed to overcome this pre-twisting that is responsible for the high stiffness before the spring can behave in accordance with its nominal stiffness. The pretension elongation of 51 mm (2 in) exceeds the original deformation required to overcome the pre-twisting effect. Considering that the starting force for the springs with such a pre-twisting together with a pretension of 51 mm (2 in) is equal to 10 times its nominal stiffness when units of in and lb are used, the initial force in the springs used here for parametric study is consistently assumed to be achieved at 10 times the corresponding spring nominal stiffnesses in units of in and lb. This explains the presence of the number “10” in Eq. 8.13. Furthermore, it is assumed that the maximum restoring force is provided by the complete spring units at a maximum displacement of 254 mm (10 in) (i.e., $\Delta_{\max}=10$ in).

In addition, Equation 8.13 can also be expressed in units of N and mm as,

$$K_s = \frac{\frac{F_{2,\max}}{2 \cdot e^{\mu_k(\pi/2 + \beta_{\max})} \cdot \sin \beta_{\max}} - f}{\Delta_{s,\max} + 254} \quad (8.14)$$

The value of the sliding friction coefficient in Equations 8.13 and 8.14, μ_k , was selected to be 0.181, which is the average of the two values used in Chapter 4 (i.e., 0.171 for the 2627 N/m spring unit and 0.190 for the 1313 N/m spring unit). The friction force between the spring and the steel tube, f , is selected as 18 N (4 lb), again the same value as in Chapter 4. The resulting stiffness is 656 N/m (3.75 lb/in) for the 0 psf load case and 2133 N/m (12.18 lb/in) for the 25 psf load case. According to the model for Isolated Floor System II described in Chapter 7, the straight lines to model the loading branch of each physical model of the spring units using the springs developed above were expressed as follows (in units of lb and in),

For each 656 N/m spring unit,

$$y = 21.037x \quad (\text{when } x \leq 3.571 \text{ in}) \quad (8.15)$$

$$y = 8.066x + 46.322 \quad (\text{when } x > 3.571 \text{ in}) \quad (8.16)$$

For each 2133 N/m spring unit,

$$y = 64.225x \quad (\text{when } x \leq 3.595 \text{ in}) \quad (8.17)$$

$$y = 25.875x + 137.902 \quad (\text{when } x > 3.595 \text{ in}) \quad (8.18)$$

The corresponding expressions of Equations 8.11 to 8.14 in units of N and mm are,

$$y = 3.684x \quad (\text{when } x \leq 90.711 \text{ mm}) \quad (8.19)$$

$$y = 1.413x + 206.04 \quad (\text{when } x > 90.711 \text{ mm}) \quad (8.20)$$

$$y = 11.247x \quad (\text{when } x \leq 91.304 \text{ mm}) \quad (8.21)$$

$$y = 4.531x + 613.19 \quad (\text{when } x > 91.304 \text{ mm}) \quad (8.22)$$

The corresponding values of the input parameters required in the IDARC2D model were determined according to the procedure shown in Chapter 7 as: for each 656 N/m spring unit: $K_0 = 3.684$ kN/m, $F_y = 334.2$ N, $\alpha_1 = 0.403$, $n = 20$, and $\eta = 0.348$; for each 2133 N/m

spring unit, $K_0 = 11.247$ kN/m, $F_y = 1027$ N, $\alpha_1 = 0.403$, $n = 20$, and $\eta = 0.336$. Note that in the model of the corresponding isolated floor system, two spring units of same properties were used in parallel. Therefore, two times of the values of K_0 and F_y were used as input of the modified hysteretic brace element in IDARC2D to simulate the behavior of two spring units.

Similar to Section 8.4.1, the average peak response of the structural fuse frame from the parametric study in this section are shown in Fig. 8.6 and 8.7, also in terms of the ductility of the SDOF structural fuse frame, respectively, for load cases of 0 psf and 25 psf. From these figures, similar observations can be made as those in Section 8.4.1. More specifically, most of the cases corresponding to elastic SDOF structural fuse frames are acceptable to achieve the structural fuse concept. However, these are not true examples of the structural fuse concept since the structural fuses have not yielded. The preferred value ranges for the parameters defining the primary structural fuse frame are also selected as $0.25 \leq \alpha \leq 0.5$ and $5 \leq R \leq 10$. Also note that the results in Figs. 8.6 and 8.7 are almost the same as to the corresponding ones shown in Fig. 8.5. This is reasonable because the mass ratio in the parametric study is only 1% and hence the interaction between the isolated floor systems and the base frames is negligible, which will be confirmed through the comparison of results between coupled and corresponding uncoupled models in following sections. Note again that the response of the isolated floor systems is not the focus of this initial parametric study, and will be addressed in following sections.

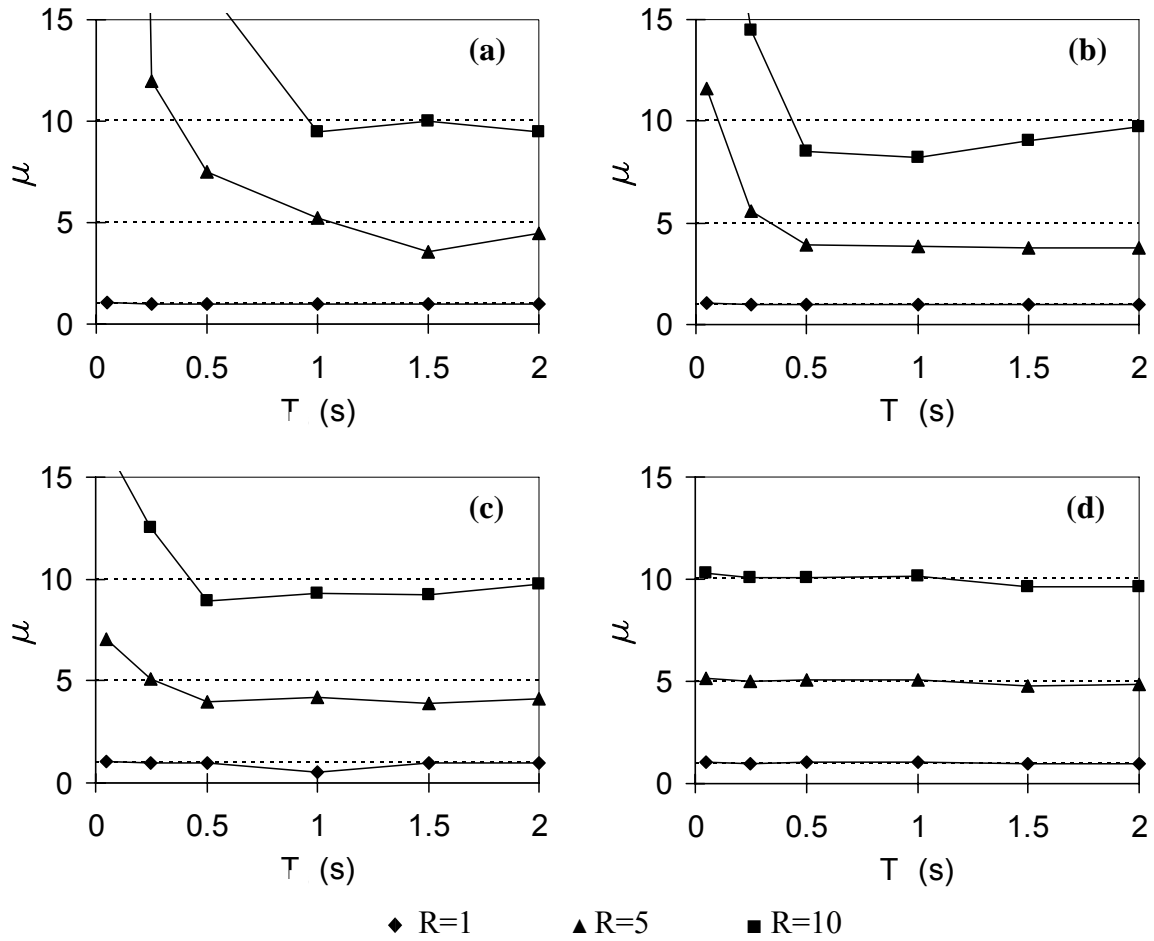


Figure 8.6 Average Peak Response of the SDOF Frame from Preliminary Parametric Study of Combined Systems Using Isolated Floor System II (0 psf Load Case): (a) to (d) respectively correspond to α value of 0, 0.25, 0.5, and 1.0

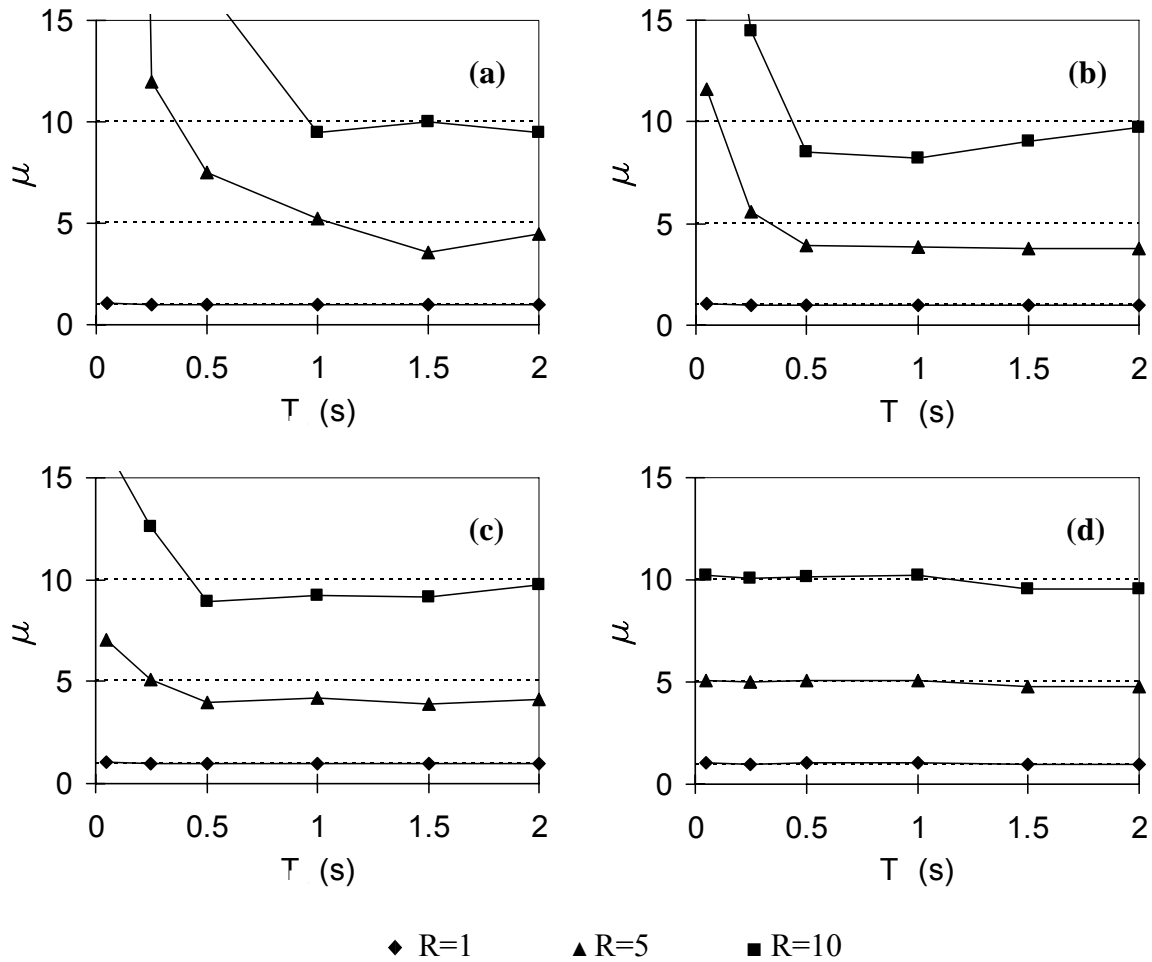


Figure 8.7 Average Peak Response of the SDOF Frame from Preliminary Parametric Study of Combined Systems Using Isolated Floor System II (25 psf Load Case): (a) to (d) respectively correspond to α value of 0, 0.25, 0.5, and 1.0

8.4.3 Isolated Floor System II under Upper Bound Load

As shown in Section 8.4.2, under a given restoring force, the acceleration response will decrease with increases in the isolated weight. Therefore, the lower bound value of the load range considered was used there to determine the stiffness of the springs used in the system. However, note that, for a given restoring force, the displacement response may increase under a bigger isolated weight and may affect the response of the structural fuse frame consequently. Therefore,

some parametric study using coupled model were done to check the response of the isolated floor system under the corresponding upper bound value (i.e., 8096 lb) of the two load range (i.e., 0 psf to 50 psf, and 25 psf to 50 psf) used for Isolated Floor System II in Section 8.4. Note that all the sets of parameters considered in Section 8.4.2 were considered here too. The only difference between the parametric study here and that in Section 8.4.2 is that the isolated weight here is changed to that corresponding to the upper bound load value. Note that the corresponding friction effect from the casters was also changed in proportion with the change of the weight of Isolated Floor System II. However, the properties of the spring units and the structural fuse frame here remained the same as in Section 8.4.2.

The results of such parametric studies are shown in Tables 8.1 and 8.2, in terms of comparison with those from the parametric study using the corresponding lower bound load values in Section 8.4.2, where “ D_{ris} ”, “ A_{absi} ”, “ D_{rs} ”, and “ A_{abss} ” are all average peak response quantities, which means that they were obtained as the average of the corresponding peak response values from the nonlinear time history analyses using the seven synthetic acceleration time histories as ground motions. They represent, respectively, the average peak response of the relative displacement response between the isolated floor system and the base frame, the absolute acceleration of the isolated floor system, the relative displacement of the frame with respect to the ground, and the absolute acceleration of the structural fuse frame.

It can be found from each table that D_{rs} in Column 10 and A_{abss} in Column 11 obtained from the parametric study using upper bound load values are almost the same as the corresponding ones in Columns 6 and 7 corresponding the lower bound load values for Isolated Floor System II. This is reasonable because the mass of the isolated floor system is still a low value relative to the mass of the structural fuse frame (although the upper bound load value was used) which will not introduce significant interaction into the combined system as presented in following sections. Also, note from each table that while the values of A_{absi} in Column 9 corresponding to the

parametric study using upper bound load values are lower than those in Column 5 from the parametric study using lower bound load values, which has been predicted above, the values of D_{ris} in Column 8 are higher than the corresponding ones in Column 4, which indicates that the relative displacement will increase under higher load values of isolated weight. Finally, it can be noted from these tables that in some cases with $T=1.0s$, and especially in most cases with $T=1.5 s$ and $2.0 s$ (except the cases where the structural fuse frame is elastic as mentioned in Section 8.4.1), the isolated floor system is not effective because the acceleration response of the isolated floor is equal or even bigger than that of the corresponding structural fuse frames or the isolated floor system hardly moves.

Table 8.1 Results from Parametric Studies Using Lower and Upper Bound Isolated Load Values (0 psf to 50 psf)

R (1)	α (2)	T (s) (3)	0 psf				50 psf			
			D _{ris} (mm) (4)	A _{absi} (g) (5)	D _{rs} (mm) (6)	A _{abss} (g) (7)	D _{ris} (mm) (8)	A _{absi} (g) (9)	D _{rs} (mm) (10)	A _{abss} (g) (11)
1	0	0.05	47.0	0.11	0.5	0.78	78.5	0.06	0.5	0.78
		0.25	83.3	0.14	15.6	1.01	116.7	0.06	15.5	1.00
		0.5	144.8	0.16	50.2	0.81	192.3	0.07	49.7	0.81
		1	179.4	0.18	99.6	0.40	196.3	0.07	98.5	0.40
		1.5	241.4	0.20	143.2	0.26	263.2	0.08	140.7	0.25
		2	240.0	0.20	191.6	0.19	304.7	0.08	185.7	0.19
	0.25	0.05	47.0	0.11	0.5	0.78	78.5	0.06	0.5	0.78
		0.25	83.3	0.14	15.6	1.01	116.7	0.06	15.5	1.00
		0.5	144.9	0.17	50.2	0.81	192.3	0.07	49.7	0.81
		1	179.6	0.18	99.9	0.40	196.6	0.07	98.7	0.40
		1.5	241.5	0.20	143.2	0.26	263.2	0.08	140.7	0.25
		2	240.7	0.20	191.6	0.19	305.0	0.08	185.7	0.19
	0.5	0.05	47.0	0.11	0.5	0.78	78.5	0.06	0.5	0.78
		0.25	83.3	0.14	15.6	1.01	116.7	0.06	15.5	1.00
		0.5	145.0	0.17	50.2	0.81	192.3	0.07	49.7	0.81
		1	198.1	0.18	100.4	0.40	197.1	0.07	98.9	0.40
		1.5	241.6	0.20	143.2	0.26	263.2	0.08	140.7	0.25
		2	241.4	0.20	191.5	0.19	305.3	0.08	185.7	0.19
	1	0.05	47.7	0.11	0.5	0.80	78.5	0.06	0.5	0.79
		0.25	83.3	0.14	15.6	1.01	116.7	0.06	15.5	1.00
0.5		145.1	0.17	50.2	0.81	192.3	0.07	49.7	0.81	
1		181.6	0.18	101.1	0.41	198.4	0.07	99.2	0.40	
1.5		241.8	0.20	143.2	0.26	263.2	0.08	140.7	0.25	
2		242.8	0.20	191.5	0.19	305.9	0.08	185.7	0.19	
5	0	0.05	44.4	0.11	12.3	0.27	75.5	0.06	12.4	0.27
		0.25	51.5	0.11	37.1	0.25	87.2	0.06	36.8	0.25
		0.5	61.2	0.12	74.8	0.20	101.4	0.06	74.4	0.20
		1	25.3	0.09	103.9	0.10	94.0	0.06	102.7	0.10
		1.5	0.0	0.07	106.6	0.07	47.8	0.05	110.5	0.07
		2	0.0	0.06	179.0	0.05	6.2	0.04	185.3	0.05
	0.25	0.05	48.7	0.11	1.1	0.57	79.3	0.06	1.1	0.57
		0.25	66.6	0.13	17.3	0.44	103.2	0.06	17.2	0.44
		0.5	81.3	0.14	38.9	0.28	122.8	0.06	38.8	0.28
		1	59.5	0.12	76.3	0.14	118.0	0.06	75.5	0.14
		1.5	20.7	0.09	112.8	0.09	101.6	0.06	112.0	0.09
		2	1.1	0.07	148.9	0.07	60.0	0.06	151.4	0.07
0.5	0.05	47.1	0.11	0.7	0.63	77.6	0.06	0.7	0.63	
	0.25	71.2	0.13	15.7	0.61	113.5	0.06	15.7	0.61	
	0.5	97.6	0.15	39.3	0.40	148.0	0.07	39.0	0.40	
	1	101.8	0.32	83.2	0.21	138.6	0.07	81.8	0.21	
	1.5	80.0	0.13	116.4	0.13	169.7	0.07	115.1	0.13	
	2	43.4	0.11	164.9	0.10	159.1	0.07	163.4	0.10	
10	0	0.05	41.1	0.11	19.9	0.24	73.9	0.06	19.9	0.24
		0.25	36.4	0.10	52.7	0.16	72.3	0.06	52.0	0.16
		0.5	27.6	0.09	82.6	0.12	74.8	0.06	82.3	0.12
		1	0.0	0.07	93.9	0.06	13.9	0.05	97.3	0.06
		1.5	0.0	0.06	148.7	0.04	0.0	0.04	152.5	0.04
		2	0.0	0.06	188.3	0.03	0.0	0.04	187.7	0.03
	0.25	0.05	50.9	0.11	1.3	0.61	82.6	0.06	1.3	0.61
		0.25	77.2	0.14	22.5	0.45	113.2	0.06	22.4	0.45
		0.5	76.7	0.13	42.2	0.24	126.3	0.06	41.9	0.23
		1	33.1	0.10	81.8	0.12	110.4	0.06	81.6	0.11
		1.5	10.2	0.08	134.6	0.08	75.0	0.05	136.3	0.08
		2	0.2	0.07	193.1	0.07	40.7	0.05	195.6	0.07
0.5	0.05	47.3	0.11	0.8	0.68	76.9	0.06	1.8	0.68	
	0.25	80.3	0.14	19.5	0.68	150.5	0.07	44.0	0.40	
	0.5	100.4	0.15	44.4	0.40	100.4	0.15	44.4	0.40	
	1	125.2	0.16	92.1	0.21	163.9	0.07	90.4	0.20	
	1.5	90.7	0.13	137.8	0.14	183.7	0.07	135.3	0.14	
	2	54.4	0.12	193.9	0.11	202.0	0.07	195.1	0.11	

Table 8.2 Results from Parametric Studies Using Lower and Upper Bound Isolated Load Values (25 psf to 50 psf)

R (1)	α (2)	T (s) (3)	25 psf				50 psf			
			D _{ris} (mm) (4)	A _{absi} (g) (5)	D _{rs} (mm) (6)	A _{abss} (g) (7)	D _{ris} (mm) (8)	A _{absi} (g) (9)	D _{rs} (mm) (10)	A _{abss} (g) (11)
1	0	0.05	58.8	0.11	0.5	0.78	69.8	0.09	0.5	0.78
		0.25	98.2	0.14	15.6	1.01	117.9	0.11	15.6	1.01
		0.5	153.9	0.16	50.3	0.81	190.3	0.12	50.2	0.81
		1	196.8	0.18	99.6	0.40	196.7	0.13	99.4	0.40
		1.5	271.1	0.21	142.3	0.26	271.6	0.14	141.9	0.26
		2	329.0	0.23	190.0	0.19	347.0	0.16	188.9	0.19
	0.25	0.05	58.8	0.11	0.5	0.78	69.8	0.09	0.5	0.78
		0.25	98.2	0.14	15.6	1.01	117.9	0.11	15.6	1.01
		0.5	154.0	0.16	50.3	0.81	190.4	0.12	50.2	0.81
		1	197.3	0.18	100.0	0.40	196.9	0.13	99.8	0.40
		1.5	271.2	0.21	142.3	0.26	271.6	0.14	141.9	0.26
		2	329.5	0.23	190.0	0.19	347.5	0.16	188.9	0.19
0.5	0.05	58.8	0.11	0.5	0.78	69.8	0.09	0.5	0.78	
	0.25	98.2	0.14	15.6	1.01	117.9	0.11	15.6	1.01	
	0.5	154.1	0.16	50.3	0.81	190.5	0.12	50.2	0.81	
	1	198.1	0.18	100.4	0.40	197.3	0.13	100.2	0.40	
	1.5	271.2	0.21	142.3	0.26	271.6	0.14	141.9	0.26	
	2	330.0	0.23	190.0	0.19	347.9	0.16	188.9	0.19	
1	0.05	58.8	0.11	0.5	0.79	69.8	0.09	0.5	0.79	
	0.25	98.3	0.14	15.6	1.01	118.0	0.11	15.6	1.01	
	0.5	154.2	0.16	50.3	0.81	190.6	0.12	50.2	0.81	
	1	200.4	0.18	101.2	0.41	198.1	0.13	100.9	0.41	
	1.5	271.3	0.21	142.3	0.26	271.6	0.14	141.9	0.26	
	2	331.0	0.23	190.0	0.19	348.8	0.16	188.9	0.19	
5	0	0.05	56.8	0.10	12.3	0.27	66.2	0.08	12.3	0.27
		0.25	68.1	0.12	37.1	0.25	80.2	0.09	37.1	0.25
		0.5	75.6	0.12	74.8	0.20	89.9	0.10	74.7	0.20
		1	65.9	0.11	103.4	0.10	85.9	0.09	103.2	0.10
		1.5	24.0	0.07	106.4	0.07	42.3	0.07	107.0	0.07
		2	0.9	0.05	179.0	0.05	6.9	0.05	179.7	0.05
	0.25	0.05	59.4	0.11	1.1	0.57	68.9	0.09	1.1	0.57
		0.25	77.9	0.12	17.3	0.44	92.7	0.10	17.3	0.44
		0.5	95.8	0.13	38.9	0.28	106.8	0.10	38.8	0.28
		1	97.4	0.14	75.9	0.14	116.5	0.10	75.8	0.14
		1.5	73.8	0.11	112.3	0.09	96.4	0.09	112.1	0.09
		2	32.1	0.08	148.7	0.07	53.6	0.08	149.1	0.07
0.5	0.05	58.2	0.11	0.7	0.62	68.4	0.09	0.7	0.63	
	0.25	84.1	0.13	15.7	0.61	99.6	0.10	15.7	0.61	
	0.5	111.9	0.14	39.3	0.40	124.4	0.11	39.2	0.40	
	1	132.1	0.15	82.8	0.21	143.4	0.11	82.6	0.21	
	1.5	153.6	0.16	115.4	0.13	173.8	0.12	115.0	0.13	
	2	121.5	0.14	164.1	0.10	152.9	0.11	163.7	0.10	
10	0	0.05	53.8	0.10	19.8	0.24	63.6	0.08	19.8	0.24
		0.25	51.3	0.10	52.7	0.16	62.7	0.08	52.7	0.16
		0.5	51.1	0.10	82.4	0.12	64.1	0.08	82.4	0.12
		1	5.1	0.05	93.9	0.06	13.7	0.05	94.5	0.06
		1.5	0.0	0.05	148.7	0.04	0.0	0.04	149.4	0.04
		2	0.0	0.04	188.3	0.03	0.0	0.04	188.4	0.03
	0.25	0.05	61.3	0.11	1.3	0.61	70.3	0.09	1.3	0.61
		0.25	83.5	0.13	22.5	0.45	100.5	0.10	22.5	0.45
		0.5	95.3	0.14	42.2	0.24	102.5	0.10	42.1	0.24
		1	81.5	0.12	81.5	0.12	103.1	0.10	81.4	0.12
		1.5	51.1	0.10	134.3	0.08	74.0	0.09	134.5	0.08
		2	23.3	0.07	192.9	0.07	40.0	0.07	193.3	0.07
0.5	0.05	57.4	0.10	0.8	0.68	67.3	0.09	0.8	0.68	
	0.25	94.5	0.14	19.5	0.68	105.6	0.10	19.5	0.68	
	0.5	114.2	0.15	44.4	0.40	123.5	0.11	44.4	0.40	
	1	161.1	0.16	91.7	0.21	163.6	0.12	91.4	0.21	
	1.5	169.0	0.17	136.9	0.14	203.6	0.13	136.3	0.14	
	2	127.7	0.14	193.3	0.11	179.7	0.12	193.4	0.11	

8.5 Selected Targeted Parametric Studies

Section 8.4 presented the results of an initial parametric study using coupled model (albeit with a low mass ratio that made it behave like uncoupled one) to determine a preferred range of the parameters defining the primary SDOF structural fuse frame. It suggested that this preferred range consists of parameter values selected as $0.25 \leq \alpha \leq 0.5$, and $5 \leq R \leq 10$. This section focuses on further parametric studies conducted using selected values from the preferred ranges of parameter for 1) checking the effect of interaction between the isolated floor system and the primary base SDOF structural fuse frame, and; 2) investigating the behavior of the combined systems under different mass ratios of the isolated floor system on top to the base structural fuse frame. The selected values of the parameter are: $\alpha = 0.25, 0.5$; $R = 5, 10$, and $T = 0.25 \text{ s}, 0.5 \text{ s}, 1.0 \text{ s}$, which brackets the parameter values used in actual design of SDOF structural fuse frames.

8.5.1 Parametric Study Using Uncoupled Model

Under the selected parameter values above and a mass ratio of 1%, some nonlinear time history analyses were done using uncoupled model to confirm that the interaction between the isolated floor system and the base structural fuse frame is negligible under those cases, through comparison with the results from the three series of preliminary parametric study presented in Section 8.4. The differences between the results from the uncoupled model and the corresponding ones from the corresponding preliminary parametric study using coupled model presented are shown in Tables 8.3 and 8.4, respectively, for systems consisting of structural fuse frames and Isolated Floor System I using polyurethane balls and systems consisting of structural fuse frames and Isolated Floor System II under 0 psf load case. In the footnotes to these two tables, the “ D_{ris} ”, “ A_{absi} ”, “ D_{rs} ”, and “ A_{abss} ” have the same meaning as mentioned in Section 8.4.3. The subscripts “coupled” and “uncoupled” indicate whether the results are obtained using coupled or uncoupled models.

Note from these two tables that the maximum difference in the results between the uncoupled and coupled model is only 5.4% for the difference in the average peak relative displacement between Isolated Floor System I and the base frame, and happens in Table 8.3 for the case $T=1.0$ s, $R=5$, and $\alpha=0.5$, for which T is the same as the natural vibration period of the Isolated Floor System I (i.e., resonant case). All the other differences are less than 3% for Isolated Floor System I, and 1.6% for Isolated Floor System II, which can be negligible. This confirms that, as expected, the interaction between the isolated floor system and the base structural fuse frame is insignificant under a low mass ratio, M_r .

Table 8.3 Difference of the Results between Uncoupled and Coupled Models for Systems Using Isolated Floor System I (Polyurethane Balls)

R (1)	α (2)	T (s) (3)	DD _{ris} * (%) (4)	DA _{absi} ** (%) (5)	DD _{rs} *** (%) (6)	DA _{abss} # (%) (7)
5	0.25	0.25	0.1	0.0	0.4	0.3
		0.5	0.3	0.0	0.3	0.2
		1	2.6	0.0	0.7	1.3
	0.5	0.25	0.1	0.0	0.3	0.3
		0.5	0.8	0.0	0.8	0.5
		1	0.9	0.0	1.3	1.1
10	0.25	0.25	0.0	0.0	0.4	0.3
		0.5	1.0	0.0	0.4	0.6
		1	5.4	0.3	-0.2	0.8
	0.5	0.25	0.1	0.0	0.4	0.3
		0.5	0.4	0.0	0.8	0.7
		1	1.2	0.0	1.5	1.3

* , $DD_{ris}=(D_{ris,uncoupled}-D_{ris,coupled})/D_{ris,coupled}\times 100\%$;

** , $Daabsi=(A_{absi,uncoupled}-A_{absi,coupled})/A_{absi,coupled}\times 100\%$;

*** , $DD_{rs}=(D_{rs,uncoupled}-D_{rs,coupled})/D_{rs,coupled}\times 100\%$;

, $DA_{abss}=(A_{abss,uncoupled}-A_{abss,coupled})/A_{abss,coupled}\times 100\%$.

Table 8.4 Difference of the Results between Uncoupled and Coupled Models for Systems Using Isolated Floor System II (Load Case of 0 psf)

R (1)	α (2)	T (s) (3)	DD _{ris} * (%) (4)	DA _{absi} ** (%) (5)	DD _{rs} *** (%) (6)	DA _{abss} # (%) (7)
5	0.25	0.25	0.1	0.1	0.2	0.3
		0.5	0.4	0.1	0.1	0.4
		1	1.0	0.4	-0.3	0.3
	0.5	0.25	0.3	0.1	0.2	0.2
		0.5	0.5	0.1	0.4	0.5
		1	1.6	0.5	0.4	0.6
10	0.25	0.25	0.2	0.1	0.3	0.4
		0.5	0.8	0.4	0.1	0.3
		1	1.2	0.3	-0.4	0.3
	0.5	0.25	0.3	0.1	0.3	0.4
		0.5	0.5	0.2	0.6	0.7
		1	1.5	0.5	0.5	0.8

* , $DD_{ris} = (D_{ris,uncoupled} - D_{ris,coupled}) / D_{ris,coupled} \times 100\%$;

** , $DA_{absi} = (A_{absi,uncoupled} - A_{absi,coupled}) / A_{absi,coupled} \times 100\%$;

*** , $DD_{rs} = (D_{rs,uncoupled} - D_{rs,coupled}) / D_{rs,coupled} \times 100\%$;

, $DA_{abss} = (A_{abss,uncoupled} - A_{abss,coupled}) / A_{abss,coupled} \times 100\%$.

8.5.2 Parametric Study on Mass Ratio

From the description of the two modeling approaches in Section 8.3, it can be noted that the only difference between these two models is that in the uncoupled model, the interaction between those two SDOF systems is not considered. Section 8.4 confirmed that the uncoupled model can provide accurate results when the mass ratio of the isolated floor system to that of the structural fuse frame is low (e.g., the cases with a mass ratio of 1% was compared above). Here, another parametric study using the selected parameter values mentioned at the beginning of Section 8.5 was conducted this time, to investigate the effect of bigger mass ratios on the response of the combined system (i.e., to investigate the effect of the interaction between the isolated floor system and the structural fuse frame on the response of the combined system). Note that to compare the behavior of the structural fuse frame and the corresponding elastic system, 1.0 was also selected as a value of α . Both the combined systems consisting of SDOF structural fuse frames and Isolated Floor System I (using polyurethane balls and rubber balls, respectively) and those consisting of SDOF structural fuse frames and Isolated Floor System II (the case of load

range of 0 psf to 50 psf) were considered. The values of the mass ratio are selected as: $M_r=0.01$, 0.03, 0.05, 0.07, 0.1, 0.2, 0.3, 0.4, 0.5, 0.6, 0.7, 0.8, 0.9, and 1.0. Note that the results for the cases with $M_r=0.01$ are taken from the study in Section 8.4.

8.5.2.1 Isolated Floor System I

A parametric study was first conducted on systems consisting of structural fuse frames and Isolated Floor System I using polyurethane balls. Note that the same friction coefficient determined for Isolated Floor System I (using polyurethane balls) in Section 8.4.1 was used here. Also, note that in this parametric study, the structural fuse frame was kept the same as in Section 8.4.1, and the only model change was for the isolated floor system. Here, it was just assumed that the floors of multiple rooms, each of which is the same as that used in Section 8.4.1, were isolated corresponding to different mass ratios. For example, for $M_r=0.01$, this case corresponds to the case in Section 8.4.1. When $M_r=0.5$, the model properties for the isolated floor system reflect the corresponding properties that would be obtained in the presence of 50 such isolated floor systems in Section 8.4.1.

The results are shown here as in Figs. 8.8 to 8.11, respectively for the average peak response of D_{ris} , D_{rs} , A_{absi} , and A_{abss} . There are three plots in each of these figures, respectively corresponding to cases with $T=0.25$ s, 0.5 s, and 1.0 s. Note from part b of each of these figures that some additional analyses were also conducted and included here (i.e., cases with additional α values of 0.125 and 0.375 under mass ratios of 0.01 and 1.0).

It can be noted from Fig. 8.8 that the average peak relative displacement between Isolated Floor System I (using polyurethane balls) and the structural fuse frame (i.e., D_{ris}) decreases in all cases with increasing values of M_r . It can also be noted that for a given value of R , D_{ris} is bigger for the cases with bigger values of α , and under a given value of α , D_{ris} is bigger for cases with bigger values for R in most cases (except the cases with parameter sets of $T=0.5$ s,

and 1.0 s, $R=5, 10$, and $\alpha=0.25$, where the reverse trend is observed). In addition, for the cases with T (i.e., 0.5 s and 1.0 s) exceeding T_s (i.e., 0.4 s) where the equal displacement rule applies per NEHRP 2003, the cases with $\alpha=1.0$ (i.e., elastic frame response cases) produced the biggest value for D_{ris} , and the cases with T (i.e., 0.25 s) lower than T_s where the equal energy rule applies per NEHRP 2003, the cases with $\alpha=1.0$ (i.e., elastic cases) produced the smallest value for D_{ris} . Finally, in comparing the three plots in Fig. 8.8, note that in most cases (i.e., except the cases with parameter sets of $T=1.0$, $R=5, 10$, and $\alpha=0.25$) the values of D_{ris} are bigger for cases with bigger T at relatively small values of M_r , and drop faster to lower values of D_{ris} at relatively big values of M_r .

From Fig. 8.9, it can be noted that, in most cases, the average peak relative displacement of the structural fuse frame to the ground (i.e., D_{rs}) first decreases when M_r is relatively low, and then increases (even to a D_{rs} value higher than the corresponding value at $M_r=1\%$) when M_r takes relatively high values. It can also be noted that for a given value of R , D_{rs} is smaller for the cases with bigger values of α . However, for a given value of α , D_{rs} is bigger for cases with bigger values of R . In addition, for the cases with T (i.e., 0.5 s and 1.0 s) exceeding T_s (i.e., 0.4 s) where the equal displacement rule applies per NEHRP 2003, the cases with $\alpha=1.0$ (i.e., elastic frame response cases) produced the biggest value for D_{rs} at relative low values of M_r , and the cases with T (i.e., 0.25 s) lower than T_s where the equal energy rule applies per NEHRP 2003, the cases with $\alpha=1.0$ (i.e., elastic cases) produced the smallest value for D_{rs} . Finally, in comparing of the three plots in Fig. 8.8, note that, with the increasing of M_r , the values of D_{rs} are bigger for cases with bigger T and go up earlier and faster to higher values of D_{rs} .

It can be found from the three plots in Fig. 8.10 that the values of A_{absi} is a constant (i.e., 0.154g) which is determined to be a function of the geometry of the working plates and the friction effects between the polyurethane balls and the concrete working surfaces and from the

edge plates as mentioned in Chapter 7. Note that there are also some cases where A_{absi} is lower than the constant value mentioned above. A closer looking into the data revealed that in these cases, the rolling balls did not roll over to the straight parts of the working surfaces of the concrete plates.

From Fig. 8.11, note that the average peak absolute acceleration response of the structural fuse frame (i.e., A_{abss}) decreases with increases in M_r . It can also be noted that for a given value of R , A_{abss} is bigger for the cases with bigger values of α . However, for a given value of α , A_{abss} is either almost equal or smaller for cases with bigger values of R (except the cases with parameter sets of $T = 0.25$ s, $R = 5, 10$, and $\alpha = 0.5$). In addition, the cases with value of α equal to 1.0 (i.e., elastic frame response cases) give the biggest values for A_{abss} in each plot of Fig. 8.11. Finally, from comparing of the three plots in Fig. 8.11, note that the values of A_{abss} are bigger for cases with smaller T .

The minimum friction coefficient for these isolated floor systems using rubber balls can be found through the same procedure for those using polyurethane balls described in Section 8.4.1. The friction coefficient equation under such cases (as done by Eq. 8.12 for systems using polyurethane balls) can be expressed as:

$$\mu = 0.00004x + 0.0507 + \frac{18.37}{x} \quad (8.23)$$

From Equation 8.19, the smallest friction coefficient can be found to be 0.105 under the load per ball of 677.7 N (152.35 lb) for Isolated Floor System I using rubber balls and was used as the friction coefficient to build the model for the selected parametric study here. The analyses conducted on combined systems using Isolated Floor System I with rubber balls investigated the behavior of this system under different mass ratios mentioned above and the parameter set of $T = 0.5$ s, $R = 5$, and $\alpha = 0.5$. The results are shown in the four parts of Fig. 8.12, respectively corresponding to the results of D_{ris} , D_{rs} , A_{absi} , and A_{abss} . The same trends mentioned above can also be observed from these figures.

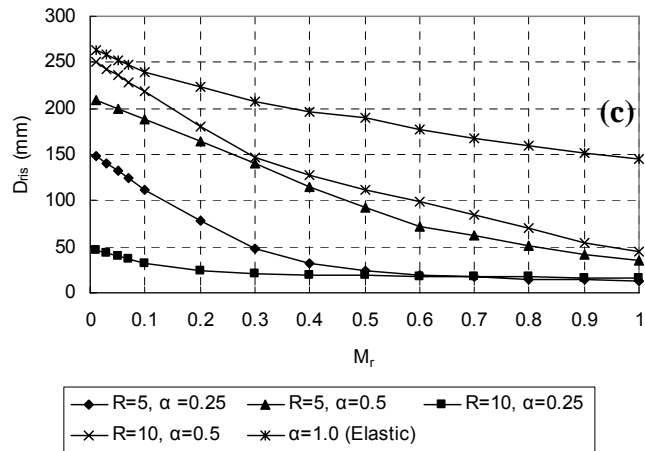
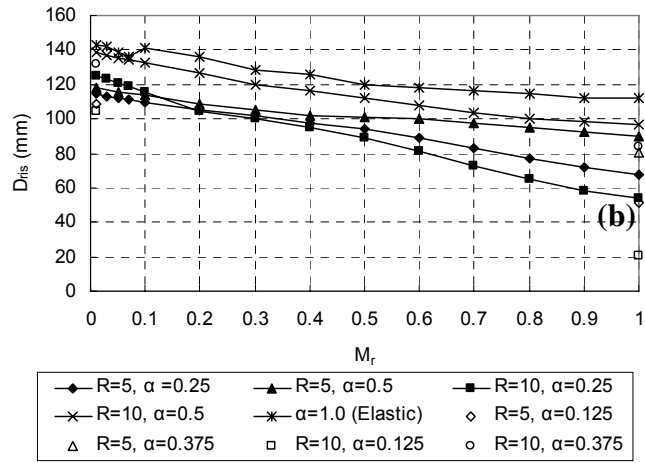
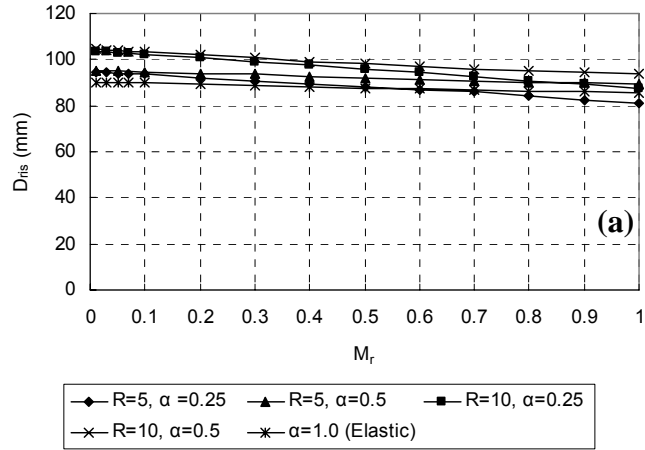


Figure 8.8 Average Peak Relative Displacement Response of Isolated Floor System I to Structural Fuse Frame (D_{ris}): (a) to (c) Respectively Correspond to Cases with $T=0.25s$, $0.5 s$, and $1.0 s$

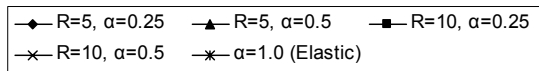
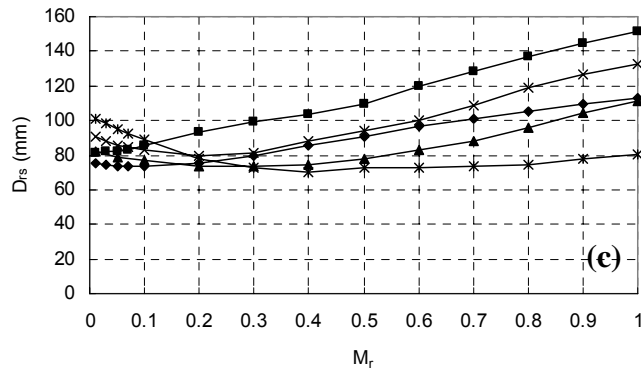
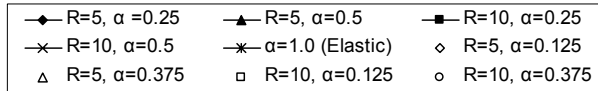
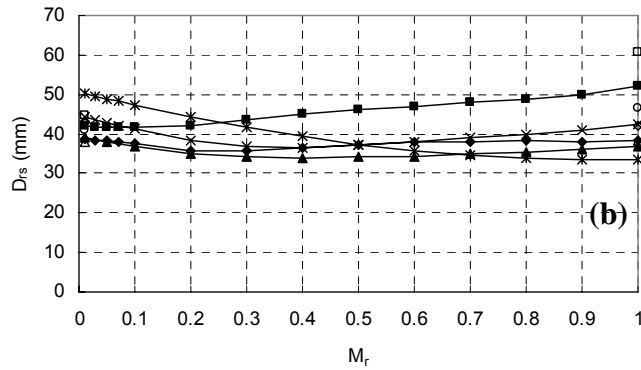
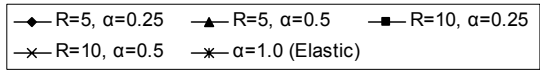
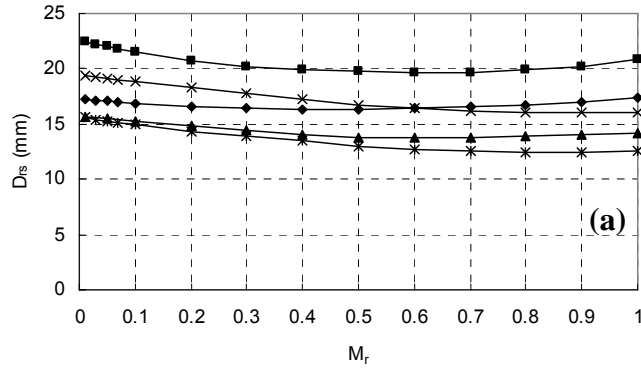


Figure 8.9 Average Peak Relative Displacement Response of Structural Fuse Frame in Systems Using Isolated Floor System I (D_{rs}): (a) to (c) Respectively Correspond to Cases with $T = 0.25s, 0.5 s,$ and $1.0 s$

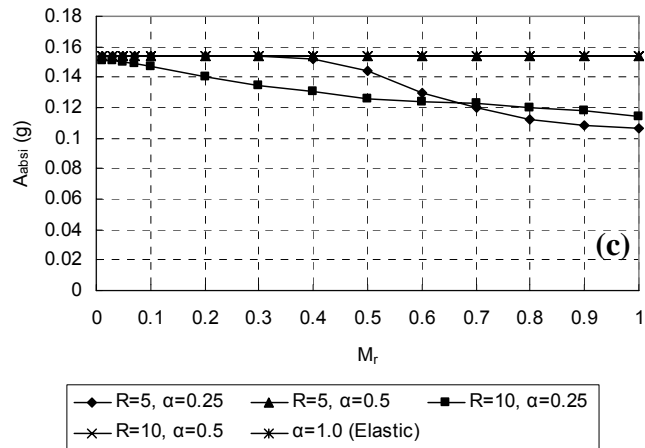
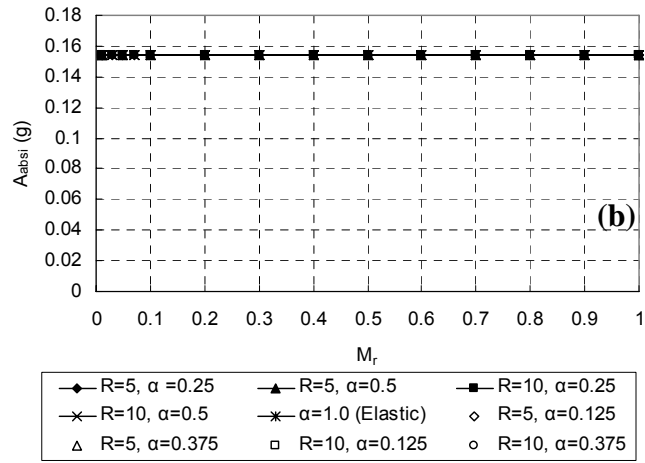
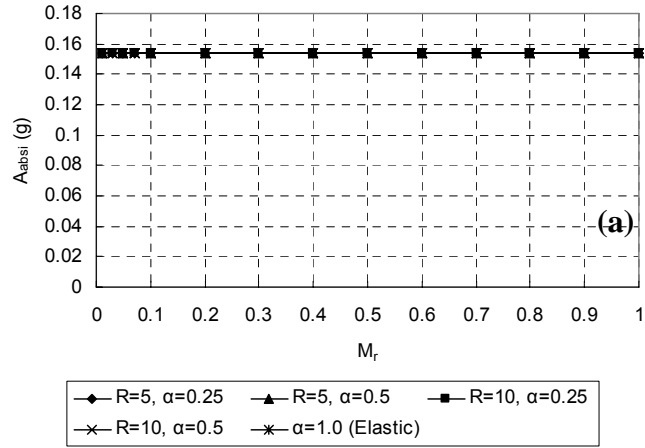


Figure 8.10 Average Peak Absolute Acceleration Response of Isolated Floor System I (A_{absi}):
(a) to (c) Respectively Correspond to Cases with $T=0.25s, 0.5 s,$ and $1.0 s$

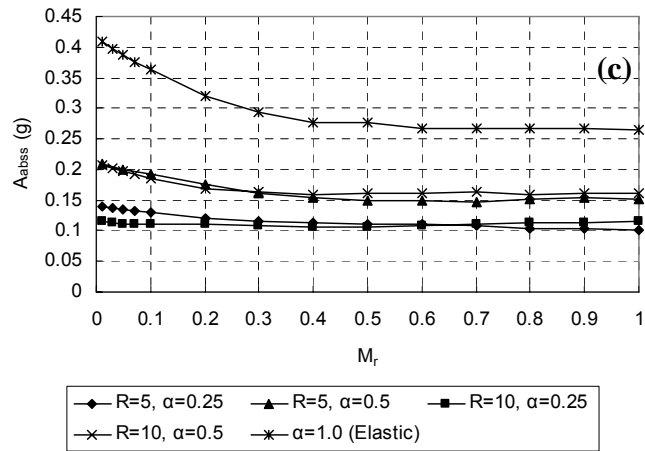
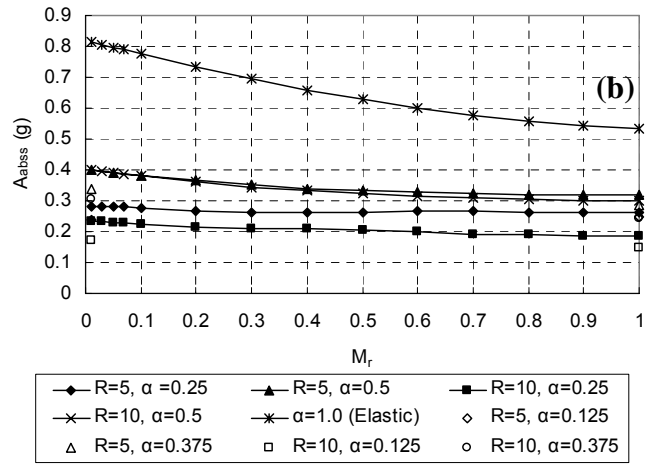
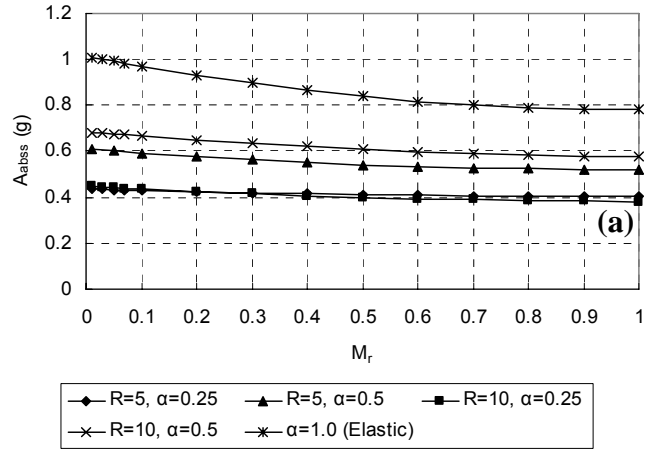


Figure 8.11 Average Peak Absolute Acceleration Response of Structural Fuse Frame in Systems Using Isolated Floor System I (A_{abss}): (a) to (c) Respectively Correspond to Cases with $T=0.25s$, $0.5s$, and $1.0s$

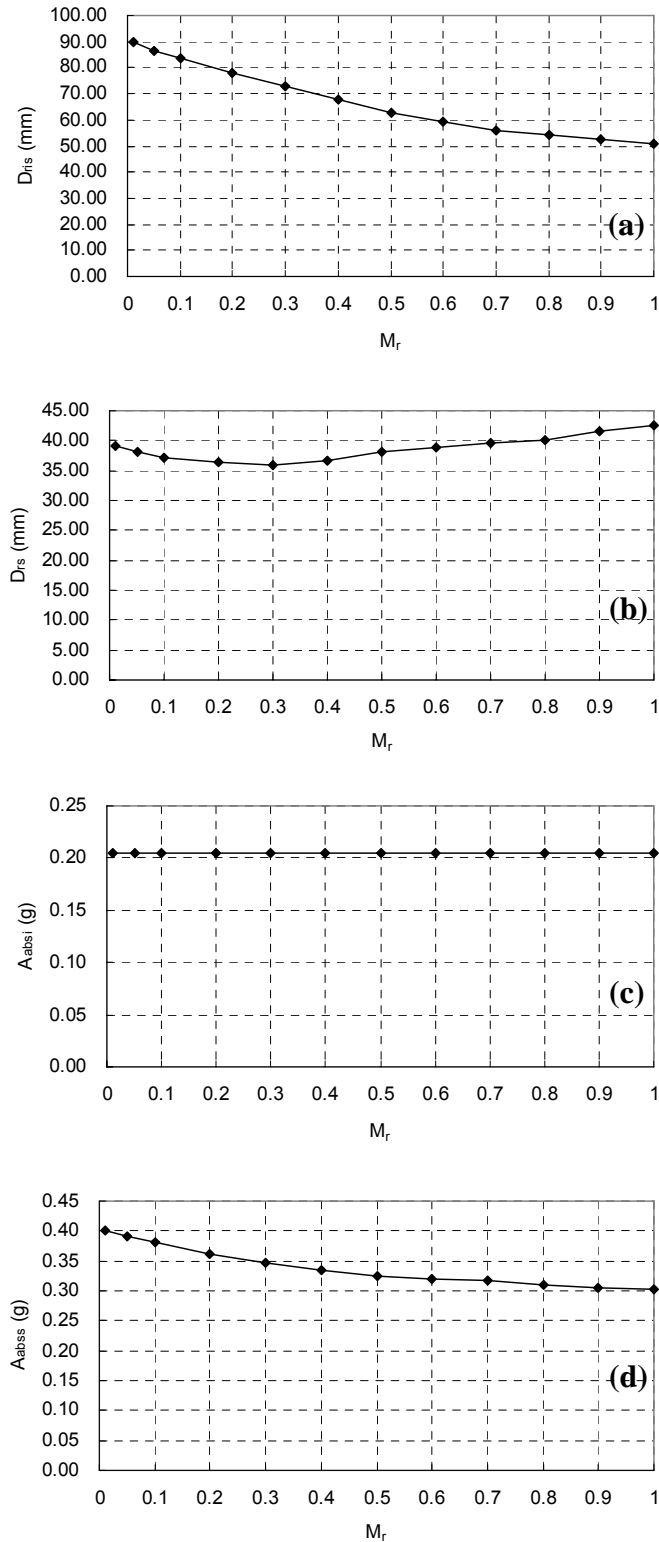


Figure 8.12 Average Peak Responses of Combined System Using Isolated Floor System I with Rubber Balls ($T=0.5$ s, $R=5$, and $\alpha=0.5$): (a) to (d) Respectively Correspond to Results of D_{ris} , D_{rs} , A_{absi} , and A_{abss}

8.5.2.2 Isolated Floor System II

Selected parameter study was then conducted on combined systems using Isolated Floor System II to investigate the effect of mass ratio, M_r , on the behavior of such combined systems. The spring units developed for the load range of 0 psf to 50 psf and the friction effects mentioned in Section 8.4.2, together with the selected parameter values described in the early part of this section, were also used here. Also, note that in this parametric study, the structural fuse frame was kept the same as in Section 8.4.2, and the only model change was for the isolated floor system. Here, it was just assumed that the floors of multiple rooms, each of which is the same as that used in Section 8.4.2, were isolated corresponding to different mass ratios. For example, for $M_r=0.01$, this case corresponds to the case in Section 8.4.2. When $M_r=0.5$, the model just use the property for the isolated floor system corresponding the total property for 50 such isolated floor systems in Section 8.4.2.

The parametric analysis results are shown in Figs. 8.13 to 8.16, respectively corresponding to the results of D_{ris} , D_{rs} , A_{absi} , and A_{abss} . In each of these figures, there are also three plots, respectively corresponding to cases of $T=0.25$ s, 0.5 s, and 1.0 s. Observations on the results are the same as those for the prior selected parametric study on combined systems using Isolated Floor System I with polyurethane balls, with the few differences outlined below:

- 1) For D_{ris} , the cases with $\alpha=1.0$ (i.e., elastic frame response cases) produced the biggest value for D_{ris} regardless of the values of T ;
- 2) The average peak absolute acceleration response (i.e., A_{absi}) of the isolated floor system decrease with the increasing in M_r as shown in Fig. 8.15, which is different than the constant value observed for cases using Isolated Floor System I;
- 3) Under a given value of R , A_{absi} is bigger for the cases with bigger values of α , and under a given value of α , D_{rs} is bigger for cases with bigger values of R (except for cases with parameter sets of $T=0.5$ s and 1.0 s, $R=5$, and $\alpha=0.25$);
- 4) In addition, the cases with $\alpha=1.0$ (i.e., elastic structural fuse frame cases) produced the

biggest value for A_{absi} in each plot of Fig. 8.15;

- 5) Finally, through the comparison of the three plots in Fig. 8.8, note that in most cases (i.e., except the cases with parameter sets of $T=1.0$, $R=5$, 10 , and $\alpha=0.25$) the values of A_{absi} are bigger for cases with bigger T at relatively small values of M_r ;

Since the other trends found here are the same as those observed from the selected parametric study on systems using Isolated Floor System I with polyurethane balls in the early stage of this section, they are not repeated here.

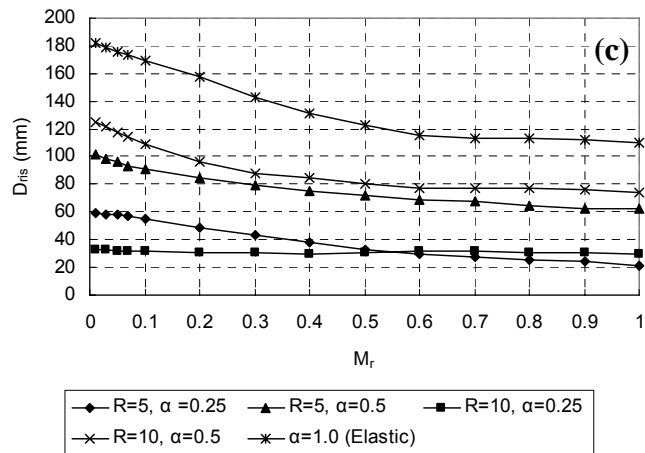
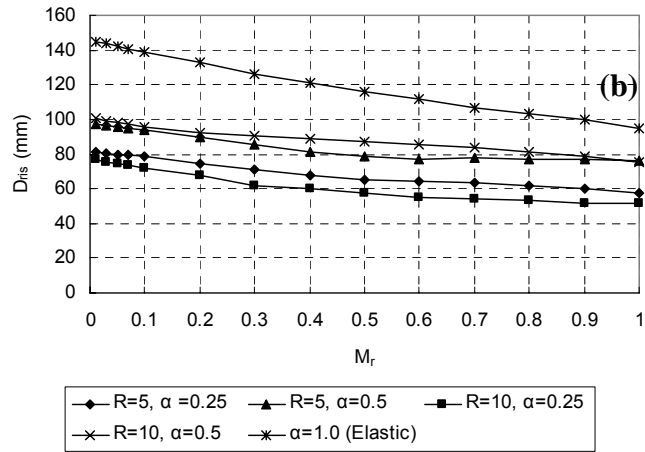
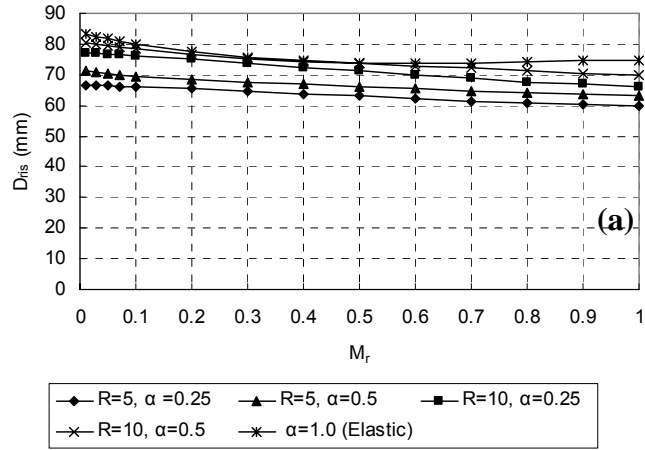


Figure 8.13 Average Peak Relative Displacement Response of Isolated Floor System II to Structural Fuse Frame (D_{ris}): (a) to (c) Respectively Correspond to Cases with $T = 0.25$ s, 0.5 s, and 1.0 s

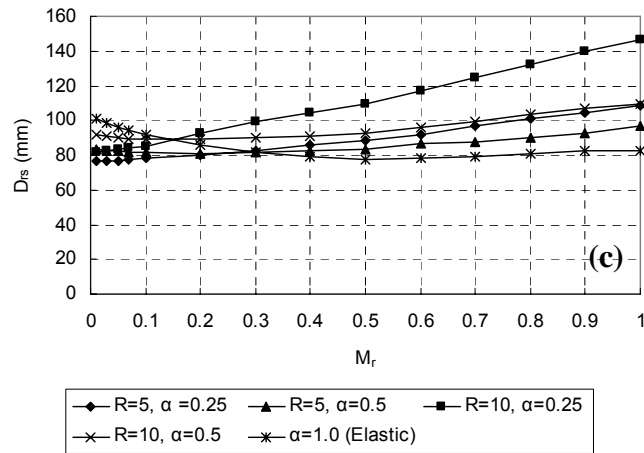
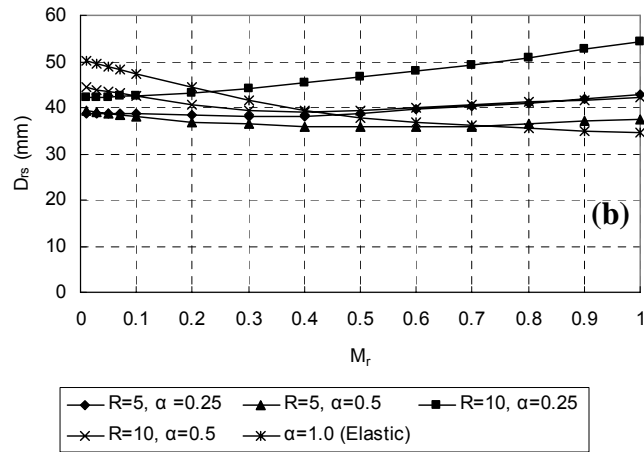
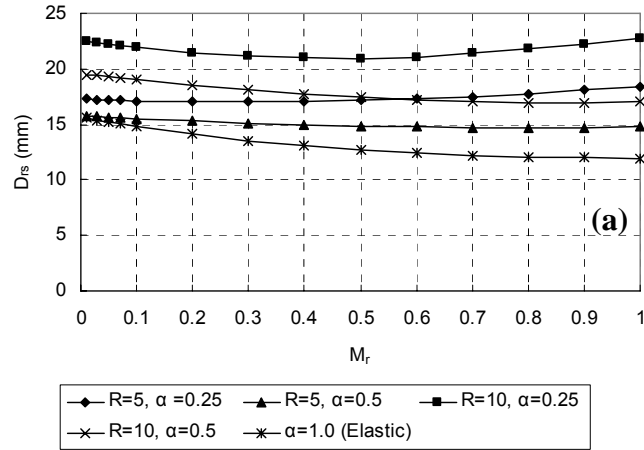


Figure 8.14 Average Peak Relative Displacement Response of Structural Fuse Frame in Systems Using Isolated Floor System II (D_{rs}): (a) to (c) Respectively Correspond to Cases with $T=0.25s, 0.5s$, and $1.0s$

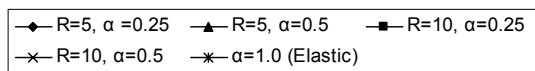
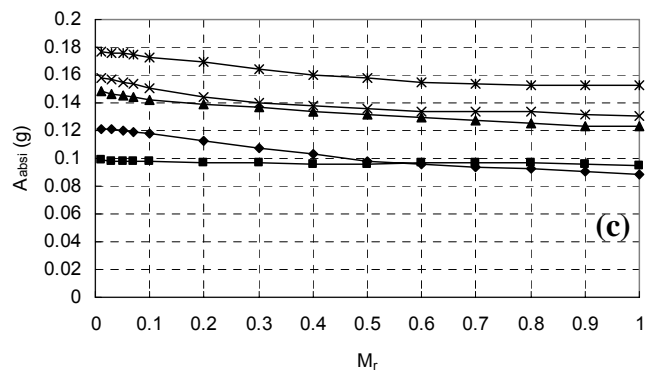
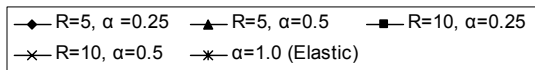
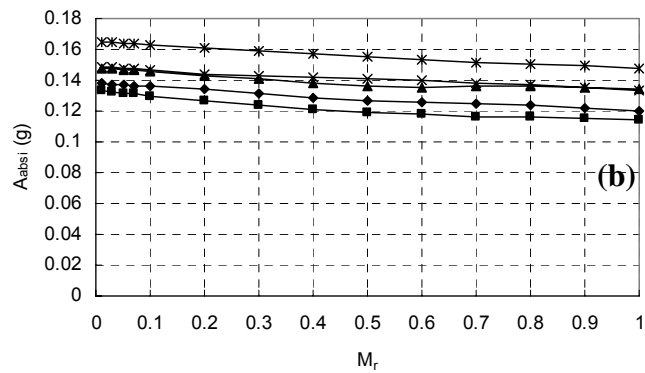
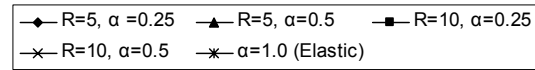
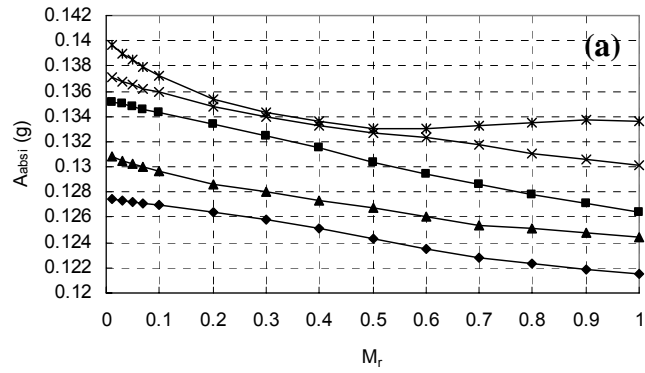


Figure 8.15 Average Peak Absolute Acceleration Response of Isolated Floor System II

(A_{absi}): (a) to (c) Respectively Correspond to Cases with $T=0.25s, 0.5s, \text{ and } 1.0s$

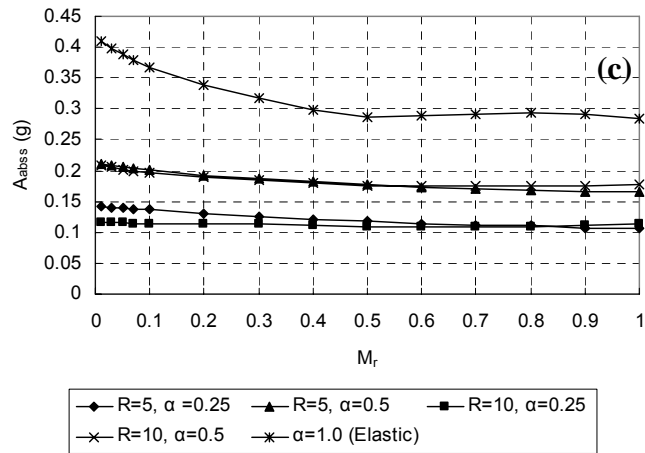
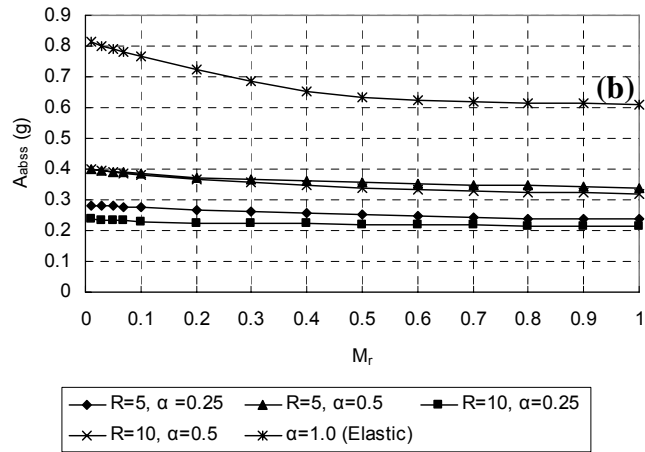
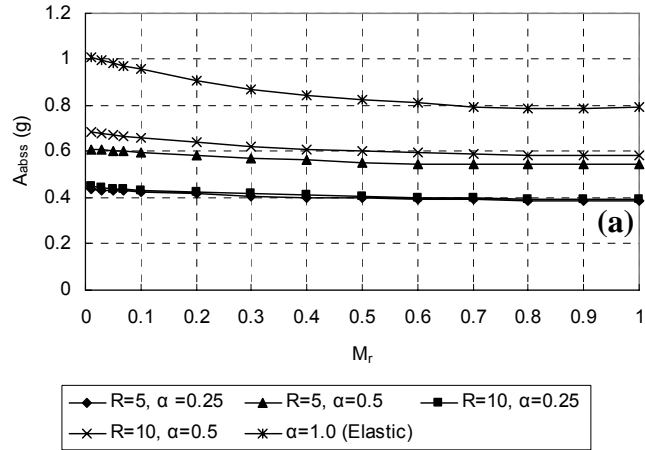


Figure 8.16 Average Peak Absolute Acceleration Response of Structural Fuse Frame in Systems Using Isolated Floor System II (A_{abs}): (a) to (c) Respectively Correspond to Cases with $T=0.25s, 0.5s$, and $1.0s$

8.5.3 Explanation of the Observed Trends

Through the selected targeted parametric study, some trends were observed in Sections 8.5.2. Furthermore, most of the trends, obtained from parametric studies on different systems, are the same. Here, some efforts are made to try to explain these trends in physical terms. Given the complexity of the nonlinearity in the structural system analysis, it is of interest to first investigate the trends in the corresponding elastic systems (i.e., both the isolated floor system and the primary SDOF structural fuse frame are assumed to be elastic). The combined system using Isolated Floor System I is used to show the corresponding trends under elastic assumptions. Mass ratio values of $M_r = 0.01, 0.05, 0.1, 0.2, 0.3, 0.4, 0.5, 0.6, 0.7, 0.8, 0.9,$ and 1.0 are used. A natural vibration period of $T=0.5$ s is selected for the structural fuse frame. Such analysis follows the process for earthquake analysis of linear systems in Chopra (2001) and complete quadratic combination (CQC) rule is used. The results are shown in Figs. 8.17 to 8.20, respectively corresponding to the results for D_{ris} , D_{rs} , A_{absi} , and A_{abss} . Note that in each of these figures, the contributions from modes, together with the total combination of the response quantities, are illustrated. It can be found that:

- 1) As shown in Fig. 8.17, with the increasing values of M_r , the contribution from Mode 1 decreases and the contribution from Mode 2 increases for D_{ris} . The total combination of D_{ris} decreases along with the increases in M_r ;
- 2) Fig. 8.18 shows that the contribution from Mode 1 increases and the contribution decreases along with the increases of M_r . The total combination of D_{rs} first decreases when M_r is relatively low, and then increases when M_r takes relatively high values;
- 3) Fig. 8.19 illustrates that for A_{absi} , the contribution from Mode 1 increases and the contribution of Mode 2 decreases with the increases of M_r . The total combination of A_{absi} decreases along with the increases in M_r ;
- 4) As shown in Fig. 8.20 with the increases in M_r , the contribution from Mode 1 decreases and the contribution from Mode 2 increases for A_{abss} . The total combination of A_{abss}

decreases along with the increases in M_r .

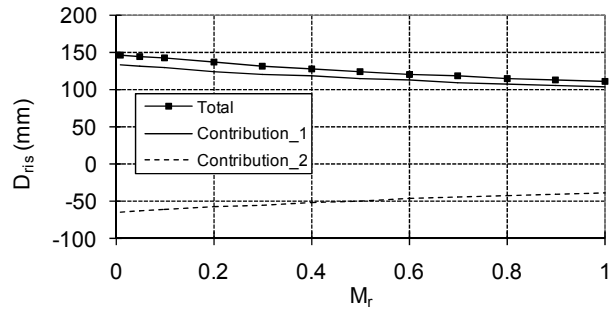


Figure 8.17 Analysis Results of Systems Using Isolated Floor System I: D_{ris}

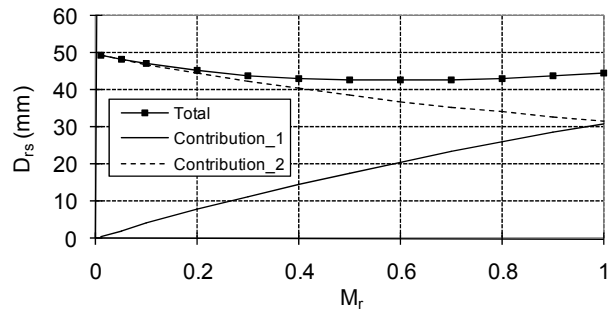


Figure 8.18 Analysis Results of Systems Using Isolated Floor System I: D_{rs}

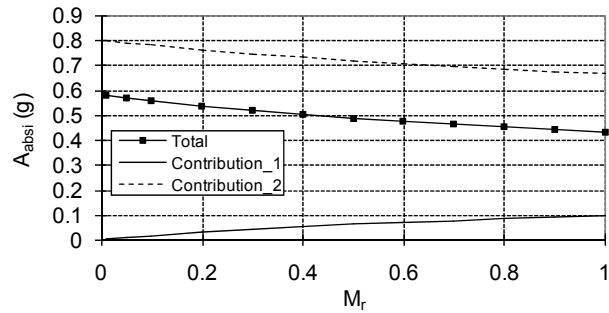


Figure 8.19 Analysis Results of Systems Using Isolated Floor System I: A_{absi}

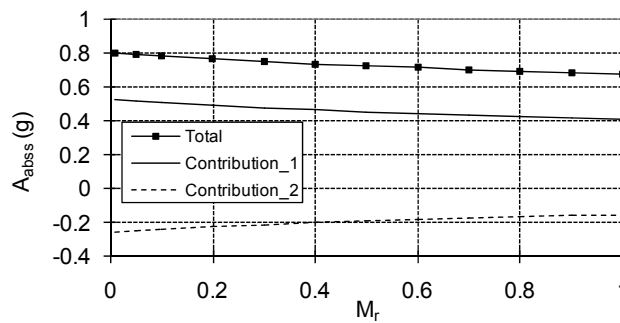


Figure 8.20 Analysis Results of Systems Using Isolated Floor System I: A_{abss}

These observations agree with the corresponding ones described in Section 8.5.2, except for A_{absi} . Along with the increases in M_r , the value of A_{absi} for Isolated Floor System I decreases instead of keeping a constant value found in Section 8.5.2. This is because the isolated floor system here is assumed to be an elastic system as mentioned at the beginning of this section while the property of the isolated floor system I was input as nonlinear behavior in Section 8.5.2.

The above shows the investigation of the behavior of elastic combined system along with the increasing values of M_r . However, this modal combination approach cannot be directly used for the analysis of combined systems with nonlinear behaviors, which may be the topic of the future research. The following shows the efforts made to explain the observations in Section 8.5.2 using different approaches.

Note that all the results presented in Section 8.5.2 are the average peak response values from the nonlinear time history analyses on the corresponding systems using the seven synthetic acceleration time histories. The trends found there are from these averaged values. In some individual cases, out of the seven cases separately subjected to the seven synthetic accelerograms, the behavior of the combined structural system shows a trend which is reverse to the one observed from the corresponding averaged value. However, the individual value in the opposite direction is so small that it cannot significantly affect the average results which are in the direction of most peak response values responding in the same direction. Also, in some cases, the trend observed at large values of M_r is reverse to the one observed at relatively small values of M_r . This is attributed to the fact that more cases among the seven cases behave in a trend which is reverse to the ones observed at relatively small values of M_r . It may be because the mass ratio affects the response phases of both the isolated floor and the base frame. Here, a couple of typical cases are used as examples to show how the phase conditions may induce different response trends. The system consisting of Isolated Floor System I using polyurethane balls with parameter set of $T=0.5$ s, $R=5$, and $\alpha=0.5$ is used in this example. The value of

M_r was separately taken as 0.01 and 1.0. Figs. 8.21 and 8.22 illustrate the responses of the isolated floor D_{ri} , the structural fuse frame D_{rs} , and the relative displacement between these two D_{ris} for these two cases, respectively. The peak response points for D_{rs} and D_{ri} are identified in these two figures. Note that the two peak values are not reached at the same time. The maximum displacement of the structural fuse frame (i.e., D_{rs}) when subjected to one of the artificial seismic motions is 41.5 mm in the case with $M_r=0.01$, and decreases to 28.0 mm in the case with $M_r=1.0$.

It can be noted from Fig. 8.21 that before D_{rs} reaches its peak value, the structural fuse frame moves in the positive direction, the isolated floor on top moves in the negative direction and the relative displacement between these two is increasing. This motion condition indicates that the isolated floor system is trying to stop the motion of the structural fuse frame in the positive direction. This corresponds to a trend of decreasing the peak value of D_{rs} and decreasing the peak value of the absolute acceleration of the structural fuse frame accordingly.

Fig. 8.22 illustrates that before D_{rs} reaches its peak value, both the structural fuse frame and the isolated floor on top move in the positive direction, and the relative displacement between these two is increasing (i.e., the isolated floor moves faster than the structural fuse frame). This motion condition indicates that the isolated floor system is trying to drag the structural fuse frame to move more in the positive direction. This corresponds to a trend of increasing the peak value of D_{rs} and increasing the peak value of the absolute acceleration of the structural fuse frame accordingly.

To show the phase change of the motion of the structural fuse frame under different M_r in a more explicit manner, the comparison of the displacement time history between the two cases with $M_r=0.01$ and 1.0 is shown in Fig. 8.23.

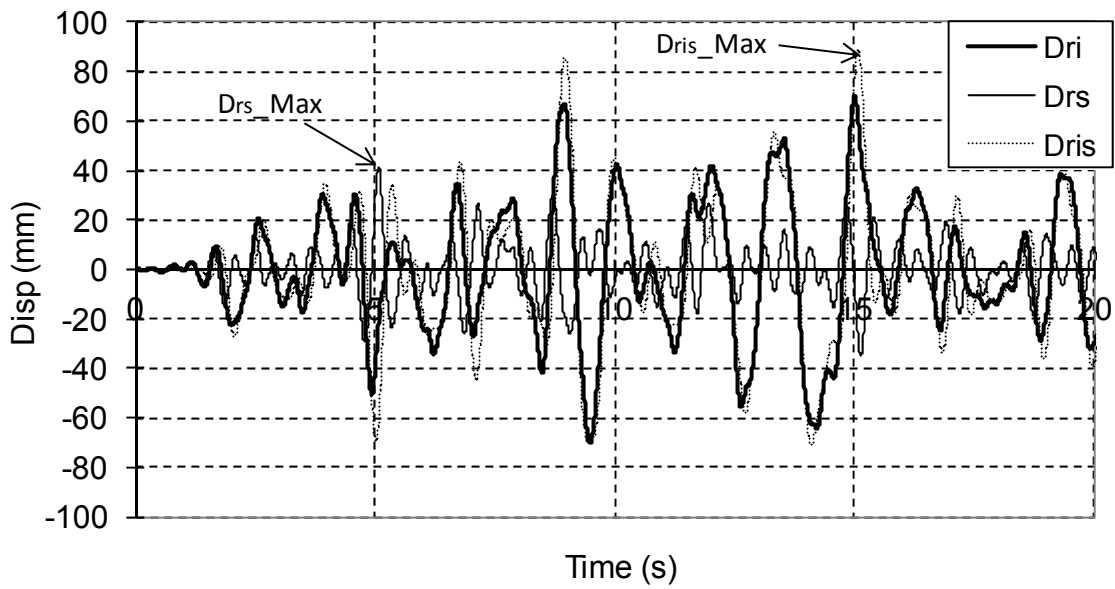


Figure 8.21 Displacement Responses of System Using Isolated Floor System I: $M_r = 0.01$

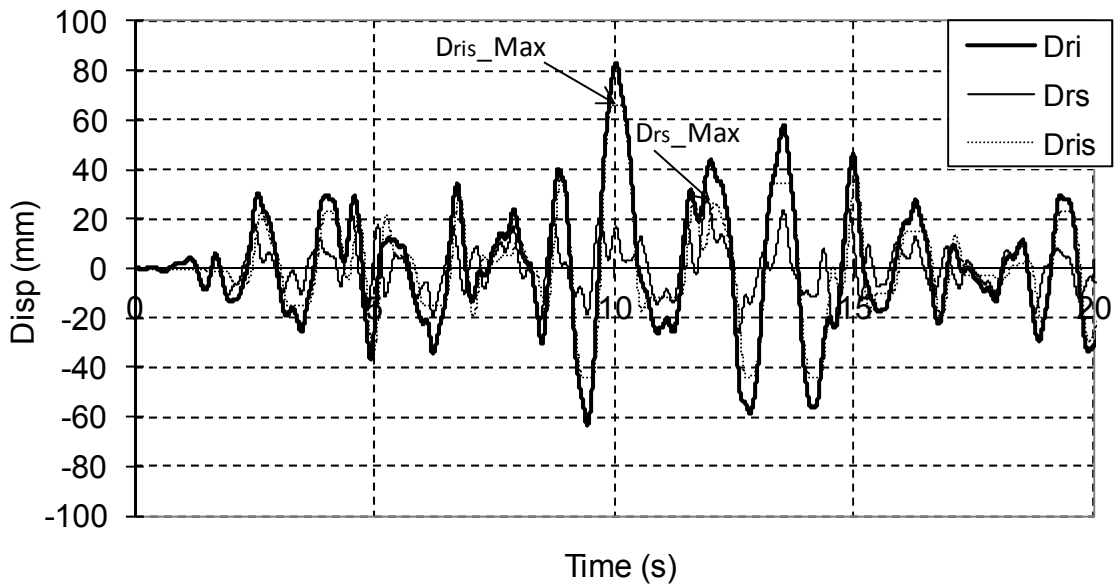


Figure 8.22 Displacement Responses of System Using Isolated Floor System I: $M_r = 1.0$

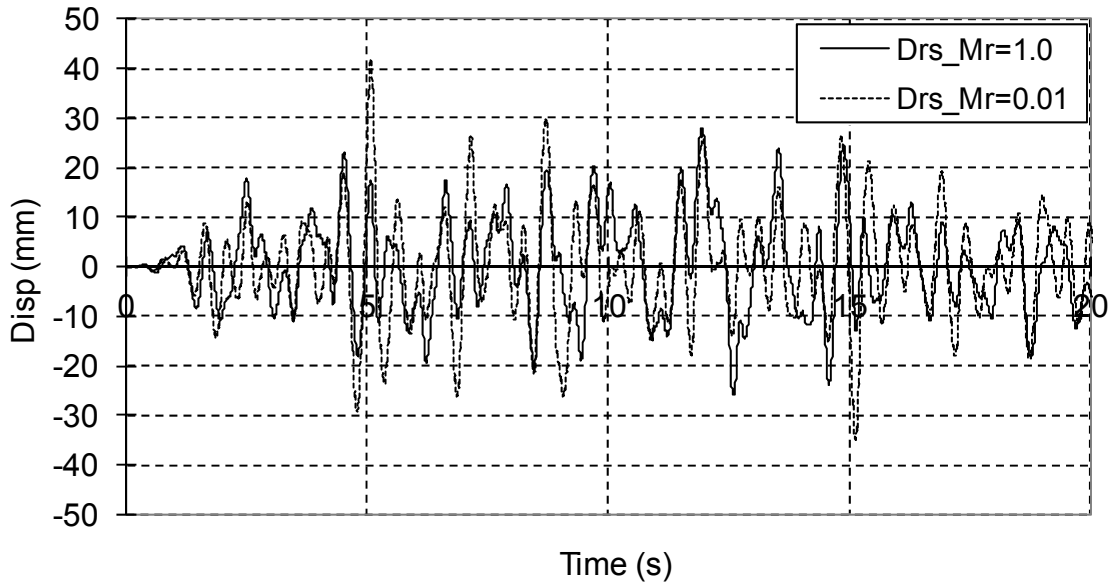


Figure 8.23 Comparison of Displacement Responses of Structural Fuse Frame

In addition, the trends observed in Section 8.5.2 can be attributed to the fact that the mass ratio introduces changes to the energy flow in the combined system. Here, as an example, the hysteretic energy flow history of a combined system consisting of a SDOF structural fuse frame and an Isolated Floor System I, using polyurethane balls with a parametric set of $T=0.5$ s, $R=10$, $\alpha=0.5$ and under mass ratios of 0.01, and 1.0, is calculated following the definition and energy calculation process described in Christopoulos and Filiatrault (2006). Such calculation is based on the results from time history analysis using one specific synthetic seismic motion as input, where the weight of the isolated floor system was selected to be 1 time and 100 times the value of 23 kN (5171 lb), corresponding to cases with $M_r=0.01$ and 1.0, respectively. The values of D_{ris} , D_{rs} are, respectively, 95.9 mm and 45.4 mm for the case with $M_r=0.01$, and 67.2 mm and 35.5 mm for the case with $M_r=1.0$. This indicates that both D_{rs} and D_{ris} decrease with the increase in M_r from 0.01 to 1.0. The calculated hysteretic energy history for both the isolated floor, Eh_Iso (which is directly related to the relative displacement response to the structural fuse frame), and the base frame, Eh_str (which is directly related to the

deformation of the structural fuse frame) are shown respectively as the two parts of Figure 8.24.

Note from Fig. 8.24 that the maximum hysteretic energy of the isolated floor system corresponding to the case with 1.0 is equal to 45 times the value for the case with $M_r=0.01$, and that the maximum hysteretic energy of the base structural fuse frame corresponding to the case with $M_r=1.0$ is 0.91 times the value for case with $M_r=0.01$.

If the response of the isolated floor when $M_r=1.0$ is the same as that when $M_r=0.01$, the maximum hysteretic energy of the isolated floor corresponding to $M_r=1.0$ should be 100 times of the hysteretic energy in the case when $M_r=0.01$. However, as mentioned above, the actual value obtained is only 45 times larger. This may be because the maximum displacement response of the isolated floor decreases in the case when $M_r=1.0$, as found from the nonlinear time history analysis results. In a similar way, if the response of the structural fuse frame when $M_r=1.0$ is the same as that when $M_r=0.01$, the maximum hysteretic energy of the structural fuse frame will be equal to that in the case when $M_r=0.01$. However, as mentioned above, the maximum hysteretic energy in the case with $M_r=1.0$ is smaller than that when $M_r=0.01$. It may be because the maximum relative displacement response, D_{rs} , of the structural fuse frame decreases in this case, as observed from the nonlinear time history analysis results. This method is called the “energy check method” in this report. As shown above, it can be used to partially explain the trends observed from results of nonlinear response history analysis. However, due to the complexity of the nonlinearity in the structural system analysis, the complete explanation (in physical terms) of all the observations found in Section 8.5.2 goes beyond the scope of the current research, and may be the subject of future research.

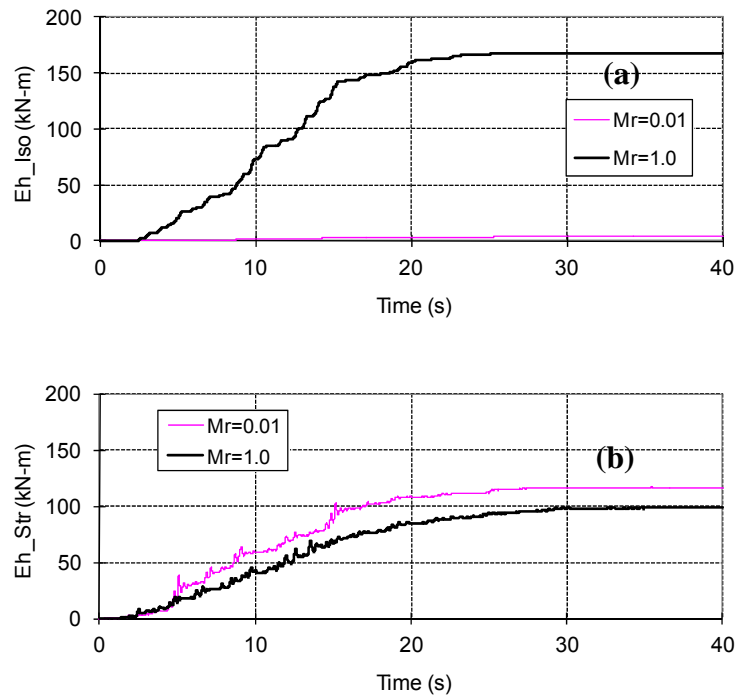


Figure 8.24 Energy Flow Time Histories: (a) and (b) Respectively Correspond to the Histories of Hysteretic Energy of the Isolated Floor System and Hysteretic Energy of the Structural Fuse Frame

8.6 Observations

This chapter presented the results of parametric studies on combined systems consisting of SDOF structural fuse frames and isolated floor systems, subjected to seven synthetic spectra compatible acceleration time histories as the ground seismic motions. An initial parametric study on combined systems respectively using Isolated Floor Systems I and II together with the primary SDOF structural fuse frame was first conducted. The coupled models and a mass ratio of 0.01 were adopted. From this initial parametric study, the acceptable range of the three parameters defining the structural fuse frame (i.e., T , R , and α) were found, and based on this range, a preferred range (in which most cases satisfying the structural fuse concept fall) for the three parameters was also recommended for the design of structural fuse frames, namely:

$5 \leq R \leq 10$, $0.25 \leq \alpha \leq 0.5$, and no limit is set for T at this time.

For the cases including Isolated Floor System II, two spring units were developed by separately using the lower bound load value of two gravity load ranges: 0 psf to 50 psf, and 25 psf to 50 psf. From the comparison of the results from cases with the lower bound load value and upper bound load value of each gravity load range, it is found that the acceleration response of the isolated floor system from cases under upper bound gravity load is smaller than that obtained from cases under the lower bound load condition. However, the displacement response under the upper bound gravity load is bigger than that using the lower bound load.

After the initial parametric study, selected targeted parametric studies were conducted. The results from the parametric study using uncoupled models and a mass ratio of 0.01 were compared with those from the corresponding cases using coupled models. It is observed that the results from these two kinds of models under a low mass ratio are almost same, confirming that the interaction between the isolated floor system and the primary SDOF structural fuse frame is insignificant when the mass ratio is small.

Using the parameter values selected from the preferred range, more parametric studies were conducted on systems, respectively using Isolated Floor System I (respectively using polyurethane and rubber balls) and II together with the structural fuse frame, to investigate the effect of the mass ratios on the response of such combined systems. A number of trends observed for the response quantities with respect to the mass ratio and the three parameters defining the structural fuse frame. These trends can be used in the design of the combined systems consisting of the isolated floor systems and the structural fuse frames which is the topic of Chapter 9.

The trends found for combined systems using Isolated Floor System I are:

- 1) For D_{ris} , it was found that, with increasing the values of the mass ratio M_r , D_{ris} decreases. Under same value of R , D_{ris} is bigger for the cases with bigger values of α ,

and under same value of α , D_{ris} is bigger for cases with bigger values of R in most cases. In addition, in most cases, the values of D_{ris} are bigger for cases with bigger T at relatively small values of M_r , and drop faster to lower values of D_{ris} at relatively big values of M_r ;

- 2) For D_{rs} , in most cases, D_{rs} first decreases when M_r is relatively low, and then increases (even to a D_{rs} value higher than the corresponding value at $M_r=1\%$) when M_r takes relatively high values. It is also found that for a given value of R , D_{rs} is smaller for the cases with bigger values of α . However, for a given value of α , D_{rs} is bigger for cases with bigger values of R . In addition, with the increase values of M_r , the values of D_{rs} are bigger for cases with bigger T and go up earlier and faster to higher values of D_{rs} ;
- 3) For A_{absi} , note that the values of A_{absi} is a constant value as long as the rolling balls run into the straight part of the working surfaces of the concrete BNC isolators' working plates, and;
- 4) For A_{abss} , note that with the increase in M_r , A_{abss} decreases. Also, for a given value of R , A_{abss} is bigger for the cases with bigger values of α . However, under a given value of α , A_{abss} is either almost equal or smaller for cases with bigger values of R in most cases. In addition, the values of A_{abss} are found to be bigger for cases with smaller T .

For cases using Isolated Floor System II, most of the observations are the same as mentioned above for systems including Isolated Floor System I except for:

- 1) The average peak absolute acceleration response (i.e., A_{absi}) of the isolated floor system decrease with the increasing in M_r , which is different from the constant value observed for cases using Isolated Floor System I;
- 2) Under a given value of R , A_{absi} is bigger for the cases with bigger values of α , and under a given value of α , D_{rs} is bigger for cases with bigger values of R ;
- 3) In most cases the values of A_{absi} are bigger for cases with bigger T at relatively small values of M_r .

Some efforts were made to explain the trends observed in the parametric studies. Given the complexity of the nonlinearity in the structural system analysis, the behavior of the elastic systems was first studied using modal the combination method. Same trends in the behavior as those from the parametric studies were found except for A_{absi} because the isolated floor was assumed to be an elastic system. For non-linear systems, both phase check and energy check methods were used to partially explain the trends observed from the parametric studies; based on those approaches, the change in the response quantities along with the change in the mass ratio were attributed to the phase change of the motions and the change in the energy flow of the systems. However, given the complexity of the nonlinearity in the structural system analysis, a complete explanation of all the trends for the response quantities found from the parametric studies needs further research.

CHAPTER 9

DESIGN METHODOLOGY FOR SYSTEMS CONSISTING OF SINGLE-DEGREE-OF-FREEDOM STRUCTURAL FUSE FRAMES AND ISOLATED FLOOR SYSTEMS

9.1 Introduction

Chapter 8 highlighted a number of trends in response as a result of parametric studies on the combined systems consisting of single-degree-of-freedom (SDOF) structural fuse frames and isolated floor systems. This chapter focuses on the development of design concepts for such combined systems based on these observed response trends and the findings in other previous chapters.

Corresponding to the two methods of modeling used in those parametric studies described in Chapter 8, two design procedures are developed in this chapter: a linear static method and a nonlinear response history method. Note that these two methods are named based on whether the isolated floor system design requires a nonlinear response history analysis. Also note that a nonlinear response history analysis is needed for the design of the SDOF structural fuse frame in both methods. The systems using Isolated Floor System I and those with Isolated Floor System II are separately considered. These two design methods are illustrated through design examples. In addition, a comparison is made between the resulting designs obtained from the two methods for each kind of isolated floor system. This comparison will show that a design obtained per the

linear static method is on the conservative side when the mass ratio (being defined as the mass of the isolated floor system divided by that of the SDOF structural fuse frame) is low. The design methodology developed in this chapter for combined systems of SDOF structural fuse frames and isolated floor systems provides a basis for the development of design concept for systems consisting of multi-degree-of-freedom (MDOF) structural fuse frames and isolated floor systems, which can be the topic of future research.

9.2 Design Methodology For Systems Consisting of SDOF Structural Fuse Frames and Isolated Floor System I

9.2.1 Linear Static Method

The linear static method has been widely used in the design of seismically isolated structure and structures with damping systems (NEHRP 2003, Lee et al. 2007). This method is also adopted here for the design of the combined systems consisting of SDOF structural fuse frames and Isolated Floor System I. Note that this method does not consider the interaction between the isolated floor system and the structural fuse frame. So it is suitable for the design case with a low mass ratio of the isolated floor system to the structural fuse frame, under which the interaction between these two SDOF systems is insignificant as observed in Chapter 8. The flow chart of this method is shown in Fig. 9.1. Note that although the design of the isolated floor system does not need a nonlinear response history analysis in this method, the design of the SDOF structural fuse frame requires a nonlinear response history analysis. The following describes each step of this design method in detail. Note that Steps 1 to 12 of the design procedure in Fig. 9.1 and the following descriptions regarding these steps are almost the same as those in Vargas and Bruneau (2006a) except for the parameters required to define the structural fuse frame and the change of orders here for steps 2 and 3 in Vargas and Bruneau (2006a).

- Step 1. Define the allowable drift as the upper limit of the lateral deformation, Δ_a , which is usually expressed as a percentage of the story height, H ;
- Step 2. The values of the parameters, α and R , are selected. From the parametric studies in Chapter 8, note that the preferred range of the values for these two parameter is: $0.25 \leq \alpha \leq 0.5$ and $5 \leq R \leq 10$;
- Step 3. Determine the elastic period limit, T_L , corresponding to the drift limit from the target design spectrum, using Eq. 9.1 for flexible cases where $T_L \geq T_s$, and Eq. 9.2 for stiff systems where $T_L < T_s$. After T_L is determined, select the elastic period of the frame, T ;

$$T_L = \frac{4\pi^2}{S_{D1}} S_d \quad (9.1)$$

$$T_L = \frac{(1-R)T_s + \sqrt{(R-1)^2 T_s^2 + \frac{16\pi^2 R \Delta_a}{S_{DS}}}}{2} \quad (9.2)$$

Eqs. 9.1 and 9.2 are derived from the following procedure. As per the provisions in NEHRP 2003, in the constant velocity region (i.e., $T \geq T_s$) of the acceleration response spectrum, the equal displacement theory applies: the maximum displacement of a given nonlinear structure is assumed approximately to be equal to the maximum displacement of the corresponding linear elastic structure. Then, the allowable drift can be converted to a corresponding period limit by Eq. 9.1 where S_d is the elastic spectral displacement equal to the design drift limit. However, for the constant acceleration range (i.e., $T < T_s$), the equal energy theory is considered. The inelastic displacement can be obtained from the spectra displacement by multiplying a factor as shown in Eq. 9.3, where S_d is the elastic spectral displacement and Δ_a is the

allowable design drift. Then, T_L can be back calculated from this equation to get Eq. 9.2;

$$\Delta_a = \frac{S_d \left[1 + (R-1) \frac{T_s}{T_L} \right]}{R} \quad (9.3)$$

Step 4 Given the mass, m , and the response modification factor, R , calculate the required yield base shear as:

$$V_y = \frac{mS_a}{R} \quad (9.4)$$

where, S_a is the spectral acceleration corresponding to the selected structural period, T .

Step 5 Following Eq. 9.5-9.7, calculate the target stiffness for the structure, K_1 , the bare frame, K_f , and the damping system, K_a , respectively,

$$K_1 = \frac{4\pi^2}{T^2} m \quad (9.5)$$

$$K_f = \alpha K_1 \quad (9.6)$$

$$K_a = (1-\alpha)K_1 \quad (9.7)$$

Step 6. Determine the yield displacement for the damping system, Δ_{ya} , and for the bare frame, Δ_{yf} , respectively, as:

$$\Delta_{ya} = \frac{V_y}{K_1} \quad (9.8)$$

$$\Delta_{yf} = R\Delta_{ya} \quad (9.9)$$

Step 7. Calculate the base shear capacity for the frame, V_{yf} , and the damping system, V_{ya} , respectively, as:

$$V_{yf} = K_f \Delta_{yf} \quad (9.10)$$

$$V_{ya} = K_a \Delta_{ya} \quad (9.11)$$

Step 8 Design the bare frame and structural fuse elements to match as close as possible to the stiffness and the base shear capacity required by Eqs. 9.6, 9.7, 9.10, and 9.11. To do this for a pinned-base single-bay, one-story SDOF frame, the lateral stiffness, K_f , shear capacity, V_{yf} can be calculated using Eqs. 9.12 and 9.13. The required beam plastic modulus, Z_B , can be obtained from Eq. 9.13 given the story height, H , and the frame steel yield stress, F_{yf} . Then, it is allowed to select a beam section with a plastic modulus as close as possible to this calculated value. From Eq. 9.12, the required moment of inertia for the column, I_C , may be calculated given the story height, H , the bay length, L , and the beam moment of inertia, I_B , corresponding to the selected plastic modulus, Z_B .

$$K_f = \frac{12EI_C}{H^3} \left[\frac{1}{2 + \frac{I_C L}{I_B H}} \right] \quad (9.12)$$

$$V_{yf} = \frac{2F_{yf}Z_B}{H} \quad (9.13)$$

For the selection of the metallic fuse element sizes and properties, a one-bay, one-story SDOF frame with a pinned-base and braced with buckling-restrained-braces (BRBs), as shown in Fig. 9.2 (from Vargas and Bruneau, 2006a), is selected as an example here. Then, as shown in Vargas and Bruneau (2006a), the metallic damper lateral stiffness, K_a , base shear capacity, V_{ya} , and yield deformation, Δ_{ya} , can be calculated following Eqs. 9.14 to 9.16. Area of BRBS can be determined from Eq. 9.14 for the selection of a plate cross sectional area. The required steel yield strength for the braces may be determined by using Eq. 9.15. For cases using other metallic energy dissipation devices mentioned, such as triangular added damping and stiffness (TADAS) devices and shear plates (SP), the selection of metallic damping element sizes and properties should follow the corresponding

equations shown in Vargas and Bruneau (2006a);

$$K_d = \frac{4A_b E}{L} \cos^3(\theta) \quad (9.14)$$

$$V_{ya} = 2F_{yd} A_b \cos(\theta) \quad (9.15)$$

$$\Delta_{ya} = \frac{F_{yd} L}{2E \cos^2(\theta)} \quad (9.16)$$

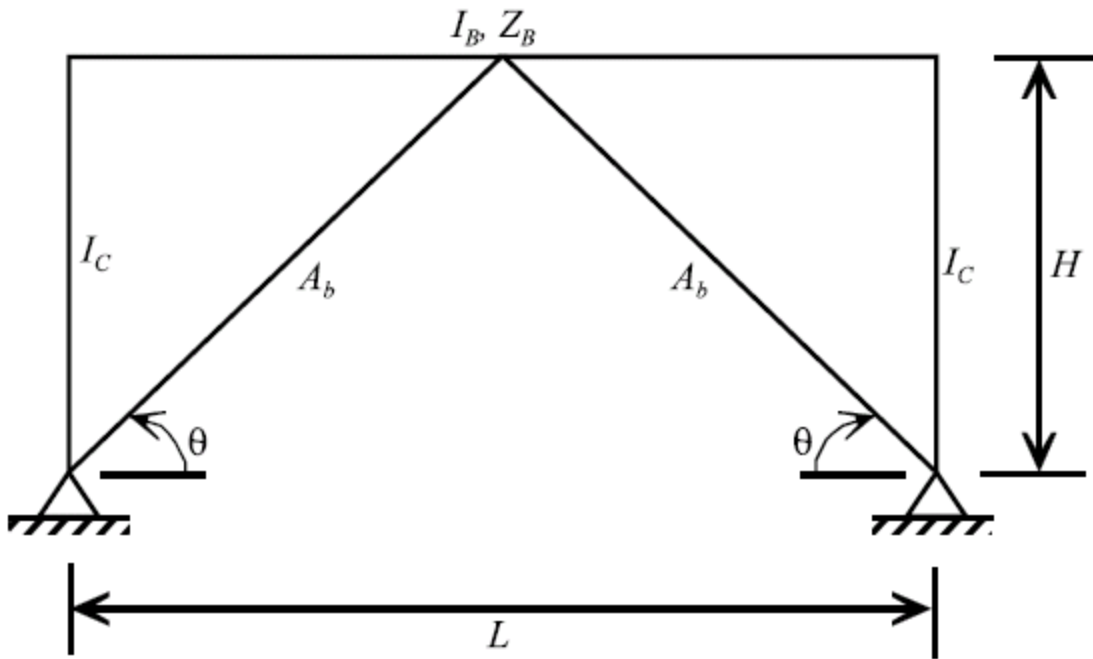


Figure 9.2 Frame and BRB Properties (from Vargas and Bruneau (2006a))

Step 9. Recalculate the values for parameters, α , R , and T , from the actual structure properties obtained in Step 8. From Chapter 8, the maximum displacement ductility, μ_{\max} is equal to the response modification factor, R , when $T \geq T_s$. Then in theory, if the R (i.e., μ_{\max}) is over the target, the bare frame will yield and the structural

fuse concept will not be valid. For cases with $T < T_S$, μ_{\max} should be calculated according to Eq. 8.6;

- Step 10. Evaluate system response by modeling and performing nonlinear response history analysis on the designed SDOF structural fuse frame;
- Step 11. Verify that the structural fuse frame response is still satisfactory. If the structural fuse concept is not satisfied, a new set of frame and metallic damper properties may be chosen to improve the system seismic behavior, and the procedure is repeated from Step 9. Alternatively, a sensitivity study as shown in Section 4.4 of Vargas and Bruneau (2006a) can be conducted for the design of new systems;
- Step 12. Verify that the new parameters calculated in Step 9 are sufficiently close to the target parameters selected at the beginning of the design process. If not, new frame and damper properties should be selected to match as close as possible the target parameters, and the procedure is repeated from Step 9. Alternatively, in a worse case, it may be necessary to change the frame geometry and might even be possible to change the system mass, although project constraints make this difficult;
- Step 13. Based on the absolute acceleration response histories at the floor level recorded from the nonlinear time history analysis of the designed structural fuse frame in Step 10, the acceleration response spectra for the floor level of the SDOF structural fuse frame is determined;
- Step 14. Determine the acceleration response limits, A_L , for the isolated floor system, and the distance between the isolated floor and surrounded walls, D_L ;
- Step 15: Determine the allowable displacement for Isolated Floor System I, D_{L1} . It is equal to the displacement capacity of the isolators (but, of course, not bigger than D_L) divided by $(1 + R_c/D_{ris})$, where R_c/D_{ris} is the rotation effect discussed in Chapter 6 for Isolated Floor System I (and in Chapter 5 for Isolated Floor System II);
- Step 16. Make layout of Concrete BNC Isolators and the isolated floor system. Also, select

ball type (i.e., polyurethane or rubber balls). For the first trial, the slope of the straight part in the working surface of the slope of the concrete BNC isolators may be selected as 1:10;

- Step 17. Check the strength of the isolators and the isolated floor system following the procedure in Appendices A and B. If the design based on the layout in Step 16 is not satisfied to support the isolated objects, it is necessary to go back to Step 16 and make a new layout and new design of the isolated floor system;
- Step 18. Calculate the self-weight of the designed isolated floor system(s) in Step 16, W_{i2} , and the friction from the edge plates f_{ie} . Note that when edge plates with sizes and weights different from those used in the characterization tests in Chapters 5 and 6, the friction from the edge plates should change accordingly;
- Step 19. Calculate the lower and upper bounds of total isolated mass, M_{iL} and M_{iU} , respectively, corresponding to the addition of the self-weight of the isolated floor system (obtained in Step 18) to the lower and upper bounds of the weight of the isolated contents, respectively;
- Step 20. Calculate the lower and upper bounds of the average load on each rolling ball, w_{iL} and w_{iU} ;
- Step 21. Determine minimum and maximum total friction coefficient based on procedure shown in Section 8.2: $\mu_{f \min}$, $\mu_{f \max}$;
- Step 22. Verify whether $\mu_{f \max} + 0.1 > A_L$. If yes, it is necessary to try the following methods to make $\mu_{f \max} + 0.1 \leq A_L$. First, note from the characterization tests shown in previous chapters that the rubber balls will provide higher friction (inducing higher peak acceleration) than polyurethane balls under a given gravity load case. Therefore, if the first trial uses rubber balls as the rolling balls and $\mu_{f \max} + 0.1 > A_L$, polyurethane

balls may be used alternatively in Step 16. The second method to make the isolated floor system satisfy $\mu_{f_{\max}} + 0.1 \leq A_L$ is to increase the number or isolator to reduce the average load on each ball corresponding to lower equivalent friction coefficient as mentioned in Chapter 7. Also note from the empirical model of the concrete BNC isolators shown in Chapter 3 that a smaller slope of the straight part of the working surface will generate a smaller peak acceleration response under a given gravity load. So the second method to satisfy $\mu_{f_{\max}} + 0.1 \leq A_L$ is to decrease the slope of the working surface. Note that if a new slope other than 1:10, Slo , is used, the relationship required to be checked in Step 22 should be $\mu_{f_{\max}} + Slo > A_L$;

- Step 23. Assume the displacement response of the isolated floor system, Δ ;
- Step 24. Calculate linear effective properties of the designed isolated floor system(s): K_{eff} , β_{eff} , and T_{eff} according to Eqs. 9.17 and 9.18, Eq. 9.19, and Eqs. 9.21 and 9.22, respectively;

The behavior of Isolated Floor System I is shown in Fig. 9.3. In this figure, the symbols of “ F_y ” and “ F_r ” correspond to the yield force of the concrete BNC isolators used in Isolated Floor System I and the friction in this system (i.e., sum of the friction from the rolling balls and that from the edge plates), respectively. “ Δ_y ” is the displacement of the isolated floor when it reaches the transition point between the spherical and straight parts of the working surface. “ Δ ” is the maximum displacement of the isolated floor system.

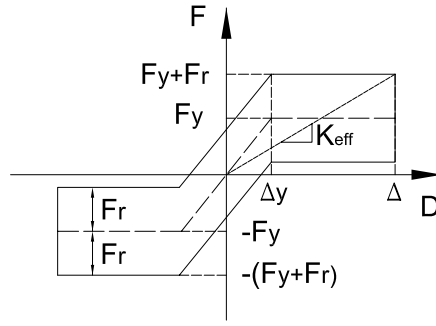


Figure 9.3 Behavior of Isolated Floor System I

Similar to expressions in Lee etc. (2007), the effective stiffness, K_{eff} , and the effective period, T_{eff} , are respectively expressed as,

$$K_{eff} = \frac{\frac{F_y \Delta}{\Delta_y} + F_r}{\Delta} \quad (\text{when } \Delta \leq \Delta_y) \quad (9.17)$$

$$K_{eff} = \frac{F_y + F_r}{\Delta} \quad (\text{when } \Delta > \Delta_y) \quad (9.18)$$

$$T_{eff} = 2\pi \sqrt{\frac{M_i}{K_{eff}}} \quad (M_i \text{ is the isolated mass}) \quad (9.19)$$

According to the formula mentioned in Chopra (2001), the equivalent damping ratio, β_{eff} , is derived for Isolated Floor System I,

$$\beta_{eff} = \frac{E_D}{4\pi E_{so}} = \frac{2F_r \Delta}{\pi K_{eff} \Delta^2} \quad (9.20)$$

Substituting Eqs. 9.17 and 9.18, respectively, into Eq. 9.20 gives;

$$\beta_{eff} = \frac{2F_r}{\pi \left(\frac{F_y \Delta}{\Delta_y} + F_r \right)} \quad (\text{when } \Delta \leq \Delta_y) \quad (9.21)$$

$$\beta_{eff} = \frac{2F_r}{\pi (F_y + F_r)} \quad (\text{when } \Delta > \Delta_y) \quad (9.22)$$

It can be noted from Eqs. 9.21 and 9.22 that the equivalent damping ratio is related to the maximum displacement when $\Delta \leq \Delta_y$, and is independent from the displacement when $\Delta > \Delta_y$.

Step 25. Determine the damping coefficient B based on the provision in NEHRP 2003 for seismic isolated structures or for structures with damping devices;

Step 26. Divide the spectral acceleration $S_{a5\%}$ (5% critical damping), which corresponds to T_{eff} in the acceleration response spectra obtained in Step 13, by the damping coefficient B found in Step 24;

Step 27. Calculate Δ_1 using Eq. 9.23:

$$\Delta_1 = \frac{S_{a5\%} T_{eff}^2}{4\pi^2 B} \quad (9.23)$$

Step 28. Check whether Δ_1 is close to Δ . If yes, go to next step. If no, go back to step 23 by assuming another value for the displacement of the isolated floor system, and repeat Steps 24 to 27;

Step 29. Check whether $\Delta > D_{L1}$. If no, the design is finished. And if yes, go to Step 30.

Step 30. There are two options when $\Delta > D_{L1}$:

- 1) Choose new target parameter values for the base structural structure and repeat Steps 2 to 29;
- 2) Select new D_L and/or A_L and repeat Steps 14 to 29.

The iteration will not end until $\Delta \leq D_{L1}$ is satisfied.

Appendix E shows the design examples which follow the design steps of this linear static method. The set of the parameters defining the structural fuse frame, $\alpha = 0.25$, $R = 5$, and $T = 0.767s$, is first used for the design of a combined system including Isolated Floor System I. After that,

new lower acceleration and displacement response limits are set for the isolated floor system and a lower allowable displacement is set for the structural fuse frame. To make the combined system work, the structural fuse frame is stiffened by using another set of the parameter values, $\alpha = 0.25$, $R = 5$, and $T = 0.386s$, and the slope of the working surface of the isolators is reduced. Also note that the latter design case is also an example where the natural vibration period of the structural fuse frame is less than the transition period of the response spectrum (i.e., T_s).

9.2.2 Nonlinear Response History Method

Compared to the linear static method where the floor acceleration response spectra and equivalent linear properties of the isolated floor system are generated as described in Section 9.2.1, the nonlinear response history method, which is the focus of this section, uses direct nonlinear analyses using coupled models consisting of both the base SDOF frame and the isolated floor system on top. Figure 9.4 illustrates the flow chart of this design method. It can be noted that Steps 1 to 12 for the design of the structural fuse frame in the nonlinear response history method are all the same as those in the linear static method. Also note that the Steps 13 to 21 for the design of isolated floor system in the nonlinear response history method are actually same as the Steps 14 to 22 in the linear static method only except for the difference in the step numbers. These steps have been described in detail in Section 9.2.1. So it is not necessary to repeat them here. The following only describes the steps in the nonlinear response history method which are different from those in the static linear method.

Step 22. Model the designed combined systems consisting of the SDOF structural fuse frame and the isolated floor system using coupled models and run nonlinear response history analysis. Note that the isolated load under which the $\mu_{f \min}$ is obtained (in order to get the worst displacement response of the isolated floor) and the isolated

load corresponding to the upper bound isolated mass M_{iU} (in order to investigate the interaction effect on the structural fuse frame) are separately used as the isolated weight for the isolated floor system in the model. Therefore, two nonlinear response history analyses need to be conducted by using the above two isolated loads, respectively;

Step 23. Verify that the structural fuse frame response is still satisfactory using the results from the nonlinear response history analysis in Step 22. As mentioned in Chapter 8, the interaction between the isolated floor system and the structural fuse frame is insignificant when the mass ratio takes low values, but can affect the response of the structural fuse frame when the mass ratio take relatively high values. If the design does not meet the structural fuse concept, choose new target values for the parameters defining the structural fuse frame and repeat Steps 2 to 22;

Step 24. Check whether the relative displacement of the isolated floor system with respect to the structural fuse frame, Δ , is bigger than the allowable displacement of the isolated floor system, D_{L1} . If no, the design is finished. And if yes, go to the next step. If yes, go to Step 25;

Step 25. There are two options when $\Delta > D_{L1}$:

- 1) Choose new target parameter values for the base structural structure and repeat Steps 2 to 24;
- 2) Select new D_L and/or A_L and repeat Steps 13 to 24.

The iteration will not end until $\Delta \leq D_{L1}$ is satisfied.

The design examples for the nonlinear response history method are shown in Appendix F. The same two sets of parameter values as in Appendix E are used for the SDOF structural fuse frame design in Appendix F.

9.2.3 Comparison of Designs

In this section, the designs using the linear static method are compared with the corresponding ones using the nonlinear response history method. This comparison is shown in Table 9.1. It can be noted that the displacement of the structural fuse frame, U_{max} , are almost same between these two design methods because the mass ratio is low and the interaction between the isolated floor and the structural fuse is insignificant. It can also be found that the relative displacement of the isolated floor with respect to the structural fuse frame, Δ , from the linear static method is bigger than that from the nonlinear response history method. This indicates the designs from the linear static method are on the conservative side when the mass ratio is low. Note that such a comparison would not be logical if the mass ratio was high, since only the second method is reliable and recommended in that case.

Table 9.1 Comparison of Designs_Combined Systems Using Isolated Floor System I

Response Quantity (1)	Linear Static Method (mm)		Nonlinear Response History Method (mm)	
	Example 1* (2)	Example 2** (3)	Example 1# (4)	Example 2## (5)
U_{max}	56.9	27.7	56.9	27.9
Δ	170.9	149.9	141.2	102.4

Notes,

and *, The parameters defining the structural fuse frame are: $\alpha = 0.25$, $R = 5$, and $T = 0.767s$;

and **, The parameters defining the structural fuse frame are: $\alpha = 0.25$, $R = 5$, and $T = 0.386s$.

9.3 Design Methodology For Systems Consisting of SDOF Structural Fuse Frames and Isolated Floor System II

9.3.1 Linear Static Method

Similar to the development of the design methodology for combined systems using Isolated Floor System I, the linear static method is also developed for the combined system using Isolated Floor System II in this section. Fig. 9.5 shows the flow chart of this design method. The

comparison between Figs. 9.5 and 9.1 shows that the Steps 1 to 19 in Fig. 9.5 are exactly same as the corresponding ones in Fig. 9.1 except for Steps 16. In the meanwhile, it can be found that the Steps 22 to 29 in Fig. 9.5 are also exactly same as the Steps 23 to 30 in Fig. 9.1 only except for the difference in the step numbers, and for Step 23 in Fig. 9.5. These steps have been described in detail in Section 9.2.1. So it is not necessary to repeat them here. The following shows the Step 16, Steps 20 and 21, and Step 23 in the linear static design method for combined systems using Isolated Floor System II, which are different from the corresponding ones in Fig. 9.1 for combined systems using Isolated Floor System I.

Step 16. Make layout of spring units and the isolated floor system;

Step 20. Determine the spring stiffness by following the procedure described in Section 8.4.2;

Step 21. Select the isolated mass, M_i , separately as the lower and upper bound, M_{iL} and M_{iU} . It means both the lower and upper bound of the isolated mass will be used for checking the requirements defined in the following steps.

Step 23. Calculate linear effective properties of the designed isolated floor system(s): K_{eff} , β_{eff} , and T_{eff} according to Eqs. 9.24 to 9.25, Eq. 9.26, and Eqs. 9.27 and 9.28, respectively. It can be noted that the expressions of these three terms are different than those for Isolated Floor System I because different kinds of isolators are used in these two systems.

The behavior of Isolated Floor System II is shown in Fig. 9.6. In this figure, the symbols of “ F_y ” and “ F_r ” correspond to the yield force of the spring units used in Isolated Floor System II and the friction in this system (i.e., sum of the friction from the casters and that from the edge plates), respectively. “ Δ_y ” is the yield displacement of the isolated floor, equal to the yield force of F_y divided by the initial stiffness of the spring units K_0 . “ F_p ” is the force contributed from the spring unit at the displacement of “ Δ ” which is the maximum displacement of the isolated floor system. All other

symbols have the same meaning as mentioned in Chapter 7 for the modeling of Isolated Floor System II.

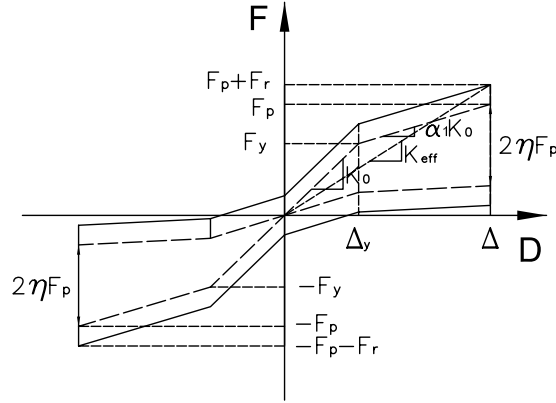


Figure 9.6 Behavior of Isolated Floor System II

Similar to the process in NEHRP 2003 and Lee et al. (2007), the effective stiffness, K_{eff} , and the effective period, T_{eff} , are respectively expressed as,

$$K_{eff} = \frac{K_0 \Delta + F_r}{\Delta} \quad (\text{when } \Delta \leq \Delta_y) \quad (9.24)$$

$$K_{eff} = \frac{F_y + \alpha_1 K_0 \left(\Delta - \frac{F_y}{K_0} \right) + F_r}{\Delta} \quad (\text{when } \Delta > \Delta_y) \quad (9.25)$$

$$T_{eff} = 2\pi \sqrt{\frac{M_i}{K_{eff}}} \quad (M_i \text{ is the isolated mass}) \quad (9.26)$$

According to the formula mentioned in Chopra (2001), the equivalent damping ratio is derived for Isolated Floor System II here,

$$\beta_{eff} = \frac{E_D}{4\pi E_{so}} = \frac{2F_r \Delta + \eta \alpha_1 K_0 \Delta^2}{\pi K_{eff} \Delta^2} \quad (\text{when } \Delta \leq \Delta_y) \quad (9.27)$$

$$\beta_{eff} = \frac{E_D}{4\pi E_{so}} = \frac{2F_r\Delta + \eta F_y\Delta + \eta \left[2F_y + \alpha_1 K_0 \left(\Delta - \frac{F_y}{K_0} \right) \right] \left(\Delta - \frac{F_y}{K_0} \right)}{\pi K_{eff} \Delta^2} \quad (\text{when } \Delta > \Delta_y) \quad (9.28)$$

Note that the K_{eff} in Eqs. 9.27 and 9.28 is expressed by Eqs. 9.24 and 9.25, respectively.

Appendix G shows the design examples which follow the design steps in this linear static method. The set of the parameters defining the structural fuse frame, $\alpha = 0.25$, $R = 10$, and $T = 0.767s$, is first used for the design of a combined system including Isolated Floor System II. After that, new lower acceleration and displacement response limits are set for the isolated floor system. To make the combined system work, the structural fuse frame is stiffened by using another set of the parameter values, $\alpha = 0.5$, $R = 5$, and $T = 0.767s$.

9.3.2 Nonlinear Response History Method

Similar to the development of the nonlinear response history method developed for combined systems using Isolated Floor System I described in Section 9.2.2, this method is also developed for the combined systems using Isolated Floor System II. Fig. 9.7 illustrates the flow chart of this design method. The comparison between Figs. 9.7 and 9.4 shows that the Steps 1 to 18 in Fig. 9.7 are exactly same as the corresponding ones in Fig. 9.4 except for Step 15. In the meanwhile, it can be found that the Steps 21 to 24 in Fig. 9.7 are also exactly same as the Steps 22 to 25 in Fig. 9.4 only except for the difference in the step numbers. These steps have been described in detail in Section 9.2.2 and are not repeated here. The following shows the Step 15 and Steps 19 and 20 in the linear static design method for combined systems using Isolated Floor System II, which are different from the corresponding ones in Fig. 9.4 for combined systems using Isolated Floor System I.

Step 15. Make layout of spring units and the isolated floor system;

- Step 19. Determine the spring stiffness by following the procedure described in Section 8.4.2;
- Step 20. Select the isolated mass, M_i , separately as the lower and upper bound, M_{iL} and M_{iU} . It means both the lower and upper bound of the isolated mass will be used to check the requirements defined in the following steps.

Incidentally, note that because sensitivity analyses presented in previous chapters demonstrated the sensitivity of response to the magnitude of the friction coefficient, an additional option to all of the above design procedures (i.e., for all the combined systems considered in Sections 9.2.1, 9.2.2, 9.3.1, and 9.3.2) is possible to consider a lower bound and a upper bound value approach to account for possible variation for possible variations in all the friction effects respectively used in the design procedure to make the designs more reliable (as typically done in conventional base isolation design).

The design examples using this nonlinear response history method are shown in Appendix H. The same two sets of the parameter values as in Appendix G are used for the SDO structural fuse frame design in Appendix H.

9.3.3 Comparison of Designs

In this section, the designs using the linear static method are compared with the corresponding ones using the nonlinear response history method. This comparison is shown in Table 9.2. It can be noted here that the displacement of the structural fuse frame, U_{max} , are almost same between these two design methods for the same reason mentioned in Section 9.2.3. It can also be found here that the relative displacement of the isolated floor with respect to the structural fuse frame, Δ_Lower from the case when the lower bound isolated load is applied and Δ_Upper from the case when the upper bound isolated load is applied, from the linear static method is bigger than that from the nonlinear response history method. As the observation in Section 9.2.3, this also

indicates the designs from the linear static method are on the conservative side when the mass ratio is low.

Table 9.2 Comparison of Designs_Combined Systems Using Isolated Floor System II

Response Quantity (1)	Linear Static Method (mm)		Nonlinear Response History Method (mm)	
	Example 1* (2)	Example 2** (3)	Example 1# (4)	Example 2## (5)
U_{max}	63.2	55.4	65.0	56.9
Δ_{Lower}	137.2	137.2	50.3	104.4
Δ_{Upper}	203.2	190.5	124.0	143.8

Notes,

and *, The parameters defining the structural fuse frame are: $\alpha = 0.25$, $R = 10$, and $T = 0.767s$;

and **, The parameters defining the structural fuse frame are: $\alpha = 0.5$, $R = 5$, and $T = 0.767s$.

Note here that even though the maximum displacements of the isolated floor systems in all the design examples considered in this chapter are satisfactory, it is recognized that in some instances (due to specific building properties or particularly severe earthquake demands), limiting the maximum displacement responses to tolerable values may be hard (or impossible) to achieve. Appendix I provides additional comments on this complex issue. The range of solutions that may work and may not work is unknown, and is the subject of future research.

9.4 Observations

This chapter developed the design methodology for the combined systems consisting both SDOF structural fuse frames and isolated floor systems. Combined systems using Isolated Floor I and II are separately considered. Both the linear static design method and nonlinear response history analysis design method are developed for each case. Note that the linear static method is only suitable for the design case with a low mass ratio because it does not consider the interaction between the two SDOF systems. The design examples show these two design methods work well. This confirms that the proposed combined solution of stiffening the primary structure using PED devices and isolating the floor of the room(s) to protect the acceleration sensitive components on

the room floor(s) of critical facilities is feasible, considering at least two kinds of possible isolated floor system. A comparison between the design examples using these two methods is made and it is found that the linear static method is on the conservative side for the design of the combined systems when the mass ratio is low. These design methods provide an important basis for the development of the design concepts for the combined systems consisting multi-degree-of-freedom (MDOF) structural fuse frames and isolated floor systems which can be the topic of further research.

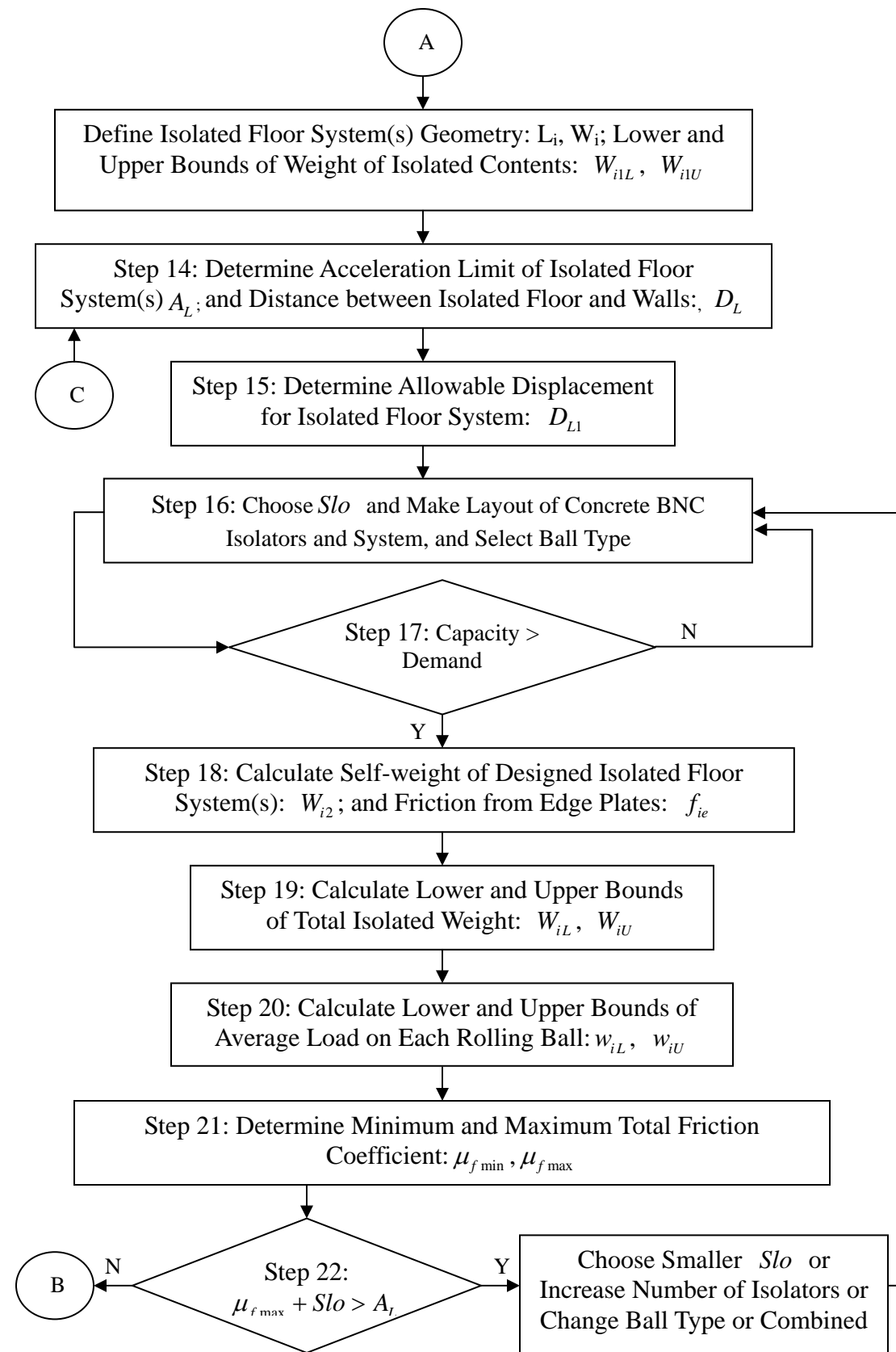


Figure 9.1 Procedure of Linear Static Design Method: Isolated Floor System I (Contd.)

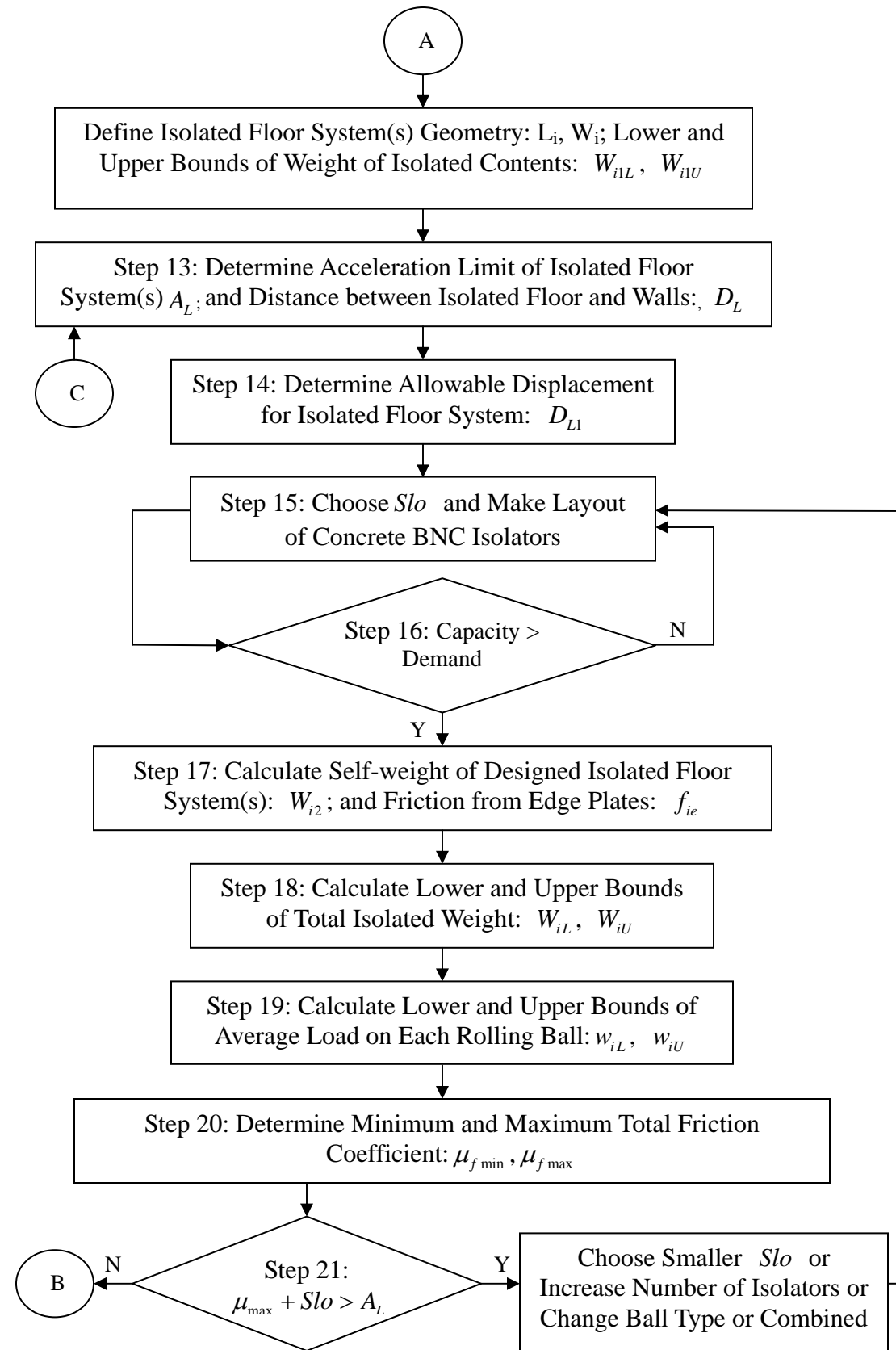


Figure 9.4 Procedure of Nonlinear Response History Design Method: Isolated Floor System I (Contd.)

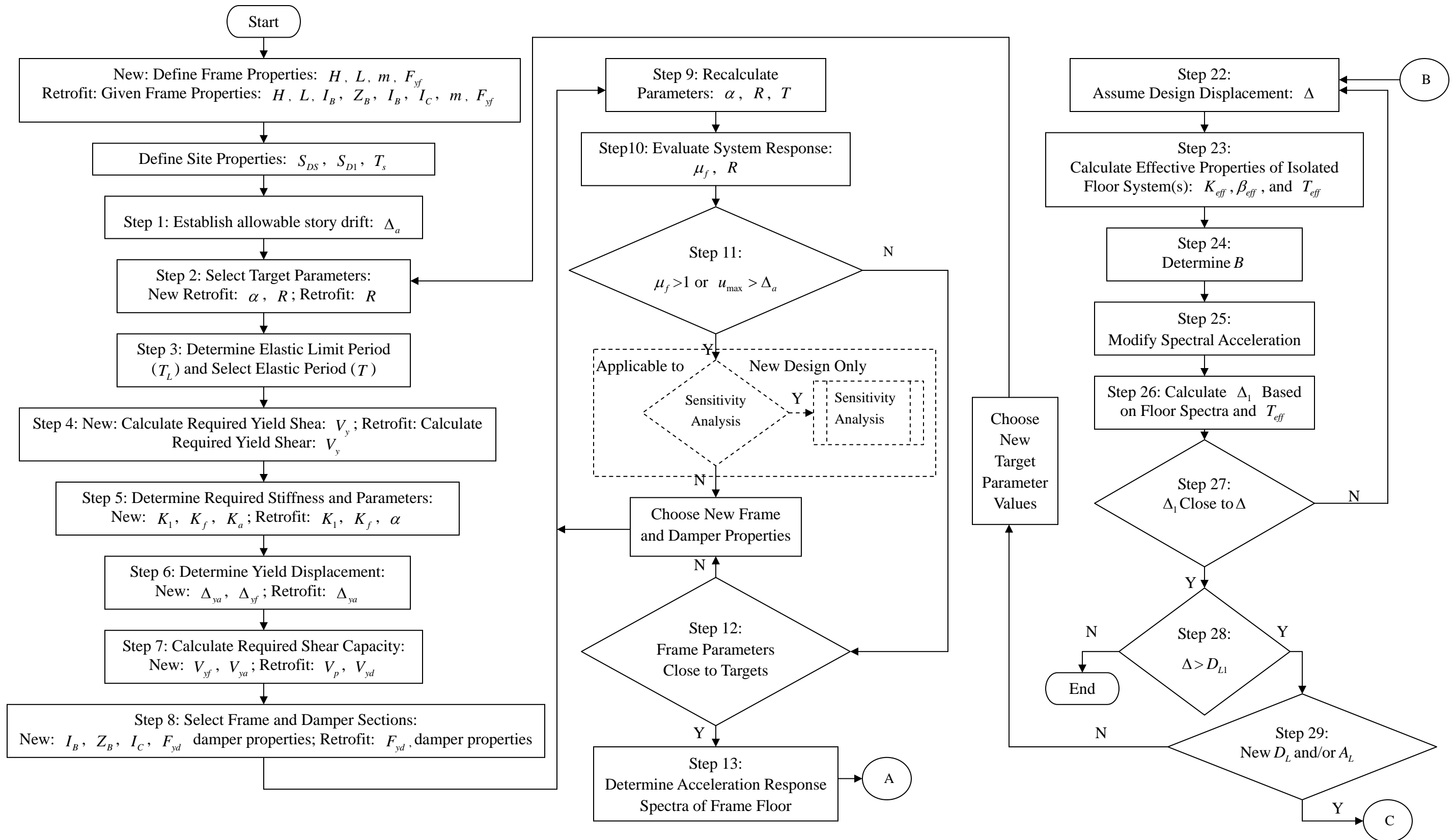


Figure 9.5 Procedure of Linear Static Design Method: Isolated Floor System II

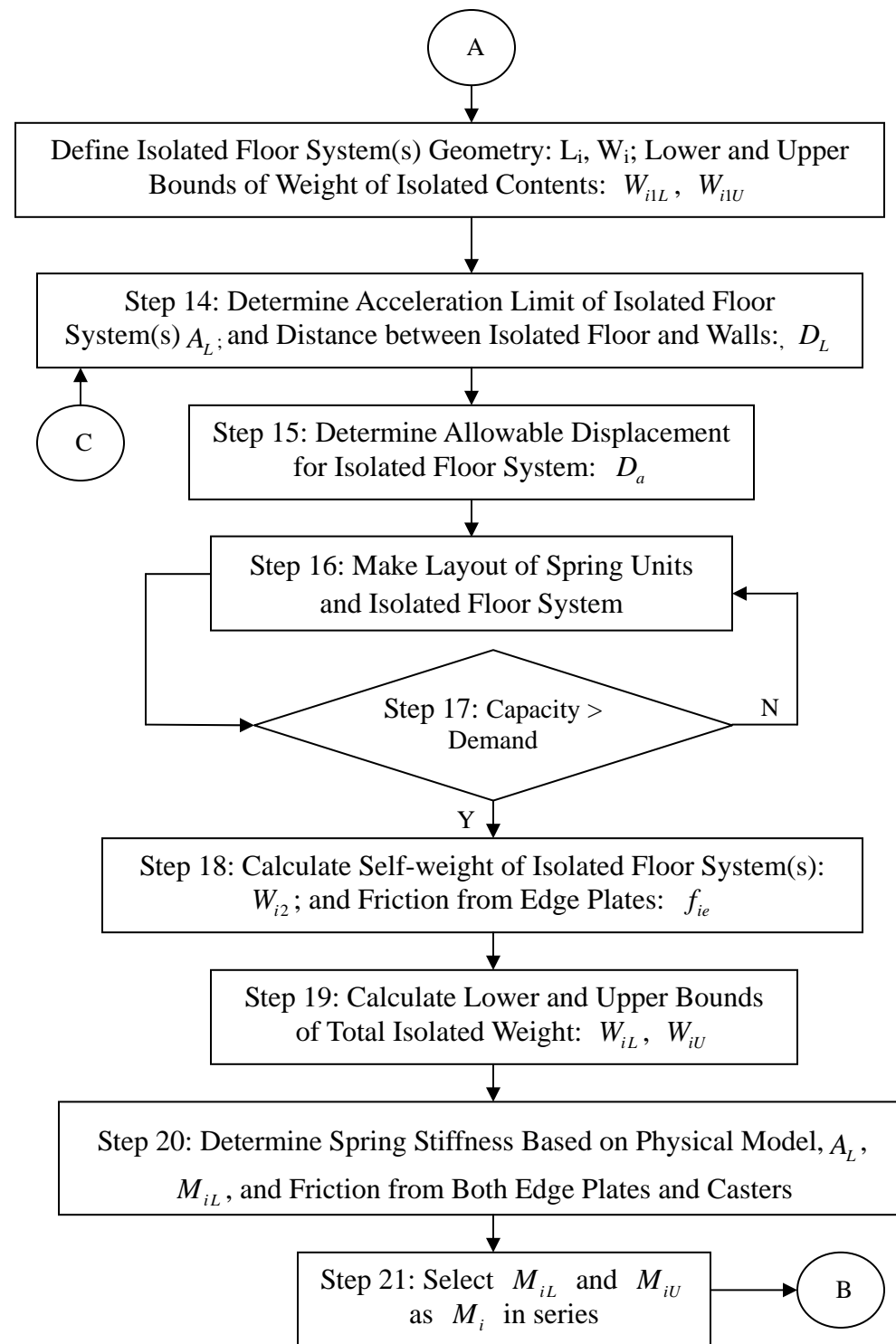


Figure 9.5 Procedure of Linear Static Design Method: Isolated Floor System II (Contd.)

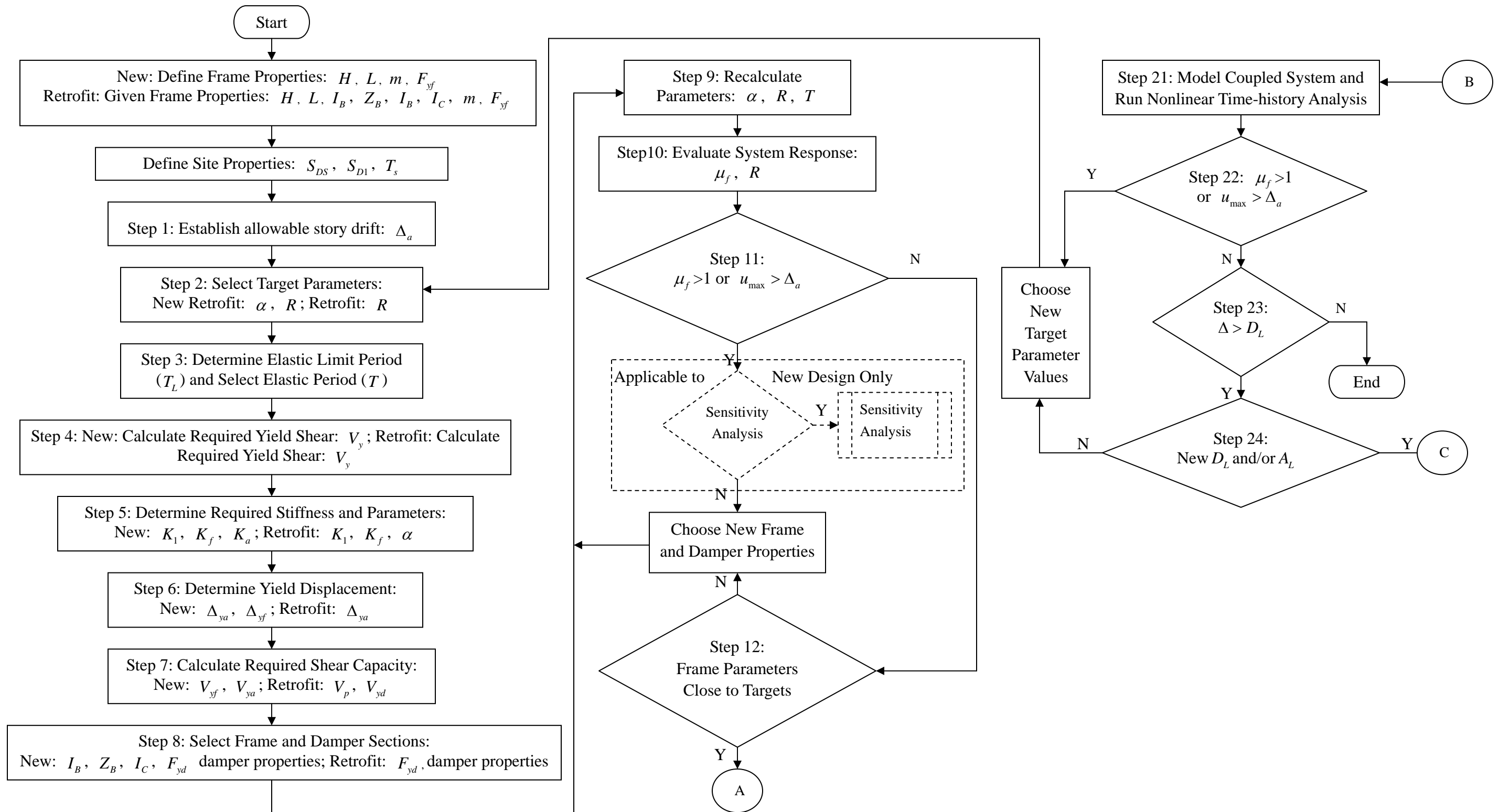


Figure 9.7 Procedure of Nonlinear Response History Design Method: Isolated Floor System II

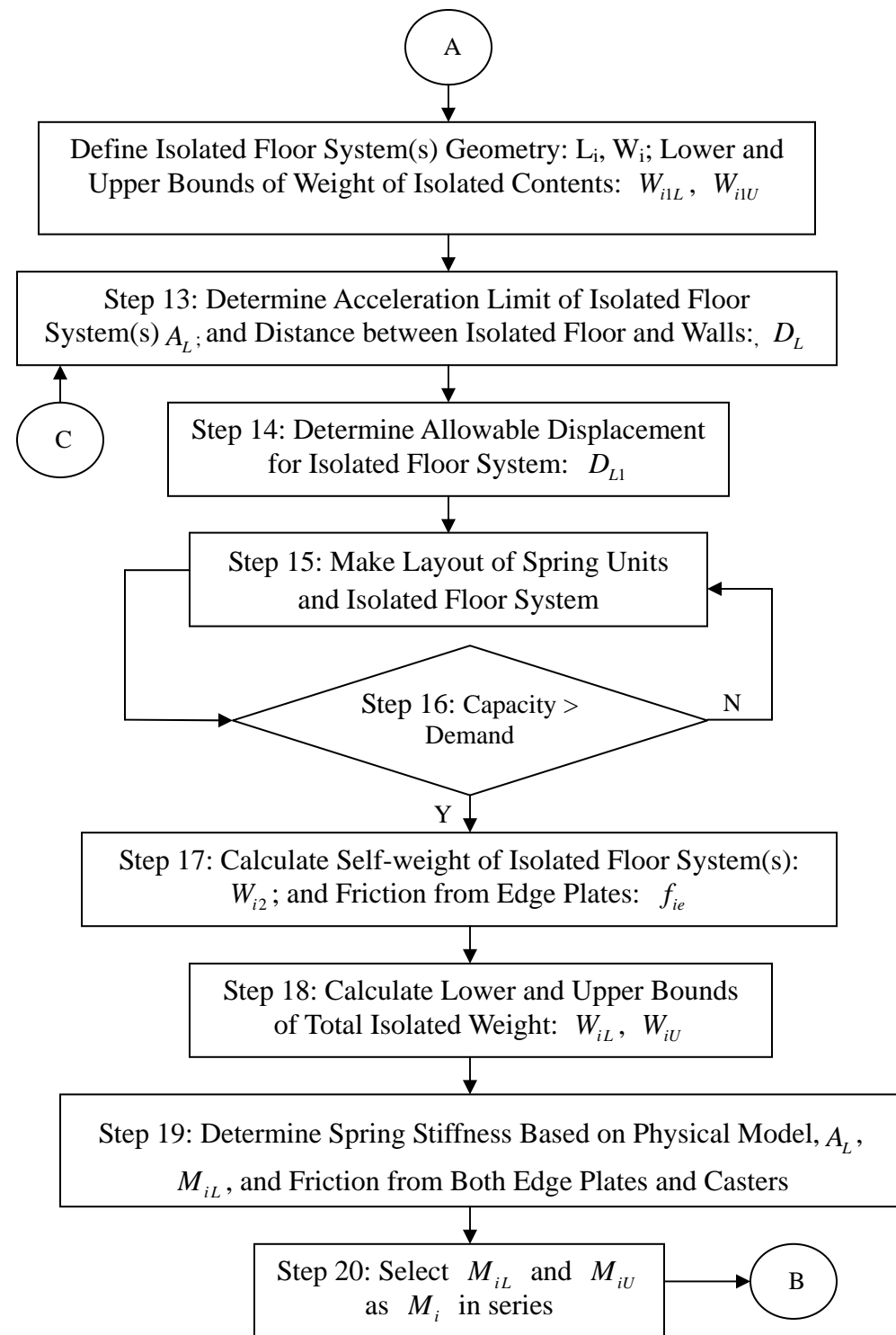


Figure 9.7 Procedure of Nonlinear Response History Design Method: Isolated Floor System II (Contd.)

CHAPTER 10

CONCLUSIONS AND FUTURE RESEARCH

General design procedures implementing the structural fuse concept were developed by various researchers. In their study, passive energy dissipation (PED) devices (such as BRBs and other hysteretic devices) have been used to stiffen the structures and act as “structural fuses”. While this concept reduces the displacement responses of the building during seismic events, studies also show that it can result in an increase in the floor acceleration response in most cases. To protect acceleration sensitive devices in buildings that would have a structural fuse frame system (which would be important in some mission critical facilities, such as hospitals), a combined concept of stiffening the structures by using special cases of PED devices and isolating the floors supporting such acceleration sensitive devices has been proposed herein. Two kinds of isolated floor systems were studied here. Both experimental and analytical studies were conducted for each type of isolated floor considered, from single isolators to complete isolated floor systems.

Isolated Floor System I used a special kind of concrete ball-in-cone (BNC) isolators. Rubber and polyurethane spherical solid balls, instead of steel balls, were respectively used as the rolling balls between the top and bottom concrete bearing plates of these BNC isolators. A multi-directional spring unit was used as isolators in Isolated Floor System II.

The test results show that:

- The design of both isolated floor systems is feasible for a broad range of design load cases;
- The mechanical behaviors of the single isolator and of the complete isolated floor systems are stable;

- The maximum acceleration response of the isolated components is a constant value for Isolated floor system I. After a specific initial displacement, the maximum acceleration response of the isolated components also reaches a plateau for Isolated Floor System II;
- The equivalent friction coefficient, accounting for the rolling friction between the rolling balls and the working surface of the concrete BNC isolator, rises with increases in the magnitude of the isolated loads;
- The rolling friction from the casters in Isolated Floor System II has been estimated and should be included in the design of Isolated Floor System II;
- The friction from the steel edge plates in both isolated floor systems has been observed and should be considered in the design of these isolated floor systems;
- The rotation effect of the isolated top part of the isolated floor systems has been estimated in both systems and should be considered in the design of these isolated floor systems;
- The walking surface of Isolated Floor System II should be smooth enough to prevent the impact between the edge plates and the tilt edges.

Based on the experimentally obtained mechanical behavior and the models (empirical or physical) respectively developed for the two kinds of isolation bearings used in the two isolated floor systems, both coupled and uncoupled models were built in computer programs to model the combined systems consisting of a base SDOF structural fuse structures and the two kinds of isolated floor systems, respectively. A three-parameter system was used for the design of the SDOF structural fuse frame. Through an initial parametric study, a preferred range of these parameter values (i.e., $0.25 \leq \alpha \leq 0.5$ and $5 \leq \mu_{\max} \leq 10$) was recommended. It is found from selected targeted parametric studies that the interaction between the isolated floor system and the structural fuse frame is insignificant when the mass ratio is low and will affect the responses of both systems when the mass ratio is high. A number of trends in the behavior of the combined systems are observed with respect to the primary parameters defining the structural fuse frame and the mass ratio between the isolated floor system and the SDOF structural fuse frame. These trends act as a basis for the development of combined design concepts. A large number of parametric studies were conducted.

Finally, combined design concepts were developed for each kind of isolated floor system, including the designs of both the base SDOF structural fuse structures and the isolated floor systems on top. Both linear static and nonlinear response history design methods were developed for each case. Both methods were found to work well, as shown through design examples. The linear static design method, which only applies when the mass ratio of the isolated floor to the SDOF structural fuse is low, is found to give results on the conservative side. These methods can be used for the integrated design of isolated floor systems in SDOF frames having structural fuses.

Based on all the findings in this report, further future research is recommended to:

- Investigate the rolling friction between balls (rubber/polyurethane) and their rolling surface (i.e., concrete in the case of the concrete BNC isolator), and develop mechanistic-based models of that phenomenon;
- Investigate the long-term performance and maintenance of the isolated floor systems;
- Explain in physical terms all the observations made from the parametric studies in this report, by expanding the scope of the parametric studies and simultaneously investigating the fundamental dynamic and seismic behavior of the coupled nonlinear systems ;
- Develop a simple method (or methods) to directly generate the floor response spectrum under any given nonlinearity the SDOF structural fuse structure, the isolated floor systems, and the interaction between these two systems;
- Expand the integrated design methodology proposed here to systems consisting of MDOF structural fuse frame and isolated floor systems;
- Parametric studies on the design procedures by using different seismic inputs to find out the range of solutions that generate satisfactory displacement responses for the isolated floor systems;
- Create a simple method (or methods) to directly generate the floor response spectrum under any given nonlinearity in both the MDOF structural fuse structure, the isolated floor systems, and the interaction between these two systems;
- Introduce new base isolation devices to also isolate nonstructural components from vertical motions (in addition to horizontal motions).

CHAPTER 11

REFERENCES

American Concrete Institute (2005). “Building Code Requirements for Structural Concrete (ACI 318-05) and Commentary (ACI 318R-05).” *Report No. ACI 318-05, ACI-318R-05*, Farmington Hills, MI.

American Society of Civil Engineering (1998), “Minimum Design Loads for Buildings and Other Structures.” *Report No. ASCE 7-98*, Reston, VA.

American Society of Civil Engineering (2010), “Minimum Design Loads for Buildings and Other Structures.” *Report No. ASCE 7-10*, Reston, VA.

American Society of Civil Engineering (2005), “Minimum Design Loads for Buildings and Other Structures.” *Report No. ASCE/SEI 7-05*, Reston, VA.

Amick, H., Bayat, A., and Kemeny, Z. (1998). “Seismic Isolation of Semiconductor Production Facilities.” *Proceedings of Seminar on Seismic Design, Retrofit, and Performance of Nonstructural Components*, ATC-29-1, Applied Technology Council, pp. 297-312.

Aristizabal-Ochoa, J. D. (1986). “Disposable Knee Bracing: Improvement in Seismic Design of Steel Frames.” *Journal of Structural Engineering*, Volume 112, No. 17, ASCE, pp. 1544-1552.

Basha, H. S. and Goel, S. C. (1996). “Ductile Truss Moment Frames.” *Los Angeles Tall Buildings Structural Design Council, Annual Meeting: Modern Analysis Techniques in Practice*, Los Angeles, California.

Biggs, J. M. and Roesset, J. M. (1970). "Seismic Analysis of Equipment Mounted on A Massive Structure." *Seismic Des. for Nuclear Power Plants*, R. J. Hansen, ed., MIT press, Cambridge, Mass., pp. 319-343.

Carter, C. J., and Iwankiw, N. R. (1998). "Improved Ductility in Seismic Steel Moment Frames with Dogbone Connections." *Second World Conference on Steel in Construction*, Elsevier Science Ltd., Paper No. 253.

Chen, Y. and Soong, T. T. (1988). "State-of-The –Art-Review: Seismic Response of Secondary Systems." *Engrg. Struct.*, Vol. 10, No. 4, 218-228.

Chopra, A. K. (2001). "Dynamics of Structures: Theory and Applications to Earthquake Engineering." Prentice-Hall, Inc., Upper Saddle River, NJ.

Christopoulos, C. and Filiatrault, A. (2006). "Principles of passive supplemental damping and seismic isolation." IUSS Press, Pavia, Italy.

Computers and Structures Inc. (2004). "CSI Analysis Reference Manual for SAP2000, ETABS^R, and SAFETM." Computers and Structures Inc., Berkeley, CA.

Constantinou, M. C., Kartoum, A., and Kelly, J. M. (1992). "Analysis of Compression of Hollow Circular Elastomeric Bearings." *Engineering Structures*, Vol. 14, No. 2, pp. 103-111.

Constantinou, M. C., Tsopelas, P., Kim, Y-S. and Okamoto, S. (1993). "NCEER Taisei Corporation Research Program on Sliding Seismic Isolation Systems for Bridges: Experimental and Analytical Study of a Friction Pendulum System (FPS)." *Report No. NCEER-93-0020*, National Center for Earthquake Engineering Research, University at Buffalo, State University of New York, Buffalo, NY.

Constantinou, M. C., Soong, T. T. and Dargush, G. F. (1998), "Passive Energy Dissipation Systems for Structural Design and Retrofit." Monograph, Multidisciplinary Center for

Earthquake Engineering Research, University at Buffalo, State University of New York, Buffalo, NY.

Constantinou, M. C., Tsopelas, P., Kasalanati, A. and Wolff, E. D. (1999), "Property Modification Factors for Seismic Isolation Bearings." *Report No. MCEER-99-0012*, Multidisciplinary Center for Earthquake Engineering Research, University at Buffalo, State University of New York, Buffalo, NY.

Demetriades, G. F., Constantinou M. C., and Reinhorn, A. M. (1992). " Study of Wire Rope Systems for Seismic Protection of Equipment in Buildings." *Report No. NCEER-92-0012*, National Center for Earthquake Engineering Research, University at Buffalo, State University of New York, Buffalo, NY.

Demetriades, G. F., Constantinou M. C., and Reinhorn, A. M. (1993). " Study of Wire Rope Systems for Seismic Protection of Equipment in Buildings." *Engineering Structures*, Vol. 15, No. 5, pp. 321-334.

Federal Emergency Management Agency (2000). "NEHRP Recommended Provisions for Seismic Regulations for New Buildings and Other Structures." *Report No. FEMA 368*, Washington, D.C..

Federal Emergency Management Agency (2000). "Global Topics on the Prestandard and Commentary for The Seismic Rehabilitation of Buildings." *Report No. FEMA 357*, Washington, D.C..

Federal Emergency Management Agency (2003). " NEHRP Recommended Provisions for Seismic Regulations for New Buildings and Other Structures." *Report No. FEMA 450*, Washington, D.C..

Fenz, D. M. and Constantinou, M. C. (2006). "Behavior of the Double Concave Friction Pendulum Bearing." *Earthquake Engrg. and Struct. Dyn.*, Vol. 35, No. 11, pp. 1403-1424, DOI: 10.1002/eqe.589.

Fenz, D. M. and Constantinou, M. C. (2008). "Mechanical Behavior of Multi-Spherical Sliding Bearings." *Report No. MCEER-08-0007*, Multidisciplinary Center for Earthquake Engineering Research, University at Buffalo, State University of New York, Buffalo, NY.

Fintel, M. and Ghosh, S. K. (1981). "The Structural Fuse: an Inelastic Approach to Seismic Design of Buildings." *Civil Engineering*. Volume 51, No. 1, ASCE, pp. 48-51.

Igusa, T. (1990). "Response Characteristics of Inelastic 2-DOF Primary-Secondary Systems." *J. Engrg. Mech.*, ASCE, Vol. 116, No. 5, pp. 1160-1174.

Igusa, T. and Der Kiureghian, A. (1985a). "Generation of Floor Response Spectra Including Oscillator-structure Interaction." *Earthquake Engrg. and Struct. Dyn.*, Vol. 13, No. 5, pp. 661-676.

Igusa, T. and Der Kiureghian, A. (1985b). "Dynamic Response of Multiply Supported Secondary Systems." *J. Engrg. Mech.*, ASCE, Vol. 111, No. 1, pp. 20-41.

International Conference of Building Officials (1997). "Uniform building code." Whittier, CA.

Kapur, K. K. and Shao, L. C. (1973). "Generation of Seismic Floor Response Spectra for Equipment Design." *Proc., ASCE Conf. Struct. Des. of Nuclear Power Plants Fac.*, ASCE, Vol. 2, pp. 29-71.

Kartoum, A. (1987). "A Contribution to the Analysis of Elastomeric Bearings." *M.S. Thesis*, Department of Civil Engineering, Drexel University, Philadelphia, PA

Kasalanati, A., Reinhorn, A., Constantinou, M., and Sanders, D. (1997). "Experimental Study of Ball-in-Cone Isolation System." *Building to last: Proceedings of Structures Congress XV*, American Society of Civil Engineers, pp. 1191-1195.

Kasalanati, A. and Constantinou, M.C. (1999). "Experimental Study of Bridge Elastomeric and Other Isolation and Energy Dissipation Systems With Emphasis on Uplift Prevention and High Velocity Near Source Seismic Excitation." *Report No. MCEER-99-0004*, Multidisciplinary Center for Earthquake Engineering Research, University at Buffalo, State University of New York, Buffalo, NY.

Kelly, J. M. (1991). "Dynamic and Failure Characteristics of Bridgestone Isolation Bearings." *Report No. UCB/EERC-91/04*, Earthquake Engineering Research Center, University of California, Berkeley.

Kelly, J.M. (2003), "Tension Buckling in Multilayer Elastomeric Bearings," *J. Engrg. Mech.*, ASCE, Vol. 129, No. 12, pp. 1363-1368.

Kemeny, Z.A., and Szidarovszky, F. (1995). "Seismic Isolation Bearings with Nonlinear Gravity Restoring." *Report No. NCEER VF01127*, National Center for Earthquake Engineering Research, University at Buffalo, State University of New York, Buffalo, NY.

Koh, C. G. and Kelly, J. M. (1987). "Effects of Axial Load on Elastomeric Bearings." *Report No. UCB/EERC-86/12*, Earthquake Engineering Research Center, University of California, Berkeley.

Kosar K., Soong, T. T., Shen, K. L., Holung, J. A., and Lin, Y. K. (1993). "Seismic Testing of Installation Methods for Computers and Data Processing Equipments." *Report No. NCEER-93-0007*, National Center for Earthquake Engineering Research, University at Buffalo, State University of New York, Buffalo, NY.

Lambrou, V. and Constantinou M. C. (1994). "Study of Seismic Isolation Systems for Computer Floors." *Report No. NCEER-94-0020*, National Center for Earthquake Engineering Research, University at Buffalo, State University of New York, Buffalo, NY.

Lee, G. C., Ou, Y., Liang, Z., Niu, T., and Song, J. (2007). "Principles and Performance of Roller Seismic Isolation Bearings for Highway Bridges." *Report No. MCEER-07-0019*, Multidisciplinary Center for Earthquake Engineering Research, University at Buffalo, State University of New York, Buffalo, NY.

Lee, M. C. and Penzien, J. (1983). "Stochastic Analysis of Structures and Piping Systems Subjected to Stationary Multiple Support Excitations." *Earthquake Engrg. and Struct. Dyn.*, Vol. 11, No. 1, pp. 91-110.

Naeim F. and Kelly, J. M. (1999). "Design of Seismic Isolated Structures." John Wiley & Sons, Inc., New York.

Peters, K. A., Schmitz, D., and Wagner, U. (1977). "Determination of Floor Response Spectra on the Basis of The Response Spectrum Method." *Nuclear Engrg. and Des.*, Vol. 44, No. 2, pp. 255-262.

Reinhorn, A. M. (2008). Private communication, University at Buffalo, The State University of New York, Buffalo, NY.

Reinhorn, A. M., Roh, H., Sivaselvan, M., Kunnath, S. K., Valles, R. E., Madan, A., Li, C., Lobo, R., and Park, Y. J. (2009). "IDARC2D Version 7.0: A Program for the Inelastic Damage Analysis of Structures." *Report No. MCEER-09-0006*, Multidisciplinary Center for Earthquake Engineering Research, University at Buffalo, State University of New York, Buffalo, NY.

Reinhorn, A. M., Park, Y. J., Kunnath, S. K., Valles, R. E., Lobo, R., Madan, A., Sivaselvan, M., and Roh, H. (2009). Download of IDARC2D Version 7.0 is available at: <http://civil.eng.buffalo.edu/idarc2d50/>.

Retamales, R. (2008). "New Experimental Capabilities and Loading Protocols for Seismic Fragility and Qualification of Nonstructural Component." *Ph.D. dissertation*, Department of Civil, Structural and Environmental Engineering, University at Buffalo, State University of New York, Buffalo, NY.

Rezai, M., Prion, H.G.L., Tremblay, R., Bouatay, N., and Timler, P. (2000). "Seismic Performance of Brace Fuse Elements for Concentrically Steel Braced Frames." *Behavior of Steel Structures in Seismic Areas*, STESSA, pp. 39-46.

Roeder, C. and Popov, E. (1977). "Inelastic Behavior of Eccentrically Braced Steel Frames under Cyclic Loadings." Report No. UCB-77/17, Earthquake Engineering Research Center, University of California, Berkeley.

Shimizu, K., Hashimoto, J., Kawai, H., and Wada, A. (1998). "Application of Damage Control Structure using Energy Absorption Panel." Paper No. T105-2, *Structural Engineering World Wide 1998*, Elsevier Science, Ltd.

Singh, M. P. (1980). "Seismic Design Input for secondary Systems." *J. Struct. Div.*, ASCE, Vol. 106, No. 2, pp. 505-517.

Singh, M. P. and Sharma, A. M. (1985). "Seismic Floor Spectra by Mode Acceleration Approach." *J. Engrg. Mech.*, ASCE, Vol. 111, No. 11, pp. 1402-1419.

Soong, T. T. (1994). "Seismic Behavior of Nonstructural Elements-State-of-The-Art Report." *Proc., 10th Eur. Conf. on Earthquake Engrg.*, Vol. 3, A. A., Balkema, Rotterdam, The Netherlands, pp. 1599-1606.

Soong, T. T., Chen, G., Wu, Z., Zhang, R.-H. and Grigoriu, M. (1993). "Assessment of The 1991 NEHR Provisions for Nonstructural Components and Recommended Revisions." *Report No.*

NCEER 93-00003, National Center for Earthquake Engineering Research, University at Buffalo, State University of New York, Buffalo.

Strongwell (2003) "Fiberglass Flooring and Decking Systems", Fiberglass Solutions, Strongwell Bristol Division, Bristol, VA

Suarez, L. E. and Singh, M. P. (1987a). "Floor Response Spectra with Structure-equipment Interaction Effects by A Mode Synthesis Approach." *Earthquake Engrg. and Struct. Dyn.*, Vol. 15, No. 2, pp. 141-158.

Suarez, L. E. and Singh, M. P. (1987b). "Seismic Response of Equipment-structure Systems." *J. Engrg. Mech.*, ASCE, Vol. 113, No. 1, pp. 16-30.

Sugiyama, S. (1998). "Application of Hysteresis Steel Dampers to Tall Building." Paper No. T190-5, *Structural Engineering World Wide 1998*, Elsevier Science, Ltd.

U.S. Department of Transportation (1977). "Rolling Resistance of Truck Tires as Measured under Equilibrium and Transient Conditions on Calspan's Tire Research Facility." *Report No. DOT-TST-78-1*, U.S. Department of Transportation, Washington, D.C..

USGS (2009). USGS Data on <http://earthquake.usgs.gov/hazards/design/buildings.php>

Valles, R. E., Reinhorn, A. M., Kunnath, S. K., Li, C., and Madan, A. (1996). "IDARC2D Version 4.0: A Program for the Inelastic Damage Analysis of Buildings." *Report No. NCEER-96-0010*, National Center for Earthquake Engineering Research, University at Buffalo, State University of New York, Buffalo, NY.

Vargas, R. E. and Bruneau, M. (2006a). "Analytical Investigation of the Structural Fuse Concept." *Report No. MCEER-06-0004*, Multidisciplinary Center for Earthquake Engineering Research, University at Buffalo, State University of New York, Buffalo, NY.

Vargas, R. E. and Bruneau, M. (2006b). "Experimental Investigation of the Structural Fuse Concept." *Report No. MCEER-06-0005*, Multidisciplinary Center for Earthquake Engineering Research, University at Buffalo, State University of New York, Buffalo, NY.

Villaverde, R. (1986). "Simplified Seismic Analysis of Secondary Systems." *J. Struct. Engrg.*, ASCE, Vol. 112, No. 3, pp. 588-604.

Villaverde, R. (1987). "Simplified Approach for the Seismic Analysis of Equipment Attached to Elastoplastic Structures." *Nuclear Engrg. and Des.*, Vol. 103, No. 3, pp. 267-279.

Villaverde, R. (1991). "Approximate Formulas to Calculate The Seismic response of Light Attachments to Buildings." *Nuclear Engrg. and Des.*, Vol. 128, No. 3, pp. 349-368.

Villaverde, R. (1997). "Seismic Design of Secondary Structures: State of The Art." *Journal of Structural Engineering*, American Society of Civil Engineers, Vol. 123, No. 8, pp. 1011-1019.

Wada, A., Connor, J.J., Kawai, H., Iwata, M., and Watanabe, A. (1992). "Damage Tolerant Structures." *Proceedings of: Fifth U.S.-Japan Workshop on the Improvement of Structural Design and Construction Practices*, ATC-15-4, Applied Technology Council, pp. 27-39.

Wada, A. and Huang, Y.H. (1995). "Preliminary Seismic Design of Damage Tolerant Tall Building Structures." *Proceedings of Symposium on a New Direction in Seismic Design*, Architectural Institute of Japan, Tokyo, Japan, pp. 77-93.

Wang, Y. K., Subudhi, M., and Bezler, P. (1983). "Comparison Study of Time History and Response Spectrum Responses for Multiply Supported Piping Systems." *Trans., 7th Int. Conf. on Struct. Mech. Reactor Technol.*, Vol. K(a), North-Holland Publishing Co., Amsterdam, The Netherland, K7/5.

Wen, Y. K. (1976). "Method for Random Vibration of Hysteretic Systems," *Journal of the Engineering Mechanics Division*, ASCE, Vol. 102, No. EM2.

Yang, T. and Whittaker, A. (2002). "MCEER Demonstration Hospitals Mathematical Models and Preliminary Analysis Results." *Thesis*, Department of Civil, Structural, and Environmental Engineering, University at Buffalo, Buffalo, NY.

MCEER Technical Reports

MCEER publishes technical reports on a variety of subjects written by authors funded through MCEER. These reports are available from both MCEER Publications and the National Technical Information Service (NTIS). Requests for reports should be directed to MCEER Publications, MCEER, University at Buffalo, State University of New York, 133A Ketter Hall, Buffalo, New York 14260. Reports can also be requested through NTIS, P.O. Box 1425, Springfield, Virginia 22151. NTIS accession numbers are shown in parenthesis, if available.

- NCEER-87-0001 "First-Year Program in Research, Education and Technology Transfer," 3/5/87, (PB88-134275, A04, MF-A01).
- NCEER-87-0002 "Experimental Evaluation of Instantaneous Optimal Algorithms for Structural Control," by R.C. Lin, T.T. Soong and A.M. Reinhorn, 4/20/87, (PB88-134341, A04, MF-A01).
- NCEER-87-0003 "Experimentation Using the Earthquake Simulation Facilities at University at Buffalo," by A.M. Reinhorn and R.L. Ketter, to be published.
- NCEER-87-0004 "The System Characteristics and Performance of a Shaking Table," by J.S. Hwang, K.C. Chang and G.C. Lee, 6/1/87, (PB88-134259, A03, MF-A01). This report is available only through NTIS (see address given above).
- NCEER-87-0005 "A Finite Element Formulation for Nonlinear Viscoplastic Material Using a Q Model," by O. Gyebe and G. Dasgupta, 11/2/87, (PB88-213764, A08, MF-A01).
- NCEER-87-0006 "Symbolic Manipulation Program (SMP) - Algebraic Codes for Two and Three Dimensional Finite Element Formulations," by X. Lee and G. Dasgupta, 11/9/87, (PB88-218522, A05, MF-A01).
- NCEER-87-0007 "Instantaneous Optimal Control Laws for Tall Buildings Under Seismic Excitations," by J.N. Yang, A. Akbarpour and P. Ghaemmaghami, 6/10/87, (PB88-134333, A06, MF-A01). This report is only available through NTIS (see address given above).
- NCEER-87-0008 "IDARC: Inelastic Damage Analysis of Reinforced Concrete Frame - Shear-Wall Structures," by Y.J. Park, A.M. Reinhorn and S.K. Kunnath, 7/20/87, (PB88-134325, A09, MF-A01). This report is only available through NTIS (see address given above).
- NCEER-87-0009 "Liquefaction Potential for New York State: A Preliminary Report on Sites in Manhattan and Buffalo," by M. Budhu, V. Vijayakumar, R.F. Giese and L. Baumgras, 8/31/87, (PB88-163704, A03, MF-A01). This report is available only through NTIS (see address given above).
- NCEER-87-0010 "Vertical and Torsional Vibration of Foundations in Inhomogeneous Media," by A.S. Veletsos and K.W. Dotson, 6/1/87, (PB88-134291, A03, MF-A01). This report is only available through NTIS (see address given above).
- NCEER-87-0011 "Seismic Probabilistic Risk Assessment and Seismic Margins Studies for Nuclear Power Plants," by Howard H.M. Hwang, 6/15/87, (PB88-134267, A03, MF-A01). This report is only available through NTIS (see address given above).
- NCEER-87-0012 "Parametric Studies of Frequency Response of Secondary Systems Under Ground-Acceleration Excitations," by Y. Yong and Y.K. Lin, 6/10/87, (PB88-134309, A03, MF-A01). This report is only available through NTIS (see address given above).
- NCEER-87-0013 "Frequency Response of Secondary Systems Under Seismic Excitation," by J.A. HoLung, J. Cai and Y.K. Lin, 7/31/87, (PB88-134317, A05, MF-A01). This report is only available through NTIS (see address given above).
- NCEER-87-0014 "Modelling Earthquake Ground Motions in Seismically Active Regions Using Parametric Time Series Methods," by G.W. Ellis and A.S. Cakmak, 8/25/87, (PB88-134283, A08, MF-A01). This report is only available through NTIS (see address given above).
- NCEER-87-0015 "Detection and Assessment of Seismic Structural Damage," by E. DiPasquale and A.S. Cakmak, 8/25/87, (PB88-163712, A05, MF-A01). This report is only available through NTIS (see address given above).

- NCEER-87-0016 "Pipeline Experiment at Parkfield, California," by J. Isenberg and E. Richardson, 9/15/87, (PB88-163720, A03, MF-A01). This report is available only through NTIS (see address given above).
- NCEER-87-0017 "Digital Simulation of Seismic Ground Motion," by M. Shinozuka, G. Deodatis and T. Harada, 8/31/87, (PB88-155197, A04, MF-A01). This report is available only through NTIS (see address given above).
- NCEER-87-0018 "Practical Considerations for Structural Control: System Uncertainty, System Time Delay and Truncation of Small Control Forces," J.N. Yang and A. Akbarpour, 8/10/87, (PB88-163738, A08, MF-A01). This report is only available through NTIS (see address given above).
- NCEER-87-0019 "Modal Analysis of Nonclassically Damped Structural Systems Using Canonical Transformation," by J.N. Yang, S. Sarkani and F.X. Long, 9/27/87, (PB88-187851, A04, MF-A01).
- NCEER-87-0020 "A Nonstationary Solution in Random Vibration Theory," by J.R. Red-Horse and P.D. Spanos, 11/3/87, (PB88-163746, A03, MF-A01).
- NCEER-87-0021 "Horizontal Impedances for Radially Inhomogeneous Viscoelastic Soil Layers," by A.S. Veletsos and K.W. Dotson, 10/15/87, (PB88-150859, A04, MF-A01).
- NCEER-87-0022 "Seismic Damage Assessment of Reinforced Concrete Members," by Y.S. Chung, C. Meyer and M. Shinozuka, 10/9/87, (PB88-150867, A05, MF-A01). This report is available only through NTIS (see address given above).
- NCEER-87-0023 "Active Structural Control in Civil Engineering," by T.T. Soong, 11/11/87, (PB88-187778, A03, MF-A01).
- NCEER-87-0024 "Vertical and Torsional Impedances for Radially Inhomogeneous Viscoelastic Soil Layers," by K.W. Dotson and A.S. Veletsos, 12/87, (PB88-187786, A03, MF-A01).
- NCEER-87-0025 "Proceedings from the Symposium on Seismic Hazards, Ground Motions, Soil-Liquefaction and Engineering Practice in Eastern North America," October 20-22, 1987, edited by K.H. Jacob, 12/87, (PB88-188115, A23, MF-A01). This report is available only through NTIS (see address given above).
- NCEER-87-0026 "Report on the Whittier-Narrows, California, Earthquake of October 1, 1987," by J. Pantelic and A. Reinhorn, 11/87, (PB88-187752, A03, MF-A01). This report is available only through NTIS (see address given above).
- NCEER-87-0027 "Design of a Modular Program for Transient Nonlinear Analysis of Large 3-D Building Structures," by S. Srivastav and J.F. Abel, 12/30/87, (PB88-187950, A05, MF-A01). This report is only available through NTIS (see address given above).
- NCEER-87-0028 "Second-Year Program in Research, Education and Technology Transfer," 3/8/88, (PB88-219480, A04, MF-A01).
- NCEER-88-0001 "Workshop on Seismic Computer Analysis and Design of Buildings With Interactive Graphics," by W. McGuire, J.F. Abel and C.H. Conley, 1/18/88, (PB88-187760, A03, MF-A01). This report is only available through NTIS (see address given above).
- NCEER-88-0002 "Optimal Control of Nonlinear Flexible Structures," by J.N. Yang, F.X. Long and D. Wong, 1/22/88, (PB88-213772, A06, MF-A01).
- NCEER-88-0003 "Substructuring Techniques in the Time Domain for Primary-Secondary Structural Systems," by G.D. Manolis and G. Juhn, 2/10/88, (PB88-213780, A04, MF-A01).
- NCEER-88-0004 "Iterative Seismic Analysis of Primary-Secondary Systems," by A. Singhal, L.D. Lutes and P.D. Spanos, 2/23/88, (PB88-213798, A04, MF-A01).
- NCEER-88-0005 "Stochastic Finite Element Expansion for Random Media," by P.D. Spanos and R. Ghanem, 3/14/88, (PB88-213806, A03, MF-A01).

- NCEER-88-0006 "Combining Structural Optimization and Structural Control," by F.Y. Cheng and C.P. Pantelides, 1/10/88, (PB88-213814, A05, MF-A01).
- NCEER-88-0007 "Seismic Performance Assessment of Code-Designed Structures," by H.H-M. Hwang, J-W. Jaw and H-J. Shau, 3/20/88, (PB88-219423, A04, MF-A01). This report is only available through NTIS (see address given above).
- NCEER-88-0008 "Reliability Analysis of Code-Designed Structures Under Natural Hazards," by H.H-M. Hwang, H. Ushiba and M. Shinozuka, 2/29/88, (PB88-229471, A07, MF-A01). This report is only available through NTIS (see address given above).
- NCEER-88-0009 "Seismic Fragility Analysis of Shear Wall Structures," by J-W Jaw and H.H-M. Hwang, 4/30/88, (PB89-102867, A04, MF-A01).
- NCEER-88-0010 "Base Isolation of a Multi-Story Building Under a Harmonic Ground Motion - A Comparison of Performances of Various Systems," by F-G Fan, G. Ahmadi and I.G. Tadjbakhsh, 5/18/88, (PB89-122238, A06, MF-A01). This report is only available through NTIS (see address given above).
- NCEER-88-0011 "Seismic Floor Response Spectra for a Combined System by Green's Functions," by F.M. Lavelle, L.A. Bergman and P.D. Spanos, 5/1/88, (PB89-102875, A03, MF-A01).
- NCEER-88-0012 "A New Solution Technique for Randomly Excited Hysteretic Structures," by G.Q. Cai and Y.K. Lin, 5/16/88, (PB89-102883, A03, MF-A01).
- NCEER-88-0013 "A Study of Radiation Damping and Soil-Structure Interaction Effects in the Centrifuge," by K. Weissman, supervised by J.H. Prevost, 5/24/88, (PB89-144703, A06, MF-A01).
- NCEER-88-0014 "Parameter Identification and Implementation of a Kinematic Plasticity Model for Frictional Soils," by J.H. Prevost and D.V. Griffiths, to be published.
- NCEER-88-0015 "Two- and Three- Dimensional Dynamic Finite Element Analyses of the Long Valley Dam," by D.V. Griffiths and J.H. Prevost, 6/17/88, (PB89-144711, A04, MF-A01).
- NCEER-88-0016 "Damage Assessment of Reinforced Concrete Structures in Eastern United States," by A.M. Reinhorn, M.J. Seidel, S.K. Kunnath and Y.J. Park, 6/15/88, (PB89-122220, A04, MF-A01). This report is only available through NTIS (see address given above).
- NCEER-88-0017 "Dynamic Compliance of Vertically Loaded Strip Foundations in Multilayered Viscoelastic Soils," by S. Ahmad and A.S.M. Israil, 6/17/88, (PB89-102891, A04, MF-A01).
- NCEER-88-0018 "An Experimental Study of Seismic Structural Response With Added Viscoelastic Dampers," by R.C. Lin, Z. Liang, T.T. Soong and R.H. Zhang, 6/30/88, (PB89-122212, A05, MF-A01). This report is available only through NTIS (see address given above).
- NCEER-88-0019 "Experimental Investigation of Primary - Secondary System Interaction," by G.D. Manolis, G. Juhn and A.M. Reinhorn, 5/27/88, (PB89-122204, A04, MF-A01).
- NCEER-88-0020 "A Response Spectrum Approach For Analysis of Nonclassically Damped Structures," by J.N. Yang, S. Sarkani and F.X. Long, 4/22/88, (PB89-102909, A04, MF-A01).
- NCEER-88-0021 "Seismic Interaction of Structures and Soils: Stochastic Approach," by A.S. Veletsos and A.M. Prasad, 7/21/88, (PB89-122196, A04, MF-A01). This report is only available through NTIS (see address given above).
- NCEER-88-0022 "Identification of the Serviceability Limit State and Detection of Seismic Structural Damage," by E. DiPasquale and A.S. Cakmak, 6/15/88, (PB89-122188, A05, MF-A01). This report is available only through NTIS (see address given above).
- NCEER-88-0023 "Multi-Hazard Risk Analysis: Case of a Simple Offshore Structure," by B.K. Bhartia and E.H. Vanmarcke, 7/21/88, (PB89-145213, A05, MF-A01).

- NCEER-88-0024 "Automated Seismic Design of Reinforced Concrete Buildings," by Y.S. Chung, C. Meyer and M. Shinozuka, 7/5/88, (PB89-122170, A06, MF-A01). This report is available only through NTIS (see address given above).
- NCEER-88-0025 "Experimental Study of Active Control of MDOF Structures Under Seismic Excitations," by L.L. Chung, R.C. Lin, T.T. Soong and A.M. Reinhorn, 7/10/88, (PB89-122600, A04, MF-A01).
- NCEER-88-0026 "Earthquake Simulation Tests of a Low-Rise Metal Structure," by J.S. Hwang, K.C. Chang, G.C. Lee and R.L. Ketter, 8/1/88, (PB89-102917, A04, MF-A01).
- NCEER-88-0027 "Systems Study of Urban Response and Reconstruction Due to Catastrophic Earthquakes," by F. Kozin and H.K. Zhou, 9/22/88, (PB90-162348, A04, MF-A01).
- NCEER-88-0028 "Seismic Fragility Analysis of Plane Frame Structures," by H.H-M. Hwang and Y.K. Low, 7/31/88, (PB89-131445, A06, MF-A01).
- NCEER-88-0029 "Response Analysis of Stochastic Structures," by A. Kardara, C. Bucher and M. Shinozuka, 9/22/88, (PB89-174429, A04, MF-A01).
- NCEER-88-0030 "Nonnormal Accelerations Due to Yielding in a Primary Structure," by D.C.K. Chen and L.D. Lutes, 9/19/88, (PB89-131437, A04, MF-A01).
- NCEER-88-0031 "Design Approaches for Soil-Structure Interaction," by A.S. Veletsos, A.M. Prasad and Y. Tang, 12/30/88, (PB89-174437, A03, MF-A01). This report is available only through NTIS (see address given above).
- NCEER-88-0032 "A Re-evaluation of Design Spectra for Seismic Damage Control," by C.J. Turkstra and A.G. Tallin, 11/7/88, (PB89-145221, A05, MF-A01).
- NCEER-88-0033 "The Behavior and Design of Noncontact Lap Splices Subjected to Repeated Inelastic Tensile Loading," by V.E. Sagan, P. Gergely and R.N. White, 12/8/88, (PB89-163737, A08, MF-A01).
- NCEER-88-0034 "Seismic Response of Pile Foundations," by S.M. Mamoon, P.K. Banerjee and S. Ahmad, 11/1/88, (PB89-145239, A04, MF-A01).
- NCEER-88-0035 "Modeling of R/C Building Structures With Flexible Floor Diaphragms (IDARC2)," by A.M. Reinhorn, S.K. Kunnath and N. Panahshahi, 9/7/88, (PB89-207153, A07, MF-A01).
- NCEER-88-0036 "Solution of the Dam-Reservoir Interaction Problem Using a Combination of FEM, BEM with Particular Integrals, Modal Analysis, and Substructuring," by C-S. Tsai, G.C. Lee and R.L. Ketter, 12/31/88, (PB89-207146, A04, MF-A01).
- NCEER-88-0037 "Optimal Placement of Actuators for Structural Control," by F.Y. Cheng and C.P. Pantelides, 8/15/88, (PB89-162846, A05, MF-A01).
- NCEER-88-0038 "Teflon Bearings in Aseismic Base Isolation: Experimental Studies and Mathematical Modeling," by A. Mokha, M.C. Constantinou and A.M. Reinhorn, 12/5/88, (PB89-218457, A10, MF-A01). This report is available only through NTIS (see address given above).
- NCEER-88-0039 "Seismic Behavior of Flat Slab High-Rise Buildings in the New York City Area," by P. Weidlinger and M. Ettouney, 10/15/88, (PB90-145681, A04, MF-A01).
- NCEER-88-0040 "Evaluation of the Earthquake Resistance of Existing Buildings in New York City," by P. Weidlinger and M. Ettouney, 10/15/88, to be published.
- NCEER-88-0041 "Small-Scale Modeling Techniques for Reinforced Concrete Structures Subjected to Seismic Loads," by W. Kim, A. El-Attar and R.N. White, 11/22/88, (PB89-189625, A05, MF-A01).
- NCEER-88-0042 "Modeling Strong Ground Motion from Multiple Event Earthquakes," by G.W. Ellis and A.S. Cakmak, 10/15/88, (PB89-174445, A03, MF-A01).

- NCEER-88-0043 "Nonstationary Models of Seismic Ground Acceleration," by M. Grigoriu, S.E. Ruiz and E. Rosenblueth, 7/15/88, (PB89-189617, A04, MF-A01).
- NCEER-88-0044 "SARCF User's Guide: Seismic Analysis of Reinforced Concrete Frames," by Y.S. Chung, C. Meyer and M. Shinozuka, 11/9/88, (PB89-174452, A08, MF-A01).
- NCEER-88-0045 "First Expert Panel Meeting on Disaster Research and Planning," edited by J. Pantelic and J. Stoyle, 9/15/88, (PB89-174460, A05, MF-A01).
- NCEER-88-0046 "Preliminary Studies of the Effect of Degrading Infill Walls on the Nonlinear Seismic Response of Steel Frames," by C.Z. Chrysostomou, P. Gergely and J.F. Abel, 12/19/88, (PB89-208383, A05, MF-A01).
- NCEER-88-0047 "Reinforced Concrete Frame Component Testing Facility - Design, Construction, Instrumentation and Operation," by S.P. Pessiki, C. Conley, T. Bond, P. Gergely and R.N. White, 12/16/88, (PB89-174478, A04, MF-A01).
- NCEER-89-0001 "Effects of Protective Cushion and Soil Compliancy on the Response of Equipment Within a Seismically Excited Building," by J.A. HoLung, 2/16/89, (PB89-207179, A04, MF-A01).
- NCEER-89-0002 "Statistical Evaluation of Response Modification Factors for Reinforced Concrete Structures," by H.H-M. Hwang and J-W. Jaw, 2/17/89, (PB89-207187, A05, MF-A01).
- NCEER-89-0003 "Hysteretic Columns Under Random Excitation," by G-Q. Cai and Y.K. Lin, 1/9/89, (PB89-196513, A03, MF-A01).
- NCEER-89-0004 "Experimental Study of 'Elephant Foot Bulge' Instability of Thin-Walled Metal Tanks," by Z-H. Jia and R.L. Ketter, 2/22/89, (PB89-207195, A03, MF-A01).
- NCEER-89-0005 "Experiment on Performance of Buried Pipelines Across San Andreas Fault," by J. Isenberg, E. Richardson and T.D. O'Rourke, 3/10/89, (PB89-218440, A04, MF-A01). This report is available only through NTIS (see address given above).
- NCEER-89-0006 "A Knowledge-Based Approach to Structural Design of Earthquake-Resistant Buildings," by M. Subramani, P. Gergely, C.H. Conley, J.F. Abel and A.H. Zaghaw, 1/15/89, (PB89-218465, A06, MF-A01).
- NCEER-89-0007 "Liquefaction Hazards and Their Effects on Buried Pipelines," by T.D. O'Rourke and P.A. Lane, 2/1/89, (PB89-218481, A09, MF-A01).
- NCEER-89-0008 "Fundamentals of System Identification in Structural Dynamics," by H. Imai, C-B. Yun, O. Maruyama and M. Shinozuka, 1/26/89, (PB89-207211, A04, MF-A01).
- NCEER-89-0009 "Effects of the 1985 Michoacan Earthquake on Water Systems and Other Buried Lifelines in Mexico," by A.G. Ayala and M.J. O'Rourke, 3/8/89, (PB89-207229, A06, MF-A01).
- NCEER-89-R010 "NCEER Bibliography of Earthquake Education Materials," by K.E.K. Ross, Second Revision, 9/1/89, (PB90-125352, A05, MF-A01). This report is replaced by NCEER-92-0018.
- NCEER-89-0011 "Inelastic Three-Dimensional Response Analysis of Reinforced Concrete Building Structures (IDARC-3D), Part I - Modeling," by S.K. Kunnath and A.M. Reinhorn, 4/17/89, (PB90-114612, A07, MF-A01). This report is available only through NTIS (see address given above).
- NCEER-89-0012 "Recommended Modifications to ATC-14," by C.D. Poland and J.O. Malley, 4/12/89, (PB90-108648, A15, MF-A01).
- NCEER-89-0013 "Repair and Strengthening of Beam-to-Column Connections Subjected to Earthquake Loading," by M. Corazao and A.J. Durrani, 2/28/89, (PB90-109885, A06, MF-A01).
- NCEER-89-0014 "Program EXKAL2 for Identification of Structural Dynamic Systems," by O. Maruyama, C-B. Yun, M. Hoshiya and M. Shinozuka, 5/19/89, (PB90-109877, A09, MF-A01).

- NCEER-89-0015 "Response of Frames With Bolted Semi-Rigid Connections, Part I - Experimental Study and Analytical Predictions," by P.J. DiCorso, A.M. Reinhorn, J.R. Dickerson, J.B. Radzinski and W.L. Harper, 6/1/89, to be published.
- NCEER-89-0016 "ARMA Monte Carlo Simulation in Probabilistic Structural Analysis," by P.D. Spanos and M.P. Mignolet, 7/10/89, (PB90-109893, A03, MF-A01).
- NCEER-89-P017 "Preliminary Proceedings from the Conference on Disaster Preparedness - The Place of Earthquake Education in Our Schools," Edited by K.E.K. Ross, 6/23/89, (PB90-108606, A03, MF-A01).
- NCEER-89-0017 "Proceedings from the Conference on Disaster Preparedness - The Place of Earthquake Education in Our Schools," Edited by K.E.K. Ross, 12/31/89, (PB90-207895, A012, MF-A02). This report is available only through NTIS (see address given above).
- NCEER-89-0018 "Multidimensional Models of Hysteretic Material Behavior for Vibration Analysis of Shape Memory Energy Absorbing Devices, by E.J. Graesser and F.A. Cozzarelli, 6/7/89, (PB90-164146, A04, MF-A01).
- NCEER-89-0019 "Nonlinear Dynamic Analysis of Three-Dimensional Base Isolated Structures (3D-BASIS)," by S. Nagarajaiah, A.M. Reinhorn and M.C. Constantinou, 8/3/89, (PB90-161936, A06, MF-A01). This report has been replaced by NCEER-93-0011.
- NCEER-89-0020 "Structural Control Considering Time-Rate of Control Forces and Control Rate Constraints," by F.Y. Cheng and C.P. Pantelides, 8/3/89, (PB90-120445, A04, MF-A01).
- NCEER-89-0021 "Subsurface Conditions of Memphis and Shelby County," by K.W. Ng, T-S. Chang and H-H.M. Hwang, 7/26/89, (PB90-120437, A03, MF-A01).
- NCEER-89-0022 "Seismic Wave Propagation Effects on Straight Jointed Buried Pipelines," by K. Elhmadi and M.J. O'Rourke, 8/24/89, (PB90-162322, A10, MF-A02).
- NCEER-89-0023 "Workshop on Serviceability Analysis of Water Delivery Systems," edited by M. Grigoriu, 3/6/89, (PB90-127424, A03, MF-A01).
- NCEER-89-0024 "Shaking Table Study of a 1/5 Scale Steel Frame Composed of Tapered Members," by K.C. Chang, J.S. Hwang and G.C. Lee, 9/18/89, (PB90-160169, A04, MF-A01).
- NCEER-89-0025 "DYNA1D: A Computer Program for Nonlinear Seismic Site Response Analysis - Technical Documentation," by Jean H. Prevost, 9/14/89, (PB90-161944, A07, MF-A01). This report is available only through NTIS (see address given above).
- NCEER-89-0026 "1:4 Scale Model Studies of Active Tendon Systems and Active Mass Dampers for Aseismic Protection," by A.M. Reinhorn, T.T. Soong, R.C. Lin, Y.P. Yang, Y. Fukao, H. Abe and M. Nakai, 9/15/89, (PB90-173246, A10, MF-A02). This report is available only through NTIS (see address given above).
- NCEER-89-0027 "Scattering of Waves by Inclusions in a Nonhomogeneous Elastic Half Space Solved by Boundary Element Methods," by P.K. Hadley, A. Askar and A.S. Cakmak, 6/15/89, (PB90-145699, A07, MF-A01).
- NCEER-89-0028 "Statistical Evaluation of Deflection Amplification Factors for Reinforced Concrete Structures," by H.H.M. Hwang, J-W. Jaw and A.L. Ch'ng, 8/31/89, (PB90-164633, A05, MF-A01).
- NCEER-89-0029 "Bedrock Accelerations in Memphis Area Due to Large New Madrid Earthquakes," by H.H.M. Hwang, C.H.S. Chen and G. Yu, 11/7/89, (PB90-162330, A04, MF-A01).
- NCEER-89-0030 "Seismic Behavior and Response Sensitivity of Secondary Structural Systems," by Y.Q. Chen and T.T. Soong, 10/23/89, (PB90-164658, A08, MF-A01).
- NCEER-89-0031 "Random Vibration and Reliability Analysis of Primary-Secondary Structural Systems," by Y. Ibrahim, M. Grigoriu and T.T. Soong, 11/10/89, (PB90-161951, A04, MF-A01).

- NCEER-89-0032 "Proceedings from the Second U.S. - Japan Workshop on Liquefaction, Large Ground Deformation and Their Effects on Lifelines, September 26-29, 1989," Edited by T.D. O'Rourke and M. Hamada, 12/1/89, (PB90-209388, A22, MF-A03).
- NCEER-89-0033 "Deterministic Model for Seismic Damage Evaluation of Reinforced Concrete Structures," by J.M. Bracci, A.M. Reinhorn, J.B. Mander and S.K. Kunnath, 9/27/89, (PB91-108803, A06, MF-A01).
- NCEER-89-0034 "On the Relation Between Local and Global Damage Indices," by E. DiPasquale and A.S. Cakmak, 8/15/89, (PB90-173865, A05, MF-A01).
- NCEER-89-0035 "Cyclic Undrained Behavior of Nonplastic and Low Plasticity Silts," by A.J. Walker and H.E. Stewart, 7/26/89, (PB90-183518, A10, MF-A01).
- NCEER-89-0036 "Liquefaction Potential of Surficial Deposits in the City of Buffalo, New York," by M. Budhu, R. Giese and L. Baumgrass, 1/17/89, (PB90-208455, A04, MF-A01).
- NCEER-89-0037 "A Deterministic Assessment of Effects of Ground Motion Incoherence," by A.S. Veletsos and Y. Tang, 7/15/89, (PB90-164294, A03, MF-A01).
- NCEER-89-0038 "Workshop on Ground Motion Parameters for Seismic Hazard Mapping," July 17-18, 1989, edited by R.V. Whitman, 12/1/89, (PB90-173923, A04, MF-A01).
- NCEER-89-0039 "Seismic Effects on Elevated Transit Lines of the New York City Transit Authority," by C.J. Costantino, C.A. Miller and E. Heymsfield, 12/26/89, (PB90-207887, A06, MF-A01).
- NCEER-89-0040 "Centrifugal Modeling of Dynamic Soil-Structure Interaction," by K. Weissman, Supervised by J.H. Prevost, 5/10/89, (PB90-207879, A07, MF-A01).
- NCEER-89-0041 "Linearized Identification of Buildings With Cores for Seismic Vulnerability Assessment," by I-K. Ho and A.E. Aktan, 11/1/89, (PB90-251943, A07, MF-A01).
- NCEER-90-0001 "Geotechnical and Lifeline Aspects of the October 17, 1989 Loma Prieta Earthquake in San Francisco," by T.D. O'Rourke, H.E. Stewart, F.T. Blackburn and T.S. Dickerman, 1/90, (PB90-208596, A05, MF-A01).
- NCEER-90-0002 "Nonnormal Secondary Response Due to Yielding in a Primary Structure," by D.C.K. Chen and L.D. Lutes, 2/28/90, (PB90-251976, A07, MF-A01).
- NCEER-90-0003 "Earthquake Education Materials for Grades K-12," by K.E.K. Ross, 4/16/90, (PB91-251984, A05, MF-A05). This report has been replaced by NCEER-92-0018.
- NCEER-90-0004 "Catalog of Strong Motion Stations in Eastern North America," by R.W. Busby, 4/3/90, (PB90-251984, A05, MF-A01).
- NCEER-90-0005 "NCEER Strong-Motion Data Base: A User Manual for the GeoBase Release (Version 1.0 for the Sun3)," by P. Friberg and K. Jacob, 3/31/90 (PB90-258062, A04, MF-A01).
- NCEER-90-0006 "Seismic Hazard Along a Crude Oil Pipeline in the Event of an 1811-1812 Type New Madrid Earthquake," by H.H.M. Hwang and C-H.S. Chen, 4/16/90, (PB90-258054, A04, MF-A01).
- NCEER-90-0007 "Site-Specific Response Spectra for Memphis Sheahan Pumping Station," by H.H.M. Hwang and C.S. Lee, 5/15/90, (PB91-108811, A05, MF-A01).
- NCEER-90-0008 "Pilot Study on Seismic Vulnerability of Crude Oil Transmission Systems," by T. Ariman, R. Dobry, M. Grigoriu, F. Kozin, M. O'Rourke, T. O'Rourke and M. Shinozuka, 5/25/90, (PB91-108837, A06, MF-A01).
- NCEER-90-0009 "A Program to Generate Site Dependent Time Histories: EQGEN," by G.W. Ellis, M. Srinivasan and A.S. Cakmak, 1/30/90, (PB91-108829, A04, MF-A01).
- NCEER-90-0010 "Active Isolation for Seismic Protection of Operating Rooms," by M.E. Talbott, Supervised by M. Shinozuka, 6/8/9, (PB91-110205, A05, MF-A01).

- NCEER-90-0011 "Program LINEARID for Identification of Linear Structural Dynamic Systems," by C-B. Yun and M. Shinozuka, 6/25/90, (PB91-110312, A08, MF-A01).
- NCEER-90-0012 "Two-Dimensional Two-Phase Elasto-Plastic Seismic Response of Earth Dams," by A.N. Yiagos, Supervised by J.H. Prevost, 6/20/90, (PB91-110197, A13, MF-A02).
- NCEER-90-0013 "Secondary Systems in Base-Isolated Structures: Experimental Investigation, Stochastic Response and Stochastic Sensitivity," by G.D. Manolis, G. Juhn, M.C. Constantinou and A.M. Reinhorn, 7/1/90, (PB91-110320, A08, MF-A01).
- NCEER-90-0014 "Seismic Behavior of Lightly-Reinforced Concrete Column and Beam-Column Joint Details," by S.P. Pessiki, C.H. Conley, P. Gergely and R.N. White, 8/22/90, (PB91-108795, A11, MF-A02).
- NCEER-90-0015 "Two Hybrid Control Systems for Building Structures Under Strong Earthquakes," by J.N. Yang and A. Daniellians, 6/29/90, (PB91-125393, A04, MF-A01).
- NCEER-90-0016 "Instantaneous Optimal Control with Acceleration and Velocity Feedback," by J.N. Yang and Z. Li, 6/29/90, (PB91-125401, A03, MF-A01).
- NCEER-90-0017 "Reconnaissance Report on the Northern Iran Earthquake of June 21, 1990," by M. Mehrain, 10/4/90, (PB91-125377, A03, MF-A01).
- NCEER-90-0018 "Evaluation of Liquefaction Potential in Memphis and Shelby County," by T.S. Chang, P.S. Tang, C.S. Lee and H. Hwang, 8/10/90, (PB91-125427, A09, MF-A01).
- NCEER-90-0019 "Experimental and Analytical Study of a Combined Sliding Disc Bearing and Helical Steel Spring Isolation System," by M.C. Constantinou, A.S. Mokha and A.M. Reinhorn, 10/4/90, (PB91-125385, A06, MF-A01). This report is available only through NTIS (see address given above).
- NCEER-90-0020 "Experimental Study and Analytical Prediction of Earthquake Response of a Sliding Isolation System with a Spherical Surface," by A.S. Mokha, M.C. Constantinou and A.M. Reinhorn, 10/11/90, (PB91-125419, A05, MF-A01).
- NCEER-90-0021 "Dynamic Interaction Factors for Floating Pile Groups," by G. Gazetas, K. Fan, A. Kaynia and E. Kausel, 9/10/90, (PB91-170381, A05, MF-A01).
- NCEER-90-0022 "Evaluation of Seismic Damage Indices for Reinforced Concrete Structures," by S. Rodriguez-Gomez and A.S. Cakmak, 9/30/90, PB91-171322, A06, MF-A01).
- NCEER-90-0023 "Study of Site Response at a Selected Memphis Site," by H. Desai, S. Ahmad, E.S. Gazetas and M.R. Oh, 10/11/90, (PB91-196857, A03, MF-A01).
- NCEER-90-0024 "A User's Guide to Strongmo: Version 1.0 of NCEER's Strong-Motion Data Access Tool for PCs and Terminals," by P.A. Friberg and C.A.T. Susch, 11/15/90, (PB91-171272, A03, MF-A01).
- NCEER-90-0025 "A Three-Dimensional Analytical Study of Spatial Variability of Seismic Ground Motions," by L-L. Hong and A.H.-S. Ang, 10/30/90, (PB91-170399, A09, MF-A01).
- NCEER-90-0026 "MUMOID User's Guide - A Program for the Identification of Modal Parameters," by S. Rodriguez-Gomez and E. DiPasquale, 9/30/90, (PB91-171298, A04, MF-A01).
- NCEER-90-0027 "SARCF-II User's Guide - Seismic Analysis of Reinforced Concrete Frames," by S. Rodriguez-Gomez, Y.S. Chung and C. Meyer, 9/30/90, (PB91-171280, A05, MF-A01).
- NCEER-90-0028 "Viscous Dampers: Testing, Modeling and Application in Vibration and Seismic Isolation," by N. Makris and M.C. Constantinou, 12/20/90 (PB91-190561, A06, MF-A01).
- NCEER-90-0029 "Soil Effects on Earthquake Ground Motions in the Memphis Area," by H. Hwang, C.S. Lee, K.W. Ng and T.S. Chang, 8/2/90, (PB91-190751, A05, MF-A01).

- NCEER-91-0001 "Proceedings from the Third Japan-U.S. Workshop on Earthquake Resistant Design of Lifeline Facilities and Countermeasures for Soil Liquefaction, December 17-19, 1990," edited by T.D. O'Rourke and M. Hamada, 2/1/91, (PB91-179259, A99, MF-A04).
- NCEER-91-0002 "Physical Space Solutions of Non-Proportionally Damped Systems," by M. Tong, Z. Liang and G.C. Lee, 1/15/91, (PB91-179242, A04, MF-A01).
- NCEER-91-0003 "Seismic Response of Single Piles and Pile Groups," by K. Fan and G. Gazetas, 1/10/91, (PB92-174994, A04, MF-A01).
- NCEER-91-0004 "Damping of Structures: Part 1 - Theory of Complex Damping," by Z. Liang and G. Lee, 10/10/91, (PB92-197235, A12, MF-A03).
- NCEER-91-0005 "3D-BASIS - Nonlinear Dynamic Analysis of Three Dimensional Base Isolated Structures: Part II," by S. Nagarajaiah, A.M. Reinhorn and M.C. Constantinou, 2/28/91, (PB91-190553, A07, MF-A01). This report has been replaced by NCEER-93-0011.
- NCEER-91-0006 "A Multidimensional Hysteretic Model for Plasticity Deforming Metals in Energy Absorbing Devices," by E.J. Graesser and F.A. Cozzarelli, 4/9/91, (PB92-108364, A04, MF-A01).
- NCEER-91-0007 "A Framework for Customizable Knowledge-Based Expert Systems with an Application to a KBES for Evaluating the Seismic Resistance of Existing Buildings," by E.G. Ibarra-Anaya and S.J. Fennes, 4/9/91, (PB91-210930, A08, MF-A01).
- NCEER-91-0008 "Nonlinear Analysis of Steel Frames with Semi-Rigid Connections Using the Capacity Spectrum Method," by G.G. Deierlein, S-H. Hsieh, Y-J. Shen and J.F. Abel, 7/2/91, (PB92-113828, A05, MF-A01).
- NCEER-91-0009 "Earthquake Education Materials for Grades K-12," by K.E.K. Ross, 4/30/91, (PB91-212142, A06, MF-A01). This report has been replaced by NCEER-92-0018.
- NCEER-91-0010 "Phase Wave Velocities and Displacement Phase Differences in a Harmonically Oscillating Pile," by N. Makris and G. Gazetas, 7/8/91, (PB92-108356, A04, MF-A01).
- NCEER-91-0011 "Dynamic Characteristics of a Full-Size Five-Story Steel Structure and a 2/5 Scale Model," by K.C. Chang, G.C. Yao, G.C. Lee, D.S. Hao and Y.C. Yeh," 7/2/91, (PB93-116648, A06, MF-A02).
- NCEER-91-0012 "Seismic Response of a 2/5 Scale Steel Structure with Added Viscoelastic Dampers," by K.C. Chang, T.T. Soong, S-T. Oh and M.L. Lai, 5/17/91, (PB92-110816, A05, MF-A01).
- NCEER-91-0013 "Earthquake Response of Retaining Walls; Full-Scale Testing and Computational Modeling," by S. Alampalli and A-W.M. Elgamal, 6/20/91, to be published.
- NCEER-91-0014 "3D-BASIS-M: Nonlinear Dynamic Analysis of Multiple Building Base Isolated Structures," by P.C. Tsopelas, S. Nagarajaiah, M.C. Constantinou and A.M. Reinhorn, 5/28/91, (PB92-113885, A09, MF-A02).
- NCEER-91-0015 "Evaluation of SEAOC Design Requirements for Sliding Isolated Structures," by D. Theodossiou and M.C. Constantinou, 6/10/91, (PB92-114602, A11, MF-A03).
- NCEER-91-0016 "Closed-Loop Modal Testing of a 27-Story Reinforced Concrete Flat Plate-Core Building," by H.R. Somaprasad, T. Toksoy, H. Yoshiyuki and A.E. Aktan, 7/15/91, (PB92-129980, A07, MF-A02).
- NCEER-91-0017 "Shake Table Test of a 1/6 Scale Two-Story Lightly Reinforced Concrete Building," by A.G. El-Attar, R.N. White and P. Gergely, 2/28/91, (PB92-222447, A06, MF-A02).
- NCEER-91-0018 "Shake Table Test of a 1/8 Scale Three-Story Lightly Reinforced Concrete Building," by A.G. El-Attar, R.N. White and P. Gergely, 2/28/91, (PB93-116630, A08, MF-A02).
- NCEER-91-0019 "Transfer Functions for Rigid Rectangular Foundations," by A.S. Veletsos, A.M. Prasad and W.H. Wu, 7/31/91, to be published.

- NCEER-91-0020 "Hybrid Control of Seismic-Excited Nonlinear and Inelastic Structural Systems," by J.N. Yang, Z. Li and A. Daniellians, 8/1/91, (PB92-143171, A06, MF-A02).
- NCEER-91-0021 "The NCEER-91 Earthquake Catalog: Improved Intensity-Based Magnitudes and Recurrence Relations for U.S. Earthquakes East of New Madrid," by L. Seeber and J.G. Armbruster, 8/28/91, (PB92-176742, A06, MF-A02).
- NCEER-91-0022 "Proceedings from the Implementation of Earthquake Planning and Education in Schools: The Need for Change - The Roles of the Changemakers," by K.E.K. Ross and F. Winslow, 7/23/91, (PB92-129998, A12, MF-A03).
- NCEER-91-0023 "A Study of Reliability-Based Criteria for Seismic Design of Reinforced Concrete Frame Buildings," by H.H.M. Hwang and H-M. Hsu, 8/10/91, (PB92-140235, A09, MF-A02).
- NCEER-91-0024 "Experimental Verification of a Number of Structural System Identification Algorithms," by R.G. Ghanem, H. Gavin and M. Shinozuka, 9/18/91, (PB92-176577, A18, MF-A04).
- NCEER-91-0025 "Probabilistic Evaluation of Liquefaction Potential," by H.H.M. Hwang and C.S. Lee," 11/25/91, (PB92-143429, A05, MF-A01).
- NCEER-91-0026 "Instantaneous Optimal Control for Linear, Nonlinear and Hysteretic Structures - Stable Controllers," by J.N. Yang and Z. Li, 11/15/91, (PB92-163807, A04, MF-A01).
- NCEER-91-0027 "Experimental and Theoretical Study of a Sliding Isolation System for Bridges," by M.C. Constantinou, A. Kartoum, A.M. Reinhorn and P. Bradford, 11/15/91, (PB92-176973, A10, MF-A03).
- NCEER-92-0001 "Case Studies of Liquefaction and Lifeline Performance During Past Earthquakes, Volume 1: Japanese Case Studies," Edited by M. Hamada and T. O'Rourke, 2/17/92, (PB92-197243, A18, MF-A04).
- NCEER-92-0002 "Case Studies of Liquefaction and Lifeline Performance During Past Earthquakes, Volume 2: United States Case Studies," Edited by T. O'Rourke and M. Hamada, 2/17/92, (PB92-197250, A20, MF-A04).
- NCEER-92-0003 "Issues in Earthquake Education," Edited by K. Ross, 2/3/92, (PB92-222389, A07, MF-A02).
- NCEER-92-0004 "Proceedings from the First U.S. - Japan Workshop on Earthquake Protective Systems for Bridges," Edited by I.G. Buckle, 2/4/92, (PB94-142239, A99, MF-A06).
- NCEER-92-0005 "Seismic Ground Motion from a Haskell-Type Source in a Multiple-Layered Half-Space," A.P. Theoharis, G. Deodatis and M. Shinozuka, 1/2/92, to be published.
- NCEER-92-0006 "Proceedings from the Site Effects Workshop," Edited by R. Whitman, 2/29/92, (PB92-197201, A04, MF-A01).
- NCEER-92-0007 "Engineering Evaluation of Permanent Ground Deformations Due to Seismically-Induced Liquefaction," by M.H. Baziar, R. Dobry and A-W.M. Elgamal, 3/24/92, (PB92-222421, A13, MF-A03).
- NCEER-92-0008 "A Procedure for the Seismic Evaluation of Buildings in the Central and Eastern United States," by C.D. Poland and J.O. Malley, 4/2/92, (PB92-222439, A20, MF-A04).
- NCEER-92-0009 "Experimental and Analytical Study of a Hybrid Isolation System Using Friction Controllable Sliding Bearings," by M.Q. Feng, S. Fujii and M. Shinozuka, 5/15/92, (PB93-150282, A06, MF-A02).
- NCEER-92-0010 "Seismic Resistance of Slab-Column Connections in Existing Non-Ductile Flat-Plate Buildings," by A.J. Durrani and Y. Du, 5/18/92, (PB93-116812, A06, MF-A02).
- NCEER-92-0011 "The Hysteretic and Dynamic Behavior of Brick Masonry Walls Upgraded by Ferrocement Coatings Under Cyclic Loading and Strong Simulated Ground Motion," by H. Lee and S.P. Prawel, 5/11/92, to be published.
- NCEER-92-0012 "Study of Wire Rope Systems for Seismic Protection of Equipment in Buildings," by G.F. Demetriades, M.C. Constantinou and A.M. Reinhorn, 5/20/92, (PB93-116655, A08, MF-A02).

- NCEER-92-0013 "Shape Memory Structural Dampers: Material Properties, Design and Seismic Testing," by P.R. Witting and F.A. Cozzarelli, 5/26/92, (PB93-116663, A05, MF-A01).
- NCEER-92-0014 "Longitudinal Permanent Ground Deformation Effects on Buried Continuous Pipelines," by M.J. O'Rourke, and C. Nordberg, 6/15/92, (PB93-116671, A08, MF-A02).
- NCEER-92-0015 "A Simulation Method for Stationary Gaussian Random Functions Based on the Sampling Theorem," by M. Grigoriu and S. Balopoulou, 6/11/92, (PB93-127496, A05, MF-A01).
- NCEER-92-0016 "Gravity-Load-Designed Reinforced Concrete Buildings: Seismic Evaluation of Existing Construction and Detailing Strategies for Improved Seismic Resistance," by G.W. Hoffmann, S.K. Kunnath, A.M. Reinhorn and J.B. Mander, 7/15/92, (PB94-142007, A08, MF-A02).
- NCEER-92-0017 "Observations on Water System and Pipeline Performance in the Limón Area of Costa Rica Due to the April 22, 1991 Earthquake," by M. O'Rourke and D. Ballantyne, 6/30/92, (PB93-126811, A06, MF-A02).
- NCEER-92-0018 "Fourth Edition of Earthquake Education Materials for Grades K-12," Edited by K.E.K. Ross, 8/10/92, (PB93-114023, A07, MF-A02).
- NCEER-92-0019 "Proceedings from the Fourth Japan-U.S. Workshop on Earthquake Resistant Design of Lifeline Facilities and Countermeasures for Soil Liquefaction," Edited by M. Hamada and T.D. O'Rourke, 8/12/92, (PB93-163939, A99, MF-E11).
- NCEER-92-0020 "Active Bracing System: A Full Scale Implementation of Active Control," by A.M. Reinhorn, T.T. Soong, R.C. Lin, M.A. Riley, Y.P. Wang, S. Aizawa and M. Higashino, 8/14/92, (PB93-127512, A06, MF-A02).
- NCEER-92-0021 "Empirical Analysis of Horizontal Ground Displacement Generated by Liquefaction-Induced Lateral Spreads," by S.F. Bartlett and T.L. Youd, 8/17/92, (PB93-188241, A06, MF-A02).
- NCEER-92-0022 "IDARC Version 3.0: Inelastic Damage Analysis of Reinforced Concrete Structures," by S.K. Kunnath, A.M. Reinhorn and R.F. Lobo, 8/31/92, (PB93-227502, A07, MF-A02).
- NCEER-92-0023 "A Semi-Empirical Analysis of Strong-Motion Peaks in Terms of Seismic Source, Propagation Path and Local Site Conditions, by M. Kamiyama, M.J. O'Rourke and R. Flores-Berrones, 9/9/92, (PB93-150266, A08, MF-A02).
- NCEER-92-0024 "Seismic Behavior of Reinforced Concrete Frame Structures with Nonductile Details, Part I: Summary of Experimental Findings of Full Scale Beam-Column Joint Tests," by A. Beres, R.N. White and P. Gergely, 9/30/92, (PB93-227783, A05, MF-A01).
- NCEER-92-0025 "Experimental Results of Repaired and Retrofitted Beam-Column Joint Tests in Lightly Reinforced Concrete Frame Buildings," by A. Beres, S. El-Borgi, R.N. White and P. Gergely, 10/29/92, (PB93-227791, A05, MF-A01).
- NCEER-92-0026 "A Generalization of Optimal Control Theory: Linear and Nonlinear Structures," by J.N. Yang, Z. Li and S. Vongchavalitkul, 11/2/92, (PB93-188621, A05, MF-A01).
- NCEER-92-0027 "Seismic Resistance of Reinforced Concrete Frame Structures Designed Only for Gravity Loads: Part I - Design and Properties of a One-Third Scale Model Structure," by J.M. Bracci, A.M. Reinhorn and J.B. Mander, 12/1/92, (PB94-104502, A08, MF-A02).
- NCEER-92-0028 "Seismic Resistance of Reinforced Concrete Frame Structures Designed Only for Gravity Loads: Part II - Experimental Performance of Subassemblages," by L.E. Aycaardi, J.B. Mander and A.M. Reinhorn, 12/1/92, (PB94-104510, A08, MF-A02).
- NCEER-92-0029 "Seismic Resistance of Reinforced Concrete Frame Structures Designed Only for Gravity Loads: Part III - Experimental Performance and Analytical Study of a Structural Model," by J.M. Bracci, A.M. Reinhorn and J.B. Mander, 12/1/92, (PB93-227528, A09, MF-A01).

- NCEER-92-0030 "Evaluation of Seismic Retrofit of Reinforced Concrete Frame Structures: Part I - Experimental Performance of Retrofitted Subassemblages," by D. Choudhuri, J.B. Mander and A.M. Reinhorn, 12/8/92, (PB93-198307, A07, MF-A02).
- NCEER-92-0031 "Evaluation of Seismic Retrofit of Reinforced Concrete Frame Structures: Part II - Experimental Performance and Analytical Study of a Retrofitted Structural Model," by J.M. Bracci, A.M. Reinhorn and J.B. Mander, 12/8/92, (PB93-198315, A09, MF-A03).
- NCEER-92-0032 "Experimental and Analytical Investigation of Seismic Response of Structures with Supplemental Fluid Viscous Dampers," by M.C. Constantinou and M.D. Symans, 12/21/92, (PB93-191435, A10, MF-A03). This report is available only through NTIS (see address given above).
- NCEER-92-0033 "Reconnaissance Report on the Cairo, Egypt Earthquake of October 12, 1992," by M. Khater, 12/23/92, (PB93-188621, A03, MF-A01).
- NCEER-92-0034 "Low-Level Dynamic Characteristics of Four Tall Flat-Plate Buildings in New York City," by H. Gavin, S. Yuan, J. Grossman, E. Pekelis and K. Jacob, 12/28/92, (PB93-188217, A07, MF-A02).
- NCEER-93-0001 "An Experimental Study on the Seismic Performance of Brick-Infilled Steel Frames With and Without Retrofit," by J.B. Mander, B. Nair, K. Wojtkowski and J. Ma, 1/29/93, (PB93-227510, A07, MF-A02).
- NCEER-93-0002 "Social Accounting for Disaster Preparedness and Recovery Planning," by S. Cole, E. Pantoja and V. Razak, 2/22/93, (PB94-142114, A12, MF-A03).
- NCEER-93-0003 "Assessment of 1991 NEHRP Provisions for Nonstructural Components and Recommended Revisions," by T.T. Soong, G. Chen, Z. Wu, R-H. Zhang and M. Grigoriu, 3/1/93, (PB93-188639, A06, MF-A02).
- NCEER-93-0004 "Evaluation of Static and Response Spectrum Analysis Procedures of SEAOC/UBC for Seismic Isolated Structures," by C.W. Winters and M.C. Constantinou, 3/23/93, (PB93-198299, A10, MF-A03).
- NCEER-93-0005 "Earthquakes in the Northeast - Are We Ignoring the Hazard? A Workshop on Earthquake Science and Safety for Educators," edited by K.E.K. Ross, 4/2/93, (PB94-103066, A09, MF-A02).
- NCEER-93-0006 "Inelastic Response of Reinforced Concrete Structures with Viscoelastic Braces," by R.F. Lobo, J.M. Bracci, K.L. Shen, A.M. Reinhorn and T.T. Soong, 4/5/93, (PB93-227486, A05, MF-A02).
- NCEER-93-0007 "Seismic Testing of Installation Methods for Computers and Data Processing Equipment," by K. Kosar, T.T. Soong, K.L. Shen, J.A. HoLung and Y.K. Lin, 4/12/93, (PB93-198299, A07, MF-A02).
- NCEER-93-0008 "Retrofit of Reinforced Concrete Frames Using Added Dampers," by A. Reinhorn, M. Constantinou and C. Li, to be published.
- NCEER-93-0009 "Seismic Behavior and Design Guidelines for Steel Frame Structures with Added Viscoelastic Dampers," by K.C. Chang, M.L. Lai, T.T. Soong, D.S. Hao and Y.C. Yeh, 5/1/93, (PB94-141959, A07, MF-A02).
- NCEER-93-0010 "Seismic Performance of Shear-Critical Reinforced Concrete Bridge Piers," by J.B. Mander, S.M. Waheed, M.T.A. Chaudhary and S.S. Chen, 5/12/93, (PB93-227494, A08, MF-A02).
- NCEER-93-0011 "3D-BASIS-TABS: Computer Program for Nonlinear Dynamic Analysis of Three Dimensional Base Isolated Structures," by S. Nagarajaiah, C. Li, A.M. Reinhorn and M.C. Constantinou, 8/2/93, (PB94-141819, A09, MF-A02).
- NCEER-93-0012 "Effects of Hydrocarbon Spills from an Oil Pipeline Break on Ground Water," by O.J. Helweg and H.H.M. Hwang, 8/3/93, (PB94-141942, A06, MF-A02).
- NCEER-93-0013 "Simplified Procedures for Seismic Design of Nonstructural Components and Assessment of Current Code Provisions," by M.P. Singh, L.E. Suarez, E.E. Matheu and G.O. Maldonado, 8/4/93, (PB94-141827, A09, MF-A02).
- NCEER-93-0014 "An Energy Approach to Seismic Analysis and Design of Secondary Systems," by G. Chen and T.T. Soong, 8/6/93, (PB94-142767, A11, MF-A03).

- NCEER-93-0015 "Proceedings from School Sites: Becoming Prepared for Earthquakes - Commemorating the Third Anniversary of the Loma Prieta Earthquake," Edited by F.E. Winslow and K.E.K. Ross, 8/16/93, (PB94-154275, A16, MF-A02).
- NCEER-93-0016 "Reconnaissance Report of Damage to Historic Monuments in Cairo, Egypt Following the October 12, 1992 Dahshur Earthquake," by D. Sykora, D. Look, G. Croci, E. Karaesmen and E. Karaesmen, 8/19/93, (PB94-142221, A08, MF-A02).
- NCEER-93-0017 "The Island of Guam Earthquake of August 8, 1993," by S.W. Swan and S.K. Harris, 9/30/93, (PB94-141843, A04, MF-A01).
- NCEER-93-0018 "Engineering Aspects of the October 12, 1992 Egyptian Earthquake," by A.W. Elgamal, M. Amer, K. Adalier and A. Abul-Fadl, 10/7/93, (PB94-141983, A05, MF-A01).
- NCEER-93-0019 "Development of an Earthquake Motion Simulator and its Application in Dynamic Centrifuge Testing," by I. Krstelj, Supervised by J.H. Prevost, 10/23/93, (PB94-181773, A-10, MF-A03).
- NCEER-93-0020 "NCEER-Taisei Corporation Research Program on Sliding Seismic Isolation Systems for Bridges: Experimental and Analytical Study of a Friction Pendulum System (FPS)," by M.C. Constantinou, P. Tsopelas, Y-S. Kim and S. Okamoto, 11/1/93, (PB94-142775, A08, MF-A02).
- NCEER-93-0021 "Finite Element Modeling of Elastomeric Seismic Isolation Bearings," by L.J. Billings, Supervised by R. Shepherd, 11/8/93, to be published.
- NCEER-93-0022 "Seismic Vulnerability of Equipment in Critical Facilities: Life-Safety and Operational Consequences," by K. Porter, G.S. Johnson, M.M. Zadeh, C. Scawthorn and S. Eder, 11/24/93, (PB94-181765, A16, MF-A03).
- NCEER-93-0023 "Hokkaido Nansei-oki, Japan Earthquake of July 12, 1993, by P.I. Yanev and C.R. Scawthorn, 12/23/93, (PB94-181500, A07, MF-A01).
- NCEER-94-0001 "An Evaluation of Seismic Serviceability of Water Supply Networks with Application to the San Francisco Auxiliary Water Supply System," by I. Markov, Supervised by M. Grigoriu and T. O'Rourke, 1/21/94, (PB94-204013, A07, MF-A02).
- NCEER-94-0002 "NCEER-Taisei Corporation Research Program on Sliding Seismic Isolation Systems for Bridges: Experimental and Analytical Study of Systems Consisting of Sliding Bearings, Rubber Restoring Force Devices and Fluid Dampers," Volumes I and II, by P. Tsopelas, S. Okamoto, M.C. Constantinou, D. Ozaki and S. Fujii, 2/4/94, (PB94-181740, A09, MF-A02 and PB94-181757, A12, MF-A03).
- NCEER-94-0003 "A Markov Model for Local and Global Damage Indices in Seismic Analysis," by S. Rahman and M. Grigoriu, 2/18/94, (PB94-206000, A12, MF-A03).
- NCEER-94-0004 "Proceedings from the NCEER Workshop on Seismic Response of Masonry Infills," edited by D.P. Abrams, 3/1/94, (PB94-180783, A07, MF-A02).
- NCEER-94-0005 "The Northridge, California Earthquake of January 17, 1994: General Reconnaissance Report," edited by J.D. Goltz, 3/11/94, (PB94-193943, A10, MF-A03).
- NCEER-94-0006 "Seismic Energy Based Fatigue Damage Analysis of Bridge Columns: Part I - Evaluation of Seismic Capacity," by G.A. Chang and J.B. Mander, 3/14/94, (PB94-219185, A11, MF-A03).
- NCEER-94-0007 "Seismic Isolation of Multi-Story Frame Structures Using Spherical Sliding Isolation Systems," by T.M. Al-Hussaini, V.A. Zayas and M.C. Constantinou, 3/17/94, (PB94-193745, A09, MF-A02).
- NCEER-94-0008 "The Northridge, California Earthquake of January 17, 1994: Performance of Highway Bridges," edited by I.G. Buckle, 3/24/94, (PB94-193851, A06, MF-A02).
- NCEER-94-0009 "Proceedings of the Third U.S.-Japan Workshop on Earthquake Protective Systems for Bridges," edited by I.G. Buckle and I. Friedland, 3/31/94, (PB94-195815, A99, MF-A06).

- NCEER-94-0010 "3D-BASIS-ME: Computer Program for Nonlinear Dynamic Analysis of Seismically Isolated Single and Multiple Structures and Liquid Storage Tanks," by P.C. Tsopelas, M.C. Constantinou and A.M. Reinhorn, 4/12/94, (PB94-204922, A09, MF-A02).
- NCEER-94-0011 "The Northridge, California Earthquake of January 17, 1994: Performance of Gas Transmission Pipelines," by T.D. O'Rourke and M.C. Palmer, 5/16/94, (PB94-204989, A05, MF-A01).
- NCEER-94-0012 "Feasibility Study of Replacement Procedures and Earthquake Performance Related to Gas Transmission Pipelines," by T.D. O'Rourke and M.C. Palmer, 5/25/94, (PB94-206638, A09, MF-A02).
- NCEER-94-0013 "Seismic Energy Based Fatigue Damage Analysis of Bridge Columns: Part II - Evaluation of Seismic Demand," by G.A. Chang and J.B. Mander, 6/1/94, (PB95-18106, A08, MF-A02).
- NCEER-94-0014 "NCEER-Taisei Corporation Research Program on Sliding Seismic Isolation Systems for Bridges: Experimental and Analytical Study of a System Consisting of Sliding Bearings and Fluid Restoring Force/Damping Devices," by P. Tsopelas and M.C. Constantinou, 6/13/94, (PB94-219144, A10, MF-A03).
- NCEER-94-0015 "Generation of Hazard-Consistent Fragility Curves for Seismic Loss Estimation Studies," by H. Hwang and J-R. Huo, 6/14/94, (PB95-181996, A09, MF-A02).
- NCEER-94-0016 "Seismic Study of Building Frames with Added Energy-Absorbing Devices," by W.S. Pong, C.S. Tsai and G.C. Lee, 6/20/94, (PB94-219136, A10, A03).
- NCEER-94-0017 "Sliding Mode Control for Seismic-Excited Linear and Nonlinear Civil Engineering Structures," by J. Yang, J. Wu, A. Agrawal and Z. Li, 6/21/94, (PB95-138483, A06, MF-A02).
- NCEER-94-0018 "3D-BASIS-TABS Version 2.0: Computer Program for Nonlinear Dynamic Analysis of Three Dimensional Base Isolated Structures," by A.M. Reinhorn, S. Nagarajaiah, M.C. Constantinou, P. Tsopelas and R. Li, 6/22/94, (PB95-182176, A08, MF-A02).
- NCEER-94-0019 "Proceedings of the International Workshop on Civil Infrastructure Systems: Application of Intelligent Systems and Advanced Materials on Bridge Systems," Edited by G.C. Lee and K.C. Chang, 7/18/94, (PB95-252474, A20, MF-A04).
- NCEER-94-0020 "Study of Seismic Isolation Systems for Computer Floors," by V. Lambrou and M.C. Constantinou, 7/19/94, (PB95-138533, A10, MF-A03).
- NCEER-94-0021 "Proceedings of the U.S.-Italian Workshop on Guidelines for Seismic Evaluation and Rehabilitation of Unreinforced Masonry Buildings," Edited by D.P. Abrams and G.M. Calvi, 7/20/94, (PB95-138749, A13, MF-A03).
- NCEER-94-0022 "NCEER-Taisei Corporation Research Program on Sliding Seismic Isolation Systems for Bridges: Experimental and Analytical Study of a System Consisting of Lubricated PTFE Sliding Bearings and Mild Steel Dampers," by P. Tsopelas and M.C. Constantinou, 7/22/94, (PB95-182184, A08, MF-A02).
- NCEER-94-0023 "Development of Reliability-Based Design Criteria for Buildings Under Seismic Load," by Y.K. Wen, H. Hwang and M. Shinozuka, 8/1/94, (PB95-211934, A08, MF-A02).
- NCEER-94-0024 "Experimental Verification of Acceleration Feedback Control Strategies for an Active Tendon System," by S.J. Dyke, B.F. Spencer, Jr., P. Quast, M.K. Sain, D.C. Kaspari, Jr. and T.T. Soong, 8/29/94, (PB95-212320, A05, MF-A01).
- NCEER-94-0025 "Seismic Retrofitting Manual for Highway Bridges," Edited by I.G. Buckle and I.F. Friedland, published by the Federal Highway Administration (PB95-212676, A15, MF-A03).
- NCEER-94-0026 "Proceedings from the Fifth U.S.-Japan Workshop on Earthquake Resistant Design of Lifeline Facilities and Countermeasures Against Soil Liquefaction," Edited by T.D. O'Rourke and M. Hamada, 11/7/94, (PB95-220802, A99, MF-E08).

- NCEER-95-0001 “Experimental and Analytical Investigation of Seismic Retrofit of Structures with Supplemental Damping: Part 1 - Fluid Viscous Damping Devices,” by A.M. Reinhorn, C. Li and M.C. Constantinou, 1/3/95, (PB95-266599, A09, MF-A02).
- NCEER-95-0002 “Experimental and Analytical Study of Low-Cycle Fatigue Behavior of Semi-Rigid Top-And-Seat Angle Connections,” by G. Pekcan, J.B. Mander and S.S. Chen, 1/5/95, (PB95-220042, A07, MF-A02).
- NCEER-95-0003 “NCEER-ATC Joint Study on Fragility of Buildings,” by T. Anagnos, C. Rojahn and A.S. Kiremidjian, 1/20/95, (PB95-220026, A06, MF-A02).
- NCEER-95-0004 “Nonlinear Control Algorithms for Peak Response Reduction,” by Z. Wu, T.T. Soong, V. Gattulli and R.C. Lin, 2/16/95, (PB95-220349, A05, MF-A01).
- NCEER-95-0005 “Pipeline Replacement Feasibility Study: A Methodology for Minimizing Seismic and Corrosion Risks to Underground Natural Gas Pipelines,” by R.T. Eguchi, H.A. Seligson and D.G. Honegger, 3/2/95, (PB95-252326, A06, MF-A02).
- NCEER-95-0006 “Evaluation of Seismic Performance of an 11-Story Frame Building During the 1994 Northridge Earthquake,” by F. Naeim, R. DiSulio, K. Benuska, A. Reinhorn and C. Li, to be published.
- NCEER-95-0007 “Prioritization of Bridges for Seismic Retrofitting,” by N. Basöz and A.S. Kiremidjian, 4/24/95, (PB95-252300, A08, MF-A02).
- NCEER-95-0008 “Method for Developing Motion Damage Relationships for Reinforced Concrete Frames,” by A. Singhal and A.S. Kiremidjian, 5/11/95, (PB95-266607, A06, MF-A02).
- NCEER-95-0009 “Experimental and Analytical Investigation of Seismic Retrofit of Structures with Supplemental Damping: Part II - Friction Devices,” by C. Li and A.M. Reinhorn, 7/6/95, (PB96-128087, A11, MF-A03).
- NCEER-95-0010 “Experimental Performance and Analytical Study of a Non-Ductile Reinforced Concrete Frame Structure Retrofitted with Elastomeric Spring Dampers,” by G. Pekcan, J.B. Mander and S.S. Chen, 7/14/95, (PB96-137161, A08, MF-A02).
- NCEER-95-0011 “Development and Experimental Study of Semi-Active Fluid Damping Devices for Seismic Protection of Structures,” by M.D. Symans and M.C. Constantinou, 8/3/95, (PB96-136940, A23, MF-A04).
- NCEER-95-0012 “Real-Time Structural Parameter Modification (RSPM): Development of Innervated Structures,” by Z. Liang, M. Tong and G.C. Lee, 4/11/95, (PB96-137153, A06, MF-A01).
- NCEER-95-0013 “Experimental and Analytical Investigation of Seismic Retrofit of Structures with Supplemental Damping: Part III - Viscous Damping Walls,” by A.M. Reinhorn and C. Li, 10/1/95, (PB96-176409, A11, MF-A03).
- NCEER-95-0014 “Seismic Fragility Analysis of Equipment and Structures in a Memphis Electric Substation,” by J-R. Huo and H.H.M. Hwang, 8/10/95, (PB96-128087, A09, MF-A02).
- NCEER-95-0015 “The Hanshin-Awaji Earthquake of January 17, 1995: Performance of Lifelines,” Edited by M. Shinozuka, 11/3/95, (PB96-176383, A15, MF-A03).
- NCEER-95-0016 “Highway Culvert Performance During Earthquakes,” by T.L. Youd and C.J. Beckman, available as NCEER-96-0015.
- NCEER-95-0017 “The Hanshin-Awaji Earthquake of January 17, 1995: Performance of Highway Bridges,” Edited by I.G. Buckle, 12/1/95, to be published.
- NCEER-95-0018 “Modeling of Masonry Infill Panels for Structural Analysis,” by A.M. Reinhorn, A. Madan, R.E. Valles, Y. Reichmann and J.B. Mander, 12/8/95, (PB97-110886, MF-A01, A06).
- NCEER-95-0019 “Optimal Polynomial Control for Linear and Nonlinear Structures,” by A.K. Agrawal and J.N. Yang, 12/11/95, (PB96-168737, A07, MF-A02).

- NCEER-95-0020 "Retrofit of Non-Ductile Reinforced Concrete Frames Using Friction Dampers," by R.S. Rao, P. Gergely and R.N. White, 12/22/95, (PB97-133508, A10, MF-A02).
- NCEER-95-0021 "Parametric Results for Seismic Response of Pile-Supported Bridge Bents," by G. Mylonakis, A. Nikolaou and G. Gazetas, 12/22/95, (PB97-100242, A12, MF-A03).
- NCEER-95-0022 "Kinematic Bending Moments in Seismically Stressed Piles," by A. Nikolaou, G. Mylonakis and G. Gazetas, 12/23/95, (PB97-113914, MF-A03, A13).
- NCEER-96-0001 "Dynamic Response of Unreinforced Masonry Buildings with Flexible Diaphragms," by A.C. Costley and D.P. Abrams, 10/10/96, (PB97-133573, MF-A03, A15).
- NCEER-96-0002 "State of the Art Review: Foundations and Retaining Structures," by I. Po Lam, to be published.
- NCEER-96-0003 "Ductility of Rectangular Reinforced Concrete Bridge Columns with Moderate Confinement," by N. Wehbe, M. Saiidi, D. Sanders and B. Douglas, 11/7/96, (PB97-133557, A06, MF-A02).
- NCEER-96-0004 "Proceedings of the Long-Span Bridge Seismic Research Workshop," edited by I.G. Buckle and I.M. Friedland, to be published.
- NCEER-96-0005 "Establish Representative Pier Types for Comprehensive Study: Eastern United States," by J. Kulicki and Z. Prucz, 5/28/96, (PB98-119217, A07, MF-A02).
- NCEER-96-0006 "Establish Representative Pier Types for Comprehensive Study: Western United States," by R. Imbsen, R.A. Schamber and T.A. Osterkamp, 5/28/96, (PB98-118607, A07, MF-A02).
- NCEER-96-0007 "Nonlinear Control Techniques for Dynamical Systems with Uncertain Parameters," by R.G. Ghanem and M.I. Bujakov, 5/27/96, (PB97-100259, A17, MF-A03).
- NCEER-96-0008 "Seismic Evaluation of a 30-Year Old Non-Ductile Highway Bridge Pier and Its Retrofit," by J.B. Mander, B. Mahmoodzadegan, S. Bhadra and S.S. Chen, 5/31/96, (PB97-110902, MF-A03, A10).
- NCEER-96-0009 "Seismic Performance of a Model Reinforced Concrete Bridge Pier Before and After Retrofit," by J.B. Mander, J.H. Kim and C.A. Ligozio, 5/31/96, (PB97-110910, MF-A02, A10).
- NCEER-96-0010 "IDARC2D Version 4.0: A Computer Program for the Inelastic Damage Analysis of Buildings," by R.E. Valles, A.M. Reinhorn, S.K. Kunnath, C. Li and A. Madan, 6/3/96, (PB97-100234, A17, MF-A03).
- NCEER-96-0011 "Estimation of the Economic Impact of Multiple Lifeline Disruption: Memphis Light, Gas and Water Division Case Study," by S.E. Chang, H.A. Seligson and R.T. Eguchi, 8/16/96, (PB97-133490, A11, MF-A03).
- NCEER-96-0012 "Proceedings from the Sixth Japan-U.S. Workshop on Earthquake Resistant Design of Lifeline Facilities and Countermeasures Against Soil Liquefaction, Edited by M. Hamada and T. O'Rourke, 9/11/96, (PB97-133581, A99, MF-A06).
- NCEER-96-0013 "Chemical Hazards, Mitigation and Preparedness in Areas of High Seismic Risk: A Methodology for Estimating the Risk of Post-Earthquake Hazardous Materials Release," by H.A. Seligson, R.T. Eguchi, K.J. Tierney and K. Richmond, 11/7/96, (PB97-133565, MF-A02, A08).
- NCEER-96-0014 "Response of Steel Bridge Bearings to Reversed Cyclic Loading," by J.B. Mander, D-K. Kim, S.S. Chen and G.J. Premus, 11/13/96, (PB97-140735, A12, MF-A03).
- NCEER-96-0015 "Highway Culvert Performance During Past Earthquakes," by T.L. Youd and C.J. Beckman, 11/25/96, (PB97-133532, A06, MF-A01).
- NCEER-97-0001 "Evaluation, Prevention and Mitigation of Pounding Effects in Building Structures," by R.E. Valles and A.M. Reinhorn, 2/20/97, (PB97-159552, A14, MF-A03).
- NCEER-97-0002 "Seismic Design Criteria for Bridges and Other Highway Structures," by C. Rojahn, R. Mayes, D.G. Anderson, J. Clark, J.H. Hom, R.V. Nutt and M.J. O'Rourke, 4/30/97, (PB97-194658, A06, MF-A03).

- NCEER-97-0003 "Proceedings of the U.S.-Italian Workshop on Seismic Evaluation and Retrofit," Edited by D.P. Abrams and G.M. Calvi, 3/19/97, (PB97-194666, A13, MF-A03).
- NCEER-97-0004 "Investigation of Seismic Response of Buildings with Linear and Nonlinear Fluid Viscous Dampers," by A.A. Seleemah and M.C. Constantinou, 5/21/97, (PB98-109002, A15, MF-A03).
- NCEER-97-0005 "Proceedings of the Workshop on Earthquake Engineering Frontiers in Transportation Facilities," edited by G.C. Lee and I.M. Friedland, 8/29/97, (PB98-128911, A25, MR-A04).
- NCEER-97-0006 "Cumulative Seismic Damage of Reinforced Concrete Bridge Piers," by S.K. Kunnath, A. El-Bahy, A. Taylor and W. Stone, 9/2/97, (PB98-108814, A11, MF-A03).
- NCEER-97-0007 "Structural Details to Accommodate Seismic Movements of Highway Bridges and Retaining Walls," by R.A. Imbsen, R.A. Schamber, E. Thorkildsen, A. Kartoum, B.T. Martin, T.N. Rosser and J.M. Kulicki, 9/3/97, (PB98-108996, A09, MF-A02).
- NCEER-97-0008 "A Method for Earthquake Motion-Damage Relationships with Application to Reinforced Concrete Frames," by A. Singhal and A.S. Kiremidjian, 9/10/97, (PB98-108988, A13, MF-A03).
- NCEER-97-0009 "Seismic Analysis and Design of Bridge Abutments Considering Sliding and Rotation," by K. Fishman and R. Richards, Jr., 9/15/97, (PB98-108897, A06, MF-A02).
- NCEER-97-0010 "Proceedings of the FHWA/NCEER Workshop on the National Representation of Seismic Ground Motion for New and Existing Highway Facilities," edited by I.M. Friedland, M.S. Power and R.L. Mayes, 9/22/97, (PB98-128903, A21, MF-A04).
- NCEER-97-0011 "Seismic Analysis for Design or Retrofit of Gravity Bridge Abutments," by K.L. Fishman, R. Richards, Jr. and R.C. Divito, 10/2/97, (PB98-128937, A08, MF-A02).
- NCEER-97-0012 "Evaluation of Simplified Methods of Analysis for Yielding Structures," by P. Tsopelas, M.C. Constantinou, C.A. Kircher and A.S. Whittaker, 10/31/97, (PB98-128929, A10, MF-A03).
- NCEER-97-0013 "Seismic Design of Bridge Columns Based on Control and Repairability of Damage," by C-T. Cheng and J.B. Mander, 12/8/97, (PB98-144249, A11, MF-A03).
- NCEER-97-0014 "Seismic Resistance of Bridge Piers Based on Damage Avoidance Design," by J.B. Mander and C-T. Cheng, 12/10/97, (PB98-144223, A09, MF-A02).
- NCEER-97-0015 "Seismic Response of Nominally Symmetric Systems with Strength Uncertainty," by S. Balopoulou and M. Grigoriu, 12/23/97, (PB98-153422, A11, MF-A03).
- NCEER-97-0016 "Evaluation of Seismic Retrofit Methods for Reinforced Concrete Bridge Columns," by T.J. Wipf, F.W. Klaiber and F.M. Russo, 12/28/97, (PB98-144215, A12, MF-A03).
- NCEER-97-0017 "Seismic Fragility of Existing Conventional Reinforced Concrete Highway Bridges," by C.L. Mullen and A.S. Cakmak, 12/30/97, (PB98-153406, A08, MF-A02).
- NCEER-97-0018 "Loss Assessment of Memphis Buildings," edited by D.P. Abrams and M. Shinozuka, 12/31/97, (PB98-144231, A13, MF-A03).
- NCEER-97-0019 "Seismic Evaluation of Frames with Infill Walls Using Quasi-static Experiments," by K.M. Mosalam, R.N. White and P. Gergely, 12/31/97, (PB98-153455, A07, MF-A02).
- NCEER-97-0020 "Seismic Evaluation of Frames with Infill Walls Using Pseudo-dynamic Experiments," by K.M. Mosalam, R.N. White and P. Gergely, 12/31/97, (PB98-153430, A07, MF-A02).
- NCEER-97-0021 "Computational Strategies for Frames with Infill Walls: Discrete and Smeared Crack Analyses and Seismic Fragility," by K.M. Mosalam, R.N. White and P. Gergely, 12/31/97, (PB98-153414, A10, MF-A02).

- NCEER-97-0022 "Proceedings of the NCEER Workshop on Evaluation of Liquefaction Resistance of Soils," edited by T.L. Youd and I.M. Idriss, 12/31/97, (PB98-155617, A15, MF-A03).
- MCEER-98-0001 "Extraction of Nonlinear Hysteretic Properties of Seismically Isolated Bridges from Quick-Release Field Tests," by Q. Chen, B.M. Douglas, E.M. Maragakis and I.G. Buckle, 5/26/98, (PB99-118838, A06, MF-A01).
- MCEER-98-0002 "Methodologies for Evaluating the Importance of Highway Bridges," by A. Thomas, S. Eshenaur and J. Kulicki, 5/29/98, (PB99-118846, A10, MF-A02).
- MCEER-98-0003 "Capacity Design of Bridge Piers and the Analysis of Overstrength," by J.B. Mander, A. Dutta and P. Goel, 6/1/98, (PB99-118853, A09, MF-A02).
- MCEER-98-0004 "Evaluation of Bridge Damage Data from the Loma Prieta and Northridge, California Earthquakes," by N. Basoz and A. Kiremidjian, 6/2/98, (PB99-118861, A15, MF-A03).
- MCEER-98-0005 "Screening Guide for Rapid Assessment of Liquefaction Hazard at Highway Bridge Sites," by T. L. Youd, 6/16/98, (PB99-118879, A06, not available on microfiche).
- MCEER-98-0006 "Structural Steel and Steel/Concrete Interface Details for Bridges," by P. Ritchie, N. Kauh and J. Kulicki, 7/13/98, (PB99-118945, A06, MF-A01).
- MCEER-98-0007 "Capacity Design and Fatigue Analysis of Confined Concrete Columns," by A. Dutta and J.B. Mander, 7/14/98, (PB99-118960, A14, MF-A03).
- MCEER-98-0008 "Proceedings of the Workshop on Performance Criteria for Telecommunication Services Under Earthquake Conditions," edited by A.J. Schiff, 7/15/98, (PB99-118952, A08, MF-A02).
- MCEER-98-0009 "Fatigue Analysis of Unconfined Concrete Columns," by J.B. Mander, A. Dutta and J.H. Kim, 9/12/98, (PB99-123655, A10, MF-A02).
- MCEER-98-0010 "Centrifuge Modeling of Cyclic Lateral Response of Pile-Cap Systems and Seat-Type Abutments in Dry Sands," by A.D. Gadre and R. Dobry, 10/2/98, (PB99-123606, A13, MF-A03).
- MCEER-98-0011 "IDARC-BRIDGE: A Computational Platform for Seismic Damage Assessment of Bridge Structures," by A.M. Reinhorn, V. Simeonov, G. Mylonakis and Y. Reichman, 10/2/98, (PB99-162919, A15, MF-A03).
- MCEER-98-0012 "Experimental Investigation of the Dynamic Response of Two Bridges Before and After Retrofitting with Elastomeric Bearings," by D.A. Wendichansky, S.S. Chen and J.B. Mander, 10/2/98, (PB99-162927, A15, MF-A03).
- MCEER-98-0013 "Design Procedures for Hinge Restrainers and Hinge Sear Width for Multiple-Frame Bridges," by R. Des Roches and G.L. Fenves, 11/3/98, (PB99-140477, A13, MF-A03).
- MCEER-98-0014 "Response Modification Factors for Seismically Isolated Bridges," by M.C. Constantinou and J.K. Quarshie, 11/3/98, (PB99-140485, A14, MF-A03).
- MCEER-98-0015 "Proceedings of the U.S.-Italy Workshop on Seismic Protective Systems for Bridges," edited by I.M. Friedland and M.C. Constantinou, 11/3/98, (PB2000-101711, A22, MF-A04).
- MCEER-98-0016 "Appropriate Seismic Reliability for Critical Equipment Systems: Recommendations Based on Regional Analysis of Financial and Life Loss," by K. Porter, C. Scawthorn, C. Taylor and N. Blais, 11/10/98, (PB99-157265, A08, MF-A02).
- MCEER-98-0017 "Proceedings of the U.S. Japan Joint Seminar on Civil Infrastructure Systems Research," edited by M. Shinozuka and A. Rose, 11/12/98, (PB99-156713, A16, MF-A03).
- MCEER-98-0018 "Modeling of Pile Footings and Drilled Shafts for Seismic Design," by I. PoLam, M. Kapuskar and D. Chaudhuri, 12/21/98, (PB99-157257, A09, MF-A02).

- MCEER-99-0001 "Seismic Evaluation of a Masonry Infilled Reinforced Concrete Frame by Pseudodynamic Testing," by S.G. Buonopane and R.N. White, 2/16/99, (PB99-162851, A09, MF-A02).
- MCEER-99-0002 "Response History Analysis of Structures with Seismic Isolation and Energy Dissipation Systems: Verification Examples for Program SAP2000," by J. Scheller and M.C. Constantinou, 2/22/99, (PB99-162869, A08, MF-A02).
- MCEER-99-0003 "Experimental Study on the Seismic Design and Retrofit of Bridge Columns Including Axial Load Effects," by A. Dutta, T. Kokorina and J.B. Mander, 2/22/99, (PB99-162877, A09, MF-A02).
- MCEER-99-0004 "Experimental Study of Bridge Elastomeric and Other Isolation and Energy Dissipation Systems with Emphasis on Uplift Prevention and High Velocity Near-source Seismic Excitation," by A. Kasalanati and M. C. Constantinou, 2/26/99, (PB99-162885, A12, MF-A03).
- MCEER-99-0005 "Truss Modeling of Reinforced Concrete Shear-flexure Behavior," by J.H. Kim and J.B. Mander, 3/8/99, (PB99-163693, A12, MF-A03).
- MCEER-99-0006 "Experimental Investigation and Computational Modeling of Seismic Response of a 1:4 Scale Model Steel Structure with a Load Balancing Supplemental Damping System," by G. Pekcan, J.B. Mander and S.S. Chen, 4/2/99, (PB99-162893, A11, MF-A03).
- MCEER-99-0007 "Effect of Vertical Ground Motions on the Structural Response of Highway Bridges," by M.R. Button, C.J. Cronin and R.L. Mayes, 4/10/99, (PB2000-101411, A10, MF-A03).
- MCEER-99-0008 "Seismic Reliability Assessment of Critical Facilities: A Handbook, Supporting Documentation, and Model Code Provisions," by G.S. Johnson, R.E. Sheppard, M.D. Quilici, S.J. Eder and C.R. Scawthorn, 4/12/99, (PB2000-101701, A18, MF-A04).
- MCEER-99-0009 "Impact Assessment of Selected MCEER Highway Project Research on the Seismic Design of Highway Structures," by C. Rojahn, R. Mayes, D.G. Anderson, J.H. Clark, D'Appolonia Engineering, S. Gloyd and R.V. Nutt, 4/14/99, (PB99-162901, A10, MF-A02).
- MCEER-99-0010 "Site Factors and Site Categories in Seismic Codes," by R. Dobry, R. Ramos and M.S. Power, 7/19/99, (PB2000-101705, A08, MF-A02).
- MCEER-99-0011 "Restraint Design Procedures for Multi-Span Simply-Supported Bridges," by M.J. Randall, M. Saiidi, E. Maragakis and T. Isakovic, 7/20/99, (PB2000-101702, A10, MF-A02).
- MCEER-99-0012 "Property Modification Factors for Seismic Isolation Bearings," by M.C. Constantinou, P. Tsopelas, A. Kasalanati and E. Wolff, 7/20/99, (PB2000-103387, A11, MF-A03).
- MCEER-99-0013 "Critical Seismic Issues for Existing Steel Bridges," by P. Ritchie, N. Kauh and J. Kulicki, 7/20/99, (PB2000-101697, A09, MF-A02).
- MCEER-99-0014 "Nonstructural Damage Database," by A. Kao, T.T. Soong and A. Vender, 7/24/99, (PB2000-101407, A06, MF-A01).
- MCEER-99-0015 "Guide to Remedial Measures for Liquefaction Mitigation at Existing Highway Bridge Sites," by H.G. Cooke and J. K. Mitchell, 7/26/99, (PB2000-101703, A11, MF-A03).
- MCEER-99-0016 "Proceedings of the MCEER Workshop on Ground Motion Methodologies for the Eastern United States," edited by N. Abrahamson and A. Becker, 8/11/99, (PB2000-103385, A07, MF-A02).
- MCEER-99-0017 "Quindío, Colombia Earthquake of January 25, 1999: Reconnaissance Report," by A.P. Asfura and P.J. Flores, 10/4/99, (PB2000-106893, A06, MF-A01).
- MCEER-99-0018 "Hysteretic Models for Cyclic Behavior of Deteriorating Inelastic Structures," by M.V. Sivaselvan and A.M. Reinhorn, 11/5/99, (PB2000-103386, A08, MF-A02).

- MCEER-99-0019 "Proceedings of the 7th U.S.- Japan Workshop on Earthquake Resistant Design of Lifeline Facilities and Countermeasures Against Soil Liquefaction," edited by T.D. O'Rourke, J.P. Bardet and M. Hamada, 11/19/99, (PB2000-103354, A99, MF-A06).
- MCEER-99-0020 "Development of Measurement Capability for Micro-Vibration Evaluations with Application to Chip Fabrication Facilities," by G.C. Lee, Z. Liang, J.W. Song, J.D. Shen and W.C. Liu, 12/1/99, (PB2000-105993, A08, MF-A02).
- MCEER-99-0021 "Design and Retrofit Methodology for Building Structures with Supplemental Energy Dissipating Systems," by G. Pekcan, J.B. Mander and S.S. Chen, 12/31/99, (PB2000-105994, A11, MF-A03).
- MCEER-00-0001 "The Marmara, Turkey Earthquake of August 17, 1999: Reconnaissance Report," edited by C. Scawthorn; with major contributions by M. Bruneau, R. Eguchi, T. Holzer, G. Johnson, J. Mander, J. Mitchell, W. Mitchell, A. Papageorgiou, C. Scaethorn, and G. Webb, 3/23/00, (PB2000-106200, A11, MF-A03).
- MCEER-00-0002 "Proceedings of the MCEER Workshop for Seismic Hazard Mitigation of Health Care Facilities," edited by G.C. Lee, M. Ettouney, M. Grigoriu, J. Hauer and J. Nigg, 3/29/00, (PB2000-106892, A08, MF-A02).
- MCEER-00-0003 "The Chi-Chi, Taiwan Earthquake of September 21, 1999: Reconnaissance Report," edited by G.C. Lee and C.H. Loh, with major contributions by G.C. Lee, M. Bruneau, I.G. Buckle, S.E. Chang, P.J. Flores, T.D. O'Rourke, M. Shinozuka, T.T. Soong, C-H. Loh, K-C. Chang, Z-J. Chen, J-S. Hwang, M-L. Lin, G-Y. Liu, K-C. Tsai, G.C. Yao and C-L. Yen, 4/30/00, (PB2001-100980, A10, MF-A02).
- MCEER-00-0004 "Seismic Retrofit of End-Sway Frames of Steel Deck-Truss Bridges with a Supplemental Tendon System: Experimental and Analytical Investigation," by G. Pekcan, J.B. Mander and S.S. Chen, 7/1/00, (PB2001-100982, A10, MF-A02).
- MCEER-00-0005 "Sliding Fragility of Unrestrained Equipment in Critical Facilities," by W.H. Chong and T.T. Soong, 7/5/00, (PB2001-100983, A08, MF-A02).
- MCEER-00-0006 "Seismic Response of Reinforced Concrete Bridge Pier Walls in the Weak Direction," by N. Abo-Shadi, M. Saiidi and D. Sanders, 7/17/00, (PB2001-100981, A17, MF-A03).
- MCEER-00-0007 "Low-Cycle Fatigue Behavior of Longitudinal Reinforcement in Reinforced Concrete Bridge Columns," by J. Brown and S.K. Kunnath, 7/23/00, (PB2001-104392, A08, MF-A02).
- MCEER-00-0008 "Soil Structure Interaction of Bridges for Seismic Analysis," I. PoLam and H. Law, 9/25/00, (PB2001-105397, A08, MF-A02).
- MCEER-00-0009 "Proceedings of the First MCEER Workshop on Mitigation of Earthquake Disaster by Advanced Technologies (MEDAT-1), edited by M. Shinozuka, D.J. Inman and T.D. O'Rourke, 11/10/00, (PB2001-105399, A14, MF-A03).
- MCEER-00-0010 "Development and Evaluation of Simplified Procedures for Analysis and Design of Buildings with Passive Energy Dissipation Systems, Revision 01," by O.M. Ramirez, M.C. Constantinou, C.A. Kircher, A.S. Whittaker, M.W. Johnson, J.D. Gomez and C. Chrysostomou, 11/16/01, (PB2001-105523, A23, MF-A04).
- MCEER-00-0011 "Dynamic Soil-Foundation-Structure Interaction Analyses of Large Caissons," by C-Y. Chang, C-M. Mok, Z-L. Wang, R. Settgast, F. Waggoner, M.A. Ketchum, H.M. Gonnermann and C-C. Chin, 12/30/00, (PB2001-104373, A07, MF-A02).
- MCEER-00-0012 "Experimental Evaluation of Seismic Performance of Bridge Restrainers," by A.G. Vlassis, E.M. Maragakis and M. Saiid Saiidi, 12/30/00, (PB2001-104354, A09, MF-A02).
- MCEER-00-0013 "Effect of Spatial Variation of Ground Motion on Highway Structures," by M. Shinozuka, V. Saxena and G. Deodatis, 12/31/00, (PB2001-108755, A13, MF-A03).
- MCEER-00-0014 "A Risk-Based Methodology for Assessing the Seismic Performance of Highway Systems," by S.D. Werner, C.E. Taylor, J.E. Moore, II, J.S. Walton and S. Cho, 12/31/00, (PB2001-108756, A14, MF-A03).

- MCEER-01-0001 “Experimental Investigation of P-Delta Effects to Collapse During Earthquakes,” by D. Vian and M. Bruneau, 6/25/01, (PB2002-100534, A17, MF-A03).
- MCEER-01-0002 “Proceedings of the Second MCEER Workshop on Mitigation of Earthquake Disaster by Advanced Technologies (MEDAT-2),” edited by M. Bruneau and D.J. Inman, 7/23/01, (PB2002-100434, A16, MF-A03).
- MCEER-01-0003 “Sensitivity Analysis of Dynamic Systems Subjected to Seismic Loads,” by C. Roth and M. Grigoriu, 9/18/01, (PB2003-100884, A12, MF-A03).
- MCEER-01-0004 “Overcoming Obstacles to Implementing Earthquake Hazard Mitigation Policies: Stage 1 Report,” by D.J. Alesch and W.J. Petak, 12/17/01, (PB2002-107949, A07, MF-A02).
- MCEER-01-0005 “Updating Real-Time Earthquake Loss Estimates: Methods, Problems and Insights,” by C.E. Taylor, S.E. Chang and R.T. Eguchi, 12/17/01, (PB2002-107948, A05, MF-A01).
- MCEER-01-0006 “Experimental Investigation and Retrofit of Steel Pile Foundations and Pile Bents Under Cyclic Lateral Loadings,” by A. Shama, J. Mander, B. Blabac and S. Chen, 12/31/01, (PB2002-107950, A13, MF-A03).
- MCEER-02-0001 “Assessment of Performance of Bolu Viaduct in the 1999 Duzce Earthquake in Turkey” by P.C. Roussis, M.C. Constantinou, M. Erdik, E. Durukal and M. Dicleli, 5/8/02, (PB2003-100883, A08, MF-A02).
- MCEER-02-0002 “Seismic Behavior of Rail Counterweight Systems of Elevators in Buildings,” by M.P. Singh, Rildova and L.E. Suarez, 5/27/02. (PB2003-100882, A11, MF-A03).
- MCEER-02-0003 “Development of Analysis and Design Procedures for Spread Footings,” by G. Mylonakis, G. Gazetas, S. Nikolaou and A. Chauncey, 10/02/02, (PB2004-101636, A13, MF-A03, CD-A13).
- MCEER-02-0004 “Bare-Earth Algorithms for Use with SAR and LIDAR Digital Elevation Models,” by C.K. Huyck, R.T. Eguchi and B. Houshmand, 10/16/02, (PB2004-101637, A07, CD-A07).
- MCEER-02-0005 “Review of Energy Dissipation of Compression Members in Concentrically Braced Frames,” by K.Lee and M. Bruneau, 10/18/02, (PB2004-101638, A10, CD-A10).
- MCEER-03-0001 “Experimental Investigation of Light-Gauge Steel Plate Shear Walls for the Seismic Retrofit of Buildings” by J. Berman and M. Bruneau, 5/2/03, (PB2004-101622, A10, MF-A03, CD-A10).
- MCEER-03-0002 “Statistical Analysis of Fragility Curves,” by M. Shinozuka, M.Q. Feng, H. Kim, T. Uzawa and T. Ueda, 6/16/03, (PB2004-101849, A09, CD-A09).
- MCEER-03-0003 “Proceedings of the Eighth U.S.-Japan Workshop on Earthquake Resistant Design of Lifeline Facilities and Countermeasures Against Liquefaction,” edited by M. Hamada, J.P. Bardet and T.D. O’Rourke, 6/30/03, (PB2004-104386, A99, CD-A99).
- MCEER-03-0004 “Proceedings of the PRC-US Workshop on Seismic Analysis and Design of Special Bridges,” edited by L.C. Fan and G.C. Lee, 7/15/03, (PB2004-104387, A14, CD-A14).
- MCEER-03-0005 “Urban Disaster Recovery: A Framework and Simulation Model,” by S.B. Miles and S.E. Chang, 7/25/03, (PB2004-104388, A07, CD-A07).
- MCEER-03-0006 “Behavior of Underground Piping Joints Due to Static and Dynamic Loading,” by R.D. Meis, M. Maragakis and R. Siddharthan, 11/17/03, (PB2005-102194, A13, MF-A03, CD-A00).
- MCEER-04-0001 “Experimental Study of Seismic Isolation Systems with Emphasis on Secondary System Response and Verification of Accuracy of Dynamic Response History Analysis Methods,” by E. Wolff and M. Constantinou, 1/16/04 (PB2005-102195, A99, MF-E08, CD-A00).
- MCEER-04-0002 “Tension, Compression and Cyclic Testing of Engineered Cementitious Composite Materials,” by K. Kesner and S.L. Billington, 3/1/04, (PB2005-102196, A08, CD-A08).

- MCEER-04-0003 "Cyclic Testing of Braces Laterally Restrained by Steel Studs to Enhance Performance During Earthquakes," by O.C. Celik, J.W. Berman and M. Bruneau, 3/16/04, (PB2005-102197, A13, MF-A03, CD-A00).
- MCEER-04-0004 "Methodologies for Post Earthquake Building Damage Detection Using SAR and Optical Remote Sensing: Application to the August 17, 1999 Marmara, Turkey Earthquake," by C.K. Huyck, B.J. Adams, S. Cho, R.T. Eguchi, B. Mansouri and B. Houshmand, 6/15/04, (PB2005-104888, A10, CD-A00).
- MCEER-04-0005 "Nonlinear Structural Analysis Towards Collapse Simulation: A Dynamical Systems Approach," by M.V. Sivaselvan and A.M. Reinhorn, 6/16/04, (PB2005-104889, A11, MF-A03, CD-A00).
- MCEER-04-0006 "Proceedings of the Second PRC-US Workshop on Seismic Analysis and Design of Special Bridges," edited by G.C. Lee and L.C. Fan, 6/25/04, (PB2005-104890, A16, CD-A00).
- MCEER-04-0007 "Seismic Vulnerability Evaluation of Axially Loaded Steel Built-up Laced Members," by K. Lee and M. Bruneau, 6/30/04, (PB2005-104891, A16, CD-A00).
- MCEER-04-0008 "Evaluation of Accuracy of Simplified Methods of Analysis and Design of Buildings with Damping Systems for Near-Fault and for Soft-Soil Seismic Motions," by E.A. Pavlou and M.C. Constantinou, 8/16/04, (PB2005-104892, A08, MF-A02, CD-A00).
- MCEER-04-0009 "Assessment of Geotechnical Issues in Acute Care Facilities in California," by M. Lew, T.D. O'Rourke, R. Dobry and M. Koch, 9/15/04, (PB2005-104893, A08, CD-A00).
- MCEER-04-0010 "Scissor-Jack-Damper Energy Dissipation System," by A.N. Sigaher-Boyle and M.C. Constantinou, 12/1/04 (PB2005-108221).
- MCEER-04-0011 "Seismic Retrofit of Bridge Steel Truss Piers Using a Controlled Rocking Approach," by M. Pollino and M. Bruneau, 12/20/04 (PB2006-105795).
- MCEER-05-0001 "Experimental and Analytical Studies of Structures Seismically Isolated with an Uplift-Restraint Isolation System," by P.C. Roussis and M.C. Constantinou, 1/10/05 (PB2005-108222).
- MCEER-05-0002 "A Versatile Experimentation Model for Study of Structures Near Collapse Applied to Seismic Evaluation of Irregular Structures," by D. Kusumastuti, A.M. Reinhorn and A. Rutenberg, 3/31/05 (PB2006-101523).
- MCEER-05-0003 "Proceedings of the Third PRC-US Workshop on Seismic Analysis and Design of Special Bridges," edited by L.C. Fan and G.C. Lee, 4/20/05, (PB2006-105796).
- MCEER-05-0004 "Approaches for the Seismic Retrofit of Braced Steel Bridge Piers and Proof-of-Concept Testing of an Eccentrically Braced Frame with Tubular Link," by J.W. Berman and M. Bruneau, 4/21/05 (PB2006-101524).
- MCEER-05-0005 "Simulation of Strong Ground Motions for Seismic Fragility Evaluation of Nonstructural Components in Hospitals," by A. Wanitkorkul and A. Filiatrault, 5/26/05 (PB2006-500027).
- MCEER-05-0006 "Seismic Safety in California Hospitals: Assessing an Attempt to Accelerate the Replacement or Seismic Retrofit of Older Hospital Facilities," by D.J. Alesch, L.A. Arendt and W.J. Petak, 6/6/05 (PB2006-105794).
- MCEER-05-0007 "Development of Seismic Strengthening and Retrofit Strategies for Critical Facilities Using Engineered Cementitious Composite Materials," by K. Kesner and S.L. Billington, 8/29/05 (PB2006-111701).
- MCEER-05-0008 "Experimental and Analytical Studies of Base Isolation Systems for Seismic Protection of Power Transformers," by N. Murota, M.Q. Feng and G-Y. Liu, 9/30/05 (PB2006-111702).
- MCEER-05-0009 "3D-BASIS-ME-MB: Computer Program for Nonlinear Dynamic Analysis of Seismically Isolated Structures," by P.C. Tsopelas, P.C. Roussis, M.C. Constantinou, R. Buchanan and A.M. Reinhorn, 10/3/05 (PB2006-111703).
- MCEER-05-0010 "Steel Plate Shear Walls for Seismic Design and Retrofit of Building Structures," by D. Vian and M. Bruneau, 12/15/05 (PB2006-111704).

- MCEER-05-0011 "The Performance-Based Design Paradigm," by M.J. Astrella and A. Whittaker, 12/15/05 (PB2006-111705).
- MCEER-06-0001 "Seismic Fragility of Suspended Ceiling Systems," H. Badillo-Almaraz, A.S. Whittaker, A.M. Reinhorn and G.P. Cimellaro, 2/4/06 (PB2006-111706).
- MCEER-06-0002 "Multi-Dimensional Fragility of Structures," by G.P. Cimellaro, A.M. Reinhorn and M. Bruneau, 3/1/06 (PB2007-106974, A09, MF-A02, CD A00).
- MCEER-06-0003 "Built-Up Shear Links as Energy Dissipators for Seismic Protection of Bridges," by P. Dusicka, A.M. Itani and I.G. Buckle, 3/15/06 (PB2006-111708).
- MCEER-06-0004 "Analytical Investigation of the Structural Fuse Concept," by R.E. Vargas and M. Bruneau, 3/16/06 (PB2006-111709).
- MCEER-06-0005 "Experimental Investigation of the Structural Fuse Concept," by R.E. Vargas and M. Bruneau, 3/17/06 (PB2006-111710).
- MCEER-06-0006 "Further Development of Tubular Eccentrically Braced Frame Links for the Seismic Retrofit of Braced Steel Truss Bridge Piers," by J.W. Berman and M. Bruneau, 3/27/06 (PB2007-105147).
- MCEER-06-0007 "REDARS Validation Report," by S. Cho, C.K. Huyck, S. Ghosh and R.T. Eguchi, 8/8/06 (PB2007-106983).
- MCEER-06-0008 "Review of Current NDE Technologies for Post-Earthquake Assessment of Retrofitted Bridge Columns," by J.W. Song, Z. Liang and G.C. Lee, 8/21/06 (PB2007-106984).
- MCEER-06-0009 "Liquefaction Remediation in Silty Soils Using Dynamic Compaction and Stone Columns," by S. Thevanayagam, G.R. Martin, R. Nashed, T. Shenthan, T. Kanagalingam and N. Ecemis, 8/28/06 (PB2007-106985).
- MCEER-06-0010 "Conceptual Design and Experimental Investigation of Polymer Matrix Composite Infill Panels for Seismic Retrofitting," by W. Jung, M. Chiewanichakorn and A.J. Aref, 9/21/06 (PB2007-106986).
- MCEER-06-0011 "A Study of the Coupled Horizontal-Vertical Behavior of Elastomeric and Lead-Rubber Seismic Isolation Bearings," by G.P. Warn and A.S. Whittaker, 9/22/06 (PB2007-108679).
- MCEER-06-0012 "Proceedings of the Fourth PRC-US Workshop on Seismic Analysis and Design of Special Bridges: Advancing Bridge Technologies in Research, Design, Construction and Preservation," Edited by L.C. Fan, G.C. Lee and L. Ziang, 10/12/06 (PB2007-109042).
- MCEER-06-0013 "Cyclic Response and Low Cycle Fatigue Characteristics of Plate Steels," by P. Dusicka, A.M. Itani and I.G. Buckle, 11/1/06 (PB2007-106987).
- MCEER-06-0014 "Proceedings of the Second US-Taiwan Bridge Engineering Workshop," edited by W.P. Yen, J. Shen, J-Y. Chen and M. Wang, 11/15/06 (PB2008-500041).
- MCEER-06-0015 "User Manual and Technical Documentation for the REDARSTM Import Wizard," by S. Cho, S. Ghosh, C.K. Huyck and S.D. Werner, 11/30/06 (PB2007-114766).
- MCEER-06-0016 "Hazard Mitigation Strategy and Monitoring Technologies for Urban and Infrastructure Public Buildings: Proceedings of the China-US Workshops," edited by X.Y. Zhou, A.L. Zhang, G.C. Lee and M. Tong, 12/12/06 (PB2008-500018).
- MCEER-07-0001 "Static and Kinetic Coefficients of Friction for Rigid Blocks," by C. Kafali, S. Fathali, M. Grigoriu and A.S. Whittaker, 3/20/07 (PB2007-114767).
- MCEER-07-0002 "Hazard Mitigation Investment Decision Making: Organizational Response to Legislative Mandate," by L.A. Arendt, D.J. Alesch and W.J. Petak, 4/9/07 (PB2007-114768).
- MCEER-07-0003 "Seismic Behavior of Bidirectional-Resistant Ductile End Diaphragms with Unbonded Braces in Straight or Skewed Steel Bridges," by O. Celik and M. Bruneau, 4/11/07 (PB2008-105141).

- MCEER-07-0004 “Modeling Pile Behavior in Large Pile Groups Under Lateral Loading,” by A.M. Dodds and G.R. Martin, 4/16/07(PB2008-105142).
- MCEER-07-0005 “Experimental Investigation of Blast Performance of Seismically Resistant Concrete-Filled Steel Tube Bridge Piers,” by S. Fujikura, M. Bruneau and D. Lopez-Garcia, 4/20/07 (PB2008-105143).
- MCEER-07-0006 “Seismic Analysis of Conventional and Isolated Liquefied Natural Gas Tanks Using Mechanical Analogs,” by I.P. Christovasilis and A.S. Whittaker, 5/1/07.
- MCEER-07-0007 “Experimental Seismic Performance Evaluation of Isolation/Restraint Systems for Mechanical Equipment – Part 1: Heavy Equipment Study,” by S. Fathali and A. Filiatrault, 6/6/07 (PB2008-105144).
- MCEER-07-0008 “Seismic Vulnerability of Timber Bridges and Timber Substructures,” by A.A. Sharma, J.B. Mander, I.M. Friedland and D.R. Allicock, 6/7/07 (PB2008-105145).
- MCEER-07-0009 “Experimental and Analytical Study of the XY-Friction Pendulum (XY-FP) Bearing for Bridge Applications,” by C.C. Marin-Artieda, A.S. Whittaker and M.C. Constantinou, 6/7/07 (PB2008-105191).
- MCEER-07-0010 “Proceedings of the PRC-US Earthquake Engineering Forum for Young Researchers,” Edited by G.C. Lee and X.Z. Qi, 6/8/07 (PB2008-500058).
- MCEER-07-0011 “Design Recommendations for Perforated Steel Plate Shear Walls,” by R. Purba and M. Bruneau, 6/18/07, (PB2008-105192).
- MCEER-07-0012 “Performance of Seismic Isolation Hardware Under Service and Seismic Loading,” by M.C. Constantinou, A.S. Whittaker, Y. Kalpakidis, D.M. Fenz and G.P. Warn, 8/27/07, (PB2008-105193).
- MCEER-07-0013 “Experimental Evaluation of the Seismic Performance of Hospital Piping Subassemblies,” by E.R. Goodwin, E. Maragakis and A.M. Itani, 9/4/07, (PB2008-105194).
- MCEER-07-0014 “A Simulation Model of Urban Disaster Recovery and Resilience: Implementation for the 1994 Northridge Earthquake,” by S. Miles and S.E. Chang, 9/7/07, (PB2008-106426).
- MCEER-07-0015 “Statistical and Mechanistic Fragility Analysis of Concrete Bridges,” by M. Shinozuka, S. Banerjee and S-H. Kim, 9/10/07, (PB2008-106427).
- MCEER-07-0016 “Three-Dimensional Modeling of Inelastic Buckling in Frame Structures,” by M. Schachter and AM. Reinhorn, 9/13/07, (PB2008-108125).
- MCEER-07-0017 “Modeling of Seismic Wave Scattering on Pile Groups and Caissons,” by I. Po Lam, H. Law and C.T. Yang, 9/17/07 (PB2008-108150).
- MCEER-07-0018 “Bridge Foundations: Modeling Large Pile Groups and Caissons for Seismic Design,” by I. Po Lam, H. Law and G.R. Martin (Coordinating Author), 12/1/07 (PB2008-111190).
- MCEER-07-0019 “Principles and Performance of Roller Seismic Isolation Bearings for Highway Bridges,” by G.C. Lee, Y.C. Ou, Z. Liang, T.C. Niu and J. Song, 12/10/07 (PB2009-110466).
- MCEER-07-0020 “Centrifuge Modeling of Permeability and Pinning Reinforcement Effects on Pile Response to Lateral Spreading,” by L.L. Gonzalez-Lagos, T. Abdoun and R. Dobry, 12/10/07 (PB2008-111191).
- MCEER-07-0021 “Damage to the Highway System from the Pisco, Perú Earthquake of August 15, 2007,” by J.S. O’Connor, L. Mesa and M. Nykamp, 12/10/07, (PB2008-108126).
- MCEER-07-0022 “Experimental Seismic Performance Evaluation of Isolation/Restraint Systems for Mechanical Equipment – Part 2: Light Equipment Study,” by S. Fathali and A. Filiatrault, 12/13/07 (PB2008-111192).
- MCEER-07-0023 “Fragility Considerations in Highway Bridge Design,” by M. Shinozuka, S. Banerjee and S.H. Kim, 12/14/07 (PB2008-111193).

- MCEER-07-0024 "Performance Estimates for Seismically Isolated Bridges," by G.P. Warn and A.S. Whittaker, 12/30/07 (PB2008-112230).
- MCEER-08-0001 "Seismic Performance of Steel Girder Bridge Superstructures with Conventional Cross Frames," by L.P. Carden, A.M. Itani and I.G. Buckle, 1/7/08, (PB2008-112231).
- MCEER-08-0002 "Seismic Performance of Steel Girder Bridge Superstructures with Ductile End Cross Frames with Seismic Isolators," by L.P. Carden, A.M. Itani and I.G. Buckle, 1/7/08 (PB2008-112232).
- MCEER-08-0003 "Analytical and Experimental Investigation of a Controlled Rocking Approach for Seismic Protection of Bridge Steel Truss Piers," by M. Pollino and M. Bruneau, 1/21/08 (PB2008-112233).
- MCEER-08-0004 "Linking Lifeline Infrastructure Performance and Community Disaster Resilience: Models and Multi-Stakeholder Processes," by S.E. Chang, C. Pasion, K. Tatebe and R. Ahmad, 3/3/08 (PB2008-112234).
- MCEER-08-0005 "Modal Analysis of Generally Damped Linear Structures Subjected to Seismic Excitations," by J. Song, Y-L. Chu, Z. Liang and G.C. Lee, 3/4/08 (PB2009-102311).
- MCEER-08-0006 "System Performance Under Multi-Hazard Environments," by C. Kafali and M. Grigoriu, 3/4/08 (PB2008-112235).
- MCEER-08-0007 "Mechanical Behavior of Multi-Spherical Sliding Bearings," by D.M. Fenz and M.C. Constantinou, 3/6/08 (PB2008-112236).
- MCEER-08-0008 "Post-Earthquake Restoration of the Los Angeles Water Supply System," by T.H.P. Tabucchi and R.A. Davidson, 3/7/08 (PB2008-112237).
- MCEER-08-0009 "Fragility Analysis of Water Supply Systems," by A. Jacobson and M. Grigoriu, 3/10/08 (PB2009-105545).
- MCEER-08-0010 "Experimental Investigation of Full-Scale Two-Story Steel Plate Shear Walls with Reduced Beam Section Connections," by B. Qu, M. Bruneau, C-H. Lin and K-C. Tsai, 3/17/08 (PB2009-106368).
- MCEER-08-0011 "Seismic Evaluation and Rehabilitation of Critical Components of Electrical Power Systems," S. Ersoy, B. Feizi, A. Ashrafi and M. Ala Saadeghvaziri, 3/17/08 (PB2009-105546).
- MCEER-08-0012 "Seismic Behavior and Design of Boundary Frame Members of Steel Plate Shear Walls," by B. Qu and M. Bruneau, 4/26/08 . (PB2009-106744).
- MCEER-08-0013 "Development and Appraisal of a Numerical Cyclic Loading Protocol for Quantifying Building System Performance," by A. Filiatrault, A. Wanitkorkul and M. Constantinou, 4/27/08 (PB2009-107906).
- MCEER-08-0014 "Structural and Nonstructural Earthquake Design: The Challenge of Integrating Specialty Areas in Designing Complex, Critical Facilities," by W.J. Petak and D.J. Alesch, 4/30/08 (PB2009-107907).
- MCEER-08-0015 "Seismic Performance Evaluation of Water Systems," by Y. Wang and T.D. O'Rourke, 5/5/08 (PB2009-107908).
- MCEER-08-0016 "Seismic Response Modeling of Water Supply Systems," by P. Shi and T.D. O'Rourke, 5/5/08 (PB2009-107910).
- MCEER-08-0017 "Numerical and Experimental Studies of Self-Centering Post-Tensioned Steel Frames," by D. Wang and A. Filiatrault, 5/12/08 (PB2009-110479).
- MCEER-08-0018 "Development, Implementation and Verification of Dynamic Analysis Models for Multi-Spherical Sliding Bearings," by D.M. Fenz and M.C. Constantinou, 8/15/08 (PB2009-107911).
- MCEER-08-0019 "Performance Assessment of Conventional and Base Isolated Nuclear Power Plants for Earthquake Blast Loadings," by Y.N. Huang, A.S. Whittaker and N. Luco, 10/28/08 (PB2009-107912).

- MCEER-08-0020 “Remote Sensing for Resilient Multi-Hazard Disaster Response – Volume I: Introduction to Damage Assessment Methodologies,” by B.J. Adams and R.T. Eguchi, 11/17/08 (PB2010-102695).
- MCEER-08-0021 “Remote Sensing for Resilient Multi-Hazard Disaster Response – Volume II: Counting the Number of Collapsed Buildings Using an Object-Oriented Analysis: Case Study of the 2003 Bam Earthquake,” by L. Gusella, C.K. Huyck and B.J. Adams, 11/17/08 (PB2010-100925).
- MCEER-08-0022 “Remote Sensing for Resilient Multi-Hazard Disaster Response – Volume III: Multi-Sensor Image Fusion Techniques for Robust Neighborhood-Scale Urban Damage Assessment,” by B.J. Adams and A. McMillan, 11/17/08 (PB2010-100926).
- MCEER-08-0023 “Remote Sensing for Resilient Multi-Hazard Disaster Response – Volume IV: A Study of Multi-Temporal and Multi-Resolution SAR Imagery for Post-Katrina Flood Monitoring in New Orleans,” by A. McMillan, J.G. Morley, B.J. Adams and S. Chesworth, 11/17/08 (PB2010-100927).
- MCEER-08-0024 “Remote Sensing for Resilient Multi-Hazard Disaster Response – Volume V: Integration of Remote Sensing Imagery and VIEWS™ Field Data for Post-Hurricane Charley Building Damage Assessment,” by J.A. Womble, K. Mehta and B.J. Adams, 11/17/08 (PB2009-115532).
- MCEER-08-0025 “Building Inventory Compilation for Disaster Management: Application of Remote Sensing and Statistical Modeling,” by P. Sarabandi, A.S. Kiremidjian, R.T. Eguchi and B. J. Adams, 11/20/08 (PB2009-110484).
- MCEER-08-0026 “New Experimental Capabilities and Loading Protocols for Seismic Qualification and Fragility Assessment of Nonstructural Systems,” by R. Retamales, G. Mosqueda, A. Filiatrault and A. Reinhorn, 11/24/08 (PB2009-110485).
- MCEER-08-0027 “Effects of Heating and Load History on the Behavior of Lead-Rubber Bearings,” by I.V. Kalpakidis and M.C. Constantinou, 12/1/08 (PB2009-115533).
- MCEER-08-0028 “Experimental and Analytical Investigation of Blast Performance of Seismically Resistant Bridge Piers,” by S.Fujikura and M. Bruneau, 12/8/08 (PB2009-115534).
- MCEER-08-0029 “Evolutionary Methodology for Aseismic Decision Support,” by Y. Hu and G. Dargush, 12/15/08.
- MCEER-08-0030 “Development of a Steel Plate Shear Wall Bridge Pier System Conceived from a Multi-Hazard Perspective,” by D. Keller and M. Bruneau, 12/19/08 (PB2010-102696).
- MCEER-09-0001 “Modal Analysis of Arbitrarily Damped Three-Dimensional Linear Structures Subjected to Seismic Excitations,” by Y.L. Chu, J. Song and G.C. Lee, 1/31/09 (PB2010-100922).
- MCEER-09-0002 “Air-Blast Effects on Structural Shapes,” by G. Ballantyne, A.S. Whittaker, A.J. Aref and G.F. Dargush, 2/2/09 (PB2010-102697).
- MCEER-09-0003 “Water Supply Performance During Earthquakes and Extreme Events,” by A.L. Bonneau and T.D. O’Rourke, 2/16/09 (PB2010-100923).
- MCEER-09-0004 “Generalized Linear (Mixed) Models of Post-Earthquake Ignitions,” by R.A. Davidson, 7/20/09 (PB2010-102698).
- MCEER-09-0005 “Seismic Testing of a Full-Scale Two-Story Light-Frame Wood Building: NEESWood Benchmark Test,” by I.P. Christovasilis, A. Filiatrault and A. Wanitkorkul, 7/22/09 (PB2012-102401).
- MCEER-09-0006 “IDARC2D Version 7.0: A Program for the Inelastic Damage Analysis of Structures,” by A.M. Reinhorn, H. Roh, M. Sivaselvan, S.K. Kunnath, R.E. Valles, A. Madan, C. Li, R. Lobo and Y.J. Park, 7/28/09 (PB2010-103199).
- MCEER-09-0007 “Enhancements to Hospital Resiliency: Improving Emergency Planning for and Response to Hurricanes,” by D.B. Hess and L.A. Arendt, 7/30/09 (PB2010-100924).

- MCEER-09-0008 “Assessment of Base-Isolated Nuclear Structures for Design and Beyond-Design Basis Earthquake Shaking,” by Y.N. Huang, A.S. Whittaker, R.P. Kennedy and R.L. Mayes, 8/20/09 (PB2010-102699).
- MCEER-09-0009 “Quantification of Disaster Resilience of Health Care Facilities,” by G.P. Cimellaro, C. Fumo, A.M. Reinhorn and M. Bruneau, 9/14/09 (PB2010-105384).
- MCEER-09-0010 “Performance-Based Assessment and Design of Squat Reinforced Concrete Shear Walls,” by C.K. Gulec and A.S. Whittaker, 9/15/09 (PB2010-102700).
- MCEER-09-0011 “Proceedings of the Fourth US-Taiwan Bridge Engineering Workshop,” edited by W.P. Yen, J.J. Shen, T.M. Lee and R.B. Zheng, 10/27/09 (PB2010-500009).
- MCEER-09-0012 “Proceedings of the Special International Workshop on Seismic Connection Details for Segmental Bridge Construction,” edited by W. Phillip Yen and George C. Lee, 12/21/09 (PB2012-102402).
- MCEER-10-0001 “Direct Displacement Procedure for Performance-Based Seismic Design of Multistory Woodframe Structures,” by W. Pang and D. Rosowsky, 4/26/10 (PB2012-102403).
- MCEER-10-0002 “Simplified Direct Displacement Design of Six-Story NEESWood Capstone Building and Pre-Test Seismic Performance Assessment,” by W. Pang, D. Rosowsky, J. van de Lindt and S. Pei, 5/28/10 (PB2012-102404).
- MCEER-10-0003 “Integration of Seismic Protection Systems in Performance-Based Seismic Design of Woodframed Structures,” by J.K. Shinde and M.D. Symans, 6/18/10 (PB2012-102405).
- MCEER-10-0004 “Modeling and Seismic Evaluation of Nonstructural Components: Testing Frame for Experimental Evaluation of Suspended Ceiling Systems,” by A.M. Reinhorn, K.P. Ryu and G. Maddaloni, 6/30/10 (PB2012-102406).
- MCEER-10-0005 “Analytical Development and Experimental Validation of a Structural-Fuse Bridge Pier Concept,” by S. El-Bahey and M. Bruneau, 10/1/10 (PB2012-102407).
- MCEER-10-0006 “A Framework for Defining and Measuring Resilience at the Community Scale: The PEOPLES Resilience Framework,” by C.S. Renschler, A.E. Frazier, L.A. Arendt, G.P. Cimellaro, A.M. Reinhorn and M. Bruneau, 10/8/10 (PB2012-102408).
- MCEER-10-0007 “Impact of Horizontal Boundary Elements Design on Seismic Behavior of Steel Plate Shear Walls,” by R. Purba and M. Bruneau, 11/14/10 (PB2012-102409).
- MCEER-10-0008 “Seismic Testing of a Full-Scale Mid-Rise Building: The NEESWood Capstone Test,” by S. Pei, J.W. van de Lindt, S.E. Pryor, H. Shimizu, H. Isoda and D.R. Rammer, 12/1/10 (PB2012-102410).
- MCEER-10-0009 “Modeling the Effects of Detonations of High Explosives to Inform Blast-Resistant Design,” by P. Sherkar, A.S. Whittaker and A.J. Aref, 12/1/10 (PB2012-102411).
- MCEER-10-0010 “L’Aquila Earthquake of April 6, 2009 in Italy: Rebuilding a Resilient City to Withstand Multiple Hazards,” by G.P. Cimellaro, I.P. Christovasilis, A.M. Reinhorn, A. De Stefano and T. Kirova, 12/29/10.
- MCEER-11-0001 “Numerical and Experimental Investigation of the Seismic Response of Light-Frame Wood Structures,” by I.P. Christovasilis and A. Filiatrault, 8/8/11 (PB2012-102412).
- MCEER-11-0002 “Seismic Design and Analysis of a Precast Segmental Concrete Bridge Model,” by M. Anagnostopoulou, A. Filiatrault and A. Aref, 9/15/11.
- MCEER-11-0003 “Proceedings of the Workshop on Improving Earthquake Response of Substation Equipment,” Edited by A.M. Reinhorn, 9/19/11 (PB2012-102413).
- MCEER-11-0004 “LRFD-Based Analysis and Design Procedures for Bridge Bearings and Seismic Isolators,” by M.C. Constantinou, I. Kalpakidis, A. Filiatrault and R.A. Ecker Lay, 9/26/11.

- MCEER-11-0005 “Experimental Seismic Evaluation, Model Parameterization, and Effects of Cold-Formed Steel-Framed Gypsum Partition Walls on the Seismic Performance of an Essential Facility,” by R. Davies, R. Retamales, G. Mosqueda and A. Filiatrault, 10/12/11.
- MCEER-11-0006 “Modeling and Seismic Performance Evaluation of High Voltage Transformers and Bushings,” by A.M. Reinhorn, K. Oikonomou, H. Roh, A. Schiff and L. Kempner, Jr., 10/3/11.
- MCEER-11-0007 “Extreme Load Combinations: A Survey of State Bridge Engineers,” by G.C. Lee, Z. Liang, J.J. Shen and J.S. O’Connor, 10/14/11.
- MCEER-12-0001 “Simplified Analysis Procedures in Support of Performance Based Seismic Design,” by Y.N. Huang and A.S. Whittaker.
- MCEER-12-0002 “Seismic Protection of Electrical Transformer Bushing Systems by Stiffening Techniques,” by M. Koliou, A. Filiatrault, A.M. Reinhorn and N. Oliveto, 6/1/12.
- MCEER-12-0003 “Post-Earthquake Bridge Inspection Guidelines,” by J.S. O’Connor and S. Alampalli, 6/8/12.
- MCEER-12-0004 “Integrated Design Methodology for Isolated Floor Systems in Single-Degree-of-Freedom Structural Fuse Systems,” by S. Cui, M. Bruneau and M.C. Constantinou, 6/13/12.



EARTHQUAKE ENGINEERING TO EXTREME EVENTS

University at Buffalo, The State University of New York

133A Ketter Hall ■ Buffalo, New York 14260-4300

Phone: (716) 645-3391 ■ Fax: (716) 645-3399

Email: mceer@buffalo.edu ■ Web: <http://mceer.buffalo.edu>



University at Buffalo *The State University of New York*

ISSN 1520-295X